

Berechnung von Massen, Zerfällen und Struktur von Hadronen mit Methoden der Gitter-QCD

Schriftliche Habilitationsleistungen

Marc Wagner

Goethe-Universität Frankfurt am Main, Institut für Theoretische Physik,
Max-von-Laue-Straße 1, D-60438 Frankfurt am Main, Germany

11. Januar 2015

vorgelegt beim Fachbereich Physik der Goethe-Universität Frankfurt am Main

Teil I

Zusammenfassende Diskussion

Die in Teil II enthaltenen Arbeiten, die über das Habilitationsthema
**“Berechnung von Massen, Zerfällen und Struktur von Hadronen mit Methoden
der Gitter-QCD”**

in thematischem Zusammenhang stehen, werden im Folgenden zusammengefasst.

Berechnung von Massen, Zerfällen und Struktur von Hadronen mit Methoden der Gitter-QCD

Marc Wagner

Goethe-Universität Frankfurt am Main, Institut für Theoretische Physik,
Max-von-Laue-Straße 1, D-60438 Frankfurt am Main, Germany

11. Januar 2015

Es wird eine Reihe von thematisch ähnlichen Arbeiten aus dem Bereich der Gitter-QCD zusammengefasst, die sich mit der Berechnung von Massen, Zerfällen und der Struktur von Hadronen befassen. In diesen Arbeiten werden verschiedene Systeme untersucht, unter anderem leichte skalare Mesonen, D - und D_s -Mesonen, Charmoniumzustände, B - und B_s -Mesonen sowie b -Baryonen. Die verwendeten Techniken decken ebenfalls ein breites Spektrum ab. Einfach strukturierte Hadronen werden mit Standard- $q\bar{q}$ - und - qqq -Erzeugungsoperatoren untersucht, während für weniger gut verstandene Hadronen, wie z.B. leichte skalare Mesonen und andere Tetraquarkkandidaten, mehrere Erzeugungsoperatoren unterschiedlicher Struktur eingesetzt werden. Außerdem werden Kräfte zwischen schweren Mesonen berechnet, die, weiterverwendet in Modellrechnungen, Hinweise auf die Existenz von Tetraquarkzuständen geben.

1 Einleitung

Bei diesem vorliegenden Teil I handelt es sich um eine zusammenfassende Diskussion der Arbeiten [1, 2, 3, 4, 5, 6, 7, 8, 9, 10, 11, 12, 13, 14, 15], die Teil der schriftlichen Habilitationsleistungen in einem kumulativen Verfahren ist. Der Inhalt, insbesondere die wesentlichen Ergebnisse der Arbeiten [1, 2, 3, 4, 5, 6, 7, 8, 9, 10, 11, 12, 13, 14, 15] werden grob skizziert und ihr Zusammenhang über das Habilitationsthema **“Berechnung von Massen, Zerfällen und Struktur von Hadronen mit Methoden der Gitter-QCD”** wird herausgearbeitet. Weitere Details sind den Arbeiten [1, 2, 3, 4, 5, 6, 7, 8, 9, 10, 11, 12, 13, 14, 15] selbst zu entnehmen, die in Teil II abgedruckt sind. Da diese Zusammenfassung eine ganze Reihe von Unterthemen abdeckt, würde eine vollständige Diskussionen existierender Literatur ihren Umfang bei weitem sprengen. Auch hierfür sei auf die Arbeiten [1, 2, 3, 4, 5, 6, 7, 8, 9, 10, 11, 12, 13, 14, 15] verwiesen.

1.1 Motivation

QCD (Quantenchromodynamik) ist die Theorie der starken Wechselwirkung. Sie beschreibt Quarks, Gluonen und die zwischen ihnen wirkenden Kräfte. Sie erklärt damit auch die Existenz der aus Quarks und Gluonen zusammengesetzten Hadronen, d.h. Mesonen, in der Regel Quark-Antiquark-Paare $q\bar{q}$, und Baryonen, gebundene Zustände von drei Quarks qqq oder drei Antiquarks $\bar{q}\bar{q}\bar{q}$.

Analytisch kann QCD nur bei hohen Energien mit Hilfe von Störungstheorie behandelt werden, da in diesem Regime die Kopplungskonstante der QCD klein ist und QCD sich ähnlich, wie eine freie Theorie verhält. Will man Rechnungen abseits von hohen Energien ausführen, z.B. Hadronmassen ausgehend von der QCD, d.h. von den elementaren Quarks und Gluonen, berechnen, ist man auf numerische Methoden, die sogenannte Gitter-QCD angewiesen.

Es gibt eine lange Reihe von interessanten Fragestellungen, die mit Hilfe von Gitter-QCD untersucht werden können, von denen im Folgenden nur einige wenige exemplarisch genannt werden. Z.B. kann durch Nachrechnen experimentell beobachteter Eigenschaften von Hadronen die QCD bzw. das Standardmodell als korrekte Theorie der Teilchenphysik verifiziert werden, zumindest bis zur experimentellen Mess- und theoretischen Rechengenauigkeit. Auf gleichem Weg kann auch versucht werden, neue Physik jenseits des Standardmodells zu entdecken. Eine andere Möglichkeit besteht darin, mit Hilfe von Gitter-QCD hadronische Zustände vorausberechnen, die experimentell noch gar nicht gemessen wurden. Ferner ist es möglich, Massen, Quantenzahlen und Struktur von experimentell weniger gut vermessenen und/oder theoretisch verstandenen Hadronen (z.B. “omitted from summary table” im “Review of Particle Physics” [16]) zu bestimmen. Des Weiteren liefern Gitter-QCD-Rechnungen Einsichten in Systeme und Bereiche, die experimentell nur schwer zugänglich sind, z.B. die Kraft zwischen einem Quark und einem Antiquark oder das Verhalten von QCD bei sehr hohen Temperaturen.

Hier werden Arbeiten aus dem Bereich der Gitter-QCD zusammengefasst und diskutiert, die sich mit der Berechnung von Massen und teilweise auch von Zerfällen von Hadronen, insbesondere von Mesonen beschäftigen. In mehreren Fällen wird auch versucht, Aussagen über die Struktur dieser Mesonen zu treffen (z.B. ob es sich um ein Quark-Antiquark-Paar oder um ein Tetraquark handelt, oder welchen Anteil am Gesamtspin die leichten Quarks und Gluonen tragen). Dabei wird ein breites Spektrum von Hadronen studiert: leichte skalare Mesonen, D - und D_s -Mesonen, Charmonium-Zustände, B - und B_s -Mesonen sowie b -Baryonen. Ein signifikanter

Teil der Untersuchungen gilt weniger gut verstandenen Mesonen, insbesondere solchen, bei denen eine 4-Quark-Struktur, also zwei Quarks und zwei Antiquarks, vermutet wird, sogenannte Tetraquark-Kandidaten. Das globale Ziel der diskutierten Arbeiten [1, 2, 3, 4, 5, 6, 7, 8, 9, 10, 11, 12, 13, 14, 15] und auch sich aktuell anschließender und zukünftiger Folgeprojekte besteht darin, ein umfassendes theoretisches Bild von Hadronen, vor allem von Mesonen, zu erhalten: präzise Ergebnisse für Massen und spezielle Zerfälle der gut verstandenen und einfach strukturierten Mesonen (z.B. pseudoskalare Mesonen) und zumindest grobe Ergebnisse und qualitative Einsichten bezüglich Massen und Struktur der weniger gut verstandenen Mesonen (radial oder orbital angeregte Mesonen, Tetraquark-Kandidaten, Resonanzen).

1.2 Gliederung

Die vorliegende zusammenfassende Diskussion ist wie folgt gegliedert. In Kapitel 2 werden Grundlagen der Gitter-QCD und -hadronspektroskopie oberflächlich skizziert. Dieses Kapitel eignet sich vor allem für Leser, die bestenfalls ein oberflächliches Wissen über Gitter-QCD mitbringen und kann von Experten problemlos übersprungen werden. Das sich anschließende kurze Kapitel 3 nennt wesentliche Eigenschaften des verwendeten Gitter-QCD-Setups, insbesondere auch der eingesetzten Wilson-Twisted-Mass-Diskretisierung. Im Hauptteil, der aus den Kapiteln 4, 5 und 6 besteht, werden die Arbeiten [1, 2, 3, 4, 5, 6, 7, 8, 9, 10, 11, 12, 13, 14, 15] zusammengefasst. Zuerst werden in Kapitel 4 Gitter-QCD-Rechnungen diskutiert, in denen Standard- $q\bar{q}$ - und - qqq -Erzeugungsoperatoren verwendet werden. Ein derartiges Vorgehen eignet sich für das Studium von Hadronen, die eine solche $q\bar{q}$ - oder qqq -Struktur aufweisen. Im folgenden Kapitel 5 wird die sehr viel aufwändigere Untersuchung von Tetraquarkkandidaten mit einer Vielzahl von Erzeugungsoperatoren unterschiedlicher Struktur besprochen. Schließlich geht es in Kapitel 6 um die Berechnung von Kräften zwischen zwei schwere Mesonen. Diese Ergebnisse werden dann in Modellrechnungen weiterverwendet, um herauszufinden, in welchen Kanälen möglicherweise Tetraquarks existieren. Kapitel 7 enthält eine kurze Zusammenfassung und einen Ausblick.

2 Grundlagen der Gitter-QCD und -hadronspektroskopie

In diesem Kapitel werden einige Elemente der QCD und der Gitter-QCD kurz wiederholt, die zum Verständnis der Arbeiten [1, 2, 3, 4, 5, 6, 7, 8, 9, 10, 11, 12, 13, 14, 15] wesentlich sind. Damit soll unter anderem die in dieser Zusammenfassung verwendete Notation eingeführt werden. Ausführliche Erklärungen, Herleitungen und technische Details können z.B. in den Lehrbüchern [17, 18, 19, 20, 21, 22, 23] oder in den Vorlesungsaufzeichnungen [24] nachgelesen werden.

2.1 Die QCD-Wirkung

Die Freiheitsgrade der QCD sind die sechs Quarkfelder

$$\psi^{(q)}(x) \equiv \psi^{(q)}(\mathbf{r}, t), \quad q \in \{u, d, s, c, t, b\} \quad (1)$$

(up (u), down (d), strange (s), charm (c), bottom (b) und top (t) bezeichnet man als Flavors) und das Gluonfeld

$$A_\mu(x) \equiv A_\mu(\mathbf{r}, t). \quad (2)$$

Diese Felder setzen sich aus einer Reihe von Komponenten zusammen, nummeriert durch verschiedene Indizes.

Die Quarkfelder $\psi_A^{a,(q)}$ besitzen einen Farbindex $a = 1, \dots, 3$ (Quarks tragen Farbladung, die in drei Sorten auftritt, bezeichnet als rot, grün und blau). Da Quarks Spin-1/2-Fermionen sind, tragen sie auch einen Spinindex $A = 1, \dots, 4$ (die vier Komponenten beschreiben Spin ‘‘up’’ und ‘‘down’’, sowie Teilchen und Antiteilchen). Außerdem existiert der bereits angesprochene Flavorindex $q = u, d, s, c, b, t$. Quarks verschiedener Flavors unterscheiden sich in ihrer Masse, $m_u \approx 2.3 \text{ MeV}$, $m_d \approx 4.8 \text{ MeV}$, $m_s \approx 95 \text{ MeV}$, $m_c \approx 1.28 \text{ GeV}$, $m_b \approx 4.18 \text{ GeV}$, $m_t \approx 173 \text{ GeV}^1$ [16].

Das Gluonfeld A_μ^a besitzt ebenfalls einen Farbindex $a = 1, \dots, 8$. Häufig ist es zweckmäßig, das Gluonfeld als Matrix $A_\mu = A_\mu^a \lambda^a / 2$ zu schreiben, wobei λ^a die acht 3×3 -Gell-Mann-Matrizen bezeichnen,

$$\lambda^1 = \begin{pmatrix} 0 & +1 & 0 \\ +1 & 0 & 0 \\ 0 & 0 & 0 \end{pmatrix}, \quad \lambda^2 = \begin{pmatrix} 0 & -i & 0 \\ +i & 0 & 0 \\ 0 & 0 & 0 \end{pmatrix}, \quad \dots \quad (3)$$

Die drei Zeilen und Spalten der Gell-Mann-Matrizen entsprechen den Quarkfarben rot, grün und blau bzw. den Farbindizes $a = 1, \dots, 3$ der Quarkfelder. Z.B. vermitteln Gluonen, die Anregungen der Feldkomponente A_μ^1 entsprechen, Kräfte zwischen roten und grünen Quarks. Da Gluonen Spin-1-Teilchen sind, gibt es auch einen Lorentz-Index $\mu = 0, \dots, 3$.

Der Quarkanteil der QCD-Wirkung² hängt sowohl von den Quarkfeldern und dem Gluonfeld

¹In dieser Zusammenfassung werden durchgehend natürliche Einheiten verwendet, d.h. $\hbar = c = 1$.

²In dieser Zusammenfassung wird ausschließlich die Euklidische Version der QCD verwendet.

ab,

$$\begin{aligned} S_{\text{quark}}[\psi, \bar{\psi}, A] &= \int d^4x \sum_f \bar{\psi}^{(q)} \left(\gamma_\mu D_\mu + m_q \right) \psi^{(q)} = \\ &= \int d^4x \sum_f \bar{\psi}_A^{a,(q)} \left(\gamma_{\mu,AB} \left(\delta^{ab} \partial_\mu - ig A_\mu^c \lambda^{c,ab} / 2 \right) + \delta^{ab} \delta_{AB} m_q \right) \psi_B^{b,(q)}. \end{aligned} \quad (4)$$

$\bar{\psi} = \psi^\dagger \gamma_0$, $D_\mu = \partial_\mu - ig A_\mu$ bezeichnet die kovariante Ableitung und g die QCD-Kopplungskonstante. γ_μ sind die bekannten 4×4 -Dirac-Matrizen, die z.B. in der Standarddarstellung

$$\gamma_0 = \begin{pmatrix} +1 & 0 \\ 0 & -1 \end{pmatrix}, \quad \gamma_j = \begin{pmatrix} 0 & +i\sigma_j \\ -i\sigma_j & 0 \end{pmatrix}, \quad (5)$$

lauten mit den Pauli-Matrizen

$$\sigma_1 = \begin{pmatrix} 0 & +1 \\ +1 & 0 \end{pmatrix}, \quad \sigma_2 = \begin{pmatrix} 0 & -i \\ +i & 0 \end{pmatrix}, \quad \sigma_3 = \begin{pmatrix} +1 & 0 \\ 0 & -1 \end{pmatrix}. \quad (6)$$

Der Gluonanteil der QCD-Wirkung hängt nur vom Gluonfeld ab,

$$S_{\text{gluon}}[A] = \frac{1}{4} \int d^4x F_{\mu\nu}^a F_{\mu\nu}^a, \quad F_{\mu\nu}^a = \partial_\mu A_\nu^a - \partial_\nu A_\mu^a + g f^{abc} A_\mu^b A_\nu^c \quad (7)$$

bzw. in Matrixschreibweise

$$\begin{aligned} S_{\text{gluon}}[A] &= \frac{1}{2} \int d^4x \text{Tr} \left(F_{\mu\nu} F_{\mu\nu} \right), \\ F_{\mu\nu} &= F_{\mu\nu}^a \frac{\lambda^a}{2} = \partial_\mu A_\nu - \partial_\nu A_\mu - ig [A_\mu, A_\nu] \end{aligned} \quad (8)$$

(f^{abc} sind die antisymmetrischen Strukturkonstanten der Gruppe SU(3), $[\lambda^a/2, \lambda^b/2] = if^{abc}\lambda^c/2$).

Die vollständige QCD-Wirkung entspricht der Summe der beiden genannten Anteile,

$$S_{\text{QCD}}[\psi, \bar{\psi}, A] = S_{\text{quark}}[\psi, \bar{\psi}, A] + S_{\text{gluon}}[A]. \quad (9)$$

2.2 Quantisierung der QCD

Die zur numerischen Umsetzung mit Hilfe von Gitter-QCD geeignete Methode der Quantisierung der QCD ist der Pfadintegralformalismus. Vakuumerwartungswerte von zeitgeordneten Produkten von Feldoperatoren können wie folgt durch Pfadintegrale ausgedrückt werden:

$$\begin{aligned} \langle \Omega | T \left\{ \mathcal{O}_1(t_1) \dots \mathcal{O}_n(t_n) \right\} | \Omega \rangle &= \frac{1}{Z} \int D\psi D\bar{\psi} \int DA \mathcal{O}_1(t_1) \dots \mathcal{O}_n(t_n) e^{-S_{\text{QCD}}[\psi, \bar{\psi}, A]}, \\ Z &= \int D\psi D\bar{\psi} \int DA e^{-S_{\text{QCD}}[\psi, \bar{\psi}, A]}, \end{aligned} \quad (10)$$

wobei

- $|\Omega\rangle$ der QCD-Grundzustand, also das Vakuum ist,
- $\int D\psi D\bar{\psi}$ die Integration über alle denkbaren Quarkfeldkonfigurationen $\psi^{(q)}$ beschreibt,
- $\int DA$ die Integration über alle denkbaren Gluonfeldkonfigurationen A_μ beschreibt,
- $\mathcal{O}_j(t_j)$ ein aus den Quarkfeldern $\psi^{(q)}(\mathbf{r})$ und $\bar{\psi}^{(q)}(\mathbf{r})$ zum Zeitpunkt t_j und dem Gluonfeld $A_\mu(\mathbf{r})$ zum Zeitpunkt t_j zusammengesetzter Operator ist,
- $T\{\dots\}$ Zeitordnung bezeichnet, d.h. die Operatoren innerhalb $\{\dots\}$ so umzuordnen sind, dass sie von links nach rechts gemäß ihren Zeitargumenten absteigend sortiert sind.

Zur Bestimmung von Hadronmassen werden Korrelationsfunktionen von Hadron-Erzeugungsoperatoren benötigt. Als Beispiel kann hier die für die Berechnung der Pionmasse erforderliche Korrelationsfunktion

$$\langle \Omega | \left(\mathcal{O}_\pi(t_2) \right)^\dagger \mathcal{O}_\pi(t_1) | \Omega \rangle = \frac{1}{Z} \int D\psi D\bar{\psi} \int DA \left(\mathcal{O}_\pi(t_2) \right)^\dagger \mathcal{O}_\pi(t_1) e^{-S_{\text{QCD}}[\psi, \bar{\psi}, A]} \quad (11)$$

mit dem Pion-Erzeugungsoperator

$$\mathcal{O}_\pi(t) \equiv \int d^3r \bar{u}(\mathbf{r}, t) \gamma_5 d(\mathbf{r}, t) \quad (12)$$

$(\gamma_5 = \gamma_0 \gamma_1 \gamma_2 \gamma_3)$ genannt werden.

2.3 Gitter-QCD: Numerische Berechnung von QCD-Pfadintegralen

QCD-Pfadintegrale (10) analytisch zu lösen scheint mit momentan bekannten Techniken der Mathematik nicht möglich zu sein. QCD-Pfadintegrale eignen sich allerdings zur numerischen Auswertung auf Hochleistungscomputersystemen. Die dazu erforderlichen Techniken werden als Gitter-QCD bezeichnet.

Die grundlegenden Ideen der Gitter-QCD sind die Folgenden:

- Die Raumzeit wird durch ein kubisches Gitter diskretisiert, $x_\mu \in \mathbb{R}^4 \rightarrow x_\mu = an_\mu$, $n_\mu \in \mathbb{Z}^4$ (a bezeichnet den Gitterabstand; siehe Abbildung 1).
- Die Raumzeit wird in Form eines 4-dimensionalen Torus periodisiert. Die Ausdehnung ist $L = aN_L$, wobei N_L die Anzahl der Gitterplätze in jeder Raumzeitrichtung bezeichnet, also insgesamt N_L^4 Gitterplätze. Folglich gilt $x_\mu \equiv x_\mu + Le_\mu^{(\nu)}$ ($e^{(\nu)}$ ist der Einheitsvektor in ν -Richtung).
- Die im Kontinuum unendliche Anzahl der Freiheitsgrade einer Quarkfeldkomponente $\psi_A^{b,(q)}$, parametrisiert durch ein kontinuierliches Raumzeitargument, ist nun auf die endliche Anzahl N_L^4 reduziert, eine Feldvariable $\psi_A^{b,(q)}(an_\mu)$ pro Gitterpunkt n_μ .

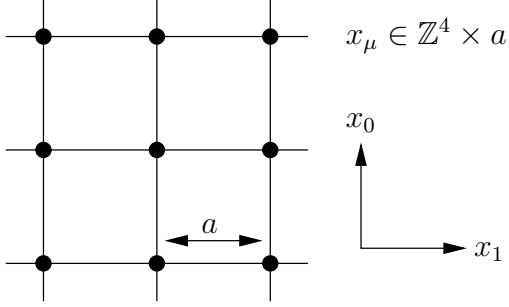


Abbildung 1: Kubische Gitterdiskretisierung der Raumzeit.

- Um die in der QCD wichtige Eichsymmetrie zu erhalten, wird nach der Diskretisierung nicht das Gluonfeld an den Gitterpunkten betrachtet, sondern sogenannte Links oder Linkvariablen $U_\nu(an_\mu) \in \text{SU}(3)$, die benachbarte Gitterpunkte n_μ und $n_\mu + e_\mu^{(\nu)}$ verbinden. Im Kontinuum entsprechen diese Links den bekannten Paralleltransportern,

$$U_\nu(an_\mu) \rightarrow P \exp \left(-ig \int_{an_\mu}^{a(n_\mu + e_\mu^{(\nu)})} dz_\rho A_\rho(z) \right), \quad (13)$$

die vom Gluonfeld abhängen.

- Es resultiert ein endlich-dimensionales Gitter-QCD-Pfadintegral

$$\begin{aligned} & \int D\psi D\bar{\psi} \int DA \rightarrow \\ & \rightarrow \prod_{n_\mu} \left(\prod_{A,b,q} \int d\psi_A^{b,(q)}(an_\mu) d\bar{\psi}_A^{b,(q)}(an_\mu) \right) \left(\prod_\nu \int dU_\nu(an_\mu) \right), \end{aligned} \quad (14)$$

das numerisch gelöst werden kann.

- Sämtliche Kontinuumsausdrücke, die Quarkfelder und das Gluonfeld enthalten, müssen durch entsprechende Gitterausdrücke approximiert werden, die sich ausschließlich aus den Quarkfeldern an den Gitterpunkten $\psi^{(q)}(an_\mu)$ und den Linkvariablen $U_\nu(an_\mu)$ zusammensetzen. Eine solche Diskretisierung ist nicht eindeutig. Gitterausdrücke müssen lediglich im Limes $a \rightarrow 0$ in die entsprechenden Kontinuumsausdrücke übergehen. Als Beispiel kann die sogenannte Wilson-Plaketten-Wirkung genannt werden, die eine Diskretisierung des Gluonanteils der QCD-Wirkung ist,

$$\begin{aligned} S_{\text{gluon}}^{\text{lattice, WP}}(U) &= \frac{1}{g^2} \sum_{n_\mu} \sum_{\rho,\sigma} \text{Tr} \left(1 - \frac{1}{2} \left(U_{\rho\sigma}(an_\mu) + U_{\rho\sigma}^\dagger(an_\mu) \right) \right) \stackrel{a \rightarrow 0}{=} \\ &\stackrel{a \rightarrow 0}{=} S_{\text{gluon}}[A] = \frac{1}{2} \int d^4x \text{Tr} \left(F_{\rho\sigma} F_{\rho\sigma} \right) \end{aligned} \quad (15)$$

mit der Plakette

$$U_{\rho\sigma}(an_\mu) \equiv U_\rho(an_\mu) U_\sigma(a(n_\mu + e_\mu^{(\rho)})) U_\rho^\dagger(a(n_\mu + e_\mu^{(\sigma)})) U_\sigma^\dagger(an_\mu) \quad (16)$$

(für eine Herleitung dieser Beziehung siehe z.B. [21]).

Wird der Gitterabstand a klein und die Gitterausdehnung L gleichzeitig groß gewählt, weichen Gitter-QCD-Ergebnisse von QCD-Ergebnissen kaum ab. Die kleinen Differenzen aufgrund von Diskretisierungs- und Periodizitätsfehlern können quantifiziert oder sogar mit Hilfe geeigneter Extrapolationen entfernt werden, wenn Gitter-QCD-Rechnungen für verschiedene Werte von a und von L ausgeführt werden.

Die Dimensionalität eines typischen Gitter-QCD-Pfadintegrals kann leicht abgeschätzt werden:

- $n_\mu \in \{0, 1, \dots, N_L - 1\}^4$: Z.B. für $N_L = 32$, $32^4 \approx 10^6$ Gitterplätze (eine typische Anzahl von Gitterplätzen für gegenwärtige Rechnungen).
- $\psi_A^{b,(q)}$: 24 Quarkfreiheitsgrade für jeden Quarkflavor (Real- und Imaginärteil von ψ , Farbe $b = 1, \dots, 3$, Spin $A = 1, \dots, 4$); ≥ 2 Flavors, d.h. mindestens u - und d -Quarks, oft auch s - und c -Quarks.
- U_ν (das Gitteräquivalent zu A_ν^a): 32 Gluonfreiheitsgrade (Farbe $a = 1, \dots, 8$, Spin $\nu = 0, \dots, 3$).
- Insgesamt ein $32^4 \times (2 \times 24 + 32) \approx 83 \times 10^6$ -dimensionales Integral.

Offensichtlich erfordern solche hochdimensionalen Integrale ausgefeilte Integrationsalgorithmen sowie Hochleistungscomputersysteme. Man verwendet stochastische Integrationsverfahren, sogenannte Monte-Carlo-Techniken, die mit Hilfe von Zufallsexperimenten eine kleine aber repräsentative Menge von Eichfeldkonfigurationen (beschrieben durch Angabe sämtlicher Linkvariablen) generieren. Repräsentativ heißt in diesem Zusammenhang gemäß dem Integrationsmaß und dem exponentiellen Gewichtungsfaktor im Pfadintegral zufällig verteilt. Liegt eine solche repräsentative Menge von Eichfeldkonfigurationen erst einmal vor, können Vakuumerwartungswerte einfach dadurch bestimmt werden, dass die entsprechende Größe auf jeder der Eichfeldkonfigurationen ausgewertet wird und die Ergebnisse gemittelt werden.

2.4 Berechnung von Hadron-Massen

2.4.1 Klassifikation von Hadronen

Hadronen und ihre Eigenschaften, wie z.B. Massen und Zerfallsraten, werden von der Particle-Data-Group zusammengestellt und regelmäßig aktualisiert [16]. Hadronische Zustände werden im Wesentlichen durch QCD-Quantenzahlen klassifiziert:

- Gesamtspin bzw. -drehimpuls J (geradzahlig für Bosonen, $J = 0, 1, 2, \dots$; ungeradzahlig für Fermionen $J = 1/2, 3/2, 5/2, \dots$).
- Parität (Raumspiegelung) $P = \pm 1$.
- Ladungskonjugation (Vertauschen von Quarks und Antiquarks) $C = \pm 1$ (nur für flavor-neutrale Mesonen).
- Flavorquantenzahlen:
Isospin: I ; $I_z = +1/2$ (u), $I_z = -1/2$ (d).
Strangeness: $S = -1$ (s), $S = +1$ (\bar{s}).

Charm: $C' = +1$ (c), $C' = -1$ (\bar{c}).
 Bottomness: $B' = -1$ (b), $B' = +1$ (\bar{b}).
 Topness: $T = +1$ (t), $T = -1$ (\bar{t}).

- Da Elektromagnetismus nicht Teil der QCD ist, wird elektrische Ladung in dieser Zusammenfassung nicht diskutiert oder berücksichtigt.

Quantenzahlen entsprechen Eigenwerten von Operatoren, die mit dem QCD-Hamilton-Operator vertauschen. Diese Operatoren generieren Symmetrietransformationen, die hadronische Zustände mit entsprechenden Quantenzahlen unverändert lassen. Typische Beispiele sind $[H, J^2] = 0$ (QCD ist rotationsinvariant) oder $[H, P] = 0$ (QCD ist symmetrisch unter Raumspiegelungen).

Ein im Rahmen der QCD stabiles Hadron mit Quantenzahlen $I(J^P)$ bzw. $I(J^{PC})$ (und S, C', B', T , die oft oft nicht explizit genannt werden, da sie aus dem jeweiligen Zusammenhang hervorgehen) entspricht einem tiefliegenden Eigenzustand des QCD-Hamilton-Operators mit diesen Quantenzahlen und seine Masse dem entsprechenden Eigenwert abzüglich der Energie des Vakuums E_Ω . Beispiele für solche stabilen Hadronen sind nicht-flavorneutrale pseudoskalare Mesonen charakterisiert durch $J^P = 0^-$ (Pion, Kaon, D -Meson, D_s -Meson, B -Meson, B_s -Meson) oder auch das Proton und das Neutron. Für das Pion $|\pi\rangle$, charakterisiert durch $I(J^P) = 1(0^-)$, gilt z.B.

- $\hat{I}^2|\pi\rangle = I(I+1)|\pi\rangle = 2|\pi\rangle$,
- $\hat{J}^2|\pi\rangle = J(J+1)|\pi\rangle = 0|\pi\rangle$,
- $\hat{P}|\pi\rangle = P|\pi\rangle = -|\pi\rangle$,

für seine Masse m_π

- $\hat{H}|\pi\rangle = E|\pi\rangle = (m_\pi + E_\Omega)|\pi\rangle \rightarrow m_\pi = E - E_\Omega$

(in diesen Gleichungen wurden Operatoren durch Dächer $\hat{}$ kenntlich gemacht, um sie von Quantenzahlen abzuheben).

Instabile Hadronen, also Hadronen, die nach kurzer Zeit in andere Hadronen zerfallen, z.B. $\kappa \equiv K_0^*(800) \rightarrow K + \pi$ mit $I(J^P) = 1/2(0^+)$, entsprechen dagegen nicht Eigenzuständen des QCD-Hamilton-Operators. Um solche sogenannten Resonanzen zu studieren, d.h. um ihre Massen und Zerfallsbreiten zu berechnen, sind sehr aufwändige numerische Rechnungen erforderlich (siehe Abschnitt 2.4.3).

Es sei außerdem angemerkt, dass Quantenzahlen ein Hadron nicht eindeutig klassifizieren. Z.B. existieren mehrere Versionen des Pions mit identischen Quantenzahlen: Sowohl der Grundzustand π^0 ($m_\pi \approx 135$ MeV) als auch die angeregten Zustände $\pi(1300)$ ($m_{\pi(1300)} \approx 1300$ MeV) und $\pi(1800)$ ($m_{\pi(1800)} \approx 1812$ MeV) werden durch $I(J^P) = 1(0^-)$ beschrieben.

2.4.2 Berechnung von Massen stabiler Hadronen

Um die Masse m_H eines stabilen Hadrons H , beschrieben durch die Quantenzahlen $I(J^P), \dots$, mit Hilfe von Gitter-QCD zu berechnen, sind zwei wesentliche Schritte auszuführen:

- (1) Definition eines geeigneten Hadron-Erzeugungsoperators.
- (2) Gitter-QCD-Berechnung der Korrelationsfunktion des Hadron-Erzeugungsoperators \mathcal{O}_H , Ablesen der Hadronmasse m_H an Hand des asymptotischen exponentiellen Abfalls der Korrelationsfunktion.

Hadron-Erzeugungsoperatoren

Ein Hadron-Erzeugungsoperator \mathcal{O}_H ist ein Operator, der sich aus den Quarkfeldern und dem Gluonfeld zusammensetzt. Wird er auf das Vakuum $|\Omega\rangle$ angewendet, generiert er einen sogenannten Testzustand $|\phi\rangle \equiv \mathcal{O}_H|\Omega\rangle$ mit den Quantenzahlen des Hadrons H , d.h. einen Zustand mit $I(J^P), \dots$. Der Testzustand sollte dem Hadron ähnlich sein, also $|\phi\rangle \approx |H\rangle$.

Im Normalfall ist es nicht möglich, einen Hadron-Erzeugungsoperator zu konstruieren, der genau das Hadron H erzeugt, also für den $|\phi\rangle = |H\rangle$ gilt. Stattdessen handelt es sich bei dem Testzustand $|\phi\rangle$ in der Regel um eine lineare Superposition sämtlicher Eigenzustände des QCD-Hamilton-Operators mit Quantenzahlen $I(J^P), \dots$ (auch von Mehrhadronzuständen),

$$|\phi\rangle = \mathcal{O}_H|\Omega\rangle = \sum_{n=0}^{\infty} a_n |I(J^P), \dots; n\rangle \quad (17)$$

(im Folgenden werden Zustandsbezeichnungen gemäß $|n\rangle \equiv |I(J^P), \dots; n\rangle$ abgekürzt; außerdem, sollen die Zustände ihren Energien entsprechend geordnet sein, d.h. aufsteigende Indizes entsprechen ansteigenden Energien bzw. Hadronmassen, $E_0 \leq E_1 \leq E_2 \leq \dots$). Der Koeffizient $a_n \equiv \langle n|\mathcal{O}_H|\Omega\rangle$ beschreibt den Überlapp des Testzustands und des Energieeigenzustands $|n\rangle$. Sein Absolutbetrag ist ein Maß dafür, in welchem Ausmaß der Hadron-Erzeugungsoperator \mathcal{O}_H den hadronischen Zustand $|n\rangle$ anregt. Häufig ist man am leichtesten hadronischen Zustand in dem durch die Quantenzahlen $I(J^P), \dots$ charakterisierten Sektor interessiert, d.h. $|H\rangle = |0\rangle$.

Beispiel: Pion, Quantenzahlen $I(J^P) = 1(0^-)$

Das Pion ist der Grundzustand im $1(0^-)$ -Sektor:

$$|H\rangle = |0\rangle = |\pi\rangle. \quad (18)$$

In einer vereinfachten Form der QCD, in der Quark-Antiquark-Paarerzeugung nicht stattfinden kann³, sind die angeregten Zustände im $1(0^-)$ -Sektor die oben genannten angeregten Versionen des Pions,

$$|n\rangle \in \left\{ |\pi(1300)\rangle, |\pi(1800)\rangle, \dots \right\}, \quad n \geq 1. \quad (19)$$

In näherungsfreier QCD, in der Quark-Antiquark-Paarerzeugung stattfinden kann, sind typischer Weise bereits viele der tiefliegenden Energieeigenzustände Mehrhadronzustände. Z.B. ist im

³Gitter-QCD-Rechnungen in dieser Näherung (der sogenannten quenched Näherung) benötigen weit weniger Rechenzeit und sind daher vor allem in der älteren Literatur häufig zu finden.

Pionsektor der erste angeregte Zustand ein 3-Pionzustand,

$$|n\rangle \in \left\{ |\pi + \pi + \pi\rangle, \dots \right\}, \quad n \geq 1. \quad (20)$$

Hadron-Erzeugungsoperatoren sind keineswegs eindeutig. Ein guter Hadron-Erzeugungsoperator \mathcal{O}_H regt im wesentlichen das Hadron H an, weitere Zustände jedoch nur in geringem Maß. Mathematisch wird dies im Fall $|H\rangle = |0\rangle$ durch $|a_n|/|a_0| \approx 0$, $n \geq 1$ beschrieben.

Ein typischer Hadron-Erzeugungsoperator für das Pion ist

$$\mathcal{O}_\pi \equiv \int d^3r \bar{u}(\mathbf{r}) \gamma_5 d(\mathbf{r}). \quad (21)$$

- Die Flavorkombination $\bar{u}(\mathbf{r})d(\mathbf{r})$ realisiert $I = 1$.
- γ_5 realisiert $J^P = 0^-$.
- $\int d^3r$ realisiert Gesamtimpuls $\mathbf{p} = 0$ (ohne $\int d^3r$ würden Hadronen mit nicht-verschwindendem Impuls in (17), (19) und (20) auftreten).

Eine dem Pion-Erzeugungsoperator (21) entsprechende Gitterversion ergibt sich geradlinig und lautet

$$\mathcal{O}_\pi \equiv \sum_{\mathbf{n}} \bar{u}(a\mathbf{n}) \gamma_5 d(a\mathbf{n}). \quad (22)$$

Um die Lesbarkeit dieser Zusammenfassung zu erleichtern, werden im weiteren Verlauf überwiegend Kontinuumsausdrücke verwendet. Die entsprechenden Gitterversionen können in den Arbeiten [1, 2, 3, 4, 5, 6, 7, 8, 9, 10, 11, 12, 13, 14, 15] nachgeschlagen werden.

Korrelationsfunktionen von Hadron-Erzeugungsoperatoren

Der Vakuumerwartungswert eines Hadron-Erzeugungsoperators \mathcal{O}_H zum Zeitpunkt t_1 und seiner hermitesch konjugierten Version \mathcal{O}_H^\dagger zum Zeitpunkt t_2 wird als Korrelationsfunktion bezeichnet:

$$C_H(\Delta t) \equiv \langle \Omega | \mathcal{O}_H^\dagger(t_2) \mathcal{O}_H(t_1) | \Omega \rangle = \frac{1}{Z} \int D\psi D\bar{\psi} \int DA \mathcal{O}_H^\dagger(t_2) \mathcal{O}_H(t_1) e^{-S_{\text{QCD}}[\psi, \bar{\psi}, A]}, \quad (23)$$

wobei $\Delta t = t_2 - t_1$.

Wie die folgende Rechnung zeigt, wird eine Korrelationsfunktion für große Zeitseparationen Δt vom Grundzustand des vom Hadron-Erzeugungsoperator \mathcal{O}_H angeregten Sektors dominiert:

$$\begin{aligned} C_H(\Delta t) &= \sum_{n=0}^{\infty} \langle \Omega | \mathcal{O}_H^\dagger(t_2) | n \rangle \langle n | \mathcal{O}_H(t_1) | \Omega \rangle = \\ &= \sum_{n=0}^{\infty} \langle \Omega | e^{+H\Delta t} \mathcal{O}_H^\dagger(t_1) e^{-H\Delta t} | n \rangle \langle n | \mathcal{O}_H(t_1) | \Omega \rangle = \end{aligned}$$

$$= \sum_{n=0}^{\infty} \underbrace{\left| \langle n | \mathcal{O}_H | \Omega \rangle \right|^2}_{=|a_n|^2} \exp \left(- \underbrace{(E_n - E_\Omega)}_{=m_n} \Delta t \right) \xrightarrow{\Delta t \rightarrow \infty} |a_0|^2 e^{-m_0 \Delta t}, \quad (24)$$

wobei (17) benutzt wurde.

Um die dem Grundzustand entsprechende Hadronmasse $m_H = m_0$ zu bestimmen, kann man die Funktion $Ae^{-m_H \Delta t}$ mit den Parametern A und m_H an die Gitter-QCD-Ergebnisse für die Korrelationsfunktion $C_H(\Delta t)$ im Bereich hinreichend großer Δt fitten. Ein Beispiel, die Bestimmung der Masse des leichtesten statisch-leichten Mesons (eine Approximation eines B -Mesons; siehe auch Abschnitt 4.1.1) ist in Abbildung 2 (links) zu sehen. Für $\Delta t/a \geq 6$ (blaue Punkte) entspricht die berechnete Korrelationsfunktion einer abfallenden Exponentialfunktion und die entsprechende statisch-leichte Mesonmasse m_H kann durch einen Fit (orange Kurve) zuverlässig bestimmt werden.

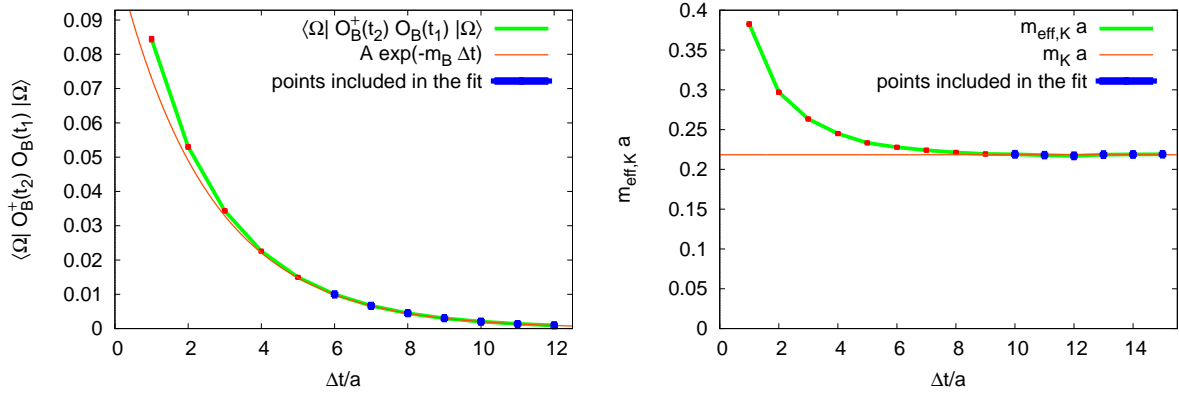


Abbildung 2: (entstammt [24]) (**links**) Korrelationsfunktion eines statisch-leichten Meson-Erzeugungsoperators als Funktion der Zeitseparation $\Delta t/a$. (**rechts**) Effektive Masse des Karons als Funktion der Zeitseparation $\Delta t/a$.

Häufig wird die Hadronmasse m_H auch mit Hilfe einer abgeleiteten Größe, der sogenannten effektiven Masse, bestimmt,

$$m_{\text{eff},H}(\Delta t) \equiv \frac{1}{a} \log \left(\frac{C_H(\Delta t)}{C_H(\Delta t + a)} \right). \quad (25)$$

Einsetzen von (24) führt auf

$$\begin{aligned} m_{\text{eff},H}(\Delta t) &= \frac{1}{a} \log \left(\frac{\sum_{n=0}^{\infty} |a_n|^2 e^{-m_n \Delta t}}{\sum_{n=0}^{\infty} |a_n|^2 e^{-m_n (\Delta t + a)}} \right) = \\ &= \frac{1}{a} \log \left(e^{+m_H a} \underbrace{\frac{1 + \sum_{n=1}^{\infty} \frac{|a_n|^2}{|a_0|^2} e^{-(m_n - m_H) \Delta t}}{1 + \sum_{n=1}^{\infty} \frac{|a_n|^2}{|a_0|^2} e^{-(m_n - m_H) (\Delta t + a)}}}_{=1+\mathcal{O}(e^{-(m_1 - m_H) \Delta t})} \right) \xrightarrow{\Delta t \rightarrow \infty} m_H. \end{aligned} \quad (26)$$

Die effektive Masse wird im Limes $\Delta t \rightarrow \infty$ zu einer Konstante, die der Hadronmasse $m_H = m_0$ entspricht. Um m_H zu bestimmen, muss lediglich eine Konstante an die Gitter-QCD-Ergebnisse für die effektive Masse $m_{\text{eff},H}(\Delta t)$ im Bereich hinreichend großer Δt gefittet werden. Ein Beispiel, die effektive Masse des Kaons, ist in Abbildung 2 (rechts) zu sehen (siehe auch Abschnitt 4.3). Für $\Delta t/a \geq 10$ kann die effektive Masse mit der Konstante m_K gefittet und so die Masse des Kaons bestimmt werden (blaue Punkte und orange Linie).

Streng genommen sind die Gleichungen (24) bis (26) nur dann korrekt, wenn die Zeitrichtung nicht periodisch, sondern unendlich ausgedehnt ist. Für ein endliches periodisches Raumzeitgitter (Ausdehnung L), sind die entsprechenden Ausdrücke komplizierter. Z.B. ist (24) durch $C_H(\Delta t) \stackrel{\Delta t \approx L/2}{\approx} |a_0|^2 (e^{-m_0 \Delta t} + e^{-m_0(L-\Delta t)})$ zu ersetzen. Details hierzu können in [25] gefunden werden.

2.4.3 Instabile Hadronen (Resonanzen)

Instabile Hadronen werden nicht nur durch Massen, sondern auch durch Zerfallsbreiten charakterisiert. Solche Resonanzparameter mit Hilfe von Gitter-QCD zu berechnen, ist sehr schwierig und recheneitaufwändig.

In einem ersten Schritt müssen dafür die Massen tiefliegender stabiler Mehrhadronenzustände mit den Quantenzahlen des instabilen Hadrons bestimmt werden. Im bereits genannten Beispiel von $\kappa \equiv K_0^*(800)$ sind dies die 2-Hadronenzustände $K + \pi$. Da es sich dabei um Eigenzustände des QCD-Hamilton-Operators handelt, kann ähnlich wie in Abschnitt 2.4.2 vorgegangen werden. Diese Massenberechnungen von Mehrhadronenzuständen müssen für eine Reihe unterschiedlich großer räumlicher Volumina wiederholt werden. Aus der so erhaltenen Volumenabhängigkeit des Spektrums können dann in einem zweiten Schritt Rückschlüsse auf die Masse und Breite von z.B. κ gezogen werden.

Theoretische Grundlagen zur Behandlung instabiler Hadronen finden sich in [26, 27, 28]. Eine moderne Gitter-QCD-Studie von κ ist [29].

2.4.4 Korrelationsmatrizen und das generalisierte Eigenwertproblem

In vielen Fällen ist es zweckmäßig nicht nur die Korrelationsfunktion eines einzelnen Hadron-Erzeugungsoperators, sondern die Korrelationsmatrix einer Reihe solcher Operatoren $\mathcal{O}_{H,1}, \dots, \mathcal{O}_{H,N}$ zu betrachten,

$$C_{H,jk}(\Delta t) \equiv \langle \Omega | \mathcal{O}_{H,j}^\dagger(t_2) \mathcal{O}_{H,k}(t_1) | \Omega \rangle. \quad (27)$$

Hierbei ist es wichtig, dass die Hadron-Erzeugungsoperatoren $\mathcal{O}_{H,j}$ Testzustände $\mathcal{O}_{H,j}|\Omega\rangle$ mit identischen Quantenzahlen generieren. Davon abgesehen unterscheiden sie sich in der Regel erheblich.

Ein gängiger Weg, Hadronmassen aus einer Korrelationsmatrix zu extrahieren, besteht darin, das generalisierte Eigenwertproblem

$$C_H(\Delta t)\mathbf{v}^{(n)}(\Delta t, t_0) = \lambda^{(n)}(\Delta t, t_0)C_H(t_0)\mathbf{v}^{(n)}(\Delta t, t_0) \quad (28)$$

zu lösen. Daraus ergeben sich effektive Massen gemäß

$$m_{\text{eff},H}^{(n)}(\Delta t, t_0) \equiv \frac{1}{a} \log \left(\frac{\lambda^{(n)}(\Delta t, t_0)}{\lambda^{(n)}(\Delta t + a, t_0)} \right). \quad (29)$$

t_0 ist ein freier Parameter, der in der Praxis nicht zu groß gewählt werden sollte, z.B. $t_0 = a$. Es lässt sich zeigen, dass diese effektiven Massen, genau wie (25), für hinreichend große Zeitseparationen Δt Plateaus aufweisen. $m_{\text{eff},H}^{(0)}$ liefert dabei den Grundzustand m_0 und $m_{\text{eff},H}^{(1)}, m_{\text{eff},H}^{(2)}, \dots$ die angeregten Zustände m_1, m_2, \dots im entsprechenden Sektor. Durch Berechnen einer Korrelationsmatrix und anschließendes Lösen des generalisierten Eigenwertproblems (28) lassen sich also auch die Massen radial angeregter Hadronen oder angeregter hadronischer Zustände bestimmen.

Die über (28) berechneten Eigenvektoren enthalten außerdem wertvolle Informationen über die Struktur der untersuchten Energieeigenzustände. Die Beträge der Komponenten von $v_j^{(n)}(\Delta t, t_0)$ stellen ein Maß dafür da, wie stark der Hadron-Erzeugungsoperator $\mathcal{O}_{H,j}$ den n -ten extrahierten Energieeigenzustand angeregt hat. Verwendet man z.B. einen Quark-Antiquark-Erzeugungsoperator ($q\bar{q}$) und einen 4-Quark-Erzeugungsoperator ($qq\bar{q}\bar{q}$) mit gleichen Quantenzahlen in einer 2×2 -Korrelationsmatrix, würde $|v_{q\bar{q}}^{(0)}| \ll |v_{qq\bar{q}\bar{q}}^{(0)}|$ auf eine Tetraquarkstruktur des Grundzustands hinweisen. Umgekehrt würde $|v_{q\bar{q}}^{(0)}| \gg |v_{qq\bar{q}\bar{q}}^{(0)}|$ andeuten, dass es sich um einen gewöhnlichen Quark-Antiquark-Zustand handelt. Solche qualitativen Untersuchungen der Struktur von Hadronen finden sich insbesondere in Abschnitt 4.2.2 und in Kapitel 5.

Eine umfangreiche Diskussion des generalisierten Eigenwertproblems bietet z.B. [30].

3 Gitter-QCD-Setup

3.1 Die Wilson-Twisted-Mass-Diskretisierung

Für die in den folgenden Kapiteln zusammengefassten Arbeiten [1, 2, 3, 4, 5, 6, 7, 8, 9, 10, 11, 12, 13, 14, 15] wurde für den Quarkanteil der QCD-Wirkung fast ausschließlich die Wilson-Twisted-Mass-Diskretisierung verwendet (siehe [31] und Referenzen darin). Teilweise wurden 2 Seequarkflavors (u - und d -Quarks), teilweise auch 2+1+1 Seequarkflavors (zusätzlich noch s - und c -Quarks) verwendet. Der Gluonanteil der Wirkung ist entweder die Symanzik-Improved-Eichwirkung [32] (für 2 Seequarkflavors) oder die Iwasaki-Eichwirkung [33] (für 2+1+1 Seequarkflavors). Ein solches Gitter-QCD-Setup ist $\mathcal{O}(a)$ -verbessert, d.h. Diskretisierungsfehler treten niemals linear, sondern höchstens quadratisch im kleinen Gitterabstand a auf. Diese $\mathcal{O}(a)$ -Verbesserung ist eine wichtige Eigenschaft, wenn man mit Hilfe von Gitterrechnungen präzise QCD-Ergebnisse erzielen will.

Ein Nachteil der Wilson-Twisted-Mass-Diskretisierung besteht darin, dass Parität sowie Isospin, Strangeness und Charm bei endlichem Gitterabstand keine exakten, sondern nur approximative Symmetrien sind. Dies hat die unschöne Konsequenz, dass Sektoren mit $P = -$ und $P = +$ aber ansonsten gleichen Quantenzahlen zu einem gemeinsamen Sektor verschmelzen. Für Mesonen mit Gesamtspin $J = 0$ in einem solchen Sektor ist z.B. das pseudoskalare Meson der Grundzustand und der skalare Paritätspartner häufig der erste angeregte Zustand im kombinierten $P = \pm$ -Sektor. Die Masse des klaren Mesons muss also als Masse eines angeregten Zustands über eine Korrelationsmatrix und Lösen des zugehörigen generalisierten Eigenwertproblems extrahiert werden, wie in Abschnitt 2.4.4 skizziert. Dies ist technisch schwieriger und hat häufig größere statistische Fehler zur Folge, als eine analoge Gitter-QCD-Massenberechnung in einer paritätserhaltenden Formulierung. Ähnliches gilt für Isospin ($I = 0$ und $I = 1$ Sektoren verschmelzen z.B. ebenfalls) sowie für Strangeness und Charm (S und C' sind keine Quantenzahlen mehr, nur noch $S - C'$, d.h. ein s -Quark kann zu einem c -Quark werden und umgekehrt). Die Verletzung von Charm hat dramatische Folgen für die Bestimmung der D -Meson-Masse (siehe [9] und Abschnitt 4.3) und anderer Hadronen die c -Quarks enthalten.

Aufgrund dieser Schwierigkeiten verwendet man in der Regel eine Wilson-Twisted-Mass-Diskretisierung der Valenz- s - und - c -Quarks, die sich von der entsprechenden oben genannten Seequarkdiskretisierung unterscheidet (siehe z.B. [10]). Diese Valenzquarkdiskretisierung, die für Simulationen, d.h. für Seequarks ungeeignet ist, verletzt nach wie vor die Parität, erhält aber zumindest Strangeness und Charm. Nur bei Einsatz eines solchen Mixed-Action-Setups ist es möglich, Präzisionsrechnungen für D - und D_s -Mesonen und Charmonium-Zustände auszuführen, wie z.B. in [6, 7] (zusammengefasst in Abschnitt 4.2).

3.2 Parameter der verwendeten Eichfeldkonfigurationen

Die zur Berechnung von Vakuumerwartungswerten verwendeten Eichfeldkonfigurationen wurden von der European-Twisted-Mass-Collaboration (ETMC) erzeugt. Technische Details der 2-Flavor-Simulationen finden sich in [34, 35], der 2+1+1-Flavor-Simulationen in [8, 9].

Aus technischen Gründen wurde die u/d -Quarkmasse unphysikalisch schwer gewählt. Es wurden aber jeweils Eichfeldkonfigurationen für mehrere unterschiedliche Werte der u/d -Quarkmasse erzeugt, so dass Extrapolationen von Ergebnissen zum physikalischen Wert der u/d -Quarkmasse

möglich sind. Die entsprechenden Pionmassen liegen etwa im Bereich $250 \text{ MeV} \dots 650 \text{ MeV}$.

Des Weiteren liegen Eichfeldkonfigurationen für drei verschieden feine Gitterabstände der Größenordnung $0.05 \text{ fm} \dots 0.09 \text{ fm}$ vor. Dies erlaubt eine Abschätzung der Diskretisierungsfehler bzw. eine Kontinuumsextrapolation.

Die Anzahl der Gitterplätze liegt zwischen $24^3 \times 48$ und $48^3 \times 96$, wobei für feine Gitterabstände und leichte Pionmassen mehr Gitterplätze verwendet wurden, um Finite-Volume-Effekte gering zu halten. Auch hier liegen für einige Gitterabstände und Pionmassen mehrere verschieden große Volumina vor, so dass Finite-Volume-Effekte quantitativ untersucht werden können.

Welche Eichfeldkonfigurationen konkret für welches Projekt verwendet wurden und in wie weit die u/d -Quarkmassen-, Gitterabstands- und Finite-Volume-Abhängigkeiten bei den entsprechenden Ergebnissen untersucht oder sogar durch Extrapolationen entfernt wurden, wird in den Zusammenfassungen der folgenden Kapitel nur in Einzelfällen diskutiert. Diese Informationen können den Arbeiten [1, 2, 3, 4, 5, 6, 7, 8, 9, 10, 11, 12, 13, 14, 15] selbst entnommen werden.

4 Hadronmassen, -zerfälle und -struktur mit $q\bar{q}$ - und qqq -Hadron-Erzeugungsoperatoren

Die in diesem Kapitel zusammengefassten Untersuchungen wurden mit typischen Hadron-Erzeugungsoperatoren durchgeführt, die im Fall von Mesonen eine Quark-Antiquark- und im Fall von Baryonen eine 3-Quark-Struktur besitzen. Eine solche Vorgehensweise ist erfolgversprechend, wenn die untersuchten Hadronen auch eine solche $q\bar{q}$ - bzw. qqq -Quarkstruktur aufweisen (also es sich z.B. nicht um Tetraquarks handelt) und sie gleichzeitig relativ stabil sind (also hadronische Zerfälle ausgeschlossen sind oder deren Effekte im Rahmen der statistischen Fehler vernachlässigbar sind; siehe hierzu auch die kurze Diskussion in Abschnitt 2.4.3).

4.1 B - und B_s -Mesonen (statisch-leichte Mesonen) und b -Baryonen (statisch-leichte Baryonen)

4.1.1 Spektrum von B - und B_s -Mesonen [1, 2]

Vorbemerkung:

Das in diesem Abschnitt zusammengefasste Projekt [1, 2] wird bewusst ausführlicher geschildert als alle weiteren diskutierten Projekte. Dies hat pädagogische Gründe und richtet sich vor allem an Leser, die kein fundiertes Wissen im Bereich der Gitter-QCD und -hadronspektroskopie mitbringen. Die umfangreichere, teilweise technische Darstellung soll die in Kapitel 2 grob skizzierten Gitter-QCD-Techniken anhand eines konkreten Beispiels ergänzen und damit besser erläutern.

B - und B_s -Mesonen bestehen aus einem schweren b -Antiquark und einem leichten u -, d - oder s -Quark, oder umgekehrt. Während die leichten Quarks mit den in Abschnitt 2.3 skizzierten Methoden behandelt werden können (konkret mit der in Abschnitt 3.1 diskutierten Wilson-Twisted-Mass-Diskretisierung), ist für das b -Antiquark ein anderer Formalismus erforderlich. Der Grund hierfür ist, dass $am_b > 1$ für typischer Weise verfügbare Gitterabstände a (siehe Abschnitt 3.2), was wiederum zu sehr großen bzw. schwer kontrollierbaren Diskretisierungsfehlern führen würde (Diskretisierungsfehler treten in Potenzen von am_q auf). Eine Möglichkeit, b -Quarks im Rahmen der Gitter-QCD zu realisieren, ist die Heavy-Quark-Effective-Theory (HQET) [36, 37]. Die führende Ordnung entspricht dem statischen Limes, d.h. unendlich schweren b -Quarks, während höhere Ordnungen Korrekturen in Form einer Potenzreihe in $1/m_b$ liefern.

Im statischen Limes, der den Abschnitt 4.1 zusammengefassten Gitter-QCD-Rechnungen zugrunde liegt, ist der Spin des statischen Quarks irrelevant, d.h. er ist nicht Teil des QCD-Hamilton-Operators. Folglich ist die Masse eines statisch-leichten Mesons nur abhängig vom Spin und Bahndrehimpuls j der leichten Freiheitsgrade, dem leichten Quark und den Gluonen. Es ist daher üblich solche Mesonen mit den Quantenzahlen j^P zu charakterisieren, wobei j halbzahlig ist. Eine ebenfalls gängige, Quarkmodellen entstammende Notation ist $S \equiv (1/2)^-$, $P_- \equiv (1/2)^+$, $P_+ \equiv (3/2)^+$, $D_- \equiv (3/2)^-$, ...

Die verwendeten statisch-leichten B - und B_s -Meson-Erzeugungsoperatoren sind von der Form

$$\mathcal{O}_{\Gamma, \psi^{(q)}}(\mathbf{r}) \equiv \bar{Q}(\mathbf{r}) \int d\hat{\mathbf{n}} U(\mathbf{r}; \mathbf{r} + d\hat{\mathbf{n}}) \Gamma(\hat{\mathbf{n}}) \psi^{(q)}(\mathbf{r} + d\hat{\mathbf{n}}). \quad (30)$$

$\bar{Q}(\mathbf{r})$ beschreibt das statische Antiquark bei \mathbf{r} , $\int d\hat{\mathbf{n}}$ bezeichnet eine Integration über eine Einheitskugel, U ist ein gerader Paralleltransporter und $\psi^{(q)}(\mathbf{r} + d\hat{\mathbf{n}})$, $q \in \{u, d, s\}$ erzeugt ein leichtes Quark bei $\mathbf{r} + d\hat{\mathbf{n}}$, also um den Abstand d versetzt zum Antiquark. Γ ist eine geeignete Kombination von Kugelflächenfunktionen und γ -Matrizen, die für definierte Quantenzahlen j^P sorgen. Die verwendeten Kombinationen Γ sind in Tabelle 1 aufgelistet. Gleichung (30) ist bildlich in Abbildung 3 dargestellt.

$\Gamma(\hat{\mathbf{n}})$	J^P	j^P	O_h	Gitter- j^P	Notation
$\gamma_5, \gamma_5 \gamma_j \hat{n}_j$ $1, \gamma_j \hat{n}_j$	$0^- [1^-]$	$(1/2)^-$	A_1	$(1/2)^-, (7/2)^-, \dots$	S
	$0^+ [1^+]$	$(1/2)^+$		$(1/2)^+, (7/2)^+, \dots$	P_-
$\gamma_1 \hat{n}_1 - \gamma_2 \hat{n}_2$ (und zyklisch) $\gamma_5 (\gamma_1 \hat{n}_1 - \gamma_2 \hat{n}_2)$ (und zyklisch)	$2^+ [1^+]$	$(3/2)^+$	E	$(3/2)^+, (5/2)^+, \dots$	P_+
	$2^- [1^-]$	$(3/2)^-$		$(3/2)^-, (5/2)^-, \dots$	D_{\pm}
$\gamma_1 \hat{n}_2 \hat{n}_3 + \gamma_2 \hat{n}_3 \hat{n}_1 + \gamma_3 \hat{n}_1 \hat{n}_2$ $\gamma_5 (\gamma_1 \hat{n}_2 \hat{n}_3 + \gamma_2 \hat{n}_3 \hat{n}_1 + \gamma_3 \hat{n}_1 \hat{n}_2)$	$3^- [2^-]$	$(5/2)^-$	A_2	$(5/2)^-, (7/2)^-, \dots$	D_+
	$3^+ [2^+]$	$(5/2)^+$		$(5/2)^+, (7/2)^+, \dots$	F_{\pm}

Tabelle 1: Statisch-leichte B - und B_s -Meson-Erzeugungsoperatoren. J^P -Zustände, die aufgrund des entkoppelten statischen Spins die gleiche Masse aufweisen, sind in eckigen Klammern angegeben.

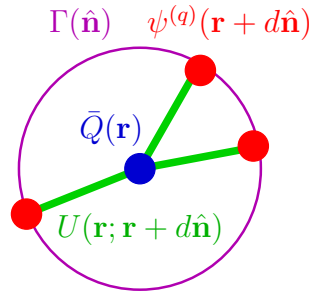


Abbildung 3: Bildliche Darstellung der verwendeten statisch-leichten B - und B_s -Meson-Erzeugungsoperatoren (Gleichung (30)).

Die Gitterversionen der Erzeugungsoperatoren (30) entstehen, indem die Integration über die Einheitskugel $\int d\hat{\mathbf{n}}$ durch eine Summe über sechs (für $j^P = 1/2, 3/2$) bzw. acht (für $j^P = 5/2$) benachbarte Gitterplätze ersetzt wird. Eine der Konsequenzen der kubischen Gitterdiskretisierung ist, dass die von diesen Erzeugungsoperatoren generierten Testzustände keine irreduzible Darstellung der Rotationsgruppe $SO(3)$ bilden, sondern nur der Untergruppe O_h der kubischen Rotationen. Folglich besitzen Gitterzustände keinen definierten Gesamtspin J bzw. j , sondern fallen in eine der irreduziblen O_h -Darstellungen, die eine unendliche Menge von Kontinuumsdrehimpulsen beinhalten (siehe Spalten " O_h " und "Gitter- j^P " in Tabelle 1).

Gitter-QCD-Rechnungen liefern typischer Weise den leichtesten Zustand eines Sektors. Dieser hat in der Regel den niedrigsten möglichen Gesamtspin. Da für die D_- - und die D_+ -Zustände genau wie die F_- - und F_+ -Zustände eine sehr ähnliche Masse zu erwarten ist (bekannt aus Modellrechnungen, z.B. [38]), kann davon ausgegangen werden, dass die entsprechenden Erzeugungsoperatoren mit Kontinuumsquantenzahlen $j^P = (3/2)^-$ und $j^P = (5/2)^+$ Testzustände generieren und Ergebnisse liefern, die Mischungen aus D_\pm und F_\pm entsprechen. Dementsprechend werden diese Erzeugungsoperatoren mit D_\pm und F_\pm bezeichnet (siehe Spalte ‘‘Notation’’ in Tabelle 1).

Um den Überlapp der Testzustände $\mathcal{O}_{\Gamma,\psi(q)}(\mathbf{r})|\Omega\rangle$ zu den untersuchten statisch-leichten Mesonzuständen zu optimieren (siehe die entsprechende Diskussion in Abschnitt 2.4.2), wurden Standard-Smeeringtechniken verwendet (APE-Smeering für räumliche Links, Gauß-Smeering für leichte Quarkfelder, HYP2-Smeering für zeitlich Links, die das statische Antiquark beschreiben; Details sind in [1] zu finden). Dieses Smearing ist essentiell, um präzise numerische Ergebnisse für statisch-leichte Mesonmassen zu erhalten.

Mit Gitter-QCD-Techniken wurden 6×6 -Korrelationsmatrizen für jeden der Kontinuumsspins $j = 1/2, 3/2, 5/2$ berechnet. Die entsprechenden sechs Erzeugungsoperatoren weisen negative und positive Parität auf (die für die leichten Quarks verwendete Wilson-Twisted-Mass-Diskretisierung bricht Parität; siehe Abschnitt 3.1) und verschiedenen Smearing-Stufen, d.h. verschiedene räumliche Ausdehnungen. Die Korrelationsmatrizen wurden dann mit Techniken analysiert, wie in Abschnitt 2.4.2 beschrieben. Die resultierenden statisch-leichten Mesonmassen sind für sich genommen allerdings bedeutungslos, da ein statisches Quark eine unendliche Masse besitzt und außerdem (im Kontinuumslimes) eine unendliche Selbstenergie zur Mesonmasse besteuert. Physisch bedeutsam sind jedoch Massendifferenzen von statisch-leichten Mesonen, da sich in diesen Größen die eben genannten Unendlichkeiten gegenseitig exakt eliminieren.

In Abbildung 4 sind Massendifferenzen statisch-leichter Mesonen $m(j^P) - m(S)$ für $q \in \{u, d\}$, also Näherungen für B -Mesonen, zu sehen. Verschiedene Farben entsprechen den Gitterabständen $a \approx 0.080$ fm (grün), $a \approx 0.064$ fm (blau) und $a \approx 0.051$ fm (magenta). Die horizontale Achse entspricht der u/d -Quarkmasse, $m_{u,d} \propto (m_\pi)^2$, wobei Rechnungen im Bereich $m_\pi \approx 284 \dots 637$ MeV ausgeführt wurden. Die sechs Plots entsprechen den Massendifferenzen $m(j^P) - m(S)$, $j^P = P_-, P_+, D_\pm, D_+, F_\pm, S^*$ (S^* bezeichnet den ersten angeregten Zustand im $(1/2)^-$ -Sektor), wie auch in den Plotüberschriften angegeben. Die Tatsache, dass die Ergebnisse für die drei verfügbaren Gitterabstände jeweils auf eine einzige Kurve fallen, zeigt an, dass Diskretisierungsfehler im Rahmen der statistischen Fehler vernachlässigbar sind. Dies war zu erwarten, da sowohl sehr feine Gitterabstände verwendet wurden, als auch die Wilson-Twisted-Mass-Diskretisierung, die garantiert, dass Diskretisierungsfehler nie linear, sondern höchstens quadratisch im kleinen Gitterabstand a auftreten (siehe die entsprechende Diskussion in Abschnitt 3.1). Analoge und qualitativ identische Plots für statisch-leichte Mesonen mit s -Quarks (Näherungen für B_s -Mesonen) finden sich in [2].

Da die Gitter-QCD-Ergebnisse für Massendifferenzen statisch-leichter Mesonen konsistent mit einer Gerade in $m_{u,d} \propto (m_\pi)^2$ sind und noch keine hinreichende Beschreibung durch effektive Feldtheorien verfügbar ist, wurde die Extrapolation zu physikalischer u/d -Quarkmasse ($m_\pi \approx 135$ MeV) linear durchgeführt. Entsprechende Ergebnisse sind in Tabelle 2 zusammengefasst.

Die angeregten statisch-leichten Mesonen $P_-, P_+, D_-, D_+, F_-, F_+$ und S^* entsprechen streng genommen nicht Eigenzuständen des QCD-Hamilton-Operators, da sie z.B. in Mehrmesonzustände

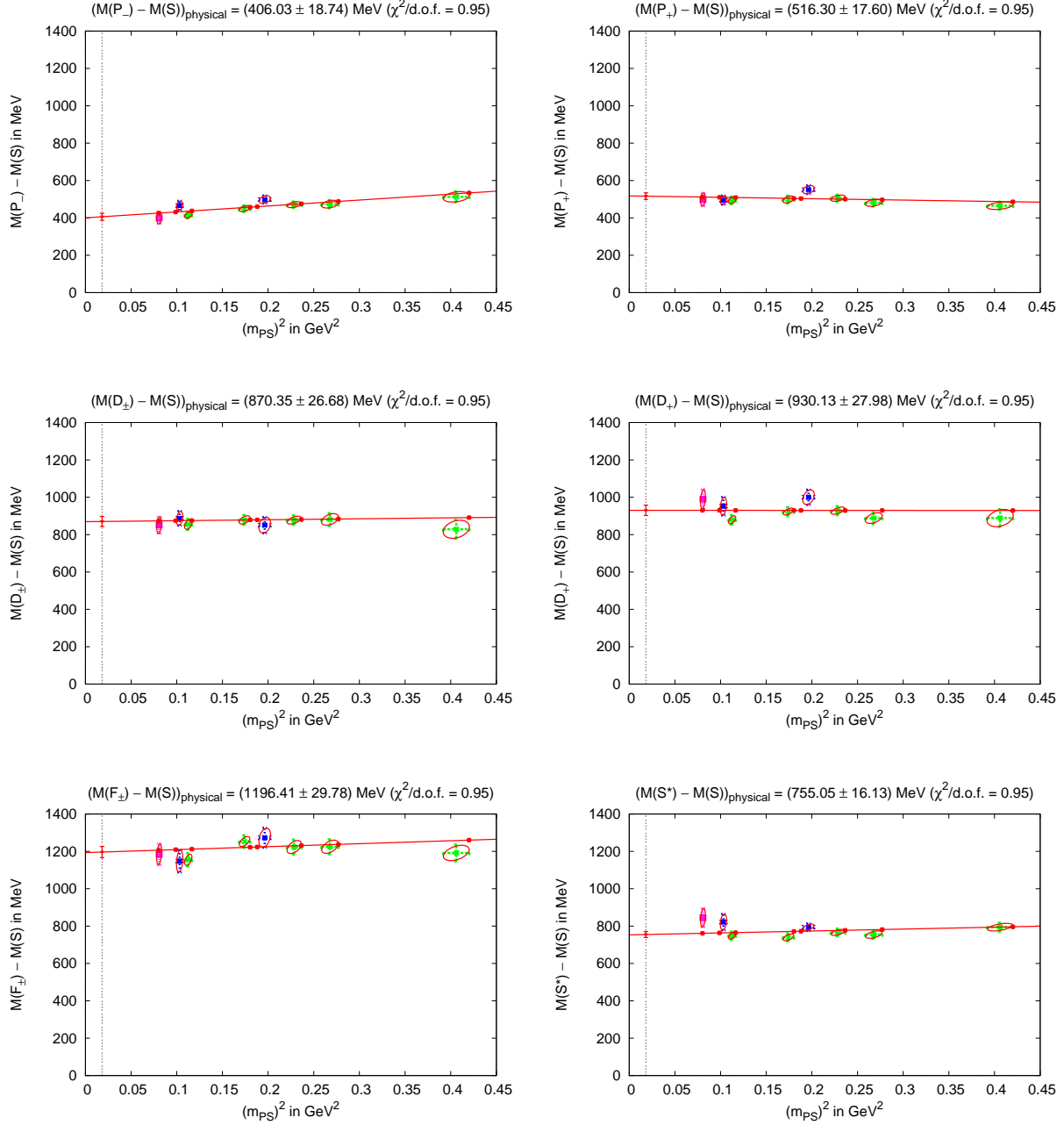


Abbildung 4: (entstammt [2]) Massendifferenzen statisch-leichter Mesonen $M(j^P) - M(S) \equiv m(j^P) - m(S)$ ($q \in \{u, d\}$, d.h. Näherungen für B -Mesonen) als Funktionen von $(m_{PS})^2 \equiv (m_\pi)^2$. Die Geraden entsprechen linearen Extrapolationen zur physikalischen u/d -Quarkmasse ($m_\pi \approx 135 \text{ MeV}$).

	P_-	P_+	D_{\pm}	D_+	F_{\pm}	S^*
B -Mesonen	406(19)	516(18)	870(27)	930(28)	1196(30)	755(16)
B_s -Mesonen	413(12)	504(12)	770(26)	960(24)	1179(37)	751(26)

Tabelle 2: Massendifferenzen statisch-leichter Mesonen $m(j^P) - m(S)$ in MeV für physikalische u/d -Quarkmasse.

$S + n \times \pi$ zerfallen können, eventuell mit entsprechendem relativen Bahndrehimpuls zwischen dem S -Meson und den Pionen, so dass die gleichen Quantenzahlen j^P vorliegen (siehe die entsprechende Diskussion in Abschnitt 2.4.1). Insbesondere für das P_- -Meson sollte ein solcher Zerfall in $S + \pi$ vergleichsweise wahrscheinlich sein, da es in einer S -Welle zerfallen kann (also kein relativer Bahndrehimpuls) und deshalb nicht von einer Drehimpulssbarriere vor dem Zerfall beschützt wird. Im Rahmen von Modellrechnungen und unter Verwendung des Matrixelements $\langle S + \pi(t_2) | P_-(t_1) \rangle$ [39, 40, 41] wurde in [2] für das P_- -Meson gezeigt, dass die über die Korrelationsmatrix bestimmte Mesonmasse vom möglichen Zerfall in $S + \pi$ nur vernachlässigbar beeinflusst wird. Aufgrund der erwähnten Drehimpulssbarriere sollte der Effekt auf die höheren Anregungen P_+ , D_- , D_+ , F_- und F_+ noch kleiner und damit ebenfalls vernachlässigbar sein.

Um Kontakt zu existierenden experimentellen Ergebnissen für B - und B_s -Mesonen herzustellen bzw. um entsprechende Vorhersagen zu treffen, ist es erforderlich, Korrekturen aufgrund der endlichen Masse des b -Quarks zu berücksichtigen. In der verwendeten HQET ist die führende Korrektur zum statischen Limes proportional zu $1/m_b$. Im Prinzip können diese Korrekturen im Rahmen der Gitter-QCD berechnet werden (siehe z.B. [42, 43, 44, 45, 46]). Dies ist aber ausgesprochen aufwändig, weshalb hier ein anderer Weg eingeschlagen wurde, nämlich die lineare Interpolation in $1/m_h$ zwischen den Gitter-QCD-Resultaten für statisch-leichte Mesonmassen und den experimentell zumindest teilweise relativ präzise gemessenen D - und D_s -Mesonmassen (m_h bezeichnet die schwere Quarkmasse, die durch die Masse des Grundzustandsmesons B bzw. D beschrieben werden kann)⁴. Abbildung 5 zeigt Interpolationen für die Quantenzahlen P_- und P_+ (diese Mesonmassen sind im D - und D_s -Sektor experimentell bekannt, weitere dagegen nicht [16]). Die entsprechenden numerischen Ergebnisse für die Massen von $B_{(s)0}^*$, $B_{(s)1}^*$, $B_{(s)1}$ und $B_{(s)2}^*$ sind in Tabelle 3 zusammengestellt.

Während eine Reihe von Fehlerquellen systematisch untersucht wurde, z.B. Gitterdiskretisierungseffekte oder Verfälschung der berechneten Mesonmassen durch mögliche Zerfälle in Mehrmesonzustände $S + n \times \pi$, ist dies für andere Fehlerquellen nicht oder nur schwer möglich. Zu nennen sind hier elektromagnetische Effekte, Isospinbrechung, Vernachlässigung höherer Ordnungen $\propto 1/(m_h)^2$ bei der Interpolation in der schweren Quarkmasse und Vernachlässigung der s -Sequarks (es wurden 2-Flavor-Eichfeldkonfigurationen verwendet; siehe Abschnitt 3.2). Eine grobe konservative Abschätzung dieser Fehlerquellen beläuft sich auf etwa 20 MeV (siehe [2]).

Vergleicht man die erzielten Gitter-QCD-Ergebnisse für Massendifferenzen von B - und B_s -Mesonen mit entsprechenden experimentellen Ergebnissen (Tabelle 3), findet man im Rahmen der Fehler keine perfekte Übereinstimmung, sondern eine Abweichung von etwa 15%. Vergleicht

⁴Ein guter Test, dass solche Interpolationen verlässliche Ergebnisse liefern, ist das Massensplitting von $m_{B^*} - m_B$. Die beschriebene Interpolation liefert mit $m_{D^*} - m_D = 141$ MeV und $m_D/m_B = 0.35$ das Ergebnis $m_{B^*} - m_B = 49$ MeV, das sehr gut mit dem experimentell bekannten $m_{B^*} - m_B = 46$ MeV übereinstimmt [16].

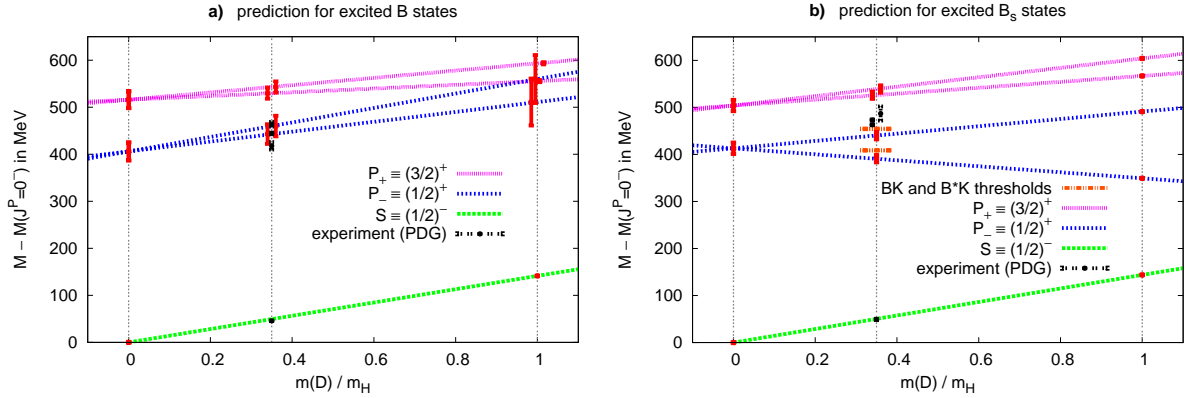


Abbildung 5: (entstammt [2]) Massendifferenzen statisch-leichter Mesonen $M - M(J^P = 0^-) \equiv m - m_{B_{(s)}}$ linear in $m(D)/m_H \equiv m_D/m_h$ zur physikalischen b -Quarkmasse interpoliert. (links) B -Mesonen. (rechts) B_s -Mesonen.

	$m - m_B$ in MeV			$m - m_{B_s}$ in MeV	
Meson	Gitter-QCD	Experiment	Meson	Gitter-QCD	Experiment
B_0^*	443(21)		B_{s0}^*	391(8)	
B_1^*	460(22)		B_{s1}^*	440(8)	
B_1	530(12)	444(2)	B_{s1}	526(8)	463(1)
B_2^*	543(12)	464(5)	B_{s2}^*	539(8)	473(1)

Tabelle 3: Gitter-QCD- und experimentelle Ergebnisse für Massendifferenzen von $B_{(s)0}^*$, $B_{(s)1}^*$, $B_{(s)1}$ und $B_{(s)2}^*$ zum Grundzustand $B_{(s)}$.

man die erzielten Gitter-QCD-Ergebnisse dagegen mit anderen unabhängigen Gitter-QCD-Studien, z.B. [47], liegt Übereinstimmung vor, wenn dies in Einheiten der typischen Skala von Gitter-QCD-Rechnungen geschieht, dem Abstand r_0 ⁵. Beziiglich r_0 in fm bzw. der Skalensetzung allgemein liegt zwischen verschiedenen Gitter-QCD-Gruppen und -Kollaborationen keine Einigkeit vor. Insbesondere für 2-Flavor-Simulationen sind die Abweichungen in der Größenordnung von ebenfalls 15% (während z.B. die ETM-Kollaboration $r_0 = 0.420$ fm findet [diese Eichfeldkonfigurationen wurden für die hier beschriebene Studie verwendet], gibt die ALPHA-Kollaboration $r_0 = 0.485$ fm an [49]). Diese Unsicherheit, deren Ursache nicht in der Gitterberechnung der B - und B_s -Mesonmassen begründet liegt, liefert eine mögliche Erklärung der in Tabelle 3 zu sehenden Abweichungen.

Die erzielten Ergebnisse für die Massen von statisch-leichten Mesonen und von B - und B_s -Mesonen sind in mehrfacher Weise von Bedeutung:

- Das Spektrum statisch-leichter Mesonen und zum Teil auch von B - und B_s -Mesonen wurde vom Gitter-QCD-Standpunkt sehr umfassend bestimmt (sechs Massendifferenzen im B -

⁵ r_0 ist über das statische Quark-Antiquark-Potential $V(r)$ gemäß $|V'(r_0)|r_0^2 \equiv 1.65$ definiert [48].

und sechs im B_s -Sektor). Diese Gitter-QCD-Ergebnisse liefern wertvolle Tests für existierende phänomenologische Modelle bzw. erleichtern deren zukünftige Konstruktion. Insbesondere zeigen die hier erzielten Gitter-QCD-Ergebnisse keine Anzeichen für eine umgekehrte Ordnung der P_- und P_+ B - und B_s -Mesonen ($B_{(s)0}^*$ und $B_{(s)1}^*$ sind deutlich leichter als $B_{(s)1}$ und $B_{(s)2}^*$). Dies ist im Widerspruch zu Ergebnissen von einer Reihe phänomenologischer Modelle [50, 51, 52, 53, 38].

- Statisch-leichte Mesonmassen wurden für zahlreiche Werte der u/d -Quarkmasse berechnet. Solche Ergebnisse sind hilfreich für die Entwicklung, den Vergleich mit und damit den Test von entsprechenden chiralen effektiven Feldtheorien.
- Die Berechnung statisch-leichter mesonischer Korrelationsfunktionen und entsprechender Mesonmassen ist ein notwendiger erster Schritt, um Zerfälle zu studieren, an denen B - und B_s -Mesonen beteiligt sind. Solche Zerfälle werden in [4, 5] untersucht und in Abschnitt 4.1.3 und Abschnitt 4.1.4 zusammengefasst.

4.1.2 Spektrum von b -Baryonen (Spektrum von Diquarks und Antidiquarks) [3]

Mit nahezu identischen Methoden, wie im vorangegangenen Abschnitt, wurde auch das Spektrum statisch-leichter Baryonen berechnet, also Baryonen die aus einem unendlich schweren Quark (eine Approximation eines b -Quarks) und zwei leichten u -, d - und/oder s -Quarks bestehen. Es wurden alle möglichen leichten Flavor-Kombinationen betrachtet, d.h. Λ_b^- , Σ_b^- , Ξ_b^- und Ω_b -Baryonen studiert, die Isospin $I \in \{0, 1/2, 1\}$ und Strangeness $S \in \{0, -1, -2\}$ entsprechen. Die entsprechenden Erzeugungsoperatoren sind von der Form

$$\mathcal{O}_{\Gamma, \psi^{(1)} \psi^{(2)}}(\mathbf{r}) \equiv \epsilon^{abc} Q^a(\mathbf{r}) \left((\psi^{b,(1)}(\mathbf{r}))^T \mathcal{C} \Gamma \psi^{c,(2)}(\mathbf{r}) \right) \quad (31)$$

mit der Ladungskonjugationsmatrix $\mathcal{C} \equiv \gamma_0 \gamma_2$. Im Gegensatz zu den Erzeugungsoperatoren für statisch-leichte Mesonen (30) setzt sich der Gesamtspin ausschließlich aus den Quarkspins zusammen, d.h. es wird kein Bahndrehimpuls mit Hilfe von Kugelflächenfunktionen und gluonischen Paralleltransportern erzeugt. Da auch hier der physikalisch relevante Spin ausschließlich von den leichten Freiheitsgraden getragen wird, ermöglichen die Erzeugungsoperatoren (31) die Berechnung von Baryonmassen in Sektoren mit $j = 0$ (d.h. Gesamtspin $J = 1/2$) und $j = 1$ (d.h. Gesamtspin $J = 1/2$ oder $J = 3/2$). Durch entsprechende Wahl von Γ kann positive und negative Parität realisiert werden. Die Erzeugungsoperatoren und die von ihnen angeregten Quantenzahlen sind in Tabelle 4 zusammengefasst (einige Erzeugungsoperatoren existieren nicht, da die rechte Seite von (31) aufgrund der Antivertauschungsrelationen für Quarkfelder verschwindet, und sind daher mit "X" markiert).

Statisch-leichte Baryonmassen sind, genau wie statisch-leichte Mesonmassen, aufgrund der unendlichen Masse und Selbstenergie des statischen Quarks zunächst physikalisch bedeutungslos. Um diese Unendlichkeiten loszuwerden, werden im Folgenden Massendifferenzen zwischen statisch-leichten Baryonen und dem leichtesten statisch leichten Meson (S -Meson bzw. B ; siehe Abschnitt 4.1.1) betrachtet, $\Delta m(S, I, j^P) \equiv m(\text{baryon} : S, I, j^P) - m_B$.

Die Extrapolationen in der u/d -Quarkmasse zum physikalischen Wert wurden analog zu denen für statisch-leichte Mesonen durchgeführt. Zur physikalischen b -Quarkmasse wurde ebenfalls in

Γ	j^P	J	I	S	Name	I	S	Name	I	S	Name
γ_5	0^+	$1/2$	0	0	Λ_b	$1/2$	-1	Ξ_b	X	X	X
$\gamma_0\gamma_5$	0^+	$1/2$	0	0	Λ_b	$1/2$	-1	Ξ_b	X	X	X
1	0^-	$1/2$	0	0		$1/2$	-1		X	X	X
γ_0	0^-	$1/2$	1	0		$1/2$	-1		0	-2	
γ_j	1^+	$1/2, 3/2$	1	0	Σ_b, Σ_b^*	$1/2$	-1		0	-2	Ω_b
$\gamma_0\gamma_j$	1^+	$1/2, 3/2$	1	0	Σ_b, Σ_b^*	$1/2$	-1		0	-2	Ω_b
$\gamma_j\gamma_5$	1^-	$1/2, 3/2$	0	0		$1/2$	-1		X	X	X
$\gamma_0\gamma_j\gamma_5$	1^-	$1/2, 3/2$	1	0		$1/2$	-1		0	-2	

Tabelle 4: Statisch-leichte Baryon-Erzeugungsoperatoren.

Anlehnung an den vorangegangenen Abschnitt mit Hilfe von experimentellen Ergebnissen für Charmbaryonen interpoliert.

Wie bereits in Abschnitt 4.1.1 erwähnt, bestehen gewisse Unstimmigkeiten bezüglich der Skalensetzung bei Gitter-QCD-Rechnungen. Z.B. wird der Gitterabstand bei den verwendeten Eichfeldkonfigurationen der ETM-Kollaboration als $a = 0.079(3)$ fm angegeben, wenn zur Skalensetzung die Pionzerfallskonstante benutzt wird [35], bzw. als $a = 0.089(5)$ fm bei Verwendung der Nukleonmasse [54]. Die Gitter-QCD-Ergebnisse für b -Baryonen werden daher für beide Versionen von a in Tabelle 5 angegeben. Erneut sei darauf hinwiesen, dass diese mit der Skalensetzung verknüpfte Unsicherheit vollkommen losgelöst von der hier vorgestellten Gitter-QCD-Berechnung statisch-leichter Baryonmassen ist. Um diese Unsicherheit weitestgehend zu eliminieren, sind in Tabelle 5 auch dimensionslose Verhältnisse

$$R(S, I, j^P) \equiv \frac{\Delta m(S, I, j^P)}{\Delta m(\Omega_b)} \quad (32)$$

angegeben. Diese Verhältnisse können als verlässliche Vorhersagen verwendet werden oder um mit theoretischen Ergebnissen anderer Gruppen oder experimentellen Daten zu vergleichen.

Die berechneten statisch-leichten Baryonmassen mit $P = +$ (siehe Tabelle 6 in [3]) stimmen im Rahmen statistischer Fehler gut mit existierenden Gitter-QCD-Studien überein [55, 56, 57]. Darüber hinaus wurden erstmals auch die Massen acht statisch-leichter Baryonzustände mit $P = -$ mit Gitter-QCD-Methoden vorhergesagt. Ein Vergleich dieser Vorhersagen mit einer phänomenologischen Modellrechnung liefert ebenfalls gute Übereinstimmung [58].

Die entsprechenden b -Baryonmassen sind in Tabelle 5 zusammengestellt. Für die experimentell bekannten Massen von b -Baryonen mit $P = +$, Λ_b , Σ_b , Σ_b^* , Ξ_b und Ω_b , liegt exzellente Übereinstimmung vor, wenn man die Verhältnisse $R(S, I, j^P)$ vergleicht. Darüberhinaus konnten auch einige $P = --$ -Massen sowie die Masse von Ξ'_b vorhergesagt werden, die bisher nicht experimentell gemessen wurden. Die $P = --$ -Massen wurden auch erstmalig mit Gitter-QCD-Methoden berechnet.

Eine konservative Abschätzung des systematischen Fehlers aufgrund der Interpolationen in der schweren Quarkmasse, von Diskretisierungsfehlern, der Vernachlässigung von s -Seequarks, elektromagnetischer Effekte und Isospinbrechung und der Verfälschung angeregter Zustände durch

S	I	J^P	$b/c\text{-Name}$	Δm^{lat} in MeV, a aus [35]	Δm^{lat} in MeV, a aus [54]	Δm^{exp} in MeV ¹	R^{lat}	R^{exp}
0	0	$(1/2)^+$	Λ_b/Λ_c	426(26)	395(25)	341(2)	0.489(27)	0.440(5)
		$(1/2)^-$	$-/\Lambda_c(2595)$	697(75)	648(69)	—	0.802(83)	—
		$(3/2)^-$	$-/\Lambda_c(2625)$	709(75)	660(69)	—	0.816(83)	—
0	1	$(1/2)^+$	$\Sigma_b/\Sigma_c(2455)$	602(29)	558(30)	532(6)	0.691(30)	0.687(11)
		$(3/2)^+$	$\Sigma_b^*/\Sigma_c(2520)$	628(29)	584(30)	553(7)	0.718(30)	0.714(11)
-1	1/2	$(1/2)^+$	Ξ_b/Ξ_c	602(21)	558(24)	511(3)	0.691(20)	0.660(8)
		$(1/2)^+$	$-/\Xi'_c$	747(25)	691(29)	—	0.857(22)	—
		$(3/2)^+$	$-/\Xi_c(2645)$	771(25)	715(29)	—	0.886(21)	—
		$(1/2)^-$	$-/\Xi_c(2790)$	1013(46)	936(48)	—	1.160(45)	—
		$(3/2)^-$	$-/\Xi_c(2815)$	1023(46)	946(48)	—	1.172(45)	—
-2	0	$(1/2)^+$	Ω_b/Ω_c	872(25)	807(31)	775(8)	1	1
		$(3/2)^+$	$-/\Omega_c(2770)$	905(25)	839(31)	—	$1.030(2)$ ¹	—

Tabelle 5: Massendifferenzen von b -Baryonen $\Delta m(S, I, J^P) = m(\text{baryon} : S, I, J^P) - m(B)$ in MeV (Skalensetzung über f_π , $a = 0.079(3)$ fm [35] und über m_N , $a = 0.089(5)$ fm [54]) und dimensionslose Verhältnisse (siehe Gleichung (32)). (¹ Dieses Ergebnis benötigt keine Gitter-QCD-Rechnung sondern ergibt sich allein aus der Interpolation in der schweren Quarkmasse.)

mögliche Zerfälle beläuft sich auf $\lesssim 25$ MeV [3]. Für die Verhältnisse $R^{\text{lat}}(S, I, j^P)$ in Tabelle 5 entspricht dies etwa einem zusätzlichen systematischen Fehler von 5%.

Neben der Berechnung und Vorhersage zahlreicher statisch-leichter Baryonmassen und b -Baryonmassen, die z.B. für den Test phänomenologischer Modelle oder die Entwicklung effektiver chiraler Feldtheorien wertvoll sind, liefern diese Ergebnisse auch wertvolle Hinweise zur Konstruktion geeigneter Tetraquark-Erzeugungsoperatoren. Diese bestehen häufig aus einem Diquark-Antidiquark-Paar, wobei sowohl Diquark als auch Antidiquark möglichst leicht sein sollten. In (31) entspricht der Anteil $\epsilon^{abc}((\psi^{b,(1)}(\mathbf{r}))^T C \Gamma \psi^{c,(2)}(\mathbf{r}))$ gerade einem Diquark, das an eine statische Farbladung $Q^a(\mathbf{r})$ gekoppelt ist. Die statisch-leichten Baryonmassen und -massendifferenzen können daher auch als Maß für die Diquark bzw. Antidiquarkmasse interpretiert werden. Die leichtesten Massen findet man für $\Gamma = \gamma_5$, weshalb (Anti-)Diquarks dieses Typs z.B. in [10, 11] zur Konstruktion von Tetraquark-Erzeugungsoperatoren für $a_0(980)$ und κ verwendet wurden (siehe auch Kapitel 5, Gleichung (51)).

4.1.3 Zerfallskonstanten f_B und f_{B_s} [4]

Vorbemerkung:

[4] beschreibt ein umfangreiches Projekt der ETM-Kollaboration, das sich im Wesentlichen in zwei Teile gliedert. Zum einen Teil, der in Kapitel 4 in [4] beschriebenen “Interpolation-Method”, habe ich wesentliche Beiträge geleistet, die im Folgenden zusammengefasst werden. Am anderen Teil, der in Kapitel 3 in [4] beschriebenen “Ratio-Method” habe ich kaum mitgewirkt.

Die Zerfallskonstanten f_B und f_{B_s} sind Standardgrößen der QCD und des Standardmodells, die eine Reihe interessanter Zerfälle parametrisieren. Als Beispiele können $B \rightarrow \tau + \nu_\tau$ und $B_s \rightarrow \mu^+ + \mu^-$ genannt werden, die beide als sensitiv bezüglich neuer Physik angesehen werden. Präzise Gitter-QCD-Vorhersagen für f_B und f_{B_s} sind daher ausgesprochen wünschenswert, um solche möglicher Weise existierende Effekte neuer Physik identifizieren zu können.

Zur Bestimmung von f_B und f_{B_s} mit der oben genannten Interpolation-Method ist es notwendig, die Matrixelemente

$$\phi_B^{\text{stat}} = \langle \Omega | \bar{Q} \gamma_5 u | B^{\text{stat}} \rangle^{\text{ren}} , \quad \phi_{B_s}^{\text{stat}} = \langle \Omega | \bar{Q} \gamma_5 s | B_s^{\text{stat}} \rangle^{\text{ren}} \quad (33)$$

zu berechnen, wobei $|B^{\text{stat}}\rangle$ und $|B_s^{\text{stat}}\rangle$ das jeweils leichteste statisch-leichte Meson, d.h. $j^P = (1/2)^-$, bezeichnen. Im Rahmen der in Abschnitt 4.1.1 beschriebenen Berechnungen statisch-leichter Mesonmassen erhält man diese Matrixelemente in ihrer nicht-renormierten Form, da sie in gewissen Korrelationsfunktionen, z.B.

$$\langle \Omega | \left(\bar{Q} \gamma_5 u \right)^\dagger(t) \left(\bar{Q} \gamma_5 u \right)(0) | \Omega \rangle, \quad (34)$$

als führende Terme auftreten (der Operator $\bar{Q} \gamma_5 u$ entspricht dem B -Meson-Erzeugungsoperator (30), wenn $\Gamma = \gamma_5$ und $r = 0$ gesetzt und keine Smearing-Techniken für Quark- und Gluonfelder verwendet werden). Diese nicht-renormierten Matrixelemente unterscheiden sich von ihren renormierten Gegenstücken um Renormierungsfaktoren, die z.B. mit Gitterstörungstheorie berechnet werden können [59]. Details der Umrechnung von nicht-renormierten Matrixelementen in renormierte im Rahmen der verwendeten Wilson-Twisted-Mass-Diskretisierung sind in [4] beschrieben.

Ähnlich wie in den beiden vorangegangenen Abschnitten 4.1.1 und 4.1.2 werden dann die Matrixelemente ϕ_B^{stat} und $\phi_{B_s}^{\text{stat}}$ und entsprechende Matrixelemente für schwere Quarkmassen im Charmbereich verwendet, um zur physikalischen b -Quarkmasse zu interpolieren. Im Gegensatz zu den Massenberechnungen von B - und B_s -Mesonen und von b -Baryonen wurden hier allerdings Gitterergebnisse statt experimenteller Ergebnisse für die Matrixelemente ϕ_B und ϕ_{B_s} im Charmbereich verwendet. Mit den Interpolationsergebnissen für $\phi_{B_s}^b$ und $\phi_B^b / \phi_{B_s}^b$ ergeben sich die Zerfallskonstanten gemäß

$$f_{B_s} = \frac{1}{\sqrt{m(B_s)}} \phi_{B_s}^b = 238(10) \text{ MeV} , \quad \frac{f_{B_s}}{f_B} = \frac{\sqrt{m(B)}}{\sqrt{m(B_s)}} \frac{\phi_{B_s}^b}{\phi_B^b} = 1.19(6). \quad (35)$$

In Kombination mit der sogenannten Ratio-Methode konnte die Präzision der Vorhersagen für f_B und f_{B_s} im Vergleich zu existierenden Vorhersagen leicht verbessert werden [60].

4.1.4 Isgur-Wise-Funktionen $\tau_{1/2}$ und $\tau_{3/2}$ und Zerfälle $B \rightarrow D^{**} + l + \nu$ [5]

Ein B -Meson kann semileptonisch in ein D^{**} -Meson zerfallen. D^{**} bezeichnet die vier D -Mesonen mit $J^P = 0^+$, $J^P = 1^+$ (tritt zweifach auf) und $J^P = 2^+$. Im in Abschnitt 4.1.1 diskutierten statischen Limes entspricht $j^P = (1/2)^+$ (bzw. P_-) dem $J^P = 0^+$ - und einem der beiden $J^P = 1^+$ -Zustände, dagegen $j^P = (3/2)^+$ (bzw. P_+) dem anderen $J^P = 1^+$ - und dem $J^P = 2^+$ -Zustand.

Dieser Zerfall ist von großem Interesse, da seit vielen Jahren ein hartnäckiger Konflikt zwischen Experiment und Theorie existiert. Während experimentelle Ergebnisse andeuten, dass der Zerfall in ein D^{**} -Meson mit $j = 1/2$ deutlich wahrscheinlicher ist als in ein D^{**} -Meson mit $j = 3/2$, liefern theoretische Rechnungen (QCD-Summenregeln, Modellrechnungen) genau die gegenteilige Aussage. Auf beiden Seiten gibt es jedoch ungeklärte Fragen und Probleme. Im Experiment ist insbesondere die Identifikation der breiten $j = 1/2$ -Zustände sehr schwierig und mag daher fehlerhaft sein. Auf der Theorie-Seite werden Modellannahmen gemacht bzw. Rechnungen nur in der ‘‘Zero-Recoil-Situation’’ ausgeführt, in der das B - und das D -Meson die gleiche Geschwindigkeit aufweisen, oder im statischen Limes, d.h. im Limes $m_b, m_c \rightarrow \infty$. Da die Zerfälle nach D^{**} etwa ein Viertel aller semileptonischen Zerfälle von B - in D -Mesonen ausmachen, ist ein gutes Verständnis von $B \rightarrow D^{**} + l + \nu$ ausgesprochen wichtig, will man den Standardmodell-Parameter V_{cb} präzise bestimmen bzw. vermessen. Eine umfangreiche Diskussion dieses sogenannten ‘‘1/2-Versus-3/2-Puzzles’’ findet sich in [61]. Eine Untersuchung dieses Zerfalls mit Methoden der Gitter-QCD ist also sehr wünschenswert und mag zur Klärung dieses lange bestehenden Konflikts beitragen.

Im statischen Limes wird der Zerfall $B \rightarrow D^{**} + l + \nu$ vollständig durch zwei Formfaktoren beschrieben, die Isgur-Wise-Funktionen $\tau_{1/2}(w)$ (Zerfall in $j^P = (1/2)^+$ bzw. P_-) und $\tau_{3/2}(w)$ (Zerfall in $j^P = (3/2)^+$ bzw. P_+) mit $w = v_B \cdot v_{D^{**}} \geq 1$ [62]. Eine bekannte QCD-Summenregel, hergeleitet im statischen Limes, lautet

$$\sum_n \left| \tau_{3/2}^{(n)}(1) \right|^2 - \left| \tau_{1/2}^{(n)}(1) \right|^2 = \frac{1}{4}, \quad (36)$$

wobei die Indizes (n) neben den Grundzuständen ($n = 0$, $\tau_{1/2,3/2} \equiv \tau_{1/2,3/2}^{(n)}$) auch sämtliche Anregungen mit den Quantenzahlen $j^P = (1/2)^+$ bzw. $j^P = (3/2)^+$ nummerieren [63]. Unter der Annahme, dass (36) in guter Näherung bereits von den Grundzuständen erfüllt wird, d.h. $|\tau_{3/2}^{(0)}(1)|^2 - |\tau_{1/2}^{(0)}(1)|^2 \approx 1/4$ gilt, legt diese Summenregel nahe, dass ein Zerfall in $j^P = (3/2)^+$ wahrscheinlicher als ein Zerfall in $j^P = (1/2)^+$ ist.

Das Ziel der im folgenden skizzierten Arbeit [5] besteht darin, die Gültigkeit dieser Annahme zu überprüfen, also $\tau_{1/2}(1)$ und $\tau_{3/2}(1)$ mit Gitter-QCD-Methoden zu berechnen. Eine Umschreibung von $\tau_{1/2}(1)$ und $\tau_{3/2}(1)$ in mit solchen Methoden zugängliche Ausdrücke findet sich in [5],

$$\tau_{1/2}(1) = \left| \frac{\langle H_0^* | \bar{Q} \gamma_5 \gamma_z D_z Q | H \rangle}{m_{H_0^*} - m_H} \right| \quad (37)$$

$$\tau_{3/2}(1) = \left| \frac{\langle H_2^* | \bar{Q} \gamma_5 (\gamma_x D_x - \gamma_y D_y) Q | H \rangle}{\sqrt{6} (m_{H_2^*} - m_H)} \right|. \quad (38)$$

Im Nenner finden sich die in Abschnitt 30 bereits berechneten Massendifferenzen statisch-leichter Mesonen, wobei $m_H \equiv m(S)$, $m_{H_0^*} \equiv m(P_-)$ und $m_{H_2^*} \equiv m(P_+)$. Die Matrixelemente im Zähler ergeben sich aus sogenannten 3-Punktfunktionen, die im Wesentlichen den Erwartungswerten von zwei statisch-leichten Mesonerzeugungsoperatoren (30) und dem Operator $\bar{Q}\gamma_5\gamma_zD_zQ$ bzw. $\bar{Q}\gamma_5(\gamma_xD_x - \gamma_yD_y)Q$ entsprechen. Wie schon im vorangegangenen Abschnitt 4.1.3 ist auch hier die Renormierung der Matrixelemente (37) und (38) bzw. der darin auftretenden Operatoren $\bar{Q}\gamma_5\gamma_zD_zQ$ und $\bar{Q}\gamma_5(\gamma_xD_x - \gamma_yD_y)Q$ notwendig. Die Renormierung wurde mit Hilfe von Gitterstörungstheorie vorgenommen und ist in [5], Kapitel 4 im Detail beschrieben.

Die Formfaktoren $\tau_{1/2}$ und $\tau_{3/2}$ wurden für verschiedene unphysikalisch schwere u/d -Quarkmassen berechnet, sind aber so gut wie unabhängig von dieser (siehe Tabelle 6). Eine lineare Extrapolation zur physikalischen u/d -Quarkmasse ist in Abbildung 6 zu sehen und liefert

$$\tau_{1/2}(1) = 0.296(26), \quad \tau_{3/2}(1) = 0.526(23). \quad (39)$$

m_π in MeV	$\tau_{1/2}$	$\tau_{3/2}$	$(\tau_{3/2})^2 - (\tau_{1/2})^2$
314	0.299(14)	0.519(13)	0.180(16)
391	0.312(10)	0.538(13)	0.193(13)
448	0.308(12)	0.522(8)	0.177(9)

Tabelle 6: $\tau_{1/2}$ und $\tau_{3/2}$ für verschiedene u/d -Quarkmassen.

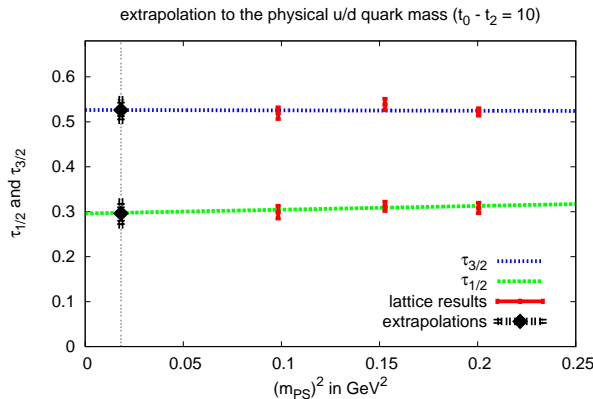


Abbildung 6: (entstammt [5]) $\tau_{1/2}$ und $\tau_{3/2}$ als Funktionen von $(m_{PS})^2 \equiv (m_\pi)^2$. Die Geraden entsprechen linearen Extrapolationen zur physikalischen u/d -Quarkmasse ($m_\pi \approx 135$ MeV).

Die erzielten Gitter-QCD-Ergebnisse (39) zeigen, dass die Summenregel (36) bereits in guter Näherung, d.h. zu etwa 80%, von den Grundzuständen erfüllt wird,

$$|\tau_{3/2}(1)|^2 - |\tau_{1/2}(1)|^2 \approx 0.17 \dots 0.21. \quad (40)$$

Diese häufig getroffenen Annahme (siehe Diskussion weiter oben in diesem Abschnitt) wurde damit erstmalig mit Hilfe von Gitter-QCD präzise und mit dynamischen leichten Quarks nach-

gewiesen. Sie ist erforderlich, um aus der Summenregel (36) zu schließen, dass ein Zerfall in $j^P = (3/2)^+$ wahrscheinlicher als ein Zerfall in $j^P = (1/2)^+$ ist.

Experimentell wurde z.B. in einer Arbeit der BELLE-Kollaboration $\tau_{3/2}(1) = 0.75$ und $\tau_{1/2}(1) = 1.28$ bestimmt [64]. Während für $j^P = (3/2)^+$ die Ergebnisse von Theorie und Experiment also zumindest von ähnlicher Größenordnung sind, liegt für $j^P = (1/2)^+$ eine starke qualitative Diskrepanz vor. Ein Grund für diese Diskrepanz könnte auf experimenteller Seite die problematische Identifikation der breiten $j = 1/2$ -Zustände sein (diese Vermutung wird auch dadurch unterstützt, dass die experimentellen Resultate $\tau_{3/2}(1) = 0.75$ und $\tau_{1/2}(1) = 1.28$ die Summenregel (36) stark verletzen). Auf theoretischer Seite könnte die Verwendung des statischen Limes anstatt endlicher b - und c -Quarkmassen zu Verzerrungen führen, genau wie die Einschränkung auf die Zero-Recoil-Situation $w = 1$. Erst wenn die Formfaktoren $\tau_{1/2}$ und $\tau_{3/2}$ auch für $w > 1$ berechnet werden, können die entsprechenden Zerfallsraten nicht nur abgeschätzt, sondern sauber berechnet werden, z.B. für $D_0^* \in D^{**}$ gemäß

$$\Gamma(B \rightarrow D_0^* + l + \nu) = \frac{G_F^2 V_{cb}^2 m_B^5 r^3}{48\pi^3} \int_1^\infty dw 4(1-r)^2(w^2-1)^{3/2} \left| \tau_{1/2}(w) \right|^2 \quad (41)$$

($r = m_D/m_B$; dieser und analoge Ausdrücke für die verbleibenden drei D^{**} -Mesonen können geradlinig analytisch berechnet werden [65, 66]). Im Prinzip ist eine solche Berechnung mit Gitter-QCD-Methoden möglich und befindet sich teilweise bereits in Arbeit [67, 68]. Voraussetzung dafür ist die Massenberechnung der vier D^{**} -Mesonen mit c -Quarks endlicher Masse sowie die Trennung und eindeutige Identifikation der beiden $J^P = 1^+$ -Zustände einmal mit $j^P = (1/2)^+$ und einmal mit $j^P = (3/2)^+$. Ein entsprechendes Gitter-QCD-Projekt ist Teil der hier zusammengefassten Arbeiten, [6, 7], und wird in Abschnitt 4.2, insbesondere in Abschnitt 4.2.2 diskutiert.

4.2 D -Mesonen, D_s -Mesonen und Charmonium [6, 7]

4.2.1 Spektrum von D -Mesonen, D_s -Mesonen und Charmonium

In [6, 7] wird das tiefliegende Spektrum von D -Mesonen, D_s -Mesonen und Charmonium-Zuständen berechnet. Die verwendeten Gitter-QCD-Methoden sind dabei sehr ähnlich, wie die zur Berechnung von statisch-leichten Mesonmassen (ausführlich beschrieben in Abschnitt 4.1.1). Im Folgenden wird daher vorwiegend auf Veränderungen und Verbesserungen gegenüber [1, 2] in diesem aktuell noch immer laufenden Projekt eingegangen.

Es werden Meson-Erzeugungsoperatoren verwendet, die ein Quark und ein Antiquark enthalten, wobei beide Quarks, $\bar{\psi}^{(1)}$ und $\psi^{(2)}$, endliche Masse besitzen, mindestens eines von beiden die Masse des c -Quarks,

$$O_{\Gamma, \bar{\psi}^{(1)} \psi^{(2)}} \equiv \int d^3r \bar{\psi}^{(1)}(\mathbf{r}) \int d\hat{\mathbf{n}} U(\mathbf{r}; \mathbf{r} + d\hat{\mathbf{n}}) \Gamma(\hat{\mathbf{n}}) \psi^{(2)}(\mathbf{r} + d\hat{\mathbf{n}}). \quad (42)$$

Folglich sind bei diesen Rechnungen auch die resultierenden Mesonmassen selbst und nicht nur Differenzen davon physikalisch aussagekräftig (das Problem mit der unendlichen Masse eines statischen Quarks und dessen unendlicher Selbstenergie tritt nicht mehr auf). Um Gesamtspin $J \geq 2$ untersuchen zu können, werden auch Erzeugungsoperatoren betrachtet, bei denen Quark

und Antiquark einen relativen Bahndrehimpuls aufweisen, realisiert durch die Integration über eine Kugel $\int d\mathbf{\hat{n}}$, die Paralleltransporter U und den Gewichtsfaktor Γ , der eine Kombination von Kugelflächenfunktionen (verantwortlich für Bahndrehimpuls L) und γ -Matrizen (verantwortlich für Spin S) ist. Neben ihren Flavorquantenzahlen werden diese Mesonen durch Gesamtspin und Parität J^P charakterisiert und im Fall von Charmonium auch noch durch Ladungskonjugation C . In Tabelle 7 sind die verwendeten Erzeugungsoperatoren zusammengestellt. Diese Liste von Erzeugungsoperatoren ist sehr umfangreich, da die tiefliegenden physikalischen Zustände optimal angeregt werden sollen und auch Aussagen über deren Struktur gewünscht sind (z.B. im Fall der D^{**} -Mesonen mit $J^P = 1^+$ welcher Anteil des Gesamtspins vom leichten Quark und von den Gluonen getragen wird).

Sämtliche Mesonmassenberechnungen wurden für jeweils zwei Werte der s -Quarkmasse und der c -Quarkmasse ausgeführt (Unterschied der beiden s - und c -Quarkmassen jeweils etwa 10%, beide in der Umgebung der physikalischen Werte). Dies liefert in linearer Näherung die Abhängigkeiten der Mesonmassen von den s - und c -Quarkmassen. Insbesondere das in Abschnitt 4.1.1 genannte Problem mit den Unstimmigkeiten und offenen Fragen die Skalensetzung bei Gitter-QCD-Rechnungen betreffend wird durch ein derartiges Vorgehen abgeschwächt. Es ist im Vorfeld der Rechnungen nicht mehr notwendig, sich auf einen speziellen Wert des Gitterabstand festzulegen und mit diesem die s - und c -Quarkmassen auf ihre physikalische Werte zu tunen. Stattdessen ist es möglich, nach Abschluss der zeitaufwändigen eigentlichen Gitter-QCD-Rechnungen ohne nennenswerten zusätzlichen Einsatz von Computerzeit eine umfangreiche Auswertung durchzuführen. Dabei können verschiedene Werte des Gitterabstands untersucht werden (z.B. Skalensetzung sowohl durch die Pionzerfallskonstante als auch durch die Nukleonmasse, wie in Abschnitt 4.1.2 erwähnt). Alternativ kann der Gitterabstand auch zunächst als unbestimmter Parameter betrachtet werden, der im Lauf der Auswertung über die berechneten D - und D_s -Meson- und Charmoniummassen gesetzt wird.

In Abbildung 7 ist der aktuelle Stand der Mesonspektren zu sehen. Verwendet wurden Eichfeldkonfigurationen, die mit 2+1+1 dynamischen Quarkflavors generiert wurden. Die leichte u/d -Quarkmasse ist erneut unphysikalisch schwer, Rechnungen für verschiedene u/d -Quarkmassen (rot: $m_\pi \approx 285$ MeV; blau: $m_\pi \approx 325$ MeV; schwarz: $m_\pi \approx 457$ MeV) ermöglichen aber eine Extrapolation zum physikalischen Wert. Die s - und die c -Quarkmasse wurde so gewählt, dass die Gitter-QCD-Ergebnisse für $2(m_K)^2 - (m_\pi)^2$ und m_D ihre physikalischen Werte annehmen (diese Größen sind so gut wie unabhängig von $m_{u,d}$, d.h. auch für unphysikalisch schwere u/d -Quarkmassen, sind die s - und c -Quarkmassen sehr nahe an ihren entsprechenden physikalischen Werten). Gegenwärtig liegen nur Ergebnisse für einen Wert des Gitterabstands vor, $a \approx 0.086$ fm, bestimmt von der ETM-Kollaboration über die Pionzerfallskonstante. Daher konnte noch keine Kontinuumsextrapolation ausgeführt werden. Dennoch lassen sich Diskretisierungsfehler zumindest grob abschätzen, da in der Wilson-Twisted-Mass-Diskretisierung jeweils zwei unterschiedliche Gitterausdrücke für jeden Kontinuums-Meson-Erzeugungsoperator existieren und sich die resultierenden Mesonmassen um Diskretisierungsfehler unterscheiden (Details sind in [7] erklärt). Diese paarweise auftretenden Ergebnisse sind in Abbildung 7 mit Kreisen bzw. Kreuzen gekennzeichnet. Ihre Differenz beträgt für die meisten D - und D_s -Meson- und Charmoniummassen um die 50 MeV, also $\approx 2.5\%$.

Experimentelle Ergebnisse sind ebenfalls in Abbildung 7 zu sehen. Die meisten Gitter-QCD-Ergebnisse stimmen nach einer Extrapolation zur physikalischen u/d -Quarkmasse im Rahmen der statistischen und grob geschätzten Diskretisierungsfehler mit diesen experimentellen Daten

	$\Gamma(\hat{\mathbf{n}})$	J	PC	$S \otimes L$	O_h
1	γ_5	0	-+		A_1
2	$\gamma_0\gamma_5$		-+		
3	1		++	$0 \otimes 0$	
4	γ_0		+-		
5	$\gamma_5\gamma_1\hat{n}_1$		--		
6	$\gamma_0\gamma_5\gamma_1\hat{n}_1$		-+		
7	$\gamma_1\hat{n}_1$		++	$1 \otimes 1$	
8	$\gamma_0\gamma_1\hat{n}_1$		++		
1	γ_1	1	--		T_1
2	$\gamma_0\gamma_1$		--		
3	$\gamma_5\gamma_1$		++	$1 \otimes 0$	
4	$\gamma_0\gamma_5\gamma_1$		+-		
5	\hat{n}_1		--		
6	$\gamma_0\hat{n}_1$		-+		
7	$\gamma_5\hat{n}_1$		+-	$0 \otimes 1$	
8	$\gamma_0\gamma_5\hat{n}_1$		+-		
9	$(\hat{\mathbf{n}} \times \vec{\gamma})_1$	2	++		E
10	$\gamma_0(\hat{\mathbf{n}} \times \vec{\gamma})_1$		++		
11	$\gamma_5(\hat{\mathbf{n}} \times \vec{\gamma})_1$		--		
12	$\gamma_0\gamma_5(\hat{\mathbf{n}} \times \vec{\gamma})_1$		-+		
13	$\gamma_1(2\hat{n}_1^2 - \hat{n}_2^2 - \hat{n}_3^2)$		--		
14	$\gamma_0\gamma_1(2\hat{n}_1^2 - \hat{n}_2^2 - \hat{n}_3^2)$		--		
15	$\gamma_5\gamma_1(2\hat{n}_1^2 - \hat{n}_2^2 - \hat{n}_3^2)$		++	$1 \otimes 2$	
16	$\gamma_0\gamma_5\gamma_1(2\hat{n}_1^2 - \hat{n}_2^2 - \hat{n}_3^2)$		+-		
1	$\hat{n}_1^2 + \hat{n}_2^2 - 2\hat{n}_3^2$	2	++		T_2
2	$\gamma_0\hat{n}_1^2 + \hat{n}_2^2 - 2\hat{n}_3^2$		-+		
3	$\gamma_5\hat{n}_1^2 + \hat{n}_2^2 - 2\hat{n}_3^2$		-+	$0 \otimes 2$	
4	$\gamma_0\gamma_5\hat{n}_1^2 + \hat{n}_2^2 - 2\hat{n}_3^2$		+-		
5	$(\gamma_1\hat{n}_1 + \gamma_2\hat{n}_2 - 2\gamma_3\hat{n}_3)$		++		
6	$\gamma_0(\gamma_1\hat{n}_1 + \gamma_2\hat{n}_2 - 2\gamma_3\hat{n}_3)$		++		
7	$\gamma_5(\gamma_1\hat{n}_1 + \gamma_2\hat{n}_2 - 2\gamma_3\hat{n}_3)$		--	$1 \otimes 1$	
8	$\gamma_0\gamma_5(\gamma_1\hat{n}_1 + \gamma_2\hat{n}_2 - 2\gamma_3\hat{n}_3)$		-+		
1	$(\gamma_2\hat{n}_1 + \gamma_1\hat{n}_2)$	2	++		
2	$\gamma_0(\gamma_2\hat{n}_1 + \gamma_1\hat{n}_2)$		++		
3	$\gamma_5(\gamma_2\hat{n}_1 + \gamma_1\hat{n}_2)$		--		
4	$\gamma_0\gamma_5(\gamma_2\hat{n}_1 + \gamma_1\hat{n}_2)$		-+		
5	$\gamma_1(\hat{n}_2^2 - \hat{n}_3^2)$		--		
6	$\gamma_0\gamma_1(\hat{n}_2^2 - \hat{n}_3^2)$		--		
7	$\gamma_5\gamma_1(\hat{n}_2^2 - \hat{n}_3^2)$		++	$1 \otimes 2$	
8	$\gamma_0\gamma_5\gamma_1(\hat{n}_2^2 - \hat{n}_3^2)$		+-		

Tabelle 7: Erzeugungsoperatoren für D -Mesonen, D_s -Mesonen und Charmonium.

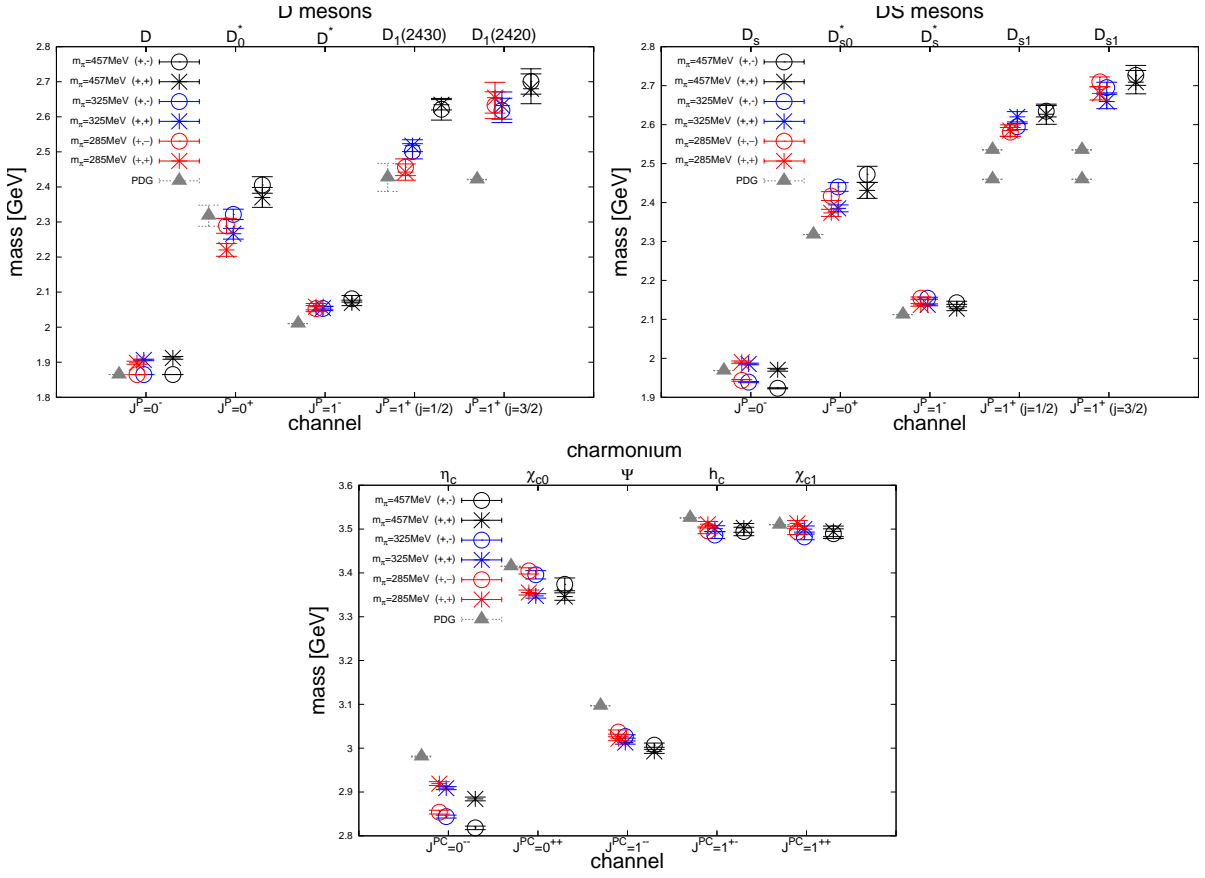


Abbildung 7: (entstammt [7]) Die Spektren von D -Mesonen, D_s -Mesonen und Charmonium für Gitterabstand $a \approx 0.086$ fm und drei verschiedene u/d -Quarkmassen, die Pionmassen $m_\pi \approx 285$ MeV (rot), $m_\pi \approx 325$ MeV (blau) und $m_\pi \approx 457$ MeV (schwarz) entsprechen.

überein. Eine umfangreiche Analyse und Diskussion wird in einer in naher Zukunft erscheinenden Arbeit enthalten sein. Auffällig und interessant ist eine vergleichsweise starke Abhängigkeit der Massen von D - und $-D_s$ -Mesonen mit Quantenzahlen $J = 0^+$ und $J = 1^+$ von der leichten u/d -Quarkmasse. Dies deutet darauf hin, dass die Gitter-QCD-Ergebnisse nicht den Massen von D_0^* und D_1 bzw. D_{s0}^* und D_{s1} entsprechen, sondern durch Beiträge der 2-Mesonenzustände $D^{(*)} + \pi$ bzw. $D_s^{(*)} + K$ mit gleichen Quantenzahlen verfälscht werden. Dies würde auch mit dem experimentellen Ergebnis übereinstimmen, dass $D_0^*(2400)$ und $D_1(2430)$ große Breiten besitzen. Insbesondere für $D_{s0}^*(2317)$ und $D_{s1}(2460)$ wird auch eine Tetraquark-Struktur diskutiert, da diese Zustände, verglichen mit Ergebnissen aus Quarkmodellen (z.B. [38]), unerwartet leicht sind. In jedem Fall wäre für diese D - und $-D_s$ -Mesonen mit $J = 0^+$ und $J = 1^+$ eine umfassendere Gitter-QCD-Studie von Interesse, bei der neben den hier verwendeten Quark-Antiquark-Erzeugungsoperatoren auch 4-Quark-Erzeugungsoperatoren verschiedenen Typs (mesonische Moleküle, Diquark-Antidiquark-Paare, 2-Mesonstruktur) verwendet werden. Entsprechende Techniken befinden sich in der Entwicklung [10, 11] und werden in Kapitel 5 zusammengefasst.

Die gezeigten und sich gegenwärtig in Berechnung befindlichen Spektren von D - und D_s -Mesonen

und Charmonium sind im Kontext aktueller und zukünftig geplanter Experimente, z.B. dem PANDA-Experiment bei FAIR, von großem Interesse. Diese Zustände werden sehr präzise vermessen werden, weshalb entsprechende theoretische QCD-Ergebnisse wünschenswert sind.

Eine weitere interessante in naher Zukunft geplante Weiterverwendung der berechneten Mesonmassen ist ihre Kombination mit den entsprechenden statisch-leichten Mesonmassen aus Abschnitt 4.1.1. Dies würde die dort verwendeten experimentellen Ergebnisse für D - und D_s -Mesonen durch Gitter-QCD-Ergebnisse ersetzen und gleichzeitig ermöglichen, Datenpunkte für mehrere unterschiedliche c -Quarkmassen im physikalischen Bereich zu erzeugen. Dies würde präzisere Extrapolation zu m_b und damit auch präzisere Ergebnisse für B - und B_s -Mesonmassen zur Folge haben. Außerdem könnten auch B - und B_s -Mesonen studiert werden, für die noch keine entsprechenden experimentellen D - und D_s -Ergebnisse vorliegen.

Da die D - und D_s -Meson- und Charmoniumspektren für verschiedene u/d -Quarkmassen und verschiedene Volumina berechnet wurden, sind auch Fits mit effektiven chiralen Theorien von Interesse. Erste Schritte in diese Richtung befinden sich bereits in Arbeit.

4.2.2 Separation und Struktur von D^{**} -Mesonen mit $J^P = 1^+$

Wie am Ende von Abschnitt 4.1.4 erwähnt, wurden erste Aktivitäten unternommen, die Isgur-Wise-Formfaktoren $\tau_{1/2}(w)$ und $\tau_{3/2}(w)$ mit b - und c -Quarks endlicher Masse zu berechnen [67, 68]. Ein notwendiger vorbereitender Schritt und gleichzeitig eine technische Herausforderung besteht darin, die finalen D^{**} -Mesonen mit entsprechenden Erzeugungsoperatoren in Form von Testzuständen zu präparieren. Wichtig ist dabei nicht nur die Massenberechnung der beiden ähnlich schweren $J^P = 1^+$ -Zustände, sondern auch eine Untersuchung ihrer Struktur, d.h. eine Identifikation dieser Zustände mit $j \approx 1/2$ bzw. $j \approx 3/2$.

Mit den im vorangegangenen Abschnitt 4.2.1 beschriebenen Techniken ist dieser vorbereitende Schritt erstmals erfolgreich mit Gitter-QCD-Methoden ausgeführt worden. Aufgrund der Paritätsbrechung der verwendeten Wilson-Twisted-Mass-Diskretisierung (siehe Abschnitt 3.1) muss das tiefliegende $J = 1$ -Spektrum, also der $J^P = 1^-$ -Grundzustand und die beiden $J^P = 1^+$ -Anregungen, aus einer Korrelationsmatrix extrahiert werden (siehe Abschnitt 2.4.4). Zu diesem Zweck wurde z.B. eine 12×12 -Korrelationsmatrix berechnet, die folgende Erzeugungsoperatoren enthält:

- für $J = 1$ und $j = 1/2$

$$\Gamma(\mathbf{n}) = \gamma_1 \gamma_5 G \quad (43)$$

(entspricht $L = 0$ und damit offensichtlich $j = 1/2$) und

$$\Gamma(\mathbf{n}) = ((\mathbf{n} \times \vec{\gamma})_1 - \hat{n}_1 \gamma_0 \gamma_5) G \quad (44)$$

(so konstruiert, dass die Kombination von $L = 1$ mit $S = 0$ bzw. $S = 1$ gerade $j = 1/2$, nicht jedoch $j = 3/2$ ergibt),

- für $J = 1$ und $j = 3/2$

$$\Gamma(\mathbf{n}) = ((\mathbf{n} \times \vec{\gamma})_1 + 2\hat{n}_1 \gamma_0 \gamma_5) G \quad (45)$$

(so konstruiert, dass die Kombination von $L = 1$ mit $S = 0$ bzw. $S = 1$ gerade $j = 3/2$, nicht jedoch $j = 1/2$ ergibt)

mit $G \in \{1, \gamma_0\}$ für $P = +$ und $G \in \{\gamma_5, \gamma_0\gamma_5\}$ für $P = -$. Dies entspricht geeigneten Linear-kombinationen der Erzeugungsoperatoren mit $J = 1$ und Indizes 1 bis 12 in Tabelle 7.

Die Analyse dieser 12×12 -Korrelationsmatrix geschieht durch Lösung eines generalisierten Eigenwertproblems (siehe Abschnitt 2.4.4). Die resultierenden Massen wurden bereits im vorangegangenen Abschnitt gezeigt (siehe Abbildung 7) und diskutiert. Die Zuordnung der Quantenzahlen zu den drei genannten $J = 1$ -Zuständen geschieht über die Komponenten der erhaltenen 12-dimensionalen Eigenvektoren. Der Übersichtlichkeit halber wurden mehrere Komponenten zu jeweils einer Größe zusammengefasst (durch Addition der Betragsquadrate der entsprechenden Komponenten):

- die sechs Operatoren (43), (44) und (45) mit $P = -$ (hellblaue Kurven in Abbildung 8),
- die beiden $j = 1/2$ -Operatoren (43) mit $P = +$ (grüne Kurven in Abbildung 8),
- die beiden $j = 1/2$ -Operatoren (44) mit $P = +$ (blaue Kurven in Abbildung 8),
- die beiden $j = 3/2$ -Operatoren (44) mit $P = +$ (magenta Kurven in Abbildung 8).

Diese Größen, die ein Maß für die Beiträge der entsprechenden Erzeugungsoperatoren zu einem extrahierten Zustand darstellen, sind in Abbildung 8 zu sehen und erlauben die folgenden Schlussfolgerungen:

- Wie erwartet ist der Grundzustand von $P = --$ -Erzeugungsoperatoren dominiert (hellblaue Kurve). Es handelt sich um das D^* -Meson ($J^P = 1^-$).
- Die erste Anregung ist klar von $P = +$ -Erzeugungsoperatoren mit $j \approx 1/2$ dominiert. Erzeugungsoperatoren mit $L = 0$ (grüne Kurve) leisten stärkeren Beitrag als Erzeugungsoperatoren mit $L = 1$ (blaue Kurve). Folglich wird diese Anregung als das breite $D_1(2430)$ -Meson identifiziert ($J^P = 1^+, j \approx 1/2$), wobei $J = 1$ hauptsächlich durch den Quarkspin realisiert wird.
- Die zweite Anregung ist klar von $P = +$ -Erzeugungsoperatoren mit $j \approx 3/2$ dominiert (magenta Kurve). Folglich wird diese Anregung als der $D_1(2420)$ -Zustand identifiziert ($J^P = 1^+, j \approx 3/2$).

In noch nicht publizierten Untersuchungen wurden weitere vier Erzeugungsoperatoren verwendet, die $L = 2$ und $S = 1$ und damit $j = 3/2$ entsprechen (Erzeugungsoperatoren mit $J = 1$ und Indizes 13 bis 16 in Tabelle 7), also eine 16×16 -Korrelationsmatrix analysiert. Die Ergebnisse bleiben qualitativ gleich, d.h. der $3/2$ -Zustand scheint im Wesentlichen $L = 1$, nicht aber $L = 2$ zu entsprechen.

Qualitativ identische Resultate erhält man im D_s -Mesonsektor.

Wie eingangs erwähnt, können diese Ergebnisse und die hierfür entwickelten Techniken direkt in einem bereits gestarteten längerfristigen Projekt zur Berechnung der Isgur-Wise-Formfaktoren $\tau_{1/2}(w)$ und $\tau_{3/2}(w)$ mit b - und c -Quarks endlicher Masse verwendet werden [67, 68].

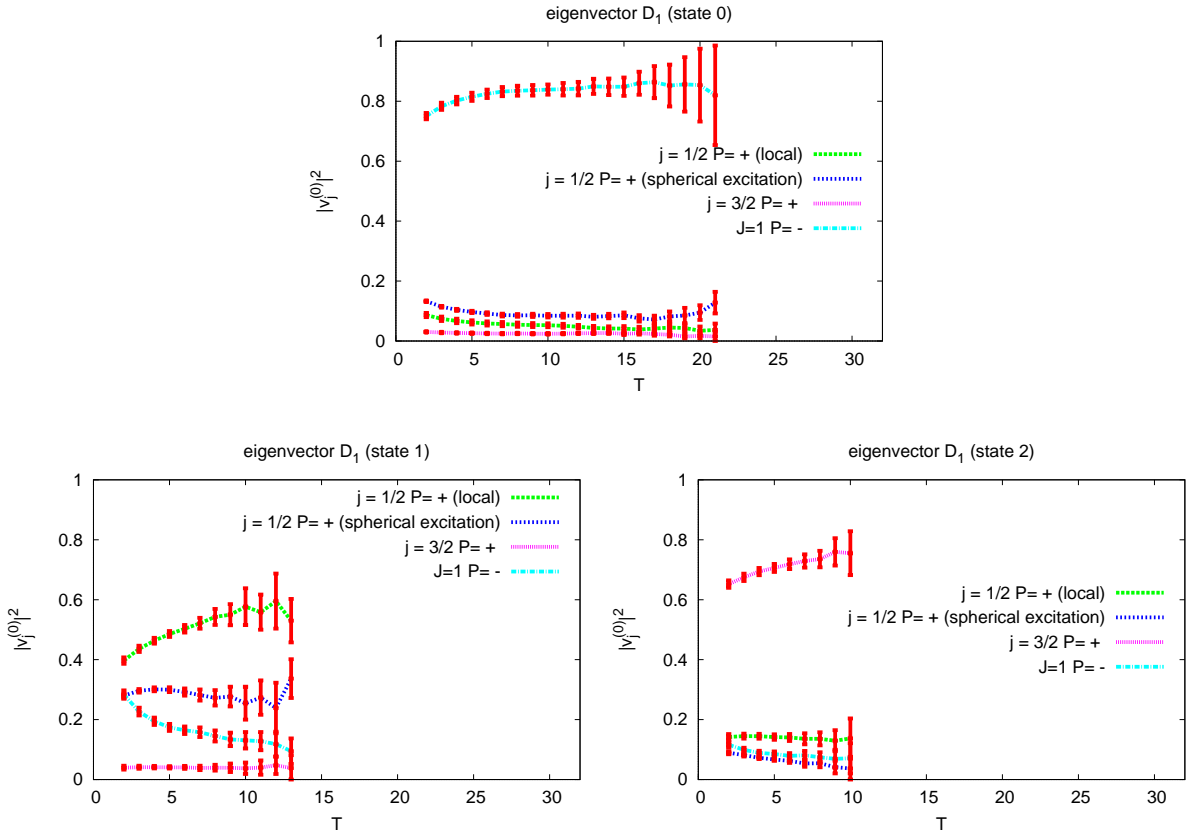


Abbildung 8: (entstammt [7]) Der ‘‘Operatorinhalt’’ der drei leichtesten D -Mesonzustände mit $J = 1$ als Funktion der Zeitseparation $\Delta t/a$. Der Grundzustand (oben) wurde als D^* ($J^P = 1^-$) identifiziert, die erste Anregung (links unten) als $D_1(2430)$ ($J^P = 1^+, j \approx 1/2$), die zweite Anregung (rechts unten) als $D_1(2420)$ ($J^P = 1^+, j \approx 3/2$).

4.3 Massenbestimmung des Kaons und des D -Mesons im unitären 2+1+1-Flavor-Wilson-Twisted-Mass-Gitter-QCD-Setup [8, 9]

Vorbemerkung:

[8] beschreibt das umfangreiche 2+1+1-Flavor-Simulationsprogramm der ETM-Kollaboration. Ich habe dazu im Wesentlichen durch Entwicklung geeigneter Techniken zur Massenbestimmung des Kaons und des D -Mesons beigetragen. Diese Techniken werden in [9] ausführlich beschrieben. Ich bin einer von drei Hauptautoren dieser Arbeit.

Die ETM-Kollaboration, der ich seit einigen Jahren angehöre, hat als eine der ersten Gitter-QCD-Kollaborationen weltweit umfangreiche Simulationen mit 2+1+1 dynamischen Quarkflavours durchgeführt [8]. Für diese Simulationen war es notwendig, die Masse der s - und c -Sequarks zumindest approximativ auf deren physikalische Werte einzustellen. Dieser Prozess ist relativ

aufwändig, da zunächst Simulationen mit geratenen nackten s - und c -Quarkmassen ausgeführt werden müssen. In einem zweiten Schritt werden dann Größen berechnet, die zeigen, wie weit entfernt m_s und m_c von ihren entsprechenden physikalischen Werten gewählt wurden. Hierfür bietet sich die Verwendung von $2(m_K)^2 - (m_\pi)^2$ sowie m_D an, da diese Größen kaum abhängig von der u/d -Quarkmasse sind. D.h. auch für unphysikalisch schwere u/d -Quarks kann m_s und m_c in guter Näherung auf physikalische Werte eingestellt werden. Diese beiden Schritte werden iteriert, d.h. abhängig von den Ergebnissen für $2(m_K)^2 - (m_\pi)^2$ und m_D werden m_s und m_c korrigiert und die Simulationen werden wiederholt.

Eine spezielle Schwierigkeit dabei ist in der verwendeten Wilson-Twisted-Mass-Diskretisierung begründet, die nicht nur Parität, sondern auch die Strange- und Charmflavorsymmetrie bricht. In anderen Worten kann sich ein s -Quark in ein c -Quark verwandeln und umgekehrt, d.h. es gibt Propagatoren von s nach \bar{c} und von c nach \bar{s} . Während Strangeness S und Charm C' bei endlichem Gitterabstand nur noch approximative Quantenzahlen sind, verschwindet diese Symmetriebrechung im Kontinuumslimes und man erhält QCD zurück. Die Simulationen werden natürlich stets bei endlichen Werten des Gitterabstands ausgeführt. Außerdem muss im vorliegenden speziellen Fall bei Berechnung von m_K und m_D (und damit indirekt $2(m_K)^2 - (m_\pi)^2$) für die s - und c -Valenzquarks die gleiche Diskretisierung wie im See verwendet werden (ein sogenanntes unitäres Setup)⁶, da die Seequarkmassen mit den physikalischen s - und c -Quarkmassen abgeglichen und auf deren Werte eingestellt werden sollen. Insgesamt führt dies zu schwerwiegenden technischen Problemen bei der Berechnung der D -Mesonmasse, da das D -Meson nicht mehr durch Symmetrien vom sehr viel leichteren Kaon oder dessen Paritätspartner unterscheidbar ist. Das D -Meson ist also ein hochgradig angeregter Zustand im kombinierten $P = --$ und $P = +-$ bzw. S - und C' -Sektor. Eine verlässliche Berechnung der D -Mesonmasse erfordert also die Analyse einer hinreichend großen Korrelationsmatrix. Dabei ist die gleichzeitige Berechnung der darunterliegenden Zustände K ($J^P = 0^-$) und $\kappa \equiv K_0^*$ ($J^P = 0^+$) notwendig. Verfälschungen durch Vielteilchenzustände, bestehend aus K oder κ und einem oder mehreren Pionen, müssen außerdem ausgeschlossen werden.

Um eine hinreichend zuverlässige und genaue Bestimmung der D -Mesonmasse unter den oben skizzierten Schwierigkeiten zu gewährleisten, wurden drei unterschiedliche Methoden entwickelt und implementiert. Sie liefern im Rahmen der statistischen und abgeschätzten systematischen Fehler identische Ergebnisse [9]. Abbildung 9 zeigt eine Bestimmung der D -Mesonmasse durch Lösen eines generalisierten Eigenwertproblems und der anschließenden Berechnung von effektiven Massen (links) und Interpretation der Eigenvektorkomponenten (rechts). Das D -Meson ist der zweite angeregte Zustand (magenta Kurve im linken Plot), was aus der deutlichen Dominanz eines Erzeugungsoperators der Struktur $\bar{c}\gamma_5 u$ geschlossen werden kann (blaue Kurve im rechten Plot). Im untersuchten Bereich der Zeitseparationen $\Delta t/a \leq 16$ ist keine Abweichung der effektiven Masse des D -Mesons von einer exponentiellen Plateauannahme erkennbar. Die Tatsache, dass die beiden anderen angesprochenen Methoden äquivalente Ergebnisse liefern (siehe Figure 10 in [9]), führt zur Schlussfolgerung, dass bei den verwendeten Erzeugungsoperatoren und Gitterabständen $a \lesssim 0.09$ fm die Twisted-Mass-Flavorbrechung schwach und eine hinreichend genaue Bestimmung der D -Mesonmasse möglich ist (relativer Fehler etwa 2.5%).

⁶Dies steht im Gegensatz zu allen anderen in dieser Zusammenfassung diskutierten Wilson-Twisted-Mass-Projekten, insbesondere z.B. der Berechnung des D -Mesonspektrums in Abschnitt 4.2.1, bei denen zumindest für die Valenzquarks eine Diskretisierung verwendet wird, die Strangeness und Charm erhält (siehe auch die Diskussion in Abschnitt 3.1).

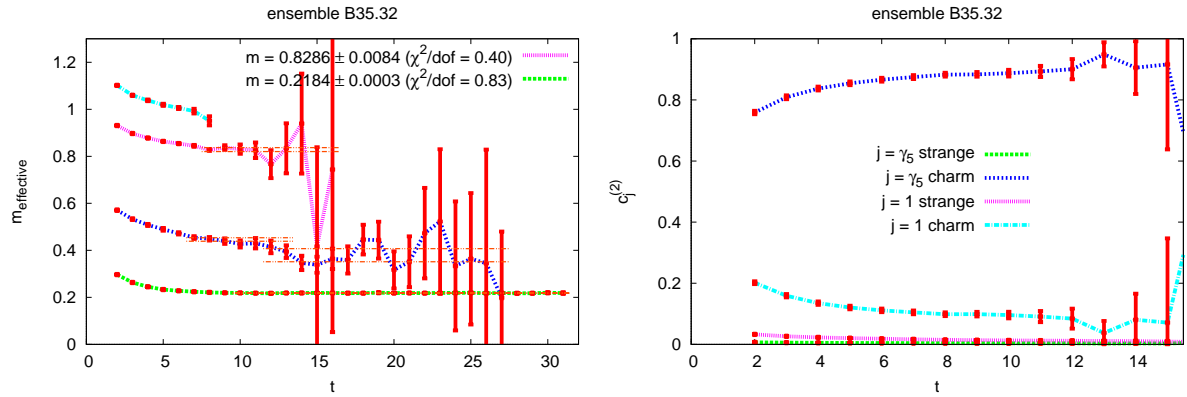


Abbildung 9: (entstammt [9]) **(links)** Effektive Massen der Zustände K (grün), $\kappa = K_0^*$ (blau), D (magenta) und D_0^* (hellblau) als Funktionen der Zeitseparation $\Delta t/a$. **(rechts)** Betragsquadrat der Eigenvektorkomponenten des zweiten angeregten Zustands (“Operatorinhalt”) als Funktionen der Zeitseparation $\Delta t/a$. Die klare Dominanz eines Erzeugungsoperators von der Struktur $\bar{c}\gamma_5 u$ erlaubt eine Identifikation dieses Zustands als D -Meson.

5 Untersuchung von Tetraquarkkandidaten mit $qq\bar{q}\bar{q}$ -Erzeugungsoperatoren [10, 11]

Die bisher geschilderten Methoden eignen sich gut zum Studium von Mesonen, die im Wesentlichen aus einem Quark und einem Antiquark aufgebaut sind. Bei einigen Mesonen, insbesondere den relativ schlecht verstandenen skalaren Mesonen, vermutet man an Stelle eines Quark-Antiquark-Paares eher einen gebundenen Zustand von vier Quarks (zwei Quarks und zwei Antiquarks), ein sogenanntes Tetraquark. Dabei werden verschiedene Anordnungen der vier Quarks diskutiert. Sind im Wesentlichen je ein Quark und ein Antiquark zu einem Meson zusammengebunden und führen die Restkräfte zwischen diesen beiden Mesonen zu einem gebundenen 4-Quarkzustand, spricht man von einem mesonischen Molekül. Sind dagegen die beiden Quarks zu einem sogenannten Diquark und die beiden Antiquarks zu einem sogenannten Antidiquark zusammengebunden und dann erst Diquark und Antidiquark zu einem Farbsinglett, spricht man von einem Diquark-Antidiquark-Paar⁷. Um solche Tetraquarkkandidaten mit Gitter-QCD-Methoden zu studieren, sind aufwändiger Verfahren und Rechnungen erforderlich.

In [10, 11] wird unter anderem das $a_0(980)$ -Meson untersucht. Es ist Teil des Nonetts leichter skalarer Mesonen mit Quantenzahlen $I(J^P) = 1(0^+)$. Diese leichten Mesonen sind theoretisch relativ schlecht verstanden und werden seit vielen Jahren als Tetraquarkkandidaten gehandelt. Zum einen ist die beobachtete Massenhierarchie der Zustände σ , $f_0(980)$, κ und $a_0(980)$ umgekehrt zu der, die man von einem Standardquarkmodell erwarten würde (siehe Abbildung 10, links und mittig). Mit einem Quark und einem Antiquark kann Isospin $I = 1$ nur mit zwei leichten Quarks realisiert werden. Im Gegensatz dazu sind für $I = 0$ sowohl zwei leichte Quarks als auch zwei s -Quarks möglich. In einem Standardquarkmodell ist die Flavor-Struktur des Nonetts also die Folgende:

$$\begin{aligned} I = 0 \quad &\rightarrow \quad \sigma \equiv \frac{1}{\sqrt{2}}(u\bar{u} + d\bar{d}) \quad , \quad f_0 \equiv s\bar{s} \\ I = 1/2 \quad &\rightarrow \quad \kappa \equiv d\bar{s}, s\bar{u}, u\bar{s}, s\bar{d} \\ I = 1 \quad &\rightarrow \quad a_0 \equiv d\bar{u}, \frac{1}{\sqrt{2}}(u\bar{u} - d\bar{d}), u\bar{d}. \end{aligned} \tag{46}$$

Darüber hinaus erklärt diese Flavorstruktur auch nicht die Massengleichheit von $f_0(980)$ und $a_0(980)$.

Nimmt man eine Tetraquarkstruktur an, speziell eine Diquark-Antidiquark-Struktur, hat das Nonett die Flavorstruktur

$$\begin{aligned} I = 0 \quad &\rightarrow \quad \sigma \equiv [ud][\bar{u}\bar{d}], \quad f_0 \equiv \frac{1}{\sqrt{2}}([su][\bar{u}\bar{s}] + [sd][\bar{d}\bar{s}]) \\ I = 1/2 \quad &\rightarrow \quad \kappa \equiv [sd][\bar{u}\bar{d}], [ud][\bar{u}\bar{s}], [su][\bar{u}\bar{d}], [ud][\bar{d}\bar{s}] \\ I = 1 \quad &\rightarrow \quad a_0 \equiv [sd][\bar{u}\bar{s}], \frac{1}{\sqrt{2}}([su][\bar{u}\bar{s}] - [sd][\bar{d}\bar{s}]), [su][\bar{d}\bar{s}] \end{aligned} \tag{47}$$

⁷An dieser Stelle sei auf eine alternative in der Literatur ebenfalls gängige Notation hingewiesen, in der Tetraquarks ausschließlich Diquark-Antidiquark-Paare bezeichnen.

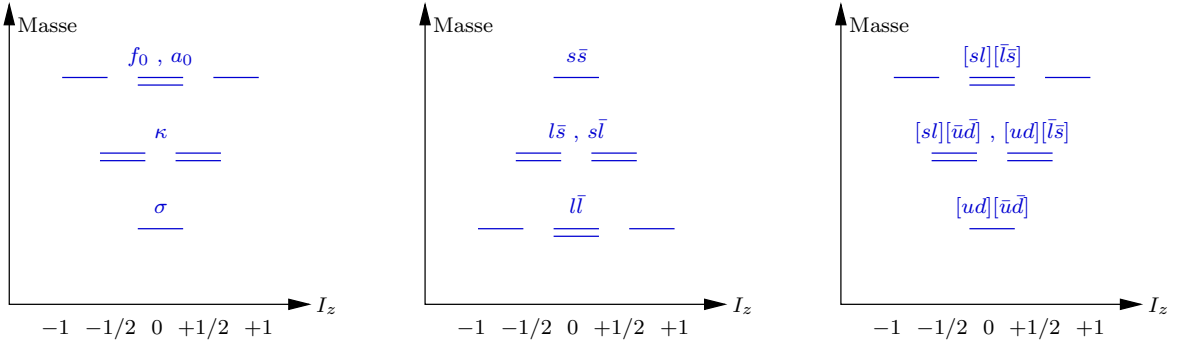


Abbildung 10: Die Flavorstruktur und Massenanordnung des leichten skalaren Nonetts ($J^P = 0^+$). (links) Experimentelle Ergebnisse. (mittig) Standardquarkmodell ($q\bar{q}$ -Struktur). (rechts) $qq\bar{q}\bar{q}$ -Quark-Struktur.

[69]. Damit lässt sich die Massenanordnung des gesamten Nonetts offensichtlich verstehen, unter anderem auch die Massengleichheit von $f_0(980)$ und $a_0(980)$ (siehe Abbildung 10, rechts).

Um herauszufinden, ob das $a_0(980)$ tatsächlich ein solcher Tetraquarkzustand ist, oder ob es sich doch im Wesentlichen um ein Quark-Antiquark-Paar handelt oder eventuell auch um eine kurzebige Resonanz, ist es erforderlich eine Reihe von Erzeugungsoperatoren mit den Quantenzahlen des $a_0(980)$ aber von verschiedener Struktur zu verwenden,

$$\mathcal{O}^{q\bar{q}} \equiv \int d^3r \left(\bar{d}(\mathbf{r})u(\mathbf{r}) \right) \quad (48)$$

$$\mathcal{O}^{K\bar{K} \text{ molecule}} \equiv \int d^3r \left(\bar{s}(\mathbf{r})\gamma_5 u(\mathbf{r}) \right) \left(\bar{d}(\mathbf{r})\gamma_5 s(\mathbf{r}) \right) \quad (49)$$

$$\mathcal{O}^{\eta_s\pi \text{ molecule}} \equiv \int d^3r \left(\bar{s}(\mathbf{r})\gamma_5 s(\mathbf{r}) \right) \left(\bar{d}(\mathbf{r})\gamma_5 u(\mathbf{r}) \right) \quad (50)$$

$$\mathcal{O}^{\text{diquark}} \equiv \int d^3r \epsilon^{abc} \left(\bar{s}^b(\mathbf{r}) \mathcal{C} \gamma_5 (\bar{d}^c(\mathbf{r}))^T \right) \epsilon^{ade} \left((u^d(\mathbf{r}))^T \mathcal{C} \gamma_5 s^e(\mathbf{r}) \right) \quad (51)$$

$$\mathcal{O}^{K+\bar{K} \text{ 2-meson}} \equiv \int d^3r_1 \left(\bar{s}(\mathbf{r}_1)\gamma_5 u(\mathbf{r}_1) \right) \int d^3r_2 \left(\bar{d}(\mathbf{r}_2)\gamma_5 s(\mathbf{r}_2) \right) \quad (52)$$

$$\mathcal{O}^{\eta_s+\pi \text{ 2-meson}} \equiv \int d^3r_1 \left(\bar{s}(\mathbf{r}_1)\gamma_5 s(\mathbf{r}_1) \right) \int d^3r_2 \left(\bar{d}(\mathbf{r}_2)\gamma_5 u(\mathbf{r}_2) \right). \quad (53)$$

Der Erzeugungsoperator $\mathcal{O}^{q\bar{q}}$ ist dabei ein Standard-Quark-Antiquark-Erzeugungsoperator (wie z.B. in Kapitel 4 durchweg verwendet). Alle weiteren Erzeugungsoperatoren beinhalten zwei Quarks und zwei Antiquarks. Bei $\mathcal{O}^{K\bar{K} \text{ molecule}}$, $\mathcal{O}^{\eta_s\pi \text{ molecule}}$ und $\mathcal{O}^{\text{diquark}}$ befinden sich die Quarks alle am gleichen Raumpunkt, d.h. diese Erzeugungsoperatoren modellieren bei Anwendung auf das Vakuum gebundene 4-Quarkzustände. $\mathcal{O}^{K\bar{K} \text{ molecule}}$ und $\mathcal{O}^{\eta_s\pi \text{ molecule}}$ haben dabei die oben diskutierte Struktur eines mesonischen Moleküls, wohingegen $\mathcal{O}^{\text{diquark}}$ einem Diquark-Antidiquark-Paar entspricht. Dabei wurden leichte pseudoskalare Mesonen $\sim \bar{q}\gamma_5 q$ verwendet bzw. die leichtesten Diquarks $\sim q^T \mathcal{C} \gamma_5 q$ und Antidiquarks $\sim \bar{q} \mathcal{C} \gamma_5 \bar{q}^T$ (siehe die entsprechende Spektrumsberechnung von statisch-leichten Baryonen in Abschnitt 4.1.2). Die letzten beiden Erzeugungsoperatoren $\mathcal{O}^{K+\bar{K} \text{ 2-meson}}$ und $\mathcal{O}^{\eta_s+\pi \text{ 2-meson}}$ generieren jeweils zwei Mesonen mit verschwindenden Impulsen, d.h. an unabhängigen Raumpunkten. Zustände, die im Wesentlichen

von diesen beiden Erzeugungsoperatoren angeregt werden, sollten nicht als gebundene 4-Quarkzustände interpretiert werden, sondern als 2-Mesonzustände.

Die den Erzeugungsoperatoren (48) bis (53) entsprechende 6×6 -Korrelationsmatrix ist in Abbildung 11 diagrammatisch skizziert (Linien entsprechen Quarkpropagatoren). Diese Korrelationsmatrix mit Methoden der Gitter-QCD zu berechnen, ist sehr schwierig und rechenteitaufwändig. Eine der Hauptursachen dafür ist, dass Quarkpropagatoren von allen Raumzeitpunkten zu allen anderen Raumzeitpunkten nur mit stochastischen Methoden abgeschätzt werden können [70, 71]⁸. Mehrere solcher stochastischer Propagatoren für ein Diagramm zu verwenden, führt in der Regel zu einem sehr großen statistischen Fehler und damit zu einem unbrauchbaren Ergebnis. Eine Alternative sind die exakten Punktpropagatoren, Propagatoren von einem ausgezeichneten Raumzeitpunkt zu allen anderen (siehe z.B. [73, 74]). Bei deren Verwendung kann allerdings die auf dem Gitter vorliegende Translationsinvarianz nicht mehr ausgenutzt werden, die wiederum wichtig ist, um vom Gluonfeld verursachte statistische Fluktuationen in den Diagrammen zu reduzieren. Einige Diagramme können aufgrund ihrer komplexen Raumzeitstruktur außerdem gar nicht ausschließlich mit Punktpropagatoren berechnet werden. Die schwierige Aufgabe besteht also darin, für jedes Diagramm die optimale Kombination von Propagatoren (stochastische oder Punktpropagatoren) zu finden, eventuell noch kombiniert mit weiteren Techniken, z.B. dem One-End-Trick [75, 76] oder sequentiellen Propagatoren [77]. Das Finden der optimalen Kombinationen erfordert die Implementation verschiedener Kombinationen von Techniken und umfangreiche numerische Testrechnungen (siehe die ausführliche Diskussion in [11]).

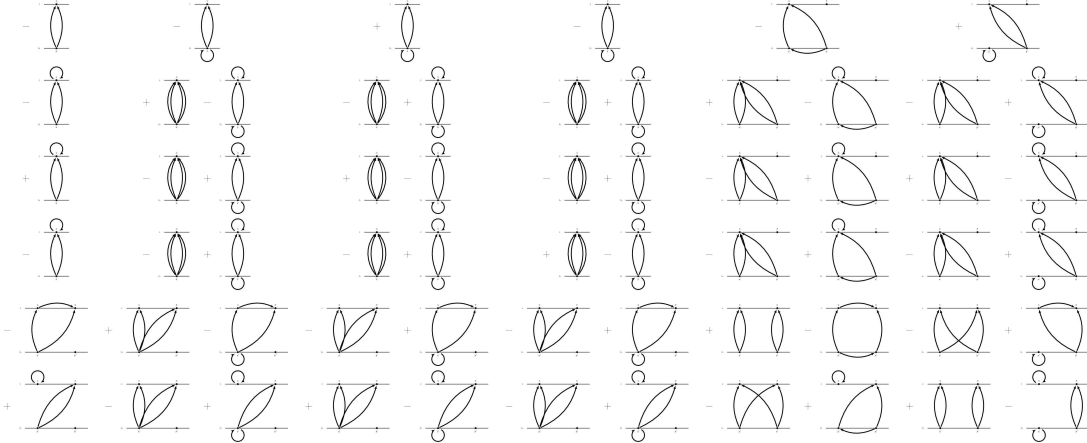


Abbildung 11: (entstammt [11]) Diagrammatische Darstellung der 6×6 -Korrelationsmatrix bestehend aus den Erzeugungsoperatoren (48) bis (53).

⁸Neben stochastischen Propagatoren existiert noch die sogenannte Destillation-Technik, um Quarkpropagatoren von allen Raumzeitpunkten zu allen anderen Raumzeitpunkten zu berechnen [72]. Diese Technik ist ebenfalls sehr aufwändig zu implementieren und eher schlecht mit den hier verwendeten Verfahren zu kombinieren. Deshalb wird sie in den hier diskutierten Arbeiten nicht verwendet.

5.1 $a_0(980)$ bei Vernachlässigung von Propagatoren innerhalb einer Zeitschicht

Die Berechnung der in Abbildung 11 gezeigten Korrelationsmatrix vereinfacht sich erheblich, wenn man Propagatoren vernachlässigt, die am gleichen Zeitpunkt starten und enden, also z.B. geschlossene Quarkloops. Während bei der Berechnung des Charmoniumspektrums (siehe Abschnitt 4.2.1) solchen Propagatoren innerhalb einer Zeitschicht kaum Bedeutung zukommt (Vernachlässigung von unverbundenen Diagrammen), ist im Fall des $a_0(980)$ -Mesons deren Einfluss nicht offensichtlich. Dennoch sind im Rahmen dieser Näherung erzielte Ergebnisse für das $a_0(980)$ -Meson zumindest qualitativ von Interesse.

Bei Vernachlässigung von Propagatoren innerhalb einer Zeitschicht sind sowohl die Anzahl der Valenzquarks als auch die Anzahl der Valenzantiquarks Erhaltungsgrößen, d.h. Korrelationen zwischen dem Quark-Antiquark-Erzeugungsoperator (48) und den 4-Quark-Erzeugungsoperatoren (49) bis (53) verschwinden. Folglich ergibt sich für die in Abbildung 11 gezeigte Korrelationsmatrix eine Blockstruktur bestehend aus einer 1×1 - und einer 5×5 -Matrix, wobei Letztere von besonderem Interesse ist, wenn man Tetraquarkkandidaten studieren will. In Abbildung 12 (links oben) sind die beiden effektiven Massen der 2×2 -Unterkorrelationsmatrix zu sehen, die aus den Erzeugungsoperatoren $\mathcal{O}^{K\bar{K} \text{ molecule}}$ und $\mathcal{O}^{\text{diquark}}$ aufgebaut ist. Die beiden Plateaus, also die resultierenden Massen, liegen zwar im Bereich von 1000 MeV, der erwarteten Masse des $a_0(980)$ -Mesons [16], sind aber von vergleichsweise schlechter Qualität. Nimmt man die beiden 2-Meson-Erzeugungsoperatoren $\mathcal{O}^{K+\bar{K} \text{ 2-meson}}$ und $\mathcal{O}^{\eta_s + \pi \text{ 2-meson}}$ hinzu, findet man die in Abbildung 12 (rechts oben) gezeigten effektiven Massen. Die beiden niedrigsten Massenplataeus sind im Wesentlichen identisch zu denen von Abbildung 12 (links oben), weisen aber sehr viel geringere Fluktuationen und statistische Fehler auf. Der zweite und der dritte angeregte Zustand liegen deutlich höher. Dies deutet drauf hin, dass die beiden beobachteten Zustände in der Gegend von 1000 MeV keine Tetraquarks sind, sondern zwei im wesentlichen nicht-wechselwirkende Mesonen. Diese Vermutung bestätigt sich bei Analyse der Eigenvektorkomponenten dieser beiden extrahierten Zustände (siehe Abbildung 12 [unten]). Während der niedrigste zu nahezu 100% ein $\eta_s + \pi$ -2-Meson-Zustand ist, ist die erste Anregung im Wesentlichen ein $K + \bar{K}$ -2-Meson-Zustand (im verwendeten Gitter-QCD-Setup mit unphysikalisch schweren u/d -Quarkmassen gilt $m_{\eta_s} + m_\pi \approx 2m_K \approx 1000$ MeV). Die Schlussfolgerung ist (unter der Annahme, dass die Vernachlässigung von Propagatoren innerhalb einer Zeitschicht die Ergebnisse zumindest qualitativ nicht beeinflusst), dass das $a_0(980)$ -Meson kein im Wesentlichen stabiles Tetraquark ist (eine umfangreichere Diskussion findet sich in [10]). Um herauszufinden, ob es sich um einen Quark-Antiquark-Zustand handelt oder eher um einen vergleichsweise instabilen 4-Quarkzustand, ist die Hinzunahme von Propagatoren innerhalb einer Zeitschicht erforderlich.

5.2 $a_0(980)$ mit Propagatoren innerhalb einer Zeitschicht

Wie bereits erwähnt ist die hinreichend präzise Gitter-QCD-Berechnung sämtlicher Diagramme der in Abbildung 11 gezeigten Korrelationsmatrix, insbesondere derer mit Propagatoren innerhalb einer Zeitschicht, sehr herausfordernd. In der Regel gibt es mehrere erfolgversprechende Varianten, ein spezielles Diagramm zu berechnen. Als Beispiel kann das in Abbildung 13 gezeigte Diagramm genannt werden, für das die folgenden Strategien denkbar sind:

- (1) Drei Punktpropagatoren und ein stochastischer Propagator (Punkt bei x , stochastischer

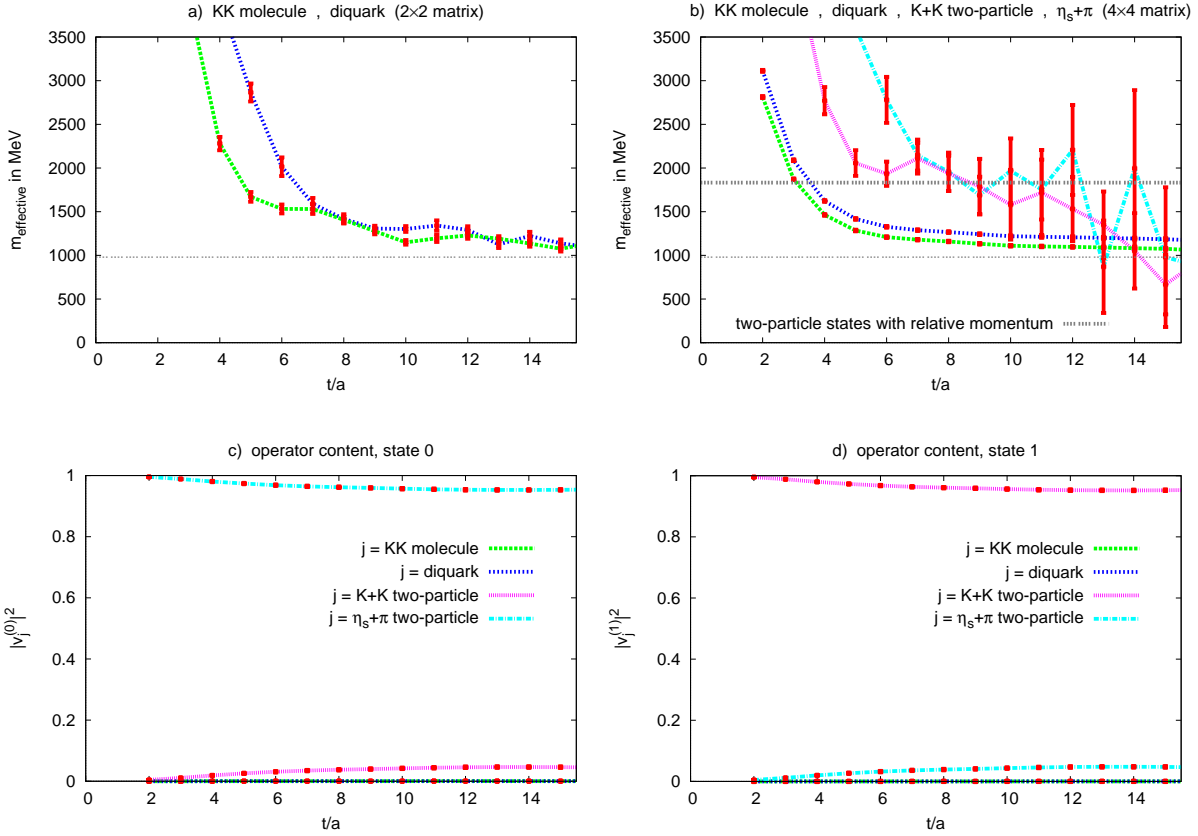


Abbildung 12: (entstammt [10]) (links oben) Effektive Massen als Funktionen der Zeitseparation $\Delta t/a$, 2×2 -Korrelationsmatrix (Erzeugungsoperatoren $\mathcal{O}^{K\bar{K}} \text{molecule}$, $\mathcal{O}^{\text{diquark}}$). (rechts oben) 4×4 -Korrelationsmatrix (Erzeugungsoperatoren $\mathcal{O}^{K\bar{K}} \text{molecule}$, $\mathcal{O}^{\text{diquark}}$, $\mathcal{O}^{K+\bar{K} \text{ 2-meson}}$, $\mathcal{O}^{\eta_s + \pi \text{ 2-meson}}$). (unten) Betragsquadrate der Eigenvektorkomponenten (“Operatorinhalt”) der beiden niedrigsten extrahierten Zustände aus der 4×4 -Korrelationsmatrix als Funktionen der Zeitseparation $\Delta t/a$.

Propagator für den unverbundenen Quarkloop bei \mathbf{x}').

- (2) One-End-Trick bei \mathbf{y}' und ein Punktpropagator für den Quarkloop bei \mathbf{x} , ein stochastischer Propagator für den unverbundenen Quarkloop bei \mathbf{x}' .
- (3) One-End-Trick bei \mathbf{y}' kombiniert mit einem stochastischen Propagator für den Quarkloop bei \mathbf{x} , ein Punktpropagator für den unverbundenen Quarkloop bei \mathbf{x}' .
- (4) One-End-Trick bei \mathbf{y}' kombiniert mit einem stochastischen Propagator für den Quarkloop bei \mathbf{x} , ein weiterer stochastischer Propagator für den unverbundenen Quarkloop bei \mathbf{x}' .

Welche dieser vier Methoden bei vergleichbarem Rechenaufwand den kleinsten statistischen Fehler liefert, lässt sich theoretisch im Vorfeld bestenfalls abschätzen. Die Implementation einiger oder aller dieser Methoden und entsprechende vergleichende Testrechnungen sind unabdingbar, will man die effizienteste Methode ausmachen. Da spätere Rechnungen sehr viel Rechenzeit auf

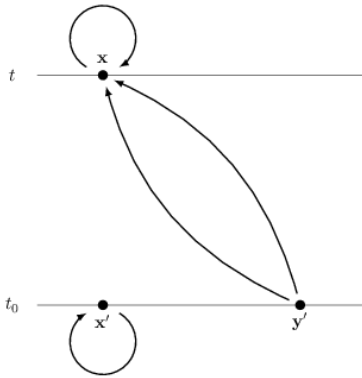


Abbildung 13: (entstammt [11]) Eines der beiden Diagramme, die zur Korrelationsfunktion von $\mathcal{O}^{\eta_s + \pi}$ 2-meson und entweder $\mathcal{O}^{K\bar{K}}$ molecule, $\mathcal{O}^{\eta_s \pi}$ molecule oder $\mathcal{O}^{\text{diquark}}$ beitragen.

Hochleistungscomputern benötigen, können derartige Untersuchungen ausgesprochen lohnend sein. Eine Diskussion einiger Diagramme und der Effizienz entsprechender Methoden sowie erste numerische Ergebnisse sind in [11] zu finden. Die Optimierung von Techniken für die komplette Berechnung der Korrelationsmatrix aus Abbildung 11 wird in einer in Kürze erscheinenden Arbeit ausführlich beschrieben werden.

Erwähnenswert ist an dieser Stelle, dass sich die hier entwickelten Techniken und Programm-codes so gut wie unverändert zum Studium nahezu beliebiger Tetraquarkkandidaten eignen. Sobald die eben angesprochenen Optimierungen abgeschlossen sind, können z.B. auch die beiden Tetraquarkkandidaten $D_{s0}^*(2317)$ und $D_{s1}(2460)$ eingehender studiert werden, die in Abschnitt 4.2.1 eher oberflächlich ausschließlich mit Quark-Antiquark-Erzeugungsoperatoren untersucht wurden. Die Bedeutung der Arbeiten [10, 11] geht also weit über das hier exemplarisch diskutierte $a_0(980)$ -Meson hinaus. Vielmehr geht es um die Vorbereitung und die Entwicklung von Techniken, mit denen langfristig eine ganze Reihe von Tetraquarkkandidaten mit Gitter-QCD-Methoden untersucht werden sollen.

Ähnliches gilt für die Berechnung von Resonanzparametern (Masse, Breite) von instabilen mesonischen Systemen. Hierfür bietet sich z.B. die sogenannte Lüscher-Methode an, die das volumenabhängige Spektrum von Streuzuständen, also 2-Mesonzuständen benötigt (siehe [26, 27, 28] und die kurze Diskussion in Abschnitt 2.4.3). Dieses Spektrum kann man voraussichtlich in vielen Fällen relativ gut mit Hilfe von Erzeugungsoperatoren mit identischer oder ähnlicher Struktur wie $\mathcal{O}^{K+\bar{K}}$ 2-meson und $\mathcal{O}^{\eta_s + \pi}$ 2-meson berechnen.

6 Kräfte zwischen schweren Mesonen, Untersuchung von $qq\bar{Q}\bar{Q}$ -Tetraquarkkandidaten [12, 13, 14, 15]

Die in Kapitel 5 beschriebenen Methoden zur Untersuchung möglicher Weise existierender Tetraquarkzustände sind sehr rechenzeitaufwändig. Eine alternative kostengünstigere Herangehensweise, die zumindest für gewisse Flavorkombinationen in guter Näherung anwendbar ist, besteht in der Berechnung von Potentialen zwischen zwei statischen Antiquarks in Anwesenheit zweier Quarks endlicher Masse. Diese Potentiale können dann in Modellrechnungen weiterverwendet werden, um zu überprüfen, ob im entsprechenden Sektor ein gebundener $qq\bar{Q}\bar{Q}$ -Zustand vorliegen kann, oder nicht.

6.1 BB -, B_sB_s - und B_cB_c -Potentiale

Zur Berechnung eines Potentials zwischen zwei statischen Antiquarks in Anwesenheit zweier Quarks endlicher Masse bieten sich Erzeugungsoperatoren der Form

$$\mathcal{O}_{\Gamma,\psi^{(1)}\psi^{(2)}} \equiv (\mathcal{C}\Gamma)_{AB} \tilde{\Gamma}_{CD} \left(\bar{Q}_C(\mathbf{r}_1) \psi_A^{(1)}(\mathbf{r}_1) \right) \left(\bar{Q}_D(\mathbf{r}_2) \psi_B^{(2)}(\mathbf{r}_2) \right) \quad (54)$$

an. $\bar{Q}(\mathbf{r}_1)$ und $\bar{Q}(\mathbf{r}_2)$ bezeichnen die statischen Antiquarks und $\psi^{(1)}(\mathbf{r}_1)$ und $\psi^{(2)}(\mathbf{r}_2)$ die “leichten” u/d -, s - oder c -Quarks, die für einen farbneutralen Testzustand $\mathcal{O}_{\Gamma,\psi^{(1)}\psi^{(2)}}|\Omega\rangle$ sorgen. Da sich jeweils ein statisches Antiquark und ein leichtes Quark den gleichen Raumpunkt teilen, kann man (54) auch als Erzeugungsoperator zweier B -Mesonen (oder B_s - bzw. B_c -Mesonen bei Verwendung von s - oder c -Quarks) betrachten und das entsprechende Potential als BB -Potential. Ohne Beschränkung der Allgemeinheit wird die Separation der statischen Antiquarks entlang der z -Achse gewählt, d.h. $\mathbf{r}_1 \equiv (0, 0, +r/2)$ und $\mathbf{r}_2 \equiv (0, 0, -r/2)$. Im statischen Limes verschwinden die schweren Quarkspins aus dem Hamilton-Operator, haben also keinen Einfluss auf Energieniveaus und damit auch nicht auf die gesuchten Potentiale. Es ist daher wichtig, die Spinindizes der leichten Quarks zu koppeln und keinesfalls leichte und statische Quarkspins zu mischen. Die Spinindizes der statischen Quarks können mit $\tilde{\Gamma} \in \{1, \gamma_0, \gamma_3\gamma_5, \gamma_1\gamma_2, \gamma_1\gamma_5, \gamma_2\gamma_5, \gamma_2\gamma_3, \gamma_1\gamma_3\}$ kontrahiert werden, wobei die konkrete Wahl von $\tilde{\Gamma}$ keinen Einfluss auf das resultierende Potential hat.

Die Separation der statischen Antiquarks bricht die Rotationssymmetrie und schränkt sie auf Drehungen um die Separationsachse, also die z -Achse ein. Da nur die beiden leichten Quarks zum Gesamtspin beitragen, ist eine der Quantenzahlen der betrachteten BB -Systeme $j_z = -1, 0, +1$. Parität $P = +, -$ ist ebenfalls eine Quantenzahl. Beschränkt man sich auf $|j_z|$ an Stelle von j_z , ist auch eine Spiegelung entlang der x -Achse (bzw. allgemein entlang einer beliebigen Achse senkrecht zur Separationsachse) eine Symmetrie mit der zugeordneten Quantenzahl $P_x = +, -$. Hinzu kommen noch Flavorquantenzahlen, z.B. im Fall zweier leichter u/d -Quarks Isospin I und die zugehörige z -Komponente. Der vollständige Satz von Quantenzahlen lautet dann $(I, I_z, |j_z|, P, P_x)$. Eine detaillierte Diskussion dieser Symmetrien und Quantenzahlen findet sich in [12, 13].

BB -Potentiale wurden über Korrelationsmatrizen und Lösen von generalisierten Eigenwertproblemen berechnet (siehe Abschnitt 2.4.4), wobei für jeden $\bar{Q}\bar{Q}$ -Abstand r eine separate Rechnung auszuführen war. Variiert man die Flavorkombination $\psi^{(1)}\psi^{(2)}$ und die leichte Spinkopplung Γ ,

erhält man Potentiale für verschiedenen Sektoren, charakterisiert z.B. durch die Quantenzahlen $(I, I_z, |j_z|, P, P_x)$. Diese Potentiale können attraktiv oder repulsiv sein und besitzen für große $\bar{Q}\bar{Q}$ -Separationen r verschiedene asymptotische Werte, entweder $2m(S)$, $m(S) + m(P_-)$ oder $2m(P_-)$ ($m(S)$ und $m(P_-)$ stehen für die Massen der entsprechenden statisch-leichten Mesonen; siehe Abschnitt 4.1.1). Die Ergebnisse sind in Tabelle 8 für leichte u/d -Quarks qualitativ zusammengefasst (“A” und “R” bezeichnen attraktiv bzw. repulsiv, “SS”, “SP” und “PP” die entsprechenden asymptotischen Werte $2m(S)$, $m(S) + m(P_-)$ und $2m(P_-)$) und in Abbildung 14 zu sehen. Der qualitative Verlauf dieser Potentiale lässt sich wie folgt verstehen:

		$\psi^{(1)}\psi^{(2)} = ud - du$		$\psi^{(1)}\psi^{(2)} = uu, ud + du, dd$	
Γ	$ j_z $	P, P_x	Typ	P, P_x	Typ
$\gamma_5 + \gamma_0\gamma_5$	0	-, +	A, SS	+, +	R, SS
$\gamma_5 - \gamma_0\gamma_5$	0	-, +	A, PP	+, +	R, PP
1	0	+, -	A, SP	-, -	R, SP
γ_0	0	-, -	R, SP	+, -	A, SP
$\gamma_3 + \gamma_0\gamma_3$	0	+, -	R, SS	-, -	A, SS
$\gamma_3 - \gamma_0\gamma_3$	0	+, -	R, PP	-, -	A, PP
$\gamma_3\gamma_5$	0	+, +	A, SP	-, +	R, SP
$\gamma_0\gamma_3\gamma_5$	0	-, +	R, SP	+, +	A, SP
$\gamma_{1/2} + \gamma_0\gamma_{1/2}$	1	+, ±	R, SS	-, ±	A, SS
$\gamma_{1/2} - \gamma_0\gamma_{1/2}$	1	+, ±	R, PP	-, ±	A, PP
$\gamma_{1/2}\gamma_5$	1	+, ∓	A, SP	-, ∓	R, SP
$\gamma_0\gamma_{1/2}\gamma_5$	1	-, ∓	R, SP	+, ∓	A, SP

Tabelle 8: Quantenzahlen der BB -Testzustände und -Potentiale. “Typ” beschreibt das qualitative Verhalten des numerisch mit Gitter-QCD bestimmten Potentials (“A”: attraktiv; “R”: repulsiv; “SS”, “SP” und “PP”: asymptotischer Potentialwert $2m(S)$, $m(S) + m(P_-)$ oder $2m(P_-)$).

- Attraktivität bzw. Repulsivität bei kurzen Abständen wird vom 1-Gluon-Exchange-Potential zwischen den statischen Antiquarks erzeugt. Je nach Quantenzahlen und aufgrund des Pauli-Prinzips befinden sich die statischen Antiquarks entweder in einem Farbtriplett oder -sextett, was Attraktivität bzw. Repulsivität zur Folge hat [15].
- Die asymptotischen Potentialwerte können verstanden werden, indem man die Erzeugungsoperatoren (54) durch statisch-leichte Meson-Erzeugungsoperatoren ähnlich zu (30) ausdrückt. Z.B. findet man für $\Gamma = 1$ und $\psi^{(1)}\psi^{(2)} = uu$

$$\begin{aligned}
 (\mathcal{C}1)_{AB} & \left(\bar{Q}_C(\mathbf{r}_1) u_A(\mathbf{r}_1) \right) \left(\bar{Q}_C(\mathbf{r}_2) u_B(\mathbf{r}_2) \right) = \\
 & = -S_\uparrow(\mathbf{r}_1) P_{-\downarrow}(\mathbf{r}_2) + S_\downarrow(\mathbf{r}_1) P_{-\uparrow}(\mathbf{r}_2) - P_{-\uparrow}(\mathbf{r}_1) S_\downarrow(\mathbf{r}_2) + P_{-\downarrow}(\mathbf{r}_1) S_\uparrow(\mathbf{r}_2)
 \end{aligned} \quad (55)$$

(S und P_- bezeichnen statisch-leichte Meson-Erzeugungsoperatoren für das S - bzw. P_- -Meson; dabei geben \uparrow und \downarrow die Ausrichtungen der leichten Quarkspins an). Dieser BB -Erzeugungsoperator generiert also Kombinationen von jeweils einem S -Meson und einem P_- -Meson. Das entsprechende BB -Potential nimmt folglich für große $\bar{Q}\bar{Q}$ -Separationen r den asymptotischen Wert $m(S) + m(P_-)$ an [12].

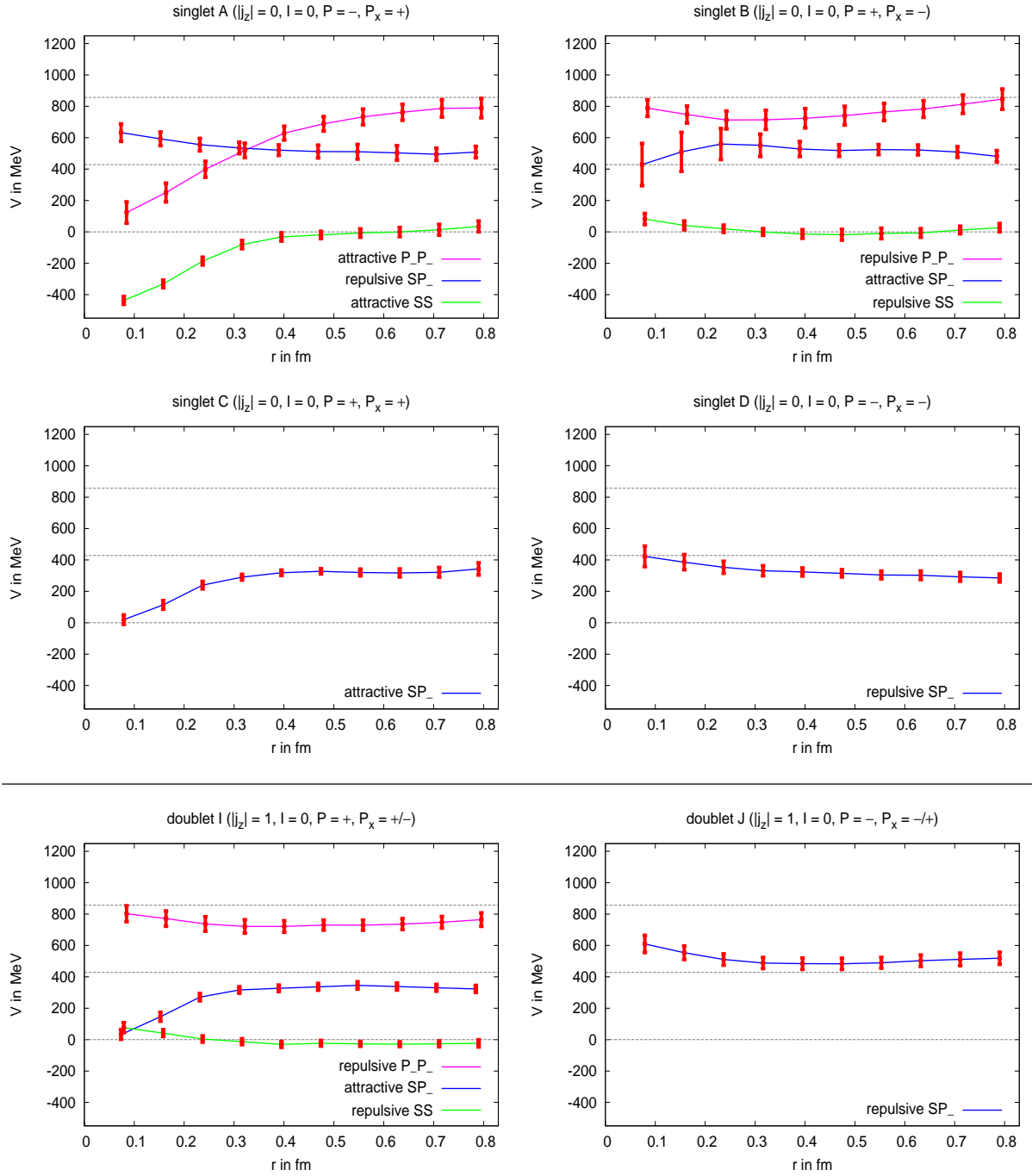


Abbildung 14: BB -Potentiale als Funktionen der $\bar{Q}\bar{Q}$ -Separation r für $I = 0$. Die Potentialwerte bei $r = a \approx 0.079$ fm weisen starke Diskretisierungsfehler auf (siehe Diskussion in [12]).

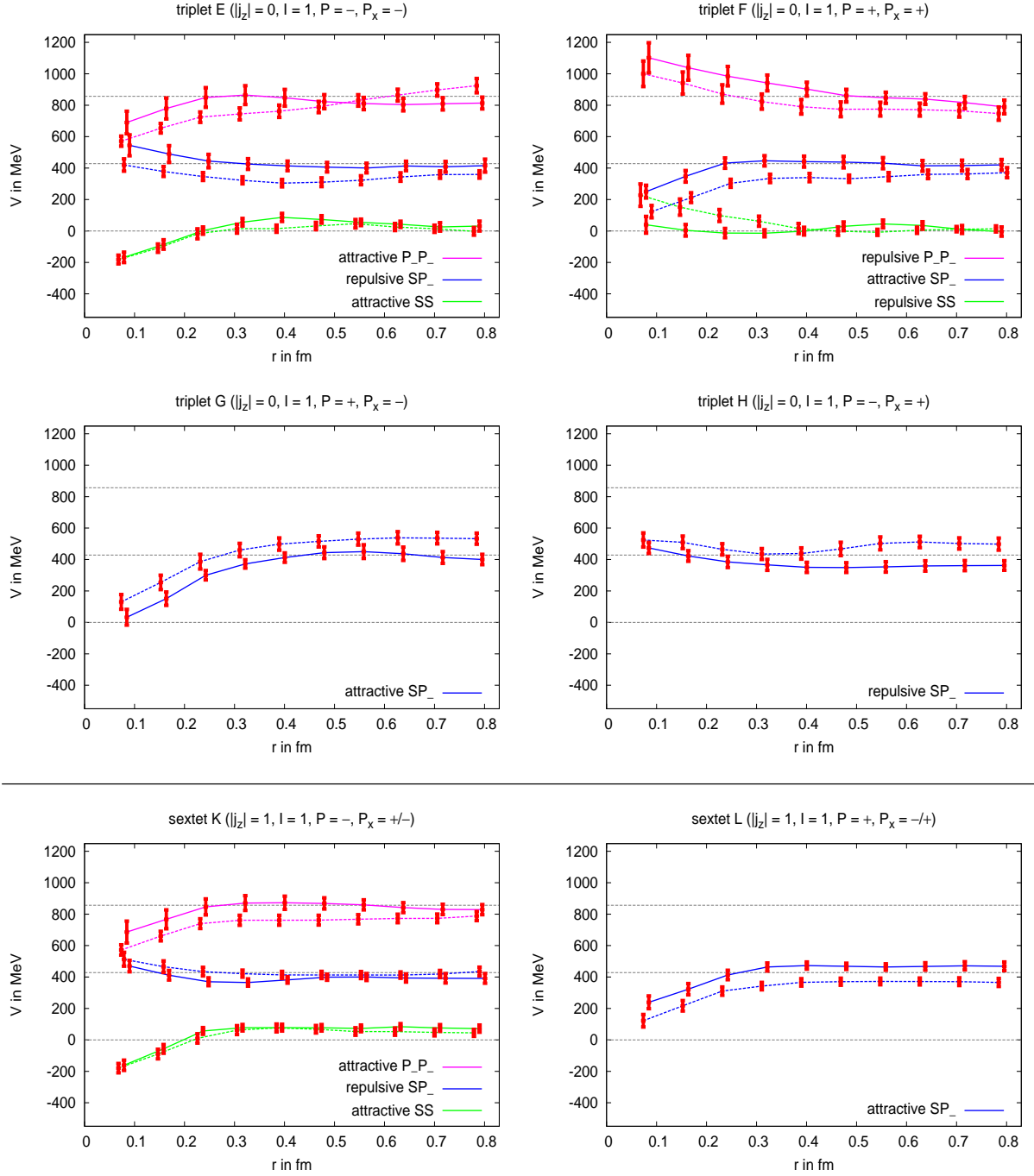


Abbildung 15: BB -Potentiale als Funktionen der $\bar{Q}\bar{Q}$ -Separation r für $I = 1$. Die Potentialwerte bei $r = a \approx 0.079$ fm weisen starke Diskretisierungsfehler auf (siehe Diskussion in [12]). Aufgrund der verwendeten Wilson-Twisted-Mass-Diskretisierung unterscheiden sich die Ergebnisse für $I_z = \pm 1$ und $I_z = 0$ um Diskretisierungseffekte. Die Differenzen der paarweise auftretenden Kurven stellen also ein Maß für Diskretisierungsfehler dar.

Auch wenn aufgrund der Wahlmöglichkeiten für Γ (16 Möglichkeiten) und $\psi^{(1)}\psi^{(2)}$ (4 Möglichkeiten bei Beschränkung auf leichte u/d -Quarks) 64 Testzustände existieren, sind die resultierenden BB -Potentiale teilweise aufgrund von Isospinsymmetrie ($I = 1$ -Tripletts) oder Rotationssymmetrie ($|j_z| = 1$ -Dubletts) entartet. Insgesamt ergibt sich die folgende Struktur [13]:

SS -Potentiale,	attraktiv:	$1(A) \oplus 3(E) \oplus 6(K)$	(10 Testzustände)
	repulsiv:	$1(B) \oplus 3(F) \oplus 2(I)$	(6 Testzustände)
SP_- -Potentiale,	attraktiv:	$1(B) \oplus 1(C) \oplus 3(E) \oplus 3(G) \oplus 2(I) \oplus 6(L)$	(16 Testzustände)
	repulsiv:	$1(A) \oplus 1(D) \oplus 3(F) \oplus 3(H) \oplus 2(J) \oplus 6(K)$	(16 Testzustände)
P_-P_- -Potentiale,	attraktiv:	$1(A) \oplus 3(E) \oplus 6(K)$	(10 Testzustände)
	repulsiv:	$1(B) \oplus 3(F) \oplus 2(I)$	(6 Testzustände)

Die Buchstaben A bis L nummerieren die Multipletts und sind in Abbildung 14 und Abbildung 15 in den Bildüberschriften angegeben. Die 64 Erzeugungsoperatoren (54) erlauben also die Berechnung von 24 unterschiedlichen BB -Potentialen.

Analoge Rechnungen wurden auch mit $\psi^{(1)}\psi^{(2)} = ss$ und $\psi^{(1)}\psi^{(2)} = cc$ an Stelle von leichten u/d -Quarks ausgeführt. Qualitativ entspricht dies $\psi^{(1)}\psi^{(2)} = uu$ bzw. $\psi^{(1)}\psi^{(2)} = dd$ und damit $I = 1$. Konzeptionell ist es natürlich auch interessant, zwei degenerierte Flavors von s -Quarks und von c -Quarks zu studieren und damit auch Ergebnisse mit ‘‘Strange-Isospin’’ $I_s = 0$ und ‘‘Charm-Isospin’’ $I_c = 0$ zu generieren (siehe Abschnitt 6.2).

Auf ähnlichem Weg können auch $B\bar{B}$ -Potentiale studiert werden, wobei hier Erzeugungsoperatoren der Form

$$\mathcal{O}_{\Gamma, \psi^{(1)}\psi^{(2)}} \equiv \Gamma_{AB} \tilde{\Gamma}_{CD} \left(\bar{Q}_C(\mathbf{r}_1) q_A^{(1)}(\mathbf{r}_1) \right) \left(\bar{q}_B^{(2)}(\mathbf{r}_2) Q_D(\mathbf{r}_2) \right) \quad (56)$$

zu verwenden sind. Dieses System ist technisch schwieriger zu untersuchen, da im Gegensatz zum BB -Fall ein extrahierter Zustand neben einer Tetraquark-Struktur auch ein $Q\bar{Q}$ -Zustand neben einem weit entfernten leichten Meson (z.B. einem Pion) sein kann, oder es im Fall von $I = 0$ sogar zur Auslöschung des leichten Quark-Antiquark-Paars kommen kann und man so unter Umständen nur das ordinäre statische Quark-Antiquark-Potential berechnet. Erste vorläufige Ergebnisse zeigen ähnliche Potentiale, wie im BB -Fall, mit dem Unterschied, dass sämtliche $B\bar{B}$ -Potentiale attraktiv sind, also keine repulsiven Kanäle existieren [15]. Wie oben skizziert kann auch dieses Ergebnis über das 1-Gluon-Exchange-Potential zwischen dem statischen Quark und dem statischen Antiquark verstanden werden, da in diesem Fall das Pauli-Prinzip einen Beitrag des stark attraktiven Farbsingletpotentials in keinem Kanal verbietet.

6.2 Modellrechnungen zur Identifikation von Tetraquark-Zuständen

Um festzustellen, ob $qq\bar{Q}\bar{Q}$ -Tetraquarkzustände existieren, wird der phänomenologisch orientierte Ansatz

$$V(r) \equiv -\frac{\alpha}{r} \exp \left(-\left(\frac{r}{d} \right)^p \right)$$

an die Gitter-QCD-Ergebnisse für die BB -Potentiale gefittet (Fitparameter α , d , und p). Von besonderem Interesse bei der Suche nach Tetraquarks sind die attraktiven Potentiale zweier

statisch-leichter Mesonen im Grundzustand S , also Potentiale mit asymptotischem Wert $2m(S)$. Hier gibt es das stärker attraktive skalare Isosinglett-Potential A und die beiden im Rahmen statistischer Fehler identischen weniger stark attraktiven Vektor-Isotriplett-Potentiale E und K . Die Fits sowohl für A als auch E und K sind in Abbildung 16 zu sehen, jeweils für u/d -, s - und c -Quarkmassen. Es ist offensichtlich, dass leichtere Quarkmassen zu stärker attraktiven Potentialen führen.

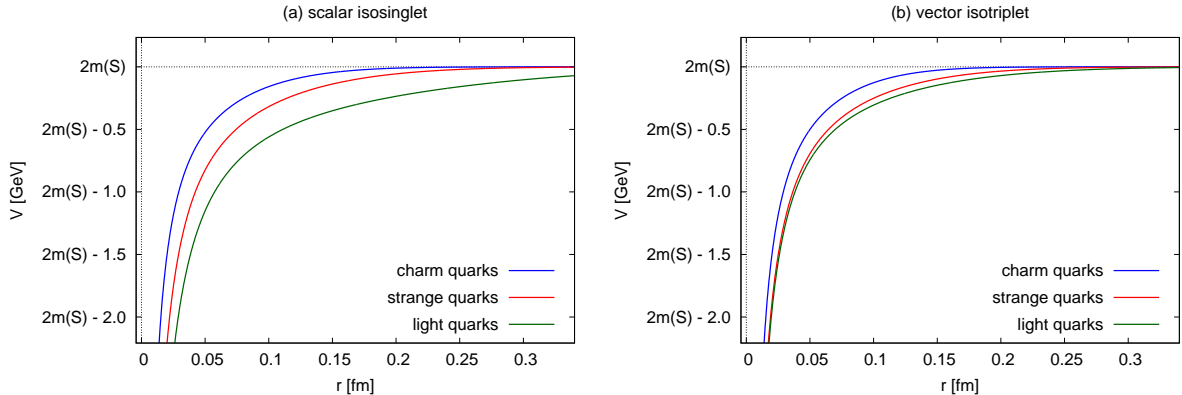


Abbildung 16: (entstammt [15]) Resultierende Fits $V(r)$ (Gleichung (57)) für attraktive BB -Potentiale für u/d -, s - und c -Quarkmassen. (**links**) Skalares Isosinglett-Potential. (**rechts**) Vektor-Isotriplett-Potential.

Um herauszufinden, ob in einem der beiden Kanäle für die untersuchten leichten Quarkmassen ein gebundener 4-Quarkzustand vorliegen kann, wurden diese Potentiale $V(r)$ in der radialen S -Wellen-Schrödinger-Gleichung

$$\left(-\frac{1}{2\mu} \frac{d^2}{dr^2} + 2m_{B_{(s,c)}} + V(r) \right) R(r) = ER(r) \quad (57)$$

mit der Wellenfunktion $\psi(\mathbf{r}) \equiv R(r)/r$ und der reduzierten Masse $\mu \equiv m_{B_{(s,c)}}/2$ verwendet. Da eine große reduzierte Masse, also schwere Quarkmassen einen gebundenen Zustand begünstigen, genau wie ein stark attraktives Potential (wie es bei leichten Quarkmassen vorliegt), gibt es zwei entgegenwirkende Effekte. Nach numerischer Lösung von (57) mit Hilfe von Standard-Shooting-Verfahren zeigt sich, dass das skalare Isosinglett-Potential A für leichte u/d -Quarks⁹ einen gebundenen Zustand beherbergt, alle anderen Kombinationen von Quarkmassen und Potentialen dagegen nicht. Auch wenn gewisse Näherungen, wie z.B. der statische Limes, verwendet wurden und Gitter-QCD mit Modellrechnungen kombiniert wurde, liefert dieses Ergebnis dennoch klare Anzeichen für die Existenz eines Tetraquarks bestehend aus zwei b -Antiquarks und zwei leichten u/d -Quarks. Das skalare Isosinglett-Potential A für leichte u/d -Quarks ist zusammen mit der radialen Wellenfunktion des gebundenen Zustands in Abbildung 17 zu sehen. Wie aus dieser Abbildung ersichtlich, beträgt der Abstand der beiden schweren Antiquarks etwa 0.25 fm.

Um zu quantifizieren, wie weit die anderen Kombinationen von Quarkmassen und Potentialen von einem Bindungszustand entfernt sind, sind in Tabelle 9 diejenigen Faktoren angegeben,

⁹Die verwendete u/d -Quarkmasse ist unphysikalisch schwer, $m_\pi \approx 340$ MeV.

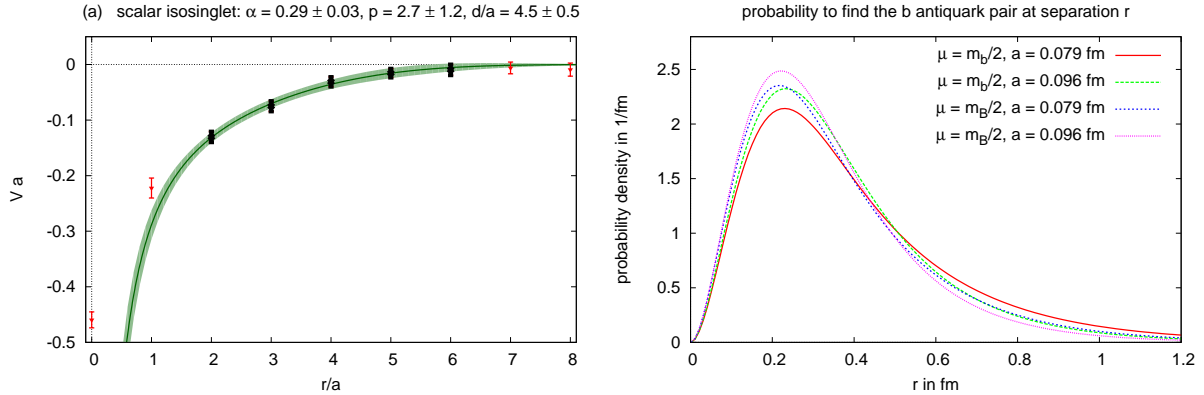


Abbildung 17: (entstammt [14]) (links) Das attraktive skalare Isosinglett-Potential für u/d -Quarkmassen als Funktion der $\bar{Q}\bar{Q}$ -Separation r/a ($a \approx 0.079 \text{ fm}$; Fit an Gitter-QCD-Resultate für $2 \leq r/a \leq 6$ [schwarze Punkte]). (rechts) Das Betragsquadrat der entsprechenden radialen Wellenfunktion $|R|^2$ als Funktion der $\bar{Q}\bar{Q}$ -Separation r .

um die die reduzierte Masse μ erhöht werden müsste, um einen Bindungszustand zu erhalten. Die aufgelisteten Faktoren zeigen, dass sich das System bei steigender leichter Quarkmasse immer weiter von einem Bindungszustand entfernt. Da die u/d -Quarkmassen unphysikalisch schwer gewählt wurden, ist es denkbar, dass bei physikalisch leichten u/d -Quarkmassen auch das Vektor-Isotriplett-Potential einen gebundenen Zustand aufweist. Dies wird Gegenstand zukünftiger Untersuchungen sein.

leichte Quarkmasse	u/d		s		c	
Konfidenzniveau für einen Bindungszustand	1σ	2σ	1σ	2σ	1σ	2σ
skalares Isosinglett-Potential	0.8	1.0	1.9	2.2	3.1	3.2
Vektor-Isotriplett-Potential	1.9	2.1	2.5	2.7	3.4	3.5

Tabelle 9: Faktoren, um die die reduzierte Masse μ erhöht werden müsste, um einen Bindungszustand mit Konfidenzniveau 1σ bzw. 2σ zu erhalten.

7 Zusammenfassung und Ausblick

Wesentliche Aspekte der thematisch ähnlichen Arbeiten [1, 2, 3, 4, 5, 6, 7, 8, 9, 10, 11, 12, 13, 14, 15] wurden zusammengefasst. Weitere Einzelheiten sind bei Bedarf den Arbeiten selbst zu entnehmen, die im folgenden Teil II vollständig abgedruckt sind.

Die in Kapitel 4 diskutierten Berechnungen von Hadronen mit $q\bar{q}$ - und qqq -Erzeugungsoperatoren sind weit fortgeschritten bzw. teilweise bereits abgeschlossen. Im Gegensatz dazu befinden sich die in Kapitel 5 und Kapitel 6 zusammengefassten Untersuchungen von Tetraquarkkandidaten eher in der Anfangsphase. Die Untersuchung solcher Systeme stellt gegenwärtig sicher eine der großen Herausforderungen im Feld der Gitter-QCD dar. Entsprechende Ergebnisse sind und wären auch weit über den Bereich der Gitter-QCD hinaus von großem Interesse, z.B. für die experimentelle Teilchenphysik und die Phänomenologie.

Eine meines Erachtens erfolgversprechende Strategie zur Untersuchung von Tetraquarkkandidaten mit Hilfe von Gitter-QCD besteht im gleichzeitigen Verfolgen der in Kapitel 5 und 6 diskutierten Ansätze. Ein erfolgreicher Einsatz der in Kapitel 5 verwendeten Methoden mag für einige Systeme Informationen über deren Struktur liefern bzw. quantitative verlässliche Ergebnisse für Resonanzparameter (Masse, Breite) liefern. Gleichzeitig erlauben die kostengünstigeren Berechnungen der Kräfte zwischen statischen Quarks bzw. statisch-leichten Mesonen und deren Weiterverwendung in Modellrechnungen aus Kapitel 6 qualitative Einsichten in die Physik von Tetraquarks.

Die Möglichkeiten zur Fortsetzung dieser Projekte sind vielfältig. Ein wichtiger sich gegenwärtig in Arbeit befindlicher Schritt ist sicher die Optimierung der Techniken zur näherungsfreien Berechnung der 6×6 -Korrelationsmatrix aus Kapitel 5 (Abbildung 11). Erst dann können verschiedene schlecht verstandene Systeme und Tetraquarkkandidaten quantitativ verlässlich untersucht werden. Ein anderer Aspekt ist die Erweiterung der Berechnung der BB -Potentiale aus Kapitel 6 auf den experimentell relevanteren aber technisch schwierigeren $B\bar{B}$ -Fall. Die Implementation und Verwendung weiterer Erzeugungsoperatoren, insbesondere solcher mit Diquark-Antidiquark-Struktur, wäre dabei ebenfalls wünschenswert.

Danksagung

Mein Dank gilt meinen Kollegen, Kollaborationspartnern, Chefs, Mentoren, Mitarbeitern, Doktoranden, Studenten und Physik-Freunden während meiner Gitter-QCD-Zeit von Mai 2007 bis heute. Besonders hervorheben möchte ich in diesem Zusammenhang Owe Philipsen, Michael Müller-Preußker, Karl Jansen, Chris Michael und Olivier Pène.

Besten Dank außerdem an Peter Eschenbrenner, Dietmar Mülhens, Francesco Giacosa und Piero Nicolini für Ratschläge und Tipps rund um das Habilitationsverfahren und die Erstellung dieser Zusammenfassung.

I acknowledge support by the Emmy Noether Programme of the DFG (German Research Foundation), grant WA 3000/1-1.

This work was supported in part by the Helmholtz International Center for FAIR within the framework of the LOEWE program launched by the State of Hesse.

Literatur

- [1] K. Jansen, C. Michael, A. Shindler and M. Wagner [ETM Collaboration], “The static-light meson spectrum from twisted mass lattice QCD,” *JHEP* **0812**, 058 (2008) [arXiv:0810.1843 [hep-lat]].
- [2] C. Michael, A. Shindler and M. Wagner [ETM Collaboration], “The continuum limit of the static-light meson spectrum,” *JHEP* **1008**, 009 (2010) [arXiv:1004.4235 [hep-lat]].
- [3] M. Wagner and C. Wiese [ETM Collaboration], “The static-light baryon spectrum from twisted mass lattice QCD,” *JHEP* **1107**, 016 (2011) [arXiv:1104.4921 [hep-lat]].
- [4] P. Dimopoulos *et al.* [ETM Collaboration], “Lattice QCD determination of m_b , f_B and f_{B_s} with twisted mass Wilson fermions,” *JHEP* **1201**, 046 (2012) [arXiv:1107.1441 [hep-lat]].
- [5] B. Blossier, M. Wagner and O. Pene [ETM Collaboration], “Lattice calculation of the Isgur-Wise functions $\tau_{1/2}$ and $\tau_{3/2}$ with dynamical quarks,” *JHEP* **0906**, 022 (2009) [arXiv:0903.2298 [hep-lat]].
- [6] M. Kalinowski and M. Wagner [ETM Collaboration], “Masses of mesons with charm valence quarks from $2+1+1$ flavor twisted mass lattice QCD,” *Acta Phys. Polon. Supp.* **6**, no. 3, 991 (2013) [arXiv:1304.7974 [hep-lat]].
- [7] M. Kalinowski and M. Wagner [ETM Collaboration], “Twisted mass lattice computation of charmed mesons with focus on D^{**} ,” *PoS LATTICE* **2013**, 241 (2013) [arXiv:1310.5513 [hep-lat]].
- [8] R. Baron *et al.* [ETM Collaboration], “Light hadrons from lattice QCD with light (u, d), strange and charm dynamical quarks,” *JHEP* **1006**, 111 (2010) [arXiv:1004.5284 [hep-lat]].
- [9] R. Baron *et al.* [ETM Collaboration], “Computing K and D meson masses with $N_f = 2+1+1$ twisted mass lattice QCD,” *Comput. Phys. Commun.* **182**, 299 (2011) [arXiv:1005.2042 [hep-lat]].
- [10] C. Alexandrou *et al.* [ETM Collaboration], “Lattice investigation of the scalar mesons $a_0(980)$ and κ using four-quark operators,” *JHEP* **1304**, 137 (2013) [arXiv:1212.1418].
- [11] A. Abdel-Rehim *et al.*, “Investigation of the tetraquark candidate $a_0(980)$: technical aspects and preliminary results,” arXiv:1410.8757 [hep-lat].
- [12] M. Wagner [ETM Collaboration], “Forces between static-light mesons,” *PoS LATTICE* **2010**, 162 (2010) [arXiv:1008.1538 [hep-lat]].
- [13] M. Wagner [ETM Collaboration], “Static-static-light-light tetraquarks in lattice QCD,” *Acta Phys. Polon. Supp.* **4**, 747 (2011) [arXiv:1103.5147 [hep-lat]].
- [14] P. Bicudo and M. Wagner, “Lattice QCD signal for a bottom-bottom tetraquark,” *Phys. Rev. D* **87**, 114511 (2013) [arXiv:1209.6274 [hep-ph]].
- [15] B. Wagenbach, P. Bicudo and M. Wagner, “Lattice investigation of heavy meson interactions,” arXiv:1411.2453 [hep-lat].

- [16] K. A. Olive *et al.* [Particle Data Group], “2014 Review of particle physics,”, Chin. Phys. C, **38**, 090001 (2014).
- [17] L. H. Ryder, “Quantum field theory,” Cambridge University Press.
- [18] M. Srednicki, “Quantum field theory,” Cambridge University Press.
- [19] M. Maggiore, “A modern introduction to quantum field theory,” Oxford University Press.
- [20] M. E. Peskin and D. V. Schroeder, “An introduction to quantum field theory,” Perseus Books.
- [21] H. J. Rothe, “Lattice gauge theories: an introduction”, World Scientific Lecture Notes.
- [22] T. DeGrand, C. DeTar, “Lattice methods for quantum chromodynamics”, World Scientific Publishing Company.
- [23] C. Gattringer and C. B. Lang, “Quantum chromodynamics on the lattice: an introductory presentation”, Springer.
- [24] M. Wagner, S. Diehl, T. Kuske and J. Weber, “An introduction to lattice hadron spectroscopy for students without quantum field theoretical background,” arXiv:1310.1760 [hep-lat].
- [25] M. Creutz, “Gauge fixing, the transfer matrix, and confinement on a lattice,” Phys. Rev. D **15**, 1128 (1977).
- [26] M. Lüscher, “Volume Dependence of the energy spectrum in massive quantum field theories. 2. Scattering states,” Commun. Math. Phys. **105**, 153 (1986).
- [27] M. Lüscher, “Two particle states on a torus and their relation to the scattering matrix,” Nucl. Phys. B **354**, 531 (1991).
- [28] M. Lüscher, “Signatures of unstable particles in finite volume,” Nucl. Phys. B **364**, 237 (1991).
- [29] C. B. Lang *et al.*, “ $K\pi$ scattering for isospin 1/2 and 3/2 in lattice QCD,” Phys. Rev. D **86**, 054508 (2012) [arXiv:1207.3204 [hep-lat]].
- [30] B. Blossier *et al.*, “On the generalized eigenvalue method for energies and matrix elements in lattice field theory,” JHEP **0904**, 094 (2009) [arXiv:0902.1265 [hep-lat]].
- [31] A. Shindler, “Twisted mass lattice QCD,” Phys. Rept. **461**, 37 (2008) [arXiv:0707.4093 [hep-lat]].
- [32] P. Weisz, “Continuum limit improved lattice action for pure Yang-Mills theory. 1.,” Nucl. Phys. B **212**, 1 (1983).
- [33] Y. Iwasaki, K. Kanaya, T. Kaneko and T. Yoshie, “Scaling in SU(3) pure gauge theory with a renormalization group improved action,” Phys. Rev. D **56**, 151 (1997) [hep-lat/9610023].
- [34] P. Boucaud *et al.* [ETM Collaboration], “Dynamical twisted mass fermions with light quarks: simulation and analysis details,” Comput. Phys. Commun. **179**, 695 (2008) [arXiv:0803.0224 [hep-lat]].

- [35] R. Baron *et al.* [ETM Collaboration], “Light meson physics from maximally twisted mass lattice QCD,” JHEP **1008**, 097 (2010) [arXiv:0911.5061 [hep-lat]].
- [36] M. Neubert, “Heavy quark symmetry,” Phys. Rept. **245**, 259 (1994) [arXiv:hep-ph/9306320].
- [37] T. Mannel, “Heavy-quark effective field theory,” Rept. Prog. Phys. **60**, 1113 (1997).
- [38] D. Ebert, R. N. Faustov and V. O. Galkin, “Heavy-light meson spectroscopy and Regge trajectories in the relativistic quark model,” arXiv:0910.5612 [hep-ph].
- [39] C. McNeile and C. Michael [UKQCD Collaboration], “Mixing of scalar glueballs and flavour-singlet scalar mesons,” Phys. Rev. D **63**, 114503 (2001) [arXiv:hep-lat/0010019].
- [40] C. McNeile, C. Michael and P. Pennanen [UKQCD Collaboration], “Hybrid meson decay from the lattice,” Phys. Rev. D **65**, 094505 (2002) [arXiv:hep-lat/0201006].
- [41] C. McNeile, C. Michael and G. Thompson [UKQCD Collaboration], “Hadronic decay of a scalar B meson from the lattice,” Phys. Rev. D **70**, 054501 (2004) [arXiv:hep-lat/0404010].
- [42] M. Bochicchio *et al.*, “Heavy quark spectroscopy on the lattice,” Nucl. Phys. B **372**, 403 (1992).
- [43] D. Guazzini, H. B. Meyer and R. Sommer [ALPHA Collaboration], “Non-perturbative renormalization of the chromo-magnetic operator in heavy quark effective theory and the B^*-B mass splitting,” JHEP **0710**, 081 (2007) [arXiv:0705.1809 [hep-lat]].
- [44] B. Blossier *et al.*, “Spectroscopy and decay constants from non-perturbative HQET at Order $1/m$,” PoS LAT **2009**, 106 (2009) [arXiv:0911.1568 [hep-lat]].
- [45] B. Blossier, M. Della Morte, N. Garron and R. Sommer, “HQET at order $1/m$: I. Non-perturbative parameters in the quenched approximation,” arXiv:1001.4783 [hep-lat].
- [46] B. Blossier *et al.*, “HQET at order $1/m$: II. Spectroscopy in the quenched approximation,” arXiv:1004.2661 [hep-lat].
- [47] T. Burch *et al.*, “Excitations of single-beauty hadrons,” Phys. Rev. D **79**, 014504 (2009) [arXiv:0809.1103 [hep-lat]].
- [48] R. Sommer, “A New way to set the energy scale in lattice gauge theories and its applications to the static force and ‘ α_s ’ in SU(2) Yang-Mills theory,” Nucl. Phys. B **411**, 839 (1994) [hep-lat/9310022].
- [49] R. Sommer, “Scale setting in lattice QCD,” PoS LATTICE **2013**, 015 (2014) [arXiv:1401.3270 [hep-lat]].
- [50] H. J. Schnitzer, “Spin structure in meson spectroscopy with an effective scalar confinement of quarks,” Phys. Rev. D **18**, 3482 (1978).
- [51] H. J. Schnitzer, “Where are the inverted multiplets of meson spectroscopy?,” Phys. Lett. B **226** (1989) 171.

- [52] D. Ebert, V. O. Galkin and R. N. Faustov, “Mass spectrum of orbitally and radially excited heavy-light mesons in the relativistic quark model,” Phys. Rev. D **57**, 5663 (1998) [Erratum-ibid. D **59**, 019902 (1999)] [arXiv:hep-ph/9712318].
- [53] N. Isgur, “Spin-orbit inversion of excited heavy quark mesons,” Phys. Rev. D **57**, 4041 (1998).
- [54] C. Alexandrou *et al.* [ETM Collaboration], “Nucleon electromagnetic form factors in twisted mass lattice QCD,” arXiv:1102.2208 [hep-lat].
- [55] W. Detmold, C. J. Lin and M. Wingate, “Bottom hadron mass splittings in the static limit from 2+1 flavour lattice QCD,” Nucl. Phys. B **818**, 17 (2009) [arXiv:0812.2583 [hep-lat]].
- [56] H. W. Lin, S. D. Cohen, N. Mathur and K. Orginos, “Bottom-hadron mass splittings from static-quark action on 2+1-flavor lattices,” Phys. Rev. D **80**, 054027 (2009) [arXiv:0905.4120 [hep-lat]].
- [57] H. W. Lin *et al.*, “Heavy-Baryon Spectroscopy from Lattice QCD,” Comput. Phys. Commun. **182**, 24 (2011) [arXiv:1002.4710 [hep-lat]].
- [58] D. Ebert, R. N. Faustov and V. O. Galkin, “Masses of excited heavy baryons in the relativistic quark model,” Phys. Lett. B **659**, 612 (2008) [arXiv:0705.2957 [hep-ph]].
- [59] B. Blossier, “Lattice renormalisation of ‘ $\mathcal{O}(a)$ improved heavy-light operators: an addendum,” Phys. Rev. D **84**, 097501 (2011) [arXiv:1106.2132 [hep-lat]].
- [60] B. Blossier *et al.* [ETM Collaboration], “A Proposal for B -physics on current lattices,” JHEP **1004**, 049 (2010) [arXiv:0909.3187 [hep-lat]].
- [61] I. I. Bigi *et al.*, “Memorino on the ‘1/2 vs. 3/2 puzzle’ in $\bar{B} \rightarrow l \bar{\nu} X_c$ – a year later and a bit wiser,” Eur. Phys. J. C **52**, 975 (2007) [arXiv:0708.1621 [hep-ph]].
- [62] N. Isgur and M. B. Wise, “Excited charm mesons in semileptonic \bar{B} decay and their contributions to a Bjorken sum rule,” Phys. Rev. D **43**, 819 (1991).
- [63] N. Uraltsev, “New exact heavy quark sum rules,” Phys. Lett. B **501**, 86 (2001) [arXiv:hep-ph/0011124].
- [64] D. Liventsev *et al.* [Belle Collaboration], “Study of $B \rightarrow D^{**}l\nu$ with full reconstruction tagging,” Phys. Rev. D **77**, 091503 (2008) [arXiv:0711.3252 [hep-ex]].
- [65] F. Jugeau, A. Le Yaouanc, L. Oliver and J. C. Raynal, “The decays $\bar{B} \rightarrow D^{**}\pi$ and the Isgur-Wise functions $\tau_{1/2}(w), \tau_{3/2}(w)$,” Phys. Rev. D **72**, 094010 (2005) [arXiv:hep-ph/0504206].
- [66] C. Riha, “Berechnung von kinematischen Faktoren in differentiellen Zerfallsraten von $B \rightarrow D^{**}$,” Bachelorarbeit im Fach Physik an der Humboldt-Universität zu Berlin (2011).
- [67] M. Atoui, “Lattice computation of $B \rightarrow D^*, D^{**}l\nu$ form factors at finite heavy masses,” arXiv:1305.0462 [hep-lat].
- [68] M. Atoui, B. Blossier, V. Morénas, O. Pène and K. Petrov, “Semileptonic $B \rightarrow D^{**}$ decays in Lattice QCD: a feasibility study and first results,” arXiv:1312.2914 [hep-lat].

- [69] R. L. Jaffe, “Exotica,” Phys. Rept. **409** (2005) 1 [hep-ph/0409065].
- [70] S. Bernardson, P. McCarty and C. Thron, “Monte Carlo methods for estimating linear combinations of inverse matrix entries in lattice QCD,” Comput. Phys. Commun. **78**, 256 (1993).
- [71] S. -J. Dong and K. -F. Liu, “Stochastic estimation with $Z(2)$ noise,” Phys. Lett. B **328**, 130 (1994) [hep-lat/9308015].
- [72] M. Peardon *et al.* [Hadron Spectrum Collaboration], “A novel quark-field creation operator construction for hadronic physics in lattice QCD,” Phys. Rev. D **80**, 054506 (2009) [arXiv:0905.2160 [hep-lat]].
- [73] T. DeGrand and C. E. Detar, “Lattice methods for quantum chromodynamics,” World Scientific (2006).
- [74] C. Gattringer and C. B. Lang, “Quantum chromodynamics on the lattice,” Lect. Notes Phys. **788** (2010).
- [75] M. Foster *et al.* [UKQCD Collaboration], “Quark mass dependence of hadron masses from lattice QCD,” Phys. Rev. D **59** (1999) 074503 [hep-lat/9810021].
- [76] C. McNeile *et al.* [UKQCD Collaboration], “Decay width of light quark hybrid meson from the lattice,” Phys. Rev. D **73** (2006) 074506 [hep-lat/0603007].
- [77] G. Martinelli and C. T. Sachrajda, “A lattice study of nucleon structure,” Nucl. Phys. B **316** (1989) 355.

Teil II

Auswahl von Veröffentlichungen

Diese Arbeiten stehen über das Habilitationsthema

“Berechnung von Massen, Zerfällen und Struktur von Hadronen mit Methoden der Gitter-QCD”

in thematischem Zusammenhang und werden in Teil I zusammengefasst. Sie sind in derselben Reihenfolge geordnet, wie sie in Teil I diskutiert werden.

- K. Jansen, C. Michael, A. Shindler and M. Wagner [ETM Collaboration], “The static-light meson spectrum from twisted mass lattice QCD,” *JHEP* **0812**, 058 (2008) [arXiv:0810.1843 [hep-lat]].
- C. Michael, A. Shindler and M. Wagner [ETM Collaboration], “The continuum limit of the static-light meson spectrum,” *JHEP* **1008**, 009 (2010) [arXiv:1004.4235 [hep-lat]].
- M. Wagner and C. Wiese [ETM Collaboration], “The static-light baryon spectrum from twisted mass lattice QCD,” *JHEP* **1107**, 016 (2011) [arXiv:1104.4921 [hep-lat]].
- P. Dimopoulos *et al.* [ETM Collaboration], “Lattice QCD determination of m_b , f_B and f_{B_s} with twisted mass Wilson fermions,” *JHEP* **1201**, 046 (2012) [arXiv:1107.1441 [hep-lat]].
- B. Blossier, M. Wagner and O. Pene [ETM Collaboration], “Lattice calculation of the Isgur-Wise functions $\tau_{1/2}$ and $\tau_{3/2}$ with dynamical quarks,” *JHEP* **0906**, 022 (2009) [arXiv:0903.2298 [hep-lat]].
- M. Kalinowski and M. Wagner [ETM Collaboration], “Masses of mesons with charm valence quarks from $2 + 1 + 1$ flavor twisted mass lattice QCD,” *Acta Phys. Polon. Supp.* **6**, no. 3, 991 (2013) [arXiv:1304.7974 [hep-lat]].
- M. Kalinowski and M. Wagner [ETM Collaboration], “Twisted mass lattice computation of charmed mesons with focus on D^{**} ,” *PoS LATTICE* **2013**, 241 (2013) [arXiv:1310.5513 [hep-lat]].
- R. Baron *et al.* [ETM Collaboration], “Light hadrons from lattice QCD with light (u, d), strange and charm dynamical quarks,” *JHEP* **1006**, 111 (2010) [arXiv:1004.5284 [hep-lat]].
- R. Baron *et al.* [ETM Collaboration], “Computing K and D meson masses with $N_f = 2 + 1 + 1$ twisted mass lattice QCD,” *Comput. Phys. Commun.* **182**, 299 (2011) [arXiv:1005.2042 [hep-lat]].
- C. Alexandrou *et al.* [ETM Collaboration], “Lattice investigation of the scalar mesons $a_0(980)$ and κ using four-quark operators,” *JHEP* **1304**, 137 (2013) [arXiv:1212.1418].
- A. Abdel-Rehim *et al.*, “Investigation of the tetraquark candidate $a_0(980)$: technical aspects and preliminary results,” submitted to *PoS LATTICE* **2014** [arXiv:1410.8757 [hep-lat]].
- M. Wagner [ETM Collaboration], “Forces between static-light mesons,” *PoS LATTICE* **2010**, 162 (2010) [arXiv:1008.1538 [hep-lat]].
- M. Wagner [ETM Collaboration], “Static-static-light-light tetraquarks in lattice QCD,” *Acta Phys. Polon. Supp.* **4**, 747 (2011) [arXiv:1103.5147 [hep-lat]].
- P. Bicudo and M. Wagner, “Lattice QCD signal for a bottom-bottom tetraquark,” *Phys. Rev. D* **87**, 114511 (2013) [arXiv:1209.6274 [hep-ph]].
- B. Wagenbach, P. Bicudo and M. Wagner, “Lattice investigation of heavy meson interactions,” accepted by *J. Phys.: Conf. Ser.* [arXiv:1411.2453 [hep-lat]].

SFB/CPP-08-82
 DESY 08-135
 LTH 809
 HU-EP-08/44

The static-light meson spectrum from twisted mass lattice QCD

Karl Jansen

DESY, Platanenallee 6, D-15738 Zeuthen, Germany
 karl.jansen@desy.de

Chris Michael, Andrea Shindler

Theoretical Physics Division, Department of Mathematical Sciences, University of Liverpool,
 Liverpool L69 3BX, UK
 c.michael@liverpool.ac.uk
 andrea.shindler@liverpool.ac.uk

Marc Wagner

Humboldt-Universität zu Berlin, Institut für Physik, Newtonstraße 15, D-12489 Berlin,
 Germany
 mcwagner@physik.hu-berlin.de



October 9, 2008

Abstract

We compute the static-light meson spectrum with $N_f = 2$ flavours of sea quarks using Wilson twisted mass lattice QCD. We consider five different values for the light quark mass corresponding to $300 \text{ MeV} \lesssim m_P \lesssim 600 \text{ MeV}$ and we present results for angular momentum $j = 1/2$, $j = 3/2$ and $j = 5/2$ and for parity $\mathcal{P} = +$ and $\mathcal{P} = -$. We extrapolate our results to physical quark masses and make predictions regarding the spectrum of B and B_s mesons.

1 Introduction

A systematic way to study B and B_s mesons from first principles is with lattice QCD. Since $am_b > 1$ at currently available lattice spacings for large volume simulations, one needs to use for the b quark a formalism such as Heavy Quark Effective Theory (HQET) or Non-Relativistic QCD. Here we follow the HQET route, which enables all sources of systematic error to be controlled.

In the static limit a heavy-light meson will be the “hydrogen atom” of QCD. Since in this limit there are no interactions involving the heavy quark spin, states are doubly degenerate, i.e. there is no hyperfine splitting. Therefore, it is common to label static-light mesons by parity \mathcal{P} and total angular momentum of the light degrees of freedom j with $j = |l \pm 1/2|$, where l denotes angular momentum and $\pm 1/2$ the spin of the light quark. An equivalent notation is given by $S \equiv (1/2)^-$, $P_- \equiv (1/2)^+$, $P_+ \equiv (3/2)^+$, $D_- \equiv (3/2)^-$, ... The total angular momentum of the static-light meson is either $J = j + 1/2$ or $J = j - 1/2$, where both states are of the same mass. Note that in contrast to parity, charge conjugation is not a good quantum number, since static-light mesons are made from non-identical quarks.

The static-light meson spectrum has been studied comprehensively by lattice methods in the quenched approximation with a rather coarse lattice spacing [1]. Lattice studies with $N_f = 2$ flavours of dynamical sea quarks have also explored this spectrum [2, 3, 4, 5, 6, 7]. Here (cf. also [8]) we use $N_f = 2$ and are able to reach lighter dynamical quark masses, which are closer to the physical u/d quark mass, so enabling a more reliable extrapolation. Note that in this formalism, mass differences in the heavy-light spectrum are $\mathcal{O}(a)$ improved so that the continuum limit is more readily accessible.

In this paper, we concentrate on the unitary sector, where valence quarks and sea quarks are of the same mass. This is appropriate for static-light mesons with a light quark, which is u/d . We also estimate masses of static-light mesons with light s quarks, albeit with a sea of two degenerate s instead of u and d . Within the twisted mass formalism, it is feasible to use $N_f = 2 + 1 + 1$ flavours of dynamical sea quarks, which will give a more appropriate focus on the static-strange meson spectrum with light sea quarks.

In HQET the leading order is just the static limit. The next correction will be of order $1/m_Q$, where m_Q is the mass of the heavy quark. This correction is expected to be relatively small for b quarks, but larger for c quarks. Lattice methods to evaluate these $1/m_Q$ contributions to the B meson hyperfine splittings have been established and tested in quenched studies [9, 10]. We intend to explore these contributions using lattice techniques subsequently. An alternative way to predict the spectrum for B and B_s mesons is to interpolate between D and D_s states, where the experimental spectrum is rather well known, and the static limit obtained by lattice QCD assuming a dependence as $1/m_Q$. Thus the splittings among B and B_s mesons should be approximately $m_c/m_b \approx 1/3$ of those among the corresponding D and D_s mesons.

For excited D_s mesons, experiment has shown that some of the states have very narrow decay widths [11]. This comes about, since the hadronic transitions to DK and D_sM (where M is a flavour singlet mesonic system, e.g. η' , $\pi\pi$ or f_0) are not allowed energetically. The isospin violating decay to $D_s\pi$ together with electromagnetic decay to $D_s\gamma$ are then responsible for the narrow width observed. A similar situation may exist for B_s decays and we investigate this here using our lattice mass determinations of the excited states. This will enable us to predict

whether narrow excited B_s mesons should be found.

As well as exploring this issue of great interest to experiment, we determine the excited state spectrum of static-light mesons as fully as possible. This will help the construction of phenomenological models and will shed light on questions such as, whether there is an inversion of the level ordering with l_+ lighter than l_- at larger l or for radial excitations as has been predicted [12, 13, 14, 15].

Since we measure the spectrum for a range of values of the bare quark mass parameter μ_q for the light quark, we could also compare with chiral effective Lagrangians appropriate to HQET. This comparison would be most appropriate applied to heavy-light decay constants in the continuum limit, so we will defer that discussion to a subsequent publication.

This paper is organised as follows. In section 2 we review some basic properties of twisted mass lattice QCD. Moreover, we discuss particularities arising in static-light computations as well as automatic $\mathcal{O}(a)$ improvement. In section 3 we present technical details regarding static-light meson creation operators and the corresponding correlation matrices we are using. We also explain how we extract the static-light spectrum from these correlation matrices and present numerical results for a range of light quark masses. We extrapolate these results both to the physical u/d quark mass and to the physical s quark mass. In section 4 we make predictions regarding the spectrum of B and B_s mesons by interpolating in the heavy quark mass to the physical b quark mass using experimental results as input. We close with a summary and a brief outlook (section 5).

2 Twisted mass lattice QCD

2.1 Simulation details

We use $L^3 \times T = 24^3 \times 48$ gauge configurations produced by the European Twisted Mass Collaboration (ETMC). The gauge action is the tree-level Symanzik (tlSym) action [16]

$$S_G[U] = \frac{\beta}{6} \left(b_0 \sum_{x,\mu \neq \nu} \text{Tr} \left(1 - P^{1 \times 1}(x; \mu, \nu) \right) + b_1 \sum_{x,\mu \neq \nu} \text{Tr} \left(1 - P^{1 \times 2}(x; \mu, \nu) \right) \right) \quad (1)$$

with the normalisation condition $b_0 = 1 - 8b_1$ and $b_1 = -1/12$. The fermionic action is the Wilson twisted mass (Wtm) action [17, 18, 19] with $N_f = 2$ degenerate flavours

$$S_F[\chi, \bar{\chi}, U] = a^4 \sum_x \bar{\chi}(x) \left(D_W + i\mu_q \gamma_5 \tau_3 \right) \chi(x), \quad (2)$$

where

$$D_W = \frac{1}{2} \left(\gamma_\mu \left(\nabla_\mu + \nabla_\mu^* \right) - a \nabla_\mu^* \nabla_\mu \right) + m_0, \quad (3)$$

∇_μ and ∇_μ^* are the standard gauge covariant forward and backward derivatives, m_0 and μ_q are the bare untwisted and twisted quark masses respectively and $\chi = (\chi^{(u)}, \chi^{(d)})$ represents the fermionic field in the so-called twisted basis. It is useful to introduce at this point the twist angle

ω given by $\tan \omega = \mu_R/m_R$, where μ_R and m_R denote the renormalised twisted and untwisted quark masses. This angle characterises the particular lattice action and must be kept fixed up to $\mathcal{O}(a)$, while performing the continuum limit.

The results presented in this paper have been obtained with gauge configurations computed at $\beta = 3.9$ corresponding to a lattice spacing $a = 0.0855(5)$ fm. We consider five different values of μ_q with m_0 tuned to its critical value at $\mu_q = 0.0040$ [20, 21, 22] (cf. Table 1, where for each value the corresponding “pion mass” m_{PS} and number of gauge configurations is listed). With this tuning our target continuum theory is given by

$$\mathcal{L} = \bar{\chi}(x) \left(\gamma_\mu D_\mu + i\mu_R \gamma_5 \tau_3 \right) \chi(x), \quad (4)$$

which is parameterised by the renormalised twisted quark mass μ_R . The tuning guarantees automatic $\mathcal{O}(a)$ improvement for physical correlation functions involving only light fermions [18]. In section 2.3 we will argue that automatic $\mathcal{O}(a)$ improvement also holds for static-light spectral quantities without additional complications.

μ_q	m_{PS} in MeV	number of gauge configurations
0.0040	314(2)	1400
0.0064	391(1)	1450
0.0085	448(1)	1350
0.0100	485(1)	900
0.0150	597(2)	1000

Table 1: bare twisted quark masses μ_q , pion masses m_{PS} and number of gauge configurations.

2.2 Static-light correlation functions

To compute correctly a static-light correlation function with the Wtm lattice action (2), we follow the general procedure described in [17] and reviewed in [19]. The procedure reads:

- (1) start with the continuum static-light correlation function you are interested in,
- (2) perform the axial rotation

$$\psi = \exp \left(i\omega \gamma_5 \tau_3 / 2 \right) \chi \quad , \quad \bar{\psi} = \bar{\chi} \exp \left(i\omega \gamma_5 \tau_3 / 2 \right) \quad (5)$$

on the fields appearing in the correlation function with a given value for ω ,

- (3) compute the resulting correlation function with the Wtm lattice action (2), with a choice of quark masses, such that $\tan \omega = \mu_R/m_R$ up to $\mathcal{O}(a)$,
- (4) perform the continuum limit with renormalisation constants computed in a massless scheme, tuning the untwisted bare quark mass in order to achieve the desired target continuum theory, i.e. the desired value of the twist angle ω .

Each value of ω defines a different discretisation, but when the continuum limit is performed the result will be exactly the initially chosen static-light correlation function in the continuum with quark mass $M_R^2 = m_R^2 + \mu_R^2$.

In the following we give an explicit example. In QCD the pseudoscalar and scalar static-light currents read

$$\mathcal{P}^{\text{stat}}(x) = \bar{Q}(x)\gamma_5\psi^{(u)}(x), \quad \mathcal{S}^{\text{stat}}(x) = \bar{Q}(x)\psi^{(u)}(x), \quad (6)$$

where Q is the static quark field¹ and $\psi^{(u)}$ is a single flavour of the light fermion doublet $\psi = (\psi^{(u)}, \psi^{(d)})$. Let us suppose we are interested in computing in continuum QCD the static-light pseudoscalar-pseudoscalar correlation function

$$\mathcal{C}_{PP} = \left\langle (\mathcal{P}^{\text{stat}})_R(x)(\mathcal{P}^{\text{stat}})_R^\dagger(y) \right\rangle_{(M_R, 0)}, \quad (7)$$

where we write an index $(M_R, 0)$ to specify that the continuum action has a vanishing twisted mass and a renormalised untwisted mass given by M_R . We perform the axial rotation (5) obtaining

$$\cos^2(\omega/2)Z_P^2C_{PP} + \sin^2(\omega/2)Z_S^2C_{SS} - i\cos(\omega/2)\sin(\omega/2)Z_PZ_S(C_{PS} - C_{SP}), \quad (8)$$

where Z_P and Z_S are the standard renormalisation constants for static-light currents computed in a massless scheme with Wilson fermions. Note that for the static-light case, $Z_V \equiv Z_P$ and $Z_A \equiv Z_S$. This correlation function has to be computed with the Wtm action (2) with quark masses tuned accordingly to the value of ω chosen. The C_{XX} correlation functions in (8) are defined in terms of currents in the twisted basis

$$C_{PP} = \left\langle P^{\text{stat}}(x)(P^{\text{stat}})^\dagger(y) \right\rangle_{(m_R, \mu_R)}, \quad C_{SS} = \left\langle S^{\text{stat}}(x)(S^{\text{stat}})^\dagger(y) \right\rangle_{(m_R, \mu_R)}, \quad \dots, \quad (9)$$

where

$$P^{\text{stat}}(x) = \bar{Q}\gamma_5\chi^{(u)}(x), \quad S^{\text{stat}}(x) = \bar{Q}(x)\chi^{(u)}(x). \quad (10)$$

Once the continuum limit of the correlation function (8) has been performed, the result will be the original correlation function (7) with $M_R^2 = m_R^2 + \mu_R^2$.

However, to compute spectral quantities it is sufficient to analyze a matrix of correlation functions of bare currents with the appropriate quantum numbers. We will discuss this in detail in section 2.4.

2.3 Automatic $\mathcal{O}(a)$ improvement of static-light meson masses

Spectral quantities like hadron masses extracted from lattice simulations of Wilson fermions will in general be affected by $\mathcal{O}(a)$ discretisation errors. In the particular case of masses extracted

¹We will discuss the static quark action in section 3.2.1.

from static-light correlation functions the $\mathcal{O}(a)$ discretisation errors come from the dimension-5-operators of the Symanzik effective action of the light and static quarks.

The Symanzik effective action for the Eichten-Hill (EH) static action contains only one term, which contributes to the $\mathcal{O}(a)$ corrections of the linearly divergent static self-energy [23]. In this paper all observables we consider are differences, where this static self-energy cancels. Moreover, this result is independent on the particular lattice static action chosen, as long as it preserves the relevant symmetries of the EH action. This is the case for our choice of static action (cf. section 3.2.1).

As a consequence, the only $\mathcal{O}(a)$ errors which could affect our results, come from the dimension-5-operators of the Symanzik effective action of the light quarks. The light quark action used in this paper is Wtm at maximal twist. It is by now well known that at maximal twist a single insertion of a dimension-5-operator of the Symanzik effective action into parity even correlation functions vanishes, because, independently on the lattice basis adopted, these operators are parity odd and the insertions have to be evaluated in the continuum theory, where parity is a preserved symmetry [18]. We can conclude that all the spectral quantities, when the static self-energy has been removed, are automatically $\mathcal{O}(a)$ improved.

2.4 Spectral decomposition and parity mixing

In this section we explain, how to analyze lattice results for static-light correlation functions obtained in the twisted basis. In particular we concentrate on the assignment of parity labels to extracted static-light meson states.

We start from the physical basis and, for simplicity, consider only two operators, the pseudoscalar and the scalar static-light current, and only two states, which we label by $|1\rangle$ and $|2\rangle$. The explanation carries over to the more general case in a straightforward way.

First consider the following matrix of correlation functions in the physical basis:

$$\mathcal{C}(t) = \begin{pmatrix} \mathcal{C}_{PP}(t) & \mathcal{C}_{PS}(t) \\ \mathcal{C}_{SP}(t) & \mathcal{C}_{SS}(t) \end{pmatrix}, \quad (11)$$

where $\mathcal{C}_{PP}(t)$ has been defined in (7) with $x = (t, \vec{0})$ and $y = (0, \vec{0})$ and analogously the others. The parity of the operators $(\mathcal{P}^{\text{stat}})_R$ and $(\mathcal{S}^{\text{stat}})_R$ is determined by the parity transformation properties of the associated field, i.e. $(\mathcal{P}^{\text{stat}})_R$ has negative parity and $(\mathcal{S}^{\text{stat}})_R$ has positive parity. Even if parity is broken at finite lattice spacing, one can still assign a parity label to each of the states we use to decompose the correlation functions [18]. If we consider only two states, the spectral decomposition will have the form

$$\mathcal{C}(T) = \begin{pmatrix} |a_1^P|^2 & (a_1^P)^* a_1^S \\ (a_1^S)^* a_1^P & |a_1^S|^2 \end{pmatrix} e^{-M_1 t} + \begin{pmatrix} |a_2^P|^2 & (a_2^P)^* a_2^S \\ (a_2^S)^* a_2^P & |a_2^S|^2 \end{pmatrix} e^{-M_2 t}, \quad (12)$$

where we have defined

$$(a_{1,2}^P)^* = \langle \Omega | \hat{\mathcal{P}}^{\text{stat}} | 1, 2 \rangle, \quad (a_{1,2}^S)^* = \langle \Omega | \hat{\mathcal{S}}^{\text{stat}} | 1, 2 \rangle. \quad (13)$$

The correlation functions \mathcal{C}_{PS} and \mathcal{C}_{SP} vanish in the continuum limit, because parity is a symmetry of QCD. This means by universality that at finite lattice spacing they are at most of

$\mathcal{O}(a)$. Since \mathcal{C}_{PP} and \mathcal{C}_{SS} are of $\mathcal{O}(1)$ in the continuum limit, we can conclude that for given n either a_n^P is of $\mathcal{O}(1)$ and a_n^S is of $\mathcal{O}(a)$ or the opposite way round [18]. We can conclude that if a_n^P is of $\mathcal{O}(1)$, the state $|n\rangle$ has the same parity as the formal parity of $\mathcal{P}^{\text{stat}}$, which in this case is negative. Moreover, a_n^S is of $\mathcal{O}(a)$ and has to vanish in the continuum limit.

We now perform the axial transformation (5). The relation between correlation functions up to discretisation errors is, for example, for \mathcal{C}_{PP}

$$\mathcal{C}_{PP} = \cos^2(\omega/2)Z_P^2 C_{PP} + \sin^2(\omega/2)Z_S^2 C_{SS} - i \cos(\omega/2) \sin(\omega/2) Z_P Z_S (C_{PS} - C_{SP}). \quad (14)$$

For the matrix of correlation functions in the twisted basis

$$C(t) = \begin{pmatrix} C_{PP}(t) & C_{PS}(t) \\ C_{SP}(t) & C_{SS}(t) \end{pmatrix} \quad (15)$$

we can also perform a spectral decomposition considering again only the states $|1\rangle$ and $|2\rangle$:

$$C(t) = \begin{pmatrix} |b_1^P|^2 & (b_1^P)^* b_1^S \\ (b_1^S)^* b_1^P & |b_1^S|^2 \end{pmatrix} e^{-M_1 t} + \begin{pmatrix} |b_2^P|^2 & (b_2^P)^* b_2^S \\ (b_2^S)^* b_2^P & |b_2^S|^2 \end{pmatrix} e^{-M_2 t}. \quad (16)$$

From (12), (14) and (16) we can conclude

$$|a_{1,2}^P|^2 = \cos^2(\omega/2)Z_P^2 |b_{1,2}^P|^2 + \sin^2(\omega/2)Z_S^2 |b_{1,2}^S|^2 + 2 \cos(\omega/2) \sin(\omega/2) Z_P Z_S \text{Im}\left((b_{1,2}^P)^* b_{1,2}^S\right) \quad (17)$$

$$|a_{1,2}^S|^2 = \cos^2(\omega/2)Z_S^2 |b_{1,2}^S|^2 + \sin^2(\omega/2)Z_P^2 |b_{1,2}^P|^2 + 2 \cos(\omega/2) \sin(\omega/2) Z_P Z_S \text{Im}\left((b_{1,2}^S)^* b_{1,2}^P\right). \quad (18)$$

If the state $|1\rangle$ has negative parity, $|a_1^S|^2$ has to vanish as $\mathcal{O}(a^2)$ in the continuum limit, while $|a_1^P|^2$ has to be of $\mathcal{O}(1)$. Since the first two terms on the right hand side of (17) are positive and non-vanishing in the continuum limit, there must be a cancellation coming from the third term. In fact we immediately see that this third term has opposite sign for $|a_{1,2}^P|^2$ compared to $|a_{1,2}^S|^2$. This allows us to identify the parity of the states $|1\rangle$ and $|2\rangle$ without knowing the exact values of the renormalisation constants and the twist angle. The criterion will be the following: if

$$\text{Im}\left((b_1^S)^* b_1^P\right) < 0, \quad (19)$$

the state $|1\rangle$ has negative parity, otherwise positive parity. The other cases follow accordingly.

This method, which we have described for a simple case, is valid independently of the number of states considered and the kind of operators studied. At finite lattice spacing it provides a way to assign a formal parity to each of the extracted states.

The method extends to all cases, where the light degrees of freedom involve fermions in the twisted basis, e.g. for static-light mesons, but also for baryons.

3 The static-light meson spectrum

3.1 Static-light trial states

3.1.1 Static-light meson creation operators in the continuum

It is convenient to discuss static-light mesons treating the static quark as a four component spinor since the symmetries of hadronic bilinears are well studied [24]. In the continuum an operator creating a static-light meson with well defined quantum numbers J , j and \mathcal{P} is given by

$$\mathcal{O}^{(\Gamma)}(\mathbf{x}) = \bar{Q}(\mathbf{x}) \int d\hat{\mathbf{n}} \Gamma(\hat{\mathbf{n}}) U(\mathbf{x}; \mathbf{x} + r\hat{\mathbf{n}}) \psi^{(u)}(\mathbf{x} + r\hat{\mathbf{n}}). \quad (20)$$

$\bar{Q}(\mathbf{x})$ represents an infinitely heavy antiquark (here a Dirac spinor) at position \mathbf{x} , $\int d\hat{\mathbf{n}}$ denotes an integration over the unit sphere, U is a straight parallel transporter and $\psi^{(u)}(\mathbf{x} + r\hat{\mathbf{n}})$ creates a light quark at position $\mathbf{x} + r\hat{\mathbf{n}}$ separated by a distance r from the antiquark (of course, using $\psi^{(d)}$ instead of $\psi^{(u)}$ would yield identical results). Γ is an appropriate combination of spherical harmonics and γ matrices coupling angular momentum and quark spin to yield well defined total angular momentum J (static quark spin included) and j (static quark spin not included) and parity \mathcal{P} . The meson creation operators used in the following are listed in Table 2.

$\Gamma(\hat{\mathbf{n}})$	$J^{\mathcal{P}}$	$j^{\mathcal{P}}$	O_h	lattice $j^{\mathcal{P}}$	notation
$\gamma_5, \gamma_5\gamma_j\hat{n}_j$	$0^- [1^-]$	$(1/2)^-$	A_1	$(1/2)^-, (7/2)^-, \dots$	S
	$0^+ [1^+]$	$(1/2)^+$		$(1/2)^+, (7/2)^+, \dots$	P_-
$\gamma_1\hat{n}_1 - \gamma_2\hat{n}_2$ (and cyclic) $\gamma_5(\gamma_1\hat{n}_1 - \gamma_2\hat{n}_2)$ (and cyclic)	$2^+ [1^+]$	$(3/2)^+$	E	$(3/2)^+, (5/2)^+, \dots$	P_+
	$2^- [1^-]$	$(3/2)^-$		$(3/2)^-, (5/2)^-, \dots$	D_{\pm}
$\gamma_1\hat{n}_2\hat{n}_3 + \gamma_2\hat{n}_3\hat{n}_1 + \gamma_3\hat{n}_1\hat{n}_2$ $\gamma_5(\gamma_1\hat{n}_2\hat{n}_3 + \gamma_2\hat{n}_3\hat{n}_1 + \gamma_3\hat{n}_1\hat{n}_2)$	$3^- [2^-]$	$(5/2)^-$	A_2	$(5/2)^-, (7/2)^-, \dots$	D_+
	$3^+ [2^+]$	$(5/2)^+$		$(5/2)^+, (7/2)^+, \dots$	F_{\pm}

Table 2: Static-light meson creation operators. The other mesonic $J^{\mathcal{P}}$ states that are degenerate with that created are noted in square brackets.

3.1.2 Static-light meson creation operators on a lattice

Here we present the construction of appropriate lattice operators to create the states of interest, following [1, 24]. When putting static-light meson creation operators (20) on a lattice, one has to replace the integration over the unit sphere by a discrete sum over lattice sites, which have the same distance from the static antiquark at position \mathbf{x} . For the operators in A_1 and E representations we use six lattice sites, i.e.

$$\mathcal{O}^{(\Gamma)}(\mathbf{x}) = \bar{Q}(\mathbf{x}) \sum_{\mathbf{n}=\pm\hat{\mathbf{e}}_1, \pm\hat{\mathbf{e}}_2, \pm\hat{\mathbf{e}}_3} \Gamma(\hat{\mathbf{n}}) U(\mathbf{x}; \mathbf{x} + r\mathbf{n}) \chi^{(u)}(\mathbf{x} + r\mathbf{n}), \quad (21)$$

whereas for those in the A_2 representation one has to use eight lattice sites, i.e.

$$\mathcal{O}^{(\Gamma)}(\mathbf{x}) = \bar{Q}(\mathbf{x}) \sum_{\mathbf{n}=\pm\hat{\mathbf{e}}_1\pm\hat{\mathbf{e}}_2\pm\hat{\mathbf{e}}_3} \Gamma(\hat{\mathbf{n}}) U(\mathbf{x}; \mathbf{x} + r\mathbf{n}) \chi^{(u)}(\mathbf{x} + r\mathbf{n}). \quad (22)$$

In the first case the spatial parallel transporters are straight paths of links, while in the second case we use “diagonal links”, which are averages over the six possible paths around a cube between opposite corners projected back to SU(3).

The states created by these lattice meson creation operators do not form irreducible representations of the rotation group SO(3), but of its cubic subgroup O_h . Therefore, these states have no well defined total angular momentum, but are linear superpositions of an infinite number of total angular momentum eigenstates. The common notation of the corresponding O_h representations together with their lowest angular momentum content are also listed in Table 2. Note that we do not consider O_h representations T_1 and T_2 , because these representations yield correlation functions, which are numerically identical to those listed (e.g. T_1 would be $\Gamma = \gamma_j$ or $\Gamma = \gamma_5 \gamma_j$, which gives the same correlations as $\Gamma = \gamma_5$ and $\Gamma = 1$, and T_2 would be $\Gamma = \gamma_1 n_2 + \gamma_2 n_1$ or $\Gamma = \gamma_5 (\gamma_1 n_2 + \gamma_2 n_1)$, which gives the same correlations as $\Gamma = \gamma_1 n_1 - \gamma_2 n_2$ and $\Gamma = \gamma_5 (\gamma_1 n_1 - \gamma_2 n_2)$).

Since the D_- and the D_+ states as well as the F_- and F_+ states are expected to have a similar mass, we do not have unambiguous lattice operators to determine D_- and F_- but rather operators, which have an admixture of D_\pm and F_\pm respectively. We label these operators as D_\pm and F_\pm (cf. Table 2).

We have also replaced the light quark fields in the physical basis $\psi^{(u)}$ by their counterparts in the twisted basis $\chi^{(u)}$. Note that trial states created by such twisted basis operators are not eigenstates of parity. Nevertheless, as we have discussed in section 2.4, it is possible to assign unambiguously a parity label to the masses extracted from the time dependence of such twisted basis correlators.

3.1.3 Smearing techniques

When performing a lattice study of the static-light meson spectrum, the following points have to be considered:

- It is imperative to use trial states with large overlap to low lying energy eigenstates. Only then the corresponding meson masses can be extracted from correlation functions at small temporal separations, where signal-to-noise ratios are acceptable.
- To determine excited states for a given O_h representation, it is necessary to have a whole set of linearly independent trial states belonging to that O_h representation.

To fulfill both requirements we use different “radii” r (cf. eqns. (21) and (22)) and apply APE smearing and Gaussian smearing also with different parameters. The resulting extended trial states have significantly better overlap to low lying energy eigenstates than their unsmeared counterparts.

APE smearing of spatial links

After N_{APE} iterations APE smeared spatial links [25] are given by

$$U^{(N_{\text{APE}})}(x, x + e_k) = P_{\text{SU}(3)} \left(U^{(N_{\text{APE}}-1)}(x, x + e_k) + \alpha_{\text{APE}} \sum_{j=\pm 1, \pm 2, \pm 3}^{j \neq \pm k} U^{(N_{\text{APE}}-1)}(x, x + e_j) \right. \\ \left. U^{(N_{\text{APE}}-1)}(x + e_j, x + e_j + e_k) U^{(N_{\text{APE}}-1)}(x + e_j + e_k, x + e_k) \right), \quad (23)$$

where $U^{(0)}$ are the original unsmeared links. α_{APE} is a weight parameter and $P_{\text{SU}(3)}$ denotes a projection back to SU(3) defined by

$$P_{\text{SU}(3)}(U) = \frac{U'}{\det(U')^{1/3}}, \quad U' = U \left(U^\dagger U \right)^{-1/2} \quad (24)$$

with $\det(U')^{1/3}$ being that root closest to 1.

Gaussian smearing of light quark operators

After N_{Gauss} iterations Gaussian smeared light quark operators [26, 27] are given by

$$\chi^{(N_{\text{Gauss}})}(x) = \\ = \frac{1}{1+6\kappa} \left(\chi^{(N_{\text{Gauss}}-1)}(x) + \kappa_{\text{Gauss}} \sum_{j=\pm 1, \pm 2, \pm 3} U^{(N_{\text{APE}})}(x, x + e_j) \chi^{(N_{\text{Gauss}}-1)}(x + e_j) \right), \quad (25)$$

where $\chi^{(0)}$ are the original unsmeared light quark operators and $U^{(N_{\text{APE}})}$ denote APE smeared spatial links.

3.2 Correlation matrices

For each O_h representation we compute 6×6 correlation matrices

$$C_{KK'}(t) = \langle \mathcal{O}^{(K)}(t) (\mathcal{O}^{(K')})^\dagger(0) \rangle, \quad (26)$$

where $\mathcal{O}^{(K)}$ is a static-light meson creation operator (cf. eqns. (21) and (22)) with K denoting its parameters, i.e. $K = (\Gamma, N_{\text{Gauss}}, r)$ (we have chosen $N_{\text{APE}} = 10$, $\alpha_{\text{APE}} = 0.5$ and $\kappa_{\text{Gauss}} = 0.5$ for all operators). Detailed information about the operator content of the correlation matrices is given in Table 3.

The width of a Gaussian smeared light quark operator (25) in lattice units is approximately given by

$$\sigma \approx \sqrt{\frac{2N_{\text{Gauss}}\kappa_{\text{Gauss}}}{1+6\kappa_{\text{Gauss}}}}. \quad (27)$$

O_h	Γ	N_{Gauss}	r	R/a	R in fm
A_1	γ_5	30	3	5.61	0.48
		60	6	9.00	0.77
	1	30	3	5.61	0.48
		60	6	9.00	0.77
	$\gamma_5 \gamma_j x_j$	30	3	5.61	0.48
	$\gamma_j x_j$	30	3	5.61	0.48
	E	30	3	5.61	0.48
		60	6	9.00	0.77
		90	3	8.74	0.75
A_2	$\gamma_1 x_1 - \gamma_2 x_2$ (and cyclic)	30	3	5.61	0.48
		60	6	9.00	0.77
		90	3	8.74	0.75
	$\gamma_5(\gamma_1 x_1 - \gamma_2 x_2)$ (and cyclic)	30	3	5.61	0.48
		60	6	9.00	0.77
		90	3	8.74	0.75
	$\gamma_1 x_2 x_3 + \gamma_2 x_3 x_1 + \gamma_3 x_1 x_2$	30	2	5.88	0.50
		60	4	9.64	0.82
		90	2	8.91	0.76
	$\gamma_5(\gamma_1 x_2 x_3 + \gamma_2 x_3 x_1 + \gamma_3 x_1 x_2)$	30	2	5.88	0.50
		60	4	9.64	0.82
		90	2	8.91	0.76

Table 3: static-light meson creation operators used for the A_1 , E and A_2 correlation matrices.

For $\kappa_{\text{Gauss}} = 0.5$ and $N_{\text{Gauss}} = (30, 60, 90)$ this amounts to $\sigma \approx (2.74, 3.87, 4.74)$. Taking also the parameter r into account one can estimate the radius of a static-light trial state: $R/a = \sqrt{r^2 + 3\sigma^2}$ for the A_1 and E representations and $R/a = \sqrt{3r^2 + 3\sigma^2}$ for the A_2 representation. The radii of the trial states used are also listed in Table 3 both in lattice units and in physical units.

Note that to identify the parity of states extracted via fitting it is important to compute correlation matrices, which contain for each operator Γ also its counterpart $\gamma_5 \Gamma$ (cf. section 2.4).

3.2.1 Quark propagators

When evaluating the correlations (26), both static quark propagators and light quark propagators appear. To improve signal-to-noise ratios, we apply the following techniques.

Static quark propagators

To improve the signal to noise ratio for static-light correlation functions, we use the HYP2 static action [28, 29, 30]. Static quark propagators are given by

$$\langle Q(x)\bar{Q}(y) \rangle_{Q,\bar{Q}} = \delta^{(3)}(\mathbf{x} - \mathbf{y}) U^{(\text{HYP2})}(x; y) \left(\Theta(y_0 - x_0) \frac{1 - \gamma_0}{2} + \Theta(x_0 - y_0) \frac{1 + \gamma_0}{2} \right), \quad (28)$$

where $\langle \dots \rangle_{Q,\bar{Q}}$ denotes the integration over the static quark fields and $U(x; y)$ is a path ordered product of HYP2 smeared links along the straight path from x to y .

Light quark propagators

To exploit translational invariance, it is imperative to use stochastic methods for the light quark propagators. The correlators can then be evaluated at a large number of source points, while only a few inversions of the lattice Dirac operator have to be performed. One very powerful method is maximal variance reduction [1]. A somewhat easier method to implement is to use stochastic sources on time slices and this has been found to give reasonable results [31]. Because we have inverted from such time-slice sources as part of our light-light meson studies [20, 21, 22], we follow this latter route, since it is computationally much quicker for us.

For each gauge configuration we use N_s stochastic $\mathcal{Z}_2 \times \mathcal{Z}_2$ sources $\xi^{(\alpha)}$, $\alpha = 1, \dots, N_s$ located on the same timeslice. For our lightest three μ_q values we take $N_s = 4$ sources, which are the same for each of the four spin components so that we can re-use previous inversions [20, 21, 22]. For our heavier two μ_q values, we had to redo the inversions so we use only $N_s = 1$ source with random values in each of the spin components.

After solving

$$D_{\text{Wtm}}^{(u)}(x; y)\phi^{(\alpha)}(y) = \xi^{(\alpha)}(x), \quad (29)$$

where $D_{\text{Wtm}}^{(u)} = D_W + i\mu_q\gamma_5$ is the twisted mass Dirac operator acting on $\chi^{(u)}$, the light quark propagator is given by the unbiased estimate

$$\langle \chi^{(u)}(x)\bar{\chi}^{(u)}(y) \rangle_{\chi,\bar{\chi}} = (D_{\text{Wtm}}^{(u)})^{-1}(x; y) \approx \sum_{\alpha=1}^{N_s} \phi^{(\alpha)}(x)(\xi^{(\alpha)})^\dagger(y), \quad (30)$$

where $\langle \dots \rangle_{\chi,\bar{\chi}}$ denotes the integration over the light quark fields.

3.3 Extracting static-light meson masses from correlation matrices

Assuming that for sufficiently large t the correlation matrix (26) can be approximated by the n lowest lying energy eigenstates $|i\rangle$, $i = 1, \dots, n$ we use the ansatz

$$\left(\mathcal{O}^{(K)} \right)^\dagger |\Omega\rangle \approx \sum_{i=1}^n b_i^K |i\rangle. \quad (31)$$

The correlation matrix (26) in terms of the ansatz is

$$C_{KK'}(t) \approx \sum_{i=1}^n (b_i^K)^* b_i^{K'} e^{-E_i t} = \tilde{C}_{KK'}(t). \quad (32)$$

The parameters E_i and b_i^K are determined by minimising

$$\chi^2 = \sum_{t=t_{\min}}^{t_{\max}} \sum_{K \leq K'} \left(\frac{C_{KK'}(t) - \tilde{C}_{KK'}(t)}{\sigma(C_{KK'}(t))} \right)^2, \quad (33)$$

where $\sigma(C_{KK'}(t))$ denotes the statistical error of $C_{KK'}(t)$.

In the following we apply this fitting procedure with $n = 4$ exponentials. To obtain physically meaningful results with small statistical errors, it is essential to determine an appropriate fitting range $t_{\min} \dots t_{\max}$. To this end, we have performed correlated fits with various fitting ranges using eigenvalue smoothed covariance matrices [32]. We have found that $t_{\min} = 3$ gives reasonable reduced χ^2 values (cf. Table 4), while data points beyond $t_{\max} = 12$ seem to be dominated by statistical noise, i.e. including them in the fits does not alter resulting meson masses nor corresponding statistical errors.

O_h	$\mu_q = 0.0040$	$\mu_q = 0.0064$	$\mu_q = 0.0085$	$\mu_q = 0.0100$	$\mu_q = 0.0150$
A_1	1.89	2.30	2.35	0.95	1.16
E	1.21	1.33	1.70	2.04	2.09
A_2	1.56	1.96	1.28	1.16	1.26

Table 4: χ^2/dof from correlated χ^2 fits for different O_h representations and different μ_q .

As has already been discussed in section 3.1.2, it is difficult to unambiguously determine the total angular momentum j of a state obtained from a lattice computation. This is, because for every O_h representation there exists an infinite number of possible total angular momentum eigenstates (cf. Table 2). In the following, we assume that the low lying states we are going to study have the lowest total angular momentum possible, i.e. we assign $j = 1/2$ to states from A_1 , $j = 3/2$ to states from E and $j = 5/2$ to states from A_2 . Parity on the other hand can directly be read off from the coefficients b_i^K (cf. section 2.4).

Since static-light meson masses diverge in the continuum limit due to the self energy of the static quark, we always consider mass differences, where this self energy cancels. Mass differences between various static-light mesons with quantum numbers j^P and the lightest static-light meson ($(1/2)^- \equiv S$ ground state) for all five μ_q values are collected in Figure 1 and Table 5. Statistical errors have been computed from 100 bootstrap samples.

To check the stability of the fitting method, we have performed computations with different parameters (number of states n , fitting range $t_{\min} \dots t_{\max}$, operator content of the correlation matrices). We have obtained results which are consistent within statistical errors.

j^P	$\mu_q = 0.0040$	$\mu_q = 0.0064$	$\mu_q = 0.0085$	$\mu_q = 0.0100$	$\mu_q = 0.0150$
$(1/2)^{-,*} \equiv S^*$	777(17)	808(19)	839(22)	780(34)	782(32)
$(1/2)^+ \equiv P_-$	389(16)	428(12)	447(10)	456(17)	495(16)
$(3/2)^+ \equiv P_+$	473(10)	496(8)	488(7)	486(12)	479(14)
$(3/2)^- \equiv D_\pm$	813(24)	828(19)	833(16)	861(27)	858(21)
$(5/2)^- \equiv D_+$	823(24)	887(14)	887(15)	862(24)	846(42)
$(5/2)^+ \equiv F_\pm$	1134(35)	1205(27)	1173(24)	1136(34)	1205(28)

Table 5: static-light mass differences $m(j^P) - m(S)$ in MeV for different μ_q .

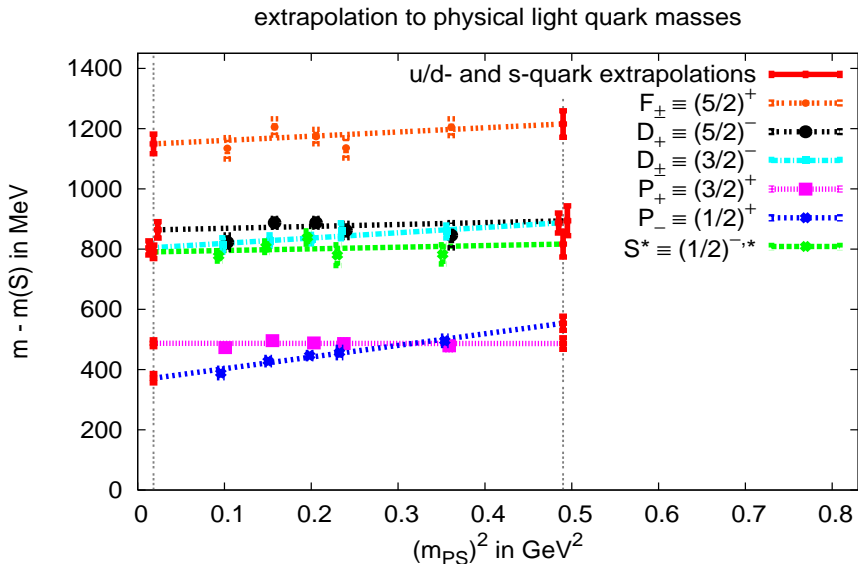


Figure 1: static-light mass differences linearly extrapolated to the physical u/d quark mass and the physical s quark mass.

3.4 Extrapolation to physical light quark masses

We linearly extrapolate our static-light mass differences in $(m_{PS})^2$ to the physical u/d quark mass ($m_{PS} = 135$ MeV) and the physical s quark mass (taken here as $m_{PS} = 700$ MeV). Results are shown in Figure 1 and Table 6. We also list the corresponding χ^2/dof values indicating that straight lines are acceptable for extrapolation. A more thorough study using extrapolations based on chiral effective theories will be attempted when we are able to extract the continuum limit of our results at each light quark mass value.

Note that we consider the unitary sector, where valence quarks and sea quarks are of the same mass. For the s quark extrapolated results this implies a sea of two degenerate s instead of a sea of u and d . If the sea-quark mass dependence of our spectra is small, as usually assumed, then our results will be a good estimate of the physical static-strange meson spectrum. This

j^P	u/d quark extrapolation: $m(j^P) - m(S)$ in MeV	s quark extrapolation: $m(j^P) - m(S)$ in MeV	χ^2/dof
$(1/2)^{-,*} \equiv S^*$	791(23)	816(43)	1.82
$(1/2)^+ \equiv P_-$	371(16)	554(23)	0.44
$(3/2)^+ \equiv P_+$	487(11)	486(19)	1.22
$(3/2)^- \equiv D_\pm$	804(23)	887(33)	0.21
$(5/2)^- \equiv D_+$	864(27)	894(50)	2.24
$(5/2)^+ \equiv F_\pm$	1149(33)	1215(44)	1.40

Table 6: static-light mass differences linearly extrapolated to the physical u/d quark mass and the physical s quark mass.

limitation can be removed, in principle, by performing similar computations on $N_f = 2 + 1 + 1$ flavour gauge configurations, which are currently being produced by ETMC [33].

We have performed a similar extrapolation for the mass difference of the P wave states. When extrapolating to the physical u/d quark mass, we find $m(P_+) - m(P_-) = 117(17)$ MeV, i.e. the $P_- \equiv (1/2)^+$ state is lighter than the $P_+ \equiv (3/2)^+$ as usually expected. When increasing the mass of the light quark, we observe a reversal of this level ordering, $m(P_-) - m(P_+) = 71(23)$ MeV at the physical s quark mass. It will be interesting to study this in the continuum limit, in particular since such a reversal is predicted by certain phenomenological models [12, 13, 14, 15].

In principle, our excited states could be two-particle states since we have dynamical sea quarks. In practice, the two-particle state is expected to be weakly coupled to the operators we use (which are constructed assuming one particle states). Some exploration of transitions to two particle static-light mesons has been made which confirms this expectation [31].

4 Predictions for B and B_s mesons

To make predictions regarding the spectrum of B and B_s mesons, we interpolate between the static-light lattice results obtained in the previous section and experimental results for charmed mesons² [11]. To this end, we assume a linear dependence in $1/m_Q$, where m_Q is the mass of the heavy quark. This interpolation introduces a possible systematic error, which, however, we consider to be smaller than the systematic errors coming from the continuum limit, the extrapolation to light quarks and the treatment of the strange sea. The most important of these systematic errors is that involved in the continuum limit and that will be quantified when we have results at finer lattice spacings.

²For the states B , D , D^* , D_0^* and D_2^* experimental results for charged as well as for uncharged mesons exist. We use the average in the following.

4.1 B mesons

Results of the interpolation between our u/d extrapolated P wave lattice results and experimental results on D mesons are shown in Figure 2a and Table 7.

- To predict $m(B_0^*) - m(B)$ and $m(B_1^*) - m(B)$, we interpolate between our static spin degenerate $P_- \equiv (1/2)^+$ state, i.e. $m(P_-) - m(S)$, and experimental data on $m(D_0^*) - m(D)$ and $m(D_1(2430)^0) - m(D)$.
- To predict $m(B_1) - m(B)$ and $m(B_2^*) - m(B)$, we interpolate between our static spin degenerate $P_+ \equiv (3/2)^+$ state, i.e. $m(P_+) - m(S)$, and experimental data on $m(D_1(2420)^0) - m(D)$ and $m(D_2^*) - m(D)$. Here we assign the D_1^0 states assuming that states with similar widths belong to the same multiplet.
- The line labeled “ $S \equiv (1/2)^-$ ” in Figure 2a shows that $m(B^*) - m(B)$ is lighter by a factor of $\approx m_c/m_b$ than $m(D^*) - m(D)$ indicating that a straight line is a suitable ansatz for interpolation and that the estimate of $m_c/m_b = 0.3$ [11] is reasonable.
- A comparison with experimental results from CDF and DØ [34, 35] on $m(B_1) - m(B)$ and $m(B_2^*) - m(B)$ shows that our lattice results are larger by $\approx 10\%$ (cf. Table 7). There is another resonance listed in [11] with unknown quantum numbers J^P , $m(B_J^*) - m(B)$, which is rather close to our $m(B_0^*) - m(B)$ and $m(B_1^*) - m(B)$ results. For a conclusive comparison it will be necessary to study the continuum limit, which will be part of an upcoming publication.

	$m - m(B)$ in MeV						$m - m(B_s)$ in MeV				
state	lattice	CDF	DØ	PDG	state	lattice	CDF	DØ	PDG		
B_0^*	413(19)				B_{s0}^*	493(16)					
B_1^*	428(19)				B_{s1}^*	535(16)					
B_1	508(8)	454(5)	441(4)		B_{s1}	510(13)	463(1)				
B_2^*	519(8)	458(6)	467(4)		B_{s2}^*	521(13)	473(1)	473(2)			
B_J^*				418(8)	B_{sJ}^*					487(16)	

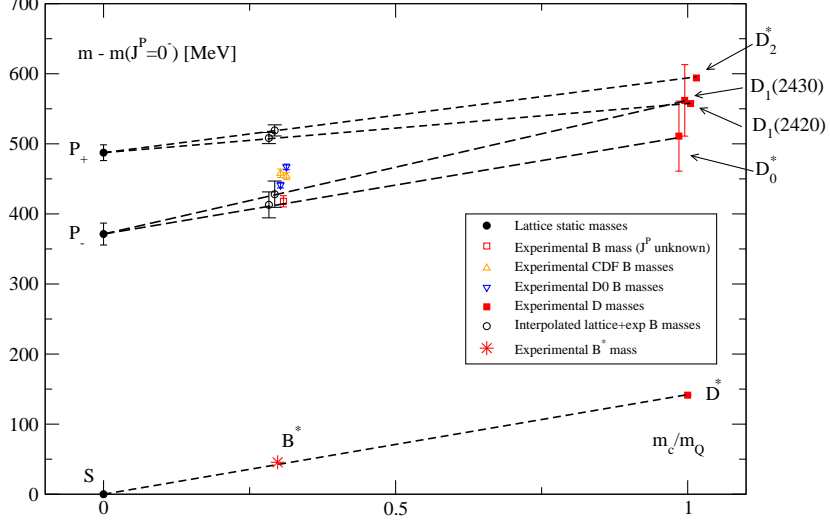
Table 7: lattice and experimental results for P wave B and B_s states. Errors on lattice results are statistical only.

4.2 B_s mesons

For B_s mesons we proceed in the same way as for B mesons, using our s quark extrapolated static-light lattice results and experimental results on D_s mesons (cf. Figure 2b and Table 7).

- To predict $m(B_{s0}^*) - m(B_s)$ and $m(B_{s1}^*) - m(B_s)$, we interpolate between our static spin degenerate $P_- \equiv (1/2)^+$ state, i.e. $m(P_-) - m(S)$, and experimental data on $m(D_{s0}^*) - m(D_s)$ and $m(D_{s1}(2460)) - m(D_s)$.

a) Excited B meson masses



b) Excited B_s meson masses

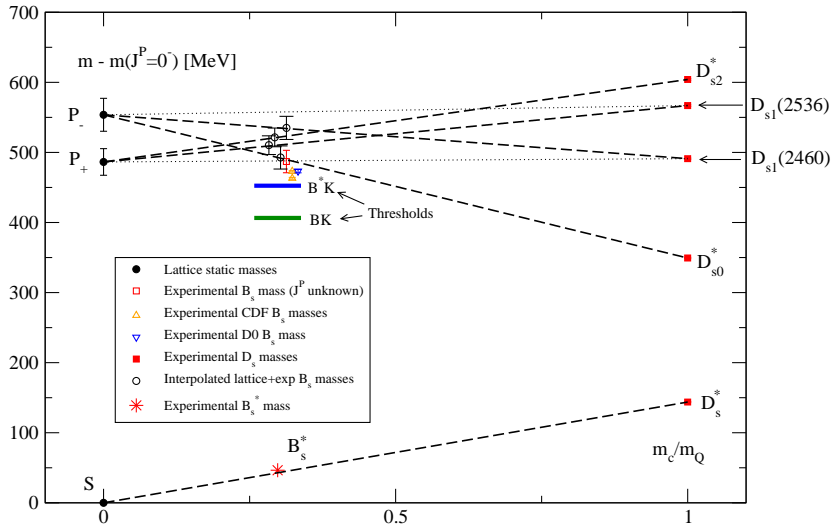


Figure 2: Static-light mass differences linearly interpolated to the physical b quark mass.

- To predict $m(B_{s1}) - m(B_s)$ and $m(B_{s2}^*) - m(B_s)$, we interpolate between our static spin degenerate $P_+ \equiv (3/2)^+$ state, i.e. $m(P_+) - m(S)$, and experimental data on $m(D_{s1}(2536)) - m(D_s)$ and $m(D_{s2}) - m(D_s)$. This time we assign the D_{s1} states according to the expectation that the splitting between D_{s1} ("j = 3/2") and D_{s2} is roughly

$m_b/m_c \approx 3.3$ times larger than that between B_{s1} and B_{s2}^* , which is according to [36] approximately 10 MeV. We also illustrate the opposite assignment in Figure 2b for completeness.

- The line labeled “ $S \equiv (1/2)^-$ ” in Figure 2b shows that $m(B_s^*) - m(B_s)$ is lighter by a factor of $\approx m_c/m_b$ than $m(D_s^*) - m(D_s)$ indicating that a straight line is a suitable ansatz for interpolation and that the estimate of $m_c/m_b = 0.3$ [11] is reasonable.
- A comparison with experimental results from CDF and DØ [36, 37] on $m(B_1) - m(B^0)$ and $m(B_2^*) - m(B^0)$ shows that our lattice results are larger by $\approx 10\%$ (cf. Table 7). There is another resonance listed in [11] with unknown quantum numbers $J^\mathcal{P}$, $m(B_{sJ}^*) - m(B_s)$, which is rather close to our $m(B_{s0}^*) - m(B_s)$ result. For a conclusive comparison it will be necessary to study the continuum limit, which will be part of an upcoming publication.
- We also plot the BK and B^*K thresholds in Figure 2b. The fact that our lattice results on the P wave states B_{s0}^* , B_{s1}^* , B_{s1} and B_{s2}^* are larger indicates that corresponding decays are energetically allowed. Therefore, one should expect that these states may have a larger width compared to the corresponding excited D_s states.

5 Conclusions

We have explored the low lying static-light meson spectrum using $N_f = 2$ flavours of sea quarks with Wtm lattice QCD. We have presented results for total angular momentum of the light degrees of freedom $j = 1/2$, $j = 3/2$ and $j = 5/2$ and for parity $\mathcal{P} = +$ and $\mathcal{P} = -$. The lattice spacing is $a = 0.0855(5)$ fm and we have considered five different values for the light quark mass corresponding to $300 \text{ MeV} \lesssim m_{\text{PS}} \lesssim 600 \text{ MeV}$.

We have extrapolated our results in $(m_{\text{PS}})^2$ both to the physical u/d quark mass and to the physical s quark mass. Moreover, we used experimental results from D and D_s mesons to interpolate in the heavy quark mass from the static case to the physical b quark mass. We are able to predict the spectrum of excited B and B_s mesons from first principles. Our formalism has lattice artifacts of order a^2 and we shall be able to control these in future work by studying smaller a values. Comparing our current predictions to available experimental results, we find agreement up to 10% with P wave B and B_s mesons.

Throughout this paper we have considered the unitary sector, where valence quarks and sea quarks are of the same mass. Particularly for our B_s results, this implies a sea of two degenerate s instead of a sea of u and d . We plan to improve this by performing similar computations on $N_f = 2 + 1 + 1$ flavour gauge configurations, which are currently produced by ETMC. Another important issue in the near future will be an investigation of the continuum limit, which amounts to considering other values for the lattice spacing. Such a study will be necessary for a conclusive comparison between lattice results and experimental results for B and B_s mesons. We also plan to compute static-light decay constants and to make a detailed comparison with chiral effective Lagrangians.

Acknowledgments

MW would like to thank Carsten Urbach for help in retrieving and handling ETMC gauge configurations. Moreover, we acknowledge useful discussions with Benoit Blossier, Tommy Burch, Vladimir Galkin, Christian Hagen, Rainer Sommer and Carsten Urbach. This work has been supported in part by the DFG Sonderforschungsbereich/Transregio SFB/TR9-03.

References

- [1] C. Michael and J. Peisa [UKQCD Collaboration], “Maximal variance reduction for stochastic propagators with applications to the static quark spectrum,” *Phys. Rev. D* **58**, 034506 (1998) [[arXiv:hep-lat/9802015](#)].
- [2] A. M. Green, J. Koponen, C. McNeile, C. Michael and G. Thompson [UKQCD Collaboration], “Excited B mesons from the lattice,” *Phys. Rev. D* **69**, 094505 (2004) [[arXiv:hep-lat/0312007](#)].
- [3] T. Burch and C. Hagen, “Domain decomposition improvement of quark propagator estimation,” *Comput. Phys. Commun.* **176**, 137 (2007) [[arXiv:hep-lat/0607029](#)].
- [4] J. Koponen, “Energies and radial distributions of B_s mesons on the lattice,” *Acta Phys. Polon. B* **38**, 2893 (2007) [[arXiv:hep-lat/0702006](#)].
- [5] J. Foley, A. O’Cais, M. Peardon and S. M. Ryan, “Radial and orbital excitations of static-light mesons,” *Phys. Rev. D* **75**, 094503 (2007) [[arXiv:hep-lat/0702010](#)].
- [6] J. Koponen [UKQCD Collaboration], “Energies of B_s meson excited states - a lattice study,” [arXiv:0708.2807 \[hep-lat\]](#).
- [7] T. Burch, C. Hagen, C. B. Lang, M. Limmer and A. Schafer, “Excitations of singly beautiful hadrons,” [arXiv:0809.1103 \[hep-lat\]](#).
- [8] K. Jansen, C. Michael, A. Shindler and M. Wagner [ETM Collaboration], “Static-light meson masses from twisted mass lattice QCD,” [arXiv:0808.2121 \[hep-lat\]](#).
- [9] M. Bochicchio, G. Martinelli, C.R. Allton, C.T Sachrajda and D.B. Carpenter, “Heavy quark spectroscopy on the lattice” *Nucl. Phys. B* **B372**, 403, (1992).
- [10] D. Guazzini, H.B. Meyer and R. Sommer [ALPHA Collaboration] “Non-perturbative renormalisation of the chromo-magnetic operator in heavy quark effective theory and the $B^* - B$ mass splitting” *JHEP* **0710**, 081 (2007) [[arXiv:0705.1809 \[hep-lat\]](#)].
- [11] W.-M. Yao *et al.* [Particle Data Group], *J. Phys. G* **33**, 1 (2006) and 2007 partial update for the 2008 edition.
- [12] H. J. Schnitzer, “Spin structure in meson spectroscopy with an effective scalar confinement of quarks,” *Phys. Rev. D* **18**, 3482 (1978).
- [13] H. J. Schnitzer, “Where are the inverted multiplets of meson spectroscopy?,” *Phys. Lett. B* **226** (1989) 171.

- [14] D. Ebert, V. O. Galkin and R. N. Faustov, “Mass spectrum of orbitally and radially excited heavy-light mesons in the relativistic quark model,” Phys. Rev. D **57**, 5663 (1998) [Erratum-ibid. D **59**, 019902 (1999)] [arXiv:hep-ph/9712318].
- [15] N. Isgur, “Spin-orbit inversion of excited heavy quark mesons,” Phys. Rev. D **57**, 4041 (1998).
- [16] P. Weisz, “Continuum Limit Improved Lattice Action For Pure Yang-Mills Theory. 1,” Nucl. Phys. B **212**, 1 (1983).
- [17] R. Frezzotti, P. A. Grassi, S. Sint and P. Weisz [Alpha collaboration], “Lattice QCD with a chirally twisted mass term,” JHEP **0108**, 058 (2001) [arXiv:hep-lat/0101001].
- [18] R. Frezzotti and G. C. Rossi, “Chirally improving Wilson fermions. I: $\mathcal{O}(a)$ improvement,” JHEP **0408**, 007 (2004) [arXiv:hep-lat/0306014].
- [19] A. Shindler, “Twisted mass lattice QCD,” Phys. Rept. **461**, 37 (2008) [arXiv:0707.4093 [hep-lat]].
- [20] Ph. Boucaud *et al.* [ETM Collaboration], “Dynamical twisted mass fermions with light quarks,” Phys. Lett. B **650**, 304 (2007) [arXiv:hep-lat/0701012].
- [21] C. Urbach [ETM Collaboration], “Lattice QCD with two light Wilson quarks and maximally twisted mass,” PoS **LAT2007**, 022 (2007) [arXiv:0710.1517 [hep-lat]].
- [22] Ph. Boucaud *et al.* [ETM Collaboration], “Dynamical twisted mass fermions with light quarks: simulation and analysis details,” arXiv:0803.0224 [hep-lat].
- [23] M. Kurth and R. Sommer [ALPHA Collaboration], “Renormalization and $\mathcal{O}(a)$ improvement of the static axial current,” Nucl. Phys. B **597**, 488 (2001) [arXiv:hep-lat/0007002].
- [24] P. Lacock, C. Michael, P. Boyle and P. Rowland [UKQCD Collaboration], “Orbitally excited and hybrid mesons from the lattice,” Phys. Rev. D **54** 6997 (1996) [arXiv:hep-lat/9605025].
- [25] M. Albanese *et al.* [APE Collaboration], “Glueball masses and string tension in lattice QCD,” Phys. Lett. B **192**, 163 (1987).
- [26] S. Gusken, “A study of smearing techniques for hadron correlation functions,” Nucl. Phys. Proc. Suppl. **17** (1990) 361.
- [27] C. Alexandrou *et al.* [ETM Collaboration], “Light baryon masses with dynamical twisted mass fermions,” Phys. Rev. D **78**, 014509 (2008) [arXiv:0803.3190 [hep-lat]].
- [28] A. Hasenfratz and F. Knechtli, “flavour symmetry and the static potential with hypercubic blocking,” Phys. Rev. D **64**, 034504 (2001) [arXiv:hep-lat/0103029].
- [29] M. Della Morte *et al.*, “Lattice HQET with exponentially improved statistical precision,” Phys. Lett. **B581**, 93, (2004) [arXiv:hep-lat/0307021].
- [30] M. Della Morte, A. Shindler and R. Sommer, “On lattice actions for static quarks,” JHEP **0508**, 051 (2005) [arXiv:hep-lat/0506008].

- [31] C. McNeile, C. Michael and G. Thompson [UKQCD Collaboration], “Hadronic decay of a scalar B meson from the lattice,” Phys. Rev. D **70**, 054501 (2004) [arXiv:hep-lat/0404010].
- [32] C. Michael and A. McKerrell, “Fitting correlated hadron mass spectrum data,” Phys. Rev. D **51**, 3745 (1995) [arXiv:hep-lat/9412087].
- [33] T. Chiarappa *et al.*, “Numerical simulation of QCD with u , d , s and c quarks in the twisted-mass Wilson formulation,” Eur. Phys. J. C **50**, 373 (2007) [arXiv:hep-lat/0606011].
- [34] R. K. Mommsen, “ B_c and excited B states: a Tevatron review,” Nucl. Phys. Proc. Suppl. **170**, 172 (2007) [arXiv:hep-ex/0612003].
- [35] V. M. Abazov *et al.* [D0 Collaboration], “Observation and properties of $L = 1$ B_1 and B_2^* mesons,” Phys. Rev. Lett. **99**, 172001 (2007) [arXiv:0705.3229 [hep-ex]].
- [36] T. Aaltonen *et al.* [CDF Collaboration], “Observation of orbitally excited B_s mesons,” Phys. Rev. Lett. **100**, 082001 (2008) [arXiv:0710.4199 [hep-ex]].
- [37] V. M. Abazov *et al.* [D0 Collaboration], “Observation and properties of the orbitally excited B_{s2}^* meson,” Phys. Rev. Lett. **100**, 082002 (2008) [arXiv:0711.0319 [hep-ex]].

The continuum limit of the static-light meson spectrum

SFB/CPP-10-30, LTH 869, IFT-UAM/CSIC-10-14, HU-EP-10/20

Chris Michael

Theoretical Physics Division, Department of Mathematical Sciences, University of Liverpool,
Liverpool L69 3BX, UK

Andrea Shindler

Istituto de Física Teórica UAM/CSIC, Universidad Autónoma de Madrid, Cantoblanco
E-28049 Madrid, Spain

Marc Wagner

Humboldt-Universität zu Berlin, Institut für Physik, Newtonstraße 15, D-12489 Berlin,
Germany



April 23, 2010

Abstract

We investigate the continuum limit of the low lying static-light meson spectrum using Wilson twisted mass lattice QCD with $N_f = 2$ dynamical quark flavours. We consider three values of the lattice spacing $a \approx 0.051 \text{ fm}, 0.064 \text{ fm}, 0.080 \text{ fm}$ and various values of the pion mass in the range $280 \text{ MeV} \lesssim m_{\text{PS}} \lesssim 640 \text{ MeV}$. We present results in the continuum limit for light cloud angular momentum $j = 1/2, 3/2, 5/2$ and for parity $\mathcal{P} = +, -$. We extrapolate our results to physical quark masses, make predictions regarding the spectrum of B and B_s mesons and compare with available experimental results.

1 Introduction

A systematic way to study B and B_s mesons from first principles is with lattice QCD. Since $am_b > 1$ at currently available lattice spacings for large volume simulations, one needs to use for the b quark a formalism such as Heavy Quark Effective Theory (HQET) [1, 2] or Non-Relativistic QCD [3]. An alternative procedure has recently been proposed [4] which is based on HQET but does not make use of the static point. Here we follow the standard HQET route, which enables all sources of systematic error to be controlled.

In the static limit a heavy-light meson will be the “hydrogen atom” of QCD. Since in this limit there are no interactions involving the heavy quark spin, states are doubly degenerate, i.e. there is no hyperfine splitting. Therefore, it is common to label static-light mesons by parity \mathcal{P} and the total angular momentum of the light degrees of freedom j with $j = |l \pm 1/2|$, where l and $\pm 1/2$ denote respectively angular momentum and spin. An equivalent notation is given by l_{\pm} , which reads $S \equiv (1/2)^-, P_- \equiv (1/2)^+, P_+ \equiv (3/2)^+, D_- \equiv (3/2)^-, D_+ \equiv (5/2)^-, F_- \equiv (5/2)^+, F_+ \equiv (7/2)^+ \dots$. The total angular momentum of a static-light meson is either $J = j + 1/2$ or $J = j - 1/2$, where both states are of the same mass. Note that in contrast to parity, charge conjugation is not a good quantum number, since static-light mesons are made from non-identical quarks.

The static-light meson spectrum has been studied comprehensively by lattice methods in the quenched approximation with a rather coarse lattice spacing [5]. Lattice studies with $N_f = 2$ flavours of dynamical sea quarks have also explored this spectrum [6, 7, 8, 9, 10, 11, 12]. Here following our initial study [13, 14], we use $N_f = 2$ flavours and are able to reach lighter dynamical quark masses, which are closer to the physical u/d quark mass, so enabling a more reliable extrapolation. Note that in our formalism, maximally twisted mass lattice QCD, mass differences in the static-light spectrum are $\mathcal{O}(a)$ improved so that the continuum limit is more readily accessible. We now extend our study to include three different lattice spacings, which gives us confidence that we are indeed extracting the continuum limit.

In this paper, we approach the B meson spectrum by concentrating on the unitary sector, where valence quarks and sea quarks are of the same mass. This is appropriate for static-light mesons with a light quark, which is u or d .

We also estimate masses of B_s mesons with s quarks of physical mass, where the s quark is treated as a valence quark in the sea of light u and d quarks (so this is a partially quenched study). We took our s quark mass values from ETMC studies of strange mesons [15, 16].

Within the twisted mass formalism, it is feasible to use $N_f = 2 + 1 + 1$ flavours of dynamical sea quarks, which would give a more appropriate focus on the static-strange meson spectrum if strange quark sea effects were significant. This is under study by ETMC.

In HQET the leading order is just the static limit. The next correction will be of order $1/m_Q$, where m_Q is the mass of the heavy quark. This correction is expected to be relatively small for b quarks, but larger for c quarks. Lattice methods to evaluate these $1/m_Q$ contributions to the B meson hyperfine splittings have been established and tested in quenched studies [17, 18, 19, 20, 21]. We intend to explore these contributions using lattice techniques subsequently. An alternative way to predict the spectrum for B and B_s mesons is to interpolate between D and D_s states, where the experimental spectrum is rather well known, and the static limit obtained by lattice QCD assuming a dependence as $1/m_Q$. Thus the splittings among B and B_s mesons

should be approximately $m_c/m_b \approx 1/3$ of those among the corresponding D and D_s mesons.

For excited D_s mesons, experiment has shown that some of the states have very narrow decay widths [22]. This comes about, since the hadronic transitions to DK and D_sM (where M is a flavour singlet mesonic system, e.g. η' , $\pi\pi$ or f_0) are not allowed energetically. The isospin violating decay to $D_s\pi$ together with electromagnetic decay to $D_s\gamma$ are then responsible for the narrow width observed. A similar situation may exist for B_s decays and we investigate this here using our lattice mass determinations of the excited states. This will enable us to predict whether narrow excited B_s mesons should be found.

As well as exploring this issue of great interest to experiment, we determine the excited state spectrum of static-light mesons as fully as possible. This will help the construction of phenomenological models and will shed light on questions such as, whether there is an inversion of the level ordering with l_+ lighter than l_- at larger l or for radial excitations as has been predicted [23, 24, 25, 26, 27].

Since we measure the spectrum for a range of values of the bare quark mass parameter μ_q for the light quark, we could also compare with chiral effective Lagrangians appropriate to HQET. This comparison would be most appropriate applied to heavy-light decay constants in the continuum limit (see ref [28]). Since that study awaits more precise renormalization constants, we do not discuss it further here.

Since we have discussed the basic methods in a previous paper [14], in this paper we present only briefly the details of our computation of static-light meson mass differences. We give a full discussion of our extrapolation to the continuum and to physical light quark masses. We also discuss the interpolation to the physical b quark mass.

2 Lattice details

We use $N_f = 2$ flavour gauge configurations produced by the European Twisted Mass Collaboration (ETMC). The gauge action is tree-level Symanzik improved [29], while the fermionic action is Wilson twisted mass at maximal twist (cf. e.g. [30] and references therein). As argued in [14] this ensures automatic $\mathcal{O}(a)$ improvement for static-light spectral quantities, e.g. mass differences of static-light mesons, the quantities we are focusing on in this work.

We use three different values of the lattice spacing $a \approx 0.051$ fm, 0.064 fm, 0.080 fm and various values of the pion mass in the range $280 \text{ MeV} \lesssim m_{\text{PS}} \lesssim 640 \text{ MeV}$. All lattice volumes are big enough to fulfill $m_{\text{PS}}L > 3.2$. The ensembles we are considering are listed in Table 1. Details regarding the generation of gauge configurations and analysis procedures for standard quantities (e.g. lattice spacing, pion mass) can be found in [31, 32].

In Table 1 we also list the number of gauges, on which we have computed static-light correlation functions, and the number and type of inversions performed to estimate light quark propagators stochastically. Note that in contrast to our previous work [13, 14] we treat B_s mesons in a partially quenched approach, where the mass of the valence quark is approximately the mass of the physical s quark, taken from the study of strange mesons using the same configurations [15, 16],

$$\bullet \quad \beta = 3.90 \quad \rightarrow \quad \mu_{q,\text{valence}} = \mu_{q,s} = 0.022,$$

β	$L^3 \times T$	μ_q	a in fm	m_{PS} in MeV	# of gauges	# and type of inversions
3.90	$24^3 \times 48$	0.0040	0.0801(14)	336(6) 417(7) 478(8) 517(9) 637(11)	1420/580 1480/- 1360/480 460/480 1000/-	(spin)/(4rand) (spin)/- (spin)/(4rand) (6rand)/(4rand) (1rand)/-
		0.0064				
		0.0085				
		0.0100				
		0.0150				
4.05	$32^3 \times 64$	0.0030	0.0638(10)	321(5) 443(7)	240/240 500/500	(4rand)/(4rand) (4rand)/(4rand)
		0.0060				
4.20	$48^3 \times 96$	0.0020	0.0514(8)	284(5)	420/420	(spin)/(4rand)

Table 1: ensembles (a and m_{PS} have been taken from [32]; # of gauges considered for B/B_s mesons; # and type of inversions for B/B_s mesons: (spin) four spin diluted timeslice sources on the same randomly chosen timeslice; (1rand) a single timeslice source on a randomly chosen timeslice; (4rand) four timeslice sources on four randomly chosen timeslices; (6rand) six timeslice sources on six randomly chosen timeslices).

- $\beta = 4.05 \rightarrow \mu_{q,\text{valence}} = \mu_{q,s} = 0.017$,
- $\beta = 4.20 \rightarrow \mu_{q,\text{valence}} = \mu_{q,s} = 0.015$,

while the sea is considerably lighter (cf. the listed μ_q values in Table 1).

3 Static-light mass differences

The determination of static-light mass differences is essentially identical to what we have done in [13, 14].

For each of our ensembles characterised by the gauge coupling β and the twisted light quark mass μ_q (cf. Table 1) and each of the lattice angular momentum representations A_1 , E and A_2 we compute 6×6 static-light correlation matrices. The corresponding meson creation operators differ in their (twisted mass) parity, in their γ matrix structure and in their spatial size. They are precisely the same we have been using before and are explained in detail in [14], section 3, Table 3.

From these correlation matrices we compute effective mass plateaux using variational methods [33, 34] (cf. [35] for exemplary plots showing the quality of our plateaus). We extract mass differences by fitting constants to these plateaus at sufficiently large temporal separations $T_{\min} \dots T_{\max}$. We determine T_{\min} and T_{\max} by requiring that the reduced χ^2 is $\mathcal{O}(1)$. T_{\min} values are listed in Table 2, while $T_{\max} = 11$ for $\beta = 3.90$ and $\beta = 4.05$ and $T_{\max} = 17$ for $\beta = 4.20$ in most cases (for some of the excited states smaller values had to be chosen, because the signal was lost in statistical noise). Note, however, that the choice of T_{\max} is essentially irrelevant for the resulting mass (on the “ T_{\max} side” of the effective mass plateau statistical errors are rather large and, therefore, data points only have a very weak effect on the fit). Since we are only interested in mass differences $\Delta M(j^{\mathcal{P}}) = M(j^{\mathcal{P}}) - M(S)$, the jackknife analysis has

been applied directly to the mass difference and not to the individual masses. The samples for $M(j^P)$ and $M(S)$ entering for such a mass difference have been obtained with the same value of T_{\min} .

		B mesons						B_s mesons					
β	μ_q	P_-	P_+	D_\pm	D_+	F_\pm	S^*	P_-	P_+	D_\pm	D_+	F_\pm	S^*
3.90	0.0040	6	6	5	4	4	4	6	6	5	5	4	4
	0.0064	6	6	5	4	4	4	-	-	-	-	-	-
	0.0085	6	6	5	4	4	4	5	5	4	4	4	4
	0.0100	6	6	5	4	4	4	5	5	4	4	4	4
	0.0150	6	6	5	4	4	4	-	-	-	-	-	-
4.05	0.0030	7	6	6	5	5	6	7	7	6	5	5	7
	0.0060	7	6	6	5	5	5	7	7	6	5	5	7
4.20	0.0020	10	10	8	7	7	9	11	9	9	8	8	11

Table 2: T_{\min} for fitting constants to effective mass plateaus.

The resulting mass differences $\Delta M(j^P)a$ (in lattice units), where $j^P \in \{P_-, P_+, D_\pm, D_+, F_\pm, S^*\}$, together with the pion masses $m_{PS}a$ (in lattice units; cf. Table 1 and [32]) and the lattice spacings a (in physical units; cf. Table 1) serve as input for the extrapolation procedure to physical u/d quark masses described in the next section.

We checked the stability of our results by varying T_{\min} by ± 1 as well as by fitting superpositions of exponentials to the elements of the correlation matrices (as done in [14]) instead of solving generalised eigenvalue problems. We found consistency within statistical errors.

4 Continuum limit and extrapolation to physical u/d quark masses

4.1 Numerical results

The mass differences $\Delta M(j^P)$ obtained for all our ensembles are plotted against $(m_{PS})^2$ ² in Figure 1 (unitary, i.e. “ B mesons”) and Figure 2 (partially quenched, i.e. “ B_s mesons”). Note that, although we use three different values of the lattice spacing, points corresponding to the same mass difference fall on a single curve. This is reassuring, since we use Wilson twisted mass lattice QCD at maximal twist, where static-light mass differences are $\mathcal{O}(a)$ improved [14]. In Table 3 and Table 4 we collect the values of the mass differences in MeV¹ for all simulation points for B and B_s mesons respectively.

For the extrapolation to physical light quark masses, we could use an effective field theory approach (Chiral HQET for instance) as used to study the decay constants [28] of the ground state. This approach has not been developed to discuss mass differences between excited states

¹The scale has been set by the pion decay constant f_π as explained in detail in [32].

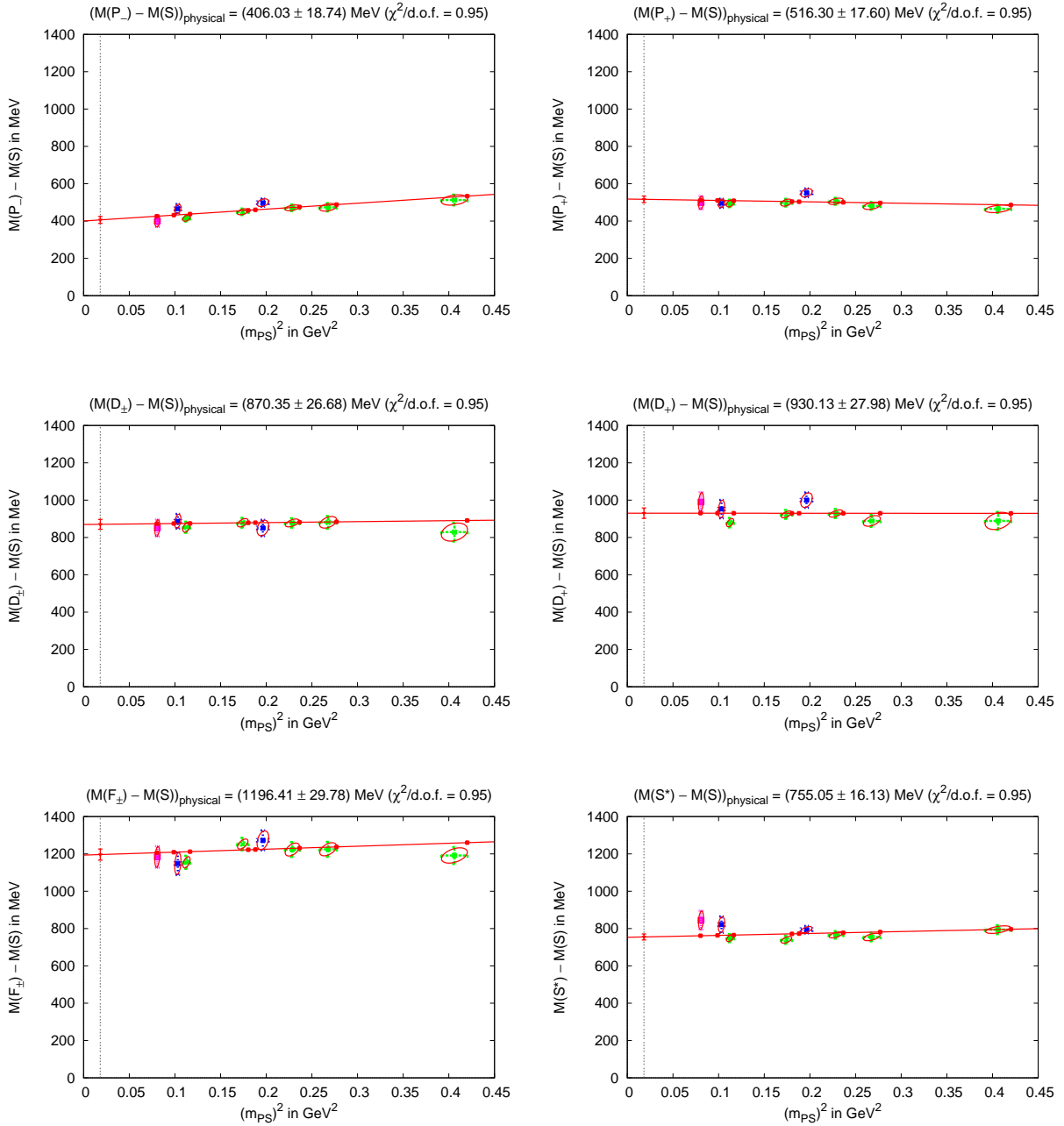


Figure 1: static-light mass differences linearly extrapolated to the physical u/d quark mass (unitary, i.e. B mesons).

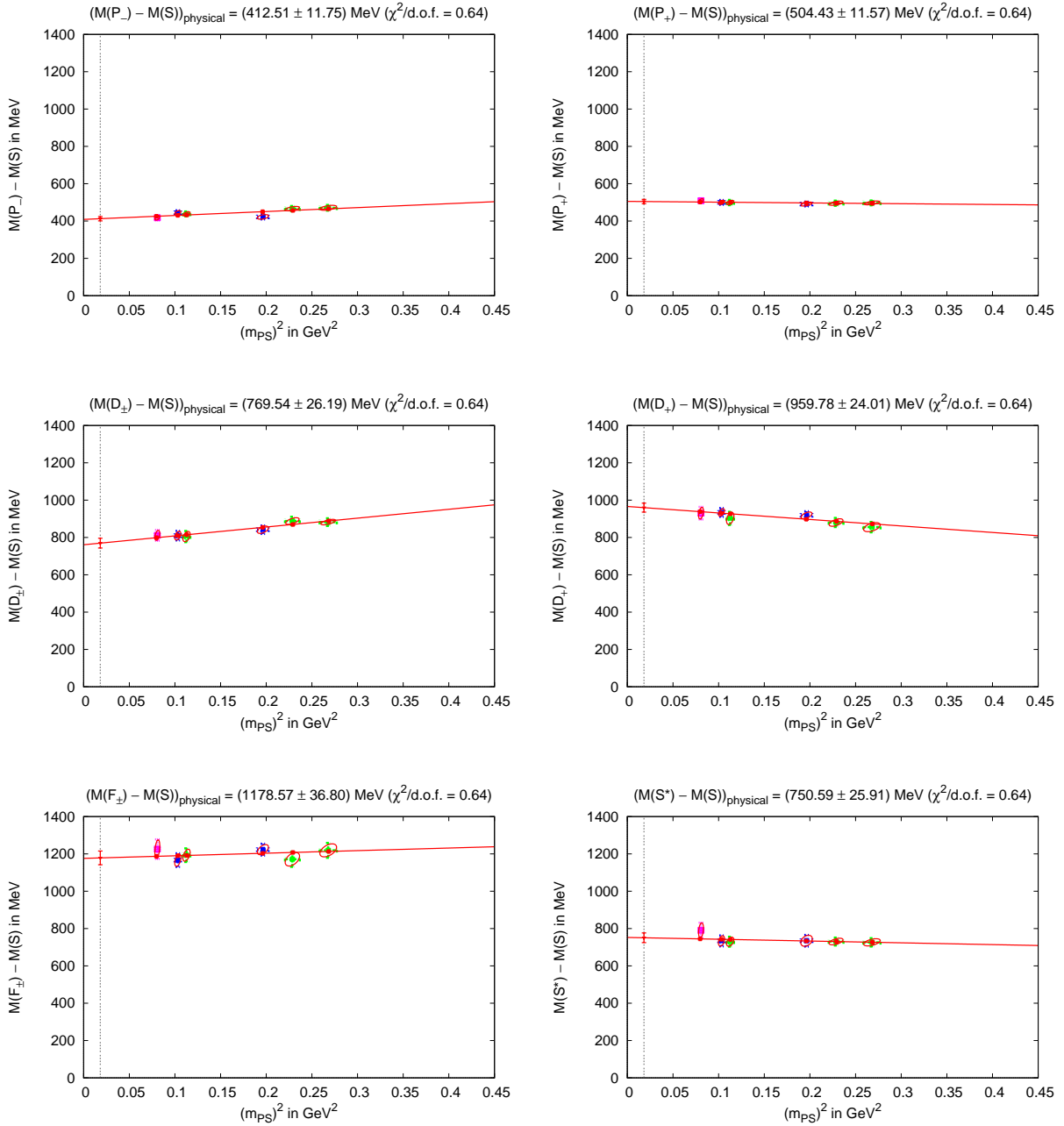


Figure 2: static-light mass differences linearly extrapolated to the physical u/d quark mass (partially quenched, i.e. B_s mesons).

β	μ_q	$\Delta M(P_-)$	$\Delta M(P_+)$	$\Delta M(D_{\pm})$	$\Delta M(D_+)$	$\Delta M(F_{\pm})$	$\Delta M(S^*)$
3.90	0.0040	415(17)	494(20)	855(30)	879(25)	1155(35)	749(22)
	0.0064	449(17)	499(20)	879(26)	924(24)	1253(33)	740(21)
	0.0085	471(17)	506(19)	878(25)	928(24)	1223(40)	766(20)
	0.0100	474(22)	481(21)	881(34)	889(32)	1225(40)	755(23)
	0.0150	513(29)	465(21)	829(50)	889(48)	1192(45)	794(24)
4.05	0.0030	465(26)	495(24)	887(39)	952(49)	1148(60)	821(44)
	0.0060	498(22)	551(23)	851(44)	1000(41)	1273(53)	794(20)
4.2	0.0020	399(31)	498(35)	851(45)	990(53)	1184(58)	845(51)

Table 3: static-light mass differences in MeV (unitary, i.e. B mesons) for all simulation points; details on the analysis procedure of the correlation functions are given in section 3.

β	μ_q	$\Delta M(P_-)$	$\Delta M(P_+)$	$\Delta M(D_{\pm})$	$\Delta M(D_+)$	$\Delta M(F_{\pm})$	$\Delta M(S^*)$
3.90	0.0040	438(13)	499(14)	805(30)	902(35)	1193(37)	729(26)
	0.0085	466(14)	495(14)	888(23)	880(24)	1171(41)	730(21)
	0.0100	471(15)	497(13)	882(20)	855(28)	1219(40)	726(22)
4.05	0.0030	444(13)	500(13)	810(26)	934(24)	1167(36)	734(29)
	0.0060	422(14)	491(13)	842(23)	918(22)	1223(32)	735(31)
4.2	0.0020	417(13)	509(13)	811(29)	930(34)	1226(52)	790(41)

Table 4: static-light mass differences in MeV (partially quenched, i.e. B_s mesons) for all simulation points; details on the analysis procedure of the correlation functions are given in section 3.

and the ground state (e.g. $M(P_-) - M(S)$), so is not appropriate here. Instead we use the simplest assumption which is supported by our results: a linear dependence.

Because our ground state mass values enter into all of the mass differences we study, we simultaneously fit to all the meson mass differences we have computed. We find that fits which are independent of the lattice spacing and which are linear in the light quark mass (represented by the mass squared of the light-light pseudoscalar meson) are acceptable, i.e. yield $\chi^2/\text{dof} \lesssim 1$.

For the B_s mesons, our results depend on the strange quark mass we choose. We have taken these values from studies of strange-light mesons [15, 16] as discussed above. The possible systematic error arising from an incorrect value for the strange quark mass is very small: because the mass differences we measure turn out to be very weakly dependent on that mass. This will be seen when we compare our results for the B and B_s mesons extrapolated to physical light quark masses.

The details of our fitting procedure are collected in appendix A.

As already mentioned both fits (one for B mesons, the other for B_s mesons) are of good quality in a sense that $\chi^2/\text{dof} \lesssim 1$. This shows that at the present level of statistical accuracy the continuum limit has already been reached at our largest value of the lattice spacing $a \approx 0.080$ fm. Moreover,

these fits enable us to extrapolate to physical u/d quark masses.

Extrapolations of static-light mass differences to physical u/d quark masses are listed in Table 5 in MeV both for B mesons and for B_s mesons. Note that both fits give $\chi^2/\text{d.o.f.} \approx 1$, i.e. are consistent with our assumption that static-light meson mass differences as functions of $(m_{\text{PS}})^2$ can be parameterised by straight lines.

	P_-	P_+	D_\pm	D_+	F_\pm	S^*	$\chi^2/\text{d.o.f.}$
B mesons	406(19)	516(18)	870(27)	930(28)	1196(30)	755(16)	0.95
B_s mesons	413(12)	504(12)	770(26)	960(24)	1179(37)	751(26)	0.64

Table 5: $M(j^P) - M(S)$ in MeV extrapolated to physical light quark masses.

To check the stability of these fits, we have varied T_{\min} by ± 1 . Within statistical errors mass differences obtained with $T_{\min} - 1$, with T_{\min} and with $T_{\min} + 1$ are in agreement.

The extrapolations are shown in Figure 1 and Figure 2. The red dots represent the maximum likelihood estimates of $\bar{\mathbf{z}} = ((m_{\text{PS}})^2, \Delta M(j^P))$ obtained during the fitting procedure. In addition to x - y -error bars we also plot covariance ellipses, which reflect the correlations between $(m_{\text{PS}})^2$ and $\Delta M(j^P)$ induced by the lattice spacing a , that is they are generated from the inverses of the corresponding 2×2 submatrices of the covariance matrix C .

4.2 Contamination of static-light meson masses by multi particle states

The radially and orbitally excited static-light mesons P_- , P_+ , D_- , D_+ , F_- , F_+ and S^* can decay into multi particle states $S + n \times \pi$ with relative angular momentum such that quantum numbers j^P are identical. In particular the P_- static-light meson is not protected by angular momentum, i.e. it can decay via an S wave into $S + \pi$, whose wave function is not suppressed at the origin. In the following we argue that the effect of $S + \pi$ states on our P_- mass is small compared to its statistical error. To this end we resort to a model presented and to numerical results obtained in [36, 37, 38].

We consider the P_- static-light meson at $\beta = 3.90$ and our lightest u/d quark mass at this β value ($\mu_q = 0.0040$). In that ensemble the masses of the P_- state and of the $S + \pi$ state are quite similar: $m(P_-)a \approx 0.57$ and $(m(S) + m(\pi))a \approx 0.53$ (we consider the case, where the pion has zero momentum). Therefore, we expect mixing of P_- and $S + \pi$ with respect to the eigenstates of the Hamiltonian H , mixing which will be different in different spatial volumes. Consequently, we do not focus on the eigenvalues of these states, but rather on $m(P_-) = \langle P_- | H | P_- \rangle / \langle |P_- \rangle$ is a state with $j^P = (1/2)^+$ created by single particle operators, e.g. operators of type $\bar{Q}u$ or $\bar{Q}d$, which we have used in the construction of trial states). At very large temporal separation the correlators we are studying will inevitably yield the eigenvalues of the Hamiltonian. At intermediate temporal separations, however, one can expect to read off $m(P_-)$ as we will explain in the following.

In [38] the effective coupling strength of the decay $P_- \rightarrow S + \pi$ has been estimated by a lattice computation: $\Gamma/k \approx 0.46$. Moreover, some evidence has been obtained that this quantity is fairly independent of the light quark mass. Using this result one can determine the mixing

element xa of the energy matrix via eqn. (5) in [38] for our situation ($L/a = 24$, $m_\pi a \approx 0.14$):

$$xa = \left(\frac{2\pi(\Gamma/k)}{3(L/a)^3(m_\pi a)} \right)^{1/2} \approx 0.023. \quad (1)$$

As detailed in [36, 37, 38] for large temporal separations the P_- correlator is of the form

$$C_{P_-}(t/a) \propto e^{-(m_{P_-}a)(t/a)} \cosh((xa)(t/a)), \quad (2)$$

while the corresponding effective mass is

$$\begin{aligned} m_{\text{effective}, P_-}(t/a)a &= -\frac{d}{d(t/a)} \ln(C_{P_-}(t/a)) = \\ &= \frac{d}{d(t/a)} \left((m_{P_-}a)(t/a) - \ln(\cosh((xa)(t/a))) \right) = m_{P_-}a - \tanh((xa)(t/a))xa. \end{aligned} \quad (3)$$

At $t/a = 12$ (the maximum temporal separation we have considered) the estimated systematic error of m_{P_-} coming from mixing with $S + \pi$ is $\tanh((xa)(t/a))xa \approx 0.0063$, i.e. roughly a 1% effect. This correction is significantly smaller than the statistical error of $m_{\text{effective}, P_-}a$ in that t region.

For the other temporal separations and/or ensembles we obtain similar estimates. We, therefore, expect that at the present level of statistical accuracy the effect of multi particle states on our static-light meson masses, in particular on P_- , is negligible.

Our conclusions are in agreement with those obtained in [9], where a study of the static-light meson spectrum with similar techniques has been performed using two different lattice volumes. No volume dependence of the eigenvectors of static-light meson states has been observed, which is a sign that contributions of multi particle states are strongly suppressed.

5 Extrapolation to the physical b quark mass

To make contact with experimentally available results on the spectrum of B mesons, we need to correct for the non-infinite mass of the b quark. In Heavy Quark Effective Theory, the leading correction will be of order $1/m_H$, where m_H is the heavy quark mass. It is possible, in principle, to evaluate the coefficients of this correction from first principles on a lattice [19, 20]. This we intend to explore in the future, but here we use a more direct method to establish the size of this small correction between static quarks and b quarks of realistic mass. These $1/m_H$ terms will break the degeneracy of mesonic states found in the static limit.

We evaluate for physical b quarks by interpolating between static heavy quarks and the charm quark, where experimental data is available. As a measure of the heavy quark mass, we take the mass of the ground state heavy-light meson (D or B). This measure is equivalent to another (such as using quark masses in some scheme) to the order $1/m_H$ we are using. One test of this interpolation can be made. The hyperfine splitting between D^* and D of 141 MeV when interpolated from the static limit (namely zero) gives for B^* and B a splitting reduced by $m(D)/m(B) = 0.35$ to 49 MeV which agrees with the observed splitting [22] of 46 MeV to within 6%.

For the fine splitting, the kinetic term (rather than the chromo-magnetic) is relevant and the experimental results for the spectrum are rather incomplete - indeed this current study is to establish the spectrum from a theoretical input. Lattice studies do confirm [19, 20] that a $1/m_H$ behavior is dominant down to masses near the charm quark mass.

We interpolate our lattice results for static-light mass differences of P and S wave states to the physical b quark mass at $m(D)/m(B) = 0.35$ linearly in $m(D)/m_H$, making use of experimental data on D and D_s mesons as input [22]. For details regarding this method of extrapolation cf. [14]. Results are listed and compared to experimental results in Table 6. The corresponding extrapolations are shown in Figure 3.

For D mesons the assignment of the two $J^P = 1^+$ states to B_1^* and B_1 is easy, because their widths differ by more than an order of magnitude (we associate the narrow state with B_1 [one of the two degenerate $j^P = (3/2)^+$ states in the static limit, which can only decay to $S + \pi$ via a D wave and is, therefore, protected by angular momentum]; the wide state with B_1^* [one of the two degenerate $j^P = (1/2)^+$ states in the static limit, which can readily decay to $S + \pi$ via an S wave]). In contrast to that the situation is less clear for D_s mesons, where both $J^P = 1^+$ states have similar (narrow) widths. Therefore, we show both possibilities in Table 6 and in Figure 3.

	$M - M(B)$ in MeV			$M - M(B_s)$ in MeV	
state	lattice	experiment	state	lattice	experiment
B_0^*	443(21)		B_{s0}^*	391(8)	
B_1^*	460(22)		B_{s1}^*	440(8)/467(8)	
B_1	530(12)	444(2)	B_{s1}	526(8)/499(8)	463(1)
B_2^*	543(12)	464(5)	B_{s2}^*	539(8)	473(1)
B_J^*		418(8)	B_{sJ}^*		487(15)

Table 6: lattice and experimental results for P wave B and B_s states (B_J^* and B_{sJ}^* denote rather vague experimental signals, which can be interpreted as stemming from several broad and narrow resonances possibly including the $j = 1/2$ P wave states B_0^* , B_1^* , B_{s0}^* and B_{s1}^* ; the two lattice values listed for B_{s1}^* and B_{s1} correspond to the two possibilities of assigning experimental $J^P = 1^+$ D results [cf. text for more details]).

Compared to our previous study [13, 14] at a single lattice spacing, the above results are similar for the B (unitary) case. For B_s mesons we now employ a partially quenched s quark which allows a more realistic treatment of the light quark sea. So our new results supersede those obtained previously for B_s . Indeed we find a significant dependence on the sea quark mass (cf. Figure 2), which is now the physical u/d quark mass, while it previously corresponded to the significantly heavier s quark mass.

In our lattice study we have extracted the continuum limit and have extrapolated to physical light quarks using a linear dependence. We have then interpolated to the physical b quark assuming that a $1/m_H$ behavior is valid down to the charm quark mass. These assumptions induce systematic errors and, in principle, they can be quantified by further lattice studies.

The assumption of a linear extrapolation to physical light quarks is sensitive to possible admixtures of two body states which become more important at lighter quark masses as thresholds

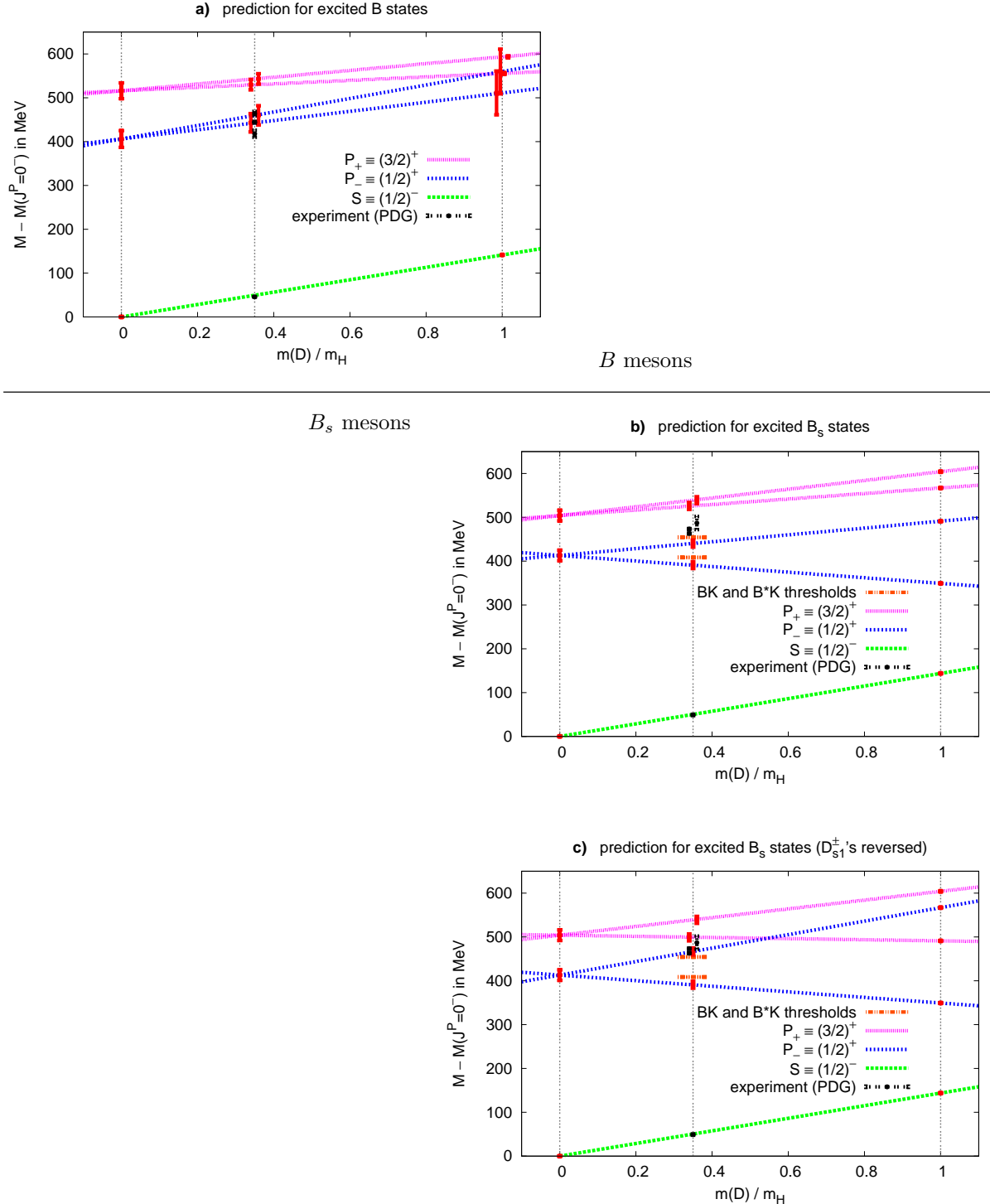


Figure 3: Static-light mass differences linearly extrapolated to the physical b quark mass. **a)** Unitary, i.e. B mesons. **b), c)** Partially quenched, i.e. B_s mesons.

for decay open. We have explored this possibility and found no evidence of such effects, so it is difficult to estimate the magnitude of a possible systematic error from this. If there was a significant difference between the light quark behavior for the ground state and an excited state, this would introduce an error on our extrapolation to the physical value which could be as large as 10 MeV.

The test of the $1/m_H$ assumption for the chromo-magnetic term, discussed above, was found to be valid within 6%. This suggests that an estimate of the systematic errors for the B and B_s meson mass splittings coming from $1/m$ effects should also be at least of order 6%. Since the $1/m$ correction to the P wave states is of order 100 MeV, this implies a systematic error of order 6 MeV.

One further possible source of systematic error is from our neglect of the strange contribution to the sea. This will be addressed in a future study making use of the $N_f = 2 + 1 + 1$ sea which includes dynamical s quarks from ETMC [39, 40].

Overall, it seems prudent to assign systematic errors on our mass differences (for P_- and P_+ relative to S) of order 20 MeV from these effects, even though we have little evidence for such effects.

The experimental determination of the spectrum of excited B and B_s mesons is quite limited [22]. Assuming that the relatively narrow states seen correspond to our P_+ state (since a $J^P = 2^+$ state must have that assignment), the mass difference we see of over 500 MeV does not agree closely with the experimental results of around 450 MeV. We do get a mass difference of around 450 MeV from our P_- states, although such states cannot have $J^P = 2^+$.

In view of this discrepancy with experimental results, it is also interesting to compare with independent existing lattice computations, in particular with the rather recent study reported in [12]. There the light quark extrapolation is only performed in the valence quark mass (from which static-light mass differences essentially seem to be independent, as can be seen by comparing our B and B_s results and also from corresponding plots and numbers presented in [12]), while the sea quark mass is kept fixed. More generally, a comparison of the dependence of static-light mass differences on the sea quark mass, which we have computed down to $m_{\text{PS}} \approx 280$ MeV, with existing lattice studies is not possible: there the number of investigated sea quark masses is rather small and they are quite heavy, around the mass of the s quark. What one can do, however, is to compare meson mass differences for a given value of the sea quark mass. Before comparing results (in physical units) with those quoted in [12] it should be noted that in [12] the scale is set by identifying r_0 with 0.49 fm, while our result for this quantity is $r_0 = 0.42$ fm [32]. Therefore, to perform a meaningful comparison, one should express all quantities in units of r_0 or equivalently scale all masses in physical units listed in [12] by a factor of around $0.49/0.42 \approx 1.14$. For the lightest sea quark mass considered in [12] corresponding to $m_{\text{PS}} \approx 461$ MeV it is most appropriate to compare with our results at $\beta = 3.90$, $\mu_q = 0.0100$ ($m_{\text{PS}} \approx 517$ MeV). For the P wave mass differences one finds

$$\frac{(m(P_-) - m(S))_{\text{ETMC}}}{(m(P_-) - m(S))_{[12]}} \approx \frac{474(29) \text{ MeV}}{454(19)(9) \text{ MeV}} \approx 1.04(11) \quad (4)$$

$$\frac{(m(P_+) - m(S))_{\text{ETMC}}}{(m(P_+) - m(S))_{[12]}} \approx \frac{481(27) \text{ MeV}}{446(17)(9) \text{ MeV}} \approx 1.08(11), \quad (5)$$

ratios, which are within statistical errors fully consistent with the expected factor 1.14.

It is interesting to note that the ratios between our lattice results and the experimental values (see Table 6) are on the same ballpark of the ratio between two values of r_0 used above, i.e. ≈ 1.14 . While there is no reason to doubt the precise determination of the lattice spacing performed in [32], it would be interesting, although beyond the scope of this paper, to investigate, whether simulations at lighter quark masses and/or with $N_f = 2 + 1 + 1$ dynamical flavours will improve the agreement with experimental results.

One interesting issue is whether the B_s states are stable to the strong decay to BK . This decay has a threshold at 408 MeV above the ground state B_s meson. Our P_- states (the upper two in Table 6) do indeed have masses which are close to (or below) this threshold. That would imply that these two states (B_{s0}^* and B_{s1}^*) should have a very small decay width. This is consistent with the experimental observation that only two candidate P wave B^* states have been seen so far: corresponding to the heavier P_+ states. All the other states B_s we study, including the S^* , lie higher than this BK threshold and so would have a strong decay open.

Moreover, our findings clearly indicate that there is no inversion of level ordering for P wave states, neither for B mesons nor for B_s mesons. B_0^* and B_1^* (B_{s0}^* and B_{s1}^*) are considerably lighter than B_1 and B_2 (B_{s1} and B_{s2}) as can be read off from Table 6 and Figure 3. This is in contrast to predictions obtained from certain phenomenological models [23, 24, 25, 26, 27] and, therefore, might provide valuable input for future model building.

6 Conclusions

We have determined the continuum limit for static-light mesons on a lattice using $N_f = 2$ flavours of light quarks. The removal of $\mathcal{O}(a)$ effects by using maximally-twisted mass fermions for meson mass differences in the static limit is confirmed.

We have investigated the light sea quark mass dependence of B and B_s mesons down to $m_{PS} \approx 280$ MeV, which is significantly lighter than what has been achieved in previous studies of static-light mesons. We find that our results are compatible with a linear extrapolation in the light quark mass to its physical value. We see no sign of any mixing with two body effects and this is consistent with our estimate that such effects should be too small to see on our lattices.

We have determined masses for a wide variety of excited states in the continuum limit and this will be a valuable resource for model builders.

We have employed the assumption of a $1/m_H$ dependence on the heavy quark mass together with experimental results for charm-light mesons to allow us to estimate the spectrum that one would obtain for physical b quarks.

Our results imply that there will be a $J^P = 0^+$ and $J^P = 1^+$ B_s meson which has a narrow width since its strong decay to BK is suppressed (or zero) due to phase space effects.

Future directions include (i) determination of f_B and f_{B_s} (for a preliminary result cf. [28]); (ii) a similar investigation regarding static-light baryons; (iii) extending these computations to $N_f = 2 + 1 + 1$ flavour ETMC gauge configurations [39, 40].

A Details of the fitting procedure

Data points $(m_{\text{PS}})^2$ and $\Delta M(j^{\mathcal{P}})$, $j^{\mathcal{P}} \in \{P_-, P_+, D_{\pm}, D_+, F_{\pm}, S^*\}$ corresponding to the same β are correlated via the lattice spacing a . We take that into account via a covariance matrix, which we estimate by resampling $m_{\text{PS}}a$, $\Delta M(j^{\mathcal{P}})a$ and a (100,000 samples). Consequently, we do not fit straight lines to the Data points $((m_{\text{PS}})^2, \Delta M(j^{\mathcal{P}}))$ individually for every static-light state $j^{\mathcal{P}}$, but perform a single correlated fit of six straight lines to the six mass differences of interest. During the fitting we take statistical errors both along the horizontal axis (errors in $(m_{\text{PS}})^2$) and along the vertical axis (errors in $\Delta M(j^{\mathcal{P}})$) into account.

The method of performing the two-dimensional fits is based on what has been used in [41].

To be able to express the corresponding equations in a compact way, we introduce the following notation:

- $\mathbf{z} = (\mathbf{x}, \mathbf{y}(1), \mathbf{y}(2), \dots)$.
- $\mathbf{x} = (((m_{\text{PS}})^2)^{(1)}, ((m_{\text{PS}})^2)^{(2)}, \dots)$ (the upper index (...) refers to both the lattice spacing and to the light quark mass).
- $\mathbf{y}(j) = ((\Delta M)^{(1)}(j), (\Delta M)^{(2)}(j), \dots)$ (the upper index (...) refers to both the lattice spacing and to the light quark mass, the index (j) refers to $j^{\mathcal{P}}$).
- C denotes the estimated covariance matrix for \mathbf{z} (a 56×56 matrix for B mesons, a 42×42 matrix for B_s mesons).
- The linear fits $y(j) = a(j)x + b(j)$ are parameterised by $a(j)$ and $b(j)$ (the quantities, which will finally allow the extrapolation to physical u/d quark masses).

The basic idea of the method is a maximum likelihood determination of the “true values” $\bar{\mathbf{z}} = (\bar{\mathbf{x}}, \bar{\mathbf{y}}(1), \bar{\mathbf{y}}(2), \dots)$. This amounts to minimizing

$$\frac{1}{2} (\mathbf{z} - \bar{\mathbf{z}})^T C^{-1} (\mathbf{z} - \bar{\mathbf{z}}) - \sum_{j,n} \lambda_n(j) (a(j)\bar{x}_n + b(j) - \bar{y}_n(j)) \quad (6)$$

with respect to $\bar{\mathbf{z}}$, $a(j)$, $b(j)$ and $\vec{\lambda}(j)$ under the constraints $\bar{y}_n(j) = a(j)\bar{x}_n + b(j)$. For \mathbf{z} we use the same resampling procedure as for estimating the covariance matrix (this is necessary, because $z_A \equiv \langle ((m_{\text{PS}})^2)^{(n)} \rangle \neq \langle (m_{\text{PS}})^{(n)}a \rangle^2 / \langle a \rangle^2$ and $z_A \equiv \langle (\Delta M)^{(n)}(j) \rangle \neq \langle (\Delta M)^{(n)}(j)a \rangle / \langle a \rangle$).

The constraint minimization is equivalent to solving a system of non-linear equations, which we do by means of the scaled-hybrid algorithm of the GSL library [42]. It needs initial parameters, which should preferably be close to the global extremum. Such initial parameters can be obtained by individual standard one-dimensional straight line fits:

- $\lambda_n(j) = 0$,
- $a(j)$ and $b(j)$ minimizing

$$\sum_n \frac{(a(j)x_n + b(j) - y_n(j))^2}{C_{y_n(j), y_n(j)}}, \quad (7)$$

- $\bar{\mathbf{x}} = \mathbf{x}$ and $\bar{\mathbf{y}}(j) = \mathbf{y}(j)$.

To judge the quality of the resulting fit, we define a “reduced χ^2 ” via

$$\frac{\chi^2}{\text{d.o.f.}} = \frac{\left(\mathbf{z} - \bar{\mathbf{z}}\right)^T C^{-1} \left(\mathbf{z} - \bar{\mathbf{z}}\right)}{\text{d.o.f.}}, \quad (8)$$

where d.o.f. is the number of entries of $\bar{\mathbf{z}}$ minus the number of $a(j)$ and $b(j)$, i.e. d.o.f. = 44 for B mesons and d.o.f. = 32 for B_s mesons respectively.

The resulting straight lines allow an extrapolation to physical u/d quark masses (corresponding to $m_{\text{PS}} = 135$ MeV). The corresponding statistical errors are obtained by repeating this fitting and extrapolation procedure 100 times with randomly sampled sets z_A (we randomly sample the input data and compute $z_A \equiv ((m_{\text{PS}})^{(n)} a)^2/a^2$ and $z_A \equiv ((\Delta M)^{(n)}(j)a)/a$) and taking the variance.

Acknowledgments

We thank Rémi Baron for running contractions at $\beta = 4.20$. We acknowledge useful discussions with Vladimir Galkin, Karl Jansen, Marcus Petschlies and Carsten Urbach.

A.S. acknowledges financial support from Spanish Consolider-Ingenio 2010 Programme CPAN (CSD 2007-00042) and from Comunidad Autónoma de Madrid, CAM under grant HEPHA-COS P-ESP-00346. This work has been supported in part by the DFG Sonderforschungsbereich/Transregio SFB/TR9-03.

This work was performed using HPC resources from GENCI/IDRIS Grant 2009-052271. We thank CCIN2P3 in Lyon and the Jülich Supercomputing Center (JSC) for having allocated to us computer time, which was used in this work. We acknowledge computing resources provided by the NW Grid at Liverpool.

References

- [1] M. Neubert, “Heavy quark symmetry,” Phys. Rept. **245**, 259 (1994) [arXiv:hep-ph/9306320].
- [2] T. Mannel, “Heavy-quark effective field theory,” Rept. Prog. Phys. **60**, 1113 (1997).
- [3] B. A. Thacker and G. P. Lepage, “Heavy quark bound states in lattice QCD,” Phys. Rev. D **43**, 196 (1991).
- [4] B. Blossier *et al.*, “A proposal for B -physics on current lattices,” arXiv:0909.3187 [hep-lat].
- [5] C. Michael and J. Peisa [UKQCD Collaboration], “Maximal variance reduction for stochastic propagators with applications to the static quark spectrum,” Phys. Rev. D **58**, 034506 (1998) [arXiv:hep-lat/9802015].

- [6] A. M. Green, J. Koponen, C. McNeile, C. Michael and G. Thompson [UKQCD Collaboration], “Excited B mesons from the lattice,” Phys. Rev. D **69**, 094505 (2004) [arXiv:hep-lat/0312007].
- [7] T. Burch and C. Hagen, “Domain decomposition improvement of quark propagator estimation,” Comput. Phys. Commun. **176**, 137 (2007) [arXiv:hep-lat/0607029].
- [8] J. Koponen, “Energies and radial distributions of B_s mesons on the lattice,” Acta Phys. Polon. B **38**, 2893 (2007) [arXiv:hep-lat/0702006].
- [9] J. Foley, A. O’Cais, M. Peardon and S. M. Ryan, “Radial and orbital excitations of static-light mesons,” Phys. Rev. D **75**, 094503 (2007) [arXiv:hep-lat/0702010].
- [10] J. Koponen [UKQCD Collaboration], “Energies of B_s meson excited states: a Lattice study,” Phys. Rev. D **78**, 074509 (2008) [arXiv:0708.2807 [hep-lat]].
- [11] T. Burch, D. Chakrabarti, C. Hagen, T. Maurer, A. Schafer, C. B. Lang and M. Limmer, “ B meson excitations with chirally improved light quarks,” PoS **LAT2007**, 091 (2007) [arXiv:0709.3708 [hep-lat]].
- [12] T. Burch, C. Hagen, C. B. Lang, M. Limmer and A. Schafer, “Excitations of single-beauty hadrons,” Phys. Rev. D **79**, 014504 (2009) [arXiv:0809.1103 [hep-lat]].
- [13] K. Jansen, C. Michael, A. Shindler and M. Wagner [ETM Collaboration], “Static-light meson masses from twisted mass lattice QCD,” PoS **LATTICE2008**, 122 (2008) [arXiv:0808.2121 [hep-lat]].
- [14] K. Jansen, C. Michael, A. Shindler and M. Wagner [ETM Collaboration], “The static-light meson spectrum from twisted mass lattice QCD,” JHEP **0812**, 058 (2008) [arXiv:0810.1843 [hep-lat]].
- [15] B. Blossier *et al.* [ETM Collaboration], “Light quark masses and pseudoscalar decay constants from $N_f = 2$ Lattice QCD with twisted mass fermions,” JHEP **0804**, 020 (2008) [arXiv:0709.4574 [hep-lat]].
- [16] B. Blossier *et al.* [ETM Collaboration], “Pseudoscalar decay constants of kaon and D -mesons from $N_f = 2$ twisted mass lattice QCD,” JHEP **0907**, 043 (2009) [arXiv:0904.0954 [hep-lat]].
- [17] M. Bochicchio, G. Martinelli, C. R. Allton, C. T. Sachrajda and D. B. Carpenter, “Heavy quark spectroscopy on the lattice,” Nucl. Phys. B **372**, 403 (1992).
- [18] D. Guazzini, H. B. Meyer and R. Sommer [ALPHA Collaboration], “Non-perturbative renormalization of the chromo-magnetic operator in heavy quark effective theory and the B^*-B mass splitting,” JHEP **0710**, 081 (2007) [arXiv:0705.1809 [hep-lat]].
- [19] B. Blossier, M. Della Morte, N. Garron, G. von Hippel, T. Mendes, H. Simma and R. Sommer, “Spectroscopy and decay constants from non-perturbative HQET at Order $1/m$,” arXiv:0911.1568 [hep-lat].
- [20] B. Blossier, M. Della Morte, N. Garron and R. Sommer, “HQET at order $1/m$: I. Non-perturbative parameters in the quenched approximation,” arXiv:1001.4783 [hep-lat].

- [21] B. Blossier, M. Della Morte, N. Garron, G. von Hippel, T. Mendes, H. Simma and R. Sommer, “HQET at order $1/m$: II. Spectroscopy in the quenched approximation,” arXiv:1004.2661 [hep-lat].
- [22] C. Amsler *et al.* [Particle Data Group], Phys. Lett. B **667**, 1 (2008) and 2009 partial update for the 2010 edition.
- [23] H. J. Schnitzer, “Spin structure in meson spectroscopy with an effective scalar confinement of quarks,” Phys. Rev. D **18**, 3482 (1978).
- [24] H. J. Schnitzer, “Where are the inverted multiplets of meson spectroscopy?,” Phys. Lett. B **226** (1989) 171.
- [25] D. Ebert, V. O. Galkin and R. N. Faustov, “Mass spectrum of orbitally and radially excited heavy-light mesons in the relativistic quark model,” Phys. Rev. D **57**, 5663 (1998) [Erratum-ibid. D **59**, 019902 (1999)] [arXiv:hep-ph/9712318].
- [26] N. Isgur, “Spin-orbit inversion of excited heavy quark mesons,” Phys. Rev. D **57**, 4041 (1998).
- [27] D. Ebert, R. N. Faustov and V. O. Galkin, “Heavy-light meson spectroscopy and Regge trajectories in the relativistic quark model,” arXiv:0910.5612 [hep-ph].
- [28] B. Blossier *et al.* [ETM Collaboration], “ f_B and f_{B_s} with maximally twisted Wilson fermions,” arXiv:0911.3757 [hep-lat].
- [29] P. Weisz, “Continuum limit improved lattice action for pure Yang-Mills theory. 1,” Nucl. Phys. B **212**, 1 (1983).
- [30] A. Shindler, “Twisted mass lattice QCD,” Phys. Rept. **461**, 37 (2008) [arXiv:0707.4093 [hep-lat]].
- [31] Ph. Boucaud *et al.* [ETM collaboration], “Dynamical twisted mass fermions with light quarks: simulation and analysis details,” Comput. Phys. Commun. **179**, 695 (2008) [arXiv:0803.0224 [hep-lat]].
- [32] R. Baron *et al.*, “Light meson physics from maximally twisted mass lattice QCD,” arXiv:0911.5061 [hep-lat].
- [33] C. Michael, “Adjoint sources in lattice gauge theory,” Nucl. Phys. B **259**, 58 (1985).
- [34] B. Blossier, M. Della Morte, G. von Hippel, T. Mendes and R. Sommer, “On the generalized eigenvalue method for energies and matrix elements in lattice field theory,” JHEP **0904**, 094 (2009) [arXiv:0902.1265 [hep-lat]].
- [35] B. Blossier, M. Wagner and O. Pene [ETM Collaboration], “Lattice calculation of the Isgur-Wise functions $\tau_{1/2}$ and $\tau_{3/2}$ with dynamical quarks,” JHEP **0906**, 022 (2009) [arXiv:0903.2298 [hep-lat]].
- [36] C. McNeile and C. Michael [UKQCD Collaboration], “Mixing of scalar glueballs and flavour-singlet scalar mesons,” Phys. Rev. D **63**, 114503 (2001) [arXiv:hep-lat/0010019].

- [37] C. McNeile, C. Michael and P. Pennanen [UKQCD Collaboration], “Hybrid meson decay from the lattice,” Phys. Rev. D **65**, 094505 (2002) [arXiv:hep-lat/0201006].
- [38] C. McNeile, C. Michael and G. Thompson [UKQCD Collaboration], “Hadronic decay of a scalar B meson from the lattice,” Phys. Rev. D **70**, 054501 (2004) [arXiv:hep-lat/0404010].
- [39] R. Baron *et al.* [ETM Collaboration], “Status of ETMC simulations with $N_f = 2 + 1 + 1$ twisted mass fermions,” PoS **LATTICE2008**, 094 (2008) [arXiv:0810.3807 [hep-lat]].
- [40] R. Baron *et al.* [ETM Collaboration], “First results of ETMC simulations with $N_f = 2+1+1$ maximally twisted mass fermions,” arXiv:0911.5244 [hep-lat].
- [41] F. Farchioni *et al.*, “Numerical simulations with two flavours of twisted-mass Wilson quarks and DBW2 gauge action,” Eur. Phys. J. C **47**, 453 (2006) [arXiv:hep-lat/0512017].
- [42] <http://www.gnu.org/software/gsl/>.

The static-light baryon spectrum from twisted mass lattice QCD

SFB/CPP-11-20, HU-EP-11/20

Marc Wagner, Christian Wiese

Humboldt-Universität zu Berlin, Institut für Physik, Newtonstraße 15, D-12489 Berlin,
Germany



April 26, 2011

Abstract

We compute the static-light baryon spectrum by means of Wilson twisted mass lattice QCD using $N_f = 2$ flavors of sea quarks. As light u/d valence quarks we consider quarks, which have the same mass as the sea quarks with corresponding pion masses in the range $340 \text{ MeV} \lesssim m_{\text{PS}} \lesssim 525 \text{ MeV}$, as well as partially quenched s quarks, which have a mass around the physical value. We consider all possible combinations of two light valence quarks, i.e. Λ , Σ , Ξ and Ω baryons corresponding to isospin $I \in \{0, 1/2, 1\}$ and strangeness $S \in \{0, -1, -2\}$ as well as angular momentum of the light degrees of freedom $j \in \{0, 1\}$ and parity $\mathcal{P} \in \{+, -\}$. We extrapolate in the light u/d and in the heavy b quark mass to the physical point and compare with available experimental results. Besides experimentally known positive parity states we are also able to predict a number of negative parity states, which have neither been measured in experiments nor previously been computed by lattice methods.

1 Introduction

In this work we report on a lattice computation of the spectrum of b baryons made from a heavy b quark and two light quarks, which are u , d and/or s .

Experimentally five b baryon states have been observed. While Λ_b has first been detected quite some time ago, Σ_b , Σ_b^* , Ξ_b and Ω_b have only been discovered recently [1, 2, 3, 4, 5]. For the mass of Ω_b there are two different results, which are not in agreement.

On the theoretical side there are a number of lattice studies of the spectrum of b baryons. Some of these consider static heavy quarks [6, 7, 8, 9, 10, 11] using Heavy Quark Effective Theory (HQET) (cf. e.g. [12, 13]), while others apply heavy quarks of finite mass [14, 15, 16] mainly by means of Non-Relativistic QCD (cf. e.g. [17]). For a recent review of lattice results on b baryon masses cf. [18].

In this work we treat the b quark in leading order of HQET, which is the static limit. In this limit there are no interactions involving the spin of the heavy quark, i.e. states are doubly degenerate. Therefore, it is common to label static-light baryons by integer spin/angular momentum j and parity \mathcal{P} of the light degrees of freedom. For the two light quarks we consider all possible combinations of u , d and s , i.e. further quantum numbers are strangeness S and isospin I . We use $N_f = 2$ flavors of dynamical quarks and study various ensembles with corresponding pion masses down to ≈ 340 MeV. Our lattice spacing $a \approx 0.079$ fm is rather fine and we use the Wilson twisted mass formulation of lattice QCD at maximal twist, which guarantees automatically $\mathcal{O}(a)$ improved spectral results. We compute all five experimentally known b baryon states. We also make predictions for Ξ'_b , which has not yet been observed, as well as for a number of negative parity static-light baryons, which have neither been measured experimentally nor been computed by lattice methods.

The next-to-leading order of HQET, which removes the degeneracy with respect to the heavy quark spin, is $\mathcal{O}(1/m_Q)$, where m_Q is the mass of the heavy quark. This correction is expected to be relatively small for b baryons, e.g. experimentally the mass difference between Σ_b and Σ_b^* is only around 21 MeV. Lattice methods to evaluate such $1/m_Q$ contributions have been established and tested in quenched studies of B mesons [19, 20, 21, 22]. We intend to explore these contributions using lattice techniques subsequently. An alternative way to predict the spectrum of b baryons is to interpolate between charmed baryons, where the experimental spectrum is rather well known, and the static limit obtained by lattice QCD assuming a dependence as $1/m_Q$. Thus the splittings among b baryons should approximately be $m_c/m_b \approx 1/3$ of those among the corresponding c baryons.

We try to determine the b baryon spectrum as fully as possible, i.e. we consider all possible light flavor combinations corresponding to $S \in \{0, -1, -2\}$ and $I \in \{0, 1\}$ as well as both parity $\mathcal{P} = +$ and $\mathcal{P} = -$. This will help the construction of phenomenological models (cf. e.g. [23]), might contribute to resolve open experimental issues (e.g. the above mentioned mass discrepancy for Ω_b) and also provide valuable input for future experiments.

This study is in many aspects similar to our recent computation of the static-light meson spectrum [24, 25]. Preliminary results have already been reported in conference proceedings [26].

The paper is organized as follows. In section 2 we briefly recapitulate our lattice setup, which is discussed in more detail in [24]. In section 3 we discuss static-light baryon trial states,

corresponding correlation matrices and how we extract the static-light baryon spectrum from these matrices as well as our extrapolation procedure to the physical u/d quark mass. In section 4 we interpolate between our static-light lattice results and experimental results for c baryons, to account for the finite mass of the b quark. We conclude with a brief summary and an outlook in section 5.

2 Lattice setup

In this work we use the same setup as for our recent computation of the static-light meson spectrum. For a more detailed presentation we refer to [24, 25].

We use $N_f = 2$ flavor gauge field configurations generated by the European Twisted Mass Collaboration (ETMC). The gauge action is tree-level Symanzik improved [27],

$$S_G[U] = \frac{\beta}{6} \left(b_0 \sum_{x,\mu \neq \nu} \text{Tr} \left(1 - P^{1 \times 1}(x; \mu, \nu) \right) + b_1 \sum_{x,\mu \neq \nu} \text{Tr} \left(1 - P^{1 \times 2}(x; \mu, \nu) \right) \right) \quad (1)$$

with $b_0 = 1 - 8b_1$ and $b_1 = -1/12$. The fermionic action is Wilson twisted mass (cf. [28, 29, 30, 31]),

$$S_F[\chi, \bar{\chi}, U] = a^4 \sum_x \bar{\chi}(x) \left(D_W + i\mu_q \gamma_5 \tau_3 \right) \chi(x), \quad (2)$$

where

$$D_W = \frac{1}{2} \left(\gamma_\mu \left(\nabla_\mu + \nabla_\mu^* \right) - a \nabla_\mu^* \nabla_\mu \right) + m_0, \quad (3)$$

∇_μ and ∇_μ^* are the gauge covariant forward and backward derivatives, m_0 and μ_q are the bare untwisted and twisted quark masses respectively, τ_3 is the third Pauli matrix acting in flavor space and $\chi = (\chi^{(u)}, \chi^{(d)})$ represents the quark fields in the so-called twisted basis. The twist angle ω is given by $\tan(\omega) = \mu_R/m_R$, where μ_R and m_R denote the renormalized twisted and untwisted quark masses. ω has been tuned to $\pi/2$ by adjusting m_0 appropriately (cf. [32] for details). As argued in [24] this ensures automatic $\mathcal{O}(a)$ improvement for static-light spectral quantities, e.g. mass differences between static-light baryons and the lightest static-light meson (the “ B/B^* meson”), the quantities we are focusing on in this work.

The ensembles of gauge field configurations we are considering are listed in Table 1. They correspond to a single value of the lattice spacing $a \approx 0.079$ fm, but various values of the pion mass in the range $340 \text{ MeV} \lesssim m_{PS} \lesssim 525 \text{ MeV}$. The lattice extension is $L^3 \times T = 24^3 \times 48$, which amounts to $L \approx 1.9$ fm and $m_{PS}L \gtrsim 3.3$. Details regarding the generation of these gauge field configurations and computation and analysis of standard quantities (e.g. lattice spacing or pion mass) can be found in [32, 33].

β	$L^3 \times T$	μ_q	a in fm	m_{PS} in MeV	# of gauges
3.90	$24^3 \times 48$	0.0040	0.079(3)	340(13)	200
		0.0064		423(16)	50
		0.0085		485(18)	50
		0.0100		525(20)	50

Table 1: ensembles of gauge field configurations (a and m_{PS} have been taken from [33]; # of gauges: number of gauge field configurations considered).

We treat static-light baryons containing valence s quarks in a partially quenched approach, where the mass of these quarks, $\mu_{q,\text{valence } s} = 0.022$, is approximately equal to the mass of the physical s quark taken from a study of strange mesons using the same gauge field configurations [34, 35]. Note that partially quenched s quarks can be realized in two ways, either with a twisted mass term $+i\mu_{q,\text{valence } s}\gamma_5$ or $-i\mu_{q,\text{valence } s}\gamma_5$ corresponding to the upper and the lower entry in the quark field doublet χ respectively. We consider both possibilities and denote them by $\chi = (\chi^{(s^+)}, \chi^{(s^-)})$.

In Table 1 we also list the number of gauge configurations, on which we have computed static-light baryon correlation functions.

3 The static-light baryon spectrum

With static-light baryons we refer to baryons made from a single static quark and two light quarks, which can either be u , d and/or s .

3.1 Static-light baryon trial states

3.1.1 Static-light baryon creation operators in the continuum

We start by discussing symmetries and quantum numbers of static-light baryons and corresponding creation operators in the continuum.

The continuum analogs of our lattice static-light baryon creation operators are

$$\mathcal{O}_{\Gamma,\psi^{(1)}\psi^{(2)}}^{\text{physical}}(\mathbf{x}) = \epsilon^{abc} Q^a(\mathbf{x}) \left((\psi^{b,(1)}(\mathbf{x}))^T \mathcal{C} \Gamma \psi^{c,(2)}(\mathbf{x}) \right), \quad (4)$$

where Q is a static quark operator and $\psi^{(n)}$ are light quark operators (in the usual physical basis). The upper indices a , b and c are color indices, $\mathcal{C} = \gamma_0 \gamma_2$ is the charge conjugation matrix and Γ is a combination of γ matrices, i.e. a 4×4 matrix acting in spin space.

Since there are no interactions involving the static quark spin, it is appropriate to label static-light baryons by the angular momentum of their light degrees of freedom j . For creation operators (4) it is determined by Γ and can either be $j = 0$ or $j = 1$. $j = 0$ states correspond to total angular momentum $J = 1/2$, while $j = 1$ states correspond to degenerate pairs of states with total angular momentum $J = 1/2$ and $J = 3/2$, respectively.

Parity is also a quantum number depending on Γ . Either $\mathcal{P} = +$ or $\mathcal{P} = -$.

The flavor quantum numbers are isospin I and strangeness S . To access all possible combinations, we consider light quark flavors $\psi^{(1)}\psi^{(2)} = ud - du$ (corresponding to $I = 0$, $S = 0$), $\psi^{(1)}\psi^{(2)} \in \{uu, dd, ud + du\}$ (corresponding to $I = 1$, $S = 0$), $\psi^{(1)}\psi^{(2)} \in \{us, ds\}$ (corresponding to $I = 1/2$, $S = -1$) and $\psi^{(1)}\psi^{(2)} = ss$ (corresponding to $I = 0$, $S = -2$).

Creation operators $\mathcal{O}_{\Gamma,\psi^{(1)}\psi^{(2)}}^{\text{physical}}$ and the quantum numbers of their associated trial states $\mathcal{O}_{\Gamma,\psi^{(1)}\psi^{(2)}}^{\text{physical}}|\Omega\rangle$ are collected in Table 2. Note that certain $\Gamma, \psi^{(1)}\psi^{(2)}$ combinations do not need to be considered, since the corresponding creation operators are identical zero due to the anticommutation property of quark operators. Such $\Gamma, \psi^{(1)}\psi^{(2)}$ combinations are either omitted from the table or marked with “X”.

3.1.2 Static-light baryon creation operators in twisted mass lattice QCD

Twisted basis lattice static-light baryon creation operators are of similar form,

$$\mathcal{O}_{\Gamma,\chi^{(1)}\chi^{(2)}}^{\text{twisted}}(\mathbf{x}) = \epsilon^{abc} Q^a(\mathbf{x}) \left((\chi^{b,(1)}(\mathbf{x}))^T \mathcal{C} \Gamma \chi^{c,(2)}(\mathbf{x}) \right), \quad (5)$$

where physical basis quark operators have been replaced by their twisted basis lattice counterparts.

Γ	j^P	J	I	S	name	I	S	name	I	S	name
γ_5	0^+	$1/2$	0	0	Λ_b	$1/2$	-1	Ξ_b	X	X	X
$\gamma_0\gamma_5$	0^+	$1/2$	0	0	Λ_b	$1/2$	-1	Ξ_b	X	X	X
1	0^-	$1/2$	0	0		$1/2$	-1		X	X	X
γ_0	0^-	$1/2$	1	0		$1/2$	-1		0	-2	
γ_j	1^+	$1/2, 3/2$	1	0	Σ_b, Σ_b^*	$1/2$	-1		0	-2	Ω_b
$\gamma_0\gamma_j$	1^+	$1/2, 3/2$	1	0	Σ_b, Σ_b^*	$1/2$	-1		0	-2	Ω_b
$\gamma_j\gamma_5$	1^-	$1/2, 3/2$	0	0		$1/2$	-1		X	X	X
$\gamma_0\gamma_j\gamma_5$	1^-	$1/2, 3/2$	1	0		$1/2$	-1		0	-2	

Table 2: continuum static-light baryon creation operators and their quantum numbers (j^P : angular momentum of the light degrees of freedom and parity; J : total angular momentum; I : isospin; S : strangeness; name: name of the corresponding b baryon(s) in [47]); operators marked with “X” are identically zero, i.e. do not exist.

In the continuum the relation between the physical and the twisted basis is given by the twist rotation $\psi = \exp(i\gamma_5\tau_3\omega/2)\chi$, where $\omega = \pi/2$ at maximal twist. At finite lattice spacing, however, issues are more complicated: the twist rotation only holds for renormalized operators and the QCD symmetries isospin and parity are explicitly broken by $\mathcal{O}(a)$. Nevertheless, it is possible to unambiguously interpret states obtained from correlation functions of twisted basis operators in terms of QCD quantum numbers as we will explain and demonstrate below.

On the lattice rotational symmetry is reduced to symmetry with respect to cubic rotations. There are only five different representations of the cubic group O_h corresponding to integer angular momentum j . $j = 0$ in the continuum corresponds to the A_1 representation on the lattice containing angular momenta $j = 0, 4, 7, \dots$, while $j = 1$ corresponds to the T_1 representation containing $j = 1, 3, 4, \dots$

While in twisted mass lattice QCD the z -component of isospin I_z is still a quantum number, isospin I and parity P are explicitly broken by the Wilson term, which is proportional to the lattice spacing. Only a specific combination of both symmetries, light flavor exchange combined with parity, is still a symmetry in twisted mass lattice QCD. We denote this symmetry by $\mathcal{P}^{(tm)}$ acting on the light twisted basis quark doublet $\chi = (\chi^{(u)}, \chi^{(d)})$ according to $\mathcal{P}^{(tm)}\chi = \gamma_0\tau_1\chi$, where τ_1 is the first Pauli matrix acting in flavor space. Consequently, the four QCD sectors labeled by $I = 0, 1$ and $P = +, -$ are pairwise combined. $\mathcal{P}^{(tm)} = +$ is a combination of $(I = 0, P = -)$ and $(I = 1, P = +)$, while $\mathcal{P}^{(tm)} = -$ is a combination of $(I = 0, P = +)$ and $(I = 1, P = -)$.

As explained in section 2 the partially quenched s quark can be realized in two ways denoted by $\chi^{(s^+)}$ and $\chi^{(s^-)}$, respectively. As a consequence baryons computed at finite lattice spacing on the one hand with s^+ quarks and on the other hand with s^- quarks, but which are otherwise identical, may differ in mass. Due to automatic $\mathcal{O}(a)$ improvement of twisted mass lattice QCD this mass splitting, however, will only be $\mathcal{O}(a^2)$, i.e. is expected to be rather small and will vanish quadratically, when approaching the continuum limit.

Since $\mathcal{P}^{(tm)}$ and I_z do not commute, they cannot simultaneously be chosen as quantum numbers. An exception are states with $I_z = 0$, which can also be classified with respect to $\mathcal{P}^{(tm)}$.

The lattice static-light baryon creation operators we have been using are collected in Table 3, Table 4 and Table 5. Creation operators are sorted according to the twisted mass lattice quantum numbers of their associated trial states, i.e. creation operators exciting states from different sectors are separated by horizontal lines. To interpret these twisted basis creation operators in terms of QCD quantum numbers, we have performed an approximate rotation to the physical basis (neglecting renormalization and using $\omega = \pi/2$). The resulting so-called pseudo physical basis creation operators together with their corresponding QCD quantum numbers are also listed in the tables.

twisted basis lattice operator				pseudo physical basis operator					
Γ	$\chi^{(1)}\chi^{(2)}$	I_z	$\mathcal{P}^{(\text{tm})}$	Γ	$\psi^{(1)}\psi^{(2)}$	I	I_z	\mathcal{P}	name
A_1 representation $\equiv j = 0, 4, 7, \dots$									
γ_5	$ud - du$	0	—	γ_5	$ud - du$	0	0	+	Λ_b
γ_0	$ud + du$	0	—	$\gamma_0\gamma_5$	$ud - du$	0	0	+	Λ_b
$\gamma_0\gamma_5$	$ud - du$	0	—	γ_0	$ud + du$	1	0	—	
1	$ud - du$	0	+	1	$ud - du$	0	0	—	
γ_0	uu/dd	+1/-1	xxx	γ_0	uu/dd	1	+1/-1	—	
T_1 representation $\equiv j = 1, 3, 4, \dots$									
$\gamma_j\gamma_5$	$ud - du$	0	+	γ_j	$ud + du$	1	0	+	Σ_b, Σ_b^*
$\gamma_0\gamma_j$	$ud + du$	0	+	$\gamma_0\gamma_j$	$ud + du$	1	0	+	Σ_b, Σ_b^*
γ_j	$ud + du$	0	+	$\gamma_j\gamma_5$	$ud - du$	0	0	—	
$\gamma_0\gamma_j\gamma_5$	$ud + du$	0	—	$\gamma_0\gamma_j\gamma_5$	$ud + du$	1	0	—	
γ_j	uu/dd	+1/-1	xxx	γ_j	uu/dd	1	+1/-1	+	Σ_b, Σ_b^*
$\gamma_0\gamma_j\gamma_5$	uu/dd	+1/-1	xxx	$\gamma_0\gamma_j$	uu/dd	1	+1/-1	+	Σ_b, Σ_b^*
$\gamma_0\gamma_j$	uu/dd	+1/-1	xxx	$\gamma_0\gamma_j\gamma_5$	uu/dd	1	+1/-1	—	

Table 3: $S = 0$ lattice static-light baryon creation operators and their quantum numbers; (j : angular momentum of the light degrees of freedom; I : isospin; I_z : z -component of isospin; \mathcal{P} : parity; $\mathcal{P}^{(\text{tm})}$: twisted mass parity [“xxx” indicates that $\mathcal{P}^{(\text{tm})}$ is not a quantum number for the corresponding trial state]; name: name of the corresponding b baryon(s) in [47]).

3.1.3 Smearing of gauge links and quark fields

To enhance the overlap of the trial states $\mathcal{O}_{\Gamma,\chi^{(1)}\chi^{(2)}}^{\text{twisted}}|\Omega\rangle$ to low lying static-light baryon states, we make extensive use of standard smearing techniques. This allows to read off static-light baryon masses from correlation functions at rather small temporal separation, where the signal-to-noise ratio is favorable.

Smearing is done in two steps. At first we replace all spatial gauge links by APE smeared versions. The parameters we have chosen are $N_{\text{APE}} = 40$ and $\alpha_{\text{APE}} = 0.5$. Then we use Gaussian smearing on the light quark fields $\chi^{(u)}$, $\chi^{(d)}$, $\chi^{(s^+)}$ and $\chi^{(s^-)}$, which resorts to the APE smeared spatial links. We consider three different smearing levels, characterized by $N_{\text{Gauss}} \in \{10, 40, 90\}$ and $\kappa_{\text{Gauss}} = 0.5$. This amounts to light quark field operators with approximate widths of

twisted basis lattice operator			pseudo physical basis operator					
Γ	$\chi^{(1)}\chi^{(2)}$	I_z	Γ	$\psi^{(1)}\psi^{(2)}$	I	I_z	\mathcal{P}	name
A_1 representation $\equiv j = 0, 4, 7, \dots$								
1	us^+/ds^-	$+1/2/-1/2$	γ_5	us/ds	$1/2$	$+1/2/-1/2$	+	Ξ_b
$\gamma_0\gamma_5$	us^+/ds^-	$+1/2/-1/2$	$\gamma_0\gamma_5$	us/ds	$1/2$	$+1/2/-1/2$	+	Ξ_b
γ_5	us^+/ds^-	$+1/2/-1/2$	1	us/ds	$1/2$	$+1/2/-1/2$	-	
γ_0	us^+/ds^-	$+1/2/-1/2$	γ_0	us/ds	$1/2$	$+1/2/-1/2$	-	
γ_5	us^-/ds^+	$+1/2/-1/2$	γ_5	us/ds	$1/2$	$+1/2/-1/2$	+	Ξ_b
γ_0	us^-/ds^+	$+1/2/-1/2$	$\gamma_0\gamma_5$	us/ds	$1/2$	$+1/2/-1/2$	+	Ξ_b
1	us^-/ds^+	$+1/2/-1/2$	1	us/ds	$1/2$	$+1/2/-1/2$	-	
$\gamma_0\gamma_5$	us^-/ds^+	$+1/2/-1/2$	γ_0	us/ds	$1/2$	$+1/2/-1/2$	-	
T_1 representation $\equiv j = 1, 3, 4, \dots$								
γ_j	us^+/ds^-	$+1/2/-1/2$	γ_j	us/ds	$1/2$	$+1/2/-1/2$	+	
$\gamma_0\gamma_j\gamma_5$	us^+/ds^-	$+1/2/-1/2$	$\gamma_0\gamma_j$	us/ds	$1/2$	$+1/2/-1/2$	+	
$\gamma_j\gamma_5$	us^+/ds^-	$+1/2/-1/2$	$\gamma_j\gamma_5$	us/ds	$1/2$	$+1/2/-1/2$	-	
$\gamma_0\gamma_j$	us^+/ds^-	$+1/2/-1/2$	$\gamma_0\gamma_j\gamma_5$	us/ds	$1/2$	$+1/2/-1/2$	-	
$\gamma_j\gamma_5$	us^-/ds^+	$+1/2/-1/2$	γ_j	us/ds	$1/2$	$+1/2/-1/2$	+	
$\gamma_0\gamma_j$	us^-/ds^+	$+1/2/-1/2$	$\gamma_0\gamma_j$	us/ds	$1/2$	$+1/2/-1/2$	+	
γ_j	us^-/ds^+	$+1/2/-1/2$	$\gamma_j\gamma_5$	us/ds	$1/2$	$+1/2/-1/2$	-	
$\gamma_0\gamma_j\gamma_5$	us^-/ds^+	$+1/2/-1/2$	$\gamma_0\gamma_j\gamma_5$	us/ds	$1/2$	$+1/2/-1/2$	-	

Table 4: $S = -1$ lattice static-light baryon creation operators and their quantum numbers; (j : angular momentum of the light degrees of freedom; I : isospin; I_z : z -component of isospin; \mathcal{P} : parity; name: name of the corresponding b baryon in [47]).

$\{1.58 \times a, 3.16 \times a, 4.74 \times a\} \approx \{0.12 \text{ fm}, 0.25 \text{ fm}, 0.37 \text{ fm}\}$ (cf. [24] for details).

Smeared static light baryon creation operators are denoted by $S^{N_{\text{Gauss}}}(\mathcal{O}_{\Gamma,\chi^{(1)}\chi^{(2)}}^{\text{twisted}})$.

3.2 Correlation matrices

For each sector characterized by strangeness S , angular momentum of the light degrees of freedom j , z -component of isospin I_z , and in certain cases twisted mass parity $\mathcal{P}^{(\text{tm})}$ we compute temporal correlation matrices

$$\begin{aligned} C_{(\Gamma_j, (\chi^{(1)}\chi^{(2)})_j, N_{\text{Gauss},j}), (\Gamma_k, (\chi^{(1)}\chi^{(2)})_k, N_{\text{Gauss},k})}(t) &= \\ &= \langle \Omega | \left(S^{N_{\text{Gauss},j}}(\mathcal{O}_{\Gamma_j, (\chi^{(1)}\chi^{(2)})_j}^{\text{twisted}}(t)) \right)^\dagger S^{N_{\text{Gauss},k}}(\mathcal{O}_{\Gamma_k, (\chi^{(1)}\chi^{(2)})_k}^{\text{twisted}}(0)) | \Omega \rangle. \end{aligned} \quad (6)$$

We consider all the creation operators listed in Table 3, Table 4 and Table 5 at three different smearing levels $N_{\text{Gauss}} \in \{10, 40, 90\}$ as explained in the previous subsection. This amounts dependent on the sector to 3×3 , 9×9 or 12×12 correlation matrices.

Static quarks are treated with the HYP2 static action [36, 37, 38], i.e. Wilson lines appearing in

twisted basis lattice operator			pseudo physical basis operator					
Γ	$\chi^{(1)}\chi^{(2)}$	I_z	Γ	$\psi^{(1)}\psi^{(2)}$	I	I_z	\mathcal{P}	name
A_1 representation			$\equiv j = 0, 4, 7, \dots$					
γ_0	s^+s^+/s^-s^-	0	γ_0	ss	0	0	-	
T_1 representation			$\equiv j = 1, 3, 4, \dots$					
γ_j	s^+s^+/s^-s^-	0	γ_j	ss	0	0	+	Ω_b
$\gamma_0\gamma_j\gamma_5$	s^+s^+/s^-s^-	0	$\gamma_0\gamma_j$	ss	0	0	+	Ω_b
$\gamma_0\gamma_j$	s^+s^+/s^-s^-	0	$\gamma_0\gamma_j\gamma_5$	ss	0	0	-	

Table 5: $S = -2$ lattice static-light baryon creation operators and their quantum numbers; (j : angular momentum of the light degrees of freedom; I : isospin; I_z : z -component of isospin; \mathcal{P} : parity; name: name of the corresponding b baryon in [47]).

static quark propagators are formed by products of HYP2 smeared temporal links (cf. [24] for details).

Light quark propagators are estimated by means of $\mathcal{Z}_2 \times \mathcal{Z}_2$ stochastic timeslice sources (cf. [24] for details). On each gauge field configuration we invert 48 independently chosen sources, all located on the same timeslice, 12 for each of the four possible light quark propagators u , d , s^+ and s^- . Multiple inversions of the same timeslice of the same gauge field configuration are beneficial with respect to statistical precision, because each correlation function contains two light quark propagators. This allows to form $12 \times 12 = 144$ statistical samples, i.e. the number of samples is the square of the number of inversions (cf. [6]).

3.3 Determination of static-light baryon masses

From correlation matrices (6) we compute effective mass plateaus by solving generalized eigenvalue problems

$$C(t)v_n(t, t_0) = \lambda_n(t, t_0)C(t_0)v_n(t, t_0), \quad m_n^{\text{eff}}(t, t_0) = \ln \frac{\lambda_n(t, t_0)}{\lambda_n(t+1, t_0)} \quad (7)$$

with $t_0 = 1$ (cf. e.g. [39, 40]). Instead of using the full 3×3 , 9×9 or 12×12 correlation matrices we have chosen “optimal submatrices” in a sense that on the one hand effective masses exhibit plateaus already at small temporal separations t and that on the other hand statistical errors on m_n^{eff} are minimized. We found that with the following choice both criteria are adequately fulfilled:

- 3×3 correlation matrices:
use 2×2 submatrices with smearing levels $N_{\text{Gauss}} \in \{40, 90\}$;
- 9×9 correlation matrices:
use 3×3 submatrices with smearing levels $N_{\text{Gauss}} = 90$;
- 12×12 correlation matrices:
use 4×4 submatrices with smearing levels $N_{\text{Gauss}} = 90$.

To demonstrate the quality of our lattice results, we show in Figure 1 examples of effective mass plateaus (at light quark mass $\mu_q = 0.0040$) corresponding to Λ_b ($S = 0, I = 0, j^P = 0^+$), Ω_b ($S = -2, I = 0, j^P = 1^+$) and its parity partner ($S = -2, I = 0, j^P = 1^-$).

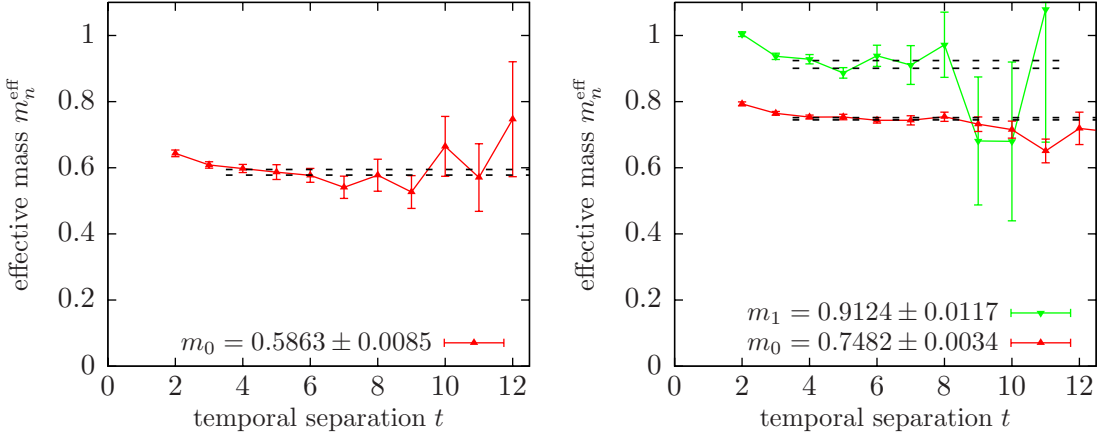


Figure 1: effective masses m_n^{eff} as functions of the temporal separation t at light quark mass $\mu_q = 0.0040$; **left:** Λ_b ($S = 0, I = 0, j^P = 0^+$) from a 3×3 correlation matrix; **right:** Ω_b ($S = -2, I = 0, j^P = 1^+$) and its parity partner ($S = -2, I = 0, j^P = 1^-$) from a 3×3 correlation matrix.

We extract static-light baryon masses by fitting constants to these plateaus in regions of sufficiently large temporal separation $t_{\min} \dots t_{\max}$. We found that $t_{\min} = 4$ yields reasonable χ^2 values, which are $\mathcal{O}(1)$ for all states investigated. t_{\max} on the other hand hardly affects the resulting static-light baryon masses (on the “ t_{\max} -side” of the effective mass plateau statistical errors are rather large and, therefore, data points have a negligible effect on the fit). The resulting fits for the examples shown in Figure 1 are indicated by dashed lines. We checked the stability of all our results by varying t_{\min} by ± 1 . We found consistency within statistical errors.

To assign appropriate QCD quantum numbers to the extracted static-light baryon states, we follow a method introduced and explained in detail in [41], section 3.1 (“Method 1: solving a generalized eigenvalue problem”). For the n -th state the components of the corresponding eigenvector $v_{n,j}$ characterize the contribution of the j -th static-light baryon creation operator entering the correlation matrix. After transforming these operators from the twisted basis to the pseudo physical basis by means of the twist rotation $\psi = \exp(i\gamma_5\tau_3\omega/2)\chi$, $\omega = \pi/2$ (cf. the right columns of Table 3, Table 4 and Table 5), one expects and finds that for each extracted state operators corresponding to only one of the two QCD sectors corresponding to the investigated twisted mass lattice QCD sector clearly dominate, while the contribution from operators from the other sector are rather small. This allows to unambiguously assign a QCD label to each extracted static-light baryon state. An example, the identification of Ω_b ($S = -2, I = 0, j^P = 1^+$) and its parity partner ($S = -2, I = 0, j^P = 1^-$), is shown in Figure 2 (cf. also Figure 1 for the corresponding effective masses both having twisted mass quantum numbers ($S = -2, j = 1, I = 0$)).

Since static-light baryon masses diverge in the continuum limit due to the self energy of the static quark, we always consider mass differences of these baryons to the lightest static-light meson (“ B/B^* meson”). In such differences the divergent self energy exactly cancels. We take the mass

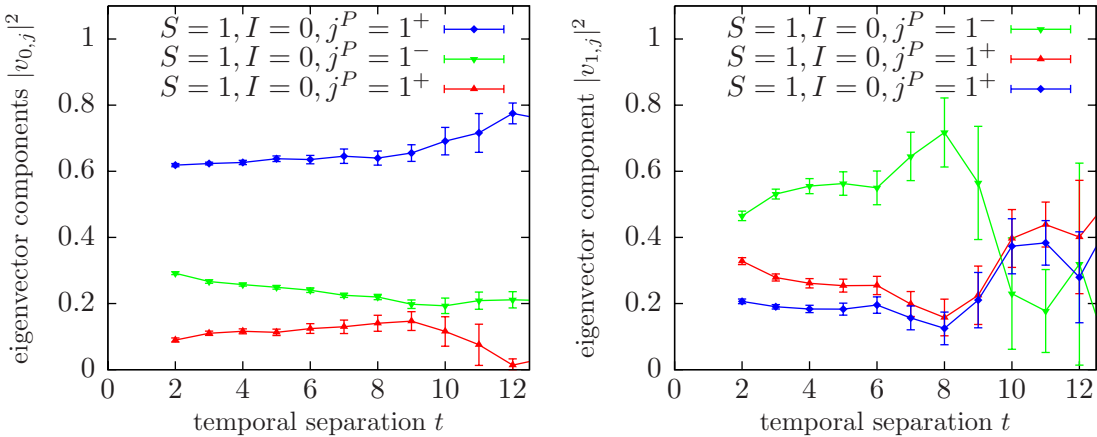


Figure 2: eigenvector components $|v_{n,j}|^2$ as functions of the temporal separation t and their associated QCD quantum numbers at light quark mass $\mu_q = 0.0040$ corresponding to the 3×3 correlation matrix with twisted mass quantum numbers ($S = -2, j = 1, I = 0$) (cf. also Figure 1); **left:** ground state identified as Ω_b ($S = -2, I = 0, j^P = 1^+$); **right:** first excited state identified as parity partner of Ω_b ($S = -2, I = 0, j^P = 1^-$).

values of the lightest static-light mesons from [25], where they have been computed using the same lattice setup. The mass differences $\Delta m^{\text{stat}}(S, I, j^P)a = (m(\text{baryon} : S, I, j^P) - m(B/B^*))a$ (in lattice units) together with the pion masses m_{PSA} (also in lattice units; cf. Table 1 and [33]) serve as input for the extrapolation procedure to the physical u/d quark mass described in the next subsection.

3.4 Extrapolation to the physical u/d quark mass

The mass differences $\Delta m^{\text{stat}}(S, I, j^P)a = (m(\text{baryon} : S, I, j^P) - m(B/B^*))a$ obtained for the four ensembles listed in Table 1, which only differ in the value of the u/d quark mass (both sea and valence), are plotted against $(m_{\text{PSA}})^2$ in Figure 3 ($S = 0, I = 0$, i.e. Λ baryons), Figure 4 ($S = 0, I = 1$, i.e. Σ baryons), Figure 5 ($S = -1$, i.e. Ξ baryons) and Figure 6 ($S = -2$, i.e. Ω baryons) and are collected in appendix A.

For the extrapolation to the physical u/d quark mass one could use an effective field theory approach (Chiral HQET for example) as used e.g. to study static-light meson decay constants [42]. However, this approach has not fully been developed to discuss mass differences $\Delta m^{\text{stat}}(S, I, j^P)a$ between excited static-light baryon states and the lightest static-light meson so is not appropriate here. Instead we use the simplest assumption, which is supported by our results: a linear dependence in $(m_{\text{PSA}})^2$.

Data points $((m_{\text{PSA}})^2, \Delta m^{\text{stat}}(S, I, j^P)a)$ are correlated via $(m_{\text{PSA}})^2$ in case they correspond to the same ensemble, i.e. to the same value of the u/d quark mass. We take that into account via a covariance matrix, which we estimate by resampling m_{PSA} and all extracted static-light mass differences $\Delta m^{\text{stat}}(S, I, j^P)a$ (10 000 000 samples). Consequently, we do not fit straight lines to the data points $((m_{\text{PSA}})^2, \Delta m^{\text{stat}}(S, I, j^P)a)$ individually for every static-light baryon state, but perform a single correlated fit of 23 straight lines to the 23 mass differences considered. During

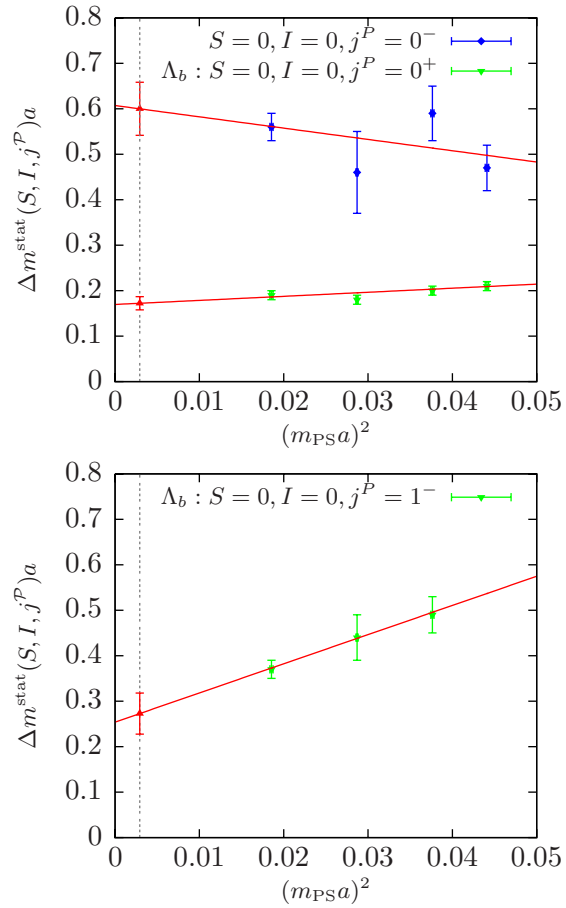


Figure 3: mass differences of $S = 0, I = 0$ static-light baryons (Λ baryons) to the lightest static-light meson as functions of $(m_{\text{PSA}})^2$; straight lines represent linear extrapolations to the physical u/d quark mass.

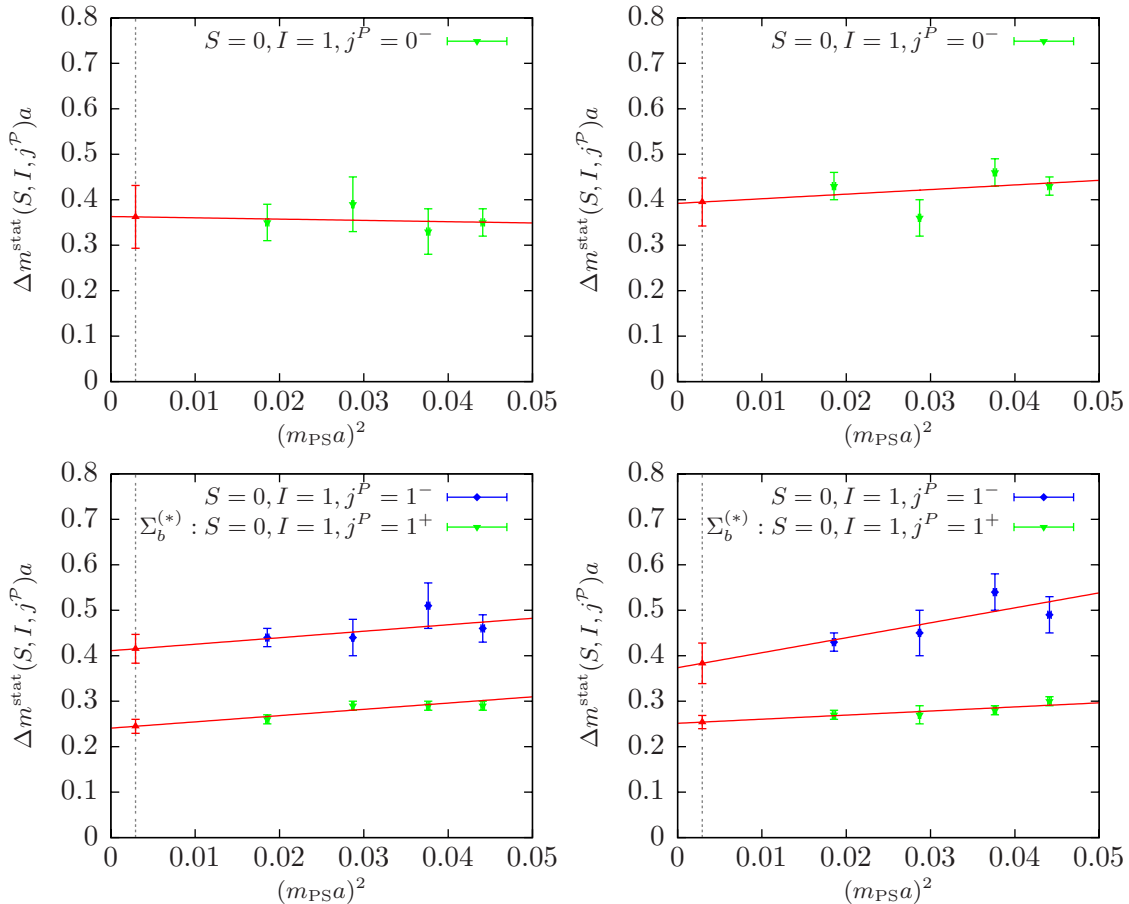


Figure 4: mass differences of $S = 0, I = 1$ static-light baryons (Σ baryons) to the lightest static-light meson as functions of $(m_{\text{PSA}})^2$; straight lines represent linear extrapolations to the physical u/d quark mass; plots in the same line only differ in I_z (**left**: $I_z = 0$; **right**: $I_z = \pm 1$).

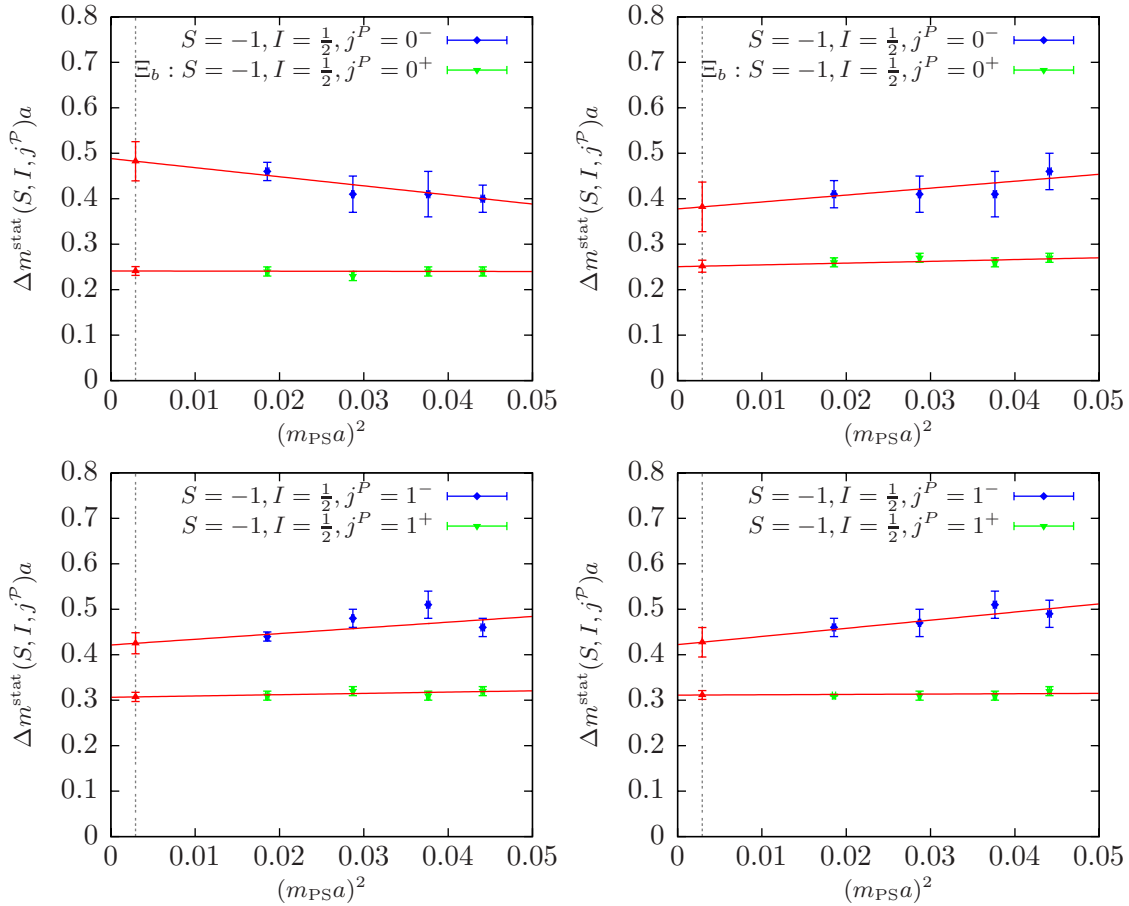


Figure 5: mass differences of $S = -1$ static-light baryons (Ξ baryons) to the lightest static-light meson as functions of $(m_{\text{PSA}})^2$; straight lines represent linear extrapolations to the physical u/d quark mass; plots in the same line only differ in the sign of the twisted mass term of the s valence quark (**left**: us^+/ds^- ; **right**: us^-/ds^+).

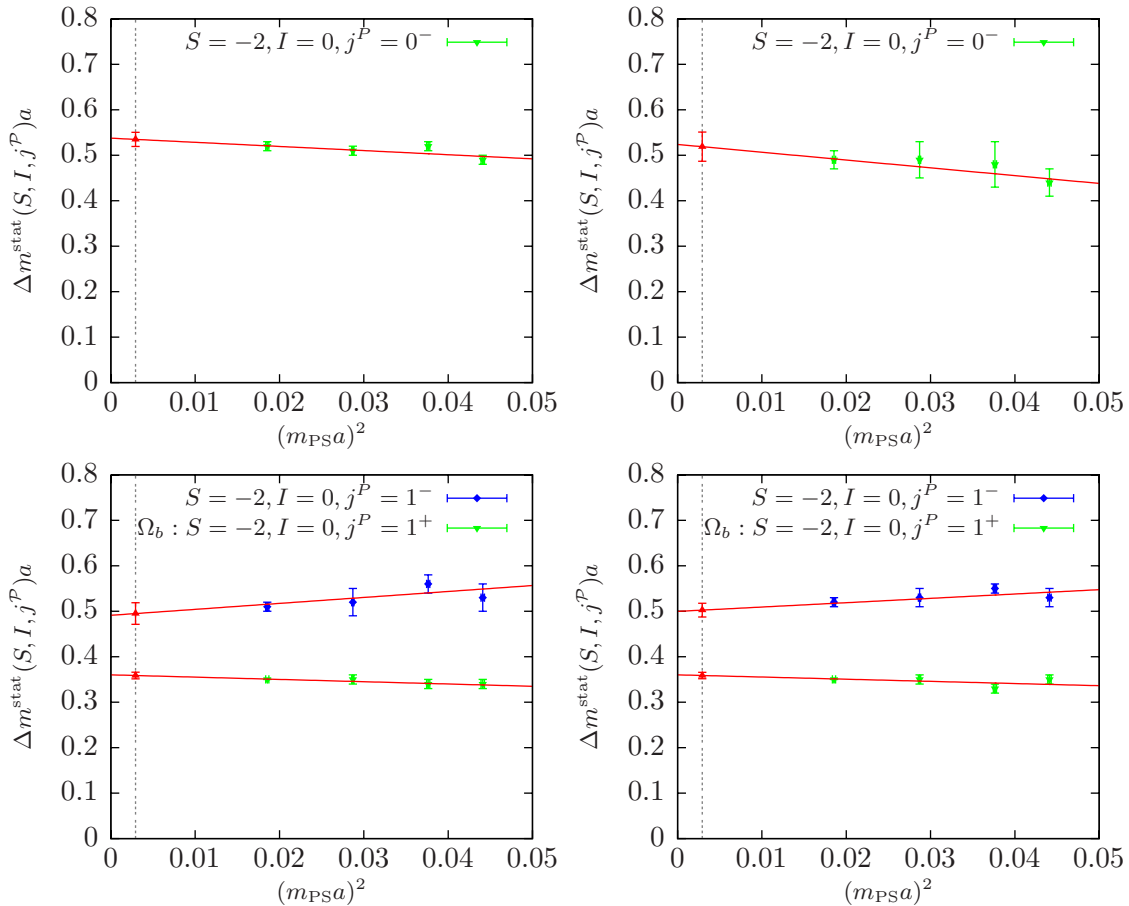


Figure 6: mass differences of $S = -2$ static-light baryons (Ω baryons) to the lightest static-light meson as functions of $(m_{\text{PSA}})^2$; straight lines represent linear extrapolations to the physical u/d quark mass; plots in the same line only differ in the signs of the twisted mass terms of the s valence quarks (**left**: s^+s^+/s^-s^- ; **right**: s^+s^-/s^-s^+).

the fitting we take statistical errors both along the horizontal axis (errors in m_{PSA}) and along the vertical axis (errors in $\Delta m^{\text{stat}}(S, I, j^{\mathcal{P}})a$) into account. The method for performing such two-dimensional fits is explained in detail in [25].

We find that a fit, which is linear in the light quark mass (represented by the mass squared of the light-light pseudoscalar meson $(m_{\text{PSA}})^2$) is acceptable, i.e. yields $\chi^2/\text{dof} \approx 0.59 \lesssim 1$. This fit enables us to extrapolate to the physical u/d quark mass, in this work taken as $m_{\text{PSA}} = 135 \text{ MeV}$ and converted to lattice units by using the lattice spacing $a = 0.079 \text{ fm}$ [33] resulting in $(m_{\text{PSA}})^2 = 0.054^2$ (cf. Figure 3, Figure 4, Figure 5 and Figure 6).

Extrapolations of static-light mass differences to the physical u/d quark mass are listed in Table 6 in MeV. Since there seems to be a controversy of around 10% regarding the value of the lattice spacing in physical units, when using on the one hand the pion mass m_π and the pion decay constant f_π and on the other hand the pion mass m_π and the nucleon mass m_N to set the scale ($a = 0.079(3) \text{ fm}$ [33] versus $a = 0.089(5) \text{ fm}$ [43]), we also list dimensionless ratios of static-light mass differences,

$$R^{\text{stat}}(S, I, j^{\mathcal{P}}) = \frac{\Delta m^{\text{stat}}(S, I, j^{\mathcal{P}})a}{\Delta m^{\text{stat}}(\Omega_b)a}. \quad (8)$$

These ratios are pretty independent of the lattice spacing and, therefore, preferable, when making predictions or when comparing to other lattice or model computations or to experimental results.

For static-light baryons with $S = -1$ and $S = -2$ our results depend on the bare s quark mass chosen. We use $\mu_{\text{q, valence}} s = 0.022$ taken from studies of strange-light mesons [34, 35] as mentioned in section 2. Possible systematic errors arising from a slightly incorrect value of the s quark mass are expected to be smaller than the corresponding statistical errors, because the mass differences we compute turn out to be rather weakly dependent on the masses of their light valence quarks (cf. Figure 3, Figure 4 and Figure 5). A possibility to estimate their magnitude for Ω_b is to estimate the slope of $m(\Omega_b)$ as a function of $\mu_{\text{q, valence}} s$ by means of the experimental results on $m(\Omega_b)$ and $m(\Sigma_b)$ and assuming a systematic error of 10% for the lattice spacing (i.e. roughly the difference obtained with the two scale setting methods [33, 43]). Then one arrives at a systematic error of around $0.1 \times (m(\Omega_b) - m(\Sigma_b)) \approx 23 \text{ MeV}$. This number is consistent with an even simpler method of estimation namely just taking a systematic error of $0.1 \times m_s$ for every s valence quark, where $m_s = 80 \text{ MeV} \dots 130 \text{ MeV}$ [47]. We intend to investigate the s quark dependence in more detail and to quantify the corresponding systematic error more precisely in a subsequent publication.

Static-light baryon states with $(S = 0, I = 1)$ and either $I_z = 0$ ($ud + du$) or $I_z = \pm 1$ (uu/dd) are not degenerate in twisted mass lattice QCD, but differ by discretization errors. These discretization errors are, however, only $\mathcal{O}(a^2)$ and, therefore, expected to be rather small. As can be seen from Table 6 $I_z = 0$ and $I_z = \pm 1$ states agree within statistical errors, which is a strong indication that discretization errors are indeed negligible. For the ratios $R^{\text{stat}}(S, I, j^{\mathcal{P}})$ and for interpolations to the physical b quark mass (cf. section 4) we subsequently use $I_z = 0$ results.

For $(S = -1, I = 1/2)$ static-light baryon states similar statements apply.

For static-light baryon states with two s quarks, i.e. $(S = -2, I = 0)$, the situation is somewhat different. On the operator level one should not use different lattice discretizations of the two s quarks, i.e. one twisted s^+ and one twisted s^- quark (for example the operator with $\Gamma = \gamma_5$,

S	I	j^P	name	flavor	Δm^{stat} in MeV, a from [33]	Δm^{stat} in MeV, a from [43]	R^{stat}	
0	0	0^+	Λ_b	$ud - du$	430(40)	382(39)	0.480(42)	
		0^-		$ud - du$	1499(156)	1330(149)	1.672(166)	
		1^-		$ud - du$	681(116)	605(106)	0.760(127)	
0	1	1^+	Σ_b, Σ_b^*	$ud + du$	611(45)	543(46)	0.682(45)	
		0^-		uu/dd	635(44)	563(45)		
				$ud + du$	905(176)	803(160)	1.010(194)	
				uu/dd	986(137)	876(127)		
		1^-		$ud + du$	1037(88)	921(87)	1.158(91)	
				uu/dd	957(117)	850(110)		
-1	$1/2$	0^+	Ξ_b	us^-/ds^+	602(33)	534(37)	0.672(30)	
		1^+		us^+/ds^-	629(41)	558(43)		
				us^-/ds^+	767(39)	681(44)	0.856(33)	
				us^+/ds^-	778(38)	690(44)		
		0^-		us^-/ds^+	1205(117)	1070(113)	1.351(123)	
				us^+/ds^-	954(141)	847(130)		
		1^-		us^-/ds^+	1062(71)	943(74)	1.185(69)	
				us^+/ds^-	1068(91)	948(89)		
-2	0	1^+	Ω_b	s^+s^+/s^-s^-	896(39)	795(48)	1	
		0^-		s^+s^-/s^-s^+	896(38)	795(47)		
				s^+s^+/s^-s^-	1336(64)	1186(75)	1.491(53)	
				s^+s^-/s^-s^+	1296(94)	1150(96)		
		1^-		s^+s^+/s^-s^-	1236(76)	1097(81)	1.380(72)	
				s^+s^-/s^-s^+	1255(61)	1114(71)		

Table 6: static-light mass differences $\Delta m^{\text{stat}}(S, I, j^P) = m(\text{baryon} : S, I, j^P) - m(B/B^*)$ in MeV (scale setting via m_π and f_π , $a = 0.079(3)$ fm [33], and via m_π and m_N , $a = 0.089(5)$ fm [43]) and dimensionless ratios of static-light mass differences (cf. (8)).

$\chi^{(1)}\chi^{(2)} = ss - ss$ clearly is identically zero, while $\Gamma = \gamma_5$, $\chi^{(1)}\chi^{(2)} = s^+s^- - s^-s^+$ would give a non-zero correlator, because there is no propagation from s^+ to s^-). Only on the level of correlators one can insert one s^+ lattice propagator and one s^- lattice propagator in a meaningful way. The corresponding masses are also listed in Table 6 and agree with their s^+s^+/s^-s^- counterparts. For the ratios $R^{\text{stat}}(S, I, j^P)$ and for interpolations to the physical b quark mass (cf. section 4) we subsequently use s^+s^+/s^-s^- results.

In principle contamination of some of the computed static-light baryon masses by multiparticle states (e.g. by a lighter static-light baryon and a pion) can at this stage not rigorously be excluded. However, from previous experience with similar lattice computations one strongly expects that the overlap of the used trial states to multiparticle states is extremely small and, therefore, that contamination of the obtained static-light baryon masses is negligible within statistical errors. A possibility to investigate this issue in detail is to compute matrix elements of two operators, where one is a “single particle baryon operator” and the other a “multiparticle operator” (cf. [44, 45, 46], where the method has been introduced and applied to glueballs and various types of mesons). Using this method we were e.g. able to confirm that the parity partner of the lightest static-light meson is essentially not affected by multiparticle states (cf. [25]).

Finally it is interesting to compare our static-light mass differences to recent results obtained by other lattice groups. In [8] three b baryon states, Λ_b , Σ_b/Σ_b^* and Ω_b , are computed. The method of scale setting used in this paper, imposing $r_0 = 0.49$ fm, can easily be applied to our lattice results, which are then in excellent agreement within statistical errors. Since in [9] and [10, 11] scale setting methods are used, which are less straightforward to adapt (via m_π , m_K and m_Ω and chiral perturbation theory [9] and via Υ [10, 11]), we directly compare the resulting mass differences in MeV. When comparing to those of our results corresponding to $a = 0.089(5)$ fm (i.e. scale setting via m_N), we also find agreement for all states computed in [9, 10, 11], Λ_b , Σ_b/Σ_b^* , Ξ_b , Ξ'_b ($S = -2$, $I = 1/2$, $j^P = 1^+$) and Ω_b .

We are also able to predict eight static-light baryon states of negative parity, for which no other lattice results seem to be available at the moment. Therefore, we compare these predictions to the quark model calculation in [23]. Also here we find agreement within statistical errors.

4 Interpolation to the physical b quark mass

To make contact with experimentally available results on the spectrum of b baryons, we need to correct for the finite mass of the b quark. In Heavy Quark Effective Theory the leading correction is $\mathcal{O}(1/m_Q)$, where m_Q is the mass of the heavy quark. It is possible in principle to compute such corrections from first principles by means of lattice QCD (cf. e.g. [21, 22]). This we intend to explore in the future, but here we use a more direct method, to establish the size of the correction between static quarks and b quarks of physically realistic mass.

We linearly interpolate in m_c/m_Q between our static-light lattice results and corresponding experimental data for charmed baryons. As a measure of the heavy quark mass m_Q we take the masses of the ground state heavy-light mesons (D or B), i.e. we interpolate to $m_c/m_b = m(D)/m(B) = 0.35$. This measure is equivalent to another (such as using quark masses in some scheme) to the order $1/m_Q$ we are considering. One test of this interpolation can be made: the hyperfine splitting between $\Sigma_c(2520)$ and $\Sigma_c(2455)$ is around 64 MeV; interpolating between this number and the static limit results in $0.35 \times 64 \text{ MeV} = 22 \text{ MeV}$, which is in fair agreement with the observed splitting of $m(\Sigma_b^*) - m(\Sigma_b) = 21 \text{ MeV}$ [47]. Results of these interpolations are collected in Table 7. Note that these m_c/m_Q corrections break the heavy spin degeneracy of static-light baryon states with $j = 1$.

4.1 Discussion of possible systematic errors

Our lattice results might be associated with certain systematic errors, which we list and briefly discuss in the following.

- Scale setting:
the dominating source of systematic error arises from the ambiguity introduced by the two methods of scale setting [33, 43], which is around 10%. Although it seems that the lattice spacing $a = 0.089(5) \text{ fm}$ determined by means of the nucleon mass seems more appropriate, when comparing to experimental results or to publications from other lattice collaborations (cf. section 3.4 and section 4.2), we strongly recommend to consider the dimensionless ratios $R^{\text{lat},b}$, where scale setting errors are essentially eliminated.
- Extrapolation to the physical u/d quark mass:
as explained in section 2 our results, which cover pion masses in the range $340 \text{ MeV} \lesssim m_{\text{PS}} \lesssim 525 \text{ MeV}$, are consistent with a linear dependence in $(m_{\text{PS}})^2$ for all static-light baryon states. Whether there are deviations at significantly lighter u/d quark masses, will be studied using corresponding ETMC gauge field configurations, which will be available soon.
- Possibly incorrect tuning of the s quark mass:
this issue has already been discussed in section 3.3, where we estimate the systematic error for static-light baryons with a single valence s quark to be around 10 MeV and for those with two valence s quarks to be around 20 MeV. Note that the extrapolation to the physical b quark mass by means of experimental results on c baryons reduces these errors by around 1/3.
- Extrapolation to the physical b quark mass:
the validity of the interpolation between static lattice results and charm experimental

S	I	J^P	b/c name	$\Delta m^{\text{lat},b}$ in MeV, a from [33]	$\Delta m^{\text{lat},b}$ in MeV, a from [43]	$\Delta m^{\text{exp},b}$ in MeV ¹	$R^{\text{lat},b}$	$R^{\text{exp},b}$ ¹
0	0	(1/2) ⁺	Λ_b/Λ_c	426(26)	395(25)	341(2)	0.489(27)	0.440(5)
		(1/2) ⁻	−/−	−	−	−	−	−
		(1/2) ⁻	−/ Λ_c (2595)	697(75)	648(69)	−	0.802(83)	−
		(3/2) ⁻	−/ Λ_c (2625)	709(75)	660(69)	−	0.816(83)	−
0	1	(1/2) ⁺	Σ_b/Σ_c (2455)	602(29)	558(30)	532(6)	0.691(30)	0.687(11)
		(3/2) ⁺	Σ_b^*/Σ_c (2520)	628(29)	584(30)	553(7)	0.718(30)	0.714(11)
		(1/2) ⁻	−/−	−	−	−	−	−
		(1/2) ⁻	−/−	−	−	−	−	−
		(3/2) ⁻	−/−	−	−	−	−	−
−1	1/2	(1/2) ⁺	Ξ_b/Ξ_c	602(21)	558(24)	511(3)	0.691(20)	0.660(8)
		(1/2) ⁺	−/ Ξ'_c	747(25)	691(29)	−	0.857(22)	−
		(3/2) ⁺	−/ Ξ_c (2645)	771(25)	715(29)	−	0.886(21)	−
		(1/2) ⁻	−/−	−	−	−	−	−
		(1/2) ⁻	−/ Ξ_c (2790)	1013(46)	936(48)	−	1.160(45)	−
		(3/2) ⁻	−/ Ξ_c (2815)	1023(46)	946(48)	−	1.172(45)	−
−2	0	(1/2) ⁺	Ω_b/Ω_c	872(25)	807(31)	775(8)	1	1
		(3/2) ⁺	−/ Ω_c (2770)	905(25)	839(31)	−	1.030(2) ²	−
		(1/2) ⁻	−/−	−	−	−	−	−
		(1/2) ⁻	−/−	−	−	−	−	−
		(3/2) ⁻	−/−	−	−	−	−	−

Table 7: b baryon mass differences $\Delta m(S, I, J^P) = m(\text{baryon} : S, I, J^P) - m(B)$ in MeV (scale setting via m_π and f_π , $a = 0.079(3)$ fm [33], and via m_π and m_N , $a = 0.089(5)$ fm [43]) and dimensionless ratios of baryon mass differences differences (cf. (8)); ¹ experimental results have been taken from [47] with exception of $m(\Omega_b)$, which has been taken from [5]; ² this number does not require any lattice result. Lines associated with quantum numbers, where no corresponding c baryons have experimentally been measured are filled with −.

results by the order $1/m_Q$ of HQET has been tested for baryons via Σ_b/Σ_b^* as explained above and for mesons via B/B^* [25]. These two tests indicate validity up to $\approx 5\%$. Since the hyperfine splitting in the b region is of order 20 MeV to 50 MeV (cf. e.g. B/B^* , B_1/B_2^* , Σ_b/Σ_b^* in [47]) one expects a corresponding systematic error of $\lesssim 2.5$ MeV.

- Electromagnetic and isospin breaking effects:
experimental results on Σ_b^- and Σ_b^+ indicate that such effects can be of order 5 MeV to 10 MeV.
- Neglect of s and c sea quarks:
the systematic error arising from our neglect of the s and c quark contribution to the sea is expected to be significantly smaller than current statistical errors. Will will address and quantify this error in a future study making use of recently generated $N_f = 2 + 1 + 1$ ETMC gauge field configurations [48, 49].
- Continuum limit:
since we use a rather fine lattice spacing and an $\mathcal{O}(a)$ improved lattice formulation (twisted mass lattice QCD at maximal twist), we expect discretization effects to be negligible. This expectation is supported by the computation and comparison of $I = 1$ states ($I_z = \pm 1$ versus $I_z = 0$), which are not degenerate in twisted mass lattice QCD, but differ by $\mathcal{O}(a^2)$. This constitutes a direct check of lattice discretization effects, for which we found no indication (cf. Table 6). Moreover, we have recently investigated the continuum limit for b mesons using the same gauge field configurations and also did not find any sign of discretization effects [25].
- Multiparticle states:
contamination of static-light baryon states by multiparticle states of the same quantum number have been discussed in section 3.3. It seems rather unlikely that they introduce a systematic error, which is significant compared to current statistical errors.

In total the sum of these systematic errors should not exceed 25 MeV, which is of the same order of magnitude as for our recent lattice results on B mesons [25], where we quoted a maximal systematic error of 20 MeV. An additional uncertainty of 10% should be assigned, when considering mass differences in MeV, i.e. $\Delta m^{\text{lat},b}(S, I, j^P)$. For the dimensionless ratios $R^{\text{lat},b}(S, I, j^P)$ collected in Table 7 the latter is not present, while the above mentioned 25 MeV translate to a systematic error of around 5%.

4.2 Comparison to experimental results

In experiments five b baryon states have been measured: Λ_b , Σ_b , Σ_b^* , Ξ_b and Ω_b . We compare our lattice results with these experimental results in Table 7. As already mentioned in the previous section the lattice spacing depends to some extent on the observables used to introduce physical units. While setting the scale via m_π and f_π [33] yields lattice results, which are around 10% to 20% larger than their experimental counterparts, using m_π and m_N [43] leads to significantly better agreement. To reduce scale setting effects as much as possible, we prefer to compare the dimensionless ratios $R^{\text{lat},b}(S, I, j^P)$ and $R^{\text{exp},b}(S, j^P, I)$, which have been defined in (8). While $R^{\text{exp},b}(S, I, j^P)$ denotes the ratio of experimentally measured b baryons, $R^{\text{lat},b}(S, I, j^P)$ is the linear m_c/m_Q interpolation between the static-light ratio from Table 6 and the corresponding

ratio of experimentally measured c baryons. As can be seen from Table 7, there is reasonable agreement between our lattice and experimental results for the four available ratios.

There are seven more b baryon states we are able to predict, but which have not yet been measured by experiment. Their values in MeV as well as the ratios $R^{\text{lat},b}(S, I, j^P)$ are also collected in Table 7.

5 Conclusions

We have computed the spectrum of static-light baryons by means of lattice QCD using $N_f = 2$ flavors of light quarks. We have considered all possible combinations of two light quarks, i.e. Λ , Σ , Ξ and Ω baryons, angular momentum/spin of the light degrees of freedom $j \in \{0, 1\}$ and both parity $\mathcal{P} = +$ and $\mathcal{P} = -$. In particular we were able to predict a number of negative parity states, which have at the moment neither been measured experimentally nor previously been computed on the lattice.

We have employed the assumption of a $1/m_Q$ dependence on the heavy quark mass together with experimental results for c baryons to allow us to estimate the spectrum that one would obtain for b quarks of finite physical mass.

The wide variety of computed states (both static-light baryons and b baryons) will be a valuable resource for model builders and might give input for future experiments.

Obvious directions to continue this research include (i) investigating the continuum limit; (ii) performing similar computations at lighter u/d quark masses; (iii) studying the dependence of Ξ and Ω baryons on the s quark mass; (iv) extending these computations to $N_f = 2 + 1 + 1$ flavor ETMC gauge field configurations [48, 49]; (v) considering non-trivial gluonic excitations allowing to study total angular momentum of the light degrees of freedom $j > 1$; (vi) replacing experimental input for c baryons by corresponding lattice results with heavy quarks of finite mass [50] and/or combining such results with a recently proposed method for lattice B physics [51] to compute the spectrum of b baryons in an alternative way.

A $\Delta m^{\text{stat}}(S, j^{\mathcal{P}}, I)a$ for all four ensembles

S	I	$j^{\mathcal{P}}$	flavor	$\Delta m^{\text{stat}}a,$ $\mu_q = 0.0040$	$\Delta m^{\text{stat}}a,$ $\mu_q = 0.0064$	$\Delta m^{\text{stat}}a,$ $\mu_q = 0.0085$	$\Delta m^{\text{stat}}a$ $\mu_q = 0.0100$
0	0	0^+	$ud - du$	0.1889(85)	0.1845(147)	0.2006(103)	0.2126(96)
		0^-	$ud - du$	0.5612(318)	0.4635(898)	0.5893(600)	0.4656(511)
		1^-	$ud - du$	0.3727(175)	0.4425(490)	0.4938(415)	—
0	1	0^-	$ud + du$	0.3519(440)	0.3878(635)	0.3336(516)	0.3524(291)
			uu/dd	0.4252(344)	0.3627(429)	0.4621(340)	0.4327(511)
		1^+	$ud + du$	0.2629(84)	0.2891(108)	0.2938(134)	0.2940(146)
			uu/dd	0.2697(79)	0.2696(194)	0.2777(121)	0.2988(128)
		1^-	$ud + du$	0.4376(162)	0.4365(393)	0.5141(472)	0.4616(314)
			uu/dd	0.4335(236)	0.4473(495)	0.5380(371)	0.4856(423)
-1	1/2	0^+	us^-/ds^+	0.2419(54)	0.2346(121)	0.2356(77)	0.2444(77)
			us^+/ds^-	0.2560(76)	0.2663(86)	0.2628(101)	0.2671(105)
		0^-	us^-/ds^+	0.4559(247)	0.4065(445)	0.4112(537)	0.4048(298)
			us^+/ds^-	0.4118(320)	0.4139(355)	0.4130(506)	0.4879(114)
		1^+	us^-/ds^+	0.3107(53)	0.3198(79)	0.3120(91)	0.3203(104)
			us^+/ds^-	0.3131(48)	0.3119(123)	0.3066(99)	0.3228(117)
		1^-	us^-/ds^+	0.4399(122)	0.4772(242)	0.5113(308)	0.4568(206)
			us^+/ds^-	0.4554(177)	0.4666(312)	0.5134(349)	0.4923(275)
-2	0	0^-	s^+s^+/s^-s^-	0.5195(90)	0.5070(143)	0.5198(122)	0.4879(114)
			s^+s^-/s^-s^+	0.4887(176)	0.4927(364)	0.4790(455)	0.4397(260)
		1^+	s^+s^+/s^-s^-	0.3508(34)	0.3488(86)	0.3357(80)	0.3422(94)
			s^+s^-/s^-s^+	0.3513(35)	0.3488(64)	0.3349(68)	0.3451(80)
		1^-	s^+s^+/s^-s^-	0.5150(117)	0.5177(287)	0.5650(235)	0.5281(272)
			s^+s^-/s^-s^+	0.5165(75)	0.5300(219)	0.5460(138)	0.5279(180)

Acknowledgments

It is a pleasure to thank Vladimir Galkin and Chris Michael for many hours of helpful discussions. We acknowledge further useful discussions with Jaume Carbonell, William Detmold, Karl Jansen, Andreas Kronfeld and Michael Müller-Preussker.

The major part of computations has been performed at the PC farm at DESY Zeuthen. We thank DESY as well as its staff for technical advice and help.

This work has been supported in part by the DFG Sonderforschungsbereich TR9 Computer-gestützte Theoretische Teilchenphysik.

References

- [1] T. Aaltonen *et al.* [CDF Collaboration], “First observation of heavy baryons Σ_b and Σ_b^* ,” Phys. Rev. Lett. **99**, 202001 (2007) [arXiv:0706.3868 [hep-ex]].
- [2] V. M. Abazov *et al.* [D0 Collaboration], “Direct observation of the strange b baryon Ξ_b^- ,” Phys. Rev. Lett. **99**, 052001 (2007) [arXiv:0706.1690 [hep-ex]].
- [3] T. Aaltonen *et al.* [CDF Collaboration], “Observation and mass measurement of the baryon Ξ_b^- ,” Phys. Rev. Lett. **99**, 052002 (2007) [arXiv:0707.0589 [hep-ex]].
- [4] V. M. Abazov *et al.* [D0 Collaboration], “Observation of the doubly strange b baryon Ω_b^- ,” Phys. Rev. Lett. **101**, 232002 (2008) [arXiv:0808.4142 [hep-ex]].
- [5] T. Aaltonen *et al.* [CDF Collaboration], “Observation of the Ω_b -baryon and measurement of the properties of the Ξ_b - and Ω_b -baryons,” Phys. Rev. D **80**, 072003 (2009) [arXiv:0905.3123 [hep-ex]].
- [6] C. Michael and J. Peisa [UKQCD Collaboration], “Maximal variance reduction for stochastic propagators with applications to the static quark spectrum,” Phys. Rev. D **58**, 034506 (1998) [arXiv:hep-lat/9802015].
- [7] W. Detmold, K. Orginos and M. J. Savage, “ BB potentials in quenched lattice QCD,” Phys. Rev. D **76**, 114503 (2007) [arXiv:hep-lat/0703009].
- [8] T. Burch, C. Hagen, C. B. Lang, M. Limmer and A. Schafer, “Excitations of single-beauty hadrons,” Phys. Rev. D **79**, 014504 (2009) [arXiv:0809.1103 [hep-lat]].
- [9] W. Detmold, C. J. Lin and M. Wingate, “Bottom hadron mass splittings in the static limit from 2+1 flavour lattice QCD,” Nucl. Phys. B **818**, 17 (2009) [arXiv:0812.2583 [hep-lat]].
- [10] H. W. Lin, S. D. Cohen, N. Mathur and K. Orginos, “Bottom-hadron mass splittings from static-quark action on 2+1-flavor lattices,” Phys. Rev. D **80**, 054027 (2009) [arXiv:0905.4120 [hep-lat]].
- [11] H. W. Lin, S. D. Cohen, L. Liu, N. Mathur, K. Orginos and A. Walker-Loud, “Heavy-Baryon Spectroscopy from Lattice QCD,” Comput. Phys. Commun. **182**, 24 (2011) [arXiv:1002.4710 [hep-lat]].

- [12] M. Neubert, “Heavy quark symmetry,” Phys. Rept. **245**, 259 (1994) [arXiv:hep-ph/9306320].
- [13] T. Mannel, “Heavy-quark effective field theory,” Rept. Prog. Phys. **60**, 1113 (1997).
- [14] R. Lewis and R. M. Woloshyn, “Bottom baryons from a dynamical lattice QCD simulation,” Phys. Rev. D **79**, 014502 (2009) [arXiv:0806.4783 [hep-lat]].
- [15] H. Na and S. Gottlieb, “Heavy baryon mass spectrum from lattice QCD with 2+1 dynamical sea quark flavors,” PoS **LATTICE2008**, 119 (2008) [arXiv:0812.1235 [hep-lat]].
- [16] S. Meinel, W. Detmold, C. J. Lin and M. Wingate, “Bottom hadrons from lattice QCD with domain wall and NRQCD fermions,” PoS **LAT2009**, 105 (2009) [arXiv:0909.3837 [hep-lat]].
- [17] B. A. Thacker and G. P. Lepage, “Heavy quark bound states in lattice QCD,” Phys. Rev. D **43**, 196 (1991).
- [18] R. Lewis, “Bottom and charmed hadron spectroscopy from lattice QCD,” arXiv:1010.0889 [hep-lat].
- [19] M. Bochicchio, G. Martinelli, C. R. Allton, C. T. Sachrajda and D. B. Carpenter, “Heavy quark spectroscopy on the lattice,” Nucl. Phys. B **372**, 403 (1992).
- [20] D. Guazzini, H. B. Meyer and R. Sommer [ALPHA Collaboration], “Non-perturbative renormalization of the chromo-magnetic operator in heavy quark effective theory and the B^*-B mass splitting,” JHEP **0710**, 081 (2007) [arXiv:0705.1809 [hep-lat]].
- [21] B. Blossier, M. della Morte, N. Garron and R. Sommer, “HQET at order $1/m$: I. Non-perturbative parameters in the quenched approximation,” JHEP **1006**, 002 (2010) [arXiv:1001.4783 [hep-lat]].
- [22] B. Blossier, M. Della Morte, N. Garron, G. von Hippel, T. Mendes, H. Simma and R. Sommer [Alpha Collaboration], “HQET at order $1/m$: II. Spectroscopy in the quenched approximation,” JHEP **1005**, 074 (2010) [arXiv:1004.2661 [hep-lat]].
- [23] D. Ebert, R. N. Faustov and V. O. Galkin, “Masses of excited heavy baryons in the relativistic quark model,” Phys. Lett. B **659**, 612 (2008) [arXiv:0705.2957 [hep-ph]].
- [24] K. Jansen, C. Michael, A. Shindler and M. Wagner [ETM Collaboration], “The static-light meson spectrum from twisted mass lattice QCD,” JHEP **0812**, 058 (2008) [arXiv:0810.1843 [hep-lat]].
- [25] C. Michael, A. Shindler and M. Wagner [ETM Collaboration], “The continuum limit of the static-light meson spectrum,” JHEP **1008**, 009 (2010) [arXiv:1004.4235 [hep-lat]].
- [26] M. Wagner and C. Wiese [ETM Collaboration], “The Spectrum of static-light baryons in twisted mass lattice QCD,” PoS **LATTICE2010**, 130 (2010) [arXiv:1008.0653 [hep-lat]].
- [27] P. Weisz, “Continuum limit improved lattice action for pure Yang-Mills theory. 1,” Nucl. Phys. B **212**, 1 (1983).

- [28] R. Frezzotti, P. A. Grassi, S. Sint and P. Weisz [Alpha collaboration], “Lattice QCD with a chirally twisted mass term,” JHEP **0108**, 058 (2001) [arXiv:hep-lat/0101001].
- [29] R. Frezzotti and G. C. Rossi, “Chirally improving Wilson fermions. 1. $\mathcal{O}(a)$ improvement,” JHEP **0408**, 007 (2004) [arXiv:hep-lat/0306014].
- [30] R. Frezzotti and G. C. Rossi, “Chirally improving Wilson fermions. 2. Four-quark operators,” JHEP **0410**, 070 (2004) [arXiv:hep-lat/0407002].
- [31] A. Shindler, “Twisted mass lattice QCD,” Phys. Rept. **461**, 37 (2008) [arXiv:0707.4093 [hep-lat]].
- [32] P. Boucaud *et al.* [ETM Collaboration], “Dynamical twisted mass fermions with light quarks: simulation and analysis details,” Comput. Phys. Commun. **179**, 695 (2008) [arXiv:0803.0224 [hep-lat]].
- [33] R. Baron *et al.* [ETM Collaboration], “Light meson physics from maximally twisted mass lattice QCD,” JHEP **1008**, 097 (2010) [arXiv:0911.5061 [hep-lat]].
- [34] B. Blossier *et al.* [ETM Collaboration], “Light quark masses and pseudoscalar decay constants from $N_f = 2$ Lattice QCD with twisted mass fermions,” JHEP **0804**, 020 (2008) [arXiv:0709.4574 [hep-lat]].
- [35] B. Blossier *et al.* [ETM Collaboration], “Pseudoscalar decay constants of kaon and D -mesons from $N_f = 2$ twisted mass lattice QCD,” JHEP **0907**, 043 (2009) [arXiv:0904.0954 [hep-lat]].
- [36] A. Hasenfratz and F. Knechtli, “flavour symmetry and the static potential with hypercubic blocking,” Phys. Rev. D **64**, 034504 (2001) [arXiv:hep-lat/0103029].
- [37] M. Della Morte *et al.*, “Lattice HQET with exponentially improved statistical precision,” Phys. Lett. **B581**, 93, (2004) [arXiv:hep-lat/0307021].
- [38] M. Della Morte, A. Shindler and R. Sommer, “On lattice actions for static quarks,” JHEP **0508**, 051 (2005) [arXiv:hep-lat/0506008].
- [39] C. Michael, “Adjoint sources in lattice gauge theory,” Nucl. Phys. B **259**, 58 (1985).
- [40] B. Blossier, M. Della Morte, G. von Hippel, T. Mendes and R. Sommer, “On the generalized eigenvalue method for energies and matrix elements in lattice field theory,” JHEP **0904**, 094 (2009) [arXiv:0902.1265 [hep-lat]].
- [41] R. Baron *et al.* [ETM Collaboration], “Computing K and D meson masses with $N_f = 2+1+1$ twisted mass lattice QCD,” Comput. Phys. Commun. **182**, 299 (2011) [arXiv:1005.2042 [hep-lat]].
- [42] B. Blossier *et al.* [ETM Collaboration], “ f_B and f_{B_s} with maximally twisted Wilson fermions,” PoS **LAT2009**, 151 (2009) [arXiv:0911.3757 [hep-lat]].
- [43] C. Alexandrou *et al.* [ETM Collaboration], “Nucleon electromagnetic form factors in twisted mass lattice QCD,” arXiv:1102.2208 [hep-lat].

- [44] C. McNeile and C. Michael [UKQCD Collaboration], “Mixing of scalar glueballs and flavour-singlet scalar mesons,” Phys. Rev. D **63**, 114503 (2001) [arXiv:hep-lat/0010019].
- [45] C. McNeile, C. Michael and P. Pennanen [UKQCD Collaboration], “Hybrid meson decay from the lattice,” Phys. Rev. D **65**, 094505 (2002) [arXiv:hep-lat/0201006].
- [46] C. McNeile, C. Michael and G. Thompson [UKQCD Collaboration], “Hadronic decay of a scalar B meson from the lattice,” Phys. Rev. D **70**, 054501 (2004) [arXiv:hep-lat/0404010].
- [47] K. Nakamura *et al.* [Particle Data Group], J. Phys. G **37**, 075021 (2010).
- [48] R. Baron *et al.*, “Light hadrons from lattice QCD with light (u, d), strange and charm dynamical quarks,” JHEP **1006**, 111 (2010) [arXiv:1004.5284 [hep-lat]].
- [49] R. Baron *et al.*, “Light hadrons from $N_f = 2 + 1 + 1$ dynamical twisted mass fermions,” PoS **LATTICE2010**, 123 (2010) [arXiv:1101.0518 [hep-lat]].
- [50] M. Papinutto, J. Carbonell, V. Drach and C. Alexandrou, “Strange and charmed baryons using $N_f = 2$ twisted mass QCD,” PoS **LATTICE2010**, 120 (2010) [arXiv:1012.2786 [hep-lat]].
- [51] B. Blossier *et al.* [ETM Collaboration], “A proposal for B -physics on current lattices,” JHEP **1004**, 049 (2010) [arXiv:0909.3187 [hep-lat]].

ROM2F/2011/08, FTUAM-11-51, IFT-UAM/CSIC-11-53,
RM3-TH/11-4, HU-EP-11/29, SFB/CPP-11-35

Lattice QCD determination of m_b , f_B and f_{B_s} with twisted mass Wilson fermions



P. Dimopoulos^(a,b), R. Frezzotti^(a,b), G. Herdoiza^(c), V. Lubicz^(d,e),
C. Michael^(f), D. Palao^(b), G. C. Rossi^(a,b), F. Sanfilippo^(g),
A. Shindler^{(h)1}, S. Simula^(e), C. Tarantino^(d,e), M. Wagner^(h)

^(a) Dip. di Fisica, Università di Roma Tor Vergata, Via della Ricerca Scientifica, I-00133 Roma, Italy

^(b) INFN, Sez. di Roma Tor Vergata, Via della Ricerca Scientifica, I-00133 Roma, Italy

^(c) Departamento de Física Teórica and Instituto de Física Teórica UAM/CSIC,
Universidad Autónoma de Madrid, Cantoblanco, E-28049 Madrid, Spain

^(d) Dip. di Fisica, Università Roma Tre, Via della Vasca Navale 84, I-00146 Roma, Italy

^(e) INFN, Sez. di Roma Tre, Via della Vasca Navale 84, I-00146 Roma, Italy

^(f) Theoretical Physics Division, Dept. of Mathematical Sciences,
University of Liverpool, Liverpool L69 7ZL, United Kingdom

^(g) Laboratoire de Physique Théorique (Bat. 210), Université Paris Sud,
Centre d'Orsay, F-91405 Orsay-Cedex, France

^(h) Humboldt Universität zu Berlin, Newtonstrasse 15, D-12489, Berlin, Germany

Abstract

We present a lattice QCD determination of the b quark mass and of the B and B_s decay constants, performed with $N_f = 2$ twisted mass Wilson fermions, by simulating at four values of the lattice spacing. In order to study the b quark on the lattice, two methods are adopted in the present work, respectively based on suitable ratios with exactly known static limit and on the interpolation between relativistic data, evaluated in the charm mass region, and the static point, obtained by simulating the HQET on the lattice. The two methods provide results in good agreement. For the b quark mass in the $\overline{\text{MS}}$ scheme and for the decay constants we obtain $\overline{m}_b(\overline{m}_b) = 4.29(14)$ GeV, $f_B = 195(12)$ MeV, $f_{B_s} = 232(10)$ MeV and $f_{B_s}/f_B = 1.19(5)$. As a byproduct of the analysis we also obtain the results for the f_D and f_{D_s} decay constants: $f_D = 212(8)$ MeV, $f_{D_s} = 248(6)$ MeV and $f_{D_s}/f_D = 1.17(5)$.

¹Heisenberg Fellow

1 Introduction

The study of physical processes involving the b quark are of utmost importance for accurate tests of the Standard Model and for searching New Physics effects. On the experimental side, B-factories have played a fundamental role in the achievement of the present accuracy and further improvements are expected and looked forward from LHCb and the planned SuperB factories. It is therefore crucial to have theoretical uncertainties well under control, in particular those of the hadronic parameters computed on the lattice.

Two particularly important cases of study are the purely leptonic decays $B \rightarrow \tau\nu_\tau$ and $B_s \rightarrow \mu^+\mu^-$. The first process is particularly sensitive to potential New Physics contributions mediated, at tree level, by charged Higgs. The relevant entries in the Standard Model prediction for the decay rate are the CKM matrix element V_{ub} , which can be extracted from the study of semileptonic $B \rightarrow \pi \ell \nu_\ell$ decays without significant New Physics contributions (for $\ell = e, \mu$), and the pseudoscalar decay constant f_B . The measured values of the $B \rightarrow \tau\nu_\tau$ decay rate deviate, at present, by about 3 sigma from the Standard Model prediction [1, 2], within relatively large experimental and theoretical uncertainties. In this respect, improving the lattice determination of f_B would be an important ingredient for increasing the chances of detecting the contribution of New Physics effects to this decay. Another golden process for the detection of potentially large New Physics contributions is the rare leptonic decay $B_s \rightarrow \mu^+\mu^-$, which is being studied with unprecedented accuracy at LHCb. In this case, the relevant hadronic parameter to be determined on the lattice, which enters the theoretical prediction of the decay rate, is the pseudoscalar decay constant f_{B_s} . The determination of both f_B and f_{B_s} , together with a prediction for the b quark mass m_b , are the scope of the present study.

With the available computer power it is not possible to simulate quark masses in the range of the physical b mass keeping, at the same time, finite volume and discretization effects under control. In order to circumvent these problems, many different methods have been proposed so far (see [3] for a recent review).

In [4] we performed an exploratory calculation of the b quark mass and the decay constants f_B and f_{B_s} by introducing suitable ratios having an exactly known static limit. In [5] a more standard method [6] was applied, using lattice QCD data with the heavy quark mass ranging from the charm region up to more than 3 GeV, together with the information coming from a calculation in the static limit point. In the following, we will refer to the two approaches as to the “ratio method” and the “interpolation method” respectively.

Here we update and finalize both the analyses, by implementing several improvements. We replace the preliminary values of the quark mass renormalization constants with the published results of [7]. We increase for some ensembles the statistics and we use more data, in particular, data at the finest lattice spacing ($\beta = 4.2$) are now included also in the analysis with the ratio method. The main improvement in the analysis based on the interpolation method consists in studying the dependence of the decay constants on the quark masses, instead of the meson masses, and performing the extrapolation to the continuum limit at fixed (reference) values of the heavy quark mass. This allows us to better disentangle discretization effects from the (physical) heavy quark mass dependence.

The use of the quark masses in the determination of f_B and f_{Bs} requires as input the value of the b quark mass, m_b , which we obtain from the ratio method.

Our results for the b quark mass in the $\overline{\text{MS}}$ scheme and for the decay constants (the latter obtained by averaging the results of the two methods) read

$$\overline{m}_b(\overline{m}_b) = 4.29(14) \text{ GeV},$$

$$f_B = 195(12) \text{ MeV}, \quad f_{Bs} = 232(10) \text{ MeV}, \quad \frac{f_{Bs}}{f_B} = 1.19(5), \quad (1)$$

which are in good agreement with our previous results [4, 5], but which have smaller uncertainties. In particular, with respect to the result $\overline{m}_b(\overline{m}_b) = 4.63(27) \text{ GeV}$ of [4], we obtain for the b quark mass a central value which is smaller by approximately one standard deviation and a reduction of the uncertainty by almost a factor two, mainly because of the improvement in the determination of the quark mass renormalization constant.

As a byproduct of the analysis we also obtain the results for the f_D and f_{Ds} decay constants

$$f_D = 212(8) \text{ MeV}, \quad f_{Ds} = 248(6) \text{ MeV}, \quad \frac{f_{Ds}}{f_D} = 1.17(5), \quad (2)$$

which update and improve our previous determination [8].

2 Simulation details

The calculation is based on the $N_f = 2$ gauge field configurations generated by the European Twisted Mass (ETM) Collaboration with the tree-level improved Symanzik gauge action [9] and the twisted mass quark action [10] at maximal twist, discussed in detail in [11]-[16]. We simulated $N_f = 2$ mass-degenerate dynamical quarks, whose mass is eventually extrapolated to the physical isospin averaged mass of the up and down quarks, $m_{u/d}$. The strange and charm quarks are quenched in the present calculation. In our lattice setup all physical quantities are $\mathcal{O}(a)$ improved [16], in particular cutoff effects related to the heavy quark mass μ_h are of order $a^2\mu_h^2$.

For further details of our simulations we refer to [17], where the same ensembles of gauge configurations were used. We recall here that data at four values of the lattice coupling, $\beta = \{3.80, 3.90, 4.05, 4.20\}$, are included in the analysis. The corresponding values of the lattice spacing, $a = \{0.098(3), 0.085(2), 0.067(2), 0.054(1)\}$ fm, have been determined in [17] together with $m_{u/d}$ using the physical values of the pion mass and decay constant as input. From [17] we also take the values of the average up/down and the strange quark masses, namely $\overline{m}_{u/d}(2 \text{ GeV}) = 3.6(2) \text{ MeV}$ and $\overline{m}_s(2 \text{ GeV}) = 95(6) \text{ MeV}$. For the quark mass renormalization constants $Z_\mu = Z_P^{-1}$ we use the results obtained in [7], i.e. $Z_P(\overline{\text{MS}}, 2 \text{ GeV}) = \{0.411(12), 0.437(7), 0.477(6), 0.501(20)\}$ at the four beta values (see also [17] for the estimate of Z_P at $\beta = 4.20$).

At variance with [17], where only the light, strange and charm quark masses were studied, a wider range of values for the valence quark masses is considered here, in order

β	$a\mu_\ell$	$a\mu_s$	$a\mu_h$	t_{min}/a
3.80	0.0080, 0.0110	0.0165, 0.0200 0.0250	0.2143, 0.2406, 0.2701, 0.3032 0.3403, 0.3819, 0.4287, 0.4812	14
3.90	0.0030, 0.0040, 0.0064, 0.0085, 0.0100	0.0150, 0.0180 0.0220	0.2049, 0.2300, 0.2582, 0.2898 0.3253, 0.3651, 0.4098, 0.4600	16
4.05	0.0030, 0.0060, 0.0080	0.0135, 0.0150, 0.0180	0.1663, 0.1867, 0.2096, 0.2352 0.2640, 0.2963, 0.3326, 0.3733	21
4.20	0.0020, 0.0065	0.0130, 0.0148 0.0180	0.1477, 0.1699, 0.1954, 0.2247 0.2584, 0.2971, 0.3417	25

Table 1: Values of simulated bare quark masses in lattice units, for the four β values, in the light ($a\mu_\ell$), strange ($a\mu_s$) and heavy ($a\mu_h$) sectors. In the last column the minimum values of time t_{min} chosen for the 2-point function fits are collected.

to get closer to the physical b quark mass. The values of the simulated valence quark masses are collected in Table 1. The values of the valence light quark mass, μ_ℓ , are always taken identical to those of their sea counterparts. The heavy quark mass μ_h ranges from approximately m_c up to $2.3 - 2.4 m_c$, being m_c the physical charm quark mass. Correlators at higher μ_h values have been simulated and were included in [5]. They are characterized by large fluctuations in the effective mass plateaux, and thus by large statistical uncertainties. As a consequence, these data turn out to be irrelevant in the fits, and we have excluded them from the present analysis.

We now proceed to describe the two approaches adopted in the present work to study the B -physics observables, namely the ratio method of [4] and the interpolation method.

3 Ratio method

3.1 The b quark mass

The b quark mass is obtained by implementing the ratio method of [4], briefly recalled hereafter. The method is suggested by the HQET asymptotic behavior of the heavy-light meson mass $M_{h\ell}$,

$$\lim_{\mu_h^{\text{pole}} \rightarrow \infty} \left(\frac{M_{h\ell}}{\mu_h^{\text{pole}}} \right) = \text{constant ,} \quad (3)$$

where μ_h^{pole} is the pole quark mass and the limit (3) is approached without corrections of $\mathcal{O}(1/\log(\mu_h^{\text{pole}}/\Lambda_{\text{QCD}}))$. The first step is to consider an appropriate sequence of heavy

quark masses, $\bar{\mu}_h^{(1)}, \bar{\mu}_h^{(2)}, \dots, \bar{\mu}_h^{(N)}$, with fixed ratio

$$\frac{\bar{\mu}_h^{(n)}}{\bar{\mu}_h^{(n-1)}} = \lambda , \quad (4)$$

and ranging from the charm mass to values somewhat below the bottom mass. Here and in the following we denote by a “bar” the quark masses renormalized in the \overline{MS} scheme and, if not otherwise specified, a renormalization scale of 2 GeV is implied.

Then one computes the following ratios that have an exactly known static limit,

$$\begin{aligned} y(\bar{\mu}_h^{(n)}, \lambda; \bar{\mu}_\ell, a) &\equiv \frac{M_{h\ell}(\bar{\mu}_h^{(n)}; \bar{\mu}_\ell, a)}{M_{h\ell}(\bar{\mu}_h^{(n-1)}; \bar{\mu}_\ell, a)} \cdot \frac{\bar{\mu}_h^{(n-1)}}{\bar{\mu}_h^{(n)}} \cdot \frac{\rho(\bar{\mu}_h^{(n-1)}, \mu^*)}{\rho(\bar{\mu}_h^{(n)}, \mu^*)} = \\ &= \lambda^{-1} \frac{M_{h\ell}(\bar{\mu}_h^{(n)}; \bar{\mu}_\ell, a)}{M_{h\ell}(\bar{\mu}_h^{(n)}/\lambda; \bar{\mu}_\ell, a)} \cdot \frac{\rho(\bar{\mu}_h^{(n)}/\lambda, \mu^*)}{\rho(\bar{\mu}_h^{(n)}, \mu^*)}, \quad n = 2, \dots, N . \end{aligned} \quad (5)$$

The function $\rho(\bar{\mu}_h, \mu^*)$ is the factor that converts the renormalized \overline{MS} quark mass (at the scale μ^*) into the pole mass,

$$\mu_h^{\text{pole}} = \rho(\bar{\mu}_h, \mu^*) \bar{\mu}_h(\mu^*) , \quad (6)$$

known up to $N^3\text{LO}$ in perturbation theory [18, 19]. The NLO expression reads

$$\begin{aligned} \rho(\bar{\mu}_h, \mu^*) &= \left[1 + \frac{16}{3} \cdot \frac{\alpha^{\overline{\text{MS}}}(\bar{\mu}_h)}{4\pi} \right] \cdot \left(\frac{\alpha^{\overline{\text{MS}}}(\bar{\mu}_h)}{\alpha^{\overline{\text{MS}}}(\mu^*)} \right)^{12/(33-2N_f)} \cdot \\ &\quad \left[1 + \left(\frac{2(4491 - 252N_f + 20N_f^2)}{3(33-2N_f)^2} \right) \frac{\alpha^{\overline{\text{MS}}}(\bar{\mu}_h) - \alpha^{\overline{\text{MS}}}(\mu^*)}{4\pi} \right] , \end{aligned} \quad (7)$$

used for $N_f = 2$ in the present analysis. We notice that the dependence on the scale μ^* cancels in the ratios of ρ factors evaluated at different heavy quark masses and thus in the y ratio defined in eq. (5).

From eq. (3) and QCD asymptotic freedom it follows that the ratios (5) have the following static limit:

$$\lim_{\bar{\mu}_h \rightarrow \infty} y(\bar{\mu}_h, \lambda; \bar{\mu}_\ell, a = 0) = 1 . \quad (8)$$

The value of the ratio λ of eq. (4), between two subsequent values of the heavy quark mass, is chosen in such a way that after a finite number of steps the heavy-light meson mass assumes the experimental value $M_B = 5.279$ GeV (we find $\lambda = 1.1762$). In order to implement this condition, the lattice data at the four lattice spacings are interpolated at the following values of the heavy quark mass,

$$\begin{aligned} \bar{\mu}_h^{(1)} &= 1.140 \text{ GeV} , \quad \bar{\mu}_h^{(2)} = \lambda \bar{\mu}_h^{(1)} = 1.341 \text{ GeV} , \quad \bar{\mu}_h^{(3)} = \lambda^2 \bar{\mu}_h^{(1)} = 1.577 \text{ GeV} , \\ \bar{\mu}_h^{(4)} &= \lambda^3 \bar{\mu}_h^{(1)} = 1.855 \text{ GeV} , \quad \bar{\mu}_h^{(5)} = \lambda^4 \bar{\mu}_h^{(1)} = 2.182 \text{ GeV} , \quad \bar{\mu}_h^{(6)} = \lambda^5 \bar{\mu}_h^{(1)} = 2.566 \text{ GeV} . \end{aligned} \quad (9)$$

Ratios of the kind defined in eq. (5) are introduced because, besides having an exactly known static limit, they are also expected [4] to have a smooth chiral and continuum limit,

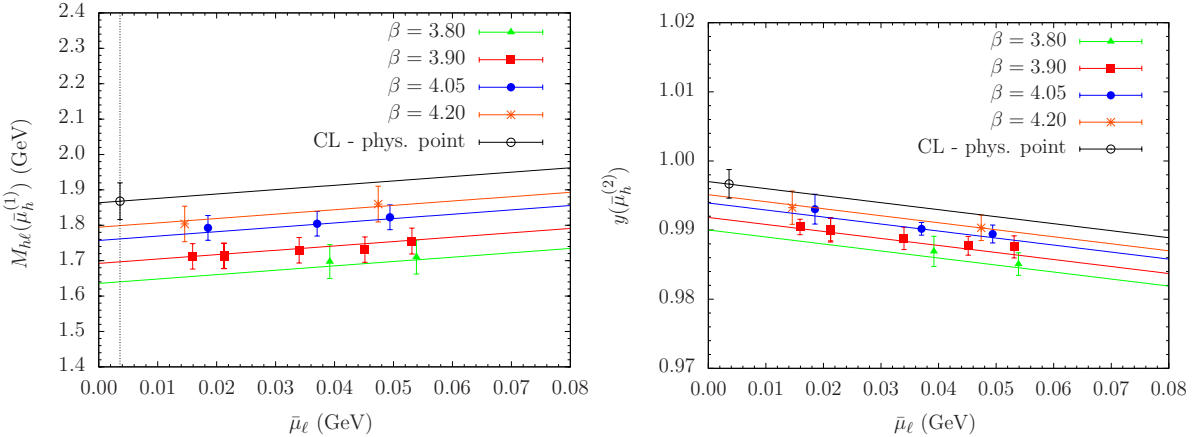


Figure 1: Light quark mass dependence of the meson mass $M_{hl}(\bar{\mu}_h^{(1)})$ (left) and of the ratio $y(\bar{\mu}_h^{(2)})$ (right) at the four values of the lattice spacing.

as shown in the right plot of fig. 1. In fig. 1 (left) we show the chiral and continuum extrapolation of the heavy-light meson mass evaluated at the first of our heavy quark masses $\bar{\mu}_h^{(1)}$, namely $M_{hl}(\bar{\mu}_h^{(1)})$, at the four available β values. We have considered the following (phenomenological) linear fit which, as shown in fig. 1, turns out to describe well the lattice data,

$$M_{hl}(\bar{\mu}_h^{(1)}) = C_1 + C_2 \bar{\mu}_l + C_3 a^2 . \quad (10)$$

After performing the continuum and chiral extrapolation of the ratios (5), we study their dependence on the inverse heavy quark mass. Inspired by HQET, we perform a polynomial fit in $1/\bar{\mu}_h$, of the form

$$y(\bar{\mu}_h) = 1 + \frac{\eta_1}{\bar{\mu}_h} + \frac{\eta_2}{\bar{\mu}_h^2} , \quad (11)$$

which imposes the constraint $y = 1$ at the static point. The fit is illustrated in fig. 2. A detailed discussion of the μ_h dependence of the ratio y , in comparison to the HQET expectation, is provided in the Appendix.

The value of the b quark mass is finally determined by considering the following equation

$$y(\bar{\mu}_h^{(2)}) y(\bar{\mu}_h^{(3)}) \dots y(\bar{\mu}_h^{(K+1)}) = \lambda^{-K} \frac{M_{hu/d}(\bar{\mu}_h^{(K+1)})}{M_{hu/d}(\bar{\mu}_h^{(1)})} \cdot \left[\frac{\rho(\bar{\mu}_h^{(1)}, \mu^*)}{\rho(\bar{\mu}_h^{(K+1)}, \mu^*)} \right] , \quad (12)$$

which should be looked at as a relation between the mass of the heavy-light meson, $M_{hu/d}(\bar{\mu}_h^{(K+1)})$, and the corresponding heavy quark mass $\bar{\mu}_h^{(K+1)}$, being $M_{hu/d}(\bar{\mu}_h^{(1)})$ the initial triggering value. The b quark mass is then determined by finding the value of K at which $M_{hu/d}(\bar{\mu}_h^{(K+1)})$ takes the experimental value of the B -meson mass, M_B . Calling K_b the solution of the resulting eq. (12) (we find $K_b = 9$), one gets for $\bar{\mu}_b = \bar{m}_b(2 \text{ GeV})$ the simple relation

$$\bar{\mu}_b = \lambda^{K_b} \bar{\mu}_h^{(1)} = 4.91(15) \text{ GeV} . \quad (13)$$

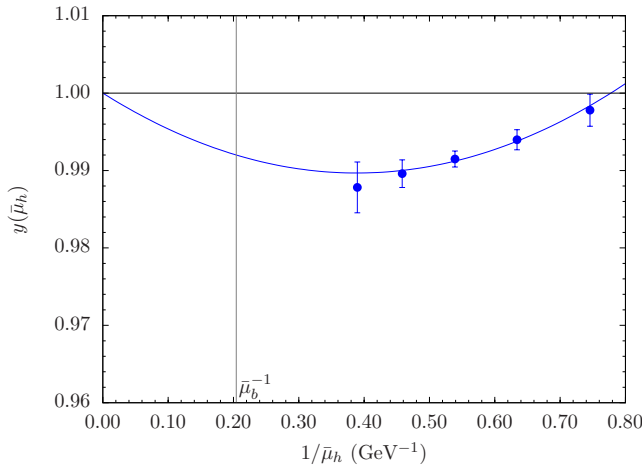


Figure 2: Heavy quark mass dependence of the ratio $y(\bar{\mu}_h)$ extrapolated to the physical value of the light quark mass and to the continuum limit. The vertical line represents the value of the physical b quark mass.

We observe that it is always possible to guarantee that the solution K_b is an integer number through a slight variation of the parameter λ and/or of the triggering mass $\bar{\mu}_h^{(1)}$.

An equivalent method consists in determining the b quark mass by studying M_{hs} instead of $M_{hu/d}$ and using in input the experimental B_s -meson mass value, $M_{Bs} = 5.366$ GeV. A very similar result is obtained from this analysis: $\bar{\mu}_b = 4.92(13)$ GeV. The small difference (0.01 GeV) with respect to eq. (13) indicates a good control of the chiral extrapolation which, in particular, in the heavy-strange meson case involves only the sea quark mass. The main effect of the uncertainty due the chiral extrapolation is accounted for by the error quoted in eq. (13), which comes from the chiral, continuum and $1/\mu_h$ fits.

In order to estimate the residual uncertainty due to discretization effects, we have tried to include in the continuum extrapolation, besides the leading $\mathcal{O}(a^2)$ correction, an additional a^4 term. We find, however, that this subleading contribution cannot be fitted with our data. Therefore, we have repeated the analysis by excluding the data at the coarsest lattice spacing ($\beta = 3.80$). The difference in the determination of the b quark mass turns out to be of 0.05 GeV.

In order to estimate the systematic error associated to the interpolation of $y(\bar{\mu}_h)$ as a function of $1/\bar{\mu}_h$, we have repeated the whole analysis by choosing a third order polynomial in $1/\bar{\mu}_h$ (rather than a second order one, as in the ansatz (11)). This change resulted in an increase of the b quark mass of about 0.5%, corresponding to a shift of $\simeq 0.02$ GeV of the central value result of eq. (13).

An additional uncertainty is introduced by the truncation of the perturbative series in the determination of the pole mass in eq. (6), which is affected by renormalon ambiguities. When comparing the results obtained with the NLO definition of the pole mass to the results found with the LO one, the difference in the b quark mass is found to be small, of about 0.01 GeV. The sensitivity to the pole mass definition, which appears in the intermediate steps, thus largely cancels out in the final determination.

We finally quote the b quark mass at the conventional renormalization scale of m_b itself

$$\bar{m}_b(m_b) = 4.29(13)(4) \text{ GeV} = 4.29(14) \text{ GeV}, \quad (14)$$

where the first error is of statistical and fitting origin and the second one is the sum in quadrature of the residual systematic uncertainties discussed above. The present result for the b quark mass has a central value which is smaller by approximately one standard deviation than the value found in [4], and an uncertainty which is reduced by almost a factor two, reflecting the various improvements implemented in the present analysis.

3.2 Decay constants

A similar strategy is employed by applying the ratio method to determine the B and B_s meson decay constants. The HQET asymptotic prediction for the decay constant is

$$\lim_{\mu_h^{\text{pole}} \rightarrow \infty} f_{h\ell} \sqrt{\mu_h^{\text{pole}}} = \text{constant}. \quad (15)$$

Therefore, the ratios with static limit equal to one of interest in this case are, for f_B and f_{B_s} , [4]

$$\begin{aligned} z(\bar{\mu}_h, \lambda; \bar{\mu}_\ell, a) &\equiv \lambda^{1/2} \frac{f_{h\ell}(\bar{\mu}_h, \bar{\mu}_\ell, a)}{f_{h\ell}(\bar{\mu}_h/\lambda, \bar{\mu}_\ell, a)} \cdot \frac{C_A^{\text{stat}}(\mu_b^*, \bar{\mu}_h/\lambda)}{C_A^{\text{stat}}(\mu_b^*, \bar{\mu}_h)} \frac{[\rho(\bar{\mu}_h, \mu^*)]^{1/2}}{[\rho(\bar{\mu}_h/\lambda, \mu^*)]^{1/2}} \\ z_s(\bar{\mu}_h, \lambda; \bar{\mu}_\ell, \bar{\mu}_s, a) &\equiv \lambda^{1/2} \frac{f_{hs}(\bar{\mu}_h, \bar{\mu}_\ell, \bar{\mu}_s, a)}{f_{hs}(\bar{\mu}_h/\lambda, \bar{\mu}_\ell, \bar{\mu}_s, a)} \cdot \frac{C_A^{\text{stat}}(\mu_b^*, \bar{\mu}_h/\lambda)}{C_A^{\text{stat}}(\mu_b^*, \bar{\mu}_h)} \frac{[\rho(\bar{\mu}_h, \mu^*)]^{1/2}}{[\rho(\bar{\mu}_h/\lambda, \mu^*)]^{1/2}}. \end{aligned} \quad (16)$$

The ratio of ρ factors (raised to the appropriate power) is present to convert \overline{MS} heavy quark masses to pole masses as in eq. (5). The factor $C_A^{\text{stat}}(\mu_b^*, \bar{\mu}_h)$, defined as

$$\Phi_{hs}(\mu_b^*) = [C_A^{\text{stat}}(\mu_b^*, \bar{\mu}_h)]^{-1} \cdot \Phi_{hs}^{\text{QCD}}(\bar{\mu}_h), \quad (17)$$

provides the matching between the decay constant in QCD for a heavy quark mass $\bar{\mu}_h$ and in HQET, and the running of the static axial current to the renormalization scale μ_b^* , and it is known up to N²LO in PT [20]. The NLO expression used in the present analysis reads

$$\begin{aligned} C_A^{\text{stat}}(\mu_b^*, \bar{\mu}_h) &= \left(\frac{\alpha^{\overline{\text{MS}}}(\bar{\mu}_h)}{\alpha^{\overline{\text{MS}}}(\mu_b^*)} \right)^{-\frac{6}{33-2N_f}} \cdot \left[1 - \left(\frac{-3951 + 300 N_f + 60 N_f^2 + (924 - 56 N_f)\pi^2}{9(33-2N_f)^2} \right) \right. \\ &\quad \left. \cdot \frac{\alpha^{\overline{\text{MS}}}(\bar{\mu}_h) - \alpha^{\overline{\text{MS}}}(\mu_b^*)}{4\pi} \right] \cdot \left[1 - \frac{8}{3} \frac{\alpha^{\overline{\text{MS}}}(\bar{\mu}_h)}{4\pi} \right], \end{aligned} \quad (18)$$

with $N_f = 2$.

In order to have better control on the chiral extrapolation, we consider as primary quantities in the present analysis the decay constant f_{B_s} , whose dependence on the light quark mass only occurs through sea effects, and the ratio f_{B_s}/f_B which provides a direct

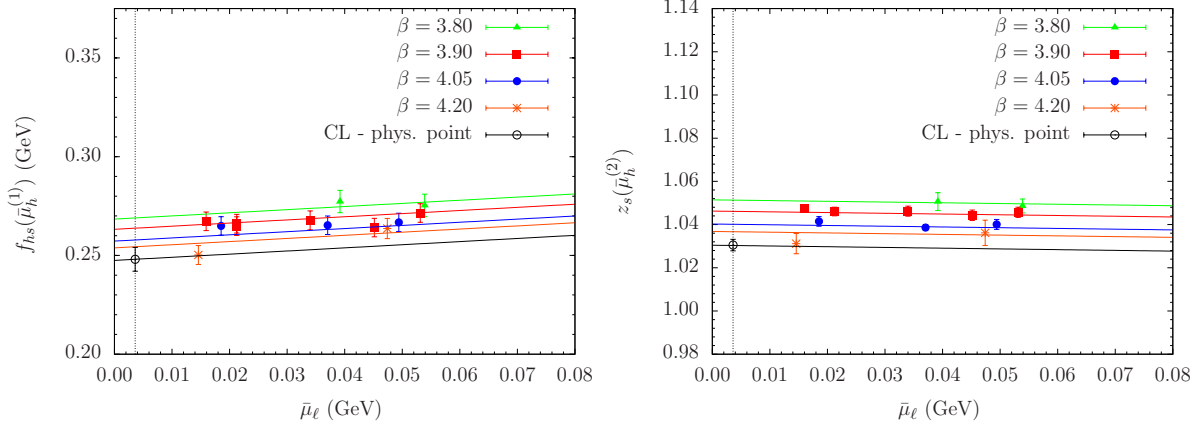


Figure 3: Light quark mass dependence of the decay constant $f_{hs}(\bar{\mu}_h^{(1)})$ (left) and of the ratio $z_s(\bar{\mu}_h^{(2)})$ (right) at the four values of the lattice spacing.

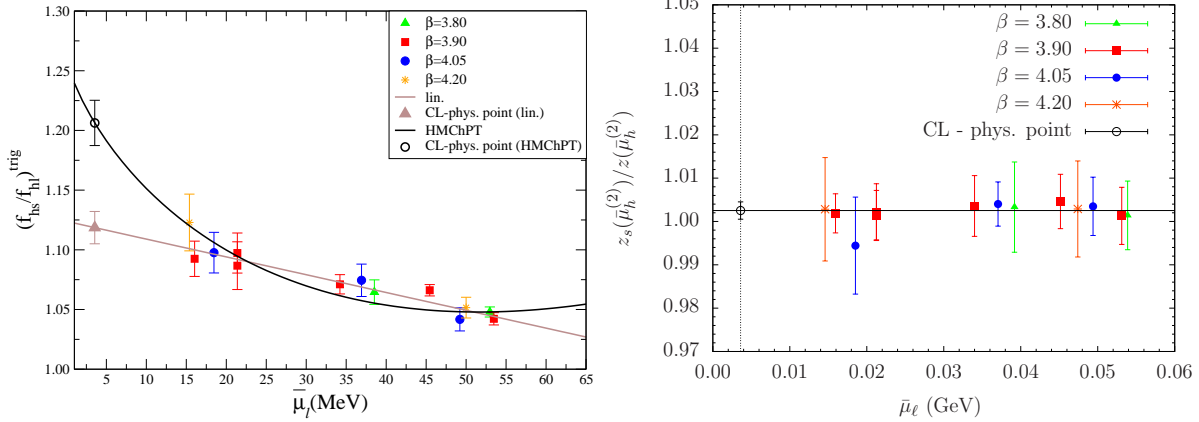


Figure 4: Light quark mass dependence of the ratio of decay constants $f_{hs}(\bar{\mu}_h^{(1)})/f_{hl}(\bar{\mu}_h^{(1)})$ (left) and of the double ratio $z_s(\bar{\mu}_h^{(2)})/z(\bar{\mu}_h^{(2)})$ (right) at the four values of the lattice spacing.

determination of the SU(3) breaking effect in the decay constant. Within the ratio method, these quantities are obtained from the ratio z_s and the double ratio z_s/z .

Both z_s and z_s/z have a smooth chiral and continuum limit, as illustrated in figs. 3 and 4. In particular, the results for the double ratio z_s/z turn out to be well described by both a linear and a constant behavior in both $\bar{\mu}_\ell$ and a^2 (see fig. 4 right). For simplicity reasons the constant fit ansatz was chosen. In the left panels of figs. 3 and 4 we show the chiral and continuum extrapolation of f_{hs} and $f_{hs}/f_{h\ell}$ at the initial (triggering) mass $\bar{\mu}_h^{(1)}$. For $f_{hs}/f_{h\ell}$, heavy meson chiral perturbation theory (HMChPT) predicts at the NLO a linear+logarithmic dependence on the light quark mass, since a chiral log controls the chiral behavior of f_B (see eq. (20) below). With our results, the logarithmic dependence cannot be appreciated, and we thus perform also a simpler linear fit in the light quark mass which turns out to describe well the lattice data. As discussed in section 5, we eventually average the results obtained from the HMChPT and the linear fits and include the difference in

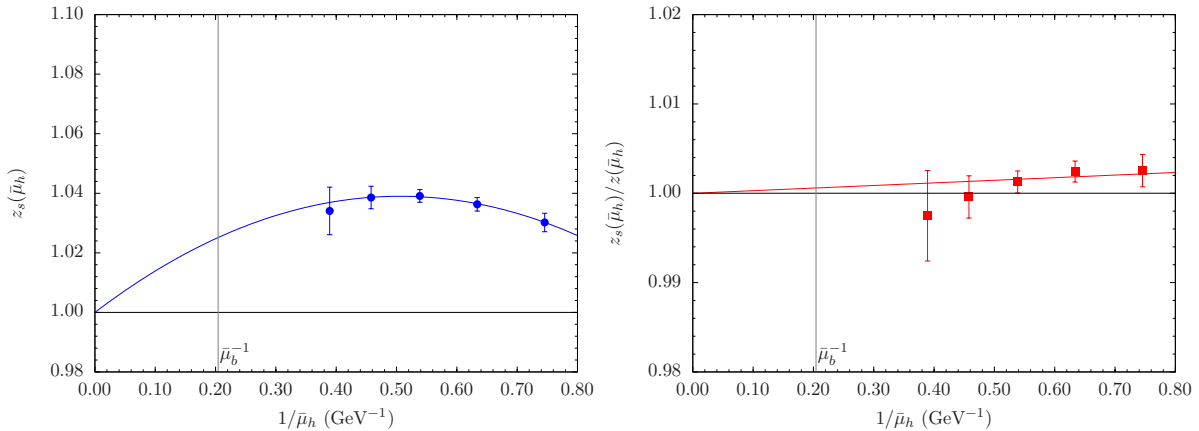


Figure 5: Heavy quark mass dependence of the ratio $z_s(\bar{\mu}_h)$ (left) and of the double ratio $z_s(\bar{\mu}_h)/z(\bar{\mu}_h)$ (right) extrapolated to the physical value of the light and strange quark masses and to the continuum limit. The vertical line represents the value of the physical b quark mass.

the systematic uncertainty. For f_{hs} , which depends on the light quark mass for sea effects only, we have implemented both a linear and a quadratic fit. They turn out to provide essentially identical results.

Finally, we study the dependence of the ratio z_s and the double ratio z_s/z on the heavy quark mass, which are shown in fig. 5. For z_s we perform a quadratic interpolation to the b quark mass as for the ratio $y(\bar{\mu}_h)$ in eq. (11) and, also in this case, a detailed discussion is provided in the Appendix. For z_s/z , the dependence on the heavy quark mass is barely visible, so that in this case we perform either a linear interpolation in $1/\bar{\mu}_h$ or we fix this ratio equal to its asymptotic heavy-quark mass limit, $z_s/z = 1$.

4 Interpolation method

As already mentioned, the interpolation method consists in interpolating to the b quark mass the relativistic results obtained for values of the heavy quark masses in the range around and above the physical charm (up to twice to three times its value) and the result evaluated in the static limit by simulating the HQET on the lattice. In this section, we describe these results by addressing, in turn, the calculation with relativistic lattice QCD in the charm mass region, the calculation within the HQET on the lattice, and the interpolation among the two sets of results.

4.1 Decay constants in relativistic QCD

The lattice relativistic data for the heavy-light and heavy-strange meson masses and decay constants are the same used for the ratio method. We considered in the analysis four values of the lattice spacing and the values of valence quark masses collected in Table 1. With respect to the preliminary results with this method presented in [5], we added an ensemble

with a lighter quark mass at $\beta = 4.2$ and, for other ensembles, we increased the statistics. Another update w.r.t to the analysis in [5] concerns the renormalization constants, which had preliminary values at the time of [5], and have been later updated and published in [7]. The main improvement, however, concerns the disentanglement of the heavy mass dependence from discretization effects. In the present analysis the extrapolation to the continuum limit is performed at fixed (renormalized) heavy quark mass. The whole analysis consists in the following steps.

First, we slightly interpolate the lattice data to reach a set of reference heavy quark masses equal at the four β values. This allows us to study discretization effects at fixed heavy quark mass. We have chosen the reference masses within the range of the simulated values. In the $\overline{\text{MS}}$ scheme, at $\mu = 2 \text{ GeV}$, the set of reference masses is $\bar{\mu}_h = \{1.25, 1.50, 1.75, 2.00, 2.25\} \text{ GeV}$.

We have then performed a combined continuum and chiral extrapolation, at fixed reference heavy quark mass. As for the ratio method, we consider as primary quantities f_{hs} and the ratio $f_{hs}/f_{h\ell}$ obtained in the present analysis from Φ_{hs} and $\Phi_{hs}/\Phi_{h\ell}$, where

$$\Phi_{hs} = f_{hs} \sqrt{M_{hs}} \quad \text{and} \quad \frac{\Phi_{hs}}{\Phi_{h\ell}} = \frac{f_{hs}}{f_{h\ell}} \sqrt{\frac{M_{hs}}{M_{h\ell}}}. \quad (19)$$

An alternative analysis based on the definition of $\Phi_{h\ell(s)}$ in terms of the pole mass, rather than the meson mass, i.e. $\Phi_{h\ell(s)} = f_{h\ell(s)} \sqrt{\mu_b^{\text{pole}}}$, has been also performed, leading to fully equivalent results.

The light quark mass dependence predicted for $\Phi_{h\ell}$ and Φ_{hs} by HMChPT [21, 22, 23] at the NLO reads

$$\begin{aligned} \Phi_{h\ell}(a, \bar{\mu}_\ell, \bar{\mu}_h) &= A_h \left[1 - \frac{3(1+3\hat{g}^2)}{4} \frac{2B_0 \bar{\mu}_\ell}{(4\pi f_0)^2} \log \left(\frac{2B_0 \bar{\mu}_\ell}{(4\pi f_0)^2} \right) + B_h \bar{\mu}_\ell + C_h a^2 \right], \\ \Phi_{hs}(a, \bar{\mu}_\ell, \bar{\mu}_s, \bar{\mu}_h) &= D_h (1 + E_h \bar{\mu}_\ell + F_h \bar{\mu}_s + G_h a^2), \end{aligned} \quad (20)$$

where we have also included in the above expressions a linear dependence on a^2 to account for leading discretization effects. The subscript h in the fit parameters of eq. (20) denotes the dependence on the heavy quark mass.

As previously discussed for the ratio method, the contribution of chiral logs in the ratio $\Phi_{hs}/\Phi_{h\ell}$, predicted by HMChPT, cannot be appreciated with our data (see fig. 4 left). Thus, in order to perform the chiral extrapolation to the physical light quark mass, we also perform a simple linear fit in $\bar{\mu}_\ell$ and eventually take the average of the two results. In the fit based on HMChPT, we take for the parameter \hat{g} the value $\hat{g} = 0.61(7)$ obtained from the experimental measurement of the $g_{D^*D\pi}$ coupling [24]. We choose this value, instead of the HQET prediction $\hat{g} = 0.44(8)$ [25, 26], as we fit data that are close to the charm mass region and in order to conservatively include in the average the maximum spread resulting from the different ways of performing the chiral extrapolation of our data. For Φ_{hs} , as for f_{hs} within the ratio method (see fig. 3 left), we have tried both a linear and a quadratic fit in $\bar{\mu}_\ell$, obtaining very similar results.

For illustration, the size of discretization effects in the calculation of Φ_{hs} is shown in fig. 6, for a simulated value of the light quark mass of about 50 MeV and with $\bar{\mu}_s \approx \bar{\mu}_s^{\text{phys}}$.

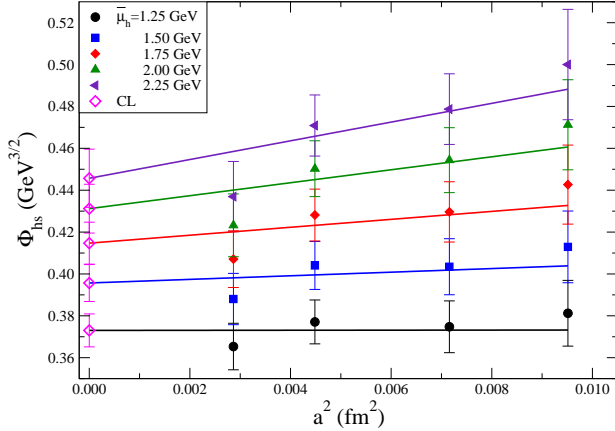


Figure 6: Dependence of Φ_{hs} on the squared lattice spacing, at the five reference values of the heavy quark mass (for a fixed value of the up/down and strange quark masses).

It is interesting to note that lattice artifacts turn out to be small. We find that this is a consequence of a partial cancellation between discretization terms in the decay constant and in the rooted meson mass, which are of similar size and opposite sign. For the same reason, the ratio $\Phi_{hs}/\Phi_{h\ell}$ turns out to be practically independent of the lattice spacing.

4.2 Decay constants in the static limit of HQET

We now summarize the procedure adopted to evaluate the static-light meson masses and decay constants, which follows and improves the analysis of [5]. We use the same setup as for the recent ETMC study of the static-light meson spectrum [27, 28]. Technical details regarding e.g. number of ETMC $N_f = 2$ gauge configurations considered, meson creation operators, corresponding correlation matrices and their analysis, smearing techniques to enhance the signal quality [29] as well as efficient propagator computation can be found in these references.

The lattice action used to describe the static quark is the HYP2 static action [29, 30, 31]

$$S_h = a^4 \sum_x \bar{\psi}_h(x) D_0 \psi_h(x) = a^3 \sum_x \bar{\psi}_h(x) [\psi_h(x) - V_{\text{HYP}}^\dagger(x - a\hat{0}, 0) \psi_h(x - a\hat{0})], \quad (21)$$

where V_{HYP} is the so-called HYP-link, which is a gauge covariant function of the gauge links located within a hypercube.

Static-light correlators have been calculated for a subset of the configuration ensembles used for the relativistic calculation, namely for two values of the lattice spacing, $\beta = 3.90$ and $\beta = 4.05$.

Due to the mixing between the pseudoscalar and the scalar currents occurring in the static-light framework, $\Phi_{B(s)}^{\text{stat}}$ is obtained as a linear combination of two matrix elements,

$$\Phi_{B_q}^{\text{stat}} = Z_P^{\text{stat}} \langle 0 | \bar{\psi}_h \gamma_5 \chi_q | B_{(q)}^{\text{stat}} \rangle + i r_q Z_S^{\text{stat}} \langle 0 | \bar{\psi}_h \chi_q | B_{(q)}^{\text{stat}} \rangle, \quad (22)$$

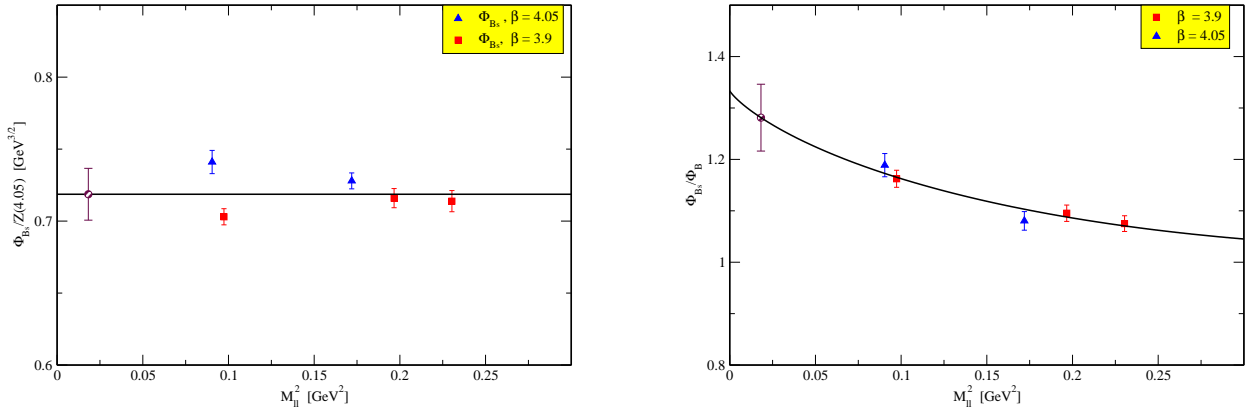


Figure 7: The combination $\Phi_{B_s}^{\text{stat}}/Z(4.05)$ (left), with $Z \equiv (Z_P^{\text{stat}} + Z_S^{\text{stat}})/2$, and the ratio $\frac{\Phi_{B_s}^{\text{stat}}}{\Phi_B^{\text{stat}}}$ (right) as a function of the (squared) light pseudoscalar meson mass. In the left plot the data at $\beta = 3.90$ have been multiplied by the appropriate factor to match the same scale for the data at $\beta = 4.05$.

where $\chi_q = e^{-ir_q(\pi/4)\gamma_5}\psi_q$ is the light quark field in the twisted basis, $r_q = \pm 1$ is the corresponding Wilson parameter, and Z_P^{stat} and Z_S^{stat} the static-light renormalization constants. In order to improve the signal quality of the lattice data we have combined the results with $r_q = +1$ and $r_q = -1$, which are identical on average due to twisted mass symmetries.

In order to check the stability of the fitting method to extract the above matrix elements, we have performed, as in [27], the computations with different parameters: number of states to be fitted in correlators, fitting time ranges, operator content of the correlation matrices. We have obtained results that are consistent within statistical errors.

For our setup (tree-level improved Symanzik gauge action and HYP2 static action) the non-perturbative values of the static-light renormalization constants are not available at present. We thus rely on the perturbative estimate at one loop [32] evaluated using a boosted coupling. It provides $Z_P^{\text{stat}} = \{0.85(8), 0.86(7)\}$ and $Z_S^{\text{stat}} = \{0.93(4), 0.94(3)\}$, at $\beta = \{3.90, 4.05\}$ respectively, in the $\overline{\text{MS}}$ scheme at the renormalization scale $1/a$. The uncertainty on $Z_{P,S}^{\text{stat}}$ has been conservatively estimated as half of the deviation from unity.

The chiral extrapolation of $\Phi_{B_s}^{\text{stat}}$ and $\Phi_{B_s}^{\text{stat}}/\Phi_B^{\text{stat}}$ has been performed, as for the relativistic data, using the HMChPT functional forms given in eq. (20), and it is shown in fig. 7 in terms of the light meson mass squared M_{ll}^2 . In this case, however, discretization terms are set to zero, as the fit includes data at only two values of the lattice spacing.

The matrix element shown in the left plot of fig. 7 is chosen to be, for better clarity, the ratio $\Phi_{B_s}^{\text{stat}}/Z$, where $Z = (Z_S^{\text{stat}} + Z_P^{\text{stat}})/2$. This quantity only depends on the ratio of renormalization constants, $Z_S^{\text{stat}}/Z_P^{\text{stat}}$, but not on their average. One can also show that the relative systematic errors due to inaccurate knowledge of $Z_S^{\text{stat}}/Z_P^{\text{stat}}$ on these matrix elements are $\Delta(Z_S^{\text{stat}}/Z_P^{\text{stat}}) \times \mathcal{O}(a)$, where $\Delta(Z_S^{\text{stat}}/Z_P^{\text{stat}})$ is the error on $Z_S^{\text{stat}}/Z_P^{\text{stat}}$ and $\mathcal{O}(a)$ denotes matrix elements which are proportional to the lattice spacing. Consequently,

the matrix elements shown in fig. 7 are only slightly affected by the systematic uncertainty on the renormalization constants due to the use of one-loop lattice perturbation theory. Of course the evaluation of Φ_{Bs}^{stat} at each lattice spacing requires the info on one renormalization constant, which is conveniently chosen as $(Z_S^{\text{stat}} + Z_P^{\text{stat}})/2$.

Fig. 7 shows that the chiral dependence on the light pseudoscalar mass is found to be very smooth for Φ_{Bs}^{stat} , and a simple constant fit is used to perform the chiral extrapolation. In order to estimate the uncertainty due to the chiral extrapolation, a linear fit is tried for comparison and the difference is included in the systematic error. For the ratio $\Phi_{Bs}^{\text{stat}}/\Phi_B^{\text{stat}}$, besides the fit based on HMChPT we have also considered both a linear (in M_u^2) and a quadratic fit. The variation of the result is found to be of the order of 5% and it is included in the systematic uncertainty.

It is clear from fig. 7 (right) that the data for the ratio $\Phi_{Bs}^{\text{stat}}/\Phi_B^{\text{stat}}$ are affected by negligible cut-off effects. Some discretization effects are visible, instead, in the left plot of fig. 7 which shows the results for Φ_{Bs}^{stat} . In order to estimate their magnitude we compare the results for Φ_{Bs}^{stat} obtained by either fitting together data at $\beta = 3.90$ and $\beta = 4.05$ or fitting data at one lattice spacing only. The difference, which turns out to be at the level of 3%, is included in the systematic uncertainty.

For Φ_{Bs}^{stat} the simulated (bare) strange quark mass is fixed to the values $a\mu_s = 0.0220$ at $\beta = 3.9$ and $a\mu_s = 0.0170$ at $\beta = 4.05$ respectively. These values correspond to the physical strange mass, as obtained from the analysis at fixed lattice spacing. The continuum limit performed in the study of [17] has later provided a value for the strange quark mass which is smaller by approximately 22% at $\beta = 3.9$ and 13% at $\beta = 4.05$. The effect of this mismatch is discussed in the following section and included in the systematic uncertainty.

As a last step in the analysis of the static data, a perturbative evolution at NLO [20] has been applied to evolve the results in the \overline{MS} scheme from the initial scale $\mu = 1/a$ to a common reference scale $\mu_b^* = 4.5$ GeV, obtaining

$$\Phi_{Bs}^{\text{stat}}(\mu_b^*) = 0.67(4) \text{ GeV}^{3/2} \quad \text{and} \quad \Phi_{Bs}^{\text{stat}}/\Phi_B^{\text{stat}} = 1.28(7). \quad (23)$$

For the B meson, eq. (23) corresponds to the result

$$\Phi_B^{\text{stat}}(\mu_b^*) = 0.52(3) \text{ GeV}^{3/2}. \quad (24)$$

As a further consistency check between the analyses based on the ratio and the interpolation methods, we have used the ratio method to predict the value of Φ_{Bs}/Φ_B in the static limit, finding $\Phi_{Bs}^{\text{stat}}/\Phi_B^{\text{stat}} = 1.20(5)$. The latter is compatible with the result in eq. (23) obtained from the direct lattice simulation in the HQET.

4.3 Interpolation of relativistic and static data

In order to perform a combined fit of relativistic and static data, we convert the relativistic values of Φ_{hs} from QCD to HQET, by using the NLO matching and evolution factor C_A^{stat} (see eqs.(17) and (18)). The renormalization scale is chosen to be $\mu_b^* = 4.5$ GeV as for the static data. Note that in the ratio $\Phi_{hs}/\Phi_{h\ell}$ the C_A^{stat} factor cancels out.

The interpolation is then performed, as shown in fig. 8, through a fit in $1/\bar{\mu}_h$, which is quadratic for Φ_{hs} (similarly to eq. (11)) and only linear for $\Phi_{hs}/\Phi_{h\ell}$, where a much

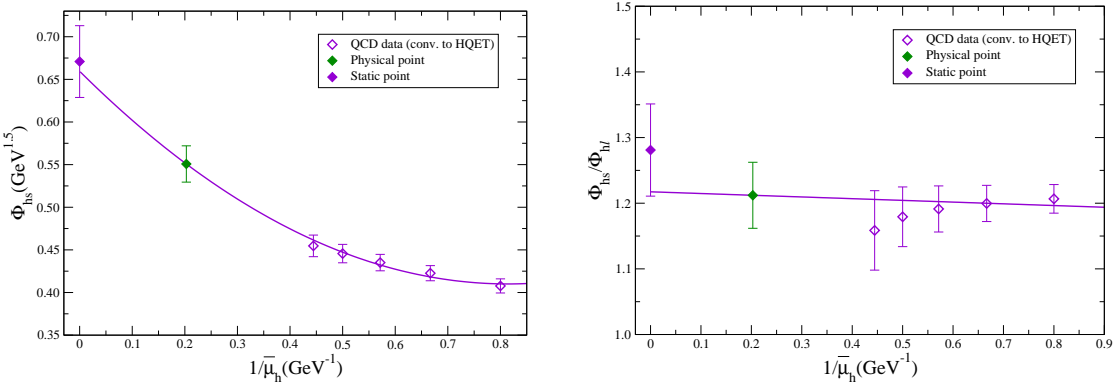


Figure 8: Dependence of Φ_{hs} (left) and $\Phi_{hs}/\Phi_{h\ell}$ (right), in the chiral and continuum limit, on the inverse of the heavy quark mass.

smoother dependence on the heavy quark mass is found, as expected. Finally, the physical results for the decay constants are obtained by inserting the “physical” value of the b quark mass determined from the ratio method, given in eqs. (13)-(14). The uncertainty on the b quark mass has been propagated by assuming a gaussian distribution of the errors.

5 Results for the decay constants

In this section we present and discuss the final results obtained for the decay constants f_{Bs} , f_{Bs}/f_B and f_B from the ratio and the interpolation methods.

As discussed in the previous sections, in order to estimate the uncertainty due to the chiral extrapolation we compare the results of two different chiral fits. This comparison is relevant in particular for the ratio $\Phi_{hs}/\Phi_{h\ell}$, from which Φ_{Bs}/Φ_B is extracted. In this case, the two fits are based either on the linear + logarithmic dependence on the light quark mass predicted by HMChPT (eq. (20)) or on a polynomial (quadratic) behavior. For Φ_{hs} we have tried both the linear fit of eq. (20) and a quadratic fit. The analogous chiral fit ansatz employed in the analysis of $f_{hs}(\bar{\mu}_h^{(1)})/f_{h\ell}(\bar{\mu}_h^{(1)})$ within the ratio method framework have been discussed in section 3.2. The results are collected in Table 2 for both the ratio and the interpolation method. The first error quoted in the table is the one coming from the fit, and includes both the statistical error and the systematic uncertainty due to the chiral and continuum extrapolation and to the interpolation to the b quark mass. The second error accounts for the additional systematic uncertainties and it has been evaluated as follows:

- Continuum limit: when performing the continuum limit, both in the ratio and the interpolation method, we consider a linear fit in a^2 . Since an additional a^4 term cannot be fitted with our data, we estimate the uncertainty due to discretization effects by excluding data at the coarsest lattice ($\beta = 3.80$). The central values for f_{Bs} change by 2 and 1 MeV for the ratio and the interpolation method respectively. The corresponding changes in the values of the ratio f_{Bs}/f_B are instead negligible.

f_{Bs} [MeV]				f_{Bs}/f_B			
Ratio Method		Interpol. Method		Ratio Method		Interpol. Method	
Lin.	Quad.	Lin.	Quad.	HMChPT	Polyn.	HMChPT	Polyn.
225(7)(4)	225(7)(4)	237(9)(4)	238(9)(4)	1.22(2)(0)	1.14(2)(0)	1.22(5)(2)	1.16(6)(2)
225(7)(4)		238(9)(4)		1.18(2)(4)		1.19(5)(3)	
232(10)				1.19(5)			

Table 2: Collection of the results obtained for f_{Bs} and f_{Bs}/f_B from the ratio and interpolation methods. The statistical and systematic uncertainties are summed in quadrature. The third and fourth lines provide info on the results obtained by extrapolating to the physical pion mass point by using different chiral fit ansatz (see text). The final values, given in the last row, are an average of the results of the two methods.

- Heavy mass dependence: Within the interpolation method we estimate the uncertainty in reaching the physical bottom mass by including, for each β , data at two larger values of μ_h , and by choosing slightly different values for the reference masses. We find that with these variations the central values obtained for f_{Bs} change by approximately 3 MeV, while the results for the ratio f_{Bs}/f_B are practically unaffected. In the context of the ratio method analysis in order to estimate the systematic error associated to the determination of $z_s(\bar{\mu}_b)$ we have varied the fit ansatz by considering either a second order or a third order polynomial in $1/\bar{\mu}_h$. This change produces only a 1 MeV decrease in the final value of $f_{Bs} \simeq 225$ MeV (see Table 2). Even smaller is the relative uncertainty in the $1/\bar{\mu}_h$ interpolation of the double ratio $z_s(\bar{\mu}_h)/z(\bar{\mu}_h)$, owing to the very flat profile of data within errors, as it is seen from fig. 5 (right).
- Pole mass: as the pole mass is affected by renormalon ambiguities, in the analysis based on the ratio method we compare the results obtained by using the NLO definition of the pole mass to the results found with the LO definition. Within the interpolation method, instead, we have also considered the alternative definition of $\Phi_{h\ell(s)}$ in terms of the pole mass (rather than the meson mass), again using either the NLO or the LO definition of the pole mass. In both cases, the differences are found to be small, at the level of 1 MeV, for the decay constants, as the sensitivity to the pole mass definition, which appears in the intermediate steps of the calculation, largely cancels out in the final determinations. The results for the ratio f_{Bs}/f_B are practically unaffected.
- Mismatch of the strange quark mass in the static simulation: as discussed in section 4.2, the static-strange correlators have been calculated with a value of the strange quark mass that was estimated from an analysis at fixed lattice spacing, and turned out to be larger with respect to the continuum limit estimate by approximately 22% at $\beta = 3.9$ and 13% at $\beta = 4.05$. In order to evaluate the systematic uncertainty due to this mismatch, we have analyzed the relativistic data for Φ_{hs} which are available

at several values of the strange quark mass. By using the continuum estimate of the strange quark mass, Φ_{B_s} decreases by approximately 2%. A similar effect can be thus expected for the static data. We have thus repeated the interpolation to the b quark mass using for the static points results smaller by 2%. We find that the B_s decay constant decreases by 3 MeV and f_{B_s}/f_B by 0.015. We conservatively ignore the sign of the variation and consider these changes as a symmetric contribution to the systematic uncertainty. This uncertainty does not affect the ratio method, since in this case the static limit of z_s and z_s/z is exactly known.

For both methods we add in quadrature the systematic uncertainties and, finally, as shown in the last row of Table 2, we average the results of the two methods obtaining

$$f_{B_s} = 232(10) \text{ MeV}, \quad \frac{f_{B_s}}{f_B} = 1.19(5), \quad (25)$$

and for the B decay constant, which is determined for each analysis as $f_B = f_{B_s}/(f_{B_s}/f_B)$,

$$f_B = 195(12) \text{ MeV}. \quad (26)$$

These values are in agreement and improve the results obtained in [4] and [5].

As a byproduct of the analysis we also obtain the decay constants for the D and D_s mesons. In order to determine these quantities, we only consider three values for the heavy quark reference masses around the physical charm quark mass. By interpolating to the physical value $\overline{m}_c(\overline{m}_c) = 1.28(4)$ GeV, obtained in [5], we find

$$f_D = 212(8) \text{ MeV}, \quad f_{D_s} = 248(6) \text{ MeV}, \quad \frac{f_{D_s}}{f_D} = 1.17(5), \quad (27)$$

to be compared with the results $f_D = 197(9)$ MeV, $f_{D_s} = 244(8)$ MeV and $f_{D_s}/f_D = 1.24(3)$ of [8]. With respect to [8], the present analysis is improved essentially for the reasons discussed for f_B and f_{B_s} , namely: the statistics is increased for some ensembles, data at the finest lattice spacing ($\beta = 4.2$) are now included, the continuum extrapolation is performed at fixed (reference) heavy quark masses. Moreover, as discussed for f_{B_s}/f_B , we perform the chiral extrapolation of f_{hs}/f_{hl} either following HMChPT or a linear dependence on μ_ℓ . In [8] the value $f_{D_s}/f_D = 1.24(3)$ was obtained from the HMChPT fit only, while the result given in eq. (27) is an average of $f_{D_s}/f_D = 1.21(2)$ from HMChPT and $f_{D_s}/f_D = 1.12(2)$ from the linear fit. By considering both results we have increased the uncertainty associated to the chiral extrapolation.

6 Conclusions

We have presented a lattice determination of the b quark mass and of the B and B_s decay constants, obtained with $N_f = 2$ twisted mass Wilson fermions. Two methods have been employed, following and improving our previous analyses in [4] and [5].

The first method is based on suitable ratios with exactly known static limit and smooth chiral and continuum limit. With respect to [4], the present analysis includes data at four

values for the lattice spacing, a larger statistics, and uses the published values for the quark mass renormalization constants [7] and for the physical up/down and strange quark masses [17].

The second method consists in interpolating between relativistic and static data. With respect to [5], we added one ensemble at $\beta = 4.2$, increased the statistics and, again, used the published values for the renormalization constants and light quark masses. A further improvement has been achieved by studying separately discretization effects and the (physical) dependence on the heavy quark mass. This has been done by performing the continuum extrapolation at fixed reference heavy quark mass.

The systematic uncertainties due to the chiral and continuum extrapolation and to the interpolation to the physical b quark mass, as well as the sensitivity to the pole mass definition, have been carefully studied. An important uncertainty affecting the determination of the ratio f_{Bs}/f_B and, in turn, of f_B , is introduced by the chiral extrapolation to the physical value of the average up/down quark mass. We note, in this respect, that given an assumption for the chiral extrapolation fitting function, i.e. either including or not the leading chiral logarithm, the results obtained for the ratio f_{Bs}/f_B by using the ratio and the interpolation method are in perfect agreement within each other (see Table 2). In order to reduce the uncertainty due to the chiral extrapolation, simulations at smaller values for the light quark masses, closer to their physical values, are needed.

The difference between the results obtained for f_{Bs} by using the ratio and the interpolation method (approximately 5%, see Table 2) provides an indication of the uncertainty due to the interpolation to the heavy b quark mass. In this respect, the main advantage of the ratio method is that the static limit of the ratios is exactly known (by definition), so that the approach does not require a dedicated lattice simulation within the HQET.

The final results for the b quark mass in the $\overline{\text{MS}}$ scheme and for the decay constants read

$$\overline{m}_b(\overline{m}_b) = 4.29(14) \text{ GeV} ,$$

$$f_B = 195(12) \text{ MeV} , \quad f_{Bs} = 232(10) \text{ MeV} , \quad \frac{f_{Bs}}{f_B} = 1.19(5) . \quad (28)$$

As a byproduct of the analysis we also obtain the results for the f_D and f_{Ds} decay constants

$$f_D = 212(8) \text{ MeV} , \quad f_{Ds} = 248(6) \text{ MeV} , \quad \frac{f_{Ds}}{f_D} = 1.17(5) , \quad (29)$$

which update and improve our previous determination [8].

The only systematic uncertainty which is not accounted for by our results is the one stemming from the missing strange and charm quark vacuum polarization effects. A comparison of our $N_f = 2$ result for the B and B_s decay constants, to existing results from $N_f = 2 + 1$ quark flavor simulations [33, 34] suggests that the error due to the partial quenching of the strange quark is smaller at present than other systematic uncertainties. In this respect we mention that simulations with $N_f = 2 + 1 + 1$ dynamical flavors are already being performed by ETMC and preliminary results for several flavor physics observables have been recently presented [35, 36].

We thank all the ETMC members for fruitful discussions and the apeNEXT computer centers in Rome for their invaluable technical help. Some computation time has been used for that project on NW-Grid in Liverpool and HLRN in Berlin. G.H. acknowledges the support from the Spanish Ministry for Education and Science project FPA2009-09017, the Consolider-Ingenio 2010 Programme CPAN (CSD2007-00042), the Comunidad Autónoma de Madrid (HEPHACOS P-ESP-00346 and HEPHACOS S2009/ESP-1473) and the European project STRONGnet (PITN-GA-2009-238353). V.L., S.S. and C.T. thank MIUR (Italy) for partial financial support under the contracts PRIN08. V.L. acknowledges the support of CNRS and the Laboratoire de Physique Théorique d'Orsay, Université Paris-Sud 11, where part of this work was completed. M.W. acknowledges support by the Emmy Noether Programme of the DFG (German Research Foundation), grant WA 3000/1-1.

Appendix: Phenomenological analysis of the ratios y and z_s

The lattice results for the ratios y and z_s derived in section 3 deviate from their static limit value, in the whole range of heavy quark masses from the charm mass value up to infinity, by only a small amount. Specifically, with the chosen value $\lambda \simeq 1.18$, the deviation is not more than 1.5% and 4% for y and z_s respectively. By looking at the best fit curves of y and z_s as functions of $1/\bar{\mu}_h$, see figs. 2 and 5 (left), one notices however a clear curvature, thus signalling a large $1/\bar{\mu}_h^2$ contribution in the heavy quark expansion compared to the linear term. In this appendix, we wish to show that this behavior is actually in good agreement with the predictions of the heavy quark expansion of $M_{h\ell}$ and f_{hs} once one employs phenomenological or lattice based estimates for the relevant coefficients.

We first discuss the phenomenological analysis of the ratio $y(\bar{\mu}_h)$ defined in eq. (5). By introducing in the expression for y the heavy quark expansion for the heavy-light pseudoscalar meson mass,

$$M_{h\ell} = \mu_h^{\text{pole}} + \bar{\Lambda} - \frac{(\lambda_1 + 3\lambda_2)}{2} \frac{1}{\mu_h^{\text{pole}}} + \mathcal{O}\left(\frac{1}{(\mu_h^{\text{pole}})^2}\right), \quad (30)$$

one finds

$$y = 1 - \bar{\Lambda} \frac{\lambda^{\text{pole}} - 1}{\mu_h^{\text{pole}}} + \left(\frac{(\lambda_1 + 3\lambda_2)}{2} (\lambda^{\text{pole}} + 1) + \bar{\Lambda}^2 \lambda^{\text{pole}} \right) \frac{\lambda^{\text{pole}} - 1}{(\mu_h^{\text{pole}})^2}, \quad (31)$$

where λ^{pole} is a smoothly varying function of $\bar{\mu}_h$ defined as $\lambda^{\text{pole}} = \mu_h^{\text{pole}}(\bar{\mu}_h)/\mu_h^{\text{pole}}(\bar{\mu}_h/\lambda) = \lambda \rho(\bar{\mu}_h)/\rho(\bar{\mu}_h/\lambda)$.

In order to estimate the ratio y we considered the following phenomenological values for the HQET parameters

$$\bar{\Lambda} = 0.39(11) \text{ GeV}, \quad \lambda_1 = -0.19(10) \text{ GeV}^2, \quad \lambda_2 = 0.12(2) \text{ GeV}^2. \quad (32)$$

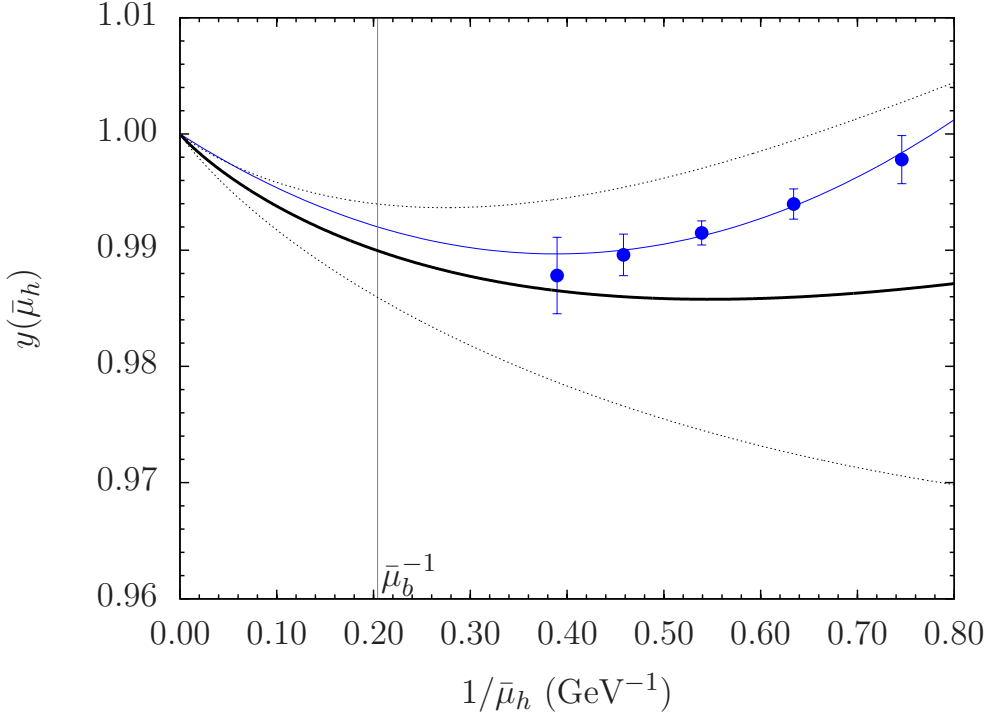


Figure 9: The lattice QCD results for y (blue points) as a function of $1/\bar{\mu}_h$ are compared to the phenomenological estimate. For the latter, the black solid and dashed curves represent the mean value and the one-standard deviation band respectively.

Notice that while λ_2 is rather precisely determined from the B-meson mass splitting $M_{B^*}^2 - M_B^2$, the values of $\bar{\Lambda}$ and λ_1 are inferred from the analysis of the inclusive semileptonic B -decays carried out in ref. [37]. Using eq. (32) we obtain the phenomenological estimate of y shown in fig. 9, which is compared to the lattice QCD results of section 3.

The above analysis shows that the lattice results for y are consistent with the phenomenological estimate. In particular, one sees that the curvature of y as a function of $1/\bar{\mu}_h$, observed in the lattice QCD data, is due to the fact that the coefficients of the linear and quadratic terms of the heavy quark expansion in eq. (31) are comparable in size and opposite in sign. As a result, the ratio y has a minimum in the region around the charm quark mass, which is the one covered by the lattice data.

A similar analysis can be also carried out for the ratio z_s , defined in eq. (16). In this case, the analysis is based on the heavy quark expansion for the pseudoscalar decay constant,

$$\Phi_{hs}(\bar{\mu}_h, \mu_b^*) = \frac{(f_{hs}\sqrt{M_{hs}})^{\text{QCD}}}{C_A^{\text{stat}}(\bar{\mu}_h, \mu_b^*)} = \Phi_0(\mu_b^*) \left(1 + \frac{\Phi_1(\mu_b^*)}{\mu_h^{\text{pole}}} + \frac{\Phi_2(\mu_b^*)}{(\mu_h^{\text{pole}})^2} \right) + \mathcal{O}\left(\frac{1}{(\mu_h^{\text{pole}})^3}\right), \quad (33)$$

where μ_b^* is the renormalization scale in the HQET. Using this expansion (and omitting

for better clarity in the following the dependence on μ_b^*), one finds

$$\begin{aligned} y_s^{1/2} z_s &= \frac{\Phi_{hs}(\bar{\mu}_h)}{\Phi_{hs}(\bar{\mu}_h/\lambda)} = \\ &= 1 - \Phi_1 \frac{\lambda^{\text{pole}} - 1}{\mu_h^{\text{pole}}} - (\Phi_2(\lambda^{\text{pole}} + 1) - \Phi_1^2 \lambda^{\text{pole}}) \frac{\lambda^{\text{pole}} - 1}{(\mu_h^{\text{pole}})^2}. \end{aligned} \quad (34)$$

The expansion for z_s can be then obtained by combining the above expression with the heavy quark expansion for the ratio y_s . The latter has the same form of eq. (31) but with HQET parameters $\bar{\Lambda}_s$, λ_{1s} and λ_{2s} depending on the strange quark mass. For the purpose of the present exercise we take

$$\bar{\Lambda}_s = \bar{\Lambda} + M_{B_s} - M_B, \quad \lambda_{1s} = \lambda_1, \quad \lambda_{2s} = \lambda_2. \quad (35)$$

We are not aware of phenomenological estimates of the HQET parameters Φ_0 , Φ_1 and Φ_2 . Therefore we consider in this case a set of values inferred from the lattice results for the heavy-light meson decay constants obtained by the HPQCD collaboration and presented in [38]. Their result for the static parameter is $\Phi_0 \simeq 0.60(4)$ GeV $^{3/2}$, which is consistent with our calculation within lattice HQET, $\Phi_0 \simeq 0.67(4)$ GeV $^{3/2}$, see eq. (23). The estimates for the parameters Φ_1 and Φ_2 can be derived, in turn, by requiring that eq. (33) provides the HPQCD determinations for f_{D_s} and f_{B_s} at the physical charm and bottom quark masses, i.e. $f_{D_s} = 249(2)$ MeV and $f_{B_s} = 224(4)$ MeV [38]. For this determination we also used the experimental values of the D_s and B_s meson masses [24] and the values of the charm and bottom quark masses obtained in section 3.1, namely $\bar{\mu}_c = 1.14(4)$ GeV and $\bar{\mu}_b = 4.91(15)$ GeV. In conclusion we considered the values

$$\Phi_0 = 0.60 \text{ GeV}^{3/2}, \quad \Phi_1 = -0.48 \text{ GeV}, \quad \Phi_2 = 0.08 \text{ GeV}^2. \quad (36)$$

The resulting phenomenological estimate of z_s corresponding to the above set of values for the HQET parameters is shown in fig. 10 and compared to our determination from section 3. By also considering that a quantitative estimate of the uncertainties on the HQET parameters is beyond the scope of the present exercise we conclude, again, that the shape of the phenomenological curve, including its curvature, is well consistent with the lattice data.

References

- [1] UTfit Collaboration, <http://www.utfit.org>
- [2] M. Bona *et al.* [UTfit Collaboration], Phys. Lett. **B687** (2010) 61-69. [arXiv:0908.3470 [hep-ph]].
- [3] C. Aubin, PoS **LAT2009** (2009) 007 [arXiv:0909.2686 [hep-lat]].
- [4] B. Blossier *et al.* [ETM Coll.], JHEP **1004** (2010) 049 [arXiv:0909.3187 [hep-lat]].

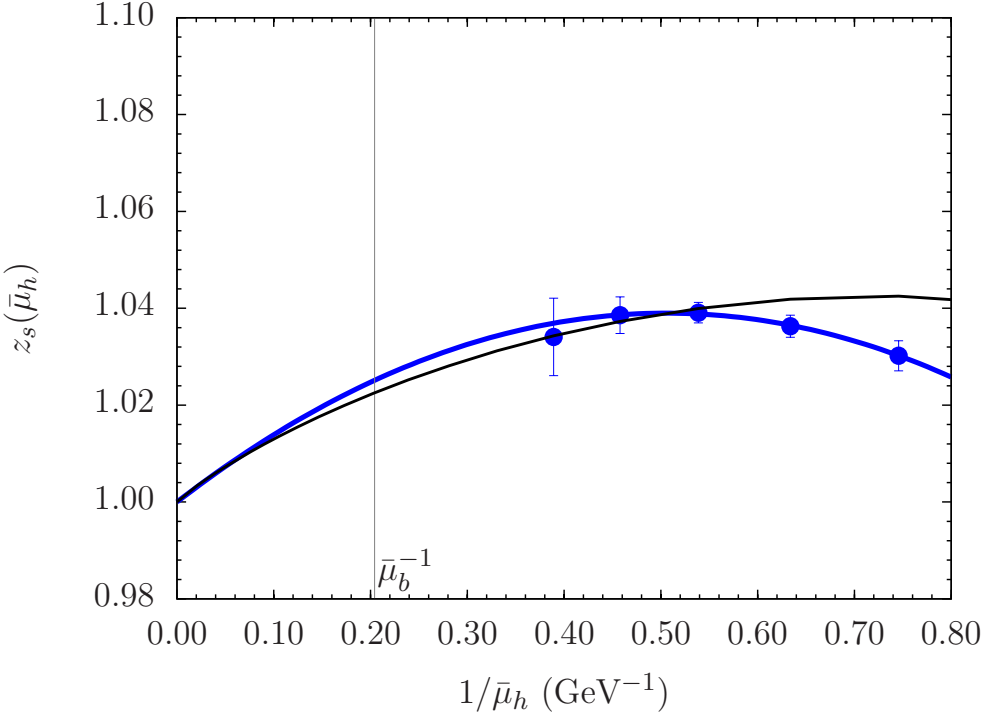


Figure 10: The lattice QCD results for z_s (blue points) as a function of $1/\bar{\mu}_h$ are compared to the phenomenological estimate (black curve).

- [5] B. Blossier *et al.* [ETM Coll.], PoS **LAT2009** (2009) 151 [arXiv:0911.3757 [hep-lat]].
- [6] C. R. Allton, C. T. Sachrajda, V. Lubicz, L. Maiani, G. Martinelli, Nucl. Phys. **B349** (1991) 598-616.
- [7] M. Constantinou *et al.*, JHEP **1008** (2010) 068 [arXiv:1004.1115 [hep-lat]].
- [8] B. Blossier *et al.* [ETM Coll.], JHEP **0907** (2009) 043 [arXiv:0904.0954 [hep-lat]].
- [9] P. Weisz, Nucl. Phys. B **212** (1983) 1.
- [10] R. Frezzotti, P. A. Grassi, S. Sint and P. Weisz [Alpha Coll.], JHEP **0108** (2001) 058 [arXiv:hep-lat/0101001].
- [11] R. Baron *et al.* [ETM Coll.], JHEP **1008** (2010) 097 [arXiv:0911.5061 [hep-lat]].
- [12] Ph. Boucaud *et al.* [ETM Coll.], Phys. Lett. B **650** (2007) 304 [arXiv:hep-lat/0701012].
- [13] Ph. Boucaud *et al.* [ETM Coll.], Comput. Phys. Commun. **179** (2008) 695 [arXiv:0803.0224 [hep-lat]].
- [14] C. Urbach [ETM Coll.], PoS **LAT2007** (2007) 022 [0710.1517 [hep-lat]].

- [15] P. Dimopoulos, R. Frezzotti, G. Herdoiza, K. Jansen, C. Michael and C. Urbach [ETM Coll.], PoS **LATTICE2008** (2008) 103 [arXiv:0810.2873 [hep-lat]].
- [16] R. Frezzotti and G. C. Rossi, JHEP **0408** (2004) 007 [hep-lat/0306014].
R. Frezzotti and G. C. Rossi, JHEP **0410** (2004) 070 [arXiv:hep-lat/0407002].
- [17] B. Blossier *et al.* [ETM Coll.], Phys. Rev. D **82** (2010) 114513 [arXiv:1010.3659 [hep-lat]].
- [18] K.G. Chetyrkin, Phys. Lett. B **404** (1997) 161;
J.A. Vermaseren, S.A. Larin and T. van Ritbergen, Phys. Lett. B **405** (1997) 327;
K.G. Chetyrkin and A. Retey, Nucl. Phys. B **583** (2000) 3. e-Print: hep-ph/9910332
- [19] N. Gray *et al.*, Z. Phys. C **48** (1990) 673;
D.J. Broadhurst, N. Gray and K. Schilcher, Z. Phys. C **52** (1991) 111;
K.G. Chetyrkin and M. Steinhauser, Phys. Rev. Lett. **83** (1999) 4001;
K. Melnikov and T. van Ritbergen, Phys. Lett. B **482** (2000) 99.
- [20] K.G. Chetyrkin and A.G. Grozin, Nucl. Phys. B **666** (2003) 289.
[arXiv:hep-ph/0303113].
- [21] J. L. Goity, Phys. Rev. D **46**, 3929 (1992) [arXiv:hep-ph/9206230].
- [22] B. Grinstein, E. E. Jenkins, A. V. Manohar, M. J. Savage and M. B. Wise, Nucl. Phys. B **380**, 369 (1992) [arXiv:hep-ph/9204207].
- [23] S. R. Sharpe and Y. Zhang, Phys. Rev. D **53** (1996) 5125 [arXiv:hep-lat/9510037].
- [24] K. Nakamura *et al.* [Particle Data Group], J. Phys. G **37** (2010) 075021.
- [25] H. Ohki, H. Matsufuru and T. Onogi, Phys. Rev. D **77**, 094509 (2008) [arXiv:0802.1563 [hep-lat]].
- [26] D. Becirevic, B. Blossier, E. Chang and B. Haas, Phys. Lett. B **679** (2009) 231
[arXiv:0905.3355 [hep-ph]].
- [27] K. Jansen, C. Michael, A. Shindler and M. Wagner [ETM Coll.], JHEP **0812**, 058 (2008) [arXiv:0810.1843 [hep-lat]].
- [28] C. Michael, A. Shindler and M. Wagner [ETM Coll.], JHEP **1008**, 009 (2010)
[arXiv:1004.4235 [hep-lat]].
- [29] M. Della Morte, A. Shindler and R. Sommer [ALPHA Coll.], JHEP **0508** (2005) 051
[arXiv:hep-lat/0506008].
- [30] A. Hasenfratz and F. Knechtli, Phys. Rev. D **64** (2001) 034504
[arXiv:hep-lat/0103029].

- [31] M. Della Morte, S. Durr, J. Heitger, H. Molke, J. Rolf, A. Shindler and R. Sommer [ALPHA Coll.], Phys. Lett. B **581** (2004) 93 [Erratum-ibid. B **612** (2005) 313] [arXiv:hep-lat/0307021].
- [32] B. Blossier, arXiv:1106.2132 [hep-lat].
- [33] E. Gamiz, C. T. H. Davies, G. P. Lepage, J. Shigemitsu and M. Wingate [HPQCD Coll.], Phys. Rev. D **80** (2009) 014503 [arXiv:0902.1815 [hep-lat]].
- [34] C. Albertus *et al.*, Phys. Rev. D **82** (2010) 014505 [arXiv:1001.2023 [hep-lat]].
- [35] R. Baron *et al.*, JHEP **1006** (2010) 111 [arXiv:1004.5284 [hep-lat]].
- [36] R. Baron *et al.* [ETM Coll.], Comput. Phys. Commun. **182** (2011) 299 [arXiv:1005.2042 [hep-lat]].
- [37] M. Gremm, A. Kapustin, Z. Ligeti, M. B. Wise, Phys. Rev. Lett. **77** (1996) 20-23.
- [38] C. Davies, plenary talk at The XXIX International Symposium on Lattice Field Theory - Lattice 2011, July 10-16, 2011, Squaw Valley, Lake Tahoe, California (USA). <http://tsailab.chem.pacific.edu/lat11/plenary/davies>

DESY 09-033
SFB/CPP-09-26
LPT-ORSAY 09-17
HU-EP-09/12

Lattice calculation of the Isgur-Wise functions $\tau_{1/2}$ and $\tau_{3/2}$ with dynamical quarks

Benoit Blossier^{a,b}, Marc Wagner^c, Olivier Pène^b

^a DESY, Platanenallee 6, D-15738 Zeuthen, Germany

^b Laboratoire de Physique Théorique (Bât.210), Université Paris-Sud XI,
Centre d'Orsay, 91405 Orsay-Cedex, France.

^c Humboldt-Universität zu Berlin, Institut für Physik, Newtonstraße 15, D-12489 Berlin,
Germany



March 13, 2009

Abstract

We perform a dynamical lattice computation of the Isgur-Wise functions $\tau_{1/2}$ and $\tau_{3/2}$ at zero recoil. We consider three different light quark masses corresponding to $300 \text{ MeV} \lesssim m_{\text{PS}} \lesssim 450 \text{ MeV}$, which allow us to extrapolate our results to the physical u/d quark mass. We find $\tau_{1/2}(1) = 0.296(26)$ and $\tau_{3/2}(1) = 0.526(23)$. Uraltsev's sum rule is saturated up to 80% by the ground state. We discuss implications regarding semileptonic decays $B \rightarrow X_c l \nu$ and the associated “1/2 versus 3/2” puzzle.

1 Introduction

The semileptonic decay of B mesons into positive parity charmed mesons (often referred to as D^{**} 's) is an important and debated issue. Important, because no accurate measurement of the V_{cb} CKM angle will be possible, if these channels, which represent about one quarter of the semileptonic decays, are not well understood. Debated, because there seems to be a persistent discrepancy between claims from theory and from experiment [1].

Two types of D^{**} 's are seen, two “narrow resonances” and a couple of “broad resonances”, grossly speaking in the same mass region. While experiments point towards a dominance of the broad resonances in semileptonic decays, theory, when using the heavy quark limit, points rather towards a dominance of the narrow resonances. To clarify the situation ref. [1] called for actions on both the experimental and the theoretical side.

The theoretical argument relies on a series of sum rules [2, 3] derived from QCD comforted by model calculations [4, 5, 6]. Lattice calculations are needed to give a more quantitative prediction stemming directly from QCD. A preliminary computation was performed in [7], but only in quenched QCD and with a marginal signal-to-noise ratio. In this letter we report on the first unquenched computation using $N_f = 2$ flavor gauge configurations with Wilson twisted quarks generated by the European Twisted Mass Collaboration (ETMC). The spectrum of heavy-light mesons in the static limit has already been reported [10, 11].

1.1 Spectrum in the heavy quark limit

We treat both b and c quarks via static Wilson lines, i.e. consider their infinite mass limit. In this limit the meson spectrum is constructed by combining the spin 1/2 of the heavy quark with the total angular momentum and parity j^P of the light degrees of freedom (light quarks and gluons) [12, 13, 14]. The two lightest negative parity mesons B and B^* (or D and D^*) are degenerate and described by the same $S \equiv (1/2)^-$ state of light particles. The lightest (non-radially excited) positive parity states can be decomposed into two degenerate doublets: $P_- \equiv (1/2)^+$ and $P_+ \equiv (3/2)^+$. The total angular momenta J^P of the P_- (P_+) mesons are 0^+ , 1^+ (1^+ , 2^+). The mixing between the two 1^+ states is suppressed in the heavy quark limit.

It is generally believed that the narrow (broad) resonances are of the P_+ (P_-) type, since in the heavy quark limit they decay into $D^{(*)}\pi$ via a D (S) wave. The D wave decays are supposed to be suppressed by a centrifugal barrier, if the final state momenta are not too large.

1.2 Decay form factors in the heavy quark limit

In the heavy quark limit the semileptonic decay of a pseudoscalar meson into D^{**} is governed by only two form factors [14], $\tau_{1/2}(w)$ and $\tau_{3/2}(w)$, where $w \equiv v_B \cdot v_{D^{**}} \geq 1$ with v_B and $v_{D^{**}}$ denoting the four-velocity of heavy-light meson H being defined by $v_H \equiv p_H/m_H$. Uraltsev has proven the following sum rule [3]:

$$\sum_n \left| \tau_{3/2}^{(n)}(1) \right|^2 - \left| \tau_{1/2}^{(n)}(1) \right|^2 = \frac{1}{4}, \quad (1)$$

where $\tau_{3/2}^{(n)}(w)$ ($\tau_{1/2}^{(n)}(w)$), $n = 0, \dots, \infty$ are the form factors for the decay into the P_+ (P_-) meson and the tower of its radial excitations¹. $w = 1$ corresponds to the zero recoil situation, i.e. the B and the D^{**} meson have the same velocity. Eqn. (1) is one of the major among many theoretical arguments in favor of the narrow resonance dominance [1].

Our goal in this paper is to make a direct lattice calculation of $\tau_{1/2}(1)$ and $\tau_{3/2}(1)$ using static quarks represented by Wilson lines [15]. However, there is the problem that the $B \rightarrow D^{**}$ decay amplitude is suppressed at $w = 1$ due to vanishing kinematical factors, which multiply $\tau_j(1)$. This is also a centrifugal barrier effect, i.e. it is impossible to give angular momentum to a meson at rest. Consequently, a computation of the weak current matrix element will trivially give zero. To overcome this difficulty, we use a method, which amounts to compute the operator matrix element based on an expression of the derivative of that matrix element in terms of the recoil four-velocity of the final meson [16, 7]. Thanks to the translational invariance in time of the heavy quark Lagrangian this is then proportional to $\tau_j(1)(m_{H^j} - m_H)$, $j = 1/2, 3/2$ (cf. eqns. (11) and (12)). The mass splittings $m_{H^{**}} - m_H$ have already been computed in the static limit with precisely the same setup we are using in this paper [10, 11], i.e. by using $N_f = 2$ ETMC gauge configurations. We are thus in a position to compute $\tau_{1/2}(1)$ and $\tau_{3/2}(1)$ and to confront it with the Uraltsev and other sum rules as well as with other non-perturbative estimates (QCD sum rules, quark models).

Our work should help to clarify the situation in the heavy quark limit. A fair comparison with experiment further needs to estimate the systematic error stemming from the heavy quark limit. After all, the charm quark is not so heavy. The authors of [5, 6] argue that large $\mathcal{O}(1/m_Q)$ corrections are present. This issue can also be addressed by lattice QCD, but in this work we restrict our computations to the static limit.

The paper is organized as follows. In section 2 we recall the method used to compute $\tau_{1/2}(1)$ and $\tau_{3/2}(1)$. In section 3 we report on the lattice calculation of $\tau_{1/2}(1)$ and $\tau_{3/2}(1)$. In section 4 we perturbatively compute the renormalization constant of the heavy-heavy current and we conclude in section 5.

2 Principle of the calculation

To compute the zero-recoil Isgur-Wise functions $\tau_{1/2}(1)$ and $\tau_{3/2}(1)$ by means of lattice QCD, we use a method proposed in [7]. We remind it here just for comfort of the reader.

The method consists in using a series of relations derived in ref. [16]. With $v' = (1, 0, 0, 0)$ and $v = v' + v_\perp$ denoting the velocities of the ingoing and outgoing mesons, where v_\perp is spatial up to higher orders in the difference $v' - v$, we assume that for some Dirac matrix Γ_l

$$\langle H^{**}(v') | \bar{Q}(v') \Gamma_l Q(v) | H^{(*)}(v) \rangle = t_l^m v_{\perp m} \tau_j(w) + \dots \quad (2)$$

Here $w \equiv v \cdot v'$, $j = 1/2, 3/2$ and $l, m = 1, 2, 3$ are spatial indices. t_l^m is a tensor, which depends on the final state (H^{**}) and the initial state (H^* or H), and $Q(v)$ is the static quark field in Heavy Quark Effective Theory. The dots represent higher order terms in $v' - v$. From

¹By definition $\tau_j(w) \equiv \tau_j^{(0)}(w)$, $j = 1/2, 3/2$.

translational invariance in time direction,

$$\begin{aligned}
& -i\partial_0 \langle H^{**}(v') | \bar{Q}(v') \Gamma_l Q(v) | H^{(*)}(v) \rangle \\
& = -i \langle H^{**}(v') | \bar{Q}(v') \left[\Gamma_l \vec{D}^0 + \overleftrightarrow{D}^0 \Gamma_l \right] Q(v) | H^{(*)}(v) \rangle \\
& = t_l^m v_{\perp m} \tau_j(w) (m_{H^{**}} - m_H) + \dots
\end{aligned} \tag{3}$$

Then we use the field equation $(v \cdot D)Q(v) = 0$:

$$D^0 Q(v') = 0, \quad D^0 Q(v) = -(D \cdot v_{\perp}) Q(v), \tag{4}$$

whence from eqn. (3)

$$i \langle H^{**}(v') | \bar{Q}(v') \Gamma_l (D \cdot v_{\perp}) Q(v) | H^{(*)}(v) \rangle = t_l^m v_{\perp m} \tau_j(w) (m_{H^{**}} - m_H) + \dots, \tag{5}$$

which, in the limit $v_{\perp} \rightarrow 0$, converges to the relation

$$i \langle H^{**}(v) | \bar{Q}(v) \Gamma_l D^m Q(v) | H^{(*)}(v) \rangle = t_l^m \tau_j(1) (m_{H^{**}} - m_H). \tag{6}$$

Applying eqn. (2) to the $J = 0$ H_0^* state we get from ref. [17]

$$\langle H_0^*(v') | A_i | H(v) \rangle \equiv -\tau_{1/2}(w) v_{\perp i}, \tag{7}$$

where A_i is the axial current in spatial direction i , and where the normalization of the states is $1/\sqrt{2m}$ times the one used in ref. [17]. From eqn. (7) follows

$$\langle H_0^*(v) | A_i D_j | H(v) \rangle = i g_{ij} (m_{H_0^*} - m_H) \tau_{1/2}(1). \tag{8}$$

Analogously for the $J = 2$ H_2^* state we have

$$\langle H_2^*(v') | A_i | H(v) \rangle \equiv \sqrt{3} \tau_{3/2}(w) \epsilon_i^{*j} v_{\perp j} + \dots, \tag{9}$$

where ϵ_i^{*j} is the polarization tensor, whence

$$\langle H_2^*(v) | A_i D_j | H(v) \rangle = -i \sqrt{3} (m_{H_2^*} - M_H) \tau_{3/2}(1) \epsilon_{ij}^*. \tag{10}$$

Finally $\tau_{1/2}(1)$ and $\tau_{3/2}(1)$ can be obtained from the following matrix elements:

$$\tau_{1/2}(1) = \left| \frac{\langle H_0^* | \bar{Q} \gamma_5 \gamma_z D_z Q | H \rangle}{m_{H_0^*} - m_H} \right| \tag{11}$$

$$\tau_{3/2}(1) = \left| \frac{\langle H_2^* | \bar{Q} \gamma_5 (\gamma_x D_x - \gamma_y D_y) Q | H \rangle}{\sqrt{6} (m_{H_2^*} - M_H)} \right|. \tag{12}$$

There is no mixing of the operators $A_i D_j$ with dimension 3 (hence linearly divergent) heavy-heavy operators to be feared on the lattice: indeed we are interested in a parity-changing transition and all dimension 3 operators have vanishing matrix elements between positive and negative parity states². There are no logarithmic divergence either thanks to the vanishing of the vector and axial currents' anomalous dimension in HQET at zero recoil. By consequence there is no conceptual issue concerning the extrapolation to the continuum limit of such a calculation. It needs only a finite renormalization constant to match the lattice result with a continuum-like scheme value, as we will discuss in Section 4.

3 Lattice computation of $\tau_{1/2}$ and $\tau_{3/2}$ at zero recoil

3.1 Simulation setup

We use $N_f = 2$ flavor $24^3 \times 48$ Wilson twisted mass gauge configurations produced by the European Twisted Mass Collaboration (ETMC). Here we only give a brief summary of the setup, which is explained in detail in [18, 19, 20].

The gauge action is tree-level Symanzik improved [21] with $\beta = 3.9$ corresponding to a lattice spacing $a = 0.0855(5)$ fm:

$$S_G[U] = \frac{\beta}{6} \left(b_0 \sum_{x,\mu \neq \nu} \text{Tr} \left(1 - P^{1 \times 1}(x; \mu, \nu) \right) + b_1 \sum_{x,\mu \neq \nu} \text{Tr} \left(1 - P^{1 \times 2}(x; \mu, \nu) \right) \right), \quad (13)$$

where $b_0 = 1 - 8b_1$ and $b_1 = -1/12$.

The fermionic action is Wilson twisted mass with two degenerate flavors [22, 23, 24]:

$$S_F[\chi, \bar{\chi}, U] = a^4 \sum_x \bar{\chi}(x) \left(D_W + i\mu_q \gamma_5 \tau_3 \right) \chi(x), \quad (14)$$

where

$$D_W = \frac{1}{2} \left(\gamma_\mu \left(\nabla_\mu + \nabla_\mu^* \right) - a \nabla_\mu^* \nabla_\mu \right) + m_0, \quad (15)$$

∇_μ and ∇_μ^* are the standard gauge covariant forward and backward derivatives, m_0 and μ_q are the bare untwisted and twisted quark masses and $\chi = (\chi^{(u)}, \chi^{(d)})$ are the fermionic fields in the twisted basis.

We consider three different values of the light quark mass, which amount to “pion masses” in the range $300 \text{ MeV} \lesssim m_{PS} \lesssim 450 \text{ MeV}$ (cf. Table 1). m_0 has been tuned to its critical value at the lightest μ_q value, i.e. at $\mu_q = 0.0040$.

²Of course the situation is different by instance for the matrix element $\langle H | \bar{h} \mathbf{D}^2 h | H \rangle$, related to the HQET parameter λ_1 or the kinetic momentum μ_π^2 for which a subtraction is necessary to its computation on the lattice [8, 9].

μ_q	m_{PS} in MeV	number of gauge configurations
0.0040	314(2)	1400
0.0064	391(1)	1450
0.0085	448(1)	1350

Table 1: twisted quark masses μ_q , pion masses m_{PS} and number of gauge configurations.

3.2 Static and light quark propagators

The propagator of a static quark is essentially a Wilson line in time direction:

$$\langle Q(x)\bar{Q}(y) \rangle_{Q,\bar{Q}} = \delta^{(3)}(\mathbf{x} - \mathbf{y}) U^{(HYP2)}(x; y) \left(\Theta(y_0 - x_0) \frac{1 - \gamma_0}{2} + \Theta(x_0 - y_0) \frac{1 + \gamma_0}{2} \right), \quad (16)$$

where $\langle \dots \rangle_{Q,\bar{Q}}$ denotes the integration over the static quark field and $U(x; y)$ is a path ordered product of links along the straight path from x to y . To improve the signal-to-noise ratio we use the HYP2 static action [25, 26, 27].

For the light quarks we use four stochastic spin diluted timeslice propagators ($\mathcal{Z}_2 \times \mathcal{Z}_2$ sources with randomly chosen components $\pm 1 \pm i$) for each gauge configuration. For details we refer to [11], where exactly the same setup has been used.

3.3 Static-light meson creation operators

In the static limit there are no interactions involving the heavy quark spin. Therefore, it is convenient to classify static-light mesons according to $j^{\mathcal{P}}$, where j denotes the angular momentum of the light degrees of freedom and \mathcal{P} parity. In particular we are interested in the sectors $j^{\mathcal{P}} = (1/2)^-$, $j^{\mathcal{P}} = (1/2)^+$ and $j^{\mathcal{P}} = (3/2)^+$. We label the corresponding static-light mesons, i.e. the ground states in these angular momentum/parity sectors, by S , P_- and P_+ respectively.

To create such static-light mesons on the lattice we use operators

$$\mathcal{O}^{(\Gamma)}(\mathbf{x}) = \bar{Q}(\mathbf{x}) \sum_{\mathbf{n}=\pm\hat{\mathbf{e}}_1, \pm\hat{\mathbf{e}}_2, \pm\hat{\mathbf{e}}_3} \Gamma(\hat{\mathbf{n}}) U(\mathbf{x}; \mathbf{x} + r\mathbf{n}) \chi^{(u)}(\mathbf{x} + r\mathbf{n}), \quad (17)$$

where \bar{Q} creates a static antiquark at position \mathbf{x} , $\chi^{(u)}$ creates a light quark in the twisted basis at position $\mathbf{x} + r\mathbf{n}$, U is a product of spatial links along the straight path between \mathbf{x} and $\mathbf{x} + r\mathbf{n}$, and Γ is a combination of spherical harmonics and γ matrices yielding a well defined behavior under cubic rotations (cf. Table 2).

To optimize the ground state overlap of these static-light meson states, we use Gaussian smearing [28] for light quark operators and APE smearing [29] for spatial links (parameters $\kappa_{\text{Gauss}} = 0.5$, $N_{\text{Gauss}} = 30$, $\alpha_{\text{APE}} = 0.5$, $N_{\text{APE}} = 10$ and $r = 3$ as in [11]).

$\Gamma(\hat{\mathbf{n}})$	O_h	j
γ_5	A_1	$1/2, 7/2, \dots$
1		$1/2, 7/2, \dots$
$\gamma_x \hat{n}_x - \gamma_y \hat{n}_y$ (and cyclic)	E	$3/2, 5/2, \dots$
$\gamma_5(\gamma_x \hat{n}_x - \gamma_y \hat{n}_y)$ (and cyclic)		$3/2, 5/2, \dots$

Table 2: static-light meson creation operators.

3.4 Static-light meson masses

Since we work in the twisted basis, where each of the operators listed in Table 2 creates both $\mathcal{P} = +$ and $\mathcal{P} = -$ states, it is convenient to determine $\mathcal{P} = +$ and $\mathcal{P} = -$ static-light meson masses from the same correlation matrix.

For S and P_- we compute the 2×2 matrix

$$\mathcal{C}_{JK}(t) = \left\langle \left(\mathcal{O}^{(\Gamma_J)}(t) \right)^\dagger \mathcal{O}^{(\Gamma_K)}(0) \right\rangle, \quad (18)$$

where $\Gamma_J \in \{\gamma_5, 1\}$, and solve the generalized eigenvalue problem

$$\mathcal{C}_{JK}(t)v_K^{(n)}(t) = \mathcal{C}_{JK}(t_0)v_K^{(n)}(t)\lambda^{(n)}(t, t_0), \quad t_0 = 1 \quad (19)$$

(cf. [30, 31]). The meson masses $m(S)$ and $m(P_-)$ are determined by performing χ^2 minimizing fits to effective mass plateaus,

$$m_{\text{effective}}^{(n)}(t) = \ln \left(\frac{\lambda^{(n)}(t, t_0)}{\lambda^{(n)}(t+1, t_0)} \right), \quad (20)$$

at large temporal separations t (as indicated in Figure 1 our fitting range is $6 \leq t \leq 11$). The parity of the corresponding states, i.e. whether it is S or P_- , can be extracted from the eigenvectors $v_J^{(n)}$ (for a detailed discussion, of how to identify parity, cf. [11]). Results of meson masses and mass differences and corresponding reduced χ^2 values are listed in Table 3.

For $m(P_+)$ we proceed analogously this time computing the 2×2 matrix (19), where $\Gamma_J \in \{\gamma_x \hat{n}_x - \gamma_y \hat{n}_y, \gamma_5(\gamma_x \hat{n}_x - \gamma_y \hat{n}_y)\}$.

By solving the generalized eigenvalue problem (19) we have also obtained appropriate linear combinations of twisted basis meson creation operators with well defined parity. To be more precise the operators

$$\mathcal{O}^{(S)} = v_{\gamma_5}^{(S)}(t)\mathcal{O}^{(\gamma_5)} + v_1^{(S)}(t)\mathcal{O}^{(1)} \quad (21)$$

$$\mathcal{O}^{(P_-)} = v_{\gamma_5}^{(P_-)}(t)\mathcal{O}^{(\gamma_5)} + v_1^{(P_-)}(t)\mathcal{O}^{(1)} \quad (22)$$

$$\mathcal{O}^{(P_+)} = v_{\gamma_x \hat{n}_x - \gamma_y \hat{n}_y}^{(P_+)}(t)\mathcal{O}^{(\gamma_x \hat{n}_x - \gamma_y \hat{n}_y)} + v_{\gamma_5(\gamma_x \hat{n}_x - \gamma_y \hat{n}_y)}^{(P_+)}(t)\mathcal{O}^{(\gamma_5(\gamma_x \hat{n}_x - \gamma_y \hat{n}_y))} \quad (23)$$

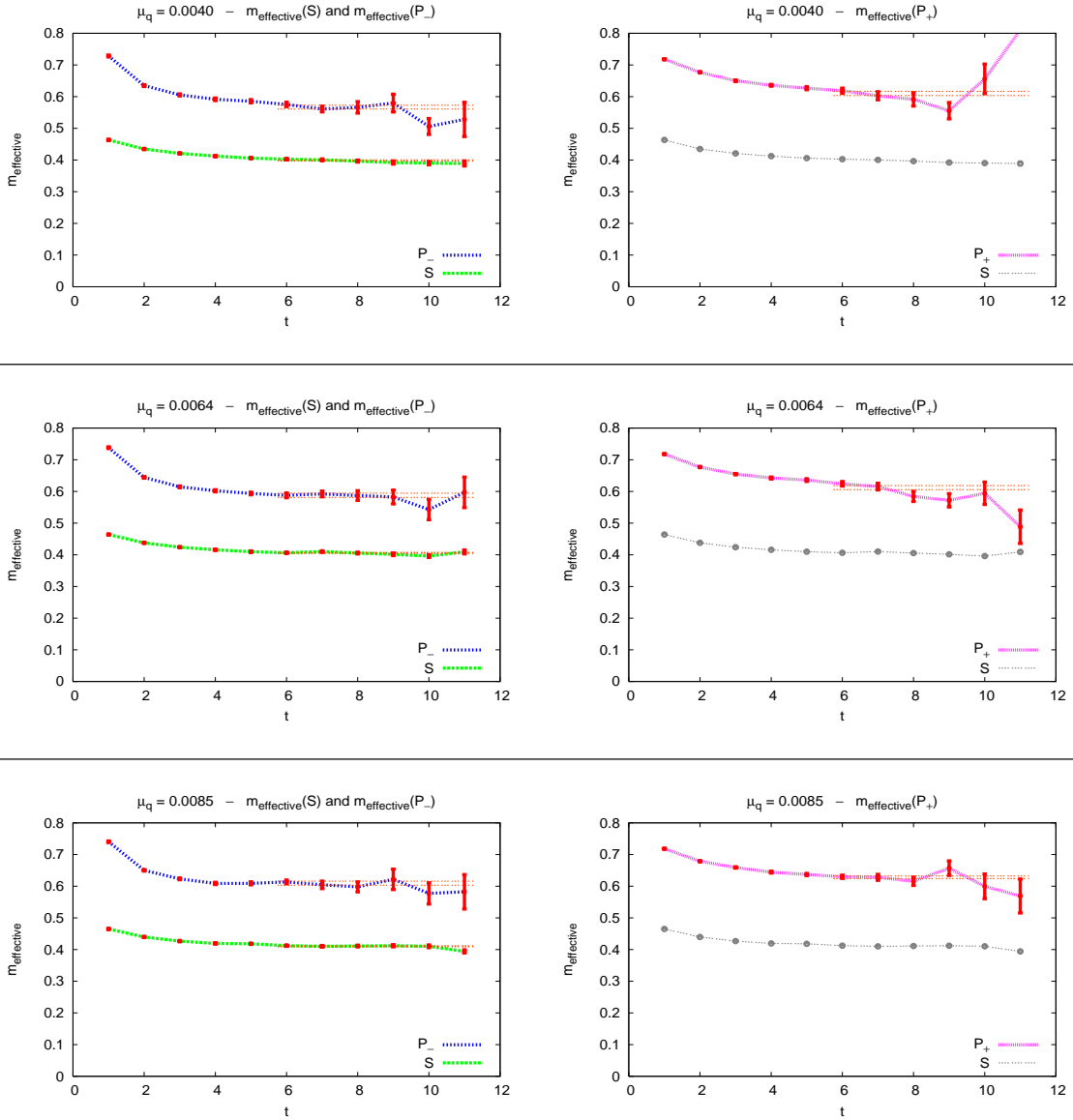


Figure 1: effective masses for S , P_- and P_+ for $\mu_q \in \{0.0040, 0.0064, 0.0085\}$.

create static-light meson states, which have the same quantum numbers j^P as the states of interest, $|S\rangle$, $|P_-\rangle$ and $|P_+\rangle$ respectively. Since the t dependence of the eigenvectors $v_j^{(n)}$ is very weak [32], results are essentially unaffected by the choice of t (we have used $t = 6$ for all results presented in the following).

μ_q	$m(S)$	χ^2/dof	$m(P_-)$	χ^2/dof	$m(P_+)$	χ^2/dof
0.0040	0.3987(19)	1.79	0.5670(60)	1.69	0.6101(66)	2.46
0.0064	0.4061(17)	1.93	0.5877(67)	0.45	0.6121(64)	3.01
0.0085	0.4104(17)	2.23	0.6095(65)	0.49	0.6283(41)	0.87

μ_q	$m(P_-) - m(S)$	$m(P_+) - m(S)$
0.0040	0.1683(65)	0.2114(62)
0.0064	0.1817(69)	0.2060(63)
0.0085	0.1991(63)	0.2179(41)

Table 3: static-light meson masses and mass differences for $\mu_q \in \{0.0040, 0.0064, 0.0085\}$.

3.5 Two-point functions and their ground state norms

After having obtained the linear combinations of twisted basis operators (21) to (23) the two-point functions

$$\left\langle \left(\mathcal{O}^{(S)}(t)\right)^\dagger \mathcal{O}^{(S)}(0) \right\rangle , \quad \left\langle \left(\mathcal{O}^{(P_-)}(t)\right)^\dagger \mathcal{O}^{(P_-)}(0) \right\rangle , \quad \left\langle \left(\mathcal{O}^{(P_+)}(t)\right)^\dagger \mathcal{O}^{(P_+)}(0) \right\rangle \quad (24)$$

are straightforward to compute.

From these two-point functions we also determine the ground state norms of the corresponding j^P sectors, $N(S)$, $N(P_-)$ and $N(P_+)$, by fitting exponentials at large temporal separations. To be more precise, we obtain e.g. $N(S)$ by fitting $N(S)^2 e^{-mt}$ to $\langle (\mathcal{O}^{(S)}(t))^\dagger \mathcal{O}^{(S)}(0) \rangle$ with $N(S)$ and m as degrees of freedom. Results and corresponding reduced χ^2 values are listed in Table 4 (fitting range $6 \leq t \leq 12$).

μ_q	$N(S)$	χ^2/dof	$N(P_-)$	χ^2/dof	$N(P_+)$	χ^2/dof
0.0040	0.3271(26)	0.21	0.2998(93)	0.33	0.1139(26)	1.43
0.0064	0.3358(20)	0.23	0.3074(87)	0.13	0.1120(27)	1.68
0.0085	0.3397(22)	0.22	0.3139(103)	0.08	0.1212(22)	0.28

Table 4: ground state norms for $\mu_q \in \{0.0040, 0.0064, 0.0085\}$.

3.6 Three-point functions and form factors $\tau_{1/2}$ and $\tau_{3/2}$

In analogy to effective masses we define effective form factors

$$\begin{aligned} & \tau_{1/2,\text{effective}}(t_0 - t_1, t_1 - t_2) \\ &= \frac{1}{Z_D} \left| \frac{N(P_-) \ N(S) \ \left\langle \left(\mathcal{O}^{(P_-)}(t_0)\right)^\dagger (\bar{Q}\gamma_5\gamma_z D_z Q)(t_1) \ \mathcal{O}^{(S)}(t_2) \right\rangle}{\left(m(P_-) - m(S)\right) \ \left\langle \left(\mathcal{O}^{(P_-)}(t_0)\right)^\dagger \mathcal{O}^{(P_-)}(t_1) \right\rangle \ \left\langle \left(\mathcal{O}^{(S)}(t_1)\right)^\dagger \mathcal{O}^{(S)}(t_2) \right\rangle} \right| \end{aligned} \quad (25)$$

$$\begin{aligned} & \tau_{3/2,\text{effective}}(t_0 - t_1, t_1 - t_2) \\ &= \frac{1}{Z_D} \left| \frac{N(P_+) N(S)}{\sqrt{6} (m(P_+) - m(S))} \frac{\left\langle \left(\mathcal{O}^{(P_+)}(t_0) \right)^\dagger (\bar{Q} \gamma_5 (\gamma_x D_x - \gamma_y D_y) Q)(t_1) \mathcal{O}^{(S)}(t_2) \right\rangle}{\left\langle \left(\mathcal{O}^{(P_+)}(t_0) \right)^\dagger \mathcal{O}^{(P_+)}(t_1) \right\rangle \left\langle \left(\mathcal{O}^{(S)}(t_1) \right)^\dagger \mathcal{O}^{(S)}(t_2) \right\rangle} \right| \end{aligned} \quad (26)$$

($Z_D = 0.976$ is a lattice renormalization constant, which we derive and discuss in detail in section 4). These effective form factors are related to $\tau_{1/2}$ and $\tau_{3/2}$ via (11) and (12):

$$\tau_{1/2}(1) = \lim_{t_0 - t_1 \rightarrow \infty, t_1 - t_2 \rightarrow \infty} \tau_{1/2,\text{effective}}(t_0 - t_1, t_1 - t_2) \quad (27)$$

$$\tau_{3/2}(1) = \lim_{t_0 - t_1 \rightarrow \infty, t_1 - t_2 \rightarrow \infty} \tau_{3/2,\text{effective}}(t_0 - t_1, t_1 - t_2). \quad (28)$$

Computation of the three-point functions appearing in (25) and (26) is again straightforward. We chose to represent the covariant derivative acting on the static quark field symmetrically by

$$D_j Q(\mathbf{x}, t) = \frac{1}{2} \left(U_j(\mathbf{x}, t) Q(\mathbf{x} + \mathbf{e}_j, t) - \left(U_j(\mathbf{x} - \mathbf{e}_j, t) \right)^\dagger Q(\mathbf{x} - \mathbf{e}_j, t) \right). \quad (29)$$

To optimally exploit our gauge configurations and propagator inversions, we average over all three-point functions, which are related by the lattice symmetries γ_5 hermiticity, parity, time reversal, charge conjugation and cubic rotations.

The resulting effective form factors $\tau_{1/2,\text{effective}}(t_0 - t_1, t_1 - t_2)$ and $\tau_{3/2,\text{effective}}(t_0 - t_1, t_1 - t_2)$ are shown in Figure 2 as functions of $t_0 - t_1$ for fixed $t_0 - t_2 \in \{10, 12\}$. Within statistical errors these effective form factors exhibit plateaus for $t_0 - t_1 \approx (t_0 - t_2)/2$, i.e. when both temporal separations, $t_0 - t_1$ and $t_1 - t_2$, are large. We determine $\tau_{1/2}$ and $\tau_{3/2}$ by performing χ^2 minimizing fits to the central three data points as indicated in Figure 2. Results for $t_0 - t_2 = 10$ and for $t_0 - t_2 = 12$, which are listed in Table 5, are in agreement within statistical errors. We consider this a strong indication that contributions from excited states at these temporal separations are essentially negligible and that the plateaus of the effective form factors indeed correspond to $\tau_{1/2}$ and $\tau_{3/2}$. In the following discussions we only quote the numbers corresponding to $t_0 - t_2 = 10$, since their statistical errors are significantly smaller than those for $t_0 - t_2 = 12$.

μ_q	$t_0 - t_2$	$\tau_{1/2}$	$\tau_{3/2}$	$\tau_{3/2}/\tau_{1/2}$	$(\tau_{3/2})^2 - (\tau_{1/2})^2$
0.0040	10	0.299(14)	0.519(13)	1.74(9)	0.180(16)
	12	0.267(26)	0.536(25)	2.01(21)	0.216(30)
0.0064	10	0.312(10)	0.538(13)	1.73(6)	0.193(13)
	12	0.278(19)	0.549(21)	1.98(14)	0.225(23)
0.0085	10	0.308(12)	0.522(8)	1.69(6)	0.177(9)
	12	0.287(24)	0.544(14)	1.90(17)	0.214(21)

Table 5: $\tau_{1/2}$ and $\tau_{3/2}$ for $t_0 - t_2 \in \{10, 12\}$ and $\mu_q \in \{0.0040, 0.0064, 0.0085\}$.

As expected from operator product expansion, $\tau_{3/2}(1)$ is significantly larger than $\tau_{1/2}(1)$. More-

over the Uraltsev sum rule [3],

$$\sum_n \left| \tau_{3/2}^{(n)}(1) \right|^2 - \left| \tau_{1/2}^{(n)}(1) \right|^2 = \frac{1}{4}, \quad (30)$$

is almost fulfilled by the ground state contributions $\tau_{1/2}^{(0)}(1) \equiv \tau_{1/2}(1)$ and $\tau_{3/2}^{(0)}(1) \equiv \tau_{3/2}(1)$.

Finally we use our results at three different light quark masses (cf. Table 1) to perform a linear extrapolation of the form factors in $(m_{\text{PS}})^2$ to the physical u/d quark mass ($m_{\text{PS}} = 135$ MeV).

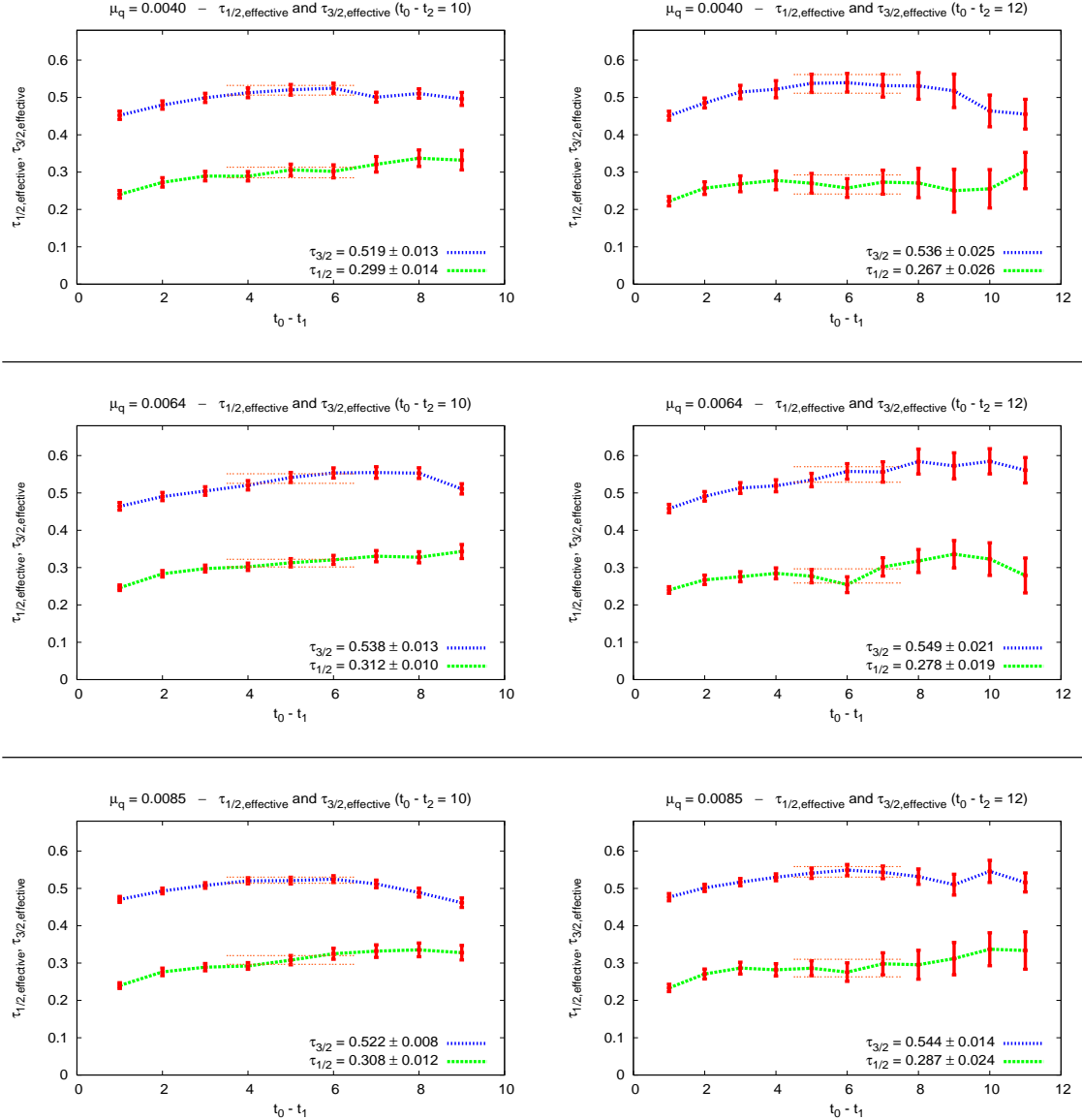


Figure 2: effective form factors $\tau_{1/2, \text{effective}}$ and $\tau_{3/2, \text{effective}}$ for $t_0 - t_2 \in \{10, 12\}$ and $\mu_q \in \{0.0040, 0.0064, 0.0085\}$.

Results are shown in Figure 3 and Table 6. The qualitative picture for u/d quark masses is the same as for the heavier masses used directly in our simulations: $\tau_{3/2}^{m_{\text{phys}}}(1) = 0.526(23)$ is significantly larger than $\tau_{1/2}^{m_{\text{phys}}}(1) = 0.296(26)$ supporting the “theory expectation” that a decay of a B meson to a $j = 3/2$ P wave D meson is more likely than to a $j = 1/2$ P wave D meson.

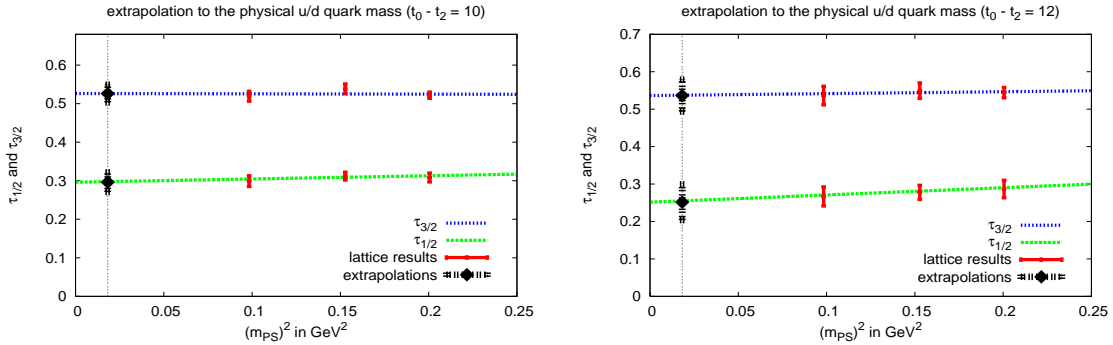


Figure 3: linear extrapolation of $\tau_{1/2}$ and $\tau_{3/2}$ to the u/d quark mass for $t_0 - t_2 \in \{10, 12\}$.

$t_0 - t_2$	$\tau_{1/2}(1)$	χ^2/dof	$\tau_{3/2}(1)$	χ^2/dof
10	0.296(26)	0.34	0.526(23)	1.43
12	0.251(48)	0.00	0.536(43)	0.12

Table 6: linear extrapolation of $\tau_{1/2}$ and $\tau_{3/2}$ to the u/d quark mass for $t_0 - t_2 \in \{10, 12\}$.

4 Perturbative renormalization of the static current $\bar{Q}\gamma_5\gamma_i D_j Q$

In this section we derive the analytical formulae and give the numerical values of the renormalization constant Z_D of the dimension 4 current $O_{ij} = \bar{Q}\gamma_5\gamma_i D_j Q$ computed at first order of perturbation theory for the HYP smeared static quark action and both the standard Wilson plaquette and the tree-level Symanzik improved gauge action.

4.1 Definitions

The bare propagator of a static quark on the lattice is

$$\begin{aligned} S^B(p) &= \frac{a}{1 - e^{-ip_4 a} + a\delta m + a\Sigma(p)} = \frac{a}{1 - e^{-ip_4 a}} \sum_n \left(-\frac{a(\delta m + \Sigma(p))}{1 - e^{-ip_4 a}} \right)^n \\ &\equiv Z_{2h} S^R(p). \end{aligned} \tag{31}$$

Choosing the renormalization conditions

$$(S^R)^{-1}(p) \Big|_{ip_4 \rightarrow 0} = ip_4, \quad \delta m = -\Sigma(p_4 = 0) \tag{32}$$

implies

$$Z_{2h} = 1 - \frac{d\Sigma}{d(ip_4)} \Big|_{ip_4 \rightarrow 0}. \quad (33)$$

The bare vertex function $V_{ij}^B(p)$ is defined as

$$\begin{aligned} V_{ij}^B(p) &= (S^B)^{-1}(p) \sum_{x,y} e^{ip(x-y)} \left\langle Q^B(x) O_{ij}^B(0) \bar{Q}^B(y) \right\rangle (S^B)^{-1}(p) \\ &= \frac{Z_D}{Z_{2h}} (S^R)^{-1}(p) \sum_{x,y} e^{ip(x-y)} \left\langle Q^R(x) O_{ij}^R(0) \bar{Q}^R(y) \right\rangle (S^R)^{-1}(p), \end{aligned} \quad (34)$$

where

$$O_{ij}^B(0) = Z_D O_{ij}^R(0). \quad (35)$$

$V_{ij}^B(p)$ can be written as

$$V_{ij}^B(p) = (1 + \delta V) \bar{u}(p) \gamma_i \gamma_5 p_j u(p) \equiv (1 + \delta V) V_{ij}^R(p). \quad (36)$$

δV is given by all the 1PI one-loop diagrams containing the vertex.

4.2 Analytical formulae and results

The notations used in this section and the Feynman rules are listed in appendix A. They are the same as in [33] except for the gluon propagator having the form

$$D_{\mu\nu} = C_0^{-1} D_{\mu\nu}^{\text{plaq}} + \Delta_{\mu\nu} \quad (37)$$

[34], where $C_0 = c_0 + 8c_1 + 16c_2 + 8c_3 \equiv 1$, $c_1 = -1/12$, $c_2 = c_3 = 0$ for the case of the tree-level Symanzik improved gauge action and

$$\Delta_{\mu\nu} = \delta_{\mu\nu} K_\mu + 4L_{\mu\nu} N_\mu N_\nu. \quad (38)$$

Finally K_μ and $L_{\mu\nu}$ are complicated expressions, which do not need to be reproduced here. The only relevant features for this work are that $\Delta_{\mu\nu}$ is regular in the infrared regime and $K_\mu = K^0 + 4N_\mu^2 K'_\mu$.

The static quark self-energy expressed at the first order of perturbation theory is given by $\Sigma(p) = -(F_1 + F_2)$, where F_1 and F_2 correspond to the diagrams shown in Figure 4(a) and (b):

$$F_1 = -\frac{4}{3a} g_0^2 \int_k h_{4i} h_{4j} D_{ij} \frac{e^{-i(k_4+2ap_4)}}{1 - e^{-i(k_4+ap_4)} + \epsilon} = F_1^{\text{plaq}} + F'_1 \quad (39)$$

$$\begin{aligned}
F_1^{\text{plaq}} &= -\frac{4}{3a}g_0^2 \int_k \frac{D_4^2 + \sum_{i=1}^3 G_{4i}^2}{2W + a^2\lambda^2} \frac{e^{-i(k_4+2ap_4)}}{1 - e^{-i(k_4+ap_4)} + \epsilon} \\
&\stackrel{ap_4 \rightarrow 0}{=} \frac{4}{3a}g_0^2 \int_{\vec{k}} \frac{D_4^2(-iE) + \sum_{i=1}^3 G_{4i}^2(-iE)}{4E\sqrt{1+E^2}} \frac{1}{1 - e^{E'}} \\
&\quad + \frac{4}{3}g_0^2 ip_4 \int_{\vec{k}} \frac{D_4^2(-iE) + \sum_{i=1}^3 G_{4i}^2(-iE)}{2E\sqrt{1+E^2}} \left[\frac{1}{e^{E'} - 1} + \frac{1}{2} \frac{1}{(e^{E'} - 1)^2} \right]
\end{aligned} \tag{40}$$

$$\begin{aligned}
F'_1 &= -\frac{4}{3a}g_0^2 \int_k h_{4i}h_{4j}\Delta_{ij} \frac{e^{-i(k_4+2ap_4)}}{1 - e^{-i(k_4+ap_4)} + \epsilon} = \\
&\stackrel{ap_4 \rightarrow 0}{=} -\frac{4}{3a}g_0^2 \int_k \frac{M_4 - iN_4}{2iN_4 + \epsilon M_4} \left(D_4^2 K^0 + N_4^2 \Lambda \right) \\
&\quad + \frac{8}{3}g_0^2 ip_4 \int_k \left[\frac{M_4 - iN_4}{2iN_4 + \epsilon M_4} + \frac{1}{2} \left(\frac{M_4 - iN_4}{2iN_4 + \epsilon M_4} \right)^2 \right] \left(D_4^2 K^0 + N_4^2 \Lambda \right) \\
&= \frac{2}{3a}g_0^2 \int_k \left(D_4^2 K^0 + N_4^2 \Lambda \right) - \frac{1}{3}g_0^2 ip_4 \int_k \left[M_4^2 \Lambda + 3 \left(D_4^2 K^0 + N_4^2 \Lambda \right) \right]
\end{aligned} \tag{41}$$

$$\begin{aligned}
N_4^2 \Lambda &= 4 \left(D_4^2 N_4^2 (K'_4 + L_{44}) + \frac{1}{4} \sum_i G_{4i}^2 (K^0 + 4N_i^2 K'_i) + 2D_4 N_4 \sum_{i=1}^3 G_{4i} N_i L_{4i} \right. \\
&\quad \left. + 2 \sum_{i,j=1}^3 G_{4i} G_{4j} N_i N_j L_{ij} \right)
\end{aligned} \tag{42}$$

$$F_2 = -\frac{1}{2} \frac{4g_0^2}{3a} e^{-iap_4} \int_k h_{4i}h_{4j} D_{ij} = F_2^{\text{plaq}} + F'_2 \tag{43}$$

$$\begin{aligned}
F_2^{\text{plaq}} &= -\frac{1}{2} \frac{4g_0^2}{3a} e^{-iap_4} \int_k \frac{D_4^2 + \sum_{i=1}^3 G_{4i}^2}{2W} \\
&\stackrel{ap_4 \rightarrow 0}{=} -\frac{1}{2} \frac{4g_0^2}{3} (1/a - ip_4) \int_k \frac{D_4^2 + \sum_{i=1}^3 G_{4i}^2}{2W}
\end{aligned} \tag{44}$$

$$F'_2 = -\frac{1}{2} \frac{4g_0^2}{3a} e^{-iap_4} \int_k h_{4i}h_{4j} \Delta_{ij} \stackrel{ap_4 \rightarrow 0}{=} -\frac{1}{2} \frac{4g_0^2}{3} (1/a - ip_4) \int_k (D_4^2 K^0 + N_4^2 \Lambda). \tag{45}$$



Figure 4: self-energy corrections.

The factor $1/2$ has been introduced to compensate the over-counting of the factor 2 in the Feynman rule of the two-gluon vertex, when a closed gluonic loop is computed.

The other terms entering the above integrals cancel, because the contour can be closed in the complex plane without including the pole $k_4 = -p_4 + i \ln(1 + \epsilon)$. Finally we can write

$$F_1 \equiv -\frac{g_0^2}{12\pi^2} \left[\left(f_1^{\text{plaq}}(\alpha_i) + f'_1(\alpha_i, c_i) \right)/a + ip_4 \left(2 \ln(a^2 \lambda^2) + f_2^{\text{plaq}}(\alpha_i) + f'_2(\alpha_i, c_i) \right) \right] \quad (46)$$

$$F_2 \equiv -\frac{g_0^2}{12\pi^2} \left(1/a - ip_4 \right) \left(f_3^{\text{plaq}}(\alpha_i) + f'_3(\alpha_i, c_i) \right). \quad (47)$$

The linearly divergent part in $1/a$ of the self-energy is given by

$$\Sigma_0(\alpha_i) = \frac{g_0^2}{12\pi^2 a} \sigma_0(\alpha_i), \quad \sigma_0 = f_1 + f'_1 + f_3 + f'_3, \quad (48)$$

while the wave function renormalization Z_{2h} reads

$$Z_{2h}(\alpha_i) = 1 + \frac{g_0^2}{12\pi^2} \left(-2 \ln(a^2 \lambda^2) + z_2(\alpha_i) \right), \quad z_2 = f_3 + f'_3 - (f_2 + f'_2). \quad (49)$$

In Table 7 we have collected the numerical values of f_i , f'_i , σ_0 and z_2 for different kinds of static quark and gluonic actions.

The vertex function V_{ij}^B is obtained by writing

$$V_{ij}^B = V_{ij}^0 + V_{ij}^1 + V_{ij}^2, \quad V_{ij}^k(\alpha_i) = \bar{u}(p) \gamma_i \gamma^5 u(p) V_j^k(\alpha_i), \quad l = 0, 1, 2 \quad (50)$$

corresponding to the diagrams (a), (b) and (c) in Figure 5. The contribution V_{ij}^0 is given by computing

$$V_j^0(\alpha_i) = -\frac{4i}{3a} g_0^2 \int_k h_{4k} h_{4l} D_{kl} \sin(k + ap)_j \frac{e^{-i(k_4 + 2ap_4)}}{(1 - e^{-i(k_4 + ap_4)} + \epsilon)^2} = V_j^{0,\text{plaq}} + V_j'^0 \quad (51)$$

$$V_j^{0,\text{plaq}} = -\frac{4i}{3a} g_0^2 \int_k \frac{D_4^2 + \sum_{i=1}^3 G_{4i}^2}{2W + a^2 \lambda^2} \sin(k + ap)_j \frac{e^{-i(k_4 + 2ap_4)}}{(1 - e^{-i(k_4 + ap_4)} + \epsilon)^2}$$

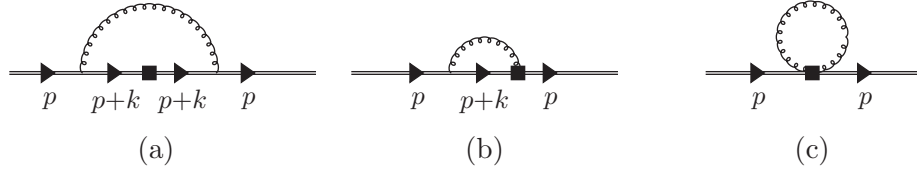


Figure 5: operator corrections.

$$\begin{aligned}
&= -\frac{4i}{3a}g_0^2 \int_k \frac{D_4^2 + \sum_{i=1}^3 G_{4i}^2}{2W + a^2\lambda^2} \left(\Gamma_j + ap_j \cos(k_j) \right) e^{-iap_4} \left(\frac{e^{-i\frac{k_4+ap_4}{2}}}{1 - e^{-i(k_4+ap_4)} + \epsilon} \right)^2 \\
&= -\frac{4i}{3a}g_0^2 \int_k \frac{D_4^2 + \sum_{i=1}^3 G_{4i}^2}{2W + a^2\lambda^2} \left(\Gamma_j + ap_j \cos(k_j) \right) (1 - iap_4) \\
&\quad \times \frac{1}{\left[2i \sin\left(\frac{k_4+ap_4}{2}\right) + e^{i\frac{k_4+ap_4}{2}} \epsilon \right]^2} \\
&= -\frac{4}{3}ig_0^2 p_j \int_k \frac{D_4^2 + \sum_{i=1}^3 G_{4i}^2}{2W + a^2\lambda^2} \frac{\cos(k_j)}{(2iN_4 + \epsilon M_4)^2}
\end{aligned} \tag{52}$$

$$\begin{aligned}
V_j'^0 &= -\frac{4i}{3a}g_0^2 \int_k h_{4k}h_{4l}\Delta_{kl} \left(\Gamma_j + ap_j \cos(k_j) \right) e^{-iap_4} \left(\frac{e^{-i\frac{k_4+ap_4}{2}}}{1 - e^{-i(k_4+ap_4)} + \epsilon} \right)^2 \\
&= -\frac{4i}{3a}g_0^2 \int_k h_{4k}h_{4l}\Delta_{kl} \left(\Gamma_j + ap_j \cos(k_j) \right) (1 - iap_4) \frac{1}{\left(2i \sin\left(\frac{k_4+ap_4}{2}\right) + e^{i\frac{k_4+ap_4}{2}} \epsilon \right)^2} \\
&= -\frac{4i}{3}g_0^2 p_j \int_k \left(D_4^2 K^0 + N_4^2 \Lambda \right) \cos(k_j) \frac{1}{(2iN_4 + \epsilon M_4)^2} = \frac{1}{3}g_0^2 ip_j \int_k \Lambda \cos(k_j).
\end{aligned}$$

The “sail diagram” has the following expression:

$$\begin{aligned}
V_j^1 &= \frac{4}{3a}g_0^2 \int_k h_{4l}D_{lj} \cos\left(\frac{k_j}{2} + ap_j\right) \frac{e^{-i\frac{k_4+ap_4}{2}}}{1 - e^{-i(k_4+ap_4)} + \epsilon} = V_j^{1,\text{plaq}} + V_j'^1 \\
V_j^{1,\text{plaq}} &= \frac{4}{3a}g_0^2 \int_k \frac{G_{4j}}{2W + a^2\lambda^2} \left(M_j - ap_j N_j \right) \left(1 - i\frac{ap_4}{2} \right) \frac{1}{2i \sin\left(\frac{k_4+ap_4}{2}\right) + e^{i\frac{k_4+ap_4}{2}} \epsilon} \\
&= -\frac{4}{3a}g_0^2 p_j \int_k \frac{G_{4j}N_j}{2W + a^2\lambda^2} \frac{1}{2iN_4 + \epsilon M_4} = \frac{2}{3}g_0^2 ip_j \int_k \frac{G'_{4j}N_j}{2W + a^2\lambda^2}, \\
G_{4j} &= N_4 G'_{4j}
\end{aligned} \tag{53}$$

$$\begin{aligned}
V_j'^1 &= \frac{4}{3a}g_0^2 \int_k h_{4l}\Delta_{lj} \left(M_j - ap_j N_j \right) \left(1 - i\frac{ap_4}{2} \right) \frac{1}{2i \sin\left(\frac{k_4+ap_4}{2}\right) + e^{i\frac{k_4+ap_4}{2}} \epsilon} \\
&= -\frac{4}{3}g_0^2 p_j \int_k \left(4D_4 N_4 N_j L_{4j} + N_4 N_j \Lambda'_j \right) N_j \frac{1}{2iN_4 + \epsilon M_4} \\
&= \frac{2}{3}g_0^2 ip_j \int_k N_j^2 \left(4D_4 L_{4j} + \Lambda'_j \right), \quad N_4 N_j \Lambda'_j = \sum_{i=1}^3 G_{4i} \Delta_{ij}.
\end{aligned} \tag{54}$$

Note that the contribution of the sail diagram to the final result must be doubled, because the gluon leg can be attached to the static line in two different ways. Eventually the tadpole diagram is given by

$$V_j^2(\alpha_i) = -\frac{1}{2!} \frac{4}{3} ig_0^2 p_j \int_k D_{44} = -\frac{ig_0^2}{12\pi^2} p_j \left(f_3(\alpha_i = 0) + f'_3(\alpha_i = 0, c_i) \right). \tag{55}$$

We finally have

$$\langle H^{**} | O_{ij}^R | H \rangle = \frac{1}{Z_{\mathcal{D}}(\alpha_i)} \langle H^{**} | O_{ij}^B | H \rangle(\alpha_i), \quad (56)$$

where

$$Z_{\mathcal{D}}(\alpha_i) = Z_{2h}(\alpha_i) \left(1 + \delta V(\alpha_i) \right) \quad (57)$$

$$\delta V(\alpha_i) \equiv \frac{g_0^2}{12\pi^2} \left(2 \ln(a^2 \lambda^2) + f_4(\alpha_i) + f'_4(\alpha_i, c_i) \right) \quad (58)$$

i.e.

$$Z_{\mathcal{D}}(\alpha_i) = 1 + \frac{g_0^2}{12\pi^2} z_d(\alpha_i), \quad z_d = z_2 + f_4 + f'_4. \quad (59)$$

The numerical values of z_d are collected in Table 7 for the different kinds of static quark and gluonic actions. With the bare coupling $g_0^2 \equiv 6/\beta$, the tree-level Symanzik improved gauge action at $\beta = 3.9$ and the HYP2 static quark action used in our simulations we obtain $Z_{\mathcal{D}}(\text{tlSym}, \text{HYP2}) = 0.976$.

	$\alpha_i = 0$	HYP1	HYP2
f_1	7.72	1.64	-1.76
$f'_1(\text{tlSym})$	2.10	0.14	0.83
f_2	-12.25	1.60	9.58
$f'_2(\text{tlSym})$	-3.43	-0.12	-1.50
f_3	12.23	4.12	5.96
$f'_3(\text{tlSym})$	-2.10	-0.14	-0.83
f_4	-12.68	-4.95	-0.56
$f'_4(\text{tlSym})$	3.56	2.04	1.67
σ_0	19.95	5.76	4.20
$z_2(\text{plaq})$	24.48	2.52	-3.62
$z_2(\text{tlSym})$	25.81	2.50	-2.96
$z_d(\text{plaq})$	11.80	-2.43	-4.19
$z_d(\text{tlSym})$	16.69	-0.41	-1.85

Table 7: numerical values of the constants $f_1, f'_1, f_2, f'_2, f_3, f'_3, f_4, f'_4, \sigma_0, z_2$ and z_d defined in the text; $\alpha_i = 0$ denotes the unsmeared Eichten-Hill static quark action, while HYP1 and HYP2 are defined in [25] and [27] respectively; “plaq” denotes the standard Wilson plaquette gauge action, while “tlSym” denotes the tree-level Symanzik improved gauge action.

5 Conclusions

We have computed the form factors $\tau_{1/2}(1)$ and $\tau_{3/2}(1)$ in the static limit, which describe (in this limit) the decay $B \rightarrow D^{**}$. This decay is presently a puzzle in the sense that sum rules

derived from QCD point towards a dominance of $\tau_{3/2}(1)$, while experimental indications point rather in the opposite direction. The aim of this paper has been to check the dominance of $\tau_{3/2}(1)$ in a quantitative way.

Our final result extrapolated to the physical u/d quark mass is given in Table 6. Since we see no systematic dependence on the temporal separation $t_0 - t_2$ except for an increase in statistical uncertainty, we keep the result at $t_0 - t_2 = 10$. To the statistical error we add a systematical error of 3% to account for the uncertainty in the computation of the renormalization constant Z_D , which was computed perturbatively. We make the “guesstimate” of 100% uncertainty on $1 - Z_D$, which turns out to be very small. Notice that this uncertainty does not apply to the ratio $\tau_{3/2}(1)/\tau_{1/2}(1)$ both having the same Z_D (cf. eqns. (25) and (26)). We have at this stage no way to estimate systematic uncertainties arising from finite lattice spacing and from finite volume. Therefore, we must consider the errors we quote as incomplete. We end up with

$$\tau_{1/2}(1) = 0.296(26), \quad \tau_{3/2}(1) = 0.526(23) \quad (60)$$

$$\frac{\tau_{3/2}(1)}{\tau_{1/2}(1)} = 1.6 \dots 1.8, \quad \left| \tau_{3/2}(1) \right|^2 - \left| \tau_{1/2}(1) \right|^2 \approx 0.17 \dots 0.21 \quad (61)$$

in fair agreement with the qualitative claim that $\tau_{3/2}$ is significantly larger than $\tau_{1/2}$. Note also that Uraltsev’s sum rule is almost saturated by the ground state contributions providing $\approx 80\%$ of the required $1/4$ (cf. eqn. (1)).

This result does not differ qualitatively from the preliminary quenched computation [7]: $\tau_{1/2} = 0.38(5)$ and $\tau_{3/2} = 0.53(8)$. However, we consider the result presented in this paper as standing on a much firmer ground, because it is unquenched, and because the signal is much clearer and more stable thanks to better analysis procedures. Our result (60) is also similar to the prediction of a Bakamjian-Thomas relativistic quark model [4], when using a Godfrey-Isgur interquark potential: $\tau_{1/2} = 0.22$ and $\tau_{3/2} = 0.54$.

Assuming that the heavy quark limit provides reliable indications and that the standard identification of narrow D^{**} resonances is correct (i.e. $D_1(2420)$ ($J = 1$) and $D_2^*(2460)$ ($J = 2$) correspond to $j = 3/2$ mesons) this points towards the expected dominance of the semileptonic decay of B mesons into these $j = 3/2$ states over the decay into $j = 1/2$ states. The latter, labeled as D_0^* ($J = 0$) and D_1' ($J = 1$) are identified to some broad structures, which are seen in the semileptonic B decay around similar masses (2200 MeV to 2600 MeV). Remember, however, that the predicted ratio of branching fractions $\text{Br}(B \rightarrow D_{3/2}^{**})/\text{Br}(B \rightarrow D_{1/2}^{**})$ is mainly governed by $(\tau_{3/2}(1)/\tau_{1/2}(1))^2$ times a rather large ratio of phase-space factors.

It is usually claimed from experiment that the decay into these broad resonances are not sub-dominant as compared to the narrow resonances. A recent analysis by BABAR [35, 36] finds significant $B \rightarrow D^{(*)}\pi l\nu$, but does not give the relative yield of narrow and broad resonances. In a recent paper by BELLE [37] the four D^{**} states are distinguished. The $B \rightarrow D_0^* l\nu$ is observed with a comparatively large signal and, assuming the heavy quark limit to be applicable, they fit $\tau_{3/2}(1) = 0.75$ and $\tau_{1/2}(1) = 1.28$. Compared to our result (60) this calls for two comments:

- (1) The $\tau_{3/2}(1)$ shows fair agreement between theory and experiment. This is encouraging, since the narrow resonances are experimentally rather well under control, i.e. the narrow resonances are well seen.

- (2) The experimental $\tau_{1/2}(1)$ is much larger than our prediction. Note, however, that BELLE does not see the other member of the $j = 1/2$ doublet, $B \rightarrow D'_1 l \nu$. This is puzzling and the discrepancy concerning $\tau_{1/2}(1)$ should not be taken as final.

In view of the impressive convergence of almost all theoretical estimates of $\tau_{1/2}(1)$ and $\tau_{3/2}(1)$, in view of our confidence that the result presented in this paper stands on a firm ground, we believe that one can consider as established that QCD predicts a clear dominance of the decay into $j = 3/2$ in the static limit.

It still remains to be solved, how to saturate the inclusive semileptonic branching ratio, in other words what to add to the $B \rightarrow D^{(*)} l \nu$ and to the narrow D^{**} resonances. The analyses performed on Class I non-leptonic $B \rightarrow D^{**}\pi$ decay do not find any trace of broad structures [38, 39]. Invoking factorization, theoretically well under control for this kind of process this naturally leads again to $\tau_{1/2}(1) < \tau_{3/2}(1)$.

Experimental work still has to be done. On the theory side, beyond doing the computation at another finer lattice spacing to be able to perform a continuum extrapolation (theoretically well defined, as recalled in Section 2), an estimate of the $1/m_c$ corrections would help a lot. To explore that issue a promising method used to study the $B \rightarrow D^{(*)} l \nu$ form factors at non-zero recoil [40, 41] might be helpful. The contributions of other states such as negative parity radial excitations should also be considered.

Let us conclude by insisting that the issue at clue is of important relevance: any accurate estimate of the V_{cb} parameter of the standard model will never be fully convincing as long as the “ $1/2$ versus $3/2$ puzzle” remains unsolved.

Acknowledgments

B.B. and O.P. thank Ikaros Bigi and the other authors of [1] for many discussions on these issues and having stimulated the present work. We also thank Vladimir Galkin, Karl Jansen, Chris Michael, David Palao and Andrea Shindler for many helpful discussions.

This work has been supported in part by the EU Contract No. MRTN-CT-2006-035482, “FLAVIAnet”, by the DFG Sonderforschungsbereich/Transregio SFB/TR9-03 and by the project ANR-NT-05-3-43577 (QCDNEXT).

We thank CCIN2P3 in Lyon and the Jülich Supercomputing Center (JSC) for having allocated to us computer time, which was used in this work.

A Feynman rules

The lattice HQET action is

$$S^{\text{HQET}} = a^3 \sum_n \left(Q^\dagger(n) \left(Q(n) - U_4^{\dagger, \text{HYP}}(n - \hat{4}) Q(n - \hat{4}) \right) + a\delta m Q^\dagger(n) Q(n) \right), \quad (62)$$

where $U_4^{\text{HYP}}(n)$ is a link built from hypercubic blocking.

We will use in the rest of this appendix the following notations taken from [42, 43, 44]:

$$\int_p \equiv \int_{-\pi/a}^{\pi/a} \frac{d^4 p}{(2\pi)^4}, \quad \int_{\vec{p}} \equiv \int_{-\pi/a}^{\pi/a} \frac{d^3 p}{(2\pi)^3}, \quad a^4 \sum_n e^{ipn} = \delta(p) \quad (63)$$

$$\int_k \equiv \int_{-\pi}^{\pi} \frac{d^4 k}{(2\pi)^4}, \quad \int_{\vec{k}} \equiv \int_{-\pi}^{\pi} \frac{d^3 k}{(2\pi)^3} \quad (64)$$

$$h(n) = \int_p e^{ipn} h(p) \quad (65)$$

$$U_\mu(n) = e^{iag_0 A_\mu^a(n) T^a} = 1 + iag_0 A_\mu^a(n) T^a - \frac{a^2 g_0^2}{2!} A_\mu^a(n) A_\mu^b(n) T^a T^b + \mathcal{O}(g_0^3) \quad (66)$$

$$U_\mu^{\text{HYP}}(n) = e^{iag_0 B_\mu^a(n) T^a} = 1 + iag_0 B_\mu^a(n) T^a - \frac{a^2 g^2}{2!} B_\mu^a(n) B_\mu^b(n) T^a T^b + \mathcal{O}(g_0^3) \quad (67)$$

$$A_\mu^a(n) = \int_p e^{ip(n+\frac{a}{2})} A_\mu^a(p), \quad B_\mu^a(n) = \int_p e^{ip(n+\frac{a}{2})} B_\mu^a(p) \quad (68)$$

$$\Gamma_\lambda = \sin(ak_\lambda) \quad (69)$$

$$c_\mu = \cos\left(\frac{a(p+p')_\mu}{2}\right), \quad s_\mu = \sin\left(\frac{a(p+p')_\mu}{2}\right) \quad (70)$$

$$M_\mu = \cos\left(\frac{k_\mu}{2}\right), \quad N_\mu = \sin\left(\frac{k_\mu}{2}\right) \quad (71)$$

$$W = 2 \sum_\lambda \sin^2\left(\frac{k_\lambda}{2}\right) \quad (72)$$

$$E^2 = \sum_{i=1}^3 N_i^2 + \frac{a^2 \lambda^2}{4}, \quad E' = 2 \arg \operatorname{sh}(E). \quad (73)$$

In Fourier space the action at $\mathcal{O}(g_0^2)$ is given by

$$\begin{aligned} S^{\text{HQET}} &= \int_p \frac{1}{a} Q^\dagger(p) (1 - e^{-ip_4 a}) Q(p) + \delta m Q^\dagger(p) Q(p) \\ &\quad + ig_0 \int_p \int_{p'} \int_q \delta(q + p' - p) Q^\dagger(p) B_4^a(q) T^a Q(p') e^{-i(p_4 + p'_4) \frac{a}{2}} \\ &\quad + \frac{ag_0^2}{2!} \int_p \int_{p'} \int_q \int_r \delta(q + r + p' - p) Q^\dagger(p) B_4^a(q) B_4^b(r) T^a T^b Q(p') e^{-i(p_4 + p'_4) \frac{a}{2}}. \end{aligned} \quad (74)$$

The block gauge fields B_μ^a can be expressed in terms of the usual gauge fields:

$$B_\mu = \sum_{n=1}^{\infty} B_\mu^{(n)}, \quad (75)$$

where $B_\mu^{(n)}$ contains n factors of A . At next to leading order, it was shown that we only need $B_\mu^{(1)}$ [45]:

$$B_\mu^{(1)}(k) = \sum_\nu h_{\mu\nu}(k) A_\nu(k) \quad (76)$$

$$h_{\mu\nu}(k) = \delta_{\mu\nu}D_\mu(k) + (1 - \delta_{\mu\nu})G_{\mu\nu}(k) \quad (77)$$

$$D_\mu(k) = 1 - d_1 \sum_{\rho \neq \mu} N_\rho^2 + d_2 \sum_{\rho < \sigma, \rho, \sigma \neq \mu} N_\rho^2 N_\sigma^2 - d_3 N_\rho^2 N_\sigma^2 N_\tau^2 \quad (78)$$

$$G_{\mu\nu}(k) = N_\mu N_\nu \left(d_1 - d_2 \frac{N_\rho^2 + N_\sigma^2}{2} + d_3 \frac{N_\rho^2 N_\sigma^2}{3} \right) \quad (79)$$

$$d_1 = \frac{2}{3}\alpha_1 \left(1 + \alpha_2(1 + \alpha_3) \right), \quad d_2 = \frac{4}{3}\alpha_1\alpha_2(1 + 2\alpha_3), \quad d_3 = 8\alpha_1\alpha_2\alpha_3. \quad (80)$$

The Feynman rules are the following:

heavy quark propagator vertex $V_{\mu,hhg}^a(p, p')$ vertex $V_{\mu\nu,hgg}^{ab}(p, p')$ gluon propagator in the Feynman gauge	$a(1 - e^{-ip_4a} + \epsilon)^{-1}$ $-ig_0 T^a \delta_{\mu 4} \sum_\rho h_{\mu\rho} e^{-i(p_4 + p'_4)\frac{a}{2}}$ $-\frac{1}{2}ag_0^2 \delta_{\mu 4} \delta_{\nu 4} \sum_{\rho, \sigma} h_{\mu\rho} h_{\nu\sigma} \{T^a, T^b\} e^{-i(p_4 + p'_4)\frac{a}{2}}$ $a^2(C_0^{-1} \delta_{\mu\nu} \delta^{ab} (2W + a^2 \lambda^2)^{-1} + \Delta_{\mu\nu})$
---	--

Note that p' and p are the in-going and the out-going fermion momenta, respectively. We also introduce an infrared regulator λ for the gluon propagator. We symmetrize the vertex $V_{\mu\nu,hgg}^{ab}$ by introducing the anti-commutator of the $SU(3)$ generators normalized by a factor 1/2. The gluon propagator and the vertices are defined with the A field. At one-loop the infrared regulator to the gluon propagator that we have chosen is legitimate, because no three-gluon vertex is involved.

References

- [1] I. I. Bigi *et al.*, “Memorino on the ‘1/2 vs. 3/2 puzzle’ in $\bar{B} \rightarrow l \bar{\nu} X_c$ – a year later and a bit wiser,” Eur. Phys. J. C **52**, 975 (2007) [arXiv:0708.1621 [hep-ph]].
- [2] A. Le Yaouanc, L. Oliver, O. Pene and J. C. Raynal, “New heavy quark limit sum rules involving Isgur-Wise functions and decay constants,” Phys. Lett. B **387**, 582 (1996) [arXiv:hep-ph/9607300].
- [3] N. Uraltsev, “New exact heavy quark sum rules,” Phys. Lett. B **501**, 86 (2001) [arXiv:hep-ph/0011124].
- [4] V. Morenas, A. Le Yaouanc, L. Oliver, O. Pene and J. C. Raynal, “Quantitative predictions for B semileptonic decays into D , D^* and the orbitally excited D^{**} in quark models a la Bakamjian-Thomas,” Phys. Rev. D **56** (1997) 5668 [arXiv:hep-ph/9706265].
- [5] D. Ebert, R. N. Faustov and V. O. Galkin, “Exclusive semileptonic decays of B mesons to orbitally excited D mesons in the relativistic quark model,” Phys. Lett. B **434**, 365 (1998) [arXiv:hep-ph/9805423].
- [6] D. Ebert, R. N. Faustov and V. O. Galkin, “Heavy quark $1/m(Q)$ contributions in semileptonic B decays to orbitally excited D mesons,” Phys. Rev. D **61**, 014016 (2000) [arXiv:hep-ph/9906415].

- [7] D. Becirevic *et al.*, “Lattice measurement of the Isgur-Wise functions $\tau_{u1/2}$ and $\tau3/2$,” *Phys. Lett. B* **609**, 298 (2005) [arXiv:hep-lat/0406031].
- [8] M. Crisafulli, V. Gimenez, G. Martinelli and C. T. Sachrajda, “First lattice calculation of the B meson binding and kinetic energies,” *Nucl. Phys. B* **457**, 594 (1995) [arXiv:hep-ph/9506210].
- [9] M. Della Morte, N. Garron, M. Papinutto and R. Sommer, “Heavy quark effective theory computation of the mass of the bottom quark,” *JHEP* **0701**, 007 (2007) [arXiv:hep-ph/0609294].
- [10] K. Jansen, C. Michael, A. Shindler and M. Wagner [ETM Collaboration], “Static-light meson masses from twisted mass lattice QCD,” *PoS LATTICE2008*, 122 (2008) [arXiv:0808.2121 [hep-lat]].
- [11] K. Jansen, C. Michael, A. Shindler and M. Wagner [ETM Collaboration], “The static-light meson spectrum from twisted mass lattice QCD,” *JHEP* **0812**, 058 (2008) [arXiv:0810.1843 [hep-lat]].
- [12] N. Isgur and M. B. Wise, “Weak decays of heavy mesons in the static quark approximation,” *Phys. Lett. B* **232**, 113 (1989).
- [13] N. Isgur and M. B. Wise, “Weak transition form-factors between heavy mesons,” *Phys. Lett. B* **237**, 527 (1990).
- [14] N. Isgur and M. B. Wise, “Excited charm mesons in semileptonic \bar{B} decay and their contributions to a Bjorken sum rule,” *Phys. Rev. D* **43**, 819 (1991).
- [15] E. Eichten and B. R. Hill, “An effective field theory for the calculation of matrix elements involving heavy quarks,” *Phys. Lett. B* **234**, 511 (1990).
- [16] A. K. Leibovich, Z. Ligeti, I. W. Stewart and M. B. Wise, “Semileptonic B decays to excited charmed mesons,” *Phys. Rev. D* **57**, 308 (1998) [arXiv:hep-ph/9705467].
- [17] N. Isgur and M. B. Wise, “Excited charm mesons in semileptonic \bar{B} decay and their contributions to a Bjorken sum rule,” *Phys. Rev. D* **43**, 819 (1991).
- [18] Ph. Boucaud *et al.* [ETM Collaboration], “Dynamical twisted mass fermions with light quarks,” *Phys. Lett. B* **650**, 304 (2007) [arXiv:hep-lat/0701012].
- [19] C. Urbach [ETM Collaboration], “Lattice QCD with two light Wilson quarks and maximally twisted mass,” *PoS LAT2007*, 022 (2007) [arXiv:0710.1517 [hep-lat]].
- [20] Ph. Boucaud *et al.* [ETM collaboration], “Dynamical twisted mass fermions with light quarks: simulation and analysis details,” *Comput. Phys. Commun.* **179**, 695 (2008) [arXiv:0803.0224 [hep-lat]].
- [21] P. Weisz, “Continuum Limit Improved Lattice Action For Pure Yang-Mills Theory. 1,” *Nucl. Phys. B* **212**, 1 (1983).
- [22] R. Frezzotti, P. A. Grassi, S. Sint and P. Weisz [Alpha collaboration], “Lattice QCD with a chirally twisted mass term,” *JHEP* **0108**, 058 (2001) [arXiv:hep-lat/0101001].

- [23] R. Frezzotti and G. C. Rossi, “Chirally improving Wilson fermions. I: O(a) improvement,” JHEP **0408**, 007 (2004) [arXiv:hep-lat/0306014].
- [24] A. Shindler, “Twisted mass lattice QCD,” Phys. Rept. **461**, 37 (2008) [arXiv:0707.4093 [hep-lat]].
- [25] A. Hasenfratz and F. Knechtli, “flavour symmetry and the static potential with hypercubic blocking,” Phys. Rev. D **64**, 034504 (2001) [arXiv:hep-lat/0103029].
- [26] M. Della Morte *et al.*, “Lattice HQET with exponentially improved statistical precision,” Phys. Lett. **B581**, 93, (2004) [arXiv:hep-lat/0307021].
- [27] M. Della Morte, A. Shindler and R. Sommer, “On lattice actions for static quarks,” JHEP **0508**, 051 (2005) [arXiv:hep-lat/0506008].
- [28] S. Gusken, “A study of smearing techniques for hadron correlation functions,” Nucl. Phys. Proc. Suppl. **17** (1990) 361.
- [29] M. Albanese *et al.* [APE Collaboration], “Glueball masses and string tension in lattice QCD,” Phys. Lett. B **192**, 163 (1987).
- [30] M. Lüscher and U. Wolff, “How to calculate the elastic scattering matrix in two-dimensional quantum field theories by numerical simulation,” Nucl. Phys. B **339**, 222 (1990).
- [31] B. Blossier, M. Della Morte, G. von Hippel, T. Mendes and R. Sommer, “On the generalized eigenvalue method for energies and matrix elements in lattice field theory,” arXiv:0902.1265 [hep-lat].
- [32] C. Gattringer, “Excited hadrons on the lattice - state of the art and future challenges,” arXiv:0711.0622 [hep-lat].
- [33] B. Blossier, A. Le Yaouanc, V. Morenas and O. Pene, “Lattice renormalization of the static quark derivative operator,” Phys. Lett. B **632**, 319 (2006) [Erratum-ibid. B **645**, 476 (2007)] [arXiv:hep-lat/0507024].
- [34] R. Horsley, H. Perlt, P. E. L. Rakow, G. Schierholz and A. Schiller [QCDSF Collaboration], “One-loop renormalisation of quark bilinears for overlap fermions with improved gauge actions,” Nucl. Phys. B **693**, 3 (2004) [Erratum-ibid. B **713**, 601 (2005)] [arXiv:hep-lat/0404007].
- [35] B. Aubert *et al.* [BABAR Collaboration], “Measurement of the branching fractions of exclusive $\bar{B} \rightarrow D/D^*/D^{(*)} \pi l^- \bar{\nu}_l$ decays in events tagged by a fully reconstructed B meson,” arXiv:0708.1738 [hep-ex].
- [36] B. Aubert *et al.* [BABAR Collaboration], “Measurement of the branching fractions of $\bar{B} \rightarrow D^{**} l^- \bar{\nu}_l$ decays in events tagged by a fully reconstructed B meson,” Phys. Rev. Lett. **101**, 261802 (2008) [arXiv:0808.0528 [hep-ex]].
- [37] D. Liventsev *et al.* [Belle Collaboration], “Study of $B \rightarrow D^{**} l \nu$ with full reconstruction tagging,” Phys. Rev. D **77**, 091503 (2008) [arXiv:0711.3252 [hep-ex]].

- [38] K. Abe *et al.* [Belle Collaboration], “Study of $B_0 \rightarrow \bar{D}_0^{(*)} \pi^+ \pi^-$ decays,” arXiv:hep-ex/0412072.
- [39] B. Aubert *et al.* [BABAR Collaboration], “Measurement of the absolute branching fractions $B \rightarrow D\pi, D^*\pi, D^{**}\pi$ with a missing mass method,” Phys. Rev. D **74**, 111102 (2006) [arXiv:hep-ex/0609033].
- [40] G. M. de Divitiis, R. Petronzio and N. Tantalo, “Quenched lattice calculation of semileptonic heavy-light meson form factors,” JHEP **0710**, 062 (2007) [arXiv:0707.0587 [hep-lat]].
- [41] G. M. de Divitiis, R. Petronzio and N. Tantalo, “Quenched lattice calculation of the vector channel $B \rightarrow D^* l \nu$ decay rate,” Nucl. Phys. B **807**, 373 (2009) [arXiv:0807.2944 [hep-lat]].
- [42] S. Capitani, “Lattice perturbation theory,” Phys. Rept. **382**, 113 (2003) [arXiv:hep-lat/0211036].
- [43] T. A. DeGrand, “One loop matching coefficients for a variant overlap action and some of its simpler relatives,” Phys. Rev. D **67**, 014507 (2003) [arXiv:hep-lat/0210028].
- [44] W. J. Lee and S. R. Sharpe, “Perturbative matching of staggered four-fermion operators with hypercubic fat links,” Phys. Rev. D **68**, 054510 (2003) [arXiv:hep-lat/0306016].
- [45] W. J. Lee, “Perturbative improvement of staggered fermions using fat links,” Phys. Rev. D **66**, 114504 (2002) [arXiv:hep-lat/0208032].

Masses of mesons with charm valence quarks from $2+1+1$ flavor twisted mass lattice QCD*

MARTIN KALINOWSKI, MARC WAGNER

Goethe-Universität Frankfurt am Main, Institut für Theoretische Physik,
Max-von-Laue-Straße 1, D-60438 Frankfurt am Main, Germany
European Twisted Mass Collaboration

We present preliminary results of an ongoing lattice QCD computation of the spectrum of D mesons and D_s mesons and of charmonium using 2+1+1 flavors of twisted mass sea and valence quarks.

PACS numbers: 12.38.Gc, 14.40.Lb.

1. Introduction

There is considerable interest in the spectrum of D and D_s mesons and of charmonium both theoretically and experimentally.

On the theory side first principles calculations are usually lattice QCD computations (for recent work cf. e.g. [1, 2, 3, 4, 5, 6]). In the last couple of years a lot of progress has been made, allowing the determination of hadron masses like the aforementioned mesons with rather high precision. For example 2+1 or even 2+1+1 flavors of dynamical quark are often used as well as small lattice spacings and improved discretizations, to keep discretization errors (in particular those, associated with the heavy charm quarks) under control. Some groups have even started to determine the resonance parameters of certain mesons from the spectrum of two-particle scattering states in finite spatial volumes (cf. e.g. [7]).

Experimentally a large number of D , D_s and charmonium states has been measured and additional and/or more precise results are expected in the near future both from existing facilities and facilities currently under construction, like the PANDA experiment at FAIR. Even though these experimental results have been extremely helpful, to improve our understanding of QCD, they also brought up new and yet unanswered questions. For example the positive parity mesons D_{s0}^* and D_{s1} are unexpectedly light,

* Presented at “Excited QCD 2013”, Bjelasnica Mountain, Sarajevo.

which is at the moment not satisfactorily understood and also quite often not reproduced by lattice QCD computations or model calculations.

Moreover, performing a precise computation of certain meson masses is often the first step for many lattice projects not primarily concerned with spectroscopy. As an example one could mention the semileptonic decay of B and B^* mesons into positive parity D mesons [8], whose masses and operator contents are an essential ingredient for any corresponding lattice computation.

This is a status report about an ongoing lattice QCD project concerned with the computation of the spectrum of mesons with at least one charm valence quark. We present preliminary results for D mesons, for D_s mesons and for charmonium states with total angular momentum $J = 0, 1$ and parity $P = -, +$. Parts of this work have already been published [9].

2. Simulation and analysis setup

We use gauge link configurations with 2+1+1 dynamical quark flavors generated by the European Twisted Mass Collaboration (ETMC) [10, 11, 12, 13, 14, 15]. Until now we have considered two ensembles (around 600 gauge link configurations per ensemble) with (unphysically heavy) values for the light u/d quark mass corresponding to $m_\pi \approx 325$ MeV, 457 MeV (lattice sizes $(L/a)^3 \times T/a = 32^3 \times 64, 24^3 \times 48$). Our results are obtained at a single lattice spacing $a \approx 0.086$ fm. Consequently, a continuum extrapolation has not yet been performed.

Meson masses are determined by computing and studying temporal correlation matrices of suitably chosen meson creation operators \mathcal{O}_j . At the moment we exclusively consider quark antiquark operators. The quark and the antiquark are combined in spin space via γ matrices and in color and position space via gauge links (discretized covariant derivatives) such that the corresponding trial states $\mathcal{O}_j|\Omega\rangle$ ($|\Omega\rangle$ denotes the vacuum) are gauge invariant and have defined total angular momentum and parity. Moreover, APE and Gaussian smearing is used, to optimize the overlap of the trial states $\mathcal{O}_j|\Omega\rangle$ to the low lying mesonic states of interest. More details regarding the construction of meson creation operators in twisted mass lattice QCD can be found e.g. in [16]. We plan to discuss these operators, their structure and their quantum numbers in detail in an upcoming publication. For the computation of the corresponding correlation matrices $\langle \mathcal{O}_j^\dagger(t)\mathcal{O}(0) \rangle$ we resort to the one-end trick (cf. e.g. [17]). Meson masses are then determined from plateaux values of corresponding effective masses, which we obtain by solving generalized eigenvalue problems (cf. e.g. [18]). Disconnected diagrams appearing in charmonium correlators are currently neglected.

For both the valence strange and charm quarks we use degenerate twisted

mass doublets, i.e. a different discretization as for the corresponding sea quarks. We do this, to avoid mixing of strange and charm quarks, which inevitably takes place in a unitary setup, and which is particularly problematic for hadrons containing charm quarks [14, 15]. The degenerate valence doublets allow two realizations for strange as well as for charm quarks, either with a twisted mass term $+i\mu_{s,c}\gamma_5$ or $-i\mu_{s,c}\gamma_5$. For a quark antiquark meson creation operator the sign combinations $(+,-)$ and $(-,+)$ for the quark q and the antiquark \bar{q} are related by symmetry, i.e. the corresponding correlators are identical. These correlators differ, however, from their counterparts with sign combinations $(+,+)$ and $(-,-)$, due to different discretization errors. In section 3 we will show for each computed meson mass both the $(+,-) \equiv (-,+)$ and the $(+,+) \equiv (-,-)$ result. The differences are $\mathcal{O}(a^2)$ due to automatic $\mathcal{O}(a)$ improvement inherent to the twisted mass formulation. These mass differences give a first impression regarding the magnitude of discretization errors at our currently used lattice spacing.

Using $(+,-) \equiv (-,+)$ correlators we have tuned the bare valence strange and charm quark masses μ_s and μ_c to reproduce the physical values of $2m_K^2 - m_\pi^2$ and m_D , quantities, which strongly depend on μ_s and μ_c , but which are essentially independent of the light u/d quark mass.

3. Numerical results

In Fig. 1 we present our results for the D and D_s meson spectrum. For every state we show five data points:

Red circles and crosses:

lattice results at $m_\pi \approx 325$ MeV, twisted mass sign combinations $(+,-) \equiv (-,+)$ and $(+,+) \equiv (-,-)$, respectively.

Blue stars and boxes:

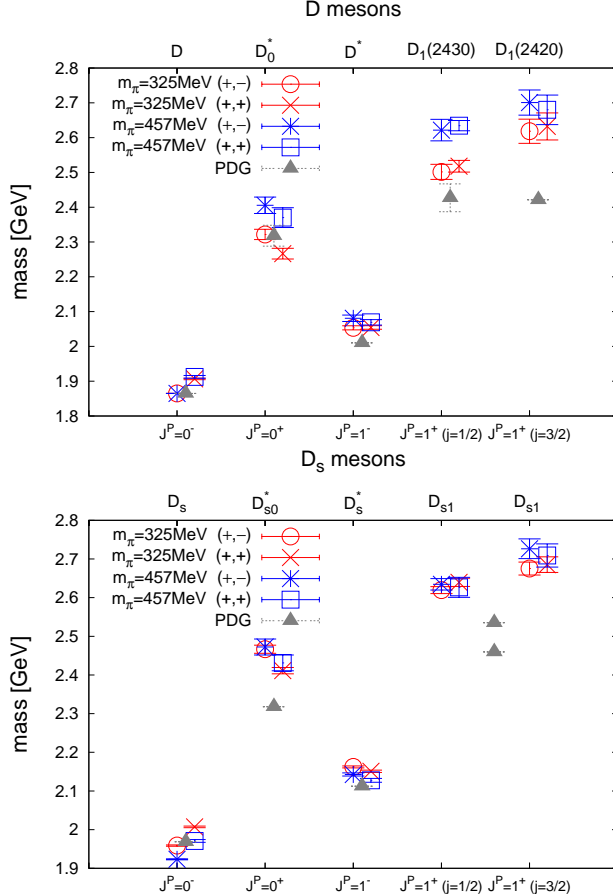
lattice results at $m_\pi \approx 457$ MeV, twisted mass sign combinations $(+,-) \equiv (-,+)$ and $(+,+) \equiv (-,-)$, respectively.

Gray triangles:

experimental result from the PDG [19].

The differences between sign combinations $(+,-) \equiv (-,+)$ and $(+,+) \equiv (-,-)$, which are $\lesssim 3\%$, indicate the magnitude of discretization errors at our currently used lattice spacing $a \approx 0.086$ fm.

While for the negative parity states lattice and experimental results agree rather well, there is a clear discrepancy in particular for the positive parity D_s states D_{s0}^* and D_{s1} . Similar findings have been reported in other lattice studies, e.g. [1, 6], and in phenomenological model calculations, e.g. [20]. This discrepancy might be an indication that these states are not predominantly $q\bar{q}$ states, but e.g. rather four quark states of molecular or tetraquark type. We plan to investigate this possibility within our setup in

Fig. 1. The D and D_s meson spectrum.

the near future. The necessary techniques have already been developed and recently been applied to light scalar mesons [21].

Another challenging, but important task is the separation of the two $J = 1^+$ states, $D_1(2420)$, $D_1(2430)$ and $D_{s1}(2460)$, $D_{s1}(2535)$, respectively. In the limit of a static charm quark one of these states has light cloud angular momentum $j = 1/2$, while the other has $j = 3/2$. To assign corresponding approximative j quantum numbers, when using charm quarks of finite mass, is e.g. important, when studying the decay of a B or B^* meson to one of the positive parity D^{**} mesons (which include the mentioned $D_1(2420)$ and $D_1(2430)$ states) in a fully dynamical setup (cf. e.g. [22, 23] for a recent lattice computation in the static limit). The correct identification of $j = 1/2$ and $j = 3/2$ states can be achieved by studying the eigenvectors obtained during the analysis of correlation matrices; the largest eigenvector compo-

nents point out the dominating operators, which, after a Clebsch-Gordan decomposition into light and heavy angular momentum contributions, can be classified according to $j = 1/2$ or $j = 3/2$.

In Fig. 2 we present our results for the charmonium spectrum. Because of the two rather heavy valence quarks, we expect considerably larger discretization errors as for the corresponding D or D_s meson states. The differences between lattice and experimental results are most prominent for the negative parity charmonium states (around 5%). We plan to explore in one of our next steps, whether discretization errors account for these differences by performing similar computations on ensembles with finer lattice spacings and by studying the continuum limit.

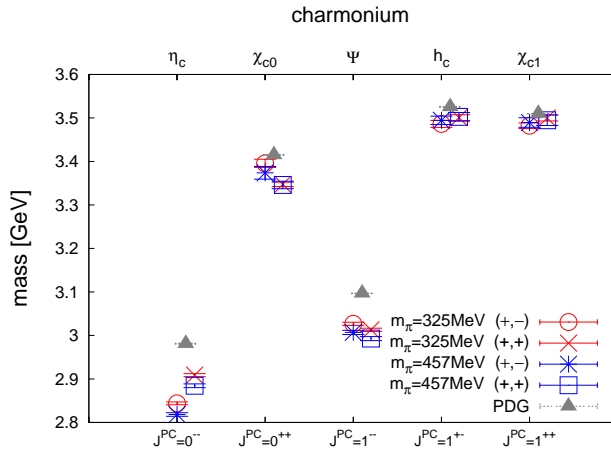


Fig. 2. The charmonium spectrum.

Acknowledgments

We thank Christian Wiese for discussions. M.K. and M.W. acknowledge support by the Emmy Noether Programme of the DFG (German Research Foundation), grant WA 3000/1-1 and by Helmholtz Graduate School HGS-HIRe for FAIR. This work was supported in part by the Helmholtz International Center for FAIR within the framework of the LOEWE program launched by the State of Hesse.

REFERENCES

- [1] D. Mohler and R. M. Woloshyn, Phys. Rev. D **84**, 054505 (2011) [arXiv:1103.5506 [hep-lat]].

- [2] Y. Namekawa *et al.* [PACS-CS Collaboration], Phys. Rev. D **84** (2011) 074505 [arXiv:1104.4600 [hep-lat]].
- [3] L. Liu *et al.* [Hadron Spectrum Collaboration], JHEP **1207**, 126 (2012) [arXiv:1204.5425 [hep-ph]].
- [4] R. J. Dowdall, C. T. H. Davies, T. C. Hammant and R. R. Horgan, Phys. Rev. D **86** (2012) 094510 [arXiv:1207.5149 [hep-lat]].
- [5] G. Bali, S. Collins and P. Perez-Rubio, J. Phys. Conf. Ser. **426** (2013) 012017 [arXiv:1212.0565 [hep-lat]].
- [6] G. Moir, M. Peardon, S. M. Ryan, C. E. Thomas and L. Liu, arXiv:1301.7670 [hep-ph].
- [7] D. Mohler, S. Prelovsek and R. M. Woloshyn, Phys. Rev. D **87**, 034501 (2013) [arXiv:1208.4059 [hep-lat]].
- [8] I. I. Bigi *et al.*, Eur. Phys. J. C **52**, 975 (2007) [arXiv:0708.1621 [hep-ph]].
- [9] M. Kalinowski and M. Wagner, PoS CONFINEMENT **10**, 303 (2012) [arXiv:1212.0403 [hep-lat]].
- [10] R. Baron *et al.* [ETM Collaboration], PoS **LATTICE2008**, 094 (2008) [arXiv:0810.3807 [hep-lat]].
- [11] R. Baron *et al.* [ETM Collaboration], PoS **LATTICE2009**, 104 (2009) [arXiv:0911.5244 [hep-lat]].
- [12] R. Baron *et al.* [ETM Collaboration], JHEP **1006**, 111 (2010) [arXiv:1004.5284 [hep-lat]].
- [13] R. Baron *et al.* [ETM Collaboration], PoS **LATTICE2010**, 123 (2010) [arXiv:1101.0518 [hep-lat]].
- [14] R. Baron *et al.* [ETM Collaboration], Comput. Phys. Commun. **182**, 299 (2011) [arXiv:1005.2042 [hep-lat]].
- [15] R. Baron *et al.* [ETM Collaboration], PoS **LATTICE2010**, 130 (2010) [arXiv:1009.2074 [hep-lat]].
- [16] K. Jansen *et al.* [ETM Collaboration], JHEP **0812**, 058 (2008) [arXiv:0810.1843 [hep-lat]].
- [17] P. Boucaud *et al.* [ETM Collaboration], Comput. Phys. Commun. **179**, 695 (2008) [arXiv:0803.0224 [hep-lat]].
- [18] B. Blossier, M. Della Morte, G. von Hippel, T. Mendes and R. Sommer, JHEP **0904**, 094 (2009) [arXiv:0902.1265 [hep-lat]].
- [19] K. Nakamura *et al.* [Particle Data Group Collaboration], “Review of particle physics,” J. Phys. G **37**, 075021 (2010) and 2011 partial update for the 2012 edition.
- [20] D. Ebert, R. N. Faustov and V. O. Galkin, Eur. Phys. J. C **66**, 197 (2010) [arXiv:0910.5612 [hep-ph]].
- [21] C. Alexandrou *et al.* [ETM Collaboration], arXiv:1212.1418 [hep-lat].
- [22] B. Blossier *et al.* [ETM Collaboration], JHEP **0906**, 022 (2009) [arXiv:0903.2298 [hep-lat]].
- [23] B. Blossier *et al.* [ETM Collaboration], PoS **LATTICE2009**, 253 (2009) [arXiv:0909.0858 [hep-lat]].

Twisted mass lattice computation of charmed mesons with focus on D^{**}

Martin Kalinowski*

Goethe University Frankfurt am Main

E-mail: kalinowm@th.physik.uni-frankfurt.de

Marc Wagner

Goethe University Frankfurt am Main

E-mail: mwagner@th.physik.uni-frankfurt.de

We present results of a 2+1+1 flavor twisted mass lattice QCD computation of the spectrum of D mesons and D_s mesons and of charmonium. Particular focus is put on the positive parity D states (so-called D^{**} mesons) with quantum numbers $J^P = 0^+, 1^+$ and 2^+ . Besides computing their masses we are also separating and classifying the two $J^P = 1^+$ states according to the angular momentum/spin of their light degrees of freedom (light quarks and gluons) $j = 1/2, 3/2$.

31st International Symposium on Lattice Field Theory LATTICE 2013

July 29 – August 3, 2013

Mainz, Germany

*Speaker.

1. Introduction

There is considerable interest in the spectrum of D and D_s mesons and of charmonium both theoretically and experimentally.

On the theory side first principles calculations are usually lattice QCD computations (for recent work cf. e.g. [1, 2, 3, 4, 5, 6, 7, 8]). In the last couple of years a lot of progress has been made, allowing the determination of hadron masses like the aforementioned mesons with rather high precision. For example 2+1 or even 2+1+1 flavors of dynamical quarks are often used as well as small lattice spacings and improved discretizations, to keep discretization errors (in particular those associated with the heavy charm quarks) under control. Some groups have even started to determine the resonance parameters of certain mesons from the spectrum of two-particle scattering states in finite spatial volumes (cf. e.g. [9, 10]).

Experimentally a large number of D , D_s and charmonium states has been measured and additional and more precise results are expected in the near future both from existing facilities and facilities currently under construction, like the PANDA experiment at FAIR. Even though these experimental results have been extremely helpful, to improve our understanding of QCD, they also brought up new and yet unanswered questions. For example the positive parity mesons D_{s0}^* and D_{s1} are unexpectedly light, which is at the moment not satisfactorily understood and also quite often not reproduced by lattice QCD computations or model calculations.

Moreover, performing a precise computation of certain meson masses is often the first step for many lattice projects not primarily concerned with spectroscopy. As an example one could mention the semileptonic decay of B and B^* mesons into positive parity D mesons [11] (so-called D^{**} mesons). Their masses and operator contents, which are discussed in detail in section 3.2, are an essential ingredient for any corresponding lattice computation.

This is mainly a status report about an ongoing lattice QCD project concerned with the computation of the spectrum of mesons with at least one charm valence quark. We present preliminary results for D mesons, for D_s mesons and for charmonium states with total angular momentum $J = 0, 1$ and parity $P = -, +$. Parts of this work have already been published [5, 8].

2. Simulation and analysis setup

We use gauge link configurations generated by the European Twisted Mass Collaboration (ETMC) with the Iwasaki gauge action and $N_f = 2 + 1 + 1$ flavors of Wilson twisted mass quarks [12, 13, 14, 15]. Until now we have considered three ensembles (around 1000 gauge link configurations per ensemble) with (unphysically heavy) values for the light u/d quark mass corresponding to $m_\pi \approx 285\text{ MeV}, 325\text{ MeV}, 457\text{ MeV}$ and lattice sizes $(L/a)^3 \times T/a = 32^3 \times 64, 32^3 \times 64, 24^3 \times 48$. Our results are obtained at a single lattice spacing $a \approx 0.086\text{ fm}$. Consequently, a continuum extrapolation has not yet been performed.

Meson masses are determined by computing and studying temporal correlation matrices of suitably chosen meson creation operators \mathcal{O}_j . At the moment we exclusively consider quark antiquark operators. The quark and the antiquark are combined in spin space via γ matrices and in color and position space via gauge links such that the corresponding trial states $\mathcal{O}_j|\Omega\rangle$ ($|\Omega\rangle$ denotes the vacuum) are gauge invariant and have defined total angular momentum and parity (cf.

section 3.2 for examples of $J = 1$ D meson creation operators and [16], in particular section 4.1, for a general discussion). Moreover, APE and Gaussian smearing is used, to optimize the overlap of the trial states $\mathcal{O}_j|\Omega\rangle$ to the low lying mesonic states of interest. We plan to discuss these operators and their structure and quantum numbers in detail in an upcoming publication. For the computation of the corresponding correlation matrices $\langle \mathcal{O}_j^\dagger(t)\mathcal{O}(0) \rangle$ we resort to the one-end trick (cf. e.g. [17]). Meson masses are then determined from plateau values of corresponding effective masses, which we obtain by solving generalized eigenvector problems (cf. e.g. [18]). Disconnected diagrams appearing in charmonium correlators are currently neglected.

One of the main advantages of the Wilson twisted mass discretization is automatic $\mathcal{O}(a)$ improvement of physical observables, e.g. hadron masses. However, parity and isospin (in case of a non-degenerate quark doublet flavor instead of isospin) are not exact symmetries. For example positive and negative parity trial states are not anymore orthogonal, which leads to additional difficulties, when doing hadron spectroscopy: positive and negative parity states have to be determined from a single correlation matrix, which is typically twice as large compared to those studied in parity and isospin symmetric lattice discretizations.

For both the valence strange and charm quarks we use degenerate twisted mass doublets, i.e. a different discretization as for the corresponding sea quarks. We do this, to avoid mixing of strange and charm quarks, which inevitably takes place in a unitary setup, and which is particularly problematic for hadrons containing charm quarks [14, 15]. The degenerate valence doublets allow two realizations for strange as well as for charm quarks, either with a twisted mass term $+i\mu_{s,c}\gamma_5$ or $-i\mu_{s,c}\gamma_5$. For a quark antiquark meson creation operator the sign combinations $(+, -)$ and $(-, +)$ for the quark q and the antiquark \bar{q} are related by symmetry, i.e. the corresponding correlators are identical. These correlators differ, however, from their counterparts with sign combinations $(+, +)$ and $(-, -)$, due to different discretization errors. In section 3 we will show for each computed meson mass both the $(+, -) \equiv (-, +)$ and the $(+, +) \equiv (-, -)$ result. The differences are $\mathcal{O}(a^2)$, due to the aforementioned automatic $\mathcal{O}(a)$ improvement inherent to the Wilson twisted mass formulation. These mass differences give a first impression regarding the magnitude of discretization errors at our currently used lattice spacing $a \approx 0.086\text{ fm}$.

Using $(+, -) \equiv (-, +)$ correlators we have tuned the bare valence strange and charm quark masses μ_s and μ_c to reproduce the physical values of $2m_K^2 - m_\pi^2$ and m_D , quantities, which strongly depend on μ_s and μ_c , but which are essentially independent of the light u/d quark mass.

3. Numerical results

3.1 The D meson, the D_s meson and the charmonium spectrum

In Figure 1 we present our results for the D and D_s meson spectrum. For every state we show six data points: different colors indicate the different light quark/pion masses of the used ensembles, the circles and crosses distinguish the twisted mass sign combinations $(+, -) \equiv (-, +)$ and $(+, +) \equiv (-, -)$, respectively. The horizontal separation of the data points have been chosen proportional to the corresponding squared pion masses.

While for the negative parity states lattice and experimental results agree rather well, there is a clear discrepancy in particular for the positive parity D_s states D_{s0}^* and D_{s1} . Similar findings have

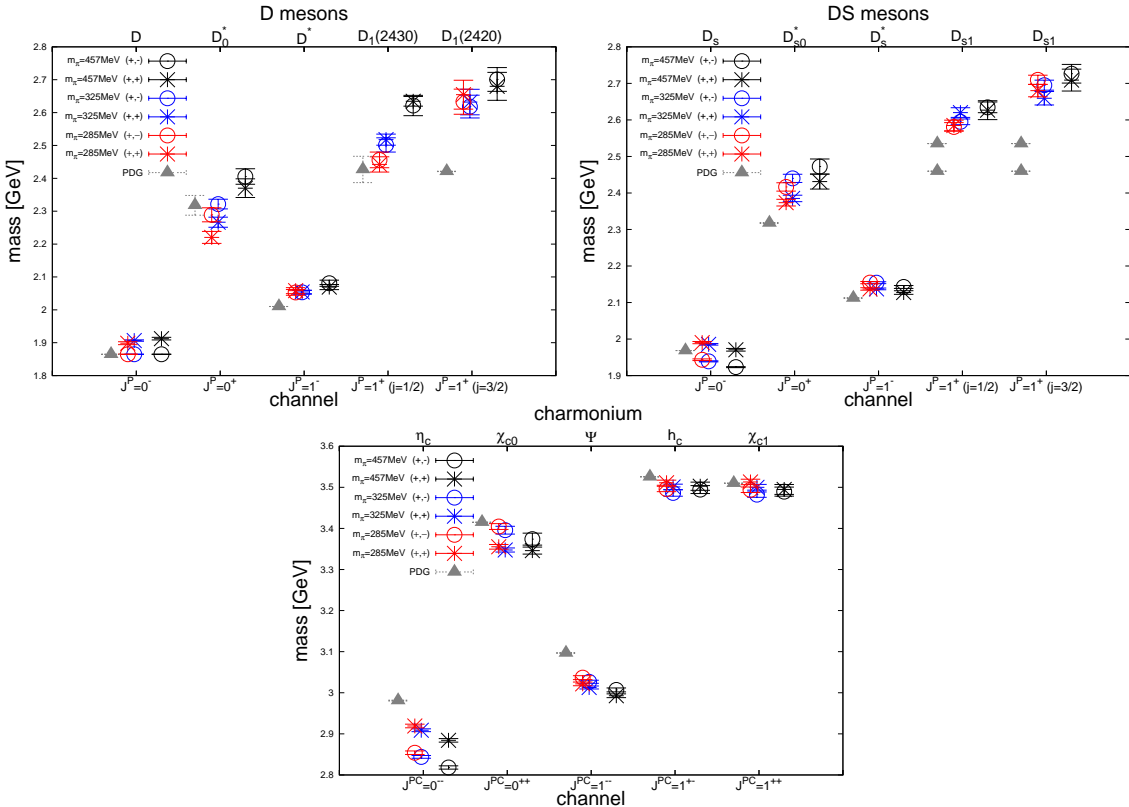


Figure 1: The D meson, the D_s meson and the charmonium spectrum for three different light quark masses corresponding to $m_\pi \approx 285\text{ MeV}, 325\text{ MeV}, 457\text{ MeV}$ and lattice spacing $a \approx 0.086\text{ fm}$.

been reported in other lattice studies, e.g. [1, 7], and in phenomenological model calculations, e.g. [20]. This discrepancy might be an indication that these states are not predominantly $q\bar{q}$ states, but e.g. rather four quark states of molecular or tetraquark type. We plan to investigate this possibility within our setup in the near future. The necessary techniques have already been developed and recently been applied to light scalar mesons [21, 22].

In Figure 1 we also present our results for the charmonium spectrum. Because of the two rather heavy valence quarks, we expect considerably larger discretization errors than for the corresponding D or D_s meson states. The differences between lattice and experimental results are most prominent for the negative parity charmonium states (around 5%). We plan to explore in one of our next steps, whether discretization errors account for these differences by performing similar computations on ensembles with finer lattice spacings and by studying the continuum limit.

3.2 $J^P = 1^+$ D mesons: separation of the two D_1 states

A challenging, but important task is the separation of the two $J = 1^+$ D meson states $D_1(2430)$ and $D_1(2420)$. In the limit of infinitely heavy charm quarks the broad $D_1(2430)$ state is expected to have light cloud angular momentum $j = 1/2$, while the narrow $D_1(2420)$ state should have $j = 3/2$ (cf. [23, 24] for a detailed discussion and computation of the static limit). Assigning corresponding j quantum numbers, when using charm quarks of finite mass, is e.g. important, when studying the decay of a B or B^* meson into one of the positive parity D^{**} mesons (which include

the mentioned $D_1(2420)$ and $D_1(2430)$ states) in a fully dynamical setup (cf. e.g. [25, 26] for a recent lattice computation in the static limit and [27] for first results obtained with dynamical charm quarks).

The correct identification of the $j \approx 1/2$ and the $j \approx 3/2$ state can be achieved by studying the eigenvectors obtained during the analysis of correlation matrices, i.e. when solving generalized eigenvector problems. After a suitable normalization of the trial states $\mathcal{O}_j|\Omega\rangle$ large eigenvector components point out the dominating meson creation operators \mathcal{O}_j , which, after a Clebsch-Gordan decomposition into light and heavy total angular momentum contributions, can be classified according to $j = 1/2$ or $j = 3/2$.

We use quark-antiquark meson creation operators

$$\mathcal{O}_\Gamma = \sum_{\mathbf{r}} \bar{c}(\mathbf{r}) \sum_{\mathbf{n}=\pm\mathbf{e}_x, \pm\mathbf{e}_y, \pm\mathbf{e}_z} U(\mathbf{r}; \mathbf{r} + \mathbf{n}) \Gamma(\mathbf{n}) u(\mathbf{r} + \mathbf{n}), \quad (3.1)$$

where \bar{c} and u are Gaussian smeared quark fields, $U(\mathbf{r}; \mathbf{r} + \mathbf{n})$ is the APE smeared link connecting \mathbf{r} and $\mathbf{r} + \mathbf{n}$ and $\Gamma(\mathbf{n})$ denotes suitably chosen linear combinations of products of γ matrices and spherical harmonics realizing the desired quantum numbers J , j and P . In total we consider 36 meson creation operators:

- for $J = 1$ and $j = 1/2$

$$\Gamma(\mathbf{n}) = \gamma_j \gamma_5 G, \quad \Gamma(\mathbf{n}) = ((\mathbf{n} \times \vec{\gamma})_j - \mathbf{n}_j \gamma_0 \gamma_5) G, \quad (3.2)$$

- for $J = 1$ and $j = 3/2$

$$\Gamma(\mathbf{n}) = ((\mathbf{n} \times \vec{\gamma})_j + 2\mathbf{n}_j \gamma_0 \gamma_5) G \quad (3.3)$$

with $j = 1, 2, 3$ and $G = 1, \gamma_0, \gamma_5, \gamma_0 \gamma_5$. Meson creation operators, which only differ in j , are related by symmetry. The resulting correlation functions have been averaged, to increase statistical accuracy. Meson creation operators with $G = 1, \gamma_0$ and with $G = \gamma_5, \gamma_0 \gamma_5$ correspond to $P = +$ and $P = -$, respectively. Due to twisted mass parity mixing (cf. section 2), these operators do not generate orthogonal trial states and, therefore, have to be included in a single 12×12 correlation matrix.

In Figure 2 we show the operator content of the three lightest $J = 1$ states as a function of the temporal separation of the correlation matrix (for a detailed explanation of such plots we refer to [14]):

- As expected the ground state is dominated by $P = -$ meson creation operators (the light blue curve corresponds to the sum of the squared eigenvector components of the six $P = -$ operators from (3.2) and (3.3), $\gamma_z[\gamma_0], ((\mathbf{n} \times \vec{\gamma})_z - \mathbf{n}_z \gamma_0 \gamma_5) \gamma_5[\gamma_0]$ and $((\mathbf{n} \times \vec{\gamma})_z + 2\mathbf{n}_z \gamma_0 \gamma_5) \gamma_5[\gamma_0]$). This confirms that the ground state is the D^* state ($J^P = 1^-$).
- The first excitation is dominated by $P = +$ meson creation operators with $j \approx 1/2$. Operators without angular momentum ($\gamma_z \gamma_5[\gamma_0]$; green curve) generate trial states with larger overlap than those with angular momentum $L = 1$ ($((\mathbf{n} \times \vec{\gamma})_z - \mathbf{n}_z \gamma_0 \gamma_5)[\gamma_0]$; dark blue curve). Consequently, the first excitation is identified as the broad $D_1(2430)$ state ($J^P = 1^+, j \approx 1/2$), where total angular momentum $J = 1$ is mainly realized by the quark spin and not by relative angular momentum $L = 1$ of the two quarks.

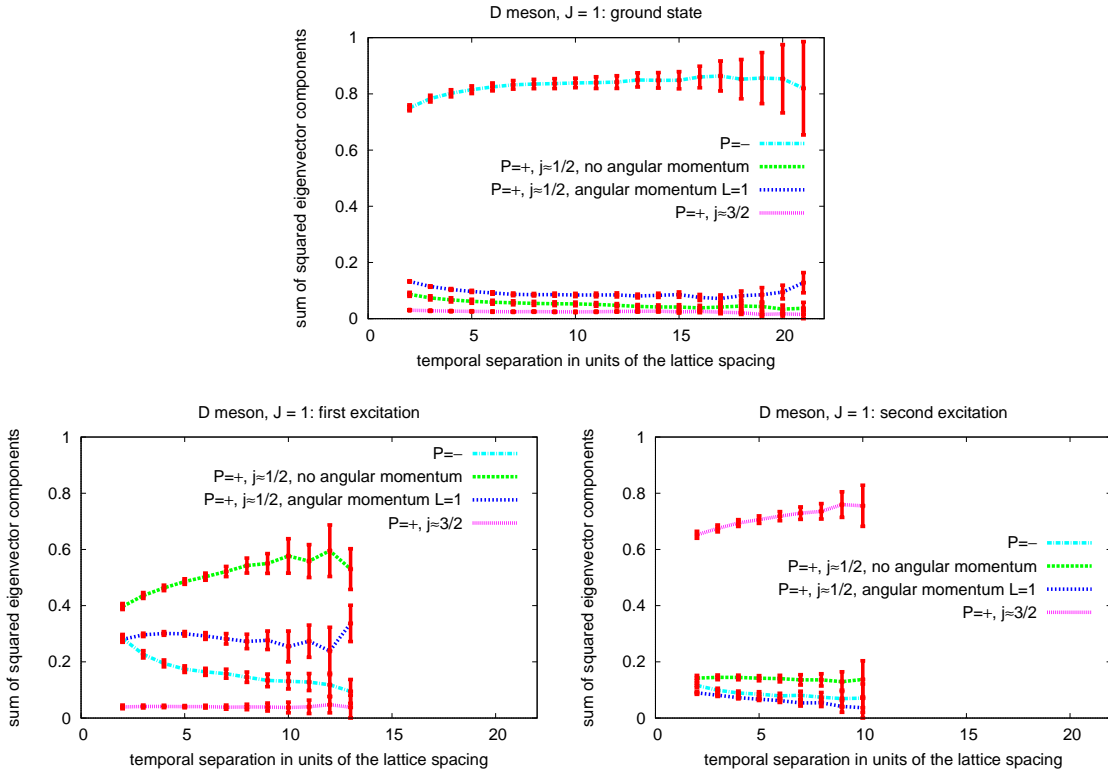


Figure 2: The operator content of the three lightest $J = 1$ D meson states. The ground state (upper plot) is identified as D^* ($J^P = 1^-$), the first excitation (left plot) as $D_1(2430)$ ($J^P = 1^+, j \approx 1/2$), the second excitation (right plot) as $D_1(2420)$ ($J^P = 1^+, j \approx 3/2$).

- Finally the second excitation, which is close in mass to the first excitation, is dominated by $P = +$ meson creation operators with $j \approx 3/2$ ($((\mathbf{n} \times \vec{\gamma})_j + 2\mathbf{n}_j \gamma_0 \gamma_5)[\gamma_0]$; magenta curve). Consequently, the second excitation is identified as the narrow $D_1(2420)$ state ($J^P = 1^+, j \approx 3/2$).

Note that one could consider even more meson creation operators, e.g. $j \approx 3/2$ operators with angular momentum $L = 2$.

An analogous analysis for D_s mesons yields qualitatively identical results.

Acknowledgments

M.K. and M.W. acknowledge support by the Emmy Noether Programme of the DFG (German Research Foundation), grant WA 3000/1-1, and by the Helmholtz Graduate School HGS-HIRE for FAIR. This work was supported in part by the Helmholtz International Center for FAIR within the framework of the LOEWE program launched by the State of Hesse.

References

- [1] D. Mohler and R. M. Woloshyn, Phys. Rev. D **84**, 054505 (2011) [arXiv:1103.5506 [hep-lat]].

- [2] Y. Namekawa *et al.* [PACS-CS Collaboration], Phys. Rev. D **84** (2011) 074505 [arXiv:1104.4600 [hep-lat]].
- [3] L. Liu *et al.* [Hadron Spectrum Collaboration], JHEP **1207**, 126 (2012) [arXiv:1204.5425 [hep-ph]].
- [4] R. J. Dowdall, C. T. H. Davies, T. C. Hammant and R. R. Horgan, Phys. Rev. D **86** (2012) 094510 [arXiv:1207.5149 [hep-lat]].
- [5] M. Kalinowski and M. Wagner, PoS ConfinementX , 303 (2012) [arXiv:1212.0403 [hep-lat]].
- [6] G. Bali, S. Collins and P. Perez-Rubio, J. Phys. Conf. Ser. **426** (2013) 012017 [arXiv:1212.0565 [hep-lat]].
- [7] G. Moir *et al.*, JHEP **1305**, 021 (2013) [arXiv:1301.7670 [hep-ph]].
- [8] M. Kalinowski and M. Wagner, Acta Phys. Polon. Supp. B **6**, 991 (2013) [arXiv:1304.7974 [hep-lat]].
- [9] D. Mohler, S. Prelovsek and R. M. Woloshyn, Phys. Rev. D **87**, 034501 (2013) [arXiv:1208.4059 [hep-lat]].
- [10] D. Mohler *et al.*, arXiv:1308.3175 [hep-lat].
- [11] I. I. Bigi *et al.*, Eur. Phys. J. C **52**, 975 (2007) [arXiv:0708.1621 [hep-ph]].
- [12] R. Baron *et al.* [ETM Collaboration], JHEP **1006**, 111 (2010) [arXiv:1004.5284 [hep-lat]].
- [13] R. Baron *et al.* [ETM Collaboration], PoS **LATTICE2010**, 123 (2010) [arXiv:1101.0518 [hep-lat]].
- [14] R. Baron *et al.* [ETM Collaboration], Comput. Phys. Commun. **182**, 299 (2011) [arXiv:1005.2042 [hep-lat]].
- [15] R. Baron *et al.* [ETM Collaboration], PoS **LATTICE2010**, 130 (2010) [arXiv:1009.2074 [hep-lat]].
- [16] J. Weber, S. Diehl, T. Kuske and M. Wagner, arXiv:1310.1760 [hep-lat].
- [17] P. Boucaud *et al.* [ETM Collaboration], Comput. Phys. Commun. **179**, 695 (2008) [arXiv:0803.0224 [hep-lat]].
- [18] B. Blossier *et al.*, JHEP **0904**, 094 (2009) [arXiv:0902.1265 [hep-lat]].
- [19] K. Nakamura *et al.* [Particle Data Group Collaboration], “Review of particle physics,” J. Phys. G **37**, 075021 (2010) and 2011 partial update for the 2012 edition.
- [20] D. Ebert, R. N. Faustov and V. O. Galkin, Eur. Phys. J. C **66**, 197 (2010) [arXiv:0910.5612 [hep-ph]].
- [21] C. Alexandrou *et al.* [ETM Collaboration], JHEP **1304**, 137 (2013) [arXiv:1212.1418].
- [22] M. Wagner *et al.* [ETM Collaboration], arXiv:1309.0850 [hep-lat].
- [23] K. Jansen, C. Michael, A. Shindler and M. Wagner [ETM Collaboration], JHEP **0812**, 058 (2008) [arXiv:0810.1843 [hep-lat]].
- [24] C. Michael, A. Shindler and M. Wagner [ETM Collaboration], JHEP **1008**, 009 (2010) [arXiv:1004.4235 [hep-lat]].
- [25] B. Blossier, M. Wagner and O. Pene [ETM Collaboration], JHEP **0906**, 022 (2009) [arXiv:0903.2298 [hep-lat]].
- [26] B. Blossier, M. Wagner and O. Pene [ETM Collaboration], PoS **LATTICE2009**, 253 (2009) [arXiv:0909.0858 [hep-lat]].
- [27] M. Atoui, arXiv:1305.0462 [hep-lat].

Light hadrons from lattice QCD with light (u, d), strange and charm dynamical quarks



ETM Collaboration, R. Baron^a, Ph. Boucaud^b, J. Carbonell^c,
 A. Deuzeman^d, V. Drach^c, F. Farchioni^e, V. Gimenez^f,
 G. Herdoiza^g, K. Jansen^g, C. McNeile^h, C. Michaelⁱ,
 I. Montvay^j, D. Palao^k, E. Pallante^d, O. Pène^b, S. Reker^d,
 C. Urbach^l, M. Wagner^m, U. Wengerⁿ

^a *CEA, Centre de Saclay, IRFU/Service de Physique Nucléaire, F-91191 Gif-sur-Yvette, France*

^b *Laboratoire de Physique Théorique (Bât. 210), CNRS et Université Paris-Sud 11, Centre d'Orsay, 91405 Orsay-Cedex, France*

^c *Laboratoire de Physique Subatomique et Cosmologie, 53 avenue des Martyrs, 38026 Grenoble, France*

^d *Centre for Theoretical Physics, University of Groningen, Nijenborgh 4, 9747 AG Groningen, the Netherlands*

^e *Institut für Theoretische Physik, Universität Münster, Wilhelm-Klemm-Straße 9, D-48149 Münster, Germany*

^f *Dep. de Física Teòrica and IFIC, Universitat de València-CSIC, Dr. Moliner 50, E-46100 Burjassot, Spain*

^g *NIC, DESY, Platanenallee 6, D-15738 Zeuthen, Germany*

^h *Department of Physics and Astronomy, The Kelvin Building, University of Glasgow, G12 8QQ Glasgow, United Kingdom*

ⁱ *Division of Theoretical Physics, University of Liverpool, L69 3BX Liverpool, United Kingdom*

^j *DESY, Notkestr. 85, D-22603 Hamburg, Germany*

^k *INFN, Sez. di Roma "Tor Vergata", Via della Ricerca Scientifica 1, I-00133 Rome, Italy*

^l *Helmholtz-Institut für Strahlen- und Kernphysik (Theorie) and Bethe Center for Theoretical Physics, Universität Bonn, 53115 Bonn, Germany*

^m *Institut für Physik, Humboldt-Universität zu Berlin, Newtonstraße 15, D-12489 Berlin, Germany*

ⁿ *Albert Einstein Center for Fundamental Physics, Institute for Theoretical Physics, University of Bern, Sidlerstr. 5, CH-3012 Bern, Switzerland*

Abstract

We present results of lattice QCD simulations with mass-degenerate up and down and mass-split strange and charm ($N_f = 2 + 1 + 1$) dynamical quarks using Wilson twisted mass fermions at maximal twist. The tuning of the strange and charm quark masses is performed at two values of the lattice spacing $a \approx 0.078$ fm and $a \approx 0.086$ fm with lattice sizes ranging from $L \approx 1.9$ fm to $L \approx 2.8$ fm. We measure with high statistical precision the light pseudoscalar mass m_{PS} and decay constant f_{PS} in a range $270 \lesssim m_{PS} \lesssim 510$ MeV and determine the low energy parameters f_0 and $\bar{l}_{3,4}$ of SU(2) chiral perturbation theory. We use the two values of the lattice spacing, several lattice sizes as well as different values of the light, strange and charm quark masses to explore the systematic effects. A first study of discretisation effects in light-quark observables and a comparison to $N_f = 2$ results are performed.

Key words: Lattice gauge theory, lattice QCD, light hadrons, charm quark, chiral perturbation theory.

PACS: 12.38.Gc, 12.39Fe

Preprint-No: DESY 10-054, HU-EP-10/18, IFIC/10-11, SFB/CPP-10-29,
LPT-Orsay 10-28, LTH873, LPSC1042, MS-TP-10-09, ROM2F/2010/08

1 Introduction and Main Results

The beginning of this century has assisted to radical improvements in theory, algorithms and supercomputer technology, leading to a far increased ability to solve non-perturbative aspects of gauge field theories in a lattice regularised framework. Following this path of improving the lattice setup, in this paper, we are reporting about our experiences and results when considering in addition to the u, d light dynamical flavours also the effects of the strange and charm sea quarks. By including a dynamical charm, we are now able to directly study its contribution to physical observables and to quantify the so far uncontrolled systematic effect present in lattice QCD simulations where the charm flavour in the sea is absent.

A number of different lattice fermion formulations are being used by several lattice groups, see refs. [1, 2] for recent reviews. Here, we adopt a particular type of Wilson fermions, known as the Wilson twisted mass formulation of lattice QCD (tmLQCD), introduced in [3, 4]. This approach is by now well established, with many physical results obtained with two light degenerate twisted mass flavours ($N_f = 2$) by our European Twisted Mass (ETM) Collaboration, see refs. [5–22]. For a review see ref. [23]. In the tmLQCD formulation a twisted mass term is added to the standard, unimproved Wilson-Dirac

operator, and the formulation becomes especially interesting when the theory is tuned to maximal twist [4]. The major advantage of the lattice theory tuned to maximal twist is the automatic $\mathcal{O}(a)$ improvement of physical observables, independently of the specific type of operator considered, implying that no additional, operator specific improvement coefficients need to be computed. Other advantages worth to mention are that the twisted mass term acts as an infrared regulator of the theory and that mixing patterns in the renormalisation procedure are expected to be simplified.

Detailed studies of the continuum-limit scaling in the quenched approximation [24–27] and with two dynamical quarks [7, 10, 17, 28] have demonstrated that, after an appropriate tuning procedure to maximal twist, lattice artefacts not only follow the expected $\mathcal{O}(a^2)$ scaling behaviour [4], but also that the remaining $\mathcal{O}(a^2)$ effects are small, in agreement with the conclusions drawn in ref. [29].

The only exception seen so far is the neutral pseudoscalar mass, which shows significant $\mathcal{O}(a^2)$ effects. This arises from the explicit breaking of both parity and isospin symmetry, which are however restored in the continuum limit with a rate of $\mathcal{O}(a^2)$ as shown in [4] and numerically confirmed in refs. [17, 30]. Moreover, a recent analysis suggests that isospin breaking effects strongly affect only a limited set of observables, namely the neutral pion mass and kinematically related quantities [31, 32].

In this paper we report on simulations with twisted mass dynamical up, down, strange and charm quarks. We realise this by adding a heavy mass-split doublet (c, s) to the light degenerate mass doublet (u, d), referring to this setup as $N_f = 2 + 1 + 1$ simulations. This formulation was introduced in [33, 34] and first explored in [35]. As for the mass-degenerate case, the use of lattice action symmetries allows to prove the automatic $\mathcal{O}(a)$ improvement of physical observables in the non-degenerate case [33, 34]. First accounts of our work were presented at recent conferences [36, 37]. Recently, results with $N_f = 2 + 1 + 1$ staggered fermions have been reported in [38–40]. The inclusion of the strange and charm degrees of freedom allows for a most complete description of light hadron physics and eventually opens the way to explore effects of a dynamical charm in genuinely strong interaction processes and in weak matrix elements.

Here, we concentrate on results in the light-quark sector using the charged pseudoscalar mass m_{PS} and decay constant f_{PS} as basic observables involving up and down valence quarks only. In fig. 1 we show the dependence of (a) $m_{\text{PS}}^2/2B_0\mu_l$ and (b) f_{PS} as a function of the mass parameter $2B_0\mu_l$, together with a fit to SU(2) chiral perturbation theory (χPT) at the smallest value of the lattice spacing of $a \approx 0.078$ fm and lattice gauge coupling $\beta = 1.95$. We summarise the fit results for the low energy constants in table 1. These are the main results of this paper.

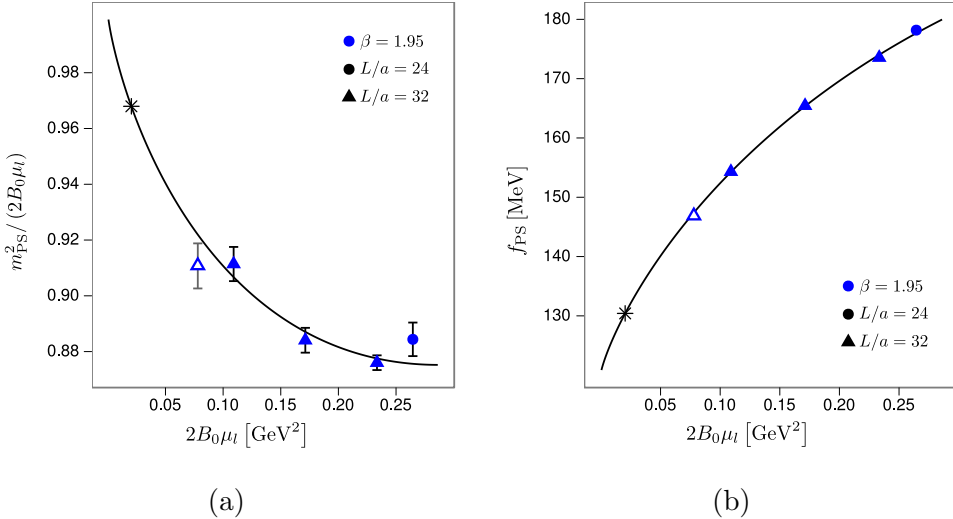


Fig. 1. (a) The charged pseudoscalar mass ratio $m_{PS}^2 / (2B_0 \mu_l)$ and (b) the pseudoscalar decay constant f_{PS} as a function of $2B_0 \mu_l$ fitted to SU(2) chiral perturbation theory, see table 1. The scale is set by the value of $2B_0 \mu_l$ at which the ratio $f_{PS}^{[L=\infty]} / m_{PS}^{[L=\infty]}$ assumes its physical value [41] $f_{\pi}/m_{\pi} = 130.4(2)/135.0$ (black star). The lattice gauge coupling is $\beta = 1.95$ and the twisted light quark mass ranges from $a\mu_l = 0.0025$ to 0.0085 , see eq. (3) for its definition, corresponding to a range of the pseudoscalar mass $270 \lesssim m_{PS} \lesssim 490$ MeV. The kaon and D meson masses are tuned to their physical value, see table 4. The lightest point (open symbol) has not been included in the chiral fit, see the discussion in section 3.2.

A comparison between data obtained with $N_f = 2 + 1 + 1$ and $N_f = 2$ flavours of quarks - see sections 3.4 and 4, and ref. [17] - reveals a remarkable agreement for the results involving light-quark observables such as the pseudoscalar mass and decay constant or the nucleon mass. This provides a strong indication in favour of the good quality of our data in this new setup. In particular, barring cancellations due to lattice discretisation errors, these results would suggest that the dynamical strange and charm degrees of freedom do not induce large effects in these light-quark observables. In the $N_f = 2$ case, data collected at four values of the lattice spacing have allowed us to properly quantify all systematic errors present in the determination of light-quark observables [17]. In this first work with $N_f = 2 + 1 + 1$ flavours, we consider data at two close values of the lattice spacing, while we defer to a forthcoming publication the inclusion of additional ensembles at a significantly lower lattice spacing and a more complete analysis of the systematic effects.

The rest of this paper is organised as follows. In section 2 we describe the gauge action and the twisted mass fermionic action for the light and heavy sectors of the theory. The realisation of $\mathcal{O}(a)$ improvement at maximal twist is also presented. In section 3 we define the simulation parameters, describe the tuning to maximal twist as well as the tuning of the strange and charm

	$\beta = 1.95$
\bar{l}_3	3.70(7)(26)
\bar{l}_4	4.67(3)(10)
f_0 [MeV]	121.14(8)(19)
f_π/f_0	1.076(2)(2)
$2B_0\mu_{u,d}/m_\pi^2$	1.032(21)(3)
$\langle r^2 \rangle_s^{\text{NLO}}$ [fm 2]	0.724(5)(23)
$r_0^\chi/a(\beta = 1.95)$	5.71(4)
$r_0^\chi(\beta = 1.95)$ [fm]	0.447(5)
$a(\beta = 1.95)$ [fm]	0.0782(6)

Table 1

Results of the fits to SU(2) χ PT for the ensemble at $\beta = 1.95$. Predicted quantities are: the low energy constants $\bar{l}_{3,4}$, the charged pseudoscalar decay constant in the chiral limit f_0 , the mass ratio $2B_0\mu_l/m_{\text{PS}}^2$ at the physical point and the pion scalar radius $\langle r^2 \rangle_s^{\text{NLO}}$. The first quoted error is from the chiral fit at $\beta = 1.95$, the second error is the systematic uncertainty that conservatively accommodates the best fitted central values of the three fits reported in table 9, section 4. The small error on the quoted lattice spacing comes exclusively from the fit at $\beta = 1.95$. The scale is set by fixing the ratio $f_{\text{PS}}^{[L=\infty]}/m_{\text{PS}}^{[L=\infty]} = f_\pi/m_\pi = 130.4(2)/135.0$ to its physical value [41]. The chirally extrapolated Sommer scale r_0^χ is determined separately and not included in the χ PT fits. For a comparison with the $N_f = 2$ ETMC results, see [17].

quark masses and the relevance of discretisation effects. Section 4 includes a discussion of the fits to SU(2) χ PT also for data on a slightly coarser lattice, $a \approx 0.086$ fm, and provides a first account of systematic uncertainties. Our conclusions and future prospects are summarised in section 5.

2 Lattice Action

The complete lattice action can be written as

$$S = S_g + S_l + S_h , \quad (1)$$

where S_g is the pure gauge action, in our case the so-called Iwasaki action [42, 43], S_l is the twisted mass Wilson action for the light doublet [3, 4] and S_h the one for the heavy doublet [33, 34].

2.1 Gauge action

The Iwasaki gauge action [42, 43] includes besides the plaquette term $U_{x,\mu,\nu}^{1\times 1}$ also rectangular (1×2) Wilson loops $U_{x,\mu,\nu}^{1\times 2}$

$$S_g = \frac{\beta}{3} \sum_x \left(b_0 \sum_{\substack{\mu,\nu=1 \\ 1 \leq \mu < \nu}}^4 \{1 - \text{Re Tr}(U_{x,\mu,\nu}^{1\times 1})\} + b_1 \sum_{\substack{\mu,\nu=1 \\ \mu \neq \nu}}^4 \{1 - \text{Re Tr}(U_{x,\mu,\nu}^{1\times 2})\} \right), \quad (2)$$

with $\beta = 6/g_0^2$ the bare inverse coupling, $b_1 = -0.331$ and the normalisation condition $b_0 = 1 - 8b_1$.

The choice of the gauge action is motivated by the non trivial phase structure of Wilson-type fermions at finite values of the lattice spacing. The phase structure of the theory has been extensively studied analytically, by means of chiral perturbation theory [44–50], and numerically [51–56]. These studies provided evidence for a first order phase transition close to the chiral point for coarse lattices. This implies that simulations at non-vanishing lattice spacing cannot be performed with pseudoscalar masses below a minimal critical value.

The strength of the phase transition has been found [53, 56] to be highly sensitive to the value of the parameter b_1 in the gauge action in eq. (2). Moreover, in [35] it was observed that its strength grows when increasing the number of flavours in the sea from $N_f = 2$ to $N_f = 2 + 1 + 1$, at otherwise fixed physical situation. Numerical studies with our $N_f = 2 + 1 + 1$ setup have shown that the Iwasaki gauge action, with $b_1 = -0.331$, provides a smoother dependence of phase transition sensitive quantities on the bare quark mass than the tree-level-improved Symanzik [57, 58] gauge action, with $b_1 = -1/12$, chosen for our $N_f = 2$ simulations.

Another way to weaken the strength of the phase transition is to modify the covariant derivative in the fermion action by smearing the gauge fields. While the main results of this work do not use smearing of the gauge fields, we report in section 3.7 on our experience when applying a stout smearing [59] procedure, see also [60].

2.2 Action for the Light Doublet

The lattice action for the mass degenerate light doublet (u, d) in the so called twisted basis reads [3, 4]

$$S_l = a^4 \sum_x \{\bar{\chi}_l(x) [D[U] + m_{0,l} + i\mu_l \gamma_5 \tau_3] \chi_l(x)\}, \quad (3)$$

where $m_{0,l}$ is the untwisted bare quark mass, μ_l is the bare twisted light quark mass, τ_3 is the third Pauli matrix acting in flavour space and

$$D[U] = \frac{1}{2} \left[\gamma_\mu (\nabla_\mu + \nabla_\mu^*) - a \nabla_\mu^* \nabla_\mu \right]$$

is the massless Wilson-Dirac operator. ∇_μ and ∇_μ^* are the forward and backward gauge covariant difference operators, respectively. Twisted mass light fermions are said to be at maximal twist if the bare untwisted mass $m_{0,l}$ is tuned to its critical value, m_{crit} , the situation we shall reproduce in our simulations. The quark doublet $\chi_l = (\chi_u, \chi_d)$ in the twisted basis is related by a chiral rotation to the quark doublet in the physical basis

$$\psi_l^{phys} = e^{\frac{i}{2}\omega_l\gamma_5\tau_3} \chi_l, \quad \bar{\psi}_l^{phys} = \bar{\chi}_l e^{\frac{i}{2}\omega_l\gamma_5\tau_3}, \quad (4)$$

where the twisting angle ω_l takes the value $|\omega_l| \rightarrow \frac{\pi}{2}$ as $|m_{0,l} - m_{\text{crit}}| \rightarrow 0$. We shall use the twisted basis throughout this paper.

2.3 Action for the Heavy Doublet

We introduce a dynamical strange quark by adding a twisted heavy mass-split doublet $\chi_h = (\chi_c, \chi_s)$, thus also introducing a dynamical charm in our framework. As shown in [34], a real quark determinant can in this case be obtained if the mass splitting is taken to be orthogonal in isospin space to the twist direction. We thus choose the construction [33, 34]

$$S_h = a^4 \sum_x \{ \bar{\chi}_h(x) [D[U] + m_{0,h} + i\mu_\sigma \gamma_5 \tau_1 + \mu_\delta \tau_3] \chi_h(x) \}, \quad (5)$$

where $m_{0,h}$ is the untwisted bare quark mass for the heavy doublet, μ_σ the bare twisted mass – the twist is this time along the τ_1 direction – and μ_δ the mass splitting along the τ_3 direction.

The bare mass parameters μ_σ and μ_δ of the non-degenerate heavy doublet are related to the physical renormalised strange and charm quark masses via [33]

$$\begin{aligned} (m_s)_R &= Z_P^{-1} (\mu_\sigma - Z_P/Z_S \mu_\delta), \\ (m_c)_R &= Z_P^{-1} (\mu_\sigma + Z_P/Z_S \mu_\delta), \end{aligned} \quad (6)$$

where Z_P and Z_S are the renormalisation constants of the pseudoscalar and scalar quark densities, respectively, computed in the massless standard Wilson theory.

A chiral rotation analogous to the one in the light sector transforms the heavy quark doublet from the twisted to the physical basis

$$\psi_h^{phys} = e^{\frac{i}{2}\omega_h\gamma_5\tau_1} \chi_h, \quad \bar{\psi}_h^{phys} = \bar{\chi}_h e^{\frac{i}{2}\omega_h\gamma_5\tau_1}, \quad (7)$$

where the twisting angle ω_h takes the value $|\omega_h| \rightarrow \frac{\pi}{2}$ as $|m_{0,h} - m_{\text{crit}}| \rightarrow 0$.

2.4 $\mathcal{O}(a)$ improvement at maximal twist

One of the main advantages of Wilson twisted mass fermions is that by tuning the untwisted bare quark mass to its critical value, automatic $\mathcal{O}(a)$ improvement of physical observables can be achieved.

Tuning the complete $N_f = 2+1+1$ action to maximal twist can in principle be performed by independently choosing the bare masses of the light and heavy sectors $am_{0,l}$ and $am_{0,h}$, resulting, however, in a quite demanding procedure. On the other hand, properties of the Wilson twisted mass formulation allow for a rather economical, while accurate alternative [4, 34, 35], where the choice $am_{0,l} = am_{0,h} \equiv 1/2\kappa - 4$ is made, and the hopping parameter κ has been introduced.

Tuning to maximal twist, i.e. $\kappa = \kappa_{\text{crit}}$, is then achieved by choosing a parity odd operator O and determine am_{crit} (equivalently κ_{crit}) such that O has vanishing expectation value. One appropriate quantity is the PCAC light quark mass [29, 52, 53]

$$m_{\text{PCAC}} = \frac{\sum_{\mathbf{x}} \langle \partial_0 A_{0,l}^a(\mathbf{x}, t) P_l^a(0) \rangle}{2 \sum_{\mathbf{x}} \langle P_l^a(\mathbf{x}, t) P_l^a(0) \rangle}, \quad a = 1, 2, \quad (8)$$

where

$$A_{\mu,l}^a(x) = \bar{\chi}_l(x) \gamma_\mu \gamma_5 \frac{\tau_a}{2} \chi_l(x), \quad P_l^a(x) = \bar{\chi}_l(x) \gamma_5 \frac{\tau_a}{2} \chi_l(x), \quad (9)$$

and we demand $m_{\text{PCAC}} = 0$. For the quenched [25] and the $N_f = 2$ case [17], this method has been found to be successful in providing the expected $\mathcal{O}(a)$ improvement and effectively reducing residual $\mathcal{O}(a^2)$ discretisation effects in the region of small quark masses [29].

The numerical precision required for the tuning of m_{PCAC} to zero has been discussed in [8]. Contrary to the $N_f = 2$ case [5, 8], where this tuning was performed once at the minimal value of the twisted light mass considered in the simulations, we now perform the tuning at each value of the twisted light quark mass μ_l and the heavy-doublet quark mass parameters μ_σ and μ_δ . This obviously leaves more freedom in the choice of light quark masses for future computations.

Although theoretical arguments tell us that $\mathcal{O}(a)$ improvement is at work in our setup, a dedicated continuum scaling study is always required to accurately quantify the actual magnitude of $\mathcal{O}(a^2)$ effects. In section 3.4 we provide a first

indication that such effects are indeed small, at least for the here considered light meson sector; currently ongoing computations at a significantly smaller lattice spacing will allow for a continuum limit scaling analysis in this setup.

3 Simulation Details

3.1 *Simulation Ensembles*

We performed simulations at two values of the lattice gauge coupling $\beta = 1.90$ and 1.95 , corresponding to values of the lattice spacing $a \approx 0.086\text{ fm}$ and $a \approx 0.078\text{ fm}$, respectively. The parameters of each ensemble are reported in table 2. The charged pion mass m_{PS} ranges from 270 MeV to 510 MeV . Simulated volumes correspond to values of $m_{\text{PS}}L$ ranging from 3.0 to 5.8 , where the smaller volumes served to estimate finite volume effects, see table 3. Physical spatial volumes range from $(1.9\text{ fm})^3$ to $(2.8\text{ fm})^3$.

As already mentioned, the tuning to κ_{crit} was performed independently for each value of the mass parameters $a\mu_l$, $a\mu_\sigma$ and $a\mu_\delta$. The mass parameters of the heavy doublet $a\mu_\sigma$ and $a\mu_\delta$ reported in table 2 are related to the strange and charm quark masses. In particular, they are fixed by requiring the simulated kaon and D meson masses to approximately take their physical values, as discussed in section 3.3. The simulation algorithm used to generate the ensembles includes in the light sector, a Hybrid Monte Carlo algorithm with multiple time scales and mass preconditioning, described in ref. [61], while in the strange-charm sector a polynomial hybrid Monte Carlo (PHMC) algorithm [62–64]; the implementation of ref. [65] is publicly available.

The positivity of the determinant of the Dirac operator is a property of the mass-degenerate Wilson twisted mass action, which does not necessarily hold in the non degenerate case for generic values of the mass parameters μ_σ and μ_δ .¹ The positivity is monitored by measuring the smallest eigenvalue $\lambda_{\text{h,min}}$ of $Q_h^\dagger Q_h$, where $Q_h = \gamma_5 \tau_3 D_h$ and D_h is the Wilson Dirac operator of the non-degenerate twisted mass action in eq. (5). We observe that $\lambda_{\text{h,min}}$ is roughly proportional to the renormalised strange quark mass squared. Since we choose the mass parameters μ_σ and μ_δ such that the strange quark takes its physical value, a spectral gap in the distribution of $Q_h^\dagger Q_h$ is observed, implying that the determinant of D_h does not change sign during the simulation. While this is sufficient for the purpose of this study, we shall provide a detailed discussion of this issue in a forthcoming publication.

¹ Notice however that the positivity of the determinant is guaranteed for $\mu_\sigma^2 > \mu_\delta^2$ [33, 34].

Ensemble	β	κ_{crit}	$a\mu_l$	$a\mu_\sigma$	$a\mu_\delta$	$(L/a)^3 \times T/a$
A30.32	1.90	0.1632720	0.0030	0.150	0.190	$32^3 \times 64$
A40.32		0.1632700	0.0040			$32^3 \times 64$
A40.24		0.1632700	0.0040			$24^3 \times 48$
A40.20		0.1632700	0.0040			$20^3 \times 48$
A50.32		0.1632670	0.0050			$32^3 \times 64$
A60.24		0.1632650	0.0060			$24^3 \times 48$
A80.24		0.1632600	0.0080			$24^3 \times 48$
A100.24		0.1632550	0.0100			$24^3 \times 48$
A100.24s		0.1631960	0.0100		0.197	$24^3 \times 48$
B25.32	1.95	0.1612420	0.0025	0.135	0.170	$32^3 \times 64$
B35.32		0.1612400	0.0035			$32^3 \times 64$
B55.32		0.1612360	0.0055			$32^3 \times 64$
B75.32		0.1612320	0.0075			$32^3 \times 64$
B85.24		0.1612312	0.0085			$24^3 \times 48$

Table 2

Summary of the $N_f = 2 + 1 + 1$ ensembles generated by ETMC at two values of the lattice coupling $\beta = 1.90$ and $\beta = 1.95$. From left to right, we quote the ensemble name, the value of inverse coupling β , the estimate of the critical value κ_{crit} , the light twisted mass $a\mu_l$, the heavy doublet mass parameters $a\mu_\sigma$ and $a\mu_\delta$ and the volume in units of the lattice spacing. Our notation for the ensemble names corresponds to X. $\mu_l.L$, with X referring to the value of β used. The run A100.24s is used to control the tuning of the strange and charm quark masses.

Ensemble	m_{PCAC}/μ_l	$m_{\text{PS}}L$	$\tau_{\text{int}}(\langle P \rangle)$	$\tau_{\text{int}}(am_{\text{PS}})$	$\tau_{\text{int}}(am_{\text{PCAC}})$
A30.32	-0.123(87)	3.97	118(55)	2.7(4)	46(19)
A40.32	-0.055(55)	4.53	103(48)	4.1(7)	51(21)
A40.24	-0.148(83)	3.48	132(57)	≤ 2	35(12)
A40.20	-0.051(91)	2.97	55(25)	2.9(7)	26(12)
A50.32	0.064(24)	5.05	50(19)	3.0(5)	21(7)
A60.24	-0.037(50)	4.15	28(8)	2.0(2)	13(4)
A80.24	0.020(19)	4.77	23(7)	2.4(3)	10(2)
A100.24	0.025(18)	5.35	18(5)	2.3(3)	13(3)
A100.24s	0.045(18)	5.31	18(5)	6.2(1.1)	18(5)
B25.32	-0.185(69)	3.42	65(25)	3.6(6)	26(9)
B35.32	0.009(34)	4.03	54(19)	5.5(8)	41(14)
B55.32	-0.069(13)	4.97	12(3)	≤ 2	8(2)
B75.32	-0.047(12)	5.77	14(4)	3.3(5)	13(3)
B85.24	-0.001(16)	4.66	15(4)	2.2(2)	11(2)

Table 3

For each ensemble, from left to right the values of m_{PCAC}/μ_l , $m_{\text{PS}}L$, the integrated autocorrelation time of the plaquette, m_{PS} and m_{PCAC} in units of the trajectory length. Every ensemble contains 5000 thermalised trajectories of length $\tau = 1$, except A40.24 which contains 8000 trajectories.

To generate correlators we use stochastic sources and improve the signal-to-noise ratio by using the “one-end trick”, following the techniques also employed in our $N_f = 2$ simulations [8]. We have constructed all meson correlators with

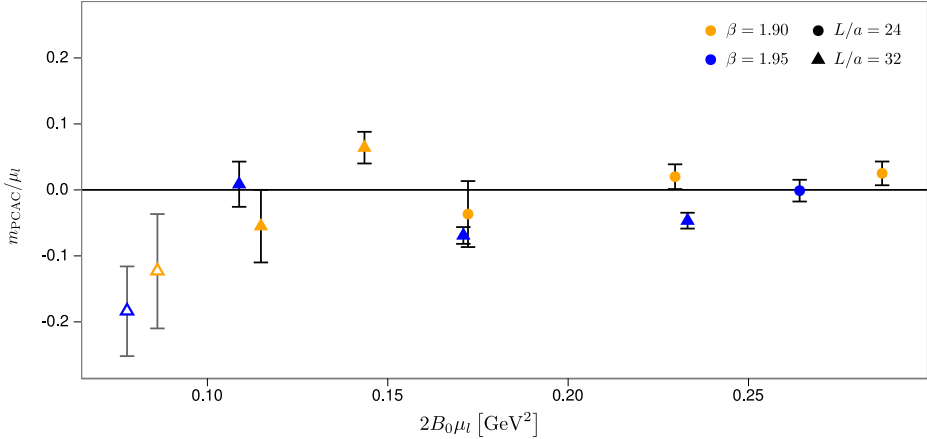


Fig. 2. The ratio m_{PCAC}/μ_l for the ensembles at $\beta = 1.90$ and 1.95 at the largest simulated volumes and as a function of $2B_0\mu_l$. For both ensembles the ratio m_{PCAC}/μ_l satisfies the 10% level criterion, except for the lightest point at $\beta = 1.90$ and $\beta = 1.95$ (open symbols), also affected by larger statistical errors. We assume $Z_A = 1$, while the actual value $Z_A \lesssim 1$ can only improve all tuning conditions.

local (L), fuzzed (F) and Gaussian smeared (S) sources and sinks. The use of smeared or fuzzed sources has stronger impact on the extraction of the kaon and D meson masses; results for the latter are reported in section 3.3, while a companion paper [66] discusses the adopted strategy for the less straightforward determination of these masses in the unitary $N_f = 2 + 1 + 1$ Wilson twisted mass formalism.

3.2 Tuning to Maximal Twist

To guarantee $\mathcal{O}(a)$ improvement of all physical observables while also avoiding residual $\mathcal{O}(a^2)$ effects with decreasing pion mass, the numerical precision of the tuning to maximal twist – quantified by the deviation from zero of m_{PCAC} – has to satisfy $|Z_A m_{\text{PCAC}}/\mu_l|_{\mu_l, \mu_\sigma, \mu_\delta} \lesssim a\Lambda_{QCD}$ [5, 8, 17]. The left-hand side contains the renormalised ratio of the untwisted mass over the twisted light-quark mass. A similar condition should be fulfilled by the error on this ratio. For the current lattice spacings, $a\Lambda_{QCD} \approx 0.1$, while the values of the axial current renormalisation factor Z_A have not yet been determined. Nevertheless, since Z_A enters as an $\mathcal{O}(1)$ multiplicative prefactor, and it is expected to be $Z_A \lesssim 1$ for our ensembles², we adopt the conservative choice $Z_A = 1$ in verifying the tuning condition.

² Preliminary determinations of Z_A from ongoing dedicated runs with four degenerate light flavours, indicate that $Z_A \sim 0.7 - 0.8$ for the ensembles considered in this work.

Satisfying this constraint clearly requires a good statistical accuracy in the determination of the PCAC mass. The values of m_{PCAC}/μ_l reported in table 3 and shown in fig. 2 are well satisfying the tuning condition to maximal twist, with the exception of the lightest mass point at $\beta = 1.90$ and $\beta = 1.95$. We notice that the autocorrelation time of m_{PCAC} reported in table 3 grows with decreasing values of the light quark mass μ_l , thus rendering the tuning more costly for the two lightest points. For the ensemble B25.32, we are currently performing a new simulation aiming at a more accurate tuning to κ_{crit} . We are also testing a reweighting procedure [36] in κ on the same ensemble, in view of applying it to the other not optimally tuned ensemble A30.32, and to future simulations. In what follows, we use the lightest mass points for consistency checks, and we exclude them from the final χ PT fits. We also remind the reader that the small deviations from zero of $a m_{\text{PCAC}}$ will only affect the $\mathcal{O}(a^2)$ lattice discretisation errors of physical observables [8].

3.3 Tuning of the Strange and Charm Quark Masses

The mass parameters μ_σ and μ_δ in the heavy doublet of the action in eq. (5) can in principle be adjusted so as to match the renormalised strange and charm quark masses by use of eq. (6). In practise, in this work, we fix the values of μ_σ and μ_δ by requiring that the simulated kaon mass m_K and D meson mass m_D approximately take their physical values.

A detailed description of the determination of the kaon and D meson masses is separately given in [66], while figures 3(a) and 3(b) show the resulting dependence of $(2m_K^2 - m_{PS}^2)$ and m_D upon the light pseudoscalar mass squared for both ensembles, and compared with the physical point. Table 4 summarises their numerical values, while the corresponding values for $a\mu_\sigma$ and $a\mu_\delta$ are given in table 2. Observe also that, in order to be able to properly tune the strange and charm quark masses to their physical values, $a\mu_\sigma$ must be chosen larger than $a\mu_\delta$, since (see eq. (6)) the ratio Z_P/Z_S is significantly smaller than one [66].

While the kaon and D meson masses at $\beta = 1.95$ are sufficiently well tuned to their physical values, the ensembles at $\beta = 1.90$ with $a\mu_\delta = 0.190$ carry a heavier kaon mass. The latter is instead visibly closer to its physical value for $a\mu_\delta = 0.197$, as can be inferred from figure 3(a). We are currently performing simulations with $a\mu_\delta = 0.197$ for other light quark masses. Moreover, another set of values of μ_σ and μ_δ are currently being used at $\beta = 1.90$ to generate ensembles with a slightly lower D meson mass and a third value of the kaon mass, in order to properly interpolate the lattice data to the physical strange quark mass.

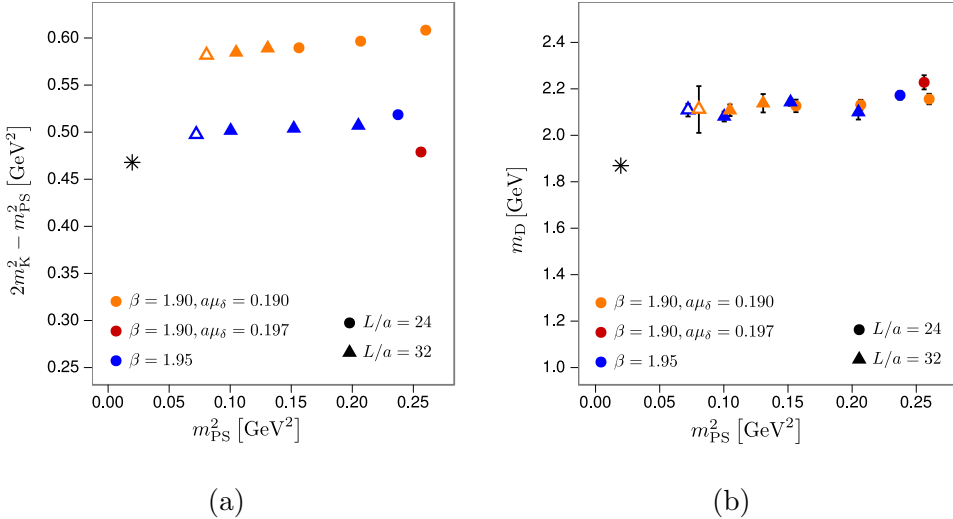


Fig. 3. (a): $2m_K^2 - m_{\text{PS}}^2$, and (b): m_D , as a function of m_{PS}^2 , for $\beta = 1.95$ (blue) and $\beta = 1.90$ (orange). The physical point is shown (black star). The kaon and D meson masses appear to be properly tuned at $\beta = 1.95$. The ensembles at $\beta = 1.90$, $\mu_\delta = 0.190$ have a larger value of the strange quark mass, while the red point at $\beta = 1.90$, $a\mu_\delta = 0.197$ appears to be well tuned. Data points have been scaled with the lattice spacing $a = 0.08585(53)$ fm for $\beta = 1.90$, and $a = 0.07820(59)$ fm for $\beta = 1.95$, obtained in this work and where the errors are only statistical.

Ensemble	β	am_K	am_D
A30.32	1.90	0.25150(29)	0.9230(440)
A40.32		0.25666(23)	0.9216(109)
A40.24		0.25884(43)	0.9375(128)
A40.20		0.26130(135)	0.8701(152)
A50.32		0.26225(38)	0.9348(173)
A60.24		0.26695(52)	0.9298(118)
A80.24		0.27706(61)	0.9319(94)
A100.24		0.28807(34)	0.9427(99)
A100.24s		0.26502(90)	0.9742(133)
B25.32	1.95	0.21240(50)	0.8395(109)
B35.32		0.21840(28)	0.8286(85)
B55.32		0.22799(34)	0.8532(62)
B75.32		0.23753(32)	0.8361(127)
B85.24		0.24476(44)	0.8650(76)

Table 4

For each ensemble, the values of the kaon mass and the D meson mass as determined in [66].

3.4 Discretisation Effects in Light-quark Observables

In this section we explore discretisation effects in the analysed light-quark observables. To this aim we also make use of the determination of the chi-

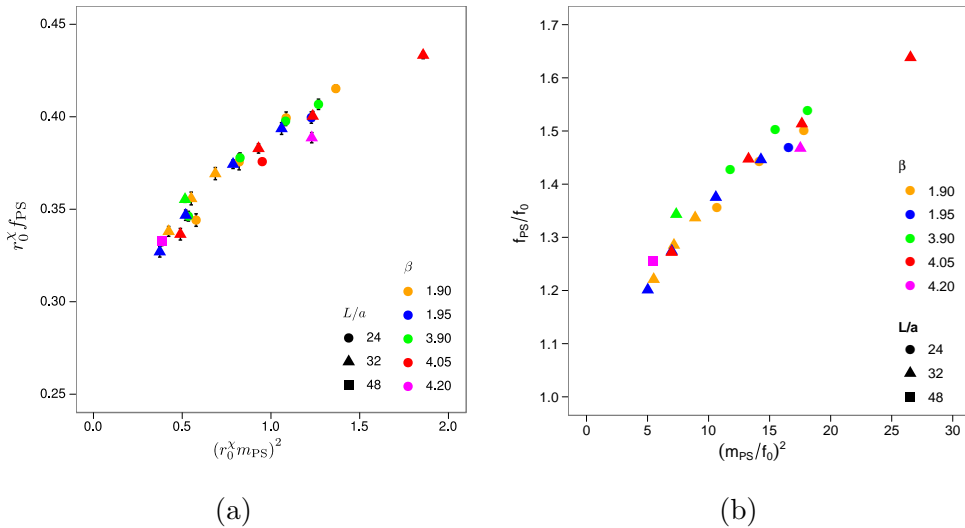


Fig. 4. The quantity αf_{PS} as a function of $(\alpha m_{\text{PS}})^2$, with (a) $\alpha = r_0^\chi$ and (b) $\alpha = 1/f_0$, for the $N_f = 2 + 1 + 1$ data at $\beta = 1.90$ and $\beta = 1.95$, and for the $N_f = 2$ data at $\beta = 3.90$, $\beta = 4.05$ and $\beta = 4.20$ in [17]. The values of r_0^χ for $N_f = 2 + 1 + 1$ are given in tables 1 and 9.

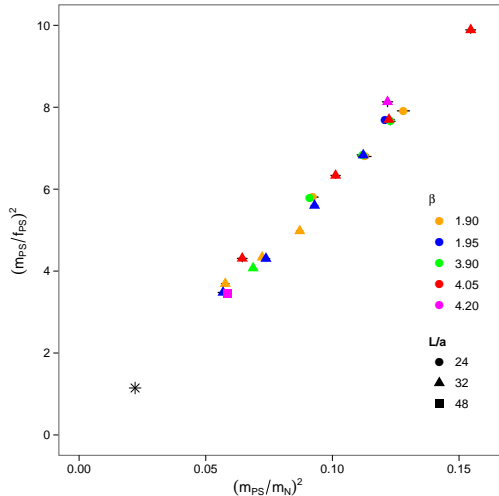


Fig. 5. The ratio $m_{\text{PS}}^2/f_{\text{PS}}^2$ as a function of m_{PS}^2/m_N^2 , for the $N_f = 2+1+1$ ensembles at $\beta = 1.90$ and $\beta = 1.95$, compared to the $N_f = 2$ data at $\beta = 3.90$, $\beta = 4.05$ and $\beta = 4.20$ [17]. The physical point is shown (black star).

rally extrapolated r_0 value for our data samples, as discussed in the following section 3.5.

In figures 4(a) and 4(b) we study the sensitivity of the charged pion mass and decay constant to possible discretisation effects, by comparing the $N_f = 2 + 1 + 1$ data at $\beta = 1.90$ and $\beta = 1.95$ and the results obtained in twisted mass simulations with two dynamical flavours [17]. The alignment of all data

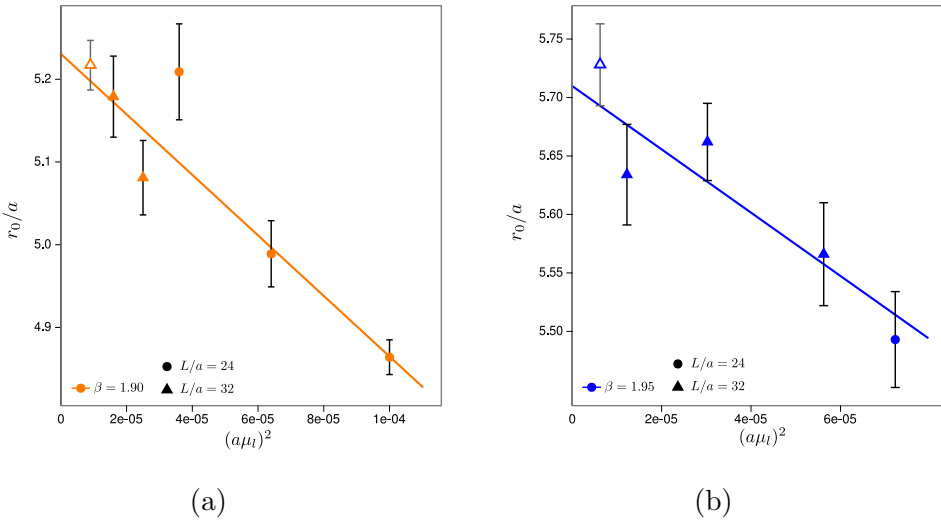


Fig. 6. The Sommer scale r_0/a as a function of $(a\mu_l)^2$ for (a) $\beta = 1.90$ and (b) $\beta = 1.95$. The lines represent a linear extrapolation in $(a\mu_l)^2$ to the chiral limit. The lightest point (open symbol) is not included in the fits and we have always used the largest available volume for a given value of the mass.

points at different values of β is in itself an indication of small discretisation effects. The comparison and good agreement with the $N_f = 2$ data seems also to suggest no significant dependence upon the inclusion of dynamical strange and charm quarks for these light observables, at least at the present level of accuracy and provided that no cancellations occur due to lattice discretisation effects. However, only a more complete study at significantly different lattice spacings will allow to draw conclusions.

In the same spirit, we show in figure 5 an analogous ratio plot where the nucleon mass data points are included. The alignment of all data and the good extrapolation to the physical point is again evident. We defer to future publications the analysis of the baryon spectrum and the study of discretisation effects in strange- and charm-quark observables.

3.5 The Sommer Scale r_0

The Sommer scale r_0 [67] is a purely gluonic quantity extracted from the static inter-quark potential. Since the knowledge of its physical value remains rather imprecise, we use the chirally extrapolated lattice data for r_0/a only as an effective way to compare results from different values of the lattice spacing. In this work, the lattice scale is extracted by performing χ PT inspired fits to the very precise data for af_{PS} and am_{PS} , and by using the physical values of m_π and f_π as inputs.

Figures 6(a) and 6(b) display the data for r_0/a at both values of the lattice coupling $\beta = 1.90$ and 1.95 , and as a function of the bare lattice mass squared. The data are reasonably well described by a quadratic dependence, as also previously found for our $N_f = 2$ ensembles. For a more detailed discussion of the possible functional forms and their theoretical interpretation see [37]. To extrapolate to the chiral limit, we have performed fits using the largest available volume at each value of the pseudoscalar mass. The chirally extrapolated values for our $N_f = 2 + 1 + 1$ ensembles are $r_0^\chi/a = 5.231(38)$ at $\beta = 1.90$ and $r_0^\chi/a = 5.710(41)$ at $\beta = 1.95$, where the lightest points of both ensembles have been excluded from the extrapolation, consistently with the fact that they do not satisfy our most stringent tuning condition to maximal twist.

In order to meaningfully compare the dependence upon the light quark mass at the two different lattice couplings $\beta = 1.90$ and 1.95 , we estimated the slope of the functional form $r_0/r_0^\chi = 1 + c_r(r_0^\chi m_{\text{PS}})^4$, where the explicit lattice spacing dependence has been removed. We observe a mild dependence on the light quark mass and similar slopes $c_r[\beta = 1.90] = -0.0379(37)$ and $c_r[\beta = 1.95] = -0.0234(69)$. It is also worth noticing that the dependence upon the light quark mass of the $N_f = 2 + 1 + 1$ data and that observed in the $N_f = 2$ case [37] are not significantly different.

3.6 Effects of Isospin Breaking

A most delicate aspect of the twisted mass formulation is the breaking of the isospin symmetry. Clear evidence for this breaking has been found in the $N_f = 2$ simulations by ETMC when comparing the neutral with the charged pion masses. Indeed, while the discretisation effects in the charged pion were observed to be very small, significant $\mathcal{O}(a^2)$ corrections appear when studying the scaling to the continuum limit of the neutral pion [17]. Notice, however, that similar effects have not been observed in other quantities that are in principle sensitive to isospin breaking but not trivially related to the neutral pion mass. These observations are supported by theoretical considerations detailed in [31, 32].

In the $N_f = 2 + 1 + 1$ case, it turns out that the isospin breaking effect in the mass difference of charged and neutral pion masses is larger than for $N_f = 2$ at fixed physical situation³, as can be inferred from table 5. On the other hand, the same theoretical considerations as in [32] do apply to the case of $N_f = 2 + 1 + 1$ flavours, and it is expected that the same class of physical observables as for $N_f = 2$ will not be significantly affected by isospin

³ Notice however that different gauge actions are used in the $N_f = 2$ and $N_f = 2 + 1 + 1$ cases as described in section 2.1.

Ensemble	β	$r_0^\chi m_{\text{PS}}^\pm$	$r_0^\chi m_{\text{PS}}^0$	c
B35.32	1.95	0.7196(57)	0.388(40)	-12.0(1.1)
B55.32		0.8861(67)	0.679(40)	-10.6(1.8)
$B_6 \ N_f = 2$	3.90	0.7113(66)	0.585(43)	-4.6(1.5)
$B_2 \ N_f = 2$		0.9001(86)	0.712(54)	-8.6(2.2)

Table 5

Measurements of the masses of the charged and the neutral pion. We compare runs at $\beta = 1.95$ and $N_f = 2$ runs [17] with comparable lattice spacing and similar charged pion masses in physical units. All masses are reported in units of the chirally extrapolated r_0 for the same ensemble, see table 9, and $r_0^\chi/a = 5.316(49)$ for $N_f = 2$. We also report on the approximate value of c , giving the slope of the a^2 dependence of the pion mass splitting.

breaking corrections. Having said that, a careful measure of this effect for each observable or class of observables is anyway mandatory. The increase of the pion mass splitting with increasing the number of flavours in the sea is in line with the observation [35] of a stronger first order phase transition when moving from $N_f = 2$ to $N_f = 2 + 1 + 1$, as discussed in section 2.1. Indeed, the endpoint of the phase transition [44, 45] corresponds to the critical value of the light twisted mass $\mu_{l,c}$ where the neutral pion mass vanishes. The mass difference can be described by $r_0^{\chi^2}((m_{\text{PS}}^0)^2 - (m_{\text{PS}}^\pm)^2) = c(a/r_0^\chi)^2$, where the coefficient c is related to $\mu_{l,c}$ [44, 45] and it is therefore a measure of the strength of the first order phase transition. Hence, a larger value of c means that simulations are to be performed at smaller values of the lattice spacing to reach, say, the physical point. Table 5 reports on the values of m_{PS}^\pm , m_{PS}^0 and c for some examples taken from the $\beta = 1.95$ ensemble and the $N_f = 2$ ensemble with the closest values of the lattice spacing and physical charged pseudoscalar mass. As anticipated, the coefficient c increases in absolute value from $N_f = 2$ to $N_f = 2 + 1 + 1$.

We are currently performing simulations at a significantly different and lower lattice spacing than the present ensembles. They will allow to determine the slope c for $N_f = 2 + 1 + 1$ more accurately and to better quantify the conditions to approach the physical point.

3.7 Stout Smeared Runs

In addition to our main simulation ensembles, we also performed runs with stout smeared gauge fields in the lattice fermionic action. The stout smearing as introduced in [59] was designed to have a smearing procedure which is analytic in the unsmeared link variables and hence well suited for HMC-type updating algorithms. In an earlier work with $N_f = 2$ quark flavours [60] we showed that using smeared gauge fields in the fermion operator is reducing the strength of the phase transition in twisted quark mass simulations and

Ensemble	β	κ_{crit}	$a\mu_l$	$a\mu_\sigma$	$a\mu_\delta$	$N_{\text{traj.}}$	r_0/a
A _{st} 40.24	1.90	0.145512	0.0040	0.170	0.185	1500	5.304(35)
A _{st} 60.24		0.145511	0.0060			3100	5.300(37)
A _{st} 80.24		0.145510	0.0080			2000	5.353(43)

Table 6

Parameters of the runs with stout smearing on $L/a = 24$, $T/a = 48$ lattices. The number of thermalised trajectories with length $\tau = 1$ is given by $N_{\text{traj.}}$. The label “st” in the ensemble name refers to the use of stout smearing, compared to the non stout-smeared ensemble in table 2.

Ensemble	am_{PS}	am_K	am_D	m_{PCAC}/μ_l
A _{st} 40.24	0.12600(93)	0.2479(18)	0.802(27)	0.0175(68)
A _{st} 60.24	0.14888(78)	0.25338(67)	0.825(26)	0.0017(50)
A _{st} 80.24	0.17156(69)	0.26198(80)	0.811(12)	0.0138(48)

Table 7

The masses in lattice units for the ensembles with one level of stout smearing.

therefore allows to reach smaller quark masses at a given lattice spacing.

The definition of the stout smeared links can be found in [59], and for the parameter ρ connecting thin to fat gauge links we choose $\rho = 0.15$. In principle, such smearing can be iterated several times, with the price of rendering the fermion action delocalised over a larger lattice region. We made a conservative choice to maintain the action well localised and performed a single smearing step. As shown in [60], this kind of smearing does not substantially change the lattice spacing, and for the sake of comparison we thus kept the same value of β as in one of the non stout-smeared runs. On the other hand, the hopping parameter has to be tuned again, since the additive renormalisation of the quark mass is expected to be smaller. The parameters of our runs are given in Table 6. These runs have been done with the two-step polynomial Hybrid Monte Carlo (TS-PHMC) update algorithm [68]. Results for the hadron masses are collected in Table 7, where the quoted errors include an estimate of the systematic error induced by variations of the fitting range. The method of estimating and combining statistical and systematic errors for the case of the kaon and D meson masses is described in [66].

As the values of m_{PCAC}/μ_l in table 7 show, the hopping parameters are well tuned to maximal twist. The masses in the run with smallest light twisted mass $a\mu_l = 0.0040$ (ensemble A_{st}40.24) satisfy $r_0 m_{\text{PS}} = 0.668(10)$, $r_0 m_K = 1.315(13)$ and $r_0 m_D = 4.25(29)$. This means that the pion is lighter than in the corresponding run without stout smearing (see table 8) and the kaon and D meson masses are closer to their physical value. The smaller pion mass should be interpreted as due to a quark mass renormalisation factor closer to one. For the same reason the tuned twisted masses in the heavy doublet $a\mu_\sigma = 0.170$, $a\mu_\delta = 0.185$ are smaller than in the runs without stout smearing. It is also interesting to compare the mass splitting of the charged and

neutral pion between runs with and without stout smearing. For the ensemble A_{st}60.24 we obtain a neutral pion mass $r_0^\chi m_{\text{PS}}^0 = 0.409(34)$ and a charged pion mass $r_0^\chi m_{\text{PS}}^\pm = 0.7861(56)$, in units of the chirally extrapolated value $r_0^\chi/a = 5.280(25)$, providing an estimate of the slope $c = -12.6(0.8)$. Notice that the mass dependence of r_0/a in table 6 is reduced as compared to the runs with no stout smearing, and a quadratic dependence on the bare quark mass has been used for the extrapolation to the chiral limit, consistently with the analysis of section 3.5. For the corresponding ensemble A60.24 without stout smearing, using data in tables 8 and 9, we obtain instead $r_0^\chi m_{\text{PS}}^0 = 0.560(37)$, $r_0^\chi m_{\text{PS}}^\pm = 0.9036(71)$, and a slope $c = -13.8(1.2)$, slightly but not significantly different from the stout-smeared case.

The runs with stout-smeared gauge links show somewhat better characteristics than the ones without stout smearing, but the improvements are not dramatic, at least with one level of stout smearing. More iterations would further accelerate the approach to lighter masses and are expected to further reduce the charged to neutral pion splitting. However, it is a delicate matter to establish how physical observables other than the spectrum will be affected. Based on these considerations and given the present pool of data, the final results in this study are obtained with non stout-smeared simulations.

4 Results: f_{PS} , m_{PS} and Chiral Fits

We concentrate in this section on the analysis of the simplest and phenomenologically relevant observables involving up and down valence quarks. These are the light charged pseudoscalar decay constant f_{PS} and the light charged pseudoscalar mass m_{PS} .

The present simulations with dynamical strange and charm quarks, sitting at, or varying around, their nature given masses, should allow for a good measure of the impact of strange and charm dynamics on the low energy sector of QCD and the electroweak matrix elements. As a first step, one can determine the low energy constants of chiral perturbation theory (χ PT). The values of $a f_{\text{PS}}$ and $a m_{\text{PS}}$ for our ensembles at $\beta = 1.95$ and $\beta = 1.90$ are summarised in table 8. In contrast to standard Wilson fermions, an exact lattice Ward identity for maximally twisted mass fermions allows for extracting the charged pseudoscalar decay constant f_{PS} from the relation

$$f_{\text{PS}} = \frac{2\mu_l}{m_{\text{PS}}^2} |\langle 0 | P_l^1(0) | \pi \rangle|, \quad (10)$$

without need to specify any renormalisation factor, since $Z_P = 1/Z_\mu$ [3]. We have performed fits to NLO SU(2) continuum χ PT at $\beta = 1.95$ and $\beta = 1.90$, separately and combined. Results are summarised in table 9.

Ensemble	$a\mu_l$	am_{PS}	af_{PS}	r_0/a	L/a
A30.32	0.0030	0.12395(36)(14)	0.06451(35)(3)	5.217(30)	32
A40.32	0.0040	0.14142(27)(42)	0.06791(18)(4)	5.179(49)	32
A40.24	0.0040	0.14492(52)(34)	0.06568(34)(7)	5.178(44)	24
A40.20	0.0040	0.14871(92)(116)	0.06194(65)(23)	-	20
A50.32	0.0050	0.15796(32)(28)	0.07048(16)(4)	5.081(45)	32
A60.24	0.0060	0.17275(45)(23)	0.07169(22)(2)	5.209(58)	24
A80.24	0.0080	0.19875(41)(35)	0.07623(21)(4)	4.989(40)	24
A100.24	0.0100	0.22293(35)(38)	0.07926(20)(4)	4.864(21)	24
A100.24s	0.0100	0.22125(58)(119)	0.07843(26)(21)	4.918(50)	24
B25.32	0.0025	0.10680(39)(27)	0.05727(36)(8)	5.728(35)	32
B35.32	0.0035	0.12602(30)(30)	0.06074(18)(8)	5.634(43)	32
B55.32	0.0055	0.15518(21)(33)	0.06557(15)(5)	5.662(33)	32
B75.32	0.0075	0.18020(27)(3)	0.06895(17)(1)	5.566(44)	32
B85.24	0.0085	0.19396(38)(54)	0.06999(20)(5)	5.493(41)	24

Table 8

Lattice measurements of the charged pseudoscalar mass am_{PS} , the charged pseudoscalar decay constant af_{PS} and the Sommer scale in lattice units r_0/a for our two ensembles at $\beta = 1.90$ (A set) and $\beta = 1.95$ (B set). The value of the light twisted mass $a\mu_l$ and the spatial length L/a are also shown. Quoted errors are given as (statistical)(systematic), with the estimate of the systematic error coming from the uncertainty related to the fitting range.

We thus simultaneously fit our data for the pseudoscalar mass and decay constant to the following formulae, where the contributions F , D and T parametrising finite size corrections, discretisation effects and NNLO χ PT effects, respectively, will be discussed below:

$$\begin{aligned} m_{\text{PS}}^2(L) &= \chi_\mu \left(1 + \xi l_3 + D_{m_{\text{PS}}^2} a^2 + \xi^2 T_{m_{\text{PS}}^2} \right) F_{m_{\text{PS}}^2} \\ f_{\text{PS}}(L) &= f_0 \left(1 - 2\xi l_4 + D_{f_{\text{PS}}} a^2 + \xi^2 T_{f_{\text{PS}}} \right) F_{f_{\text{PS}}}, \end{aligned} \quad (11)$$

with the pseudoscalar mass squared at tree level defined as $\chi_\mu \equiv 2 B_0 \mu_l$ and the chiral expansion parameter by $\xi \equiv \chi_\mu / (4\pi f_0)^2$. The low energy constants l_3 and l_4 receive renormalization corrections according to $\bar{l}_i = l_i + \ln [\Lambda^2/\chi_\mu]$, with Λ the reference scale. During the fitting procedure, where all quantities are defined in lattice units, we set the reference scale to a single lattice spacing to let its constant logarithmic contribution vanish. Once the scale of the simulation has been set, the low energy constants are rescaled to the scale of the physical pion mass to recover the physical values \bar{l}_3 and \bar{l}_4 .

Systematic errors can arise from several sources: finite volume effects, neglecting of higher orders in χ PT and finite lattice spacing effects. These different corrections are accounted for explicitly in eq. (11). Finite volume corrections are described by the rescaling factors denoted by $F_{m_{\text{PS}}^2}$ and $F_{f_{\text{PS}}}$, computed in the continuum theory. Notice that the discretisation effects present in the

neutral pion mass, see section 3.6, generate peculiar finite volume corrections which have been recently analysed in ref. [69]. We shall comment on them later. We investigated the effectiveness of one loop continuum χ PT finite volume corrections, as first computed in [70], which do not introduce any additional low energy constants. However, the resummed expressions derived by Colangelo, Dürr and Haefeli (CDH) in [71] describe the finite volume effects in our simulations better, be it at the expense of the introduction of two new free parameters, and are thus adopted for this analysis. To $\mathcal{O}(\xi^2)$, these corrections read

$$\begin{aligned} F_{m_{\text{PS}}^2} &= \left[1 - \sum_{n=1}^{\infty} \frac{\rho_n}{2\lambda_n} (\xi I_m^{(2)} + \xi^2 I_m^{(4)}) \right]^2 \\ F_{f_{\text{PS}}} &= 1 + \sum_{n=1}^{\infty} \frac{\rho_n}{\lambda_n} (\xi I_f^{(2)} + \xi^2 I_f^{(4)}), \end{aligned} \quad (12)$$

with geometric contributions defined as

$$\begin{aligned} I_m^{(2)} &= -2K_1(\lambda_n) \\ I_m^{(4)} &= \left(\frac{101}{9} - \frac{13}{3}\pi + 8l_1 + \frac{16}{3}l_2 - 5l_3 - 4l_4 \right) K_1(\lambda_n) + \\ &\quad \left(-\frac{238}{9} + \frac{61}{6}\pi - \frac{16}{3}l_1 - \frac{64}{3}l_2 \right) \frac{K_2(\lambda_n)}{\lambda_n} \\ I_f^{(2)} &= -4K_1(\lambda_n) \\ I_f^{(4)} &= \left(\frac{29}{18} - \frac{29}{12}\pi + 4l_1 + \frac{8}{3}l_2 - 6l_4 \right) K_1(\lambda_n) + \\ &\quad \left(-\frac{307}{9} + \frac{391}{24}\pi - \frac{16}{3}l_1 - \frac{64}{3}l_2 \right) \frac{K_2(\lambda_n)}{\lambda_n}. \end{aligned} \quad (13)$$

The K_i are the modified Bessel functions and the low energy constants l_1 and l_2 again receive renormalisation corrections. Equations (12) and (13) use the shorthand notation $\lambda_n = \sqrt{n}m_{\text{PS}}L$. The ρ_n in eq. (12) are a set of multiplicities, counting the number of ways n^2 can be distributed over three spatial directions⁴. Because the finite volume corrections in the case of the volumes used in the chiral fits are fairly small to begin with and subsequent terms quickly decrease, the sums over n can be truncated rather aggressively without real loss of precision. It is therefore unnecessary, in practise, to go beyond the lowest contributions. The parameters l_1 and l_2 , which are in fact low energy constants appearing at NLO in χ PT, cannot be determined well from the small finite volume corrections alone. Priors are therefore introduced as additional contributions to the χ^2 , weighting the deviation of the parameters from

⁴ These values are straightforwardly precomputed to any order, but are also given in, *e.g.* [71].

their phenomenological values by the uncertainties in the latter. The values used as priors are -0.4(6) for \bar{l}_1 and 4.3(1) for \bar{l}_2 [71], as reported in table 9. We used the largest available volumes for each ensemble, in the χ PT fits. For those points, the difference between the finite volume and the infinite volume values estimated via CDH formulae for f_{PS} and m_{PS}^2 are within 1%, except for the runs B85.24 and A60.24 (see table 2 and table 8), where they are about 1.5% for both quantities.

Because of the automatic $\mathcal{O}(a)$ improvement of the twisted mass action at maximal twist, the leading order discretisation artefacts in the chiral formulae of (11) are at least of $\mathcal{O}(a^2)$, and $\mathcal{O}(a^2\mu)$ for m_{PS}^2 . The mass and decay constant of the charged pion have been studied up to NLO [44, 45, 50] in the context of twisted mass chiral perturbation theory ($\text{tm}\chi$ PT). The regime of quark masses and lattice spacings at which we have performed the simulations is such that $\mu_l \gtrsim a\Lambda_{\text{QCD}}^2$. In the associated power counting, at maximal twist, the NLO $\text{tm}\chi$ PT expressions for the charged pion mass and decay constant preserve their continuum form. The inclusion of the terms proportional to $D_{m_{\text{PS}}, f_{\text{PS}}}^2$, parametrising the lattice artifacts in eq. (11), represents an effective way of including sub-leading discretisation effects appearing at NNLO. The finite lattice spacing artefacts can of course not be determined using only data from a single lattice spacing. In addition, including these terms when analysing data with an insufficient range in a , may lead to mixing of these degrees of freedom with continuum parameters and thereby destabilise the fits. Hence, these terms were neglected for the separate fits, but included to arrive at a qualitative estimate of these systematic effects in a combined fit to the data at both lattice spacings.

Finite size effects on our data at finite lattice spacing can be analysed in the context of twisted mass chiral perturbation theory as recently proposed in ref. [69].⁵ However, our present limited set of data with only a small number of different volumes all of them at a single value of the lattice spacing, is not sufficient to apply such an analysis. We plan, however, to perform dedicated runs on different volumes to confront our data to the finite size effect formulae of ref. [69] and to estimate in particular the size of the pion mass splitting in this alternative way.

Finally, results from continuum χ PT at NNLO can be included to examine the effect of the truncation at NLO. They are given by

⁵ Notice that, in principle, after performing the continuum limit at fixed physical volume, finite size effects can be analysed by means of continuum χ PT.

$$\begin{aligned} T_{m_{\text{PS}}^2} &= \frac{17}{102} (49 + 28 l_1 + 32 l_2 - 9 l_3) + 4 k_m \\ T_{f_{\text{PS}}} &= -\frac{1}{6} (23 + 14 l_1 + 16 l_2 + 6 l_3 - 6 l_4) + 4 k_f. \end{aligned} \quad (14)$$

Two new parameters k_m and k_f enter these corrections. Again, a limited range of input pion masses may lead to poorly constrained values of these newly introduced parameters, some degree of mixing among different orders and fit instabilities. To retain predictive power and stability, additional priors are given for k_m and k_f , both priors set to $0(1)$, analogously to what is done for l_1 and l_2 in the CDH finite volume corrections.

To set the scale at each lattice spacing, we determine $a\mu_{\text{phys}}$, the value of $a\mu_l$ at which the ratio $\sqrt{m_{\text{PS}}^2(L = \infty)/f_{\text{PS}}(L = \infty)}$ assumes its physical value. We can then use the value of f_{PS} , or equivalently m_{PS} , to calculate the lattice spacing a in fm from the corresponding physical value. We also perform a chiral fit combining the two different lattice spacings. With only two different values of β , that are in fact fairly close to each other, a proper continuum limit analysis cannot be performed. Instead, we treat this combined fit as a check on the presence of lattice artefacts and the overall consistency of the data. Without a scaling variable, such as the Sommer scale r_0 , the data from different lattice spacings cannot be directly combined. Rather, the ratios of lattice spacings and light quark mass renormalisation constants ($Z_\mu = 1/Z_P$), as well as the renormalised B_0 parameter are left free in the fit.

In order to estimate the statistical errors affecting our fitted parameters, we generate at each of the μ_l values 1000 bootstrap samples for m_{PS} and f_{PS} extracted from the bare correlators, organised by blocks. For each sample, and combining all masses, we fit m_{PS}^2 and f_{PS} simultaneously as a function of μ_l . The parameter set from each of these fits is then a separate bootstrap sample for the purposes of determining the error on our fit results. By resampling f_{PS} and m_{PS} on a per-configuration basis, correlations between these quantities are taken into account.

Our final results for the separate and combined fits are summarised in table 9. The χ PT fit ansätze provide a satisfactory description of the lattice data, with a $\chi^2/\text{d.o.f} = 5.68/3 \simeq 1.9$ at $\beta = 1.95$, $\chi^2/\text{d.o.f} = 4.31/5 \simeq 0.9$ at $\beta = 1.90$, and $16.9/11 \simeq 1.5$ for the combined fit. We also predict the scalar radius of the pion at next to leading order

$$\langle r^2 \rangle_s^{\text{NLO}} = \frac{12}{(4\pi f_0)^2} \left(\bar{l}_4 - \frac{13}{12} \right). \quad (15)$$

The numerical values in table 9 for the combined fit show a very good agreement with the results from the separate fits, and with errors at the percent level throughout. The fits for f_{PS} and m_{PS} at $\beta = 1.95$ are displayed in fig-

	$\beta = 1.90$	$\beta = 1.95$	combined	priors
\bar{l}_3	3.435(61)	3.698(73)	3.537(47)	-
\bar{l}_4	4.773(21)	4.673(25)	4.735(17)	-
\bar{l}_1	-0.296(104)	-0.430(93)	-0.309(139)	-0.4(6)
\bar{l}_2	4.260(12)	4.329(15)	4.325(10)	4.3(1)
f_0 [MeV]	120.956(70)	121.144(83)	121.031(54)	-
f_π/f_0	1.0781(18)	1.0764(18)	1.0774(17)	-
$2B_0\mu_{u,d}/m_\pi^2$	1.029(16)	1.032(21)	1.030(13)	-
$\langle r^2 \rangle_s^{\text{NLO}}$ [fm 2]	0.7462(43)	0.7237(51)	0.7375(34)	-
$r_0^\chi/a(\beta = 1.90)$	5.231(38)	-	5.231(37)	-
$r_0^\chi/a(\beta = 1.95)$	-	5.710(41)	5.710(42)	-
$r_0^\chi(\beta = 1.90)$ [fm]	0.4491(43)	-	0.4505(40)	-
$r_0^\chi(\beta = 1.95)$ [fm]	-	0.4465(48)	0.4439(39)	-
$a(\beta = 1.90)$ [fm]	0.08585(53)	-	0.08612(42)	-
$a(\beta = 1.95)$ [fm]	-	0.07820(59)	0.07775(39)	-

Table 9

Results of the fits to SU(2) χ PT for the ensembles at $\beta = 1.95$ and $\beta = 1.90$, separate and combined. The largest available volumes are used for each ensemble. Predicted quantities are: the low energy constants $\bar{l}_{3,4}$ (while $\bar{l}_{1,2}$ are introduced with priors), the charged pseudoscalar decay constant in the chiral limit f_0 , the mass ratio $2B_0\mu_l/m_{\text{PS}}^2$ at the physical point and the pion scalar radius $\langle r^2 \rangle_s^{\text{NLO}}$. The scale is set by fixing the ratio $f_{\text{PS}}^{[L=\infty]}/m_{\text{PS}}^{[L=\infty]} = f_\pi/m_\pi = 130.4(2)/135.0$ to its physical value [41]. The chirally extrapolated Sommer parameter r_0^χ is determined separately and not included in the chiral fits. For a comparison with the $N_f = 2$ ETMC results, see [17].

ures 1(a) and (b), while in figures 7(a) and (b) we show the analogous fits at $\beta = 1.90$. Figures 8(a) and (b) show the results for the fit combining the two β values.

The data presented here do not allow yet for a complete account of the systematic effects, but we extract estimates of their magnitude by extending the fits with additional terms as written down in eq. (11). Checks were done for χ PT NNLO terms and $\mathcal{O}(a^2)$ corrections separately. Including NNLO corrections does not lower the total χ^2 of the fit, while we do observe a shift of several standard deviations for the lower order parameters already present in the NLO fit. Using these shifted values to obtain the implied NLO approximation produces fits with much larger values of χ^2 . We conclude that the current data lack the precision and range in quark masses to constrain NNLO effects, the added degrees of freedom mix with NLO effects and destabilise the fit instead. In practise, we conclude that the systematic error from the truncation of χ PT is unobservable at the current level of precision. Inclusion of $\mathcal{O}(a^2)$ corrections leads to similar observations, as the difference between the lattice spacings and the statistical accuracy of the data is too small to result in a stable fit. The fit mixes $D_{f_{\text{PS}}}$ and $D_{m_{\text{PS}}^2}$ on the one hand and f_0 , B_0 and the rescaling in the lattice spacing and the quark mass on the other.

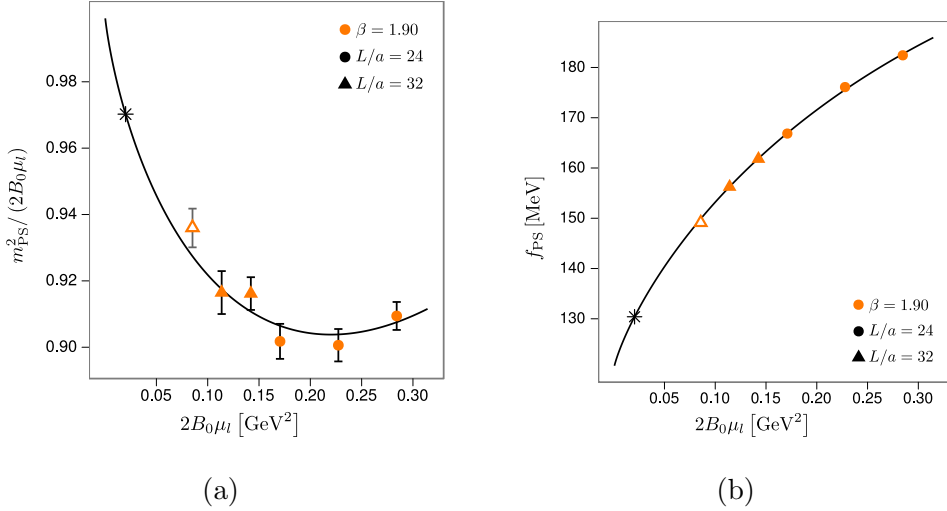


Fig. 7. (a) The charged pseudoscalar mass ratio $m_{\text{PS}}^2 / (2B_0 \mu_l)$ and (b) the pseudoscalar decay constant f_{PS} as a function of $2B_0 \mu_l$, for the ensemble at $\beta = 1.90$, fitted to SU(2) chiral perturbation theory, eq. (11). The scale is set by $a\mu_{\text{phys}}$, the value of $a\mu_l$ at which the ratio $f_{\text{PS}}^{[L=\infty]} / m_{\text{PS}}^{[L=\infty]}$ assumes its physical value [41] $f_\pi / m_\pi = 130.4(2) / 135.0$ (black star). The light twisted masses used in the fit range from $a\mu_l = 0.004$ to 0.010 . The lightest point (open symbol) lies outside our most conservative tuning criterion to maximal twist, and is not included in the fit.

The chirally extrapolated Sommer scale r_0^χ has been determined separately, using a fit of r_0/a with quadratic dependence on the bare light quark mass, as shown in figures 6(a) and 6(b), and using the lattice spacing determined by the chiral fits. As also reported in table 9, the obtained values are $r_0^\chi = 0.4491(43)$ fm at $\beta = 1.90$ and $r_0^\chi = 0.4465(48)$ fm at $\beta = 1.95$, where only statistical errors are quoted. For consistency, we also verified that a combined chiral fit with the inclusion of r_0/a , as data points and additional fit parameter, gives results anyway in agreement with the strategy adopted here.

For our final estimates of the low energy constants $\bar{l}_{3,4}$ and the chiral value of the pseudoscalar decay constant f_0 we use the predictions from the $\beta = 1.95$ ensemble based on two important observations. First, the strange quark mass in this ensemble is better tuned to the physical value. Secondly a reduced isospin breaking is observed at this finer lattice spacing. The results for the $\beta = 1.90$ ensemble and the combined fits serve instead as an estimation of systematic uncertainties. As a result of the current $N_f = 2 + 1 + 1$ simulations we thus quote

$$\bar{l}_3 = 3.70(7)(26) \quad \bar{l}_4 = 4.67(3)(10), \quad (16)$$

and $f_0 = 121.14(8)(19)$ MeV, where the first error comes from the chiral fit at $\beta = 1.95$, while the second quoted error conservatively accommodates the central values from the $\beta = 1.90$ and combined fits as a systematic uncertainty. The predictions for \bar{l}_3 and \bar{l}_4 are in good agreement and with our two-flavour predictions [17] and with other recent lattice determinations [2, 72].

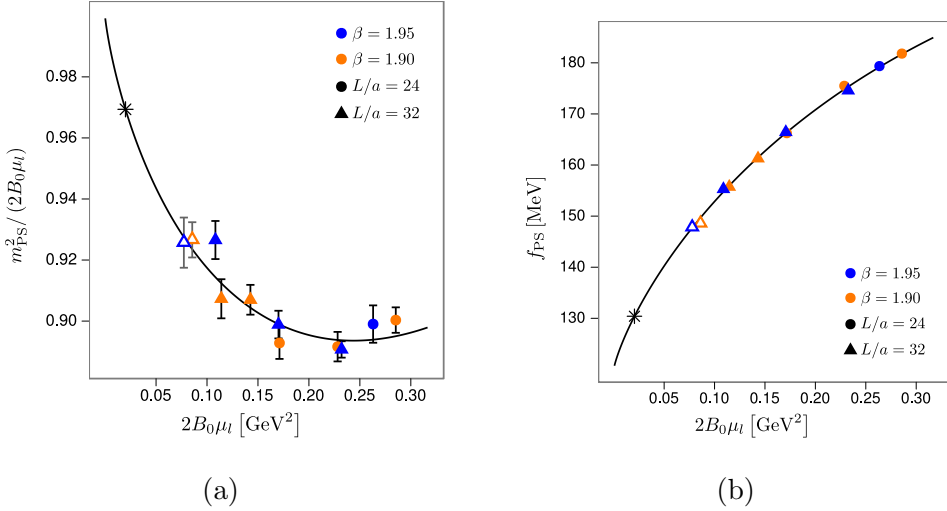


Fig. 8. (a) The charged pseudoscalar mass ratio $(m_{PS}/2B_0\mu_l)^2$ and (b) the pseudoscalar decay constant f_{PS} as a function of $2B_0\mu_l$, for the combined ensembles at $\beta = 1.90$ and $\beta = 1.95$, and fitted to eq. (11). The scale is set as in figure 7 (black star). The light twisted masses used in the fit range from $a\mu_l = 0.0035$ to 0.010 . The lightest point at $\beta = 1.90$ (open orange symbol) and at $\beta = 1.95$ (open blue symbol) lie outside our most conservative tuning criterion to maximal twist, and are not included in the fit.

5 Conclusions and Outlook

In this paper we have presented the first results of lattice QCD simulations with mass-degenerate up, down and mass-split strange and charm dynamical quarks using Wilson twisted mass fermions at maximal twist. This study constitutes a first step in our effort to describe low energy strong dynamics and electroweak matrix elements by fully taking into account the effects of a strange and a charm quark.

We have considered ensembles at slightly different lattice spacings simulated with Iwasaki gauge action at $\beta = 1.95$ with $a \approx 0.078$ fm and $\beta = 1.90$ with $a \approx 0.086$ fm. The charged pseudoscalar masses range from 270 to 510 MeV and we performed fits to SU(2) chiral perturbation theory with all data at a value of $m_{PS}L \gtrsim 4$. This analysis provides a prediction for the low energy constants $\bar{l}_3 = 3.70(7)(26)$ and $\bar{l}_4 = 4.67(3)(10)$, for the charged pseudoscalar decay constant in the chiral limit $f_0 = 121.14(8)(19)$ MeV and for the scalar radius at next-to-leading order $\langle r^2 \rangle_s^{\text{NLO}} = 0.724(5)(23)$ fm 2 . A companion paper [66] describes the less straightforward determination of the kaon and D-meson masses for the same ensembles.

We have compared our results in the light meson sector with those obtained for $N_f = 2$ flavours of maximally twisted mass fermions, ref. [17]. There,

an extrapolation to the continuum limit, a study of finite size effects and checks against higher order χ PT have been performed, leading to a controlled determination of systematic errors. The comparison we have carried through does not show any significant difference between $N_f = 2$ and $N_f = 2 + 1 + 1$ flavours, at least at the present level of accuracy. These results would suggest that effects of the strange and charm quarks are suppressed for these light observables, as it should be expected. The same comparison has also been used for a first investigation of lattice discretisation errors. As figures 4(a) and 4(b) show, the $N_f = 2 + 1 + 1$ data are completely consistent with the corresponding ones obtained for $N_f = 2$, where the discretisation effects have turned out to be very small. Thus, it can be expected that also for the case of $N_f = 2 + 1 + 1$ flavours the lattice spacing effects will be small, at least for the light meson sector considered here. Notice however that, at the present level of accuracy, there is still the possibility that cancellations occur between physical contributions due to dynamical strange and charm quarks and lattice discretisation effects. A more accurate study at a significantly lower lattice spacing will allow to draw conclusions.

One aspect of the twisted mass formulation is the breaking of isospin symmetry. Its effect is likely to be most pronounced in the lightest sector, where lattice discretisation effects at $\mathcal{O}(a^2)$, affecting the neutral pseudoscalar mass only, generate a mass splitting between the charged and the neutral pseudoscalar mesons. While this mass splitting for $N_f = 2 + 1 + 1$ flavours has been found here to be larger than in the $N_f = 2$ simulations at fixed physical situation, we do not find further effects in other quantities computed so far. This observation is supported by theoretical arguments [31, 32] and consistent with our experience in the $N_f = 2$ flavour case.

We consider the present results to be encouraging to proceed with the $N_f = 2 + 1 + 1$ flavour research programme of ETMC. In particular, we want to perform the non-perturbative renormalisation with dedicated runs for $N_f = 4$ mass-degenerate flavours, an activity which we have started already. Furthermore, we want to compute the quark mass dependence of many physical quantities towards the physical point where the pion assumes its experimentally measured value. We are currently performing simulations at a significantly different and lower lattice spacing than the present ensembles. Both strategies, smaller quark masses and smaller lattice spacings, will allow us to estimate systematic effects on a quantitative level and to obtain in this way accurate physical results in our $N_f = 2 + 1 + 1$ flavour simulations with statistical and systematical errors fully under control.

Acknowledgements

We want to thank the whole ETMC for a very fruitful and enjoyable collaboration. In particular, we gratefully acknowledge valuable suggestions and discussions with Benoît Blossier, Roberto Frezzotti, Andreas Nube, Giancarlo Rossi and Enno Scholz.

The computer time for this project was made available to us by the John von Neumann-Institute for Computing (NIC) on the JUMP, Juropa and Ju-gene systems in Jülich and apeNEXT system in Zeuthen, BG/P and BG/L in Groningen, by BSC on Mare-Nostrum in Barcelona (www.bsc.es), and by the computer resources made available by CNRS on the BlueGene system at GENCI-IDRIS Grant 2009-052271 and CCIN2P3 in Lyon. We thank these computer centres and their staff for all technical advice and help.

V.G. and D.P. thank the MICINN (Spain) for partial support under grant FPA2008-03373. This work has been supported in part by the DFG Sonderforschungsbereich/ Transregio SFB/TR9-03 and the EU Integrated Infrastructure Initiative Hadron Physics (I3HP) under contract RII3-CT-2004-506078. We also thank the DEISA Consortium (co-funded by the EU, FP6 project 508830), for support within the DEISA Extreme Computing Initiative.

References

- [1] K. Jansen, PoS **LATTICE2008**, 010 (2008), [arXiv:0810.5634 \[hep-lat\]](https://arxiv.org/abs/0810.5634).
- [2] E. E. Scholz, [arXiv:0911.2191 \[hep-lat\]](https://arxiv.org/abs/0911.2191).
- [3] **ALPHA** Collaboration, R. Frezzotti, P. A. Grassi, S. Sint and P. Weisz, JHEP **08**, 058 (2001), [hep-lat/0101001](https://arxiv.org/abs/hep-lat/0101001).
- [4] R. Frezzotti and G. C. Rossi, JHEP **08**, 007 (2004), [hep-lat/0306014](https://arxiv.org/abs/hep-lat/0306014).
- [5] **ETM** Collaboration, P. Boucaud *et al.*, Phys. Lett. **B650**, 304 (2007), [arXiv:hep-lat/0701012](https://arxiv.org/abs/hep-lat/0701012).
- [6] **ETM** Collaboration, B. Blossier *et al.*, JHEP **04**, 020 (2008), [arXiv:0709.4574 \[hep-lat\]](https://arxiv.org/abs/0709.4574).
- [7] **ETM** Collaboration, C. Urbach, PoS **LAT2007**, 022 (2007), [arXiv:0710.1517 \[hep-lat\]](https://arxiv.org/abs/0710.1517).
- [8] **ETM** Collaboration, P. Boucaud *et al.*, Comput. Phys. Commun. **179**, 695 (2008), [arXiv:0803.0224 \[hep-lat\]](https://arxiv.org/abs/0803.0224).
- [9] K. Cichy, J. Gonzalez Lopez, K. Jansen, A. Kujawa and A. Shindler, Nucl. Phys. **B800**, 94 (2008), [arXiv:0802.3637 \[hep-lat\]](https://arxiv.org/abs/0802.3637).

- [10] **ETM** Collaboration, C. Alexandrou *et al.*, Phys. Rev. **D78**, 014509 (2008), arXiv:0803.3190 [hep-lat].
- [11] **ETM** Collaboration, K. Jansen, C. Michael, A. Shindler and M. Wagner, JHEP **12**, 058 (2008), arXiv:0810.1843 [hep-lat].
- [12] **ETM** Collaboration, K. Jansen, C. Michael and C. Urbach, Eur. Phys. J. **C58**, 261 (2008), arXiv:0804.3871 [hep-lat].
- [13] R. Frezzotti, V. Lubicz and S. Simula, Phys. Rev. **D79**, 074506 (2009), arXiv:0812.4042 [hep-lat].
- [14] **ETM** Collaboration, B. Blossier *et al.*, JHEP **07**, 043 (2009), arXiv:0904.0954 [hep-lat].
- [15] **ETM** Collaboration, K. Jansen, C. McNeile, C. Michael and C. Urbach, Phys. Rev. **D80**, 054510 (2009), arXiv:0906.4720 [hep-lat].
- [16] **ETM** Collaboration, C. McNeile, C. Michael and C. Urbach, Phys. Lett. **B674**, 286 (2009), arXiv:0902.3897 [hep-lat].
- [17] **ETM** Collaboration, R. Baron *et al.*, arXiv:0911.5061 [hep-lat].
- [18] **ETM** Collaboration, C. Alexandrou *et al.*, Phys. Rev. **D80**, 114503 (2009), arXiv:0910.2419 [hep-lat].
- [19] **ETM** Collaboration, B. Blossier *et al.*, arXiv:arXiv:0909.3187 [hep-lat].
- [20] **European Twisted Mass** Collaboration, B. Blossier, M. Wagner and O. Pene, JHEP **06**, 022 (2009), arXiv:0903.2298 [hep-lat].
- [21] **ETM** Collaboration, M. Constantinou *et al.*, arXiv:arXiv:1004.1115 [hep-lat].
- [22] **ETM** Collaboration, C. Michael, A. Shindler and M. Wagner, arXiv:1004.4235 [hep-lat].
- [23] A. Shindler, Phys. Rept. **461**, 37 (2008), arXiv:0707.4093 [hep-lat].
- [24] **XLF** Collaboration, K. Jansen, A. Shindler, C. Urbach and I. Wetzorke, Phys. Lett. **B586**, 432 (2004), hep-lat/0312013.
- [25] **XLF** Collaboration, K. Jansen, M. Papinutto, A. Shindler, C. Urbach and I. Wetzorke, Phys. Lett. **B619**, 184 (2005), hep-lat/0503031.
- [26] **XLF** Collaboration, K. Jansen, M. Papinutto, A. Shindler, C. Urbach and I. Wetzorke, JHEP **09**, 071 (2005), hep-lat/0507010.
- [27] A. M. Abdel-Rehim, R. Lewis and R. M. Woloshyn, Phys. Rev. **D71**, 094505 (2005), hep-lat/0503007.
- [28] **ETM** Collaboration, P. Dimopoulos, R. Frezzotti, G. Herdoiza, C. Urbach and U. Wenger, PoS **LAT2007**, 102 (2007), arXiv:0710.2498 [hep-lat].

- [29] R. Frezzotti, G. Martinelli, M. Papinutto and G. C. Rossi, JHEP **04**, 038 (2006), [hep-lat/0503034](#).
- [30] **χ_{LF}** Collaboration, K. Jansen *et al.*, Phys. Lett. **B624**, 334 (2005), [hep-lat/0507032](#).
- [31] R. Frezzotti and G. Rossi, PoS **LAT2007**, 277 (2007), [arXiv:0710.2492 \[hep-lat\]](#).
- [32] **ETM** Collaboration, P. Dimopoulos, R. Frezzotti, C. Michael, G. C. Rossi and C. Urbach, Phys. Rev. **D81**, 034509 (2010), [arXiv:0908.0451 \[hep-lat\]](#).
- [33] R. Frezzotti and G. C. Rossi, JHEP **10**, 070 (2004), [hep-lat/0407002](#).
- [34] R. Frezzotti and G. C. Rossi, Nucl. Phys. Proc. Suppl. **128**, 193 (2004), [hep-lat/0311008](#).
- [35] T. Chiarappa *et al.*, Eur. Phys. J. **C50**, 373 (2007), [arXiv:hep-lat/0606011](#).
- [36] **ETM** Collaboration, R. Baron *et al.*, PoS **LATTICE2008**, 094 (2008), [arXiv:0810.3807 \[hep-lat\]](#).
- [37] **ETM** Collaboration, R. Baron *et al.*, PoS **LATT2009**, 104 (2009), [arXiv:0911.5244 \[hep-lat\]](#).
- [38] **MILC** Collaboration, A. Bazavov *et al.*, PoS **LATTICE2008**, 033 (2008), [arXiv:arXiv:0903.0874 \[hep-lat\]](#).
- [39] **MILC** Collaboration, A. Bazavov *et al.*, PoS **LAT2009**, 123 (2009), [arXiv:arXiv:0911.0869 \[hep-lat\]](#).
- [40] **MILC** Collaboration, A. Bazavov *et al.*, [arXiv:1004.0342 \[hep-lat\]](#).
- [41] **Particle Data Group** Collaboration, C. Amsler *et al.*, Phys. Lett. **B667**, 1 (2008).
- [42] Y. Iwasaki, Nucl. Phys. **B258**, 141 (1985).
- [43] Y. Iwasaki, K. Kanaya, T. Kaneko and T. Yoshie, Phys. Rev. **D56**, 151 (1997), [arXiv:hep-lat/9610023](#).
- [44] G. Münster and C. Schmidt, Europhys. Lett. **66**, 652 (2004), [arXiv:hep-lat/0311032](#).
- [45] S. R. Sharpe and J. M. S. Wu, Phys. Rev. **D71**, 074501 (2005), [hep-lat/0411021](#).
- [46] S. Aoki and O. Bär, Phys. Rev. **D70**, 116011 (2004), [hep-lat/0409006](#).
- [47] S. R. Sharpe and J. M. S. Wu, Phys. Rev. **D70**, 094029 (2004), [hep-lat/0407025](#).
- [48] G. Münster, JHEP **09**, 035 (2004), [hep-lat/0407006](#).
- [49] G. Münster, C. Schmidt and E. E. Scholz, Nucl. Phys. Proc. Suppl. **140**, 320 (2005), [hep-lat/0409066](#).

- [50] L. Scorzato, Eur. Phys. J. **C37**, 445 (2004), [hep-lat/0407023](#).
- [51] F. Farchioni *et al.*, Eur. Phys. J. **C39**, 421 (2005), [hep-lat/0406039](#).
- [52] F. Farchioni *et al.*, Nucl. Phys. Proc. Suppl. **140**, 240 (2005), [hep-lat/0409098](#).
- [53] F. Farchioni *et al.*, Eur. Phys. J. **C42**, 73 (2005), [hep-lat/0410031](#).
- [54] F. Farchioni *et al.*, PoS **LAT2005**, 072 (2006), [hep-lat/0509131](#).
- [55] F. Farchioni *et al.*, Eur. Phys. J. **C47**, 453 (2006), [arXiv:hep-lat/0512017](#).
- [56] F. Farchioni *et al.*, Phys. Lett. **B624**, 324 (2005), [arXiv:hep-lat/0506025](#).
- [57] P. Weisz, Nucl. Phys. **B212**, 1 (1983).
- [58] P. Weisz and R. Wohlert, Nucl. Phys. **B236**, 397 (1984).
- [59] C. Morningstar and M. J. Peardon, Phys. Rev. **D69**, 054501 (2004), [arXiv:hep-lat/0311018](#).
- [60] K. Jansen *et al.*, PoS **LAT2007**, 036 (2007), [arXiv:0709.4434 \[hep-lat\]](#).
- [61] C. Urbach, K. Jansen, A. Shindler and U. Wenger, Comput. Phys. Commun. **174**, 87 (2006), [hep-lat/0506011](#).
- [62] R. Frezzotti and K. Jansen, Phys. Lett. **B402**, 328 (1997), [hep-lat/9702016](#).
- [63] R. Frezzotti and K. Jansen, Nucl. Phys. **B555**, 395 (1999), [hep-lat/9808011](#).
- [64] T. Chiarappa, R. Frezzotti and C. Urbach, PoS **LAT2005**, 103 (2006), [arXiv:hep-lat/0509154](#).
- [65] K. Jansen and C. Urbach, Comput. Phys. Commun. **180**, 2717 (2009), [arXiv:0905.3331 \[hep-lat\]](#).
- [66] **ETM** Collaboration, R. Baron *et al.*, (2010), in preparation.
- [67] R. Sommer, Nucl. Phys. **B411**, 839 (1994), [hep-lat/9310022](#).
- [68] I. Montvay and E. Scholz, Phys. Lett. **B623**, 73 (2005), [hep-lat/0506006](#).
- [69] G. Colangelo, U. Wenger and J. M. S. Wu, [arXiv:1003.0847 \[hep-lat\]](#).
- [70] J. Gasser and H. Leutwyler, Phys. Lett. **B184**, 83 (1987).
- [71] G. Colangelo, S. Dürr and C. Haefeli, Nucl. Phys. **B721**, 136 (2005), [hep-lat/0503014](#).
- [72] S. Necco, PoS **CONFINEMENT8**, 024 (2008), [arXiv:0901.4257 \[hep-lat\]](#).

Computing K and D meson masses with $N_f = 2 + 1 + 1$ twisted mass lattice QCD

SFB/CPP-09-31, LPSC1049, MS-TP-10-10, DESY 10-055, LTH874, LPT-Orsay 10-30,
 HU-EP-10/19

Remi Baron^a, Philippe Boucaud^b, Jaume Carbonell^c, Vincent Drach^c,
 Federico Farchioni^d, Gregorio Herdoiza^e, Karl Jansen^e, Chris Michael^f,
 Istvan Montvay^g, Elisabetta Pallante^h, Olivier Pène^b, Siebren Reker^h,
 Carsten Urbachⁱ, Marc Wagner^j, Urs Wenger^k

^a CEA, Centre de Saclay, IRFU/Service de Physique Nucléaire, F-91191 Gif-sur-Yvette, France

^b Laboratoire de Physique Théorique (Bât. 210), CNRS et Université Paris-Sud XI, Centre
 d'Orsay, 91405 Orsay-Cedex, France

^c Laboratoire de Physique Subatomique et Cosmologie, 53 avenue des Martyrs, 38026
 Grenoble, France

^d Universität Münster, Institut für Theoretische Physik, Wilhelm-Klemm-Straße 9, D-48149
 Münster, Germany

^e NIC, DESY, Platanenallee 6, D-15738 Zeuthen, Germany

^f Division of Theoretical Physics, University of Liverpool, L69 3BX Liverpool, United Kingdom

^g Deutsches Elektronen-Synchrotron DESY, Notkestr. 85, D-22603 Hamburg, Germany

^h Centre for Theoretical Physics, University of Groningen, Nijenborgh 4, 9747 AG Groningen,
 the Netherlands

ⁱ Helmholtz-Institut für Strahlen- und Kernphysik (Theorie) and Bethe Center for Theoretical
 Physics, Universität Bonn, 53115 Bonn, Germany

^j Humboldt-Universität zu Berlin, Institut für Physik, Newtonstraße 15, D-12489 Berlin,
 Germany

^k Albert Einstein Center for Fundamental Physics, Institute for Theoretical Physics,
 University of Bern, Sidlerstr. 5, CH-3012 Bern, Switzerland



May 12, 2010

Abstract

We discuss the computation of the mass of the K and D mesons within the framework of $N_f = 2 + 1 + 1$ twisted mass lattice QCD from a technical point of view. These quantities are essential, already at the level of generating gauge configurations, being obvious candidates to tune the strange and charm quark masses to their physical values. In particular, we address the problems related to the twisted mass flavor and parity symmetry breaking, which arise when considering a non-degenerate (c, s) doublet. We propose and verify the consistency of three methods to extract the K and D meson masses in this framework.

1 Introduction

The framework of maximally twisted mass fermions as an $\mathcal{O}(a)$ improved lattice formulation [47] has been proved to be highly successful in recent years. The European Twisted Mass Collaboration (ETMC) has adopted this formulation and has carried through a broad research program with $N_f = 2$ flavors of mass-degenerate quarks in various areas of lattice QCD including light meson physics [1, 2, 3], spectroscopy of light baryons [4, 5], strange and charm physics [6, 7, 8], B -physics [9, 10], spectroscopy of static-light mesons [11, 12], Isgur-Wise functions [13], meson [14, 15, 16] and nucleon [17] form factors, moments of parton distribution functions [18], neutral [19] and η' [20] mesons, $\omega - \rho$ mass splitting [21], the vacuum polarization tensor [22], pion scattering lengths [23], an investigation of the ρ meson as a resonance [24] or the non-perturbative renormalization of quark bilinear operators [25].

Particular emphasis has been laid on the cut-off effects appearing at $\mathcal{O}(a^2)$ in the twisted mass formulation at maximal twist. These effects have been studied theoretically at tree-level of perturbation theory [26], and within the Symanzik approach [32, 33]. These analyses suggest that isospin breaking effects strongly affect only a limited set of observables, namely the neutral pion mass and kinematically related quantities [33]. The same effects have been numerically investigated in the quenched approximation [27, 28, 29], with two dynamical flavors [3, 4, 5, 30, 31] and with $N_f = 2 + 1 + 1$ [38]. All numerical results up to date are in agreement with the theoretical conclusions.

The studies collected so far suggest that the twisted mass formulation at maximal twist is a viable realization of QCD on the lattice, with the major advantage of automatic $\mathcal{O}(a)$ improvement of physical observables, independently of the specific type of operator considered. Other advantages worth to mention are that the twisted mass term acts as an infrared regulator of the theory and that mixing patterns in the renormalisation procedure are expected to be simplified. It is hence natural to go one step further and include dynamical strange and charm quarks in the simulations. The theoretical ground for this has been provided in ref. [34] and first feasibility studies have been performed in ref. [35]. In the last years, we have initiated a comprehensive research program with dynamical $N_f = 2 + 1 + 1$ flavors of quarks. Encouraging preliminary results were reported in [36, 37], while a companion paper [38] presents a more detailed analysis of the light meson sector for the ensembles used in this paper.

A difficulty arises in $N_f = 2 + 1 + 1$ maximally twisted mass lattice QCD when adding a strange and a charm quark, due to the explicit violation of the strange and charm flavor quantum number conservation. At any non-vanishing value of the lattice spacing, the latter leads to the contamination of correlators by unphysical contributions from intermediate states carrying the wrong quantum numbers. Moreover, transitions that are not allowed in continuum QCD become possible, the consequence being that stable states in the continuum with respect to strong interactions, such as the D meson, become resonances.

In this paper, we provide algorithmic and methodological tools to tackle the problem. In particular, we present three techniques, a generalized eigenvalue problem, multiple exponential fits, and enforcing parity and flavor symmetry restoration, to compute the physical K and D meson masses. As we will demonstrate below, we find that with all three methods these masses can be extracted and results agree among the three methods. The paper is conceived as a technical report on these methods, which can in general be applied whenever flavor symmetry breaking occurs. Efforts to implement these techniques in combination with a flavor diagonal

Osterwalder-Seiler valence quark action, see e.g. [6, 34, 42, 43], are ongoing.

The paper is organized as follows. In section 2 we define the setup, the operators used, and the optimization of the correlation matrices. Section 3 describes the determination of the K and D meson masses with the three methods. We conclude in section 4.

2 Simulation setup

2.1 $N_f = 2 + 1 + 1$ twisted mass lattice QCD

This work is based on sets of configurations generated by the ETM collaboration [36, 37] with the Iwasaki gauge action [44] and $N_f = 2 + 1 + 1$ flavors of twisted mass quarks. The light degenerate (u, d) quark doublet is described by the standard twisted mass action [45]

$$S_{F,\text{light}}[\chi^{(l)}, \bar{\chi}^{(l)}, U] = a^4 \sum_x \bar{\chi}^{(l)}(x) \left(D_W(m_0) + i\mu\gamma_5\tau_3 \right) \chi^{(l)}(x), \quad (1)$$

while for the (c, s) doublet the twisted mass formulation for non-degenerate quarks of [46] has been used:

$$S_{F,\text{heavy}}[\chi^{(h)}, \bar{\chi}^{(h)}, U] = a^4 \sum_x \bar{\chi}^{(h)}(x) \left(D_W(m_0) + i\mu_\sigma\gamma_5\tau_1 + \tau_3\mu_\delta \right) \chi^{(h)}(x). \quad (2)$$

In both cases D_W denotes the standard Wilson Dirac operator

$$D_W(m_0) = \frac{1}{2} \left(\gamma_\mu \left(\nabla_\mu + \nabla_\mu^* \right) - a \nabla_\mu^* \nabla_\mu \right) + m_0, \quad (3)$$

while $\chi^{(l)} = (\chi^{(u)}, \chi^{(d)})$ and $\chi^{(h)} = (\chi^{(c)}, \chi^{(s)})$ are the quark fields in the so-called twisted basis. For reasons explained in [35] the same value of the standard quark mass parameter m_0 has been used in both sectors.

When tuning the theory to maximal twist, automatic $\mathcal{O}(a)$ improvement for physical quantities applies [46, 47]. This tuning has been done by adjusting m_0 such that the PCAC quark mass in the light quark sector vanishes [38],

$$am_{\chi^{(l)}}^{\text{PCAC}} = \frac{\sum_x \langle \partial_0^* A_0^{(l)+}(x) P^{(l)-}(y) \rangle}{2 \sum_x \langle P^{(l)+}(x) P^{(l)-}(y) \rangle} = 0, \quad (4)$$

with the bilinears defined as

$$A_\mu^{(l)+} = \bar{\chi}^{(u)} \gamma_\mu \gamma_5 \chi^{(d)} , \quad P^{(l)+} = \bar{\chi}^{(u)} \gamma_5 \chi^{(d)} , \quad P^{(l)-} = \bar{\chi}^{(d)} \gamma_5 \chi^{(u)}. \quad (5)$$

At maximal twist, in a massless quark renormalization scheme, the renormalized quark masses are related to the bare parameters μ_σ and μ_δ by [46]

$$m_s^R = Z_P^{-1} \left(\mu_\sigma - \frac{Z_P}{Z_S} \mu_\delta \right) , \quad m_c^R = Z_P^{-1} \left(\mu_\sigma + \frac{Z_P}{Z_S}, \mu_\delta \right) \quad (6)$$

where Z_P and Z_S are the renormalization constants of the non-singlet pseudoscalar and scalar densities in a massless quark scheme, namely for $N_f = 4$ massless Wilson lattice QCD.

The values of μ_σ and μ_δ have been adjusted in our simulations by requiring that the simulated kaon and D meson mass approximately assume their physical values [38]. For this study we consider two ensembles, one from each of the currently simulated β values, $\beta = 1.90$ and $\beta = 1.95$ [36, 37, 38], with a light pseudoscalar mass $m_{PS} \approx 320$ MeV in both cases, see Table 1.

Ensemble	β	$(L/a)^3 \times T/a$	$a\mu$	κ	$a\mu_\sigma$	$a\mu_\delta$	a in fm	m_{PS} in MeV	# of gauges
A40.32	1.90	$32^3 \times 64$	0.0040	0.163270	0.150	0.190	0.086	324	1003
B35.32	1.95	$32^3 \times 64$	0.0035	0.161240	0.135	0.170	0.078	318	1042

Table 1: Summary of the ensembles considered in this paper, more details in [36, 37, 38].

2.2 Meson creation operators and trial states

2.2.1 Quantum numbers, physical basis and twisted basis

We are concerned with computing the mass of the K meson, m_K , and of the D meson, m_D , within the setup defined by eqs. (1) to (3). Both mesons have total angular momentum $J = 0$ and parity $\mathcal{P} = -$. Their quark content is e.g. $\bar{K}^0 \equiv \bar{d}s$ and $D^+ \equiv \bar{d}c$.

Neither heavy flavor nor parity are exact symmetries in $N_f = 2 + 1 + 1$ twisted mass lattice QCD at finite lattice spacing. In particular, the τ_1 -coupling term in eq. (2) violates the conservation of the strange and charm flavor quantum numbers. Consequently, instead of four different heavy-light meson sectors $(s, -)$, $(s, +)$, $(c, -)$ and $(c, +)$ there is only a single mixed flavor-parity sector $(s/c, -/+)$. Problems arise in particular when one tries to determine m_D . In continuum QCD the D meson is the lowest state in the $(c, -)$ sector, while in our setup it is a highly excited state in the combined sector $(s/c, -/+)$. Notice that, besides the K meson, there are a radially excited K state ($K(1460)$), possibly strange mesons with positive parity ($K_0^*(800)$, $K_0^*(1430)$) and a number of multi particle states $K/K_0^* + n \times \pi$ [48]. Hence, for a clean extraction of m_D one has to consider sufficiently large correlation matrices, which are able to resolve all these low lying states. This is possible in principle. In practice, the separation of the excited states would require the determination of correlation matrices with extremely high statistical precision. At our currently available statistics, this route seems not to be viable.

Our approach is instead based on the observation that parity and heavy flavor symmetries are restored in the continuum limit, where the twisted mass theory is expected to reproduce QCD with $N_f = 2 + 1 + 1$ quark flavors. In this limit, operators with definite parity [47] and flavor quantum numbers projecting onto the physical meson states can be reconstructed (cf. section 3.3). As it is shown in the following, these operators can be defined as linear combinations of bilinears of the lattice quark fields in the twisted basis.

In the continuum, or in any chirality preserving lattice formulation [45], the twist transformation

relating the physical quark fields ψ and the twisted quark fields χ reads

$$\psi^{(l)} = e^{i\omega_l \gamma_5 \tau_3 / 2} \chi^{(l)}, \quad \bar{\psi}^{(l)} = \bar{\chi}^{(l)} e^{i\omega_l \gamma_5 \tau_3 / 2} \quad (7)$$

$$\psi^{(h)} = e^{i\omega_h \gamma_5 \tau_1 / 2} \chi^{(h)}, \quad \bar{\psi}^{(h)} = \bar{\chi}^{(h)} e^{i\omega_h \gamma_5 \tau_1 / 2}, \quad (8)$$

where $\omega_{l,h}$ are the twist angles in the light and heavy quark sector, respectively. Analogous relations hold for operators projecting, in the continuum limit, on trial states with definite heavy flavor and parity quantum numbers. In the physical basis, such operators can be chosen according to¹

$$\mathcal{O}_{\text{ph}} = \begin{pmatrix} \mathcal{O}_{\text{ph}}^{(s,\gamma_5)} \\ \mathcal{O}_{\text{ph}}^{(c,\gamma_5)} \\ \mathcal{O}_{\text{ph}}^{(s,1)} \\ \mathcal{O}_{\text{ph}}^{(c,1)} \end{pmatrix} = \begin{pmatrix} +i\bar{\psi}^{(d)} \gamma_5 \psi^{(s)} \\ -i\bar{\psi}^{(d)} \gamma_5 \psi^{(c)} \\ +\bar{\psi}^{(d)} \psi^{(s)} \\ -\bar{\psi}^{(d)} \psi^{(c)} \end{pmatrix} \quad (9)$$

The twist rotations in eqs. (7) and (8) relate the twisted basis operators

$$\mathcal{O}_{\chi} = \begin{pmatrix} \mathcal{O}_{\chi}^{(s,\gamma_5)} \\ \mathcal{O}_{\chi}^{(c,\gamma_5)} \\ \mathcal{O}_{\chi}^{(s,1)} \\ \mathcal{O}_{\chi}^{(c,1)} \end{pmatrix} = \begin{pmatrix} +i\bar{\chi}^{(d)} \gamma_5 \chi^{(s)} \\ -i\bar{\chi}^{(d)} \gamma_5 \chi^{(c)} \\ +\bar{\chi}^{(d)} \chi^{(s)} \\ -\bar{\chi}^{(d)} \chi^{(c)} \end{pmatrix} \quad (10)$$

to the physical operators of eq. (9) as follows

$$\mathcal{O}_{\text{ph}} = \mathcal{M}(\omega_l, \omega_h) \mathcal{O}_{\chi}, \quad \mathcal{O}_{\text{ph}}^{\dagger} = \mathcal{O}_{\chi}^{\dagger} \mathcal{M}^T(\omega_l, \omega_h), \quad (11)$$

with the orthogonal twist rotation matrix given by

$$\mathcal{M}(\omega_l, \omega_h) = \begin{pmatrix} \cos \frac{\omega_l}{2} \cos \frac{\omega_h}{2} & -\sin \frac{\omega_l}{2} \sin \frac{\omega_h}{2} & -\sin \frac{\omega_l}{2} \cos \frac{\omega_h}{2} & -\cos \frac{\omega_l}{2} \sin \frac{\omega_h}{2} \\ -\sin \frac{\omega_l}{2} \sin \frac{\omega_h}{2} & \cos \frac{\omega_l}{2} \cos \frac{\omega_h}{2} & -\cos \frac{\omega_l}{2} \sin \frac{\omega_h}{2} & -\sin \frac{\omega_l}{2} \cos \frac{\omega_h}{2} \\ \sin \frac{\omega_l}{2} \cos \frac{\omega_h}{2} & \cos \frac{\omega_l}{2} \sin \frac{\omega_h}{2} & \cos \frac{\omega_l}{2} \cos \frac{\omega_h}{2} & -\sin \frac{\omega_l}{2} \sin \frac{\omega_h}{2} \\ \cos \frac{\omega_l}{2} \sin \frac{\omega_h}{2} & \sin \frac{\omega_l}{2} \cos \frac{\omega_h}{2} & -\sin \frac{\omega_l}{2} \sin \frac{\omega_h}{2} & \cos \frac{\omega_l}{2} \cos \frac{\omega_h}{2} \end{pmatrix}. \quad (12)$$

However, when using the Wilson lattice formulation, the operators in eq. (10), with and without a γ_5 matrix, renormalize differently due to the explicit breaking of chiral symmetry. This implies that, to be able to build a representation of the chiral group, renormalization factors must explicitly be taken into account, and eq. (11) only holds for the renormalized counterparts

$$\mathcal{O}_{\text{ph}}^R = \mathcal{M}(\omega_l, \omega_h) \mathcal{O}_{\chi}^R, \quad (\mathcal{O}_{\text{ph}}^R)^{\dagger} = (\mathcal{O}_{\chi}^R)^{\dagger} \mathcal{M}^T(\omega_l, \omega_h), \quad (13)$$

where the bilinears in eq. (10) have been replaced by their renormalized versions,

$$\mathcal{O}_{\chi}^R = \text{diag}(Z_P, Z_P, Z_S, Z_S) \mathcal{O}_{\chi} = \begin{pmatrix} Z_P \mathcal{O}_{\chi}^{(s,\gamma_5)} \\ Z_P \mathcal{O}_{\chi}^{(c,\gamma_5)} \\ Z_S \mathcal{O}_{\chi}^{(s,1)} \\ Z_S \mathcal{O}_{\chi}^{(c,1)} \end{pmatrix}, \quad (14)$$

¹For definiteness we identify the light flavor with d .

and Z_P and Z_S are the same renormalization factors as in (6). At maximal twist, i.e. $\omega_l = \omega_h = \pi/2$, one has

$$\begin{pmatrix} \mathcal{O}_{\text{ph}}^{(s,\gamma_5)} \\ \mathcal{O}_{\text{ph}}^{(c,\gamma_5)} \\ \mathcal{O}_{\text{ph}}^{(s,1)} \\ \mathcal{O}_{\text{ph}}^{(c,1)} \end{pmatrix}^R = \frac{1}{2} \begin{pmatrix} 1 & -1 & -1 & -1 \\ -1 & 1 & -1 & -1 \\ 1 & 1 & 1 & -1 \\ 1 & 1 & -1 & 1 \end{pmatrix} \begin{pmatrix} Z_P \mathcal{O}_{\chi}^{(s,\gamma_5)} \\ Z_P \mathcal{O}_{\chi}^{(c,\gamma_5)} \\ Z_S \mathcal{O}_{\chi}^{(s,1)} \\ Z_S \mathcal{O}_{\chi}^{(c,1)} \end{pmatrix}. \quad (15)$$

A third definition of the quark fields will be useful in the following (where maximal twist applies), obtained by rotating the lattice χ -fields via eqs. (7) and (8), where now $\omega_l = \omega_h = \pi/2$. The rotated fields would reproduce the physical ones in a theory with exact chiral symmetry and $Z_P = Z_S$. In the present formulation with broken chiral symmetry, they define instead a “pseudo physical basis” (ppb). We denote the rotated fields with $\psi_{\text{ppb}}^{(l,h)}$ and introduce the operator bilinears in this basis

$$\mathcal{O}_{\text{ppb}} = \begin{pmatrix} \mathcal{O}_{\text{ppb}}^{(s,\gamma_5)} \\ \mathcal{O}_{\text{ppb}}^{(c,\gamma_5)} \\ \mathcal{O}_{\text{ppb}}^{(s,1)} \\ \mathcal{O}_{\text{ppb}}^{(c,1)} \end{pmatrix} = \begin{pmatrix} +i\bar{\psi}_{\text{ppb}}^{(d)} \gamma_5 \psi_{\text{ppb}}^{(s)} \\ -i\bar{\psi}_{\text{ppb}}^{(d)} \gamma_5 \psi_{\text{ppb}}^{(c)} \\ +\bar{\psi}_{\text{ppb}}^{(d)} \psi_{\text{ppb}}^{(s)} \\ -\bar{\psi}_{\text{ppb}}^{(d)} \psi_{\text{ppb}}^{(c)} \end{pmatrix} = \frac{1}{2} \begin{pmatrix} 1 & -1 & -1 & -1 \\ -1 & 1 & -1 & -1 \\ 1 & 1 & 1 & -1 \\ 1 & 1 & -1 & 1 \end{pmatrix} \begin{pmatrix} \mathcal{O}_{\chi}^{(s,\gamma_5)} \\ \mathcal{O}_{\chi}^{(c,\gamma_5)} \\ \mathcal{O}_{\chi}^{(s,1)} \\ \mathcal{O}_{\chi}^{(c,1)} \end{pmatrix}, \quad (16)$$

otherwise written as

$$\mathcal{O}_{\text{ppb}} = \mathcal{M}(\pi/2, \pi/2) \mathcal{O}_{\chi} \equiv \mathcal{M}_{\text{mt}} \mathcal{O}_{\chi}. \quad (17)$$

The physical operators defined in eq. (13), and eq. (15) at maximal twist, project onto states that converge to states with definite flavor and parity quantum numbers in the continuum limit. Since we aim to determine the ground states of the physical system, in at least two of the four sectors, it is appropriate to first build the correlation matrices in terms of the building blocks given in eq. (10). We also project to zero momentum by summing over all lattice sites at fixed Euclidean time t ,

$$\mathcal{O}_{\chi}^{(h,\Gamma)}(t) = \eta_{\Gamma} \sum_{\mathbf{x}} \bar{\chi}^{(d)}(\mathbf{x}, t) \Gamma \chi^{(h)}(\mathbf{x}, t), \quad h \in \{s, c\}, \quad \Gamma \in \{\gamma_5, 1\} \quad (\eta_1 = \pm 1, \eta_{\gamma_5} = \pm i). \quad (18)$$

The corresponding trial states

$$|\phi_{\chi}^{(h,\Gamma)}(t)\rangle = \left(\mathcal{O}_{\chi}^{(h,\Gamma)}(t) \right)^{\dagger} |\Omega\rangle \quad (19)$$

enter the correlation matrices

$$C_{(h_2,\Gamma_2),(h_1,\Gamma_1)}(t_2 - t_1) = \langle \phi_{\chi}^{(h_2,\Gamma_2)}(t_2) | \phi_{\chi}^{(h_1,\Gamma_1)}(t_1) \rangle = \langle \Omega | \left(\mathcal{O}_{\chi}^{(h_2,\Gamma_2)}(t_2) \right) \left(\mathcal{O}_{\chi}^{(h_1,\Gamma_1)}(t_1) \right)^{\dagger} | \Omega \rangle, \quad (20)$$

and we introduce the shorthand matrix notation for later use

$$C(t_2 - t_1) = \langle \mathcal{O}(t_2) \otimes (\mathcal{O}(t_1))^{\dagger} \rangle. \quad (21)$$

Notice also that, due to the discrete symmetries of the twisted mass action in eqs. (1) and (2), the correlation $C(t_2 - t_1)$ is a real and symmetric matrix. Eqs. (18) to (21) can also be generalized to the case of more operators, as for example operators with different levels of smearing (see the next section) or Dirac structure. In this case $C(t_2 - t_1)$ will be a $D \times D$ matrix ($D = 4 \times n$) defined by the larger operator set. An application of this kind will be considered in section 3.2. One can easily obtain another set of independent meson creation operators with identical quantum numbers by replacing $\Gamma \rightarrow \gamma_0 \Gamma$. We found, however, that the corresponding trial states have worse overlaps to the low lying states of interest. Therefore, we do not consider these operators in the following. To improve the signal-to-noise ratio, we have computed the correlators in eq. (20) by using the one-end trick [1, 2].

2.2.2 Operator optimization by means of smearing

To optimize the overlap of the trial states in eq. (19) with the physical K and D mesons, we resort to standard smearing techniques. We use Gaussian smeared quark fields, with APE smeared spatial links. Additional details can be found in [11], where the same setup has been used.

We have optimized the smearing by computing effective masses at $t = 1$ and $t_0 = 1$ (cf. (25)), where excited states are suppressed the least, for different values of N_{Gauss} , and $\kappa_{\text{Gauss}} = 0.5$, $N_{\text{APE}} = 10$, $\alpha_{\text{APE}} = 0.5$ kept fixed. This optimization is essentially independent on the lattice volume and on the light quark mass. Results for $\beta = 3.90$, $L^3 \times T = 24^3 \times 48$ and $\mu = 0.0040$ are reported in Figure 1. Although the suppression of excited states only weakly depends on N_{Gauss} and, therefore, on the width of the corresponding trial states, it is obvious that the D meson has a somewhat smaller width than the K meson. Since the D meson is heavier and hence more difficult to compute, we focus on optimizing the overlap with the D meson state and choose $N_{\text{Gauss}} = 30$. An estimate of the corresponding trial state radius R can be obtained via [11]

$$\frac{R}{a} = \left(\frac{N_{\text{Gauss}} \kappa_{\text{Gauss}}}{1 + 6\kappa_{\text{Gauss}}} \right)^{1/2}, \quad (22)$$

yielding $R_K \approx 7a \approx 0.60 \text{ fm}$ and $R_D \approx 5a \approx 0.43 \text{ fm}$ (cf. Figure 1b). A similar optimization for the parameter N_{APE} shows essentially no dependence on the ground state overlap. This is exemplified in Figure 2 corresponding to $\beta = 3.90$, $L^3 \times T = 24^3 \times 48$ and $\mu = 0.0100$.

We end up with the following optimized set of smearing parameters for ensemble A40.32:

$$N_{\text{Gauss}} = 30, \quad \kappa_{\text{Gauss}} = 0.5, \quad N_{\text{APE}} = 10, \quad \alpha_{\text{APE}} = 0.5. \quad (23)$$

Given the rather mild dependence of the ground state overlap on N_{Gauss} and N_{APE} , we use the set of parameters in eq. (23) also for the ensemble B35.32, with only slightly different lattice spacing. Sometimes in the following of this paper, we will also consider correlation matrices made of local operators, or mixed local and smeared operators. However, the final determination of all masses will exclusively be obtained with the correlation matrix made of the smeared operators, with the optimized smearing parameters of eq. (23).

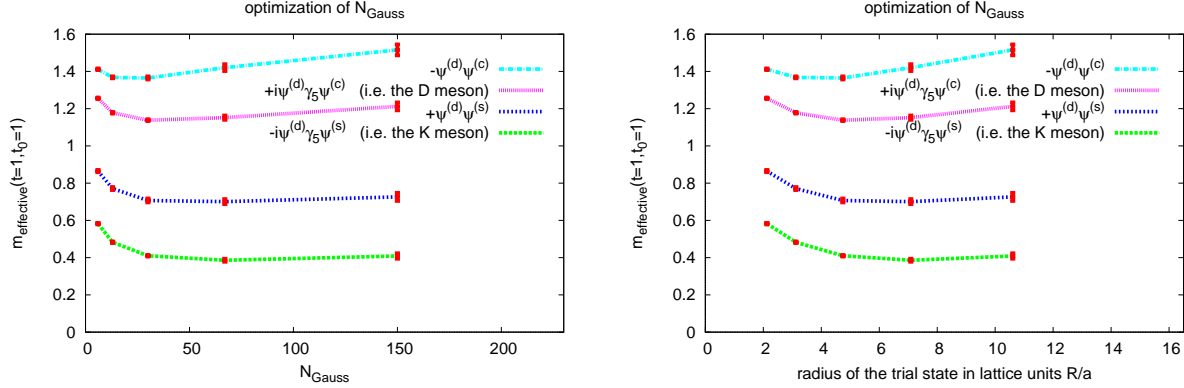


Figure 1: **a)** The effective masses $m_{\text{effective}}^{(n)}(t = 1, t_0 = 1)$ (cf. eq. (25)) for the trial states defined in eq. (19) as functions of N_{Gauss} for $\beta = 3.90$, $L^3 \times T = 24^3 \times 48$ and $\mu = 0.0040$ with $\kappa_{\text{Gauss}} = 0.5$, $N_{\text{APE}} = 10$, $\alpha_{\text{APE}} = 0.5$. **b)** The same effective masses as a function of the radius of the trial states in lattice units R/a with $\kappa_{\text{Gauss}} = 0.5$.

3 Computation of m_K and m_D

In contrast to parity and flavor conserving lattice formulations, as the standard Wilson lattice QCD, it is not possible to compute correlation functions restricted to a single parity and heavy flavor sector in our $N_f = 2 + 1 + 1$ twisted mass framework, as outlined in section 2.2.1. While the determination of m_K is anyway straightforward, since the kaon is the lowest state in the combined heavy flavor and parity sector, the extraction of m_D remains rather problematic, being the D meson a highly excited state. Besides computing m_K with high precision, we attempt in the following to estimate m_D without computing the full low-lying spectrum. We present and compare three different methods, all based on the fact that both heavy flavor symmetry and parity are only weakly broken, by terms of $\mathcal{O}(a)$. The three methods yield a consistent picture.

3.1 Method 1: solving a generalized eigenvalue problem

We consider 4×4 correlation matrices, as defined in eq. (20), computed with the twisted basis operators of eq. (10) and the optimized smearing parameters given in eq. (23). We then solve the generalized eigenvalue problem

$$\sum_k C_{jk}(t) v_k^{(n)}(t, t_0) = \sum_k C_{jk}(t_0) v_k^{(n)}(t, t_0) \lambda^{(n)}(t, t_0) , \quad t \equiv t_2 - t_1 \quad (24)$$

where k runs over the set (h, Γ) , $h = c, s$, $\Gamma = \pm$, and obtain the four effective masses $m_{\text{effective}}^{(n)}$, with $n = 0, \dots, 3$, by solving [49]

$$\frac{\lambda^{(n)}(t, t_0)}{\lambda^{(n)}(t+1, t_0)} = \frac{e^{-m_{\text{effective}}^{(n)}(t, t_0)t} + e^{-m_{\text{effective}}^{(n)}(t, t_0)(T-t)}}{e^{-m_{\text{effective}}^{(n)}(t, t_0)(t+1)} + e^{-m_{\text{effective}}^{(n)}(t, t_0)(T-(t+1))}} , \quad (25)$$

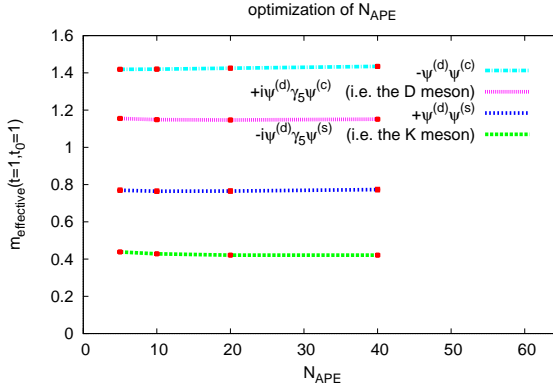


Figure 2: The effective masses $m_{\text{effective}}^{(n)}(t = 1, t_0 = 1)$ as in Figure 1, as a function of N_{APE} for $\beta = 3.90$, $L^3 \times T = 24^3 \times 48$ and $\mu = 0.0100$ with $\alpha_{\text{APE}} = 0.5$, $N_{\text{Gauss}} = 30$, $\kappa_{\text{Gauss}} = 0.5$.

with T the temporal extension of the periodic lattice.

To interpret these effective masses, we assume that heavy flavor and parity breaking effects are small. Indeed they are only $\mathcal{O}(a)$, since they originate from the flavor non-diagonal and parity odd Wilson term, which is proportional to the lattice spacing. Consequently, for vanishing lattice spacing, where heavy flavor and parity are exact symmetries, these correlation matrices would be diagonal in the physical basis, because the operators in eq. (9) would excite orthogonal trial states. Thus, solving the generalized eigenvalue problem as stated in eq. (24) would directly provide the four effective masses with definite heavy flavor and parity. In particular, one of them would have associated quantum numbers $(c, -)$ and would approach a plateau for large temporal separation to be identified with the D meson mass.

At finite lattice spacing in the presence of heavy flavor and parity breaking the four effective masses will approach the masses of the four lowest states in the mixed sector $(s/c, -/+)$ for large temporal separations. The D meson is not among those states: K and K_0^* , the radial excitations and $K/K_0^* + n \times \pi$ states are lighter than the D . At intermediate times, however, one of the four effective masses should still be dominated by the D meson and the corresponding plateau will give a measure of m_D .

To identify the heavy flavor and parity content of the four effective masses, we first note that the trial state corresponding to the n -th effective mass is

$$|\phi_\chi^{(n)}(t)\rangle = \sum_k v_k^{(n)}(t, t_0) \left(\mathcal{O}_\chi^{(k)}(t) \right)^\dagger |\Omega\rangle , \quad (26)$$

When the relations $\omega_l = \omega_h = \pi/2$ and $Z_P/Z_S = 1$ are approximately fulfilled, one can rotate to the pseudo physical basis. By inserting eq. (16) into the trial state in (26) and using the orthogonality of the twist rotation matrix \mathcal{M}_{mt} at maximal twist of eq. (17), yields

$$|\phi_\chi^{(n)}(t)\rangle = \sum_k \left(\mathcal{M}_{\text{mt}} v^{(n)}(t, t_0) \right)_k \left(\mathcal{O}_{\text{ppb}}^{(k)}(t) \right)^\dagger |\Omega\rangle . \quad (27)$$

By sorting the terms in eq. (27) according to the pseudo physical basis states $(\mathcal{O}_{\text{ppb}}^{(k)})^\dagger |\Omega\rangle$, the approximate heavy flavor and parity contents of the trial state corresponding to the n -th effective mass can be read off, and it is given by $c_{(h,\Gamma)}^{(n)} \propto |(\mathcal{M}_{\text{mt}} v^{(n)}(t, t_0))_{(h,\Gamma)}|^2$. Explicitly,

$$c_{(s,\gamma_5)}^{(n)} = \frac{1}{N} \left| +v_{(s,\gamma_5)}^{(n)} - v_{(c,\gamma_5)}^{(n)} - v_{(s,1)}^{(n)} - v_{(c,1)}^{(n)} \right|^2 \quad (28)$$

$$c_{(c,\gamma_5)}^{(n)} = \frac{1}{N} \left| -v_{(s,\gamma_5)}^{(n)} + v_{(c,\gamma_5)}^{(n)} - v_{(s,1)}^{(n)} - v_{(c,1)}^{(n)} \right|^2 \quad (29)$$

$$c_{(s,1)}^{(n)} = \frac{1}{N} \left| +v_{(s,\gamma_5)}^{(n)} + v_{(c,\gamma_5)}^{(n)} + v_{(s,1)}^{(n)} - v_{(c,1)}^{(n)} \right|^2 \quad (30)$$

$$c_{(c,1)}^{(n)} = \frac{1}{N} \left| +v_{(s,\gamma_5)}^{(n)} + v_{(c,\gamma_5)}^{(n)} - v_{(s,1)}^{(n)} + v_{(c,1)}^{(n)} \right|^2, \quad (31)$$

where N is a suitable normalization such that

$$c_{(s,\gamma_5)}^{(n)} + c_{(c,\gamma_5)}^{(n)} + c_{(s,1)}^{(n)} + c_{(c,1)}^{(n)} = 1. \quad (32)$$

To give a specific example, if $c_{(c,\gamma_5)}^{(n)} \simeq 1$, while $c_{(s,\gamma_5)}^{(n)} \simeq c_{(s,1)}^{(n)} \simeq c_{(c,1)}^{(n)} \simeq 0$, the n -th state would be interpreted as the D meson. In the continuum limit, where parity and heavy flavor symmetry are restored, each state will have one associated coefficient $c_{(h,\Gamma)}^{(n)} = 1$, and all others vanishing.

Figure 3 shows the first four effective masses $m_{\text{effective}}^{(n)}$ ($n = 0, \dots, 3$) as functions of t for the ensembles A40.32 (left) and B35.32 (right), while Figure 4 shows the approximate heavy flavor and parity contents of those states for the ensemble A40.32, measured by the coefficients in eqs. (28) to (31). As expected, each one of the effective masses is strongly dominated by and, therefore, should correspond to one of the sectors $(s, -)$, $(s, +)$, $(c, -)$ and $(c, +)$, which are approximately projected by the pseudo physical basis operators associated to the labels (s, γ_5) , $(s, 1)$, (c, γ_5) and $(c, 1)$, respectively.

To extract the numerical values for m_K and m_D , we perform χ^2 minimizing fits to the corresponding effective mass plateaus. The fitting intervals $[t_{\min}, t_{\max}]$ are chosen as follows:

- $t_{\max} = T/2 - 1 = 31$ for the K meson.
- For all the other states t_{\max} is the largest t before which the corresponding effective mass is lost in statistical noise (cf. Table 2).
- t_{\min} is the smallest t fulfilling the following two requirements:
 - $t_0 + 1 \leq t_{\min} \leq t_{\max}$.
 - All fitting intervals $[t_{\min}, t'_{\max}]$, with $t_{\min} + 1 \leq t'_{\max} \leq t_{\max}$, yield a $\chi^2/\text{dof} \leq (\chi^2/\text{dof})_{\max}$, and we require $(\chi^2/\text{dof})_{\max} = 2.0$.

By choosing t_{\min} in this way we prevent that effective masses at large t with large statistical errors effectively increase the number of degrees of freedom, while not contributing to the χ^2 ; in practice, the inclusion of these points would allow to fit ranges with too small values of t_{\min} , outside the plateau region.

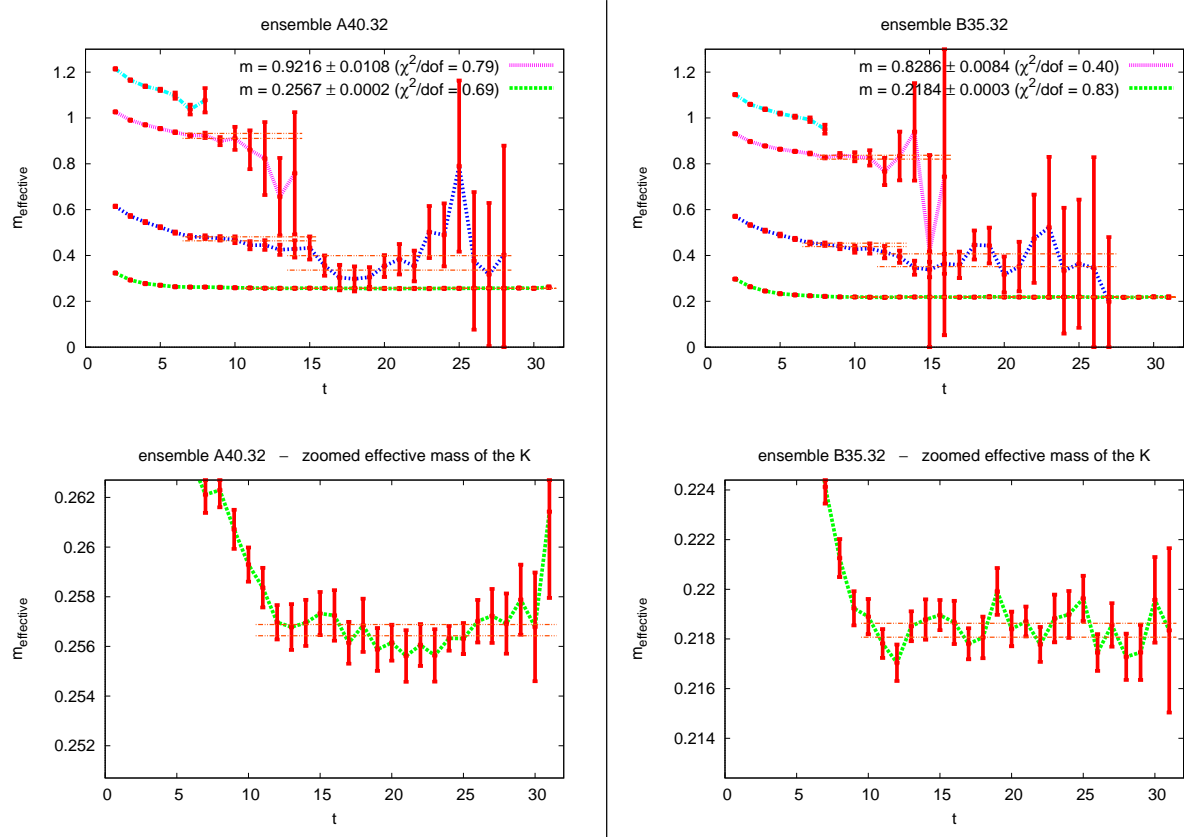


Figure 3: The four effective masses $m_{\text{effective}}^{(n)}$ as functions of t ($t_0 = 1$) for the ensemble A40.32 (left) and B35.32 (right). The zoomed in effective masses for the K meson are also shown in the bottom graphs.

Within this method, a systematic error is associated to the determination of the D meson mass, due to the fact that the effective mass plateau of the $(c, -)$ dominated state will finally decay to lighter strange states at large times, as a consequence of the heavy flavor and parity breaking.

We account for this error by taking the difference with a fit in the range $[t_{\min} - 1, t_{\max}]$, and we combine statistical and systematic uncertainties in quadrature, where the statistical error is obtained by a standard Jackknife analysis.

The results for m_K , m_D and the $(s, +)$ state, which for brevity we denote from now on as K_0^* , are collected in Table 2.

As can also be inferred from Figure 3, we obtain excellent results for m_K . For both ensembles the effective mass plateaus extend over more than twenty points, their statistical errors are essentially independent of t and the relative errors on m_K are $\approx 10^{-3}$. For m_D the situation is more problematic. As shown in Figure 3, the corresponding effective masses are soon lost in statistical noise, before they reach unambiguously identifiable plateaus. As mentioned above, we add for this a systematic uncertainty. The dominantly $(s, +)$ state does not exhibit a true plateau either. One rather observes two different plateaus, and we thus list two results for $m_{K_0^*}$ in Table 2, corresponding to two different fitting ranges. A possible explanation might be that

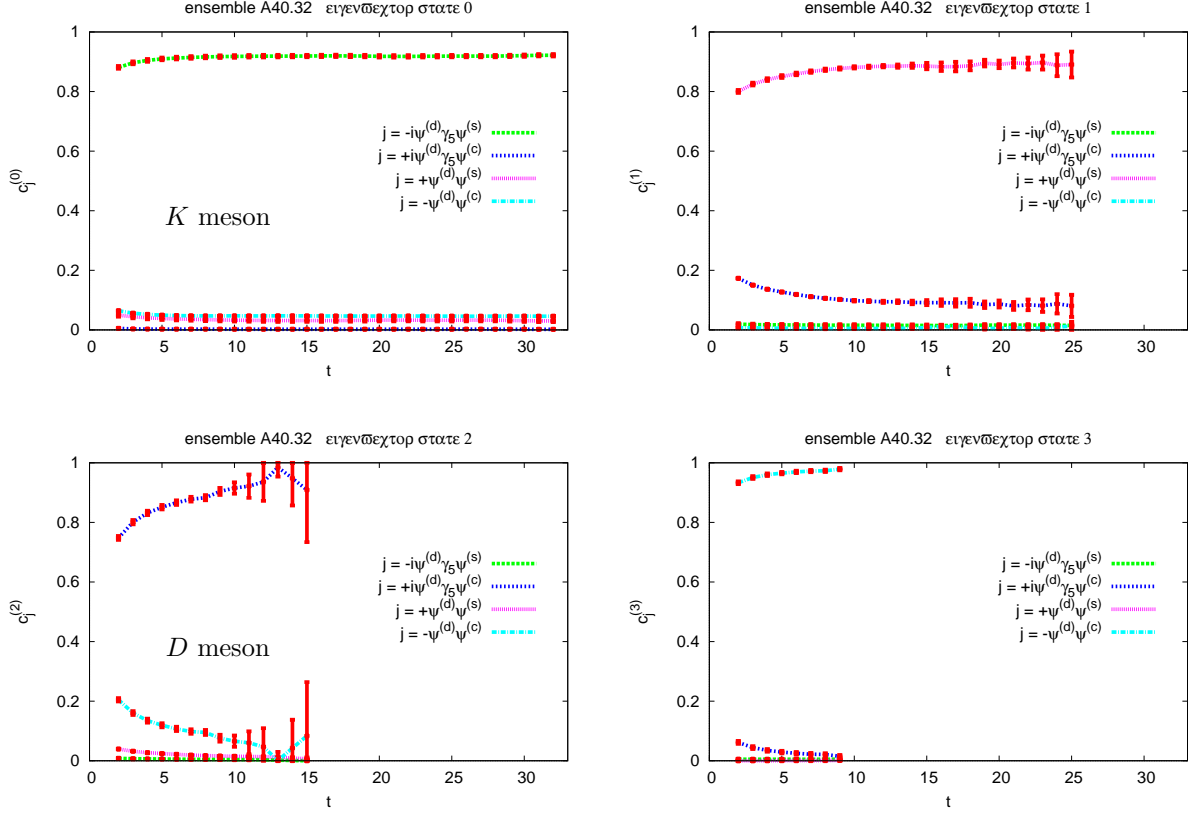


Figure 4: Approximate flavor and parity content of the four extracted states as a function of t ($t_0 = 1$) for the ensemble A40.32. Top left: $n = 0$, mainly $(s, -)$, i.e. the K meson. Top right: $n = 1$, mainly $(s, +)$. Bottom left: $n = 2$, mainly $(c, -)$, i.e. the D meson. Bottom right: $n = 3$, mainly $(c, +)$. The time ranges are the same as for the corresponding effective masses shown in Figure 3.

at small temporal separations $t \lesssim 10$ a positive parity strange meson is seen, while at larger t the lighter $K + \pi$ state, with the same strong quantum numbers, dominates. This is also supported by the fact that at larger values of the light quark mass a single plateau of rather good quality is recovered, see also the results in section 3.3.

3.2 Method 2: fitting the correlation matrix by exponentials

A complementary approach to determine the heavy-light meson masses is to fit the elements of the correlation matrix of eq. (20) by decomposing them in terms of the eigenstates of the Hamiltonian (i.e. the transfer matrix). We consider here the general case with different smearing levels, where $C(t_2 - t_1)$, defined in eq. (20), is a $D \times D$ matrix. When denoting the energy

am_K	t range	χ^2/dof	$am_{K_0^*}$	t range	χ^2/dof	am_D	t range	χ^2/dof
Ensemble A40.32								
0.2567(2)	11 – 31	0.69	0.368(32) 0.473(15)	14 – 28 7 – 15	0.92 1.65	0.922(11)	7 – 14	0.79
Ensemble B35.32								
0.2184(3)	10 – 31	0.83	0.379(28) 0.446(7)	12 – 27 7 – 13	0.54 1.55	0.829(8)	8 – 16	0.40

Table 2: The masses of the K , K_0^* and D mesons in lattice units obtained by solving a generalized eigenvalue problem (errors comprise statistical and systematic errors, which are added in quadrature). The range and the quality of the fit is also shown.

eigenstates by $|n\rangle$, $n = 1, 2, \dots, M$, the matrix elements of $C(t_2 - t_1)$ can be written as

$$C_{ij}(t_2 - t_1) = \sum_{n=1}^M (i|n)_{t_2} (j|n)_{t_1} \quad (33)$$

with

$$(i|n)_t \equiv \langle \Omega | \mathcal{O}_\chi^{(i)}(t) | n \rangle = \langle n | (\mathcal{O}_\chi^{(i)}(t))^\dagger | \Omega \rangle, \quad (34)$$

where $i = 1, \dots, D$ labels the operators inserted in the correlation matrix and $n = 1, \dots, M$ counts the eigenstates. Since we consider bosonic operators, we have a periodic time dependence on the time extension of the lattice T that can be written as follows

$$(i|n)_{t_2} (j|n)_{t_1} = (i|n)(j|n) \left(\exp(-(t_2 - t_1)E_n) + \exp(-(T - t_2 + t_1)E_n) \right). \quad (35)$$

Here, E_n is the energy of the eigenstate $|n\rangle$ and $(i|n) \equiv (i|n)_0$. In general, the number of energy eigenstates is as large as the dimension of the Hilbert space of states. However, for large temporal separations $t_2 - t_1, (T - t_2 + t_1) \gg 1$ a few lowest energy states will dominate to a good approximation. In this limit, and in analogy with the case of fitting a single correlation function with the contributions from a few states, one can fit the matrix of correlation functions with the contributions from the set of dominant lowest energy states. In fact, the relevant number of energy eigenstates M is small. The number N_P of parameters in the fit and the number N_C of independent entries of $C(t_2 - t_1)$ to be fitted are given by

$$N_P = M(D+1), \quad N_C = (t_{\max} - t_{\min} + 1) \frac{D(D+1)}{2}, \quad (36)$$

where also here t_{\min} and t_{\max} define the fitting time interval, with $(t_2 - t_1) \in [t_{\min}, t_{\max}]$. The minimal set of operators for determining the heavy-light meson masses is given in this case by the 4×4 correlation matrix in terms of the operators in eq. (10). The minimal set of states we are interested in consists of the K and D mesons. At finite lattice spacing, due to the heavy flavor

and parity breaking, the D meson is not stable and does not correspond to an energy eigenstate of the lattice theory. However, using the same arguments of section 3.1, the D should dominate the spectral decomposition of eq. (33) at intermediate temporal separations. In case of fitting the correlation matrix by several exponentials, essential contributions of the lower sectors in the D meson channel can be monitored by considering the scalar products of the linear combination of the operators obtained from the fit with the rows of the maximal twist matrix.

Using the pseudo physical basis operators of eq. (15), one obtains for the coefficients $(i|n)$:

$$(i|n) \equiv \langle \Omega | \mathcal{O}_\chi^{(i)}(0) | n \rangle = \sum_j \left(\mathcal{M}_{\text{mt}} \right)_{ji} \langle \Omega | \mathcal{O}_{\text{ppb}}^{(j)}(0) | n \rangle . \quad (37)$$

Again, assuming that $\omega_l = \omega_h \approx \pi/2$ and $Z_P/Z_S = 1$ are approximately verified, the operators \mathcal{O}_{ppb} should reproduce the physical operators associated to the four channels $(s, -)$, $(s, +)$, $(c, -)$, $(c, +)$ to a good approximation. In particular, the operator with the same quantum numbers of the state $|n\rangle$ should dominate the sum in (37). We therefore conclude

$$(i|n) \simeq G_n \left(\mathcal{M}_{\text{mt}} \right)_{ni} \quad (38)$$

to a good approximation, where the proportionality constant G_n is the matrix element of the physical operator:

$$G_n \equiv \langle \Omega | \mathcal{O}_{\text{ph}}^{(n)}(0) | n \rangle . \quad (39)$$

It turns out that it is enough to require that the relative signs of the vector components $(i|n)$ agree with the signs in the rows of maximal twist rotation matrix \mathcal{M}_{mt} . (A more stringent condition on the alignment with the rows of the maximal twist matrix could be imposed by requiring the scalar products of the linear combinations of the operators obtained from the fit with the rows of the maximal twist matrix to be close to 1, but such a requirement does not essentially change the results for the D meson mass.)

Based on the experience with varying the number of states, we determine the K meson mass with a single intermediate state, while good fits for the D meson mass can be obtained for time separations around $t_2 - t_1 \simeq 10 - 12$, by using three intermediate states. Taking four states gives compatible results, but the signal is lost at smaller distances with consequently larger errors. Larger correlation matrices have also been investigated, for instance, 8×8 matrices spanned by four Gaussian smeared operators of type (10) and the corresponding four local operators. In this case stable fits with one, three or four states can also be obtained.

We minimize the uncorrelated χ^2

$$\chi^2 = \sum_{i=1}^{N_C} \left(\frac{f_i(p_1, p_2, \dots, p_{N_P}) - \bar{X}_i}{\delta X_i} \right)^2 , \quad (40)$$

where the index i runs over the independent matrix elements to be fitted, \bar{X}_i and δX_i are the mean value and the error of the matrix element i respectively, and $f_i(p_1, p_2, \dots, p_{N_P})$ is the fitting function depending on N_P parameters defined by eqs. (33) to (35). We determined the

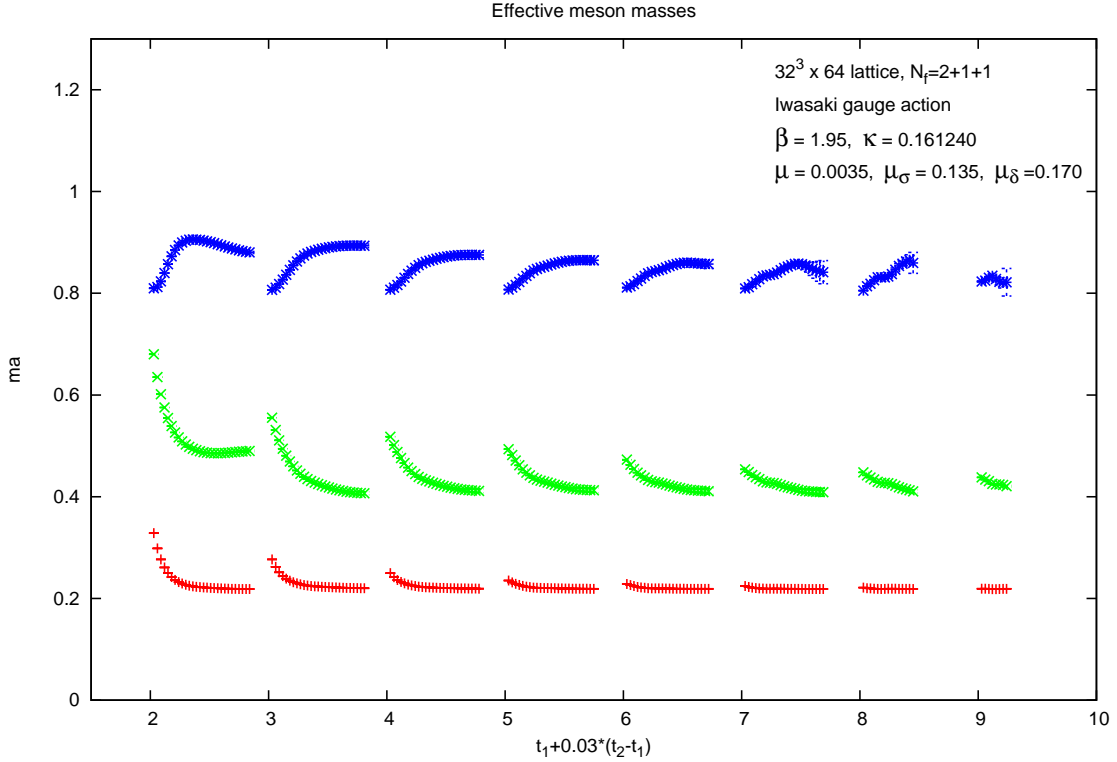


Figure 5: Masses for the K , (bottom), K_0^* (middle) and D (top) channels obtained from a 3×4 fit, i.e. a 4×4 matrix with 3 states, for the ensemble $B35.32$. The fit interval is $[t_1, t_2]$, with values shown by the abscissa. Errors on the masses are also plotted but in most cases are within the symbol size – as shown by the figure.

errors of the matrix elements δX_i and of the fit parameters δp_i by the method in ref. [50]. Figure 5 illustrates how the extracted masses depend on the fit intervals. We also studied the correlated χ^2 following refs. [51, 52]

$$\chi_c^2 = \sum_{i,j=1}^{N_C} \left(f_i(p) - \bar{X}_i \right) M_{ij} \left(f_j(p) - \bar{X}_j \right), \quad (41)$$

where $M_{ij} = N \mathcal{C}_{ij}^{-1}$, with N input data and the estimated covariance matrix

$$\mathcal{C}_{ij} = \frac{1}{N-1} \sum_{n=1}^N \left(X_{i,n} - \bar{X}_i \right) \left(X_{j,n} - \bar{X}_j \right). \quad (42)$$

It turned out, however, that on our data samples the covariance matrix has a large number of almost degenerate tiny eigenvalues of the order of magnitude 10^{-16} , which cannot be properly determined within the present statistical accuracy. The small eigenvalues can be smoothed [51, 52], at the price of introducing an uncertainty in the value of χ_c^2 . For this reason, we decided

to minimize the uncorrelated χ^2 , and to use the correlated one χ_c^2 to estimate systematic errors, see below.

Relative errors of the elements of our correlation matrices are typically of $\mathcal{O}(10^{-2})$. This results in rather small errors for the fit parameters on a given time interval: masses have relative errors of $\mathcal{O}(10^{-2})$ to $\mathcal{O}(10^{-3})$, while the components of the energy eigenvectors have errors $\mathcal{O}(10^{-2})$. A good fit has to satisfy for our case the following requirements:

1. The quantum number pattern of the fitting operators has to be as expected, i.e. the relative signs of the components of the fitted vectors are the same as those of the rows of the maximal twist matrix.
2. We exclude the results from fit intervals, where the relative errors of the masses are substantially higher than the typical errors. With our statistics, this means 1% for the K meson mass and 5% for the other masses. Only a few fit intervals turn out to be affected by this choice.
3. The fit ranges $[t_{min}, t_{max}]$ are restricted by applying cuts in t_{min} and $(t_{max} - t_{min})$ such that a reasonable ‘‘plateau’’ of the fit values emerges, always keeping a sufficiently large number of fit ranges in the sample, typically about 30 to 80.

After selecting a set of good fits by these criteria a histogram distribution of the fit values has been defined by attributing a weight $\exp(-\chi_c^2/\text{dof})$ to the entries in case of the kaon, and a weight $1/(\chi_c^2/\text{dof})$ in the other channels. The exponential suppression is in general preferable, since it gives robust results but can only be applied for very good fits and plateaus, which is the case for the kaon. In order to combine statistical and systematic errors, the entries in the distribution were not attributed to a single point but uniformly to the points on the interval $[p_i - \delta p_i, p_i + \delta p_i]$. For each final quantity, the quoted value is then the position of the median of the resulting distribution. The error is given by a symmetric interval around the median such that 68% of the distribution is contained in it.

We report on single-state, three-state, and four-state fits with a 4×4 correlation matrix of Gaussian smeared operators. For completeness, we also show the results of three-state fits with an 8×8 matrix of Gaussian smeared and local operators. All results are summarized in Table 3.

As shown in table 3 the four-state fit to a 4×4 matrix gives one state in each of the channels $J^P = 0^-$ and $J^P = 0^+$, with both strange and charmed quarks. On the other hand, errors are typically larger and/or the light states have higher masses than in the 1×4 and 3×4 fits. Therefore, as final results we quote the K meson mass from the 1×4 fit and the D meson mass from the 3×4 fit.

One can verify a posteriori how well the quantum number content of each fitted vector corresponds to the expected one. This is simply given by the scalar product of the unit vector in the direction of the fitted vector with the row of the matrix in eq. (15) that gives the expected vector in the continuum limit at maximal twist. For this, we remind that the K meson, strange 0^+ state, D meson and charmed 0^+ state correspond to the rows 1, 3, 2 and 4, respectively. Table 4 shows that the fitted vectors are actually well saturated by the expected quantum numbers, with scalar products close to 1 in all cases.

Ensemble	$M \times D$	am_K	$am_{K_0^*}$	am_D	$am_{D_0^*}$
A40.32	1x4	0.25542(67)			
	3x4	0.25853(88)	0.448(13)	0.903(20)	
	4x4	0.26272(62)	0.4905(60)	0.939(46)	1.09(15)
	3x8	0.2627(23)	0.478(18)	0.885(22)	
B35.32	1x4	0.21766(64)			
	3x4	0.21864(51)	0.422(11)	0.835(20)	
	4x4	0.2226(69)	0.449(24)	0.896(70)	1.19(10)
	3x8	0.2203(13)	0.4369(94)	0.814(18)	

Table 3: Masses of the K , K_0^* , D and D_0^* in lattice units, resulting from the fits to the correlation matrices with several eigenstates for the ensembles A40.32 and B35.32. The label $M \times D$ means a fit with M eigenstates to a $D \times D$ matrix.

Ensemble	$M \times D$	z_K	$z_{K_0^*}$	z_D	$z_{D_0^*}$
A40.32	1x4	0.98659(6)			
	3x4	0.9871(2)	0.9896(17)	0.9392(78)	
	4x4	0.9870(2)	0.9845(23)	0.9929(1)	0.9830(133)
B35.32	1x4	0.98518(8)			
	3x4	0.9847(1)	0.9772(33)	0.9518(94)	
	4x4	0.9848(1)	0.9770(21)	0.9777(86)	0.9732(110)

Table 4: Saturation of the fitted states with the expected quantum numbers, for the four-states fits of table 3, measured by the scalar product z (see text). A value $z = 1$ indicates complete saturation. Mean values and errors for z are determined analogously to masses.

3.3 Method 3: parity and flavor symmetry restoration

This third method is a generalization of the “parity restoration method” originally introduced for the twisted mass formulation with two degenerate quarks [53, 54, 55]. In the $N_f = 2$ setup the twist angle can be determined by requiring that the operators reproducing the correct definition of the chiral currents in the continuum limit (physical chiral currents) possess the appropriate transformation properties under parity. This condition allows to fix the twist angle for the degenerate light quark doublet and the correctly normalized physical currents. We generalize the method to the case of bilinear densities with mixed heavy-light flavor composition, used here for the determination of the K and D meson masses. A first account of this method can be found in [35]. As an outcome, approximations of the physical operators in eq. (9) can be constructed, from which the masses in the four heavy-flavor and parity channels can be extracted by conventional techniques.

Consider the four-by-four correlation matrix of the renormalized lattice operators in eq. (14):

$$C^R(t_2 - t_1) = \langle \mathcal{O}^R(t_2) \otimes (\mathcal{O}^R(t_1))^\dagger \rangle. \quad (43)$$

After rewriting the renormalized lattice operators in terms of the bare ones one obtains

$$C^R(t_2 - t_1) = \text{diag}\left(Z_P, Z_P, Z_S, Z_S\right) C(t_2 - t_1) \text{diag}\left(Z_P, Z_P, Z_S, Z_S\right), \quad (44)$$

where $C(t_2 - t_1)$ is the correlation matrix defined in eq. (20), the starting point of the previous two methods. The transformation properties of the correlation matrix (43) can be read from eq. (13), implying that the correlation matrix of the physical operators (9) is given by

$$\begin{aligned} C_{\text{ph}}^R &= \mathcal{M}(\omega_l, \omega_h) C^R \mathcal{M}^T(\omega_l, \omega_h) = \\ &\quad \mathcal{M}(\omega_l, \omega_h) \text{diag}\left(Z_P, Z_P, Z_S, Z_S\right) C \text{diag}\left(Z_P, Z_P, Z_S, Z_S\right) \mathcal{M}^T(\omega_l, \omega_h), \end{aligned} \quad (45)$$

where, we recall, the general orthogonal twist rotation matrix $\mathcal{M}(\omega_l, \omega_h)$ is given by (12). Since we are working at maximal twist, we are supposed to insert $\omega_l = \omega_h = \pi/2$ in the rotation matrix of eq. (45). However, differently from the previous two methods and accounting for the presence of $\mathcal{O}(a)$ effects, we treat the two twist angles, along with the renormalization factors Z_P and Z_S , as free parameters. We will return to this point in the following. These free parameters can be determined by imposing that the physical operators indeed possess the appropriate parity and flavor quantum numbers of their associated channel. This in particular implies that the physical correlation matrix of eq. (45) should be diagonal

$$\left(C_{\text{ph}}^R\right)_{jk} = 0, \quad j \neq k. \quad (46)$$

Since $C(t_2 - t_1)$ is a symmetric matrix (see section 2.2.1), the matrix in eq. (45) is by construction symmetric and eq. (46) actually amounts to only six independent conditions. The latter can be rearranged as follows

$$\frac{Z_P^2}{Z_S^2} = -\frac{C_{34}}{C_{12}} \quad (47)$$

$$\text{ctg}(\omega_l) = +\frac{(+C_{11} - C_{22})(Z_P/Z_S) + (-C_{33} + C_{44})(Z_S/Z_P)}{2(C_{13} - C_{24})} \quad (48)$$

$$\text{ctg}(\omega_h) = +\frac{(+C_{11} - C_{22})(Z_P/Z_S) + (+C_{33} - C_{44})(Z_S/Z_P)}{2(C_{14} - C_{23})} \quad (49)$$

$$\begin{aligned} \tan(\omega_l + \omega_h) &= \\ &= -\frac{C_{14} + C_{23} + C_{13} + C_{24}}{(+C_{11} + C_{22})(Z_P/Z_S) + (-C_{33} - C_{44})(Z_S/Z_P)/2 + C_{12}(Z_P/Z_S) - C_{34}(Z_S/Z_P)} \end{aligned} \quad (50)$$

$$\begin{aligned} \tan(\omega_l - \omega_h) &= \\ &= +\frac{C_{14} + C_{23} - C_{13} - C_{24}}{(+C_{11} + C_{22})(Z_P/Z_S) + (-C_{33} - C_{44})(Z_S/Z_P)/2 - C_{12}(Z_P/Z_S) + C_{34}(Z_S/Z_P)} \end{aligned} \quad (51)$$

$$\frac{\tan(\omega_l)}{\tan(\omega_h)} = -\frac{C_{13} + C_{24}}{C_{14} + C_{23}}. \quad (52)$$

Observe that the right hand sides of (48) to (52) are fully determined by the ratio Z_P/Z_S , i.e. they do not depend individually on either Z_P or Z_S .

In Figure 6 we report on the ratios of correlators on the right hand sides of the conditions (47) to (52) as functions of the time separation $t \equiv t_2 - t_1$, for the ensemble A40.32 and the original operators without Gaussian smearing. The ratios appear to approach a plateau after a transient: from these plateaus we determine the unknown parameters Z_P/Z_S , ω_l and ω_h .

Notice that the time dependence of the ratios is an $\mathcal{O}(a)$ discretization effect, and therefore not predicted by eqs. (47)-(52), which were derived in the continuum limit. For large times the lightest eigenstate of the lattice transfer matrix, corresponding to the kaon in the continuum, is supposed to saturate the spectral decomposition of the correlation matrix $C(t_2 - t_1)$ (see eqs. (33) and (34)). Assuming a single intermediate state, the six conditions (47)-(52) are not independent any more and in particular the first three of relations (47)-(49) are equivalent to (50)-(52). Parity and flavor restoration amounts in this case to requiring that the three physical operators associated to the heavier channels have no projection on the lightest state, namely

$$\sum_{\mathbf{x}} \langle \Omega | \mathcal{O}_{\text{ph}}^{(s,1)}(\mathbf{x}, t) | K \rangle = \sum_{\mathbf{x}} \langle \Omega | \mathcal{O}_{\text{ph}}^{(c,\gamma_5)}(\mathbf{x}, t) | K \rangle = \sum_{\mathbf{x}} \langle \Omega | \mathcal{O}_{\text{ph}}^{(c,1)}(\mathbf{x}, t) | K \rangle = 0. \quad (53)$$

We also observe that this procedure, which relies on asymptotic times, is supposed to be optimal from the point of view of the cutoff effects: at large times, contribution from high-mass intermediate states, which are expected to introduce large discretization effects in the correlator, is suppressed. A similar argument was used when tuning the theory to maximal twist in the light sector, see [2].

We determine Z_P/Z_S , ω_l and ω_h by using the relations (47-49), while the remaining relations serve for cross checking of the results. The latter are reported in Table 5. We observe an excellent agreement between the different determinations of the twist angles from (48-49) and (50-51), respectively, confirming that a single intermediate state contributes. The quality of the agreement deteriorates, of course, when the parameters are estimated at smaller temporal separations outside the asymptotic region. Notice that the ratio $\tan(\omega_l)/\tan(\omega_h)$ is in all cases compatible with zero, since $\omega_h \approx \pi/2$. Note instead that the value of the light twist angle

eqs.	Z_P/Z_S	eqs.	ω_l/π	ω_h/π	$\tan(\omega_l)/\tan(\omega_h)$
ensemble A40.32					
(47)	0.6575(14)	(48-49)	0.6504(21)	0.4980(8)	-0.012(5)
(47)	same value	(50-51)	0.6498(22)	0.4990(10)	-0.006(5)
(47)	same value	(52)	—	—	-0.009(5)
ensemble B35.32					
(47)	0.6793(22)	(48-49)	0.6453(34)	0.5005(8)	0.003(5)
(47)	same value	(50-51)	0.6467(29)	0.5007(9)	0.005(6)
(47)	same value	(52)	—	—	0.005(5)

Table 5: summary of different determinations of the ratio of renormalization factors and of the twist angles with point-like operators (no Gaussian smearing); the first and third column indicate the equations used for the determination of the quantities in the corresponding line.

in Table 5 significantly deviates from the expected value $\pi/2$. In order to understand this discrepancy it is useful to recall that the theory is tuned to maximal twist by requiring the vanishing of the untwisted PCAC quark mass $m_{\chi^{(l)}}^{\text{PCAC}}$ in the light quark sector, see eq. (4)).

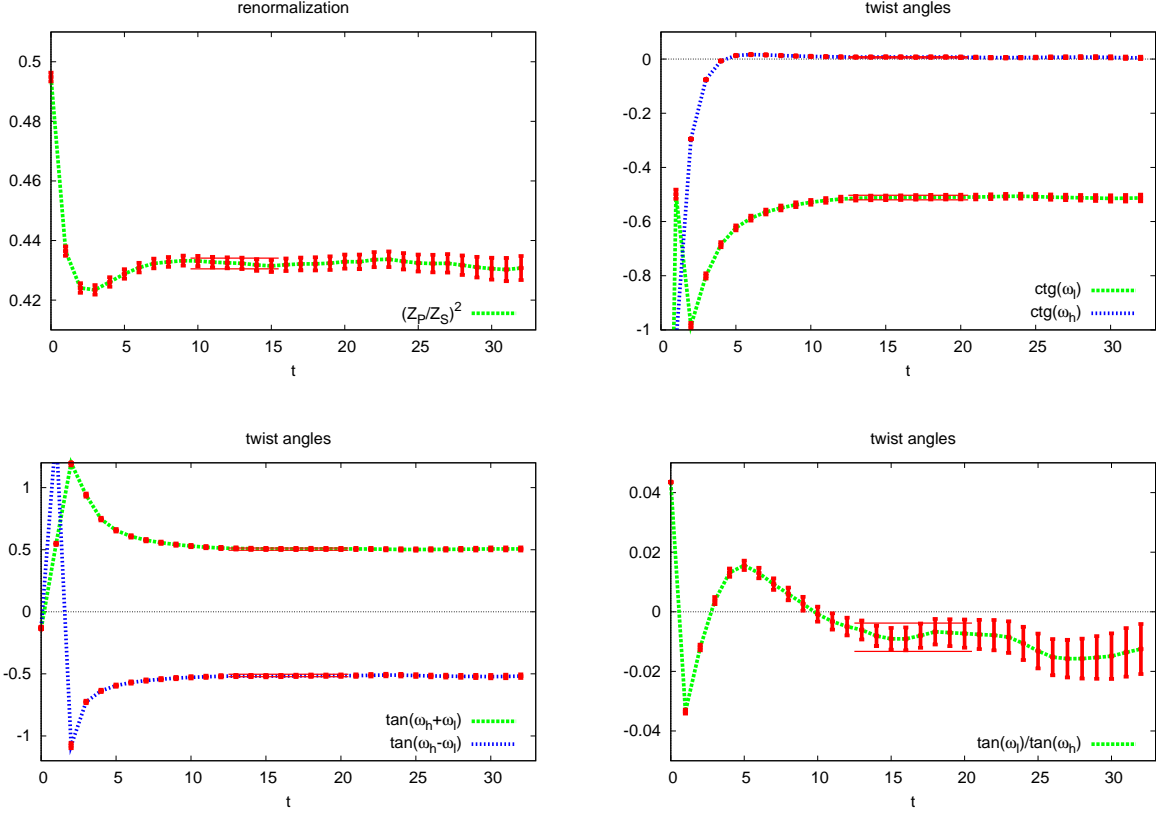


Figure 6: ratios of correlators corresponding to the right hand sides of the conditions (47) to (52) as functions of the temporal separation t for ensemble A40.32 with point-like operators (i.e. no Gaussian smearing); the lines indicate the fits in the asymptotic regime.

This can be shown to be equivalent [55] to requiring parity restoration in the light quark sector. One constructs in this case the physical vector current as follows [55]

$$V_{ph}^{(l)+}(x) \propto \cos(\omega_l) Z_V V^{(l)+}(x) - i \sin(\omega_l) Z_A A^{(l)+}(x), \quad (54)$$

where the bilinear of the lattice fields $A^{(l)+}(x)$ is defined in eq. (5) and, analogously,

$$V_\mu^{(l)+} = \bar{\chi}^{(u)} \gamma_\mu \chi^{(d)}, \quad (55)$$

and Z_A , Z_V are the respective renormalization constants in the massless scheme. The twist angle ω_l is fixed in this case by the condition

$$\sum_{\mathbf{x}} \langle \Omega | V_0^{(l)+}(\mathbf{x}, t) | \pi \rangle = 0, \quad (56)$$

from which one obtains

$$\text{ctg}(\omega_l) = \frac{Z_A m_{\chi^{(l)}}^{\text{PCAC}}}{\mu}. \quad (57)$$

From this we can conclude that our maximal twist condition $m_{\chi^{(l)}}^{\text{PCAC}} = 0$ amounts to $\omega_l = \pi/2$, if the condition (56) is assumed. This must be confronted with the conditions (53) presently used to fix the twist angles ω_l ². We conclude that the deviation of ω_l from $\pi/2$ should be attributed to different $\mathcal{O}(a)$ effects in the pion and kaon sectors.

We stress that the prescription of eq. (4), which is based on the charged pion state, is to be preferred for tuning the theory to maximal twist, since it ensures the smallest $\mathcal{O}(a^2)$ discretization errors in physical quantities [32]. Nevertheless, for the determination of the masses in the heavy-light meson sector, we use the values of the twist angles obtained from (47) to (52), since they deliver optimal projecting operators as defined in eq. (13), with the smallest heavy flavor and parity violations. The relation in (57) can also be enforced for the present determination of the light twist angle with heavy-light quark bilinears, and the cutoff effects can be absorbed in a lattice redefinition of the PCAC quark mass, $\tilde{m}_{\chi^{(l)}}^{\text{PCAC}} = m_{\chi^{(l)}}^{\text{PCAC}} + \mathcal{O}(a)$. For the ensemble A40.32, we get for instance $Z_A \tilde{m}_{\chi^{(l)}}^{\text{PCAC}} / \mu \approx -0.5$, a pretty large value³. The analogous of relation (57) for the heavy twist angle reads

$$\text{ctg}(\omega_h) = \frac{Z_A \tilde{m}_{\chi^{(l)}}^{\text{PCAC}}}{\mu_\sigma}. \quad (58)$$

The heavy twisted mass μ_σ replaces the light twisted mass μ , explaining why ω_h is very close to $\pi/2$: since $\mu_\sigma \gg \mu$, the non-zero value of $\tilde{m}_{\chi^{(l)}}^{\text{PCAC}}$ only results in a small deviation of ω_h from maximal twist. When inserting the above estimate in (58) we indeed obtain $\omega_h = 0.4956$.

The ratio of normalization factors Z_P/Z_S and the twist angles ω_l and ω_h allow to determine the physical operators up to an overall renormalization (bare physical operators). We choose this renormalization to be Z_P , so that (cf. eqs. (13) and (14))

$$\mathcal{O}_{\text{ph}}^{\text{bare}} \equiv Z_P^{-1} \mathcal{O}_{\text{ph}}^R = \mathcal{M}(\omega_l, \omega_h) \text{diag}\left(Z_P/Z_S, Z_P/Z_S, 1, 1\right) \mathcal{O}_\chi. \quad (59)$$

Observe that in the case of the negative parity densities, eq. (59) corresponds to the conventional relation between renormalized and bare operators

$$\mathcal{O}_{\text{ph}}^{(h,\gamma_5)\text{bare}} = Z_P^{-1} \mathcal{O}_{\text{ph}}^{(h,\gamma_5)R}; \quad (60)$$

on the other hand, the conventional definition for the bare scalar densities, for which

$$\mathcal{O}_{\text{ph}}^{(h,1)\text{bare, conv.}} = Z_S^{-1} \mathcal{O}_{\text{ph}}^{(h,1)R} \quad (61)$$

holds, is related to the definition (59) by a finite renormalization

$$\mathcal{O}_{\text{ph}}^{(h,1)\text{bare, conv.}} = Z_P/Z_S \mathcal{O}_{\text{ph}}^{(h,1)\text{bare}}. \quad (62)$$

²In the asymptotic regime, where only the kaon state is considered as intermediate state, the light twist angle ω_l is fixed by the vanishing of the first two matrix elements in (53); this is so because, in this regime, the two conditions can be proven to imply in particular relations (47) and (48) (analogously, ω_h is fixed in particular by the vanishing of the second and third matrix element).

³For comparison, in the tuning procedure we require $Z_A |m_{\chi^{(l)}}^{\text{PCAC}}| / \mu \leq 0.1$.

Of course, with Z_P/Z_S at hand both definitions can be computed.

Figure 7 shows the diagonal and off-diagonal correlators of the bare physical operators for the ensemble B35.32 with Gaussian smearing, which are the ones used for the final computation of all masses. A general feature is that starting from time separation $t \gtrsim 5$ most of the off-diagonal elements become small and compatible with zero within statistical errors. An exception is the matrix element $\langle \mathcal{O}_{\text{ph}}^{(c,\gamma_5)} (\mathcal{O}_{\text{ph}}^{(s,1)})^\dagger \rangle$, which remains large and comparable in size with the two smallest diagonal elements in the $(c, -/+)$ sectors. At the moment we have no explanation for this observation.

It should also be noted that, following the arguments of [47, 46], $\mathcal{O}(a)$ improvement can only be expected for the diagonal elements of the physical correlation matrix. Since the twist angles and the ratio Z_P/Z_S are obtained from conditions on the off-diagonal elements, one should a priori expect $\mathcal{O}(a)$ discretization errors for these quantities. However, it should be stressed that for physical quantities such as meson masses and decay constants, which are extracted from the diagonal matrix elements, $\mathcal{O}(a)$ improvement is at work. The mass of the low-lying state in each

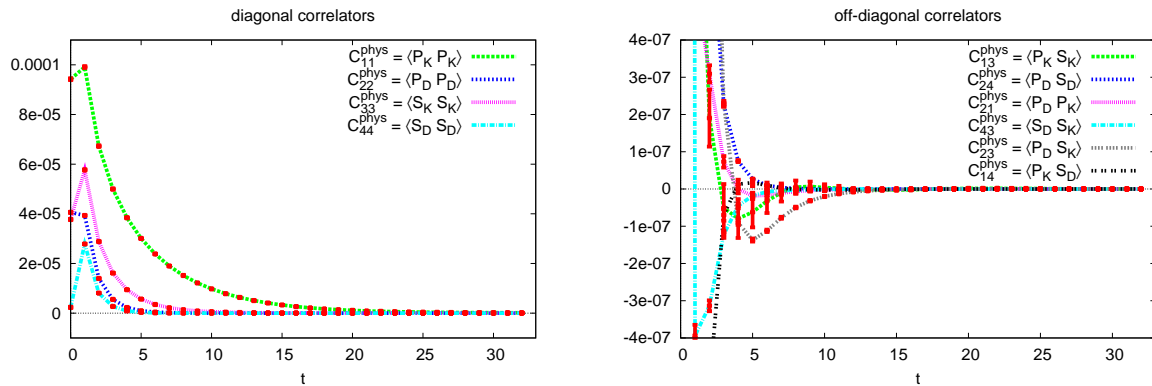


Figure 7: Bare physical correlators for the ensemble B35.32 with Gaussian smeared operators.

of the four different channels can now be extracted by standard techniques from the diagonal correlator of the appropriate operator in (59). The effective masses for the four channels and the two ensembles are reported in Figure 8, for negative parity, and Figure 9, for positive parity. The final values for all masses are obtained by applying single-mass fits with a cosh function in the asymptotic regime. Also in this case the statistical error of the fitting parameters is determined by the linearization method of [50]. The starting time t_{\min} for the fits was chosen by requiring $\chi^2/\text{dof} \lesssim 1$.

The plateaus for the charmed meson states are generally quite short, since the noise sets in early, typically around $t \gtrsim 11$. This is, however, expected. For those temporal separations the D correlator is only a small fraction of the kaon correlator, as shown in the left panel of Figure 7. On the other hand, the D correlator results from a linear combination of the correlators of the twisted basis χ -field bilinears in eq. (10), all dominated by the kaon. This means that the condition (53) can only be fulfilled through a cancellation of large terms, one of the results being the comparably small D correlator. The latter inherits the statistical fluctuations of the original bilinears and a large relative error is the consequence. As already stated many times in this

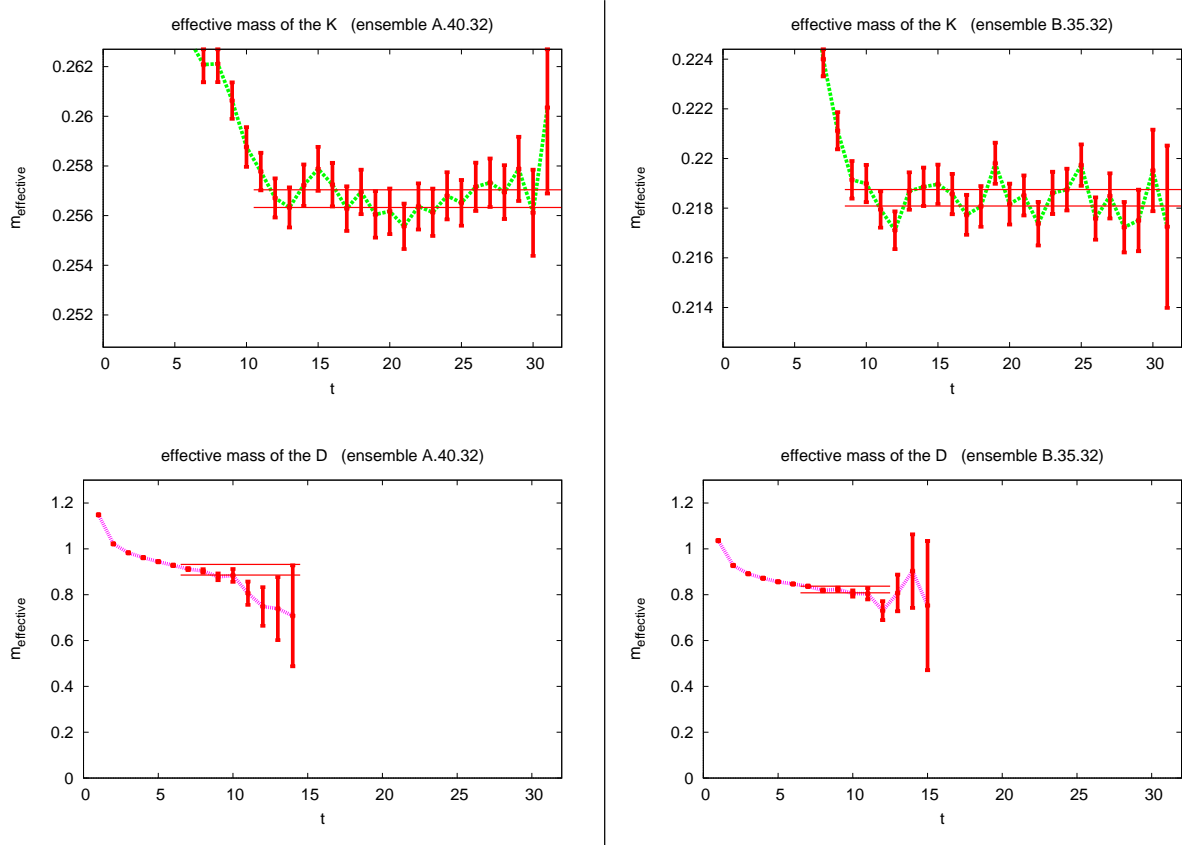


Figure 8: The effective masses in the pseudoscalar channel, with Gaussian smeared operators, for the ensembles A40.32 (left) and B35.32 (right). The error bands indicate the total error, statistical plus systematic.

paper, this is an inherent problem in our twisted mass setup, where the D is actually a highly excited state in the mixed ($s/c, -/+$) heavy-light meson sector.

In the case of the D meson we attempt to estimate the systematic error produced by possible residual contributions of excited states and the influence of an unphysical mixing with the rather light K_0^* state⁴. We apply a procedure analogous to the one of section 3.2, and consider the spread of results by including all good fits (those with high significance) obtained by varying the fit interval $[t_{\min}, t_{\max}]$. The resulting systematic error is much larger than the statistical one, and decreases on the finer lattice. This is reflected by the better quality of plateaus for the ensemble B35.32, as compared to A40.32, see Figure 8.

The numerical results for all masses are listed in Table 6. For K_0^* different plateaus could be identified for the effective mass. In this case the value for each plateau is reported. It is unclear at this stage, whether this multi plateau behavior reflects the physical structure of QCD states in this sector, or is just a statistical effect, as also discussed at the end of section 3.1.

We conclude the illustration of this method by briefly discussing its generalization to the case of

⁴The mixing with the kaon has been eliminated by construction.

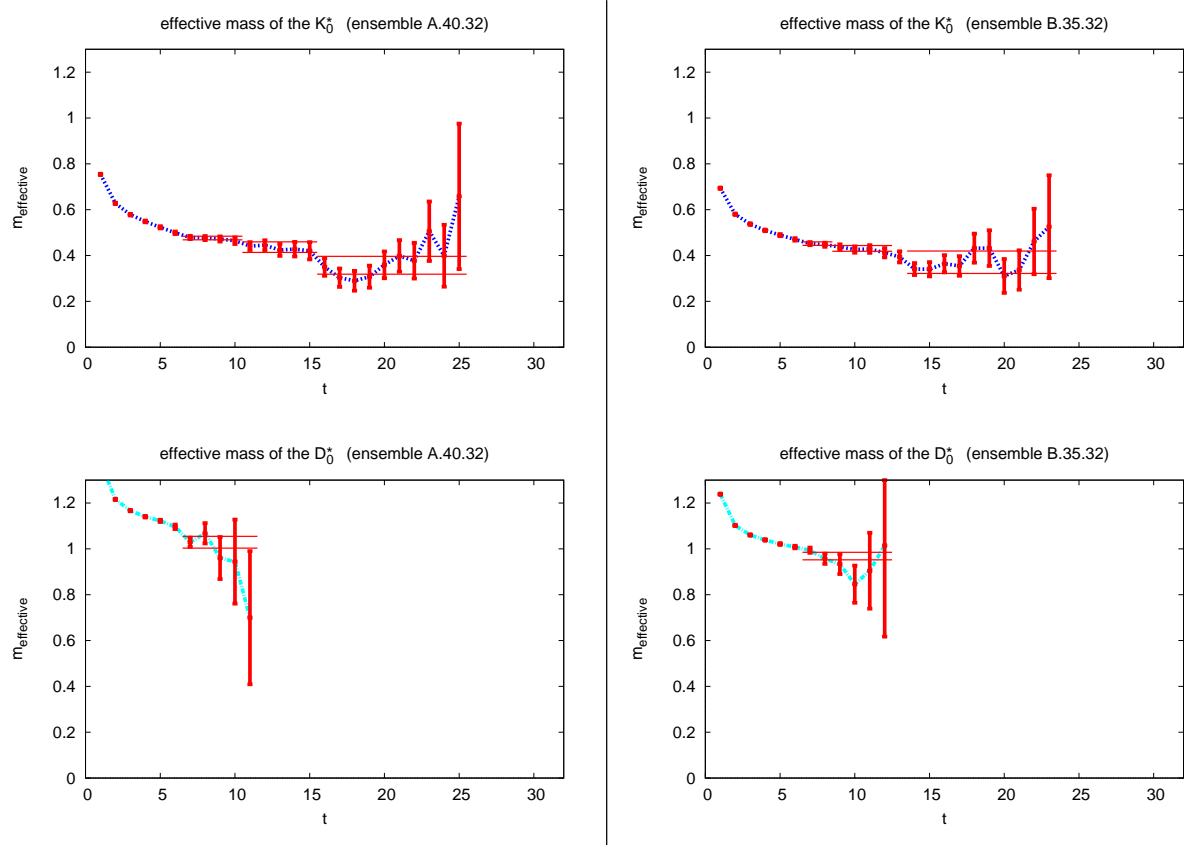


Figure 9: The effective masses in the scalar channel, with Gaussian smeared operators, for the ensembles A40.32 (left) and B35.32 (right). The error bands indicate the total error, statistical plus systematic.

$4 \times n$ operators, the immediate application being the one considered in the previous section with both local and smeared operators. The obvious route would just be to diagonalize each 4×4 correlation sub-matrix with homogeneous composition (e.g. local or smeared operators only) as we have done so far. As a result, the twist angles and the Z_P/Z_S factors are obtained for each set; observe that the Z_P/Z_S factors are heavily affected by the smearing, which brings the former closer to one. Also the twist angles are expected to differ, due to different $\mathcal{O}(a)$ effects for local and smeared operators. Once these parameters are known, the physical correlation matrices with mixed local/smeared operators can be reconstructed, too. However, this procedure is not expected to be optimal for the latter correlation matrices, since the parameters are adjusted to optimize the correlation matrices with homogeneous composition. A better way would be to apply an independent diagonalization, with new parameters, of the matrices with mixed local/smeared composition.

Ensemble	am_K	t_1, t_2	$am_{K_0^*}$	am_D	$am_{D_0^*}$
A40.32	0.25668(35)	7-8	0.452(8)	0.909(4)(22)	1.029(26)
		9-12	0.431(12)		
		14-32	0.37(5)		
B35.32	0.21842(33)	7-10	0.476(8)	0.823(4)(14)	0.968(16)
		11-15	0.437(23)		
		16-32	0.358(39)		

Table 6: Masses of the K , K_0^* , D and D_0^* mesons in lattice units, obtained with the parity and flavor restoration method, and using Gaussian smeared operators. The third row contains the temporal separations used for the determination of $m_{K_0^*}$.

4 Conclusions

We have proposed and compared three methods to determine m_K and m_D in $N_f = 2 + 1 + 1$ twisted mass lattice QCD. The computation of these masses is less straightforward in this case, since parity and flavor are not good quantum numbers. We have therefore explored strategies to extract the desired states and have developed three distinct methods all of which exploit the exponential fall-off of correlation matrices for suitably chosen heavy-light meson creation operators. Method 1 amounts to solving a generalized eigenvalue problem, method 2 is equivalent to fitting a linear superposition of exponentials and method 3 transforms the correlators to the physical basis by means of the twist rotation. Results for m_K and m_D obtained with the three methods and for both ensembles investigated here are summarized in Table 7 and visualized in Figure 10. Since the kaon is the lightest state in the combined $(s/c, -/+)$ sector, the

	Method 1	Method 2	Method 3
Ensemble A40.32			
am_K	0.2567(2)	0.25554(88)	0.25668(35)
am_D	0.922(11)	0.901(21)	0.909(22)
Ensemble B35.32			
am_K	0.2184(3)	0.21768(84)	0.21842(33)
am_D	0.829(8)	0.835(20)	0.823(15)

Table 7: Comparison of the results for m_K and m_D obtained with the three methods exposed in this work, for both ensembles.

computation of its mass is rather simple and we obtain precise values for m_K with errors $\lesssim 0.4\%$ including statistical and systematical uncertainties. Moreover, within these errors all three methods yield very compatible results which is very reassuring.

In contrast to m_K , the mass of the D meson is difficult to determine, because in our twisted mass setup the D meson is a highly excited state in the combined $(s/c, -/+)$ sector. However, also in this case our three methods yield results, which are in excellent agreement within the combined statistical and systematical errors, whose relative magnitudes are $\lesssim 2.5\%$. Therefore, we are

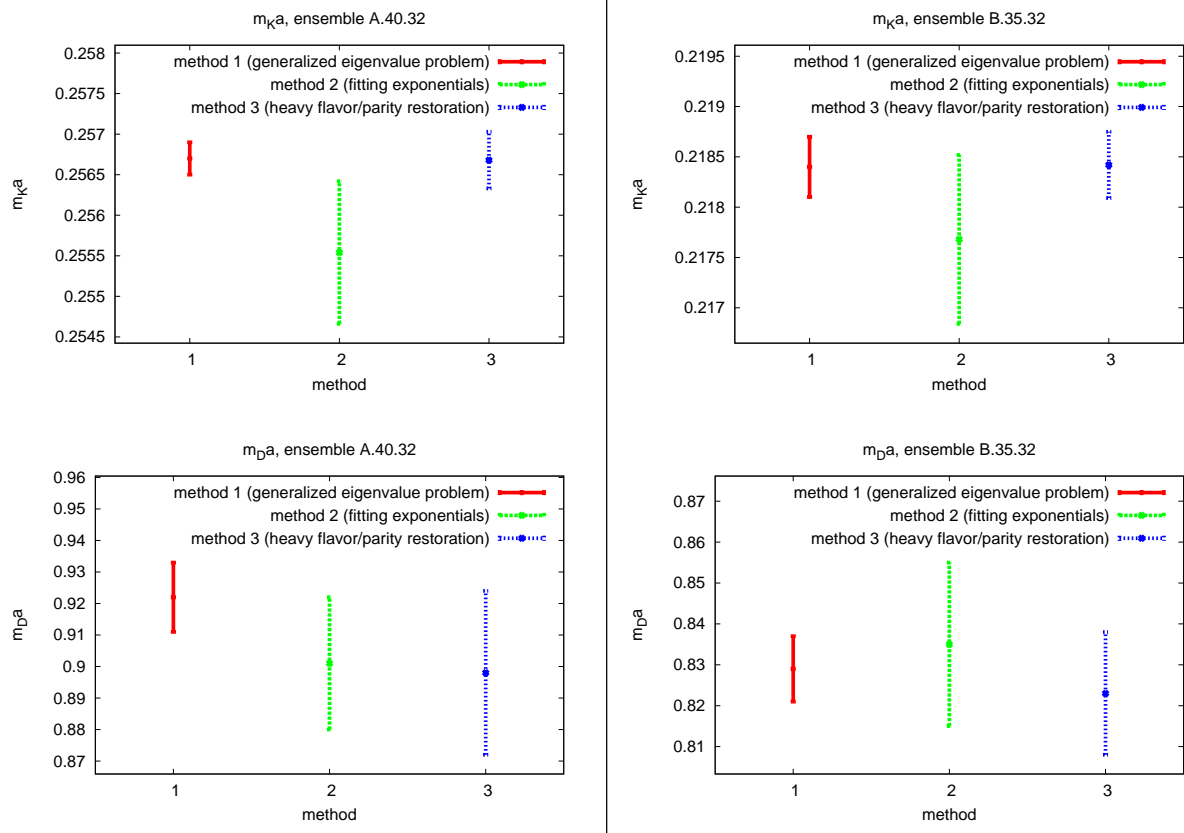


Figure 10: Comparison of the results for m_K (top) and m_D (bottom) obtained with the three methods exposed in this work, for both ensembles. The results for methods 1 to 3 are shown from left to right.

confident that we are able to obtain reliable estimates for m_D without resolving all the low lying (multi particle) states below the D meson. The latter would require to compute correlation matrices with a significantly larger operator basis and with extremely high statistical precision, an endeavor, which hardly seems to be feasible. It is therefore very important that already with the much smaller correlator matrix employed here, one can obtain a satisfactory estimate of the D meson mass.

The errors we obtain with our three methods differ by factors of around 2 to 4, originating from the fact that the three methods estimate the systematic error in different ways. While method 2 (fitting exponentials) tends to yield the largest error, its procedure to determine the systematic error is also the most conservative: the error is computed from the spread of a large set of fit results corresponding to different fitting ranges. In contrast to that method 1 (solving a generalized eigenvalue problem) estimates the corresponding error by just taking two “neighboring fitting ranges” into account. Consequently, the total error is somewhat smaller.

We stress that as far as K physics is concerned, our analysis shows that this sector can be analyzed in the unitary setup without problems. This provides a very good perspective to compute corresponding decay constants and also the strange baryon spectrum in the future. For

charm physics, the situation is different and it will be quite difficult to extract reliable physics results in the charm sector from the unitary setup. Here, we plan to employ a mixed action approach by using an Osterwalder-Seiler (OS) valence quark action [34]. This has the advantage [56] that there is no flavor mixing and that the valence quarks stay as close as possible to the sea twisted mass quarks, e.g. there is no need to re-tune κ to realize maximal twist. The idea is to match the K and D meson masses between the unitary setup and the valence OS quarks. After this matching step further physical quantities such as decay constants will then be computed with OS quarks. The matching condition will guarantee that in the continuum limit we recover the situation of a unitary setup. Of course, it needs to be seen, whether discretization errors in this strategy remain small. Investigations in this direction are in progress.

With respect to the matching of K and D meson masses between the unitary setup and the valence OS quarks, the outcome of our work in this paper is extremely important. The fact that we can compute the K meson with high accuracy and the D meson with acceptable precision in the unitary setup is a necessary prerequisite to allow for applying such a matching condition.

Instead of matching the K and D meson masses in the sea and valence sectors, one can directly match the renormalized strange and charm quark masses [34]. The latter can be determined in the sea sector by using eq. (6). Only the finite ratio Z_P/Z_S is needed as an input for the matching. We have shown in this paper one possible way to determine this quantity, which is specific for the twisted mass setup. In compliance with the massless quark renormalization scheme, however, the extrapolated value of Z_P/Z_S for four massless quarks is required. We mention here that the ETMC has started a dedicated program to evaluate the renormalization constants for our $N_f = 2 + 1 + 1$ setup in the massless quark limit. Once the relevant renormalization constants will be available, this information will be used for an alternative tuning of the mass parameters in the valence sector. This can result in different values of the valence quark masses with respect to the procedure relying on the hadron masses, and hence to different cut-off effects for the resulting mixed action theory. Employing both matching conditions can therefore be used to have independent computations for physical observables and will provide a most valuable cross-check of the way this setup approaches the continuum limit.

Acknowledgments

The computer time for this project was made available to us by the John von Neumann-Institute for Computing (NIC) on the JUMP, Juropa and Jugene systems in Jülich and apeNEXT system in Zeuthen, BG/P and BG/L in Groningen, by BSC on Mare-Nostrum in Barcelona (www.bsc.es), and by the computer resources made available by CNRS on the BlueGene system at GENCI-IDRIS Grant 2009-052271 and CCIN2P3 in Lyon. We thank these computer centers and their staff for all technical advice and help.

This work has been supported in part by the DFG Sonderforschungsbereich/ Transregio SFB/TR9-03 and the EU Integrated Infrastructure Initiative Hadron Physics (I3HP) under contract RII3-CT-2004-506078. We also thank the DEISA Consortium (co-funded by the EU, FP6 project 508830), for support within the DEISA Extreme Computing Initiative (www.deisa.org).

References

- [1] **ETM** Collaboration, Ph. Boucaud *et al.*, “Dynamical twisted mass fermions with light quarks,” Phys. Lett. B **650**, 304 (2007) [arXiv:hep-lat/0701012].
- [2] **ETM** Collaboration, Ph. Boucaud *et al.*, “Dynamical twisted mass fermions with light quarks: simulation and analysis details,” Comput. Phys. Commun. **179**, 695 (2008) [arXiv:0803.0224 [hep-lat]].
- [3] **ETM** Collaboration, R. Baron *et al.*, “Light meson physics from maximally twisted mass lattice QCD,” arXiv:0911.5061 [hep-lat].
- [4] **ETM** Collaboration, C. Alexandrou *et al.*, “Light baryon masses with dynamical twisted mass fermions,” Phys. Rev. D **78**, 014509 (2008) [arXiv:0803.3190 [hep-lat]].
- [5] **ETM** Collaboration, C. Alexandrou *et al.*, “The low-lying baryon spectrum with two dynamical twisted mass fermions,” Phys. Rev. D **80**, 114503 (2009) [arXiv:0910.2419 [hep-lat]].
- [6] **ETM** Collaboration, B. Blossier *et al.*, “Light quark masses and pseudoscalar decay constants from $N_f = 2$ lattice QCD with twisted mass fermions,” JHEP **0804**, 020 (2008) [arXiv:0709.4574 [hep-lat]].
- [7] **ETM** Collaboration, B. Blossier *et al.*, “Pseudoscalar decay constants of kaon and D -mesons from $N_f = 2$ twisted mass lattice QCD,” JHEP **0907**, 043 (2009) [arXiv:0904.0954 [hep-lat]].
- [8] **ETM** Collaboration, V. Bertone *et al.*, “Kaon oscillations in the Standard Model and Beyond using $N_f = 2$ dynamical quarks,” PoS **LAT2009** (2009) 258. [arXiv:0910.4838 [hep-lat]].
- [9] **ETM** Collaboration, B. Blossier *et al.*, “A proposal for B -physics on current lattices,” arXiv:0909.3187 [hep-lat].
- [10] **ETM** Collaboration, B. Blossier *et al.*, “ f_B and f_{B_s} with maximally twisted Wilson fermions,” [arXiv:0911.3757 [hep-lat]].
- [11] **ETM** Collaboration, K. Jansen, C. Michael, A. Shindler and M. Wagner, “The Static-light meson spectrum from twisted mass lattice QCD,” JHEP **0812**, 058 (2008) [arXiv:0810.1843 [hep-lat]].
- [12] **ETM** Collaboration, C. Michael, A. Shindler and M. Wagner, “The continuum limit of the static-light meson spectrum,” arXiv:1004.4235 [hep-lat].
- [13] **ETM** Collaboration, B. Blossier, M. Wagner and O. Pène, “Lattice calculation of the Isgur-Wise functions $\tau_{1/2}$ and $\tau_{3/2}$ with dynamical quarks,” JHEP **0906**, 022 (2009) [arXiv:0903.2298 [hep-lat]].
- [14] **ETM** Collaboration, R. Frezzotti, V. Lubicz and S. Simula, “Electromagnetic form factor of the pion from twisted-mass lattice QCD at $N_f = 2$,” Phys. Rev. D **79**, 074506 (2009) [arXiv:0812.4042 [hep-lat]].

- [15] **ETM** Collaboration, V. Lubicz, F. Mescia, S. Simula *et al.*, “ $K \rightarrow \pi \ell \nu$ semileptonic form factors from two-flavor lattice QCD,” Phys. Rev. **D80** (2009) 111502. [arXiv:0906.4728 [hep-lat]].
- [16] **ETM** Collaboration, S. Di Vita *et al.*, “Vector and scalar form factors for K - and D -meson semileptonic decays from twisted mass fermions with $N_f = 2$,” PoS **LAT2009** (2009) 257. [arXiv:0910.4845 [hep-lat]].
- [17] **ETM** Collaboration, C. Alexandrou *et al.*, “Nucleon form factors with dynamical twisted mass fermions,” PoS **LATTICE2008**, 139 (2008) [arXiv:0811.0724 [hep-lat]].
- [18] **ETM** Collaboration, R. Baron, S. Capitani, J. Carbonell, K. Jansen, Z. Liu, O. Pene and C. Urbach, “Moments of meson distribution functions with dynamical twisted mass fermions,” PoS **LAT2007**, 153 (2007) [arXiv:0710.1580 [hep-lat]].
- [19] **ETM** Collaboration, C. Michael and C. Urbach, “Neutral mesons and disconnected diagrams in twisted mass QCD,” PoS **LAT2007**, 122 (2007) [arXiv:0709.4564 [hep-lat]].
- [20] **ETM** Collaboration, K. Jansen, C. Michael and C. Urbach, “The η' meson from lattice QCD,” Eur. Phys. J. C **58**, 261 (2008) [arXiv:0804.3871 [hep-lat]].
- [21] **ETM** Collaboration, C. McNeile, C. Michael and C. Urbach, “The ω - ρ meson mass splitting and mixing from lattice QCD,” Phys. Lett. B **674**, 286 (2009) [arXiv:0902.3897 [hep-lat]].
- [22] **ETM** Collaboration, D. B. Renner and X. Feng, “Hadronic contribution to $g - 2$ from twisted mass fermions,” PoS **LATTICE2008**, 129 (2008) [arXiv:0902.2796 [hep-lat]].
- [23] **ETM** Collaboration, X. Feng, K. Jansen and D. B. Renner, “The $\pi^+ \pi^+$ scattering length from maximally twisted mass lattice QCD,” Phys. Lett. B **684**, 268 (2010) [arXiv:0909.3255 [hep-lat]].
- [24] **ETM** Collaboration, X. Feng, K. Jansen and D. B. Renner, “Scattering from finite size methods in lattice QCD,” arXiv:0910.4871 [hep-lat].
- [25] **ETM** Collaboration, M. Constantinou *et al.*, “Non-perturbative renormalization of quark bilinear operators with $N_f = 2$ (tmQCD) Wilson fermions and the tree-level improved gauge action,” arXiv:1004.1115 [hep-lat].
- [26] K. Cichy, J. Gonzalez Lopez, K. Jansen, A. Kujawa and A. Shindler, “Twisted mass, overlap and Creutz fermions: cut-off effects at tree-level of perturbation theory,” Nucl. Phys. B **800**, 94 (2008) [arXiv:0802.3637 [hep-lat]].
- [27] **χ_{LF}** Collaboration, K. Jansen, M. Papinutto, A. Shindler, C. Urbach and I. Wetzorke, “Light quarks with twisted mass fermions,” Phys. Lett. B **619**, 184 (2005) [arXiv:hep-lat/0503031].
- [28] **χ_{LF}** Collaboration, K. Jansen, M. Papinutto, A. Shindler, C. Urbach and I. Wetzorke, “Quenched scaling of Wilson twisted mass fermions,” JHEP **0509**, 071 (2005) [arXiv:hep-lat/0507010].
- [29] A. M. Abdel-Rehim, R. Lewis and R. M. Woloshyn, “Spectrum of quenched twisted mass lattice QCD at maximal twist,” Phys. Rev. D **71**, 094505 (2005) [arXiv:hep-lat/0503007].

- [30] **ETM** Collaboration, C. Urbach, “Lattice QCD with two light Wilson quarks and maximally twisted mass,” PoS **LAT2007** (2007) 022 [arXiv:0710.1517 [hep-lat]].
- [31] **ETM** Collaboration, P. Dimopoulos, R. Frezzotti, G. Herdoiza, C. Urbach and U. Wenger, “Scaling and low energy constants in lattice QCD with $N_f = 2$ maximally twisted Wilson quarks,” PoS **LAT2007** (2007) 102 [arXiv:0710.2498 [hep-lat]].
- [32] R. Frezzotti, G. Martinelli, M. Papinutto and G. C. Rossi, “Reducing cutoff effects in maximally twisted lattice QCD close to the chiral limit,” JHEP **0604** 038 (2006) [arXiv:hep-lat/0503034].
- [33] **ETM** Collaboration, P. Dimopoulos, R. Frezzotti, C. Michael, G. C. Rossi and C. Urbach, “ $\mathcal{O}(a^2)$ cutoff effects in lattice Wilson fermion simulations,” Phys. Rev. D **81**, 034509 (2010) [arXiv:0908.0451 [hep-lat]].
- [34] R. Frezzotti and G. C. Rossi, “Chirally improving Wilson fermions. II: Four-quark operators,” JHEP **0410** (2004) 070 [arXiv:hep-lat/0407002].
- [35] T. Chiarappa *et al.*, “Numerical simulation of QCD with u , d , s and c quarks in the twisted-mass Wilson formulation,” Eur. Phys. J. C **50**, 373 (2007) [arXiv:hep-lat/0606011].
- [36] **ETM** Collaboration, R. Baron *et al.*, “Status of ETMC simulations with $N_f = 2 + 1 + 1$ twisted mass fermions,” PoS **LATTICE2008**, 094 (2008) [arXiv:0810.3807 [hep-lat]].
- [37] **ETM** Collaboration, R. Baron *et al.*, “First results of ETMC simulations with $N_f = 2+1+1$ maximally twisted mass fermions,” arXiv:0911.5244 [hep-lat].
- [38] **ETM** Collaboration, R. Baron *et al.*, “Light hadrons from lattice QCD with light (u, d), strange and charm dynamical quarks”, arXiv:1004.5284 [hep-lat].
- [39] **MILC** Collaboration, A. Bazavov *et al.*, “HISQ action in dynamical simulations,” PoS **LATTICE2008** (2008) 033 [arXiv:0903.0874 [hep-lat]].
- [40] **MILC** Collaboration, A. Bazavov *et al.*, “Progress on four flavor QCD with the HISQ action,” PoS **LAT2009** (2009) 123 [arXiv:0911.0869 [hep-lat]].
- [41] **MILC** Collaboration, A. Bazavov *et al.*, “Scaling studies of QCD with the dynamical HISQ action,” [arXiv:1004.0342 [hep-lat]].
- [42] C. Pena, S. Sint and A. Vladikas, “Twisted mass QCD and lattice approaches to the Delta($I = 1/2$ rule),” JHEP **0409** (2004) 069 [arXiv:hep-lat/0405028].
- [43] A. M. Abdel-Rehim, R. Lewis, R. M. Woloshyn and J. M. S. Wu, “Strange quarks in quenched twisted mass lattice QCD,” Phys. Rev. D **74** (2006) 014507 [arXiv:hep-lat/0601036].
- [44] Y. Iwasaki, “Renormalization group analysis of lattice theories and improved lattice action: two-dimensional non-linear $\mathcal{O}(N)$ sigma model,” Nucl. Phys. B **258**, 141 (1985).
- [45] **ALPHA** Collaboration, R. Frezzotti, P. A. Grassi, S. Sint and P. Weisz, “Lattice QCD with a chirally twisted mass term,” JHEP **0108**, 058 (2001) [arXiv:hep-lat/0101001].

- [46] R. Frezzotti and G. C. Rossi, “Twisted-mass lattice QCD with mass non-degenerate quarks,” Nucl. Phys. Proc. Suppl. **128** (2004) 193 [arXiv:hep-lat/0311008].
- [47] R. Frezzotti and G. C. Rossi, “Chirally improving Wilson fermions. I: $\mathcal{O}(a)$ improvement,” JHEP **0408**, 007 (2004) [arXiv:hep-lat/0306014].
- [48] C. Amsler *et al.* [Particle Data Group], Phys. Lett. B **667**, 1 (2008) and 2009 partial update for the 2010 edition.
- [49] **ALPHA** Collaboration, B. Blossier, M. Della Morte, G. von Hippel, T. Mendes and R. Sommer, “On the generalized eigenvalue method for energies and matrix elements in lattice field theory,” JHEP **0904**, 094 (2009) [arXiv:0902.1265 [hep-lat]].
- [50] **ALPHA** Collaboration, U. Wolff, “Monte Carlo errors with less errors,” Comput. Phys. Commun. **156**, 143 (2004) [Erratum-ibid. **176**, 383 (2007)] [arXiv:hep-lat/0306017].
- [51] C. Michael, “Fitting correlated data,” Phys. Rev. D **49**, 2616 (1994) [arXiv:hep-lat/9310026].
- [52] C. Michael and A. McKerrell, “Fitting Correlated Hadron Mass Spectrum Data,” Phys. Rev. D **51**, 3745 (1995) [arXiv:hep-lat/9412087].
- [53] F. Farchioni *et al.*, “Exploring the phase structure of lattice QCD with twisted mass quarks,” Nucl. Phys. Proc. Suppl. **140**, 240 (2005) [arXiv:hep-lat/0409098].
- [54] F. Farchioni *et al.*, “The phase structure of lattice QCD with Wilson quarks and renormalization group improved gluons,” Eur. Phys. J. C **42**, 73 (2005) [arXiv:hep-lat/0410031].
- [55] F. Farchioni *et al.*, “Numerical simulations with two flavours of twisted-mass Wilson quarks and DBW2 gauge action,” Eur. Phys. J. C **47**, 453 (2006) [arXiv:hep-lat/0512017].
- [56] R. Frezzotti, private communication (2008).

Lattice investigation of the scalar mesons $a_0(980)$ and κ using four-quark operators

Constantia Alexandrou^{1,2}, Jan Oliver Daldrop³, Mattia Dalla Brida⁴,
 Mario Gravina¹, Luigi Scorzato⁵, Carsten Urbach³, Marc Wagner⁶

¹ Department of Physics, University of Cyprus, P.O. Box 20537, 1678 Nicosia, Cyprus

² Computation-based Science and Technology Research Center, Cyprus Institute,
 20 Kavafi Str., Nicosia 2121, Cyprus

³ Helmholtz-Institut für Strahlen- und Kernphysik (Theorie) and
 Bethe Center for Theoretical Physics, Universität Bonn, D-53115 Bonn, Germany

⁴ School of Mathematics, Trinity College Dublin, Dublin 2, Ireland

⁵ ECT*, Strada delle Tabarelle, 286, I-38123, Trento, Italy

⁶ Goethe-Universität Frankfurt am Main, Institut für Theoretische Physik,
 Max-von-Laue-Straße 1, D-60438 Frankfurt am Main, Germany



December 6, 2012

Abstract

We carry out an exploratory study of the isospin one $a_0(980)$ and the isospin one-half κ scalar mesons using $N_f = 2 + 1 + 1$ Wilson twisted mass fermions at one lattice spacing. The valence strange quark is included as an Osterwalder-Seiler fermion with mass tuned so that the kaon mass matches the corresponding mass in the unitary $N_f = 2+1+1$ theory. We investigate the internal structure of these mesons by using a basis of four-quark interpolating fields. We construct diquark-diquark and molecular-type interpolating fields and analyse the resulting correlation matrices keeping only connected contributions. For both channels, the low-lying spectrum is found to be consistent with two-particle scattering states. Therefore, our analysis shows no evidence for an additional state that can be interpreted as either a tetraquark or a tightly-bound molecular state.

1 Introduction

The Naive Quark Model (NQM) is – despite its simplicity – surprisingly successful in qualitatively describing the experimentally observed meson and baryon spectrum. This success has led us to think of mesons and baryons as $q\bar{q}$ and qqq bound states, respectively. In particular, no mesonic state incompatible with the quantum numbers of a $q\bar{q}$ system has been confirmed, yet. However, there are a few exceptions [1, 2] which cannot be described in the NQM. One prominent example is the Roper resonance, another not less prominent one is the presence of too many scalar states (i.e with quantum numbers $J^{PC} = 0^{++}$) with mass below 2 GeV as compared to the expectation from the NQM. These scalars are the $f_0(600)$ or σ , $f_0(980)$, $f_0(1370)$, $f_0(1500)$ and $f_0(1710)$ with isospin 0, the $K_0^*(800)$ or κ and $K_0^*(1430)$ with isospin 1/2, and the $a_0(980)$ and $a_0(1450)$ with isospin 1.

This excess of states compared to the NQM expectation suggests that the picture of mesons as $q\bar{q}$ bound states is too simplistic and it has to be complemented by other quarkonic and gluonic structures. Consequently, it has been speculated that some of these particles are tetraquark states, i.e. bound states of two quarks and two antiquarks, or predominantly gluonic in nature. For example, according to one favoured interpretation [2], the states $f_0(1370)$, $f_0(1710)$, $K_0^*(1430)$ and $a_0(1450)$ might indeed have dominant $q\bar{q}$ components, as expected in the NQM but the state $f_0(1500)$ might be, predominantly, the lightest (0^{++}) glueball [3], and the lightest of the scalar states might constitute a nonet with a dominant tetraquark contribution [4, 5, 1, 6, 7, 8]. While such an interpretation is adopted by other authors, e.g. [9], there are also different scenarios discussed in the literature, as for example in [10, 11].

Experimentally, many of the aforementioned scalar resonances are difficult to resolve as they have large decay widths and several decay channels that sometimes open up only within a short energy interval. The question whether a physical state is dominated by a $q\bar{q}$, a tetraquark, a glueball or other hybrid wavefunctions is then typically investigated through the analysis of its production and decay modes. These are directly accessible in experiments and can be often measured rather accurately. This justifies the high experimental activity [11, 12] in investigating the composition of these states. It is thus crucial to develop a deeper theoretical understanding for the internal structure of these states.

A theoretical understanding from first principles requires a non-perturbative method. Since Quantum Chromodynamics (QCD) is the theory of strongly coupled quarks and gluons, such a non-perturbative method is provided by lattice QCD. But investigating the states in lattice QCD is also a challenging endeavour: the distinction between scattering states, resonances and bound states is subtle on a Euclidean lattice with finite spacetime volume. In fact, there is no continuum spectrum in a finite spatial volume and the Hamiltonian has only discrete eigenvalues. In order to disentangle these different physical phenomena it is necessary to study the volume dependence of the discrete eigenvalues of the Hamiltonian [13, 14, 15, 16]. In particular, the coefficients of the large volume expansion of the discrete eigenvalues are related to the phase shifts of the scattering process. Moreover, as the volume increases, the eventual resonances produce "avoided level crossings" of eigenvalues¹.

This method requires the extraction of more than the ground state in a channel with given quantum numbers. These excited states are increasingly difficult to extract with sufficient

¹Note, however, that also the threshold may display the same phenomenon [17].

precision, even though the field has recently seen tremendous progress in the methodology. An additional complication is the appearance of fermionic disconnected contributions, which are notoriously noisy. Therefore, the available lattice results on scalar mesons and possibly existing tetraquark states are still limited (cf. e.g. [18, 19, 20, 21, 22, 23, 24, 25]). Certainly more and in particular independent investigations are needed to gain a better understanding of these scalar states.

In this paper we perform an exploratory study of the $a_0(980)$ and the κ using Wilson twisted mass fermions. It is the first study of this kind with $N_f = 2 + 1 + 1$ dynamical quark flavours, using gauge configurations provided by the European Twisted Mass (ETM) collaboration [26, 27, 28, 29]. Note that in particular the dynamical strange quark might be important for studying scalar resonances. In this exploratory investigation we address the question, whether or not these states could be consistent with a tetraquark or a molecule interpretation. We focus on the precise computation of correlation functions of operators with quantum numbers of the $a_0(980)$ and κ mesons using four quark interpolating fields ignoring fermionic disconnected contributions. The latter implies that there is no mixing among four quark, two-quark and gluonic states. Apart from obvious technical advantages and having a testbed of our method, there is another important reason for working in this approximation: in [20] bound states close to threshold in the $I = 0$ and the $I = 1/2$ channels have been found in the same approximation. These bound states, found in addition to the expected scattering states, were interpreted as a possible indication for a tetraquark nature of the corresponding states. In our study, performed with a similar operator basis, but a different lattice discretisation, we do not observe such a bound state in the $I = 1/2$ channel. Moreover, we also do not observe it in the $I = 1$ channel, which was not considered in [20]. Note that parts of this work have recently been presented in a conference proceeding [30].

The reason for focussing on the a_0 and the κ are the following: the a_0 has isospin $I = 1$, i.e. when choosing $I_z = \pm 1$ only a single disconnected contribution is ignored. The κ meson, on the other hand, mixes only with the $K + \pi$ channel.

The paper is organised as follows: in section 2 we introduce the lattice formulation followed by a discussion of the operator basis in section 3; the results of our study are discussed in section 4 and we conclude in the last section.

2 Lattice setup

2.1 Lattice actions

This work is based on gauge link configurations generated by the ETM collaboration [26, 27, 28, 29] with the Iwasaki gauge action [31] and $N_f = 2 + 1 + 1$ flavours of twisted mass quarks.

The light degenerate (u, d) quark doublet is described by the standard Wilson twisted mass action [32],

$$S_{\text{light}}[\chi^{(l)}, \bar{\chi}^{(l)}, U] = a^4 \sum_x \bar{\chi}^{(l)}(x) \left(D_W(m_0) + i\mu\gamma_5\tau_3 \right) \chi^{(l)}(x), \quad (1)$$

while for the heavy (c, s) sea quark doublet the twisted mass formulation for non-degenerate

quarks of [33] has been used,

$$S_{\text{heavy}}[\chi^{(h)}, \bar{\chi}^{(h)}, U] = a^4 \sum_x \bar{\chi}^{(h)}(x) \left(D_W(m_0) + i\mu_\sigma \gamma_5 \tau_1 + \tau_3 \mu_\delta \right) \chi^{(h)}(x). \quad (2)$$

In both cases D_W denotes the standard Wilson Dirac operator,

$$D_W(m_0) = \frac{1}{2} \left(\gamma_\mu \left(\nabla_\mu + \nabla_\mu^* \right) - a \nabla_\mu^* \nabla_\mu \right) + m_0, \quad (3)$$

while $\chi^{(l)} = (\chi^{(u)}, \chi^{(d)})$ and $\chi^{(h)} = (\chi^{(c)}, \chi^{(s)})$ are the quark fields in the so-called twisted basis. For reasons explained in [34] the same value of the standard quark mass parameter m_0 has been used in both sectors.

When tuning the theory to maximal twist, automatic $\mathcal{O}(a)$ improvement for physical quantities applies [33, 35]. This tuning has been done by adjusting m_0 such that the PCAC quark mass in the light quark sector vanishes (cf. [28] for details).

At maximal twist in a massless quark renormalisation scheme the renormalised quark masses are related to the bare parameters μ_σ and μ_δ by

$$m_s^R = Z_P^{-1} \left(\mu_\sigma - \frac{Z_P}{Z_S} \mu_\delta \right), \quad m_c^R = Z_P^{-1} \left(\mu_\sigma + \frac{Z_P}{Z_S} \mu_\delta \right) \quad (4)$$

[33], where Z_P and Z_S are the renormalisation constants of the non-singlet pseudoscalar and scalar densities. In our simulations the values of μ_σ and μ_δ have been adjusted by requiring that the resulting lattice kaon and D meson masses approximately assume their physical values [28, 36, 37].

For the computation of observables we use a twisted mass discretisation for valence s quarks, which is different from the sea s quarks (2). It is given by (1) with $\chi^{(l)} \rightarrow \chi^{(s)} = (\chi^{(s^+)}, \chi^{(s^-)})$ and $\mu_l \rightarrow \mu_s$. We do this, to avoid the problem of mixing between s and c quarks, which is discussed in detail in [36, 37]. Note that there are two possibilities to realize a valence s quark, $\chi^{(s^+)}$ and $\chi^{(s^-)}$, which differ in the sign of the twisted mass term, $\pm i\mu_s \gamma_5$. Strategies and consequences of choosing s^+ or s^- are discussed in detail in sections 3.1.2 and 3.2.2. The bare strange quark mass μ_s has been chosen such that kaon masses computed within this mixed action setup with flavour structure $\bar{s}^+ d$ and $\bar{s}^- u$ (which are degenerate and known to have less discretisation errors than their $\bar{s}^+ u$ and $\bar{s}^- d$ counterparts [40, 41, 42]) agree with kaon masses computed in the unitary setup [36, 37], i.e. using (2) also for valence s quarks.

In this work we consider six gauge link ensembles with simulation parameters given in Table 1. They differ in the space-time volume $(L/a)^3 \times T/a$ and in the light u/d quark mass μ_l . The lattice spacing $a \approx 0.086$ fm is the same for all ensembles. More details regarding these ensembles can be found in [28].

The discussion of meson and four-quark creation operators (cf. section 3) and their quantum numbers is more convenient with quark fields in the “physical basis”, (u, d) and (s^+, s^-) . This physical basis is related to the “twisted basis” $(\chi^{(u)}, \chi^{(d)})$ and $(\chi^{(s^+)}, \chi^{(s^-)})$ introduced in (1) and (2) according to

$$\begin{pmatrix} u \\ d \end{pmatrix} = e^{i\gamma_5 \tau_3 \omega/2} \begin{pmatrix} \chi^{(u)} \\ \chi^{(d)} \end{pmatrix}, \quad \begin{pmatrix} s^+ \\ s^- \end{pmatrix} = e^{i\gamma_5 \tau_3 \omega/2} \begin{pmatrix} \chi^{(s^+)} \\ \chi^{(s^-)} \end{pmatrix}, \quad (5)$$

Ensemble	β	$(L/a)^3 \times T/a$	μ_l	μ_σ	μ_δ	μ_s	a (fm)	m_{PS} (MeV)	# of configs
A30.32	1.90	$32^3 \times 64$	0.0030	0.150	0.190	0.02280	0.086	284	672
A40.32		$32^3 \times 64$	0.0040			0.02322		324	200
A40.24		$24^3 \times 48$	0.0040			0.02300		332	1259
A40.20		$20^3 \times 48$	0.0040			0.02308		341	500
A50.32		$32^3 \times 64$	0.0050			0.02336		362	431
A80.24		$24^3 \times 48$	0.0080			0.02328		455	1225

Table 1: Gauge link ensembles considered in this paper. The notation follows [28].

where ω is the twist angle, which we have tuned to maximal twist, i.e. $\omega = \pi/2$.

When computing temporal correlation functions $\langle \mathcal{O}_j^\dagger(t_2) \mathcal{O}_k(t_1) \rangle$, where \mathcal{O}_j and \mathcal{O}_k are e.g. meson or four-quark creation operators, we only consider quark propagators connecting time t_1 and t_2 , but ignore propagation of quarks within the same timeslice, e.g. from t_1 to t_1 . For mesons this amounts to neglecting so-called disconnected diagrams. For four-quark operators e.g. of tetraquark or two-meson type both singly and doubly disconnected contributions (cf. (b) and (c) of Figure 1) are omitted. Consequences of not considering disconnected diagrams are discussed in the following sections.

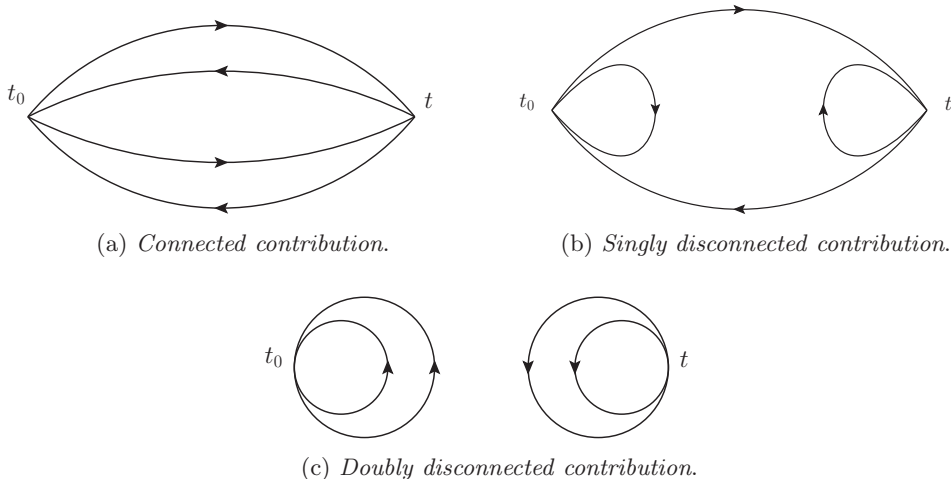


Figure 1: Relevant contributions to a four-quark operator two point function.

Finally it should be mentioned that at finite lattice spacing isospin and parity are not good quantum numbers in twisted mass lattice QCD. These symmetries are broken by terms proportional to $\mathcal{O}(a)$. Consequently, when doing spectroscopy, one has to take mixing with states of opposite parity and different isospin into account. Of course, in the continuum limit these symmetries are restored and QCD is recovered. Mixing in the context of $a_0(980)$ and κ is discussed in detail in sections 3.1.1 and 3.2.1.

2.2 The pseudoscalar meson spectrum

Since a pair of pseudoscalar mesons is rather light and can have the same quantum numbers as the scalar mesons $a_0(980)$ and κ , these are the most relevant scattering states to consider. Their masses are approximately equal to the sum of the two masses of the corresponding individual mesons. Therefore, a precise and comprehensive knowledge of the meson spectrum is important for our analysis.

As we ignore disconnected contributions, the $\eta \equiv \bar{u}u + \bar{d}d$ meson and the neutral $\pi \equiv \bar{u}u - \bar{d}d$ become degenerate and there is an η/η' -like meson with valence quark structure $\bar{s}s$, but no light $\bar{u}u$ or $\bar{d}d$ valence quarks, which we denote by η_s .

Another particularity stems from the valence action used for the strange quarks discussed above. The kaon and the η_s can be constructed using s^+ and/or s^- strange quarks, resulting in different values for the meson masses at finite value of the lattice spacing. Similarly, in Wilson twisted mass lattice QCD the neutral (connected-only) and charged pion mass values differ.

All meson masses relevant for our investigation are collected in Table 2.

ensemble	$m_{\pi(\bar{u}d, \bar{d}u)}$	$m_{\pi(\bar{u}u - \bar{d}d)}$	$m_{K(\bar{s}^+d, \bar{s}^-u)}$	$m_{K(\bar{s}^+u, \bar{s}^-d)}$	$m_{\eta_s(\bar{s}^+s^-)}$	$m_{\eta_s(\bar{s}^+s^+, \bar{s}^-s^-)}$
A30.32	284(1)	494(6)	576(7)	704(2)		876(1)
A40.20	341(2)		599(3)		774(2)	
A40.24	332(1)	530(7)	593(1)	723(2)		882(1)
A40.32	324(7)		588(5)		779(2)	
A50.32	362(7)		601(9)		783(2)	
A80.24	455(1)	625(3)	635(1)	753(1)		885(1)

Table 2: The pseudoscalar meson spectrum in MeV with disconnected diagrams neglected. Omitted mass values are not needed in the context of the tetraquark study presented in this paper.

3 Creation operators and analysis details

In this study we exclusively consider creation operators with four quarks (two quarks and two antiquarks). The structure of our four-quark operators is oriented at phenomenological expectations and ranges from four-quark bound states (molecules formed by two mesons and bound diquark-antidiquark pairs) to two essentially non-interacting mesons (two-particle operators).

Of course, standard quark-antiquark operators, e.g. $\bar{d}u$ for $a_0(980)$ and $\bar{s}u$ for κ , would also be of interest. However, since we neglect disconnected diagrams (cf. section 2.1), such two-quark operators do not generate overlap to trial states created by four-quark operators. Consequently, in our setup four-quark operators and quark-antiquark operators probe different sectors, which is, why we do not consider the latter in the following. In a subsequent improved study we plan to include disconnected diagrams and to combine two- and four-quark operators in a single correlation matrix.

Information regarding the used four-quark operators is summarised in Table 3. The operators

will be discussed in more detail below.

ensemble	quark smearing	gauge smearing	type	Dirac structure	
				$a_0(980)$	κ
A30.32			$K\bar{K}$ molecule	$\gamma_5, \gamma_\mu, \gamma_\mu\gamma_5$	—
A40.24	Gaussian	APE	$\eta_s\pi$ molecule	γ_5	—
			$K\pi$ molecule	—	$\gamma_5, \gamma_\mu, \gamma_\mu\gamma_5$
			diquark	$C\gamma_5, C$	$C\gamma_5, C$
A80.24			$K\bar{K}$ molecule	γ_5	—
			diquark	$C\gamma_5$	—
			$K + \bar{K}$ two-particle	γ_5	—
			$\eta_s + \pi$ two-particle	γ_5	—
A40.20			$K\bar{K}$ molecule	γ_5, γ_μ	—
			$\eta_s\pi$ molecule	γ_5	—
			diquark	$C\gamma_5, C$	—
A40.32	Gaussian	APE	$K\bar{K}$ molecule	γ_5, γ_μ	—
			$\eta_s\pi$ molecule	γ_5	—
			diquark	$C\gamma_5, C$	—
A50.32	Gaussian	APE	$K\bar{K}$ molecule	γ_5, γ_μ	—
			diquark	$C\gamma_5, C$	—

Table 3: Four-quark creation operators.

3.1 Creation operators, $a_0(980)$ sector (quantum numbers $I(J^P) = 1(0^+)$)

The expected low-lying spectrum in the $a_0(980)$ sector (≈ 1000 MeV) is the following:

- A two-particle $\eta + \pi$ and a two-particle $\eta' + \pi$ state.
 - In nature:
 - * Mass $m(\eta + \pi) \approx 548$ MeV + 140 MeV = 688 MeV [12].
 - * Mass $m(\eta' + \pi) \approx 958$ MeV + 140 MeV = 1098 MeV [12].
 - In our lattice setup:
 - * Due to neglect of disconnected diagrams η has flavour structure $\bar{u}u + \bar{d}d$ and is degenerate with the neutral pion (cf. section 2.2); the $\eta + \pi$ state is orthogonal to any trial state obtained by using an operator containing s quarks, i.e. can be ignored in the following.
 - * Due to neglect of disconnected diagrams η' becomes η_s (cf. section 2.2); masses $m(\eta_s + \pi) \approx m(\eta_s) + m(\pi)$ depend on the gauge link ensemble and can be read off from Table 2.
- A two-particle $K + \bar{K}$ state.
 - In nature: mass $m(K + \bar{K}) \approx 2 \times 496$ MeV = 992 MeV [12].

- In our lattice setup: masses $m(K + \bar{K}) \approx 2m(K)$ depend on the gauge link ensemble and can be read off from Table 2.
- Possibly a bound $a_0(980)$ state (might be of quark-antiquark, molecule or diquark-antidiquark type), mass $m(a_0(980)) = 980 \pm 20$ MeV [12].

To be able to resolve these low-lying states, we consider the following operators:

- Molecule type operators:

$$\mathcal{O}_{a_0(980)}^{K\bar{K} \text{ molecule}} = \sum_{\mathbf{x}} (\bar{s}(\mathbf{x})\gamma_5 u(\mathbf{x})) (\bar{d}(\mathbf{x})\gamma_5 s(\mathbf{x})) \quad (6)$$

$$\mathcal{O}_{a_0(980)}^{\eta_s\pi \text{ molecule}} = \sum_{\mathbf{x}} (\bar{s}(\mathbf{x})\gamma_5 s(\mathbf{x})) (\bar{d}(\mathbf{x})\gamma_5 u(\mathbf{x})); \quad (7)$$

since pseudoscalar mesons (mesons with spin structure γ_5) are the lightest mesons in a given flavour sector, one expects possible molecular bound states to be of pseudoscalar-pseudoscalar type. We also consider molecule type operators with γ_5 replaced by γ_j and by $\gamma_j\gamma_5$. These operators enlarge our correlation matrices and allow us to study also excited states, in particular two-particle states with relative momentum (cf. section 4).

- Diquark type operator:

$$\mathcal{O}_{a_0(980)}^{\text{diquark}} = \sum_{\mathbf{x}} (\epsilon^{abc} \bar{s}^b(\mathbf{x}) C \gamma_5 \bar{d}^{c,T}(\mathbf{x})) (\epsilon^{ade} u^{d,T}(\mathbf{x}) C \gamma_5 s^e(\mathbf{x})); \quad (8)$$

diquarks with spin structure γ_5 are known to be the lightest [1, 38, 39], which is, why we use γ_5 in this operator. We also consider diquark type operators with γ_5 replaced by 1. As before, the main reason is to enlarge our correlation matrices allowing us to study also excited states.

- Two-particle type operators:

$$\mathcal{O}_{a_0(980)}^{K+\bar{K} \text{ two-particle}} = \left(\sum_{\mathbf{x}} \bar{s}(\mathbf{x})\gamma_5 u(\mathbf{x}) \right) \left(\sum_{\mathbf{y}} \bar{d}(\mathbf{y})\gamma_5 s(\mathbf{y}) \right) \quad (9)$$

$$\mathcal{O}_{a_0(980)}^{\eta_s+\pi \text{ two-particle}} = \left(\sum_{\mathbf{x}} \bar{s}(\mathbf{x})\gamma_5 s(\mathbf{x}) \right) \left(\sum_{\mathbf{y}} \bar{d}(\mathbf{y})\gamma_5 u(\mathbf{y}) \right); \quad (10)$$

these operators resemble states with two non-interacting mesons and, therefore, should be particularly suited to resolve two-particle $K + \bar{K}$ and $\eta_s + \pi$ states. Note that terms with $\mathbf{x} = \mathbf{y}$ in (9) and (10) also appear in the molecule operators (6) and (7), which is, why two-particle $K + \bar{K}$ and $\eta_s + \pi$ states can also be resolved, even though only molecule and diquark operators are used. However, the generated overlap to two-particle states is significantly larger, when two-particle operators are applied, which in turn results in a signal of better statistical quality (cf. the numerical results in section 4.1).

3.1.1 Mixing due to twisted mass symmetry breaking

In twisted mass lattice QCD both parity P and isospin I are broken by $\mathcal{O}(a)$. Consequently, one has to take mixing with states of opposite parity and different isospin into account. When there is mixing with rather light states (lighter than those one is interested in), problems arise: correlators are slightly contaminated by weakly decaying exponentials, which become dominant at large temporal separations, at which masses are usually determined.

Before we discuss mixing due to twisted mass symmetry breaking, it is important, to understand the effects arising by neglecting disconnected diagrams in more detail. In such a setup the valence quark flavour structure is conserved, i.e. quark-antiquark pairs can neither be created nor annihilated. For $a_0(980)$ this implies that any state that mixes with the trial states created by our operators (cf. (6) to (10)) must have valence quark flavour structure $u\bar{d}s\bar{s}$.

This observation is particularly important, when discussing parity mixing, because at first glance there seem to be states of opposite (negative) parity, which are light, namely pions $I(J^P) = 1(0^-)$. However, since pions only have a u and a \bar{d} valence quark, but no $s\bar{s}$ pair, they are orthogonal to any state we probe with our four-quark operators. On the other hand $u\bar{d}s\bar{s}$ four-quark states with negative parity are expected to be rather heavy, e.g. could be a pseudoscalar meson and a scalar meson like $K + \kappa$.

Since the z -component of isospin I_z is a quantum number, and since we study the $I_z = +1$ sector, isospin mixing can only take place with $I \geq 2$ states. In principle there could be mixing with rather light $I = 2 \pi + \pi$ states, but as mentioned above this is prevented by neglecting disconnected diagrams, which enforce valence flavour structure $u\bar{d}s\bar{s}$, i.e. $I = 1$ and $I_z = +1$.

To summarise, for the $a_0(980)$ sector $I(J^P) = 1(0^+)$ mixing due to twisted mass symmetry breaking is not expected to cause any problems. This is confirmed by our numerical results (no additional unexpected states are observed, the effective mass plateaux quality is good and does not seem to be contaminated by mixing; cf. section 4).

3.1.2 Different twisted mass realizations of the s quark

In our mixed action setup the s quark can be realized with either a twisted mass term $+i\mu_s \gamma_5$ or $-i\mu_s \gamma_5$ denoted by s^+ and s^- , respectively (cf. also section 2.1). Consequently, the $s\bar{s}$ pair appearing in our creation operators can be $s^+\bar{s}^+$, $s^-\bar{s}^-$, $s^+\bar{s}^-$ or $s^-\bar{s}^+$. In the continuum limit all four choices yield identical results. At finite lattice spacing, however, results are different due to discretisation errors.

For mesons, it is known that using a quark and an antiquark with different twisted mass signs significantly reduces discretisation errors [40, 41, 42]. With this in mind $s^+\bar{s}^-$ should be the optimal choice for the operators (6), (9) and (10).

It is not clear, whether this mixed realization is optimal also for diquarks (operator (8)). For this reason, we also used $s^+\bar{s}^+$ (or $s^-\bar{s}^-$, which yields exactly the same result). Another advantage is the possibility to also compute disconnected diagrams (which we plan to do in the near future), which is not possible, when using $s^+\bar{s}^-$.

Performing computations both with $s^+\bar{s}^+$ as well as with $s^-\bar{s}^-$ is not only a valuable cross check of numerical results, but also provides a first estimate of the magnitude of discretisation errors

at our current value of the lattice spacing. In section 4 numerical results are presented and discussed in this context.

3.2 Creation operators, κ sector (quantum numbers $I(J^P) = 1/2(0^+)$)

The expected low-lying spectrum in the κ sector (≈ 700 MeV) is the following:

- A two-particle $K + \pi$ state.
 - In nature: mass $m(K + \pi) \approx 496$ MeV + 140 MeV = 636 MeV [12].
 - In our lattice setup: masses $m(K + \pi) \approx m(K) + m(\pi)$ depend on the gauge link ensemble and can be read off from Table 2.
- Possibly a bound κ state (might be of quark-antiquark, molecule or diquark-antidiquark type), mass $m = 682 \pm 29$ MeV [12]. Such a state has been observed in the lattice study reported in [20], but not in the one in [43]. Note that disconnected contributions are neglected in our calculations, like in [20].

To be able to resolve these low-lying states, we proceed similar as for $a_0(980)$ and consider the following operators:

- Molecule type operator:

$$\begin{aligned} \mathcal{O}_\kappa^{K\pi \text{ molecule}} &= \\ &= \sum_{\mathbf{x}} \left(\left(\bar{s}(\mathbf{x})\gamma_5 u(\mathbf{x}) \right) \left(\bar{u}(\mathbf{x})\gamma_5 u(\mathbf{x}) \right) + \left(\bar{s}(\mathbf{x})\gamma_5 d(\mathbf{x}) \right) \left(\bar{d}(\mathbf{x})\gamma_5 u(\mathbf{x}) \right) \right. \\ &\quad \left. + \left(\bar{s}(\mathbf{x})\gamma_5 s(\mathbf{x}) \right) \left(\bar{s}(\mathbf{x})\gamma_5 u(\mathbf{x}) \right) \right); \end{aligned} \quad (11)$$

to be able to check and compare with results of a recent similar lattice tetraquark study of κ [20], we also consider molecule type operators with γ_5 replaced by γ_j and by $\gamma_j\gamma_5$. Such a structure corresponds to a bound state of a pair of vector mesons (γ_j) and pair of axial vector mesons ($\gamma_j\gamma_5$), which are significantly heavier than pseudoscalar mesons (γ_5). Therefore, we do not expect them to be very helpful to resolve low lying states, which is confirmed by our numerical results (cf. section 4.3). They are, however, useful for the extraction of excited states.

- Diquark type operator:

$$\mathcal{O}_\kappa^{\text{diquark}} = \sum_{\mathbf{x}} \left(\epsilon^{abc} \bar{s}^b(\mathbf{x}) C \gamma_5 \bar{d}^{c,T}(\mathbf{x}) \right) \left(\epsilon^{ade} d^{d,T}(\mathbf{x}) C \gamma_5 u^e(\mathbf{x}) \right); \quad (12)$$

note that γ_5 diquark flavour combinations $[\bar{s}\bar{u}][uu]$ and $[\bar{s}\bar{s}][su]$ do not exist, due to the Grassmann property of the quark fields, i.e. $[uu] = [\bar{s}\bar{s}] = 0$. Hence, in contrast to the molecule operator (11) there is no sum over light quark flavours in the diquark operator (12); as before, we also consider diquark type operators with γ_5 replaced by 1; since a diquark with spin structure 1 is known to be heavier than a diquark with spin structure γ_5 [38, 39], we mainly use it to resolve excited states.

Both our numerical results for $a_0(980)$ and the above mentioned lattice study of κ [20] indicate that two-particle scattering states can be resolved with four-quark operators, where all quarks are located at the same point (e.g. operators (11) and (12)). Therefore, in contrast to our study of $a_0(980)$ we do not consider operators of two-particle type. This allows to save a significant amount of computer time, because two-particle operators require different inversions of the Dirac operator (timeslice propagators instead of point propagators; cf. section 3.3.2).

3.2.1 Mixing due to twisted mass symmetry breaking

In contrast to the $a_0(980)$ sector, mixing introduces additional low-lying states in the κ sector, which have to be understood and resolved. These additional states have their origin in two-particle $K + \pi$ states with $I = 3/2$ (an $I = 1/2$ kaon and an $I = 1$ pion can either form an $I = 1/2$ or $I = 3/2$ state).

In QCD, where isospin is conserved, these states are degenerate. One can linearly combine the degenerate $I_z \in \{-1/2, +1/2\}$ kaons and $I_z = \{-1, 0, +1\}$ pions with appropriate Clebsch Gordan coefficients to form states with defined isospin $I = 1/2$ and $I = 3/2$. Note, however, that any other linear combination is still an eigenstate of the QCD Hamiltonian, i.e. when discussing eigenstates of the Hamiltonian defined isospin is an option, but not a necessity.

In twisted mass lattice QCD isospin is broken by $\mathcal{O}(a)$, i.e. u and d as well as s^+ and s^- quarks are treated differently. The important consequence in the context of this discussion is that the $I_z = -1/2$ kaon \bar{s}^+d is lighter than the $I_z = +1/2$ kaon \bar{s}^+u . Similarly there is a splitting of pion masses, where the $I_z = \pm 1$ pions ($\bar{d}u$ and $\bar{u}d$) are lighter than their $I_z = 0$ counterparts ($\bar{u}u - \bar{d}d$). While in QCD any linear combination of these kaons and pions is an eigenstate of the Hamiltonian, this splitting determines specific linear combinations, which are eigenstates in twisted mass lattice QCD: there is a $(K + \pi) \equiv (\bar{s}^+u + (\bar{u}u - \bar{d}d))$ state and a $(K + \pi) \equiv (\bar{s}^+d + \bar{d}u)$ state; the two mesons in the first state are heavier than the two mesons in the second state (cf. Table 2). Note that both combinations have $I = 1/2$ and $I = 3/2$ contributions of the same order of magnitude, i.e. are not even close to isospin eigenstates. Thus, when determining the low lying spectrum, one needs to resolve $I = 1/2$ as well as $I = 3/2$ $K + \pi$ states.

To summarise, for the κ sector $I(J^P) = 1/2(0^+)$ mixing due to twisted mass symmetry breaking will double the number of two-particle $K + \pi$ states contained in our correlation matrices. This theoretical expectation is confirmed by our numerical results (cf. section 4).

3.2.2 Different twisted mass realizations of the s quark

As mentioned in the previous section, we realize the s quark via s^+ .

Using s^- would yield on a quantitative level slightly different numerical results. The reason is that one would observe a $(K + \pi) \equiv (s^-u + (\bar{u}u - \bar{d})d)$ state and a $(K + \pi) \equiv (s^-d + \bar{d}u)$ state, i.e. each of the two states contains one ‘‘heavy version’’ of a meson and one ‘‘light version’’ of a meson. Of course, in the continuum limit s^+ and s^- yield identical results.

The results presented in this paper exclusively correspond to s^+ .

3.3 Computation of correlation matrices

We compute separate correlation matrices for $a_0(980)$ and κ ,

$$C_{jk}(t_2 - t_1) = \langle (\mathcal{O}_j(t_2))^\dagger \mathcal{O}_k(t_1) \rangle, \quad (13)$$

where \mathcal{O}_j and \mathcal{O}_k denote the creation operators (6) to (12). Technical details of these computations are explained in the following.

3.3.1 Smearing techniques

To improve the overlap to the low-lying states of interest, we use Gaussian smearing of quark fields [44, 45] with APE smeared spatial links [46]. Detailed equations can be found e.g. in [47]. We use APE smearing parameters $\alpha_{\text{APE}} = 0.5$ and $N_{\text{APE}} = 20$. Gaussian smearing is done with $\kappa_{\text{Gauss}} = 0.5$ and $N_{\text{Gauss}} = 50$ for most ensembles. Only for A40.20 we used $N_{\text{Gauss}} = 30$ instead of $N_{\text{Gauss}} = 50$. For lattice spacing $a \approx 0.086$ fm these parameters are inside a region, in which the overlap between mesonic trial states and the K and D meson is rather large [36].

3.3.2 Propagator computation

For correlation matrix elements (13), where both \mathcal{O}_j and \mathcal{O}_k are molecule and/or diquark operators, we use point source inversions, i.e. twelve inversions per gauge link configuration and quark flavour. This yields point-to-all propagators, which are exact, but which do not allow to exploit spatial translational invariance of the correlation matrix elements, to increase their statistical precision. In order to reduce correlations, however, we have chosen a random position for the source vector for each gauge configuration.

For correlation matrix elements, where at least one of the operators \mathcal{O}_j and \mathcal{O}_k is a two-particle operator, the situation is different: here the standard one-end trick [48] can be applied twice, allowing a stochastic estimation of timeslice-to-all propagators. For each application of the one-end-trick we generated an independent stochastic timeslice source with $\mathcal{Z}_2 \times \mathcal{Z}_2$ noise, where the source time slice has been chosen randomly for each gauge configuration. Computing correlation matrix elements with stochastic timeslice-to-all propagators is rather efficient, because they allow to exploit spatial translational invariance, which in turn reduces gauge noise significantly. Moreover, correlations between two two-particle operators require timeslice-to-all propagators, which are prohibitively expensive to compute using point source inversions.

3.4 Analysis of correlation matrices

To extract energy levels from $N \times N$ correlation matrices, we solve the generalised eigenvalue problem

$$C(t)\vec{v}^n(t) = \lambda^n(t, t_0)C(t_0)\vec{v}^n(t), \quad n = 0, \dots, N-1 \quad (14)$$

(cf. e.g. [49] and references therein). For a lattice with infinite temporal extension T the eigenvalues $\lambda^n(t, t_0)$ are proportional to $e^{-E_n t}$ for sufficiently large t , where E_n are the energies of the N lowest energy eigenstates.

However, for lattices with periodic finite temporal extensions and sectors, where light two-particle states exist (in our case two pseudoscalar mesons; cf. sections 3.1 and 3.2), the interpretation of the eigenvalues $\lambda^n(t, t_0)$ is no longer simple. For example a diagonal correlator $C_{jj}(t)$, which is dominated by a two-particle state with energy E_n shows the following behaviour for $0 \ll t \ll T$ [20, 50, 18]:

$$C_{jj}(t) = |A_j^n|^2 \left(e^{-E_n t} + e^{-E_n(T-t)} \right) + |B_j^n|^2 \left(e^{-m_1 t} e^{-m_2(T-t)} + e^{-m_2 t} e^{-m_1(T-t)} \right), \quad (15)$$

where m_1 and m_2 denote the masses of the corresponding single-particle states and A_j^n and B_j^n are operator dependent and problem specific constants. The “ B_j^n term” corresponds to the “ m_1 particle” traveling forward in time, while the “ m_2 particle” is traveling backwards in time, and vice versa. This term leads to a drastic and characteristic deviation of effective masses from their plateaux values at larger temporal separations. For example in Figure 2b this effect is clearly visible for $t/a \gtrsim 15$.

In [20] eq. (15) was fitted to the eigenvalues $\lambda^n(t, t_0)$ to extract the energy levels E_n . In this project, however, several two-particle states with rather different single-particle masses contribute: in the $a_0(980)$ sector $K + \bar{K}$ and $\eta_s + \pi$ are the relevant states (cf. section 3.1); for κ , due to twisted mass symmetry breaking, light and heavy kaons and pions need to be considered (cf. section 3.2). Since a proper treatment of all these two-particle states yields an equation significantly more complicated than (15) with too many parameters to perform stable fits, we follow a different route.

First note that the B_j^n term in (15) is suppressed by $\approx e^{-\min(m_1, m_2)T}$. Since A_j^n and B_j^n are of the same order of magnitude, the B_j^n term becomes irrelevant for sufficiently small t or $T - t$. Hence, we extract the energy levels considering small temporal separations only. We restrict all our effective mass analyses to $t, T - t \lesssim T/4$, which seems to be a rather conservative choice. Possibly present excited state contributions are taken into account by fitting two exponentials to each of the eigenvalues $\lambda^n(t, t_0)$ of interest, fitting range $t_{\min} \leq t \leq t_{\max}$. t_0 , t_{\min} and t_{\max} have been chosen such that $\chi^2/\text{dof} \lesssim 1$. Moreover, we varied the values of t_0 , t_{\min} and t_{\max} to check and confirm the stability of our fitting results.

4 Numerical results and their interpretation

4.1 $a_0(980)$: tetraquark and two-particle operators, ensemble A40.20

We start by discussing $a_0(980)$ ($I(J^P) = 1/2(0^+)$) results obtained using ensemble A40.20 (cf. Table 1). This ensemble with rather small spatial extension ($L \approx 1.72$ fm) is particularly suited to distinguish two-particle states with relative momentum from states with two particles at rest and from possibly existing $a_0(980)$ tetraquark states (two-particle states with relative momentum have a rather large energy because one quantum of momentum $p_{\min} = 2\pi/L \approx 720$ MeV).

Figure 2a shows effective mass plots from a 2×2 correlation matrix with a $K\bar{K}$ molecule operator (6) and a diquark-antidiquark operator (8), flavour combination $s^+\bar{s}^-$ (cf. section 3.1.2). The corresponding energies extracted from the two plateaus are given in Table 4 and they are consistent both with the expectation for possibly existing $a_0(980)$ tetraquark states and with

two-particle $K + \bar{K}$ and $\eta_s + \pi$ states, where both particles are at rest ($m(K + \bar{K}) \approx 2m(K) \approx 1198$ MeV; $m(\eta_s + \pi) \approx m(\eta_s) + m(\pi) \approx 1115$ MeV; cf. Table 2).

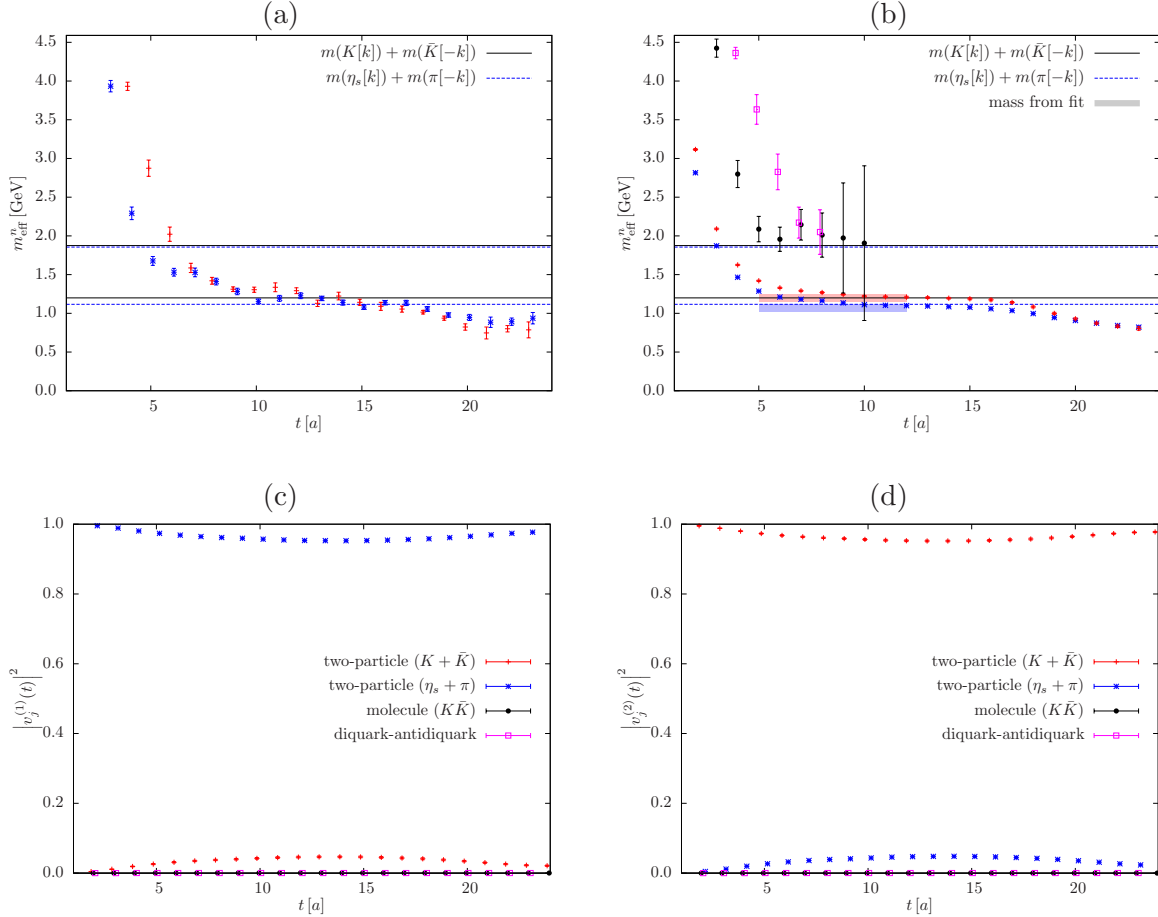


Figure 2: $a_0(980)$ sector, A40.20 ensemble. **(a)** Effective masses as a function of the temporal separation, 2×2 correlation matrix (local operators: $K\bar{K}$ molecule, diquark-antidiquark, eqs. (6) and (8)). Horizontal lines indicate the expected two-particle $K + \bar{K}$ and $\eta_s + \pi$ energy levels. **(b)** 4×4 correlation matrix (local operators: $K\bar{K}$ molecule, diquark-antidiquark, two-particle $K + \bar{K}$, two-particle $\eta_s + \pi$, eqs. (6) to (10)). **(c), (d)** Squared eigenvector components of the two low-lying states from **(b)** as a function of the temporal separation.

Increasing this correlation matrix to 4×4 by adding two-particle $K + \bar{K}$ and $\eta_s + \pi$ operators (eqs. (9) and (10)) yields the effective mass results shown in Figure 2b. Two additional states are observed with energies given in Table 4. From this 4×4 analysis we conclude the following:

- We do not observe a third low-lying state around 1000 MeV, even though we provide operators, which are of tetraquark type as well as of two-particle type. This suggests that the two low-lying states are the expected two-particle $K + \bar{K}$ and $\eta_s + \pi$ states, while no additional stable $a_0(980)$ tetraquark state is detected.
- The effective masses of the two low-lying states are of much better quality in Figure 2b than in Figure 2a. We attribute this to the two-particle $K + \bar{K}$ and $\eta_s + \pi$ operators,

which appear to create larger overlap to those states than the tetraquark operators. This in turn confirms the interpretation of the two low-lying states as two-particle states.

- To investigate the overlap in a more quantitative way, we show the squared eigenvector components of the two low-lying states in Figure 2c and Figure 2d (cf. [37] for a more detailed discussion of such eigenvector components). Clearly, the lowest state is of $\eta_s + \pi$ type, whereas the second lowest state is of $K + \bar{K}$ type. On the other hand, the two tetraquark operators are essentially irrelevant for resolving those states, i.e. they do not seem to contribute any structure, which is not already present in the two-particle operators. These eigenvector plots give additional strong support of the above interpretation of the two low lying states as two-particle states.
- The energy of two-particle excitations with one relative quantum of momentum can be estimated by

$$m(1+2, p = p_{\min}) \approx \sqrt{m(1)^2 + p_{\min}^2} + \sqrt{m(2)^2 + p_{\min}^2}, \quad p_{\min} = \frac{2\pi}{L}. \quad (16)$$

Inserting $m(K)$, $m(\eta_s)$ and $m(\pi)$ from Table 2, yields $m(K + \bar{K}, p = p_{\min}) \approx 1873 \text{ MeV}$ and $m(\eta_s + \pi, p = p_{\min}) \approx 1853 \text{ MeV}$ for the A40.20 ensemble. These numbers are consistent with the effective mass plateaus of the second and third excitation in Figure 2b. Consequently, we also interpret them as two-particle states.

Figure 2a and Figure 2b also demonstrate an important technical aspect: two-particle states can be resolved by tetraquark operators, i.e. two-particle operators are not necessarily needed, to extract the full spectrum. Since we are mainly interested in possibly existing states with a strong tetraquark component, we restrict the correlation matrices computed for other ensembles to four-quark operators (cf. Table 3). This allows to save a significant amount of computer time, because two-particle operators require different inversions of the Dirac operator (timeslice propagators instead of point propagators; cf. section 3.3.2).

4.2 $a_0(980)$: tetraquark operators, many ensembles

We have analysed the six ensembles listed in Table 1 with respect to $a_0(980)$ in a similar way as explained in section 4.1.

As already mentioned above the main difference is that this time we exclusively use tetraquark operators (6) to (8), but no two-particle operators (9) and (10). To be able to resolve more than two low-lying states, we supplement the molecule operators and the diquark-antidiquark operator by versions, where γ_5 has been replaced by γ_j and $\gamma_j\gamma_5$ (molecule) and by 1 (diquark-antidiquark). More detailed information including e.g. smearing parameters, number of gauge link configurations, etc. are collected in Table 3.

On a qualitative level our findings agree for all ensembles, i.e. are as reported in the previous subsection (effective mass plots are collected in Figure 3): there are always two low-lying states, whose masses are consistent with the expected masses of the two-particle $K + \bar{K}$ and $\eta_s + \pi$ states (cf. Figure 4 and Table 4); higher excitations (the third, forth, etc. extracted state) are in all cases significantly heavier and consistent with two-particle excitations with one relative quantum of momentum (cf. eq. (16)).

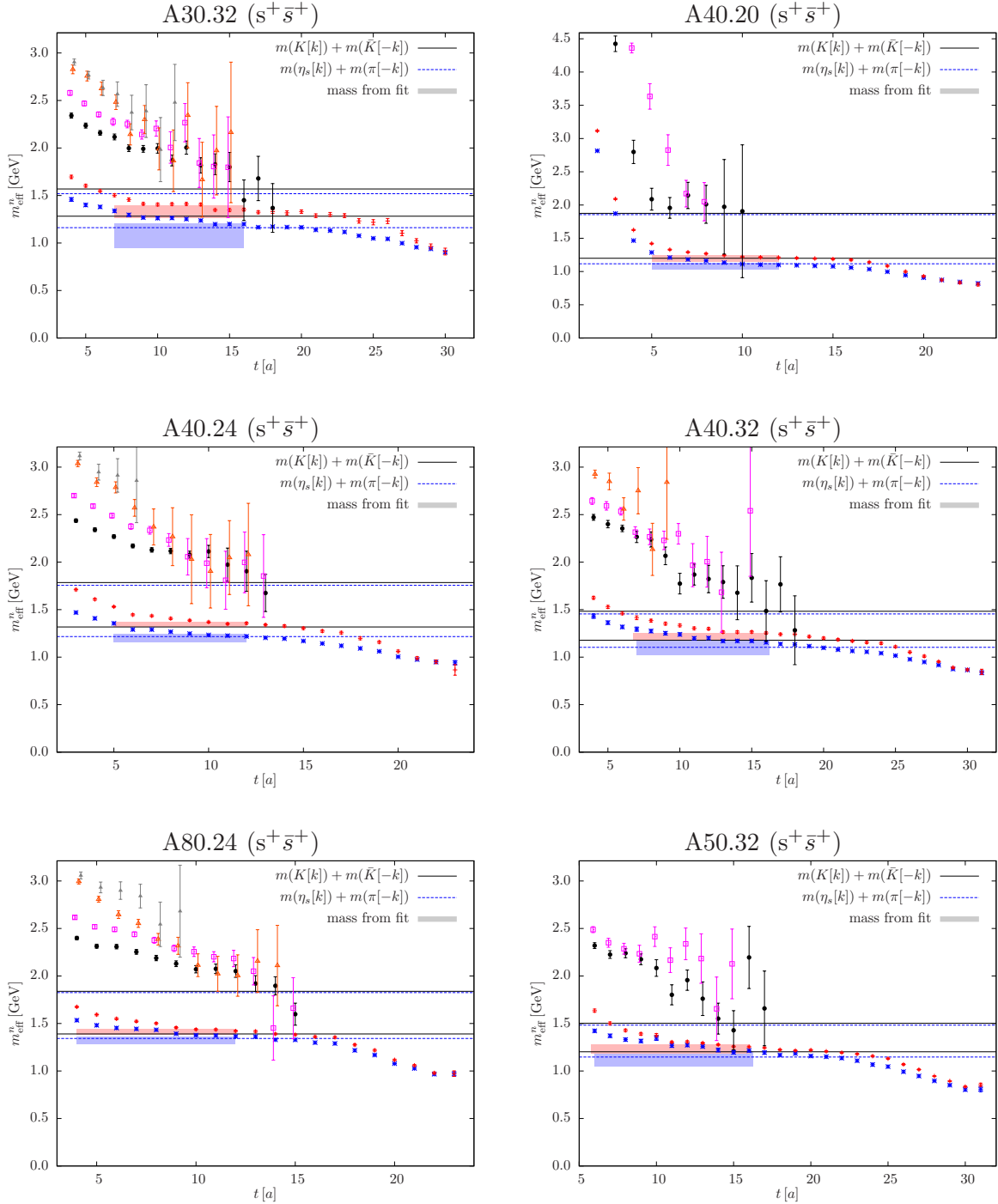


Figure 3: $a_0(980)$ sector, various ensembles, some of them with twisted mass strange quarks $s^+\bar{s}^+$, others with $s^+\bar{s}^-$. Effective masses as a function of the temporal separation. Horizontal lines indicate the expected two-particle $K + \bar{K}$ and $\eta_s + \pi$ energy levels.

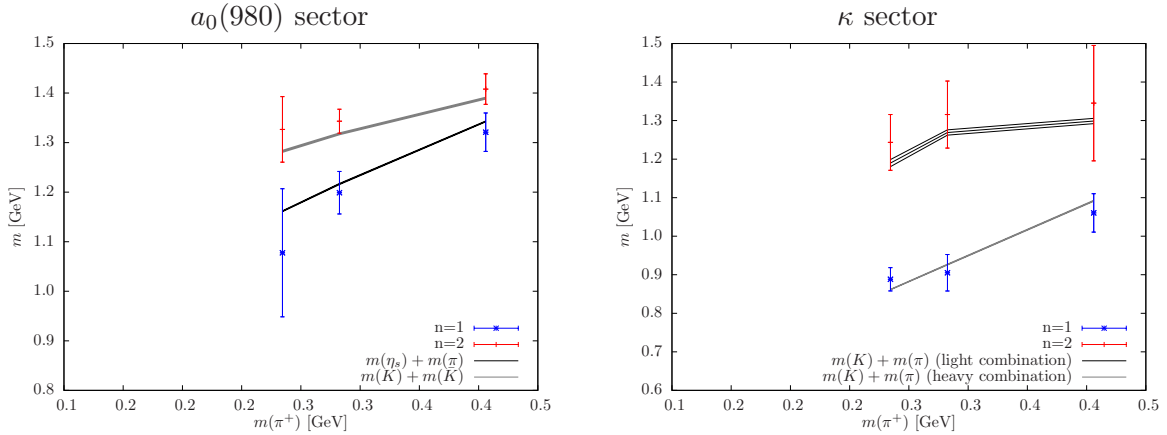


Figure 4: The two lowest energy levels E_0 and E_1 obtained by our simulations in the $a_0(980)$ ($s^+\bar{s}^+$ only) and in the κ sector (cf. also Table 4) as a function of m_{π^+} . Additionally, the energy levels of the non-interacting states are included as solid lines.

	ensemble	t_0	t_{\min}	t_{\max}	E_0 in MeV	E_1 in MeV
$a_0(980)$ ($s^+\bar{s}^+$)	A40.24	2	5	12	1199(43)	1343(24)
	A30.32	3	7	16	1078(129)	1327(66)
	A80.24	3	4	12	1321(39)	1408(31)
$a_0(980)$ ($s^+\bar{s}^-$)	A40.20	1	5	12	1073(48)	1195(51)
	A40.32	3	7	16	1098(77)	1210(40)
	A50.32	5	6	16	1130(77)	1236(48)
κ	A30.32	3	7	16	888(30)	1243(72)
	A40.24	3	5	12	905(47)	1316(87)
	A80.24	3	5	12	1060(50)	1345(150)

Table 4: The two lowest energy levels E_0 and E_1 in the $a_0(980)$ and in the κ sector (cf. also Figure 4).

To summarise, in the lattice setup and ensembles we are studying there is no indication of any additional low-lying tetraquark state.

4.3 κ : tetraquark operators, many ensembles

The analysis for the κ sector ($I(J^P) = 1/2(0^+)$) closely parallels the analysis of the $a_0(980)$ sector presented above.

We consider correlation matrices containing a $K\pi$ molecule operator (11) and analogue versions with γ_5 replaced by γ_j and $\gamma_j\gamma_5$ as well as an diquark-antidiquark operator ((12) and a similar operator with γ_5 replaced by 1). More detailed information including e.g. smearing parameters, number of gauge link configurations, etc. are collected in Table 3.

As has been explained in section 3.2.1 in twisted mass lattice QCD isospin I is not a quantum

number. Therefore, it is not sufficient to only resolve $I = 1/2$ two-particle $K + \pi$ states. One has to take into account also mixing with $I = 3/2$ two-particle $K + \pi$ states, i.e. it is necessary to resolve these two types of low-lying two-particle states at the same time.

Effective mass plots for ensembles A30.32, A40.24 and A80.24 (cf. Table 1) are shown in Figure 5 together with the expected energy levels of two-particle $K + \pi$ states (obtained via eq. (16) and the meson masses collected in Table 2). While effective mass plateaus are consistent with these expected two-particle energy levels, there is no indication of any additional low lying state, i.e. of a possibly existing bound κ state. While this is suggested by experimental data, it contradicts the findings of a similar recent lattice study of κ [20]. Currently we have no explanation for this qualitative discrepancy of two rather similar lattice computations (same operators, no disconnected diagrams, similar quark masses).

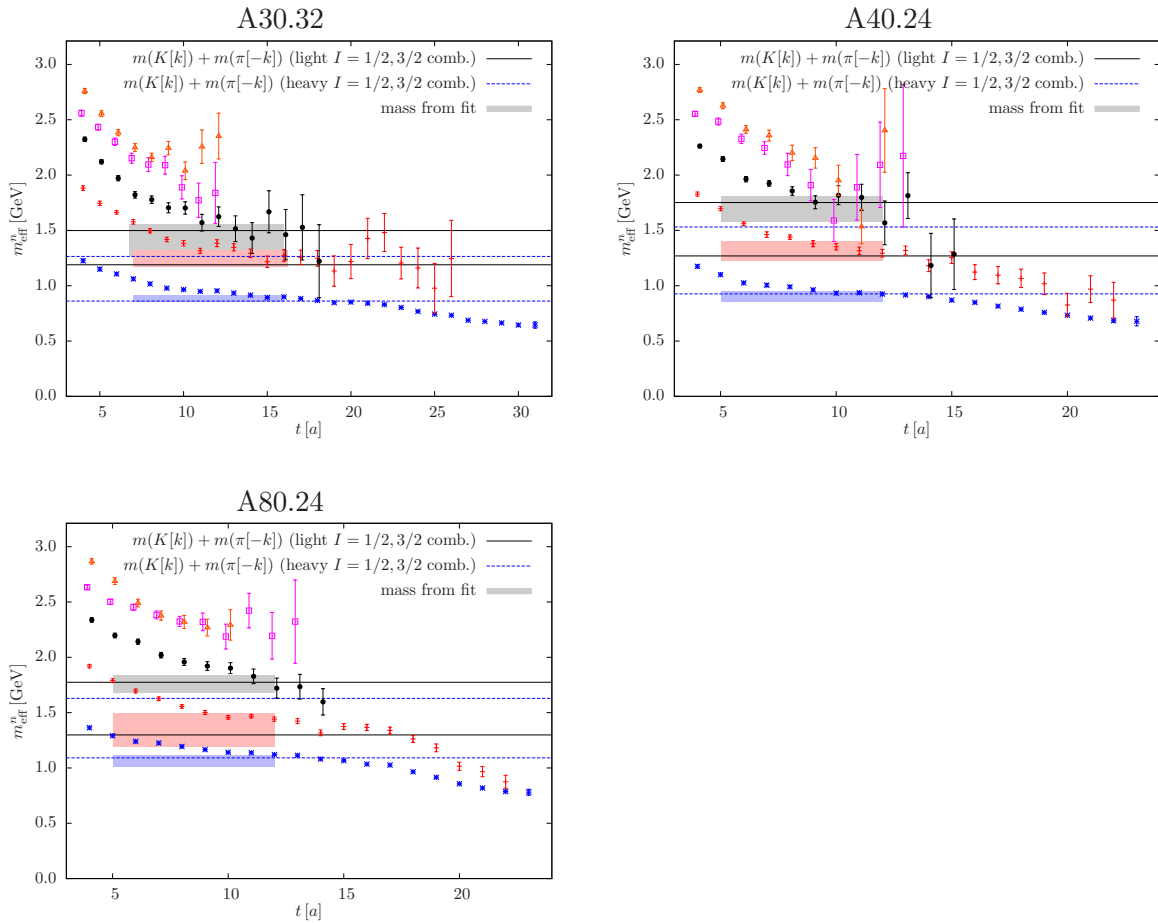


Figure 5: κ sector, various ensembles. Effective masses as a function of the temporal separation. Horizontal lines indicate the expected two-particle $K + \pi$ energy levels.

Results for the two lowest energy levels are collected in Figure 4 and Table 4.

5 Conclusions and outlook

This work represents a first necessary step in the long term project of studying the scalar mesons and their properties on the lattice. The main goal of this work was to develop and test those techniques that can be effectively exploited for studying the contribution of four-quark operators in mesons, especially in the context of the twisted mass formulation of lattice QCD.

In particular we computed the low-lying spectrum in the $a_0(980)$ and κ sectors by employing trial states designed to have a substantial overlap with both two-particle and possibly existing tetraquark states. With our ensembles we did not see additional states beside those that can be identified with the expected two-particle spectrum. In fact for all our ensembles we observed two low lying states in correspondence with the $K + \bar{K}$ and $\eta_s + \pi$ thresholds in the $a_0(980)$ sector and the $K + \pi$ ($I = 1/2$ and $I = 3/2$) threshold in the κ sector. The next states appear roughly consistent with excitations of the first quantum of momentum ($2\pi/L$) on top of those thresholds. This is somewhat difficult to reconcile with the additional state found by [20] in the κ , in spite of the rather similar lattice setups.

We find that the low lying spectrum has essentially exclusively overlap to two-particle trial states. This suggests that the states that we see are, indeed, the expected two-particles states at the threshold and not tightly bound states either of molecular type or diquark-antidiquark type.

On the basis of this, we can conclude that either our choice of operators has negligible overlap with the wave function of the resonances $a_0(980)$ and κ , or that our volumes are not large enough to identify those states.

These conclusions can be strengthened by studying more volumes, by introducing twisted boundary conditions [51] and by studying further trial states of different type. As for the latter, it will be crucial to combine four quarks with traditional quark-antiquark operators, but disconnected diagrams will be necessary for that. As for the volume dependence, we plan to use the finite volume formulae of Lüscher [52, 13, 53, 14, 15] and their extensions to multiple channels developed in [54, 55, 56, 57]. At present, our limited number of volumes is insufficient for such an analysis. Corresponding computations are in progress.

Another possible development consists in studying four-quark states that include the charm quark. This is a natural extension thanks also to the presence of a dynamical charm quark in the ETMC gauge configurations. This direction is also being explored in particular in the context of the tetraquark candidates D_{s0}^* and D_{s1}^* .

Acknowledgements

It is a great pleasure to thank Akaki Rusetsky for many enlightening discussions. We also acknowledge helpful discussions with Vladimir Galkin, Vincent Mathieu, Francesco Di Renzo and Christian Wiese. We thank Konstantin Ott nad for providing analysis code, and Marco Cristoforetti for his contribution in a preliminary phase of this project.

M.G. was supported by the Marie-Curie European training network ITN STRONGnet grant PITN-GA-2009-238353. L.S. and acknowledge support from the AuroraScience project funded by the Province of Trento and INFN. M.D.B. is currently funded by the Irish Research Council,

acknowledges support by STRONGnet and the AuroraScience project, and is grateful for the hospitality at ECT* and the University of Cyprus, where part of this work was carried out. M.W. acknowledges support by the Emmy Noether Programme of the DFG (German Research Foundation), grant WA 3000/1-1. This work is supported in part by the DFG and the NSFC through funds provided to the Sino-German CRC 110 “Symmetries and the Emergence of Structure in QCD”. For parts of this project we used computer time that was made available to us by the John von Neumann-Institute for Computing (NIC) on the JUDGE system in Jülich. In particular we thank U.-G. Meißner for granting us access on JUDGE. This work was partly supported by funding received from the Cyprus Research Promotion Foundation under contracts PENEK/0609/17 and KY-ΓΑ/0310/02 and the infrastructure project Cy-Tera co-funded by the European Regional Development Fund and the Republic of Cyprus through the Research Promotion Foundation (Project Cy-Tera NEA ΥΠΟΔΟΜΗ/ΣΤΡΑΤΗ/0308/31). This work was supported in part by the Helmholtz International Center for FAIR within the framework of the LOEWE program launched by the state of Hesse. J.D and C.U. were supported by the Bonn-Cologne Graduate School (BCGS) of Physics and Astronomie.

Part of the computations presented here were performed on the Aurora system in Trento.

References

- [1] R. L. Jaffe, “Exotica,” *Phys. Rept.* **409**, 1 (2005) [*Nucl. Phys. Proc. Suppl.* **142**, 343 (2005)] [arXiv:hep-ph/0409065].
- [2] C. Amsler and N. A. Tornqvist, “Mesons beyond the naive quark model,” *Phys. Rept.* **389**, 61 (2004).
- [3] C. J. Morningstar and M. J. Peardon, “The glueball spectrum from an anisotropic lattice study,” *Phys. Rev. D* **60**, 034509 (1999) [hep-lat/9901004].
- [4] R. L. Jaffe, “Multi-quark hadrons. 1. The phenomenology of (2 quark 2 anti-quark) mesons,” *Phys. Rev. D* **15**, 267 (1977).
- [5] R. L. Jaffe, “Multi-quark hadrons. 2. Methods,” *Phys. Rev. D* **15**, 281 (1977).
- [6] L. Maiani, F. Piccinini, A. D. Polosa and V. Riquer, “A New look at scalar mesons,” *Phys. Rev. Lett.* **93**, 212002 (2004) [hep-ph/0407017].
- [7] A. H. Fariborz, R. Jora and J. Schechter, “Toy model for two chiral nonets,” *Phys. Rev. D* **72**, 034001 (2005) [hep-ph/0506170].
- [8] F. Giacosa, “Strong and electromagnetic decays of the light scalar mesons interpreted as tetraquark states,” *Phys. Rev. D* **74**, 014028 (2006) [hep-ph/0605191].
- [9] D. Parganlija, P. Kovacs, G. Wolf, F. Giacosa and D. H. Rischke, “Meson vacuum phenomenology in a three-flavor linear sigma model with (axial-)vector mesons,” arXiv:1208.0585 [hep-ph].
- [10] V. Crede and C. A. Meyer, *Prog. Part. Nucl. Phys.* **63**, 74 (2009) [arXiv:0812.0600 [hep-ex]].

- [11] E. Klempert and A. Zaitsev, “Glueballs, hybrids, multiquarks. experimental facts versus QCD inspired concepts,” Phys. Rept. **454**, 1 (2007) [arXiv:0708.4016 [hep-ph]].
- [12] K. Nakamura et al. [Particle Data Group Collaboration], “Review of particle physics,” J. Phys. G **37**, 075021 (2010) and 2011 partial update for the 2012 edition.
- [13] M. Lüscher, “Volume Dependence of the energy spectrum in massive quantum field theories. 2. Scattering states,” Commun. Math. Phys. **105**, 153 (1986).
- [14] M. Lüscher, “Two particle states on a torus and their relation to the scattering matrix,” Nucl. Phys. B **354**, 531 (1991).
- [15] M. Lüscher, “Signatures of unstable particles in finite volume,” Nucl. Phys. B **364**, 237 (1991).
- [16] U. J. Wiese, “Identification of resonance parameters from the finite volume energy spectrum,” Nucl. Phys. Proc. Suppl. **9**, 609 (1989).
- [17] M. Döring, U. G. Meißner, E. Oset and A. Rusetsky, “Scalar mesons moving in a finite volume and the role of partial wave mixing,” arXiv:1205.4838 [hep-lat].
- [18] S. Prelovsek and D. Mohler, “A Lattice study of light scalar tetraquarks,” Phys. Rev. D **79**, 014503 (2009) [arXiv:0810.1759 [hep-lat]].
- [19] K. Jansen *et al.* [ETM Collaboration], “Meson masses and decay constants from unquenched lattice QCD,” Phys. Rev. D **80**, 054510 (2009) [arXiv:0906.4720 [hep-lat]].
- [20] S. Prelovsek, T. Draper, C. B. Lang, M. Limmer, K. -F. Liu, N. Mathur and D. Mohler, “Lattice study of light scalar tetraquarks with $I = 0, 2, 1/2, 3/2$: are σ and κ tetraquarks?,” Phys. Rev. D **82**, 094507 (2010) [arXiv:1005.0948 [hep-lat]].
- [21] C. Alexandrou and G. Koutsou, “The static tetraquark and pentaquark potentials,” Phys. Rev. D **71**, 014504 (2005) [hep-lat/0407005].
- [22] F. Okiharu, H. Suganuma and T. T. Takahashi, “Detailed analysis of the tetraquark potential and flip-flop in SU(3) lattice QCD,” Phys. Rev. D **72**, 014505 (2005) [hep-lat/0412012].
- [23] M. Wagner [ETM Collaboration], “Static-static-light-light tetraquarks in lattice QCD,” Acta Phys. Polon. Supp. **4**, 747 (2011) [arXiv:1103.5147 [hep-lat]].
- [24] P. Bicudo and M. Wagner, “Lattice QCD signal for a bottom-bottom tetraquark,” arXiv:1209.6274 [hep-ph].
- [25] M. Kalinowski and M. Wagner, “Strange and charm meson masses from twisted mass lattice QCD,” arXiv:1212.0403 [hep-lat].
- [26] **ETM** Collaboration, R. Baron *et al.*, “Status of ETMC simulations with $N_f = 2 + 1 + 1$ twisted mass fermions,” PoS **LATTICE2008**, 094 (2008) [arXiv:0810.3807 [hep-lat]].
- [27] **ETM** Collaboration, R. Baron *et al.*, “First results of ETMC simulations with $N_f = 2+1+1$ maximally twisted mass fermions,” PoS **LATTICE2009**, 104 (2009) [arXiv:0911.5244 [hep-lat]].

- [28] **ETM** Collaboration, R. Baron *et al.*, “Light hadrons from lattice QCD with light (u, d), strange and charm dynamical quarks,” JHEP **1006**, 111 (2010) [arXiv:1004.5284 [hep-lat]].
- [29] **ETM** Collaboration, R. Baron *et al.*, “Light hadrons from $N_f = 2+1+1$ dynamical twisted mass fermions,” PoS **LATTICE2010**, 123 (2010) [arXiv:1101.0518 [hep-lat]].
- [30] J. O. Daldrop, C. Alexandrou, M. D. Brida, M. Gravina, L. Scorzato, C. Urbach and M. Wagner, “Lattice investigation of the tetraquark candidates $a_0(980)$ and κ ,” PoS **LATTICE 2012**, 161 (2012) [arXiv:1211.5002 [hep-lat]].
- [31] Y. Iwasaki, “Renormalization group analysis of lattice theories and improved lattice action: two-dimensional non-linear $\mathcal{O}(N)$ sigma model,” Nucl. Phys. B **258**, 141 (1985).
- [32] **ALPHA** Collaboration, R. Frezzotti, P. A. Grassi, S. Sint and P. Weisz, “Lattice QCD with a chirally twisted mass term,” JHEP **0108**, 058 (2001) [arXiv:hep-lat/0101001].
- [33] R. Frezzotti and G. C. Rossi, “Twisted-mass lattice QCD with mass non-degenerate quarks,” Nucl. Phys. Proc. Suppl. **128** (2004) 193 [arXiv:hep-lat/0311008].
- [34] T. Chiarappa *et al.*, “Numerical simulation of QCD with u, d, s and c quarks in the twisted-mass Wilson formulation,” Eur. Phys. J. C **50**, 373 (2007) [arXiv:hep-lat/0606011].
- [35] R. Frezzotti and G. C. Rossi, “Chirally improving Wilson fermions. I: $\mathcal{O}(a)$ improvement,” JHEP **0408**, 007 (2004) [arXiv:hep-lat/0306014].
- [36] **ETM** Collaboration, R. Baron *et al.*, “Computing K and D meson masses with $N_f = 2 + 1+1$ twisted mass lattice QCD,” Comput. Phys. Commun. **182**, 299 (2011) [arXiv:1005.2042 [hep-lat]].
- [37] **ETM** Collaboration, R. Baron *et al.*, “Kaon and D meson masses with $N_f = 2 + 1 + 1$ twisted mass lattice QCD,” PoS **LATTICE2010**, 130 (2010) [arXiv:1009.2074 [hep-lat]].
- [38] C. Alexandrou, P. de Forcrand and B. Lucini, “Evidence for diquarks in lattice QCD,” Phys. Rev. Lett. **97**, 222002 (2006) [hep-lat/0609004].
- [39] M. Wagner *et al.* [ETM Collaboration], “The static-light baryon spectrum from twisted mass lattice QCD,” JHEP **1107**, 016 (2011) [arXiv:1104.4921 [hep-lat]].
- [40] S. R. Sharpe and J. M. S. Wu, “Twisted mass chiral perturbation theory at next-to-leading order,” Phys. Rev. D **71**, 074501 (2005) [hep-lat/0411021].
- [41] R. Frezzotti, G. Martinelli, M. Papinutto and G. C. Rossi, “Reducing cutoff effects in maximally twisted lattice QCD close to the chiral limit,” JHEP **0604**, 038 (2006) [hep-lat/0503034].
- [42] B. Blossier *et al.* [European Twisted Mass Collaboration], “Light quark masses and pseudoscalar decay constants from $N_f = 2$ lattice QCD with twisted mass fermions,” JHEP **0804**, 020 (2008) [arXiv:0709.4574 [hep-lat]].
- [43] C. B. Lang, L. Leskovec, D. Mohler and S. Prelovsek, “ $K\pi$ scattering for isospin 1/2 and 3/2 in lattice QCD,” arXiv:1207.3204 [hep-lat].

- [44] S. Gusken, “A study of smearing techniques for hadron correlation functions,” Nucl. Phys. Proc. Suppl. **17** (1990) 361.
- [45] C. Alexandrou *et al.* [ETM Collaboration], “Light baryon masses with dynamical twisted mass fermions,” Phys. Rev. D **78**, 014509 (2008) [arXiv:0803.3190 [hep-lat]].
- [46] M. Albanese *et al.* [APE Collaboration], “Glueball masses and string tension in lattice QCD,” Phys. Lett. B **192**, 163 (1987).
- [47] K. Jansen, C. Michael, A. Shindler and M. Wagner [ETM Collaboration], “The static-light meson spectrum from twisted mass lattice QCD,” JHEP **0812**, 058 (2008) [arXiv:0810.1843 [hep-lat]].
- [48] M. Foster *et al.* [UKQCD Collaboration], “Quark mass dependence of hadron masses from lattice QCD,” Phys. Rev. D **59**, 074503 (1999) [hep-lat/9810021].
- [49] B. Blossier, M. Della Morte, G. von Hippel, T. Mendes and R. Sommer, “On the generalized eigenvalue method for energies and matrix elements in lattice field theory,” JHEP **0904** (2009) 094 [arXiv:0902.1265 [hep-lat]].
- [50] W. Detmold, K. Orginos, M. J. Savage and A. Walker-Loud, “Kaon Condensation with Lattice QCD,” Phys. Rev. D **78** (2008) 054514 [arXiv:0807.1856 [hep-lat]].
- [51] P. F. Bedaque, “Aharonov-Bohm effect and nucleon nucleon phase shifts on the lattice,” Phys. Lett. B **593**, 82 (2004) [nucl-th/0402051].
- [52] M. Lüscher, “Volume dependence of the energy spectrum in massive quantum field theories. 1. Stable particle states,” Commun. Math. Phys. **104**, 177 (1986).
- [53] M. Lüscher and U. Wolff, “How to calculate the elastic scattering matrix in two-dimensional quantum field theories by numerical simulation,” Nucl. Phys. B **339**, 222 (1990).
- [54] M. Lage, U. -G. Meißner and A. Rusetsky, “A method to measure the antikaon-nucleon scattering length in lattice QCD,” Phys. Lett. B **681**, 439 (2009) [arXiv:0905.0069 [hep-lat]].
- [55] V. Bernard, M. Lage, U. -G. Meißner and A. Rusetsky, “Scalar mesons in a finite volume,” JHEP **1101**, 019 (2011) [arXiv:1010.6018 [hep-lat]].
- [56] E. Oset, M. Döring, U. G. Meißner and A. Rusetsky, “Chiral unitary theory of scalar mesons in a finite volume,” arXiv:1108.3923 [hep-lat].
- [57] M. Döring, U. -G. Meißner, E. Oset and A. Rusetsky, “Unitarized chiral perturbation theory in a finite volume: scalar meson sector,” Eur. Phys. J. A **47**, 139 (2011) [arXiv:1107.3988 [hep-lat]].

Investigation of the tetraquark candidate $a_0(980)$: technical aspects and preliminary results

Abdou Abdel-Rehim^{*1}, Constantia Alexandrou^{1,2}, Joshua Berlin^{†3}, Mattia Dalla Brida⁴, Mario Gravina⁵, Marc Wagner³

a.abdel-Rehim@cyi.ac.cy, alexand@ucy.ac.cy,
berlin@th.physik.uni-frankfurt.de, mattia.dallabrida@gmail.com,
mario.gravina@fis.unical.it, mwagner@th.physik.uni-frankfurt.de

¹*Computation-based Science and Technology Research Center, The Cyprus Institute,
20 Kavafi Street, 2121 Nicosia, Cyprus*

²*Department of Physics, University of Cyprus, P.O. Box 20537, 1678 Nicosia, Cyprus*

³*Goethe-Universität Frankfurt am Main, Institut für theoretische Physik,
Max-von-Laue-Straße 1, D-60438 Frankfurt am Main, Germany*

⁴*School of Mathematics, Trinity College Dublin, Dublin 2, Ireland,
& NIC, DESY, Platanenallee 6, 15738 Zeuthen, Germany*

⁵*Università della Calabria, Via Pietro Bucci, 87036 Arcavacata di Rende Cosenza, Italy*

We discuss technical aspects and first results of a lattice QCD study of the $a_0(980)$ state. We employ various interpolating operators of quark-antiquark, mesonic molecule, diquark-antidiquark and two-meson type. Both connected and disconnected contributions including diagrams with closed fermion loops are computed. To keep statistical errors small, it is essential to optimize the computation of these diagrams by choosing that combination of techniques most appropriate for each type of diagram from the correlation matrix of interpolating operators. We illustrate, how this can be done, by discussing certain diagrams in detail. We also present preliminary results corresponding to a 4×4 submatrix computed with 2+1 flavors of clover fermions.

*The 32nd International Symposium on Lattice Field Theory
23-28 June, 2014
Columbia University New York, NY*

^{*}Speaker.

[†]Speaker.

1. Introduction

Our understanding of the light scalar meson sector ($J^P = 0^+$) is incomplete [1, 2, 3]. The observed mass ordering of the states σ , $f_0(980)$, κ and $a_0(980)$ appears inverted from what would be naively expected from conventional quark models (cf. Fig. 1a and Fig. 1b). Using a single quark and a single antiquark isospin $I = 1$ can only be realized with two light quarks, whereas for $I = 0$ either two light quarks or two strange quarks are possible. Thus in the conventional quark model the flavor structure of these scalar mesons would be the following SU(3) flavor nonet [4]:

$$\begin{aligned} I = 0 &\rightarrow \sigma = \frac{1}{\sqrt{2}}(u\bar{u} + d\bar{d}) , f_0 = s\bar{s} \\ I = 1/2 &\rightarrow \kappa^+ = u\bar{s} , \kappa^0 = d\bar{s} , \bar{\kappa}^0 = s\bar{d} , \kappa^- = s\bar{u} \\ I = 1 &\rightarrow a_0^+ = u\bar{d} , a_0^0 = \frac{1}{\sqrt{2}}(u\bar{u} - d\bar{d}) , a_0^- = d\bar{u}. \end{aligned} \quad (1.1)$$

Moreover, such an assignment does not explain the mass degeneracy of $f_0(980)$ and $a_0(980)$ and it is hard to understand, why σ and κ are broader than $f_0(980)$ and $a_0(980)$.

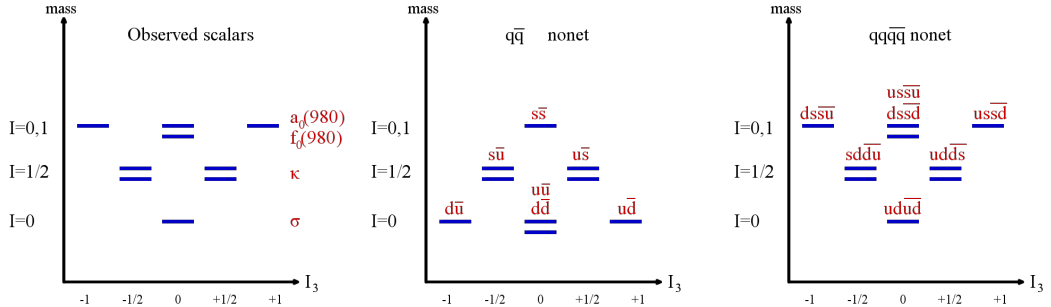


Figure 1: The spectrum of light scalar mesons ($J^P = 0^+$). From left to right: (a) Experimental results. (b) Conventional quark model (quark-antiquark structure). (c) Assuming a four-quark structure.

Alternatively one can assume a four-quark structure with quark content

$$\begin{aligned} I = 0 &\rightarrow \sigma = u\bar{d}\bar{u}\bar{d} , f_0 = \frac{1}{\sqrt{2}}(u\bar{u}\bar{s}\bar{s} + d\bar{s}\bar{d}\bar{s}) \\ I = 1/2 &\rightarrow \kappa^+ = u\bar{d}\bar{d}\bar{s} , \kappa^0 = u\bar{d}\bar{u}\bar{s} , \bar{\kappa}^0 = u\bar{s}\bar{u}\bar{d} , \kappa^- = d\bar{s}\bar{u}\bar{d} \\ I = 1 &\rightarrow a_0^+ = u\bar{s}\bar{d}\bar{s} , a_0^0 = \frac{1}{\sqrt{2}}(u\bar{u}\bar{s}\bar{s} - d\bar{s}\bar{d}\bar{s}) , a_0^- = d\bar{s}\bar{u}\bar{s}. \end{aligned} \quad (1.2)$$

Within this interpretation both the mass degeneracy of $f_0(980)$ and $a_0(980)$ and the mass ordering of the whole nonet is simple to understand (cf. Fig. 1c). The rather large width of σ and κ is also easier to explain, since the decay channels to $\pi + \pi$ and $K + \pi$, respectively, are OZI allowed.

A number of lattice QCD studies of light scalar mesons have been published in the last couple of years [5, 6, 7, 8, 9, 10]. In this work we continue our investigation of the light scalar nonet [11, 12, 13, 14, 15, 16] focusing on the study of the $a_0(980)$ state. We use a variety of interpolating operators with the aim to shed some light on the structure of the $a_0(980)$. The interpolators include a conventional quark-antiquark operator as well as different types of four quark operators with

mesonic molecule, diquark-antidiquark and two-meson structure. In the corresponding correlation matrix several diagrams with disconnected pieces or with closed fermion loops are present, which are particularly difficult to compute. To obtain an acceptable signal-to-noise ratio, it is imperative to identify the most efficient strategy of computation for each diagram. In section 2 and section 3 we will describe these technical aspects in detail. In section 4 the lattice setup is discussed and first numerical results are presented.

2. Interpolating operators and correlation matrix

Our variational basis of interpolating operators \mathcal{O}^j entering the correlation matrix

$$C_{jk}(t) = \left\langle \mathcal{O}^j(t) \mathcal{O}^{k\dagger}(0) \right\rangle \quad (2.1)$$

is the following:

$$\mathcal{O}^1 = \mathcal{O}^{q\bar{q}} = \sum_{\mathbf{x}} (\bar{d}_{\mathbf{x}} u_{\mathbf{x}}) \quad (2.2)$$

$$\mathcal{O}^2 = \mathcal{O}^{K\bar{K}, \text{point}} = \sum_{\mathbf{x}} (\bar{s}_{\mathbf{x}} \gamma_5 u_{\mathbf{x}}) (\bar{d}_{\mathbf{x}} \gamma_5 s_{\mathbf{x}}) \quad (2.3)$$

$$\mathcal{O}^3 = \mathcal{O}^{\eta_s \pi, \text{point}} = \sum_{\mathbf{x}} (\bar{s}_{\mathbf{x}} \gamma_5 s_{\mathbf{x}}) (\bar{d}_{\mathbf{x}} \gamma_5 u_{\mathbf{x}}) \quad (2.4)$$

$$\mathcal{O}^4 = \mathcal{O}^{Q\bar{Q}} = \sum_{\mathbf{x}} \epsilon_{abc} (\bar{s}_{\mathbf{x},b} (C \gamma_5) \bar{d}_{\mathbf{x},c}^T) \epsilon_{ade} (u_{\mathbf{x},d}^T (C \gamma_5) s_{\mathbf{x},e}) \quad (2.5)$$

$$\mathcal{O}^5 = \mathcal{O}^{K\bar{K}, \text{2-part}} = \sum_{\mathbf{x}, \mathbf{y}} (\bar{s}_{\mathbf{x}} \gamma_5 u_{\mathbf{x}}) (\bar{d}_{\mathbf{y}} \gamma_5 s_{\mathbf{y}}) \quad (2.6)$$

$$\mathcal{O}^6 = \mathcal{O}^{\eta_s \pi, \text{2-part}} = \sum_{\mathbf{x}, \mathbf{y}} (\bar{s}_{\mathbf{x}} \gamma_5 s_{\mathbf{x}}) (\bar{d}_{\mathbf{y}} \gamma_5 u_{\mathbf{y}}), \quad (2.7)$$

where C is the charge conjugation matrix. The first interpolating operator $\mathcal{O}^{q\bar{q}}$ is the conventional quark-antiquark “quark model interpolator”. Since the rest of the interpolating operators have four-quarks, the off-diagonal elements $C_{1,j}$ and $C_{j,1}$, $j = 2, \dots, 6$ of the correlation matrix will have closed fermion loops or propagators that start and end on the same timeslice. The interpolating operators $\mathcal{O}^{K\bar{K}, \text{point}}$, $\mathcal{O}^{\eta_s \pi, \text{point}}$ and $\mathcal{O}^{Q\bar{Q}}$ are four-quark operators with all quark fields located on the same point in space. The first two have a mesonic molecule structure ($K\bar{K}$ and $\eta_s \pi$), whereas the third has diquark-antidiquark structure (here we use the lightest diquark and antidiquark corresponding to spin structure $C \gamma_5$ [4, 17, 18]) and is expected to have a large overlap with a possibly existing tetraquark state. The last two interpolating operators $\mathcal{O}^{K\bar{K}, \text{2-part}}$ and $\mathcal{O}^{\eta_s \pi, \text{2-part}}$ are also made of two mesons, but each meson has been projected to zero momentum, i.e. their positions are independent from each other.

The matrix elements C_{jk} can be expressed in terms of quark propagators and represented diagrammatically. For example the C_{11} matrix element is given by

$$C_{11}(t) = \left\langle \mathcal{O}^{q\bar{q}}(t) \mathcal{O}^{q\bar{q}\dagger}(0) \right\rangle = - \sum_{\mathbf{x}, \mathbf{y}} \left\langle \text{Tr} \left(\gamma_5 G^d(\mathbf{x}, t; \mathbf{y}, 0)^\dagger \gamma_5 G^u(\mathbf{x}, t; \mathbf{y}, 0) \right) \right\rangle, \quad (2.8)$$

where $G^{u/d}$ denotes the u/d propagator and the trace is over the spin and color components. This expression corresponds to the diagram shown in Fig. 2a. Similarly one can write the matrix elements C_{22} and C_{33} as

$$\begin{aligned} C_{22}(t) &= \left\langle \mathcal{O}^{K\bar{K}, \text{point}}(t) \mathcal{O}^{K\bar{K}, \text{point}}(0)^\dagger \right\rangle = \\ &= \sum_{\mathbf{x}, \mathbf{y}} \left\langle \text{Tr} \left(G^s(\mathbf{x}, t; \mathbf{y}, 0)^\dagger G^u(\mathbf{x}, t; \mathbf{y}, 0) \right) \text{Tr} \left(G^d(\mathbf{x}, t; \mathbf{y}, 0)^\dagger G^s(\mathbf{x}, t; \mathbf{y}, 0) \right) \right\rangle \\ &\quad - \sum_{\mathbf{x}, \mathbf{y}} \left\langle \text{Tr} \left(\gamma_5 G^u(\mathbf{x}, t; \mathbf{y}, 0) \gamma_5 G^s(\mathbf{y}, 0; \mathbf{y}, 0) G^d(\mathbf{x}, t; \mathbf{y}, 0)^\dagger G^s(\mathbf{x}, t; \mathbf{x}, t) \right) \right\rangle \end{aligned} \quad (2.9)$$

$$\begin{aligned} C_{33}(t) &= \left\langle \mathcal{O}^{\eta_s \pi, \text{point}}(t) \mathcal{O}^{\eta_s \pi, \text{point}}(0)^\dagger \right\rangle = \\ &= \sum_{\mathbf{x}, \mathbf{y}} \left\langle \text{Tr} \left(G^s(\mathbf{x}, t; \mathbf{y}, 0)^\dagger G^s(\mathbf{x}, t; \mathbf{y}, 0) \right) \text{Tr} \left(G^d(\mathbf{x}, t; \mathbf{y}, 0)^\dagger G^u(\mathbf{x}, t; \mathbf{y}, 0) \right) \right\rangle \\ &\quad - \sum_{\mathbf{x}, \mathbf{y}} \left\langle \text{Tr} \left(\gamma_5 G^s(\mathbf{y}, 0; \mathbf{y}, 0) \right) \text{Tr} \left(G^d(\mathbf{x}, t; \mathbf{y}, 0)^\dagger G^u(\mathbf{x}, t; \mathbf{y}, 0) \right) \text{Tr} \left(\gamma_5 G^s(\mathbf{x}, t; \mathbf{x}, t) \right) \right\rangle, \end{aligned} \quad (2.10)$$

where the second terms in (2.9) and (2.10) contain closed fermion loops. In our diagrammatic language, which displays the spacetime structure, but does not take into account spin and color indices, C_{22} and C_{33} are represented by the same diagram (cf. Fig. 2b).

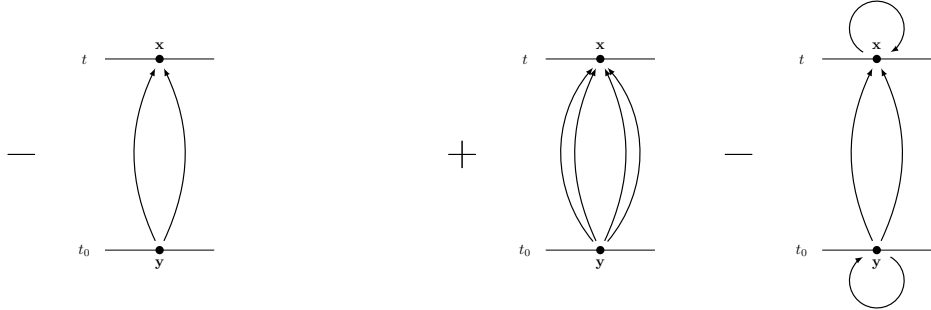


Figure 2: Diagrammatic representation of correlation matrix elements. From left to right: (a) C_{11} , eq. (2.8). (b) C_{22} and C_{33} , eq. (2.9) and eq. (2.10).

After applying this procedure to all matrix elements of the 6×6 correlation matrix C_{jk} one arrives at the diagrammatic matrix representation shown in Fig. 3. One can easily see the necessity of computing closed fermion loops and timeslice propagators, e.g. for the correlations of $\mathcal{O}^{q\bar{q}}$ and four-quark interpolating operators (first row and first column).

3. Techniques to compute the correlation matrix elements

In this section we discuss and compare different methods to compute propagators and the correlation matrix elements C_{jk} . For each diagram one should choose the optimal combination of techniques in a sense that the required CPU time is minimized and/or the signal-to-noise ratio is maximized.

There are four ways to compute quark propagators and correlators, which we try to combine most efficiently for each diagram:

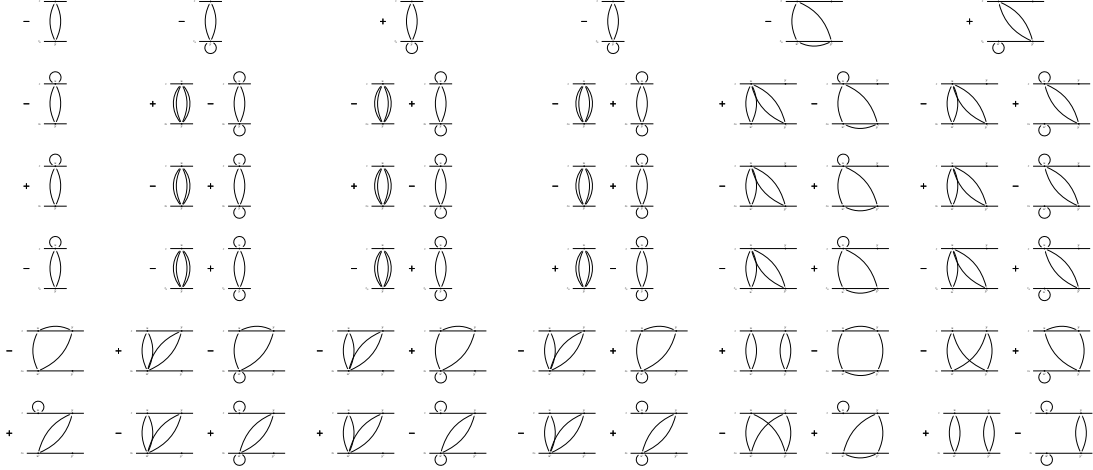


Figure 3: Diagrammatic representation of the 6×6 correlation matrix C_{jk} corresponding to the interpolating operators (2.2) to (2.7).

a) **Fixed-source propagators:** (for details cf. e.g. [19, 20])

A straightforward method to compute propagators $G(x; x_0)$ from a single point in spacetime x_0 to any other point in spacetime x (therefore, also called point-to-all propagators). Fixed-source propagators are prohibitively expensive, when a diagram involves sums over both ends of the propagator, i.e. $\sum_{\mathbf{x}, \mathbf{x}_0}$.

b) **Stochastic timeslice-to-all propagators:** (for details cf. e.g. [21, 22])

Using stochastic $Z(2) \times Z(2)$ noise on a single timeslice t_0 one can stochastically estimate propagators $G(x; \mathbf{x}_0, t_0)$ from any point in space \mathbf{x}_0 at time t_0 to any other point in spacetime x . This technique is particularly useful, when computing closed fermion loops, i.e. diagrams involving $\sum_{\mathbf{x}} G(\mathbf{x}, t; \mathbf{x}, t)$.

c) **One-end trick:** (for details cf. e.g. [23, 24])

An efficient method to stochastically estimate a pair of propagators combined by a spatial sum $\sum_{\mathbf{x}_0}$ at time t_0 , i.e. expressions containing $\sum_{\mathbf{x}_0} G(x; \mathbf{x}_0, t_0) G^\dagger(\mathbf{x}_0, t_0; y)$. If more than two propagators are involved in the sum, the one-end trick is not applicable.

d) **Sequential propagators:** (cf. e.g. [25])

Another possibility to compute a pair of propagators combined by a spatial sum $\sum_{\mathbf{x}_0}$ at time t_0 , i.e. expressions containing $\sum_{\mathbf{x}_0} G(x; \mathbf{x}_0, t_0) G^\dagger(\mathbf{x}_0, t_0; y)$, which does not necessarily involve stochastic sources. Again, if more than two propagators are involved in the sum, it is not possible to compose two of them into a sequential propagator.

These techniques can be combined in many different ways. An example is the combination of a sequential propagator d) and the one-end trick c) to compute the “triangular diagram” C_{15} as

sketched in the following:

$$C_{15} = - \left\langle \sum_{\mathbf{x}} \sum_{\mathbf{x}'} \gamma_{5\alpha\beta} G_{\beta\gamma}^u(\mathbf{x}, t; \mathbf{x}', t') \gamma_{5\gamma\delta} \underbrace{\sum_{\mathbf{y}'} G_{\delta\varepsilon}^s(\mathbf{x}', t'; \mathbf{y}', t') G_{\varepsilon\alpha}^d(\mathbf{y}', t'; \mathbf{x}, t)}_{\text{sequential propagator } G_{\delta\alpha}^{\text{sequential}}(\mathbf{x}', t'; \mathbf{x}, t)} \right\rangle. \quad (3.1)$$

one-end trick

The sequential propagator replaces two of the quark propagators $G_{\delta\varepsilon}^s(\mathbf{x}', t'; \mathbf{y}', t')$ and $G_{\varepsilon\alpha}^d(\mathbf{y}', t'; \mathbf{x}, t)$. Then the one-end trick is used to contract it properly with the third quark propagator $G_{\beta\gamma}^u(\mathbf{x}, t; \mathbf{x}', t')$. This approach yields a much better signal-to-noise ratio than e.g. combining three stochastic time-slice-to-all propagators. Another diagram, for which this strategy is very efficient, is the “rectangular diagram” in C_{55} .

3.1 Selecting the optimal method

Each diagram in Fig. 3 can be computed in a variety of ways. A priori it is usually not clear, which combination of techniques a), b), c) and d) is most efficient. Consider for example the diagram with the two closed fermion loops contributing to C_{46} (cf. Fig. 4). Options to evaluate this diagram numerically include the following:

- (1) Compute three fixed-source propagators and a stochastic propagator (fixed-source at \mathbf{x} , stochastic propagator for the disconnected loop at \mathbf{x}').
- (2) Use the one-end trick at \mathbf{y}' and a fixed-source propagator for the loop at \mathbf{x} to compute the big connected piece, use a stochastic propagator for the disconnected loop at \mathbf{x}').
- (3) Use the one-end trick at \mathbf{y}' and a stochastic propagator for the loop at \mathbf{x} to compute the big connected piece, use a fixed-source propagator for the disconnected loop at \mathbf{x}').
- (4) Use the one-end trick at \mathbf{y}' and a stochastic propagator for the loop at \mathbf{x} to compute the big connected piece, use another stochastic propagator for the disconnected loop at \mathbf{x}').

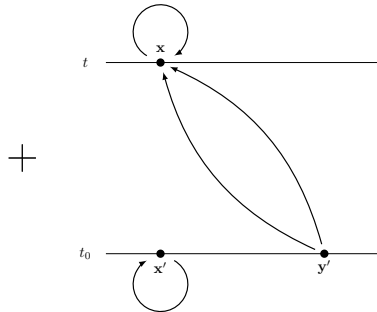


Figure 4: Diagram contributing to C_{46} .

The last option (4) involves two stochastic propagators. In general increasing the number of stochastic propagators quickly leads to a poor signal-to-noise ratio. Therefore (4) is not expected to be an efficient method. Using a single stochastic propagator and the one-end trick (options (2) and (3)) might still be comparable to option (1), where also a stochastic propagator is involved. It probably needs an exploratory numerical study before (2) and (3) should be discarded. Whether (2) and (3) perform on a similar level or one is superior to the other, is also not obvious. Probably option (1) is the most efficient choice, since only one of the four propagators is treated by stochastic methods.

3.2 An example of a numerical comparison of methods

In the following we demonstrate that different methods might yield significantly different signal-to-noise ratios. To this end we compute the four correlation matrix elements C_{j1} , $j = 1, 2, 3, 4$. For C_{11} we use

- (1) two fixed-source propagators (blue points in Fig. 5a),
- (2) the one-end trick (red points in Fig. 5a).

For C_{j1} , $j = 2, 3, 4$ we use

- (1) two fixed-source propagators (fixed source, where only two propagators join) and a stochastic timeslice-to-all propagator for the closed fermion loop (blue points in Fig. 5b to Fig. 5d),
- (2) the one-end trick and a stochastic timeslice-to-all propagator for the closed fermion loop (red points in Fig. 5b to Fig. 5d).

For all four diagrams the statistical errors obtained with methods (2) are roughly twice as large as those obtained with methods (1). Note, however, that for the latter the number of samples is larger by the factor 25 (2,500 samples compared to 100 samples). Moreover, for each sample in (1) 12 sources for light u/d propagators had to be inverted, while for (2) 2 inversion were sufficient (inversions for s propagators are comparably cheap and, therefore, not taken into account). Consequently, at roughly fixed computational costs (2) yields a signal-to-noise ratio, which is larger by a factor $\approx \sqrt{25 \times 6}/2 \approx 6$ compared to (1).

4. Numerical results

4.1 Lattice setup

Using the methods described in the previous sections we have analyzed [26] $N_f = 2 + 1$ Wilson clover gauge link configurations generated by the PACS-CS collaboration [27]. The lattice size is $32^3 \times 64$, the lattice spacing $a \approx 0.09$ fm. We have considered two ensembles corresponding to $m_\pi \approx 300$ MeV (500 gauge link configurations; referred to as “ensemble-A”) and $m_\pi \approx 150$ MeV (198 gauge link configurations; referred to as “ensemble-B”).

To improve the overlap with low lying states generated by our interpolating operators (2.2) to (2.7), Gaussian smeared quark fields with APE smeared links are used. For ensemble-A we average

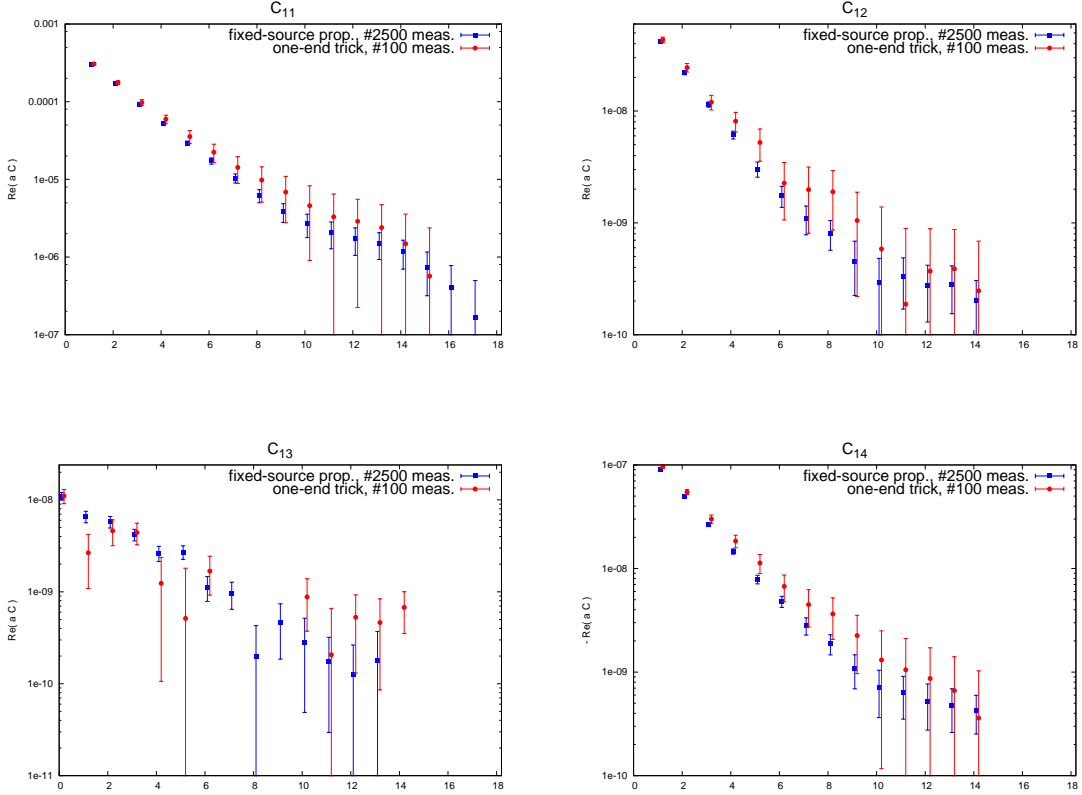


Figure 5: Numerical comparison of methods for C_{j1} , $j = 1, 2, 3, 4$.

each diagram C_{jk} , $j, k = 1, 2, 3, 4$ over 5 different source locations for each gauge link configuration, while for ensemble-B such an averaging has not been done yet. When there is a single closed fermion loop in a diagram, it is estimated with a stochastic timeslice-to-all propagator. When there are two closed fermion loops, we use a stochastic timeslice-to-all propagator for one of them and a fixed-source propagator for the other (cf. [13] for a detailed discussion). Propagators connecting the two timeslices are also fixed-source propagators (i.e. we use method (1) from subsection 3.2).

We have extracted effective masses and energy levels from the 4×4 submatrix corresponding to interpolating operators (2.2) to (2.5) by solving a standard generalized eigenvalue problem, with reference time $t_r = 1$,

$$C(t)v_n(t, t_r) = \lambda_n(t, t_r)C(t_r)v_n(t, t_r) \quad , \quad E_n \stackrel{t \text{ large}}{\equiv} E_n^{\text{eff}}(t, t_r) = \frac{1}{a} \ln \left(\frac{\lambda_n(t, t_r)}{\lambda_n(t + a, t_r)} \right). \quad (4.1)$$

4.2 Results for ensemble-A

For ensemble-A our current results have smaller statistical errors than for ensemble-B, because of a larger number of samples (2,500 compared to 198) and the heavier pion ($m_\pi \approx 300$ MeV).

4.2.1 Ignoring diagrams with closed fermion loops

In Fig. 6 we show results ignoring diagrams with closed fermion loops (statistical errors are then significantly smaller). The 4×4 correlation matrix is then equivalent to a 1×1 matrix corresponding to the quark antiquark interpolator (2.2) and an independent 3×3 matrix corresponding to the four-quark bound state interpolators (2.3) to (2.5).

The effective mass corresponding to the 1×1 matrix indicates an energy level in the region of the $a_0(980)$ ($980 \text{ MeV} \times a \approx 0.45$). The statistical errors, however, are quite large, which might be an indication that this state is not predominantly of quark-antiquark type.

The lowest state extracted from the 3×3 matrix is dominated by a $\eta_s\pi$ interpolator and the second lowest state by the $K\bar{K}$ interpolator (cf. the right plot in Fig. 6 showing the eigenvector components $|v_n|^2$). This is in agreement with our recent study of the $a_0(980)$ using Wilson twisted mass quarks [11, 12, 13, 14, 15, 16].

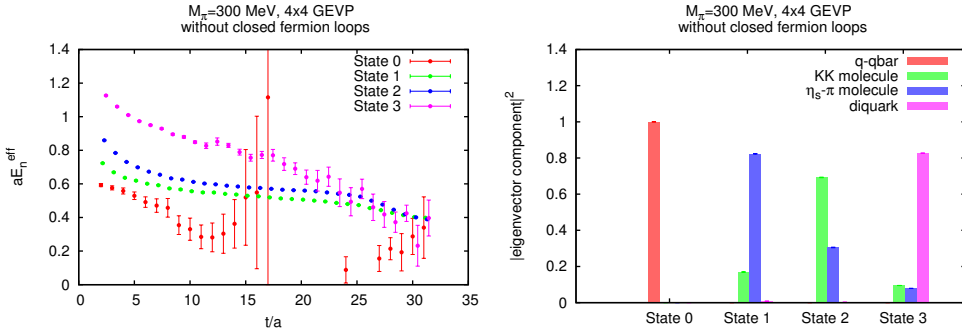


Figure 6: Effective masses (left) and eigenvector components (right) for ensemble-A ignoring diagrams with closed fermion loops.

4.2.2 Including diagrams with closed fermion loops

In Fig. 7 we show results, where also diagrams with closed fermion loops are included. It is obvious that these diagrams significantly increase statistical errors. The plots in the first row correspond to a 3×3 matrix, where only the four-quark bound state interpolators (2.3) to (2.5) are included. The results shown in the second row were obtained from a 4×4 matrix, where also the quark-antiquark interpolator (2.2) has been considered. Note that, when taking closed fermion loops into account, the 4×4 matrix cannot be decomposed into independent 1×1 and 3×3 matrices.

The lowest state extracted from the 3×3 matrix is dominated by the diquark-antidiquark interpolator, which is in strong qualitative discrepancy to the 3×3 result obtained without closed fermion loops. The first and second excitation are of $\eta_s\pi$ and of $K\bar{K}$ type and seem to correspond to the lowest two states, when closed fermion loops are ignored. When advancing to the 4×4 matrix, the nature of the ground state changes from diquark-antidiquark to quark-antiquark type. The first and second excitation remain similar. These observations might be an indication that there is an additional state (besides $\eta_s + \pi$ and $K + \bar{K}$ two-meson states) in the mass region of the $a_0(980)$. This state seems to be more quark-antiquark-like than diquark-antidiquark-like.

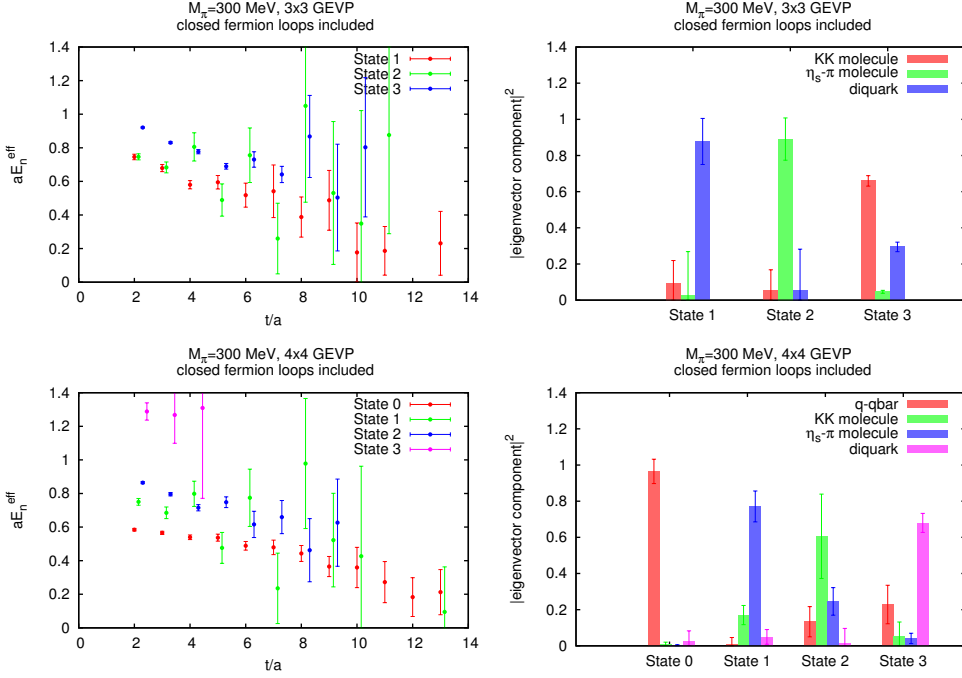


Figure 7: Effective masses (left) and eigenvector components (right) for ensemble-A including diagrams with closed fermion loops.

Since at the moment the statistical errors are quite large, this interpretation is ambiguous. To clarify the situation and to possibly resolve a bound $a_0(980)$ state, we are currently extending the correlation matrix to include the two-meson interpolators (2.6) to (2.7), which are known to result in less noisy correlators [12].

4.3 Results for ensemble-B

The results obtained for ensemble-B are shown in Fig. 8 and Fig. 9. There are only 198 samples at the moment and, hence, the results are more noisy, in particular when including closed fermion loops. The overall picture, however, is consistent with the one obtained for ensemble-A with respect to the operator content of the extracted states.

5. Conclusions and outlook

We presented technical aspects and preliminary results of our lattice QCD study of the scalar meson $a_0(980)$ using a variety of interpolating operators, e.g. of quark-antiquark, of mesonic molecule and of diquark-antidiquark type. Two $N_f = 2 + 1$ ensembles of Wilson clover gauge link configurations have been analyzed, one at near physical pion mass $m_\pi \approx 150$ MeV. Contributions from closed fermion loops, which are technically challenging to compute, have been taken into account.

Our main goal is to identify and study the $a_0(980)$ state and understand its quark sub-structure. Our current results indicate that including quark-antiquark interpolators as well as diagrams with

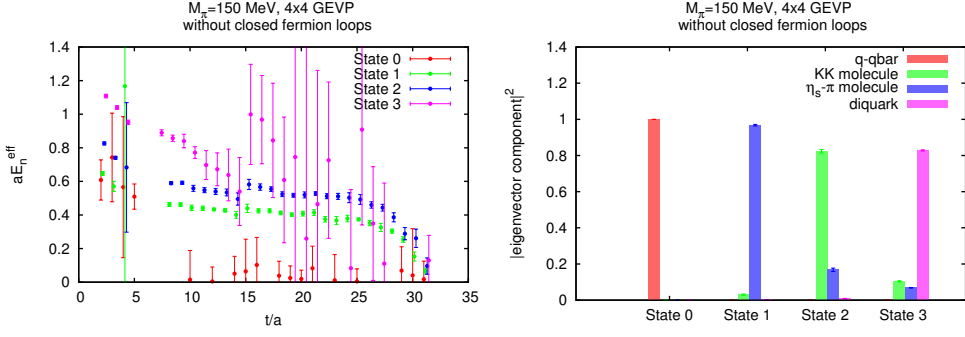


Figure 8: Effective masses (left) and eigenvector components (right) for ensemble-A ignoring diagrams with closed fermion loops.

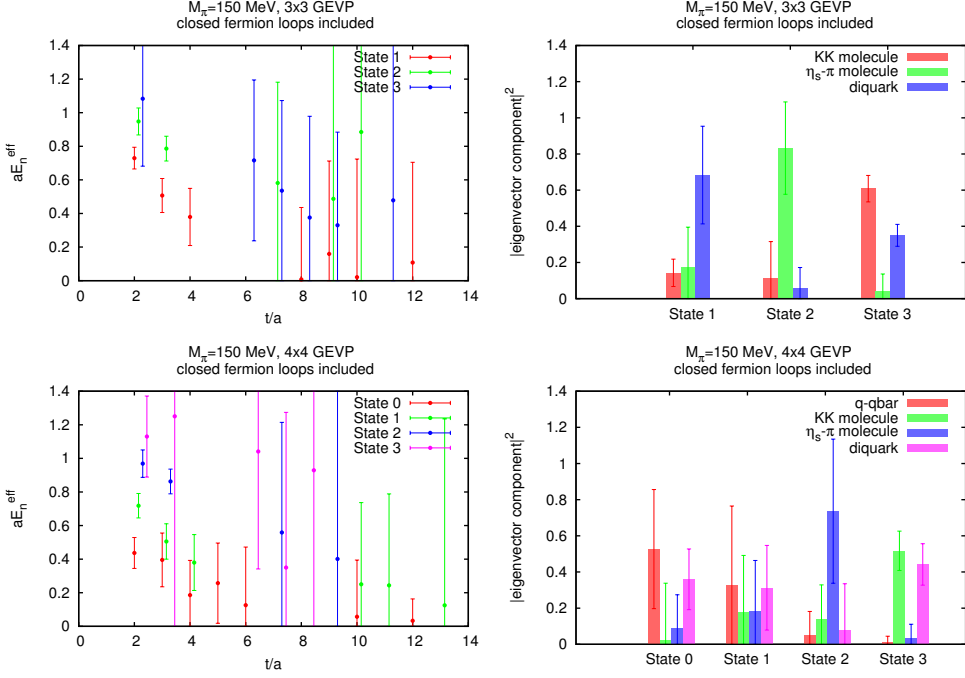


Figure 9: Effective masses (left) and eigenvector components (right) for ensemble-A including diagrams with closed fermion loops.

closed fermion loops have an important effect on the extracted spectrum. Currently we are working on reducing the statistical errors, which we plan to achieve in two ways: first, we will include explicitly scattering states of $\eta_s + \pi$ and $K + \bar{K}$ type; second we implement more advanced combinations of techniques, in particular making extensive use of the one-end trick.

Acknowledgments

M.D.B. is funded by the Irish Research Council and is grateful for the hospitality at the Uni-

versity of Cyprus, the Cyprus Institute, and DESY Zeuthen, where part of this work was carried out. The work of M.G. was supported by the European Commission, European Social Fund and Calabria Region, that disclaim any liability for the use that can be done of the information provided in this paper. M.W. acknowledges support by the Emmy Noether Programme of the DFG (German Research Foundation), grant WA 3000/1-1. This work was supported in part by the Helmholtz International Center for FAIR within the framework of the LOEWE program launched by the State of Hesse.

References

- [1] J. R. Peláez, AIP Conf. Proc. **1606**, 189 (2014).
- [2] J. R. Peláez, PoS ConfinementX (2012) 019 [arXiv:1301.4431 [hep-ph]].
- [3] C. Amsler, S. Eidelman, T. Gutsche, C. Hanhart, S. Spanier and N. A. Törnqvist, “Note on scalar mesons below 2 GeV” (2014) [<http://pdg.lbl.gov/2014/reviews/rpp2014-rev-scalar-mesons.pdf>]
- [4] R. L. Jaffe, Phys. Rept. **409** (2005) 1 [hep-ph/0409065].
- [5] C. Bernard, C. E. DeTar, Z. Fu and S. Prelovsek, Phys. Rev. D **76**, 094504 (2007) [arXiv:0707.2402 [hep-lat]].
- [6] C. Gattringer, L. Y. Glozman, C. B. Lang, D. Mohler and S. Prelovsek, Phys. Rev. D **78** (2008) 034501 [arXiv:0802.2020 [hep-lat]].
- [7] S. Prelovsek, arXiv:0804.2549 [hep-lat].
- [8] K. F. Liu, arXiv:0805.3364 [hep-lat].
- [9] M. Wakayama and C. Nonaka, PoS LATTICE **2012**, 276 (2012) [arXiv:1211.2072 [hep-lat]].
- [10] S. Prelovsek, L. Leskovec, C. B. Lang and D. Mohler, Phys. Rev. D **88** (2013) 5, 054508 [arXiv:1307.0736 [hep-lat]].
- [11] J. O. Daldrop *et al.* [ETM Collaboration], PoS LATTICE **2012**, 161 (2012) [arXiv:1211.5002 [hep-lat]].
- [12] C. Alexandrou *et al.* [ETM Collaboration], JHEP **1304**, 137 (2013) [arXiv:1212.1418].
- [13] M. Wagner *et al.* [ETM Collaboration], PoS ConfinementX, 108 (2012) [arXiv:1212.1648 [hep-lat]].
- [14] M. Wagner *et al.* [ETM Collaboration], Acta Phys. Polon. Supp. **6**, no. 3, 847 (2013) [arXiv:1302.3389 [hep-lat]].
- [15] M. Wagner *et al.*, PoS LATTICE **2013**, 162 (2012) [arXiv:1309.0850 [hep-lat]].
- [16] M. Wagner *et al.*, J. Phys. Conf. Ser. **503**, 012031 (2014) [arXiv:1310.6905 [hep-lat]].
- [17] C. Alexandrou, P. de Forcrand and B. Lucini, Phys. Rev. Lett. **97**, 222002 (2006) [hep-lat/0609004].
- [18] M. Wagner *et al.* [ETM Collaboration], JHEP **1107**, 016 (2011) [arXiv:1104.4921 [hep-lat]].
- [19] T. DeGrand and C. E. Detar, World Scientific (2006).
- [20] C. Gattringer and C. B. Lang, Lect. Notes Phys. **788** (2010).
- [21] S. Bernardson, P. McCarty and C. Thron, “ries in lattice QCD,” Comput. Phys. Commun. **78**, 256 (1993).

- [22] S. -J. Dong and K. -F. Liu, Phys. Lett. B **328**, 130 (1994) [hep-lat/9308015].
- [23] M. Foster *et al.* [UKQCD Collaboration], Phys. Rev. D **59** (1999) 074503 [hep-lat/9810021].
- [24] C. McNeile *et al.* [UKQCD Collaboration], Phys. Rev. D **73** (2006) 074506 [hep-lat/0603007].
- [25] G. Martinelli and C. T. Sachrajda, Nucl. Phys. B **316** (1989) 355.
- [26] R. G. Edwards *et al.* [SciDAC and LHPD and UKQCD Collaborations], Nucl. Phys. Proc. Suppl. **140** (2005) 832 [hep-lat/0409003].
- [27] S. Aoki *et al.* [PACS-CS Collaboration], Phys. Rev. D **79**, 034503 (2009) [arXiv:0807.1661 [hep-lat]].

Forces between static-light mesons

Marc Wagner*

Humboldt-Universität zu Berlin, Institut für Physik, Newtonstraße 15, D-12489 Berlin, Germany

E-mail: mcwagner@physik.hu-berlin.de



The isospin, spin and parity dependent potential of a pair of static-light mesons is computed using Wilson twisted mass lattice QCD with two flavors of degenerate dynamical quarks. From the results a simple rule can be deduced stating, which isospin, spin and parity combinations correspond to attractive and which to repulsive forces.

*The XXVIII International Symposium on Lattice Field Theory, Lattice2010
June 14-19, 2010
Villasimius, Italy*

*Speaker.

1. Introduction

Lattice computations of the potential of a pair of static-light mesons (in the following also referred to as B mesons) are of interest, because they constitute first principles determinations of a hadronic force. Until now interactions between static-light mesons have exclusively been studied in the quenched approximation [1, 2]. Here I report on the status of an investigation with two flavors of dynamical Wilson twisted mass quarks. Forces are not only studied between the lightest static-light mesons (denoted by S), but also first excitations are taken into account (denoted by P_-). Note that there is another ongoing study of static-light meson interactions with dynamical quarks, which has also been reported during this conference [3].

2. Trial states and quantum numbers

2.1 Static-light mesons

Here I consider static-light mesons, which are made from a static antiquark \bar{Q} and a light quark $\psi \in \{u, d\}$. Consequently, isospin $I = 1/2$ and $I_z \in \{-1/2, +1/2\}$. Since there are no interactions involving the static quark spin, it is appropriate to classify static-light mesons by the angular momentum of their light degrees of freedom j . I do not consider non-trivial gluonic excitations, hence $j = 1/2$ and $j_z = \{-1/2, +1/2\}$, which is the spin of the light u/d quark. Parity is also a quantum number, $\mathcal{P} \in \{+, -\}$.

The lightest static-light meson has quantum numbers $j^{\mathcal{P}} = (1/2)^-$ (denoted by S). The first excitation, which is $\approx 400\text{MeV}$ heavier, has quantum numbers $j^{\mathcal{P}} = (1/2)^+$ (denoted by P_-). Examples of corresponding static-light meson trial states are $\bar{Q}\gamma_5\psi|\Omega\rangle$ and $\bar{Q}\gamma_j\psi|\Omega\rangle$ for S mesons and $\bar{Q}\psi|\Omega\rangle$ and $\bar{Q}\gamma_j\gamma_5\psi|\Omega\rangle$ for P_- mesons respectively.

For a more detailed discussion of static-light mesons I refer to [4, 5].

2.2 BB systems

The aim of this work is to determine the potential of a pair of B mesons as a function of their separation R (without loss of generality I choose the axis of separation to be the z axis). To this end one has to compute the energy of eigenstates of the Hamiltonian containing two static antiquarks $\bar{Q}(\mathbf{r}_1)$ and $\bar{Q}(\mathbf{r}_2)$, $\mathbf{r}_1 = (0, 0, -R/2)$ and $\mathbf{r}_2 = (0, 0, +R/2)$, which define the positions of the two B mesons, and which will be surrounded by light quarks and gluons.

These BB states are characterized by several quantum numbers. Since there are two light u/d valence quarks, isospin $I \in \{0, 1\}$ and $I_z \in \{-1, 0, +1\}$. Due to the separation of the static antiquarks along the z axis, rotational symmetry is restricted to rotations around this axis. Consequently, states can be classified by the z component of total angular momentum. However, as already mentioned in section 2.1 there are no interactions involving the static quark spin. Therefore, it is appropriate to label BB states by the z component of the angular momentum of the light degrees of freedom $j_z \in \{-1, 0, +1\}$. Parity is also a symmetry and, therefore, a quantum number, $\mathcal{P} \in \{+, -\}$. For states with $j_z = 0$ there is an additional symmetry, reflection along an axis perpendicular to the axis of separation (without loss of generality I choose the x axis). The corresponding quantum number is $\mathcal{P}_x \in \{+, -\}$. When using $|j_z|$ instead of j_z , \mathcal{P}_x is a quantum

number for all states. To summarize, BB states can be characterized by the following five quantum numbers: $(I, I_z, |j_z|, \mathcal{P}, \mathcal{P}_x)$.

I use BB trial states

$$(\mathcal{C}\Gamma)_{AB} \left(\bar{Q}_C(\mathbf{r}_1) \psi_A^{(1)}(\mathbf{r}_1) \right) \left(\bar{Q}_C(\mathbf{r}_2) \psi_B^{(2)}(\mathbf{r}_2) \right) |\Omega\rangle, \quad (2.1)$$

where the lower indices A , B and C denote spinor indices, $\mathcal{C} = \gamma_0\gamma_2$ is the charge conjugation matrix and Γ is a combination of γ matrices. Note that it is essential to couple the light degrees of freedom of both mesons in spinor space, because these degrees of freedom determine the quantum number $|j_z|$. Proceeding in a naive way by coupling light and static degrees of freedom in both B mesons separately will not result in a well defined angular momentum $|j_z|$ and, therefore, will mix different sectors. To obtain $I = 0$, the flavors of the light quarks have to be chosen according to $\psi^{(1)}\psi^{(2)} = ud - du$, while for $I = 1$ three possibilities exist, $\psi^{(1)}\psi^{(2)} \in \{uu, dd, ud + du\}$. BB trial states are collected in Table 1 together with their quantum numbers.

		$\psi^{(1)}\psi^{(2)} = ud - du$		$\psi^{(1)}\psi^{(2)} = ud + du$		$\psi^{(1)}\psi^{(2)} \in \{uu, dd\}$	
Γ	$ j_z $	$\mathcal{P}, \mathcal{P}_x$	result	$\mathcal{P}, \mathcal{P}_x$	result	$\mathcal{P}, \mathcal{P}_x$	result
γ_5	0	-, +	A, SS	+, +	R, SS	+, +	R, SS
$\gamma_0\gamma_5$	0	-, +	A, SS	+, +	R, SS	+, +	R, SS
1	0	+, -	A, SP	-, -	R, SP	-, -	R, SP
γ_0	0	-, -	R, SP	+, -	A, SP	+, -	A, SP
γ_3	0	+, -	R, SS	-, -	A, SS	-, -	A, SS
$\gamma_0\gamma_3$	0	+, -	R, SS	-, -	A, SS	-, -	A, SS
$\gamma_3\gamma_5$	0	+, +	A, SP	-, +	R, SP	-, +	R, SP
$\gamma_0\gamma_3\gamma_5$	0	-, +	R, SP	+, +	A, SP	+, +	A, SP
$\gamma_{1/2}$	1	+, ±	R, SS	-, ±	A, SS	-, ±	A, SS
$\gamma_0\gamma_{1/2}$	1	+, ±	R, SS	-, ±	A, SS	-, ±	A, SS
$\gamma_{1/2}\gamma_5$	1	+, ∓	A, SP	-, ∓	R, SP	-, ∓	R, SP
$\gamma_0\gamma_{1/2}\gamma_5$	1	-, ∓	R, SP	+, ∓	A, SP	+, ∓	A, SP

Table 1: quantum numbers of BB trial states; due to explicit isospin breaking, $(I = 1, I_z = 0)$ and $(I = 1, I_z = \pm 1)$ states are not degenerate in twisted mass lattice QCD (cf. section 3) and, therefore, listed separately; “result” characterizes the shapes of the numerically computed BB potentials (A: attractive potential; R: repulsive potential; SS: lower asymptotic value $2m(S)$; SP: higher asymptotic value $m(S) + m(P_-)$; cf. section 4).

3. Lattice setup

I use $24^3 \times 48$ gauge field configurations generated by the European Twisted Mass Collaboration (ETMC). The fermion action is $N_f = 2$ Wilson twisted mass,

$$S_F[\chi, \bar{\chi}, U] = a^4 \sum_x \bar{\chi}(x) \left(D_W + i\mu_q \gamma_5 \tau_3 \right) \chi(x) \quad (3.1)$$

[6, 7], where D_W is the standard Wilson Dirac operator and $\chi = (\chi^{(u)}, \chi^{(d)})$ is the light quark doublet in the so-called twisted basis. In the continuum the twisted basis is related to the physical basis by the twist rotation $\psi = e^{i\gamma_5 \tau_3 \omega/2} \chi$, where ω is the twist angle. ω has been tuned to maximal twist, i.e. $\omega = \pi/2$, where static-light mass differences are automatically $\mathcal{O}(a)$ improved. The gauge action is tree-level Symanzik improved [8]. I use $\beta = 3.9$ and $\mu_q = 0.0040$ corresponding to a lattice spacing $a = 0.079(3)$ fm and a pion mass $m_{PS} = 340(13)$ MeV [9]. For details regarding these gauge field configurations I refer to [10, 11].

In twisted mass lattice QCD at finite lattice spacing SU(2) isospin is explicitly broken to U(1), i.e. I_z is still a quantum number, but I is not. Moreover, parity \mathcal{P} has to be replaced by twisted mass parity $\mathcal{P}^{(tm)}$, which is parity combined with light flavor exchange. The consequence is that twisted mass BB sectors are either labeled by $(I_z, |j_z|, \mathcal{P}^{(tm)} \mathcal{P}_x^{(tm)})$ for $I_z = \pm 1$ or by $(I_z, |j_z|, \mathcal{P}^{(tm)}, \mathcal{P}_x^{(tm)})$ for $I_z = 0$. A comparison with the set of quantum numbers discussed in section 2.2 shows that in the twisted mass formalism there are only half as many BB sectors as in QCD, i.e. QCD BB sectors are pairwise combined. Nevertheless, it is possible to unambiguously interpret states obtained from twisted mass correlation functions in terms of QCD quantum numbers. The method has successfully been applied in the context of static-light mesons [12] and is explained in detail for kaons and D mesons in [13]. For a detailed discussion of twisted mass symmetries in the context of BB systems I refer to an upcoming publication [14].

When computing correlation functions, I use several techniques to improve the signal quality including operator optimization by means of APE and Gaussian smearing and stochastic propagators combined with timeslice dilution. These techniques are very similar to those used in a recent study of the static-light meson spectrum [4, 5] and will also be explained in detail in [14].

In contrast to spectrum calculations for static-light mesons [4, 5] and static-light baryons [15], where we have always used the HYP2 static action, I perform computations both with the HYP2 static action and with unsmeared links representing the world lines of the static antiquarks. In particular for small $\bar{Q}\bar{Q}$ separations $R \lesssim 2a$ ultraviolet fluctuations are important, which are, however, filtered out, when using HYP smeared links. The effect of HYP smearing is shown in Figure 1. For all results presented in the following potential values corresponding to $R \leq 2a$ have been computed by means of unsmeared links, while for larger separations HYP smearing has been applied to improve the signal-to-noise ratio.

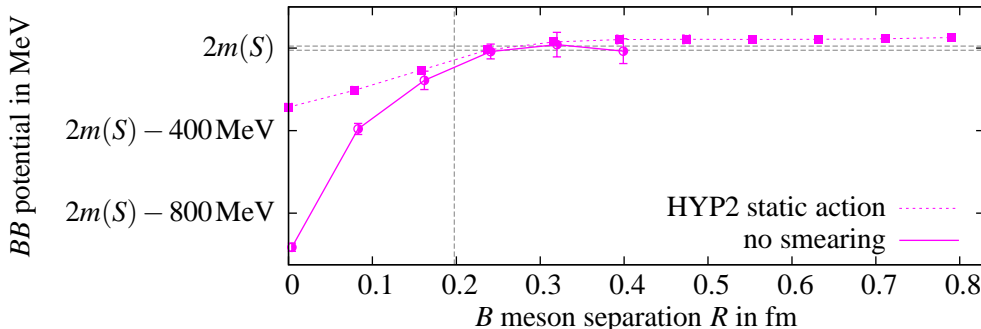


Figure 1: the BB potential corresponding to $\psi^{(1)} \psi^{(2)} = uu$, $\Gamma = \gamma_3$ computed with unsmeared links and with the HYP2 static action.

4. Numerical results

The BB potentials presented and discussed in the following have been obtained by fitting constants to effective mass plateaus obtained from temporal correlation functions of trial states (2.1). In twisted mass lattice QCD there are 24 independent $I_z = 0$ trial states (i.e. trial states not related by symmetries) and 12 independent $I_z = \pm 1$ trial states, i.e. 36 resulting potentials, which are not related by symmetries (cf. Table 1). Some of these potentials are quite similar, while others are not. In total there are four significantly different types of potentials: two of them are attractive, the other two are repulsive; two have asymptotic values for large separations R , which are larger by around 400 MeV compared to the other two (cf. the “result” columns of Table 1). For each of the four types an example is plotted in Figure 2.

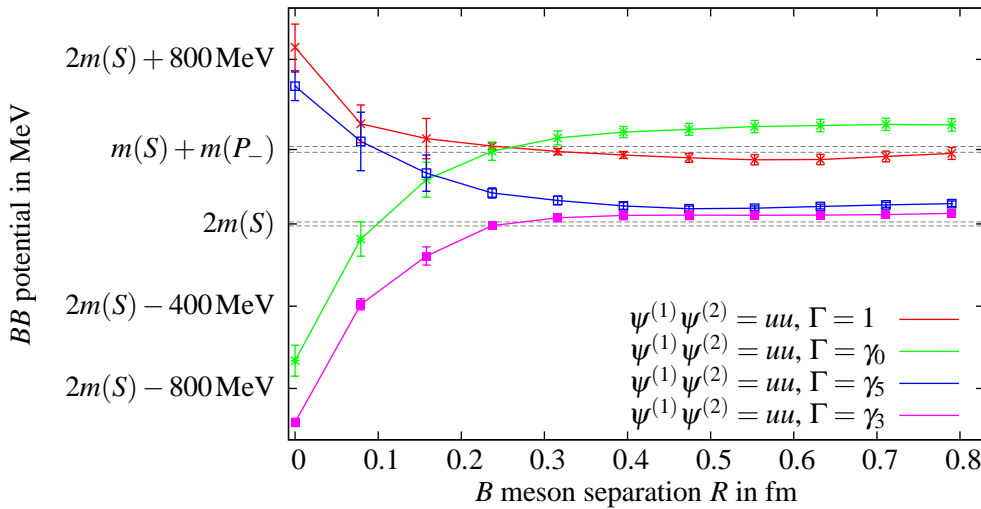


Figure 2: examples of BB potentials as functions of the separation R .

To understand the asymptotic behavior, it is convenient to express the BB creation operators appearing in (2.1) in terms of static-light meson creation operators. For the potentials shown in Figure 2 one finds after some linear algebra

$$\begin{aligned} (\mathcal{C}1)_{AB} & \left(\bar{Q}_C(\mathbf{r}_1) u_A(\mathbf{r}_1) \right) \left(\bar{Q}_C(\mathbf{r}_2) u_B(\mathbf{r}_2) \right) = \\ & = -S_\uparrow(\mathbf{r}_1) P_{-\downarrow}(\mathbf{r}_2) + S_\downarrow(\mathbf{r}_1) P_{-\uparrow}(\mathbf{r}_2) - P_{-\uparrow}(\mathbf{r}_1) S_\downarrow(\mathbf{r}_2) + P_{-\downarrow}(\mathbf{r}_1) S_\uparrow(\mathbf{r}_2) \end{aligned} \quad (4.1)$$

$$\begin{aligned} (\mathcal{C}\gamma_0)_{AB} & \left(\bar{Q}_C(\mathbf{r}_1) u_A(\mathbf{r}_1) \right) \left(\bar{Q}_C(\mathbf{r}_2) u_B(\mathbf{r}_2) \right) = \\ & = -S_\uparrow(\mathbf{r}_1) P_{-\downarrow}(\mathbf{r}_2) + S_\downarrow(\mathbf{r}_1) P_{-\uparrow}(\mathbf{r}_2) + P_{-\uparrow}(\mathbf{r}_1) S_\downarrow(\mathbf{r}_2) - P_{-\downarrow}(\mathbf{r}_1) S_\uparrow(\mathbf{r}_2) \end{aligned} \quad (4.2)$$

$$\begin{aligned} (\mathcal{C}\gamma_5)_{AB} & \left(\bar{Q}_C(\mathbf{r}_1) u_A(\mathbf{r}_1) \right) \left(\bar{Q}_C(\mathbf{r}_2) u_B(\mathbf{r}_2) \right) = \\ & = -S_\uparrow(\mathbf{r}_1) S_\downarrow(\mathbf{r}_2) + S_\downarrow(\mathbf{r}_1) S_\uparrow(\mathbf{r}_2) - P_{-\uparrow}(\mathbf{r}_1) P_{-\downarrow}(\mathbf{r}_2) + P_{-\downarrow}(\mathbf{r}_1) P_{-\uparrow}(\mathbf{r}_2) \end{aligned} \quad (4.3)$$

$$\begin{aligned} (\mathcal{C}\gamma_3)_{AB} & \left(\bar{Q}_C(\mathbf{r}_1) u_A(\mathbf{r}_1) \right) \left(\bar{Q}_C(\mathbf{r}_2) u_B(\mathbf{r}_2) \right) = \\ & = -iS_\uparrow(\mathbf{r}_1) S_\downarrow(\mathbf{r}_2) - iS_\downarrow(\mathbf{r}_1) S_\uparrow(\mathbf{r}_2) + iP_{-\uparrow}(\mathbf{r}_1) P_{-\downarrow}(\mathbf{r}_2) + iP_{-\downarrow}(\mathbf{r}_1) P_{-\uparrow}(\mathbf{r}_2). \end{aligned} \quad (4.4)$$

At large separations R the BB potentials are expected to approach the sum of the masses of the two individual B mesons. When considering (4.1) to (4.4) and Figure 2, one can see that the two potentials with the lower asymptotic value ($\psi^{(1)}\psi^{(2)} = uu$, $\Gamma = \gamma_5$ and $\psi^{(1)}\psi^{(2)} = uu$, $\Gamma = \gamma_3$) contain SS combinations. These are significantly lighter than the also present P_-P_- combinations and should, therefore, dominate the correlation functions and effective masses at large temporal separations. The asymptotic value of the corresponding potentials should be around $2m(S)$, which is the case. In contrast to that the other two potentials with the higher asymptotic value ($\psi^{(1)}\psi^{(2)} = uu$, $\Gamma = 1$ and $\psi^{(1)}\psi^{(2)} = uu$, $\Gamma = \gamma_0$) exclusively contain SP_- combinations. Their asymptotic value is expected at around $m(S) + m(P_-)$, which is also reflected by Figure 2.

This expansion of BB creation operators in terms of static-light meson creation operators also provides an explanation, why potentials computed with different operators, but which have identical quantum numbers, are of different type. An example is given by $\psi^{(1)}\psi^{(2)} = uu$, $\Gamma = \gamma_3$ and $\psi^{(1)}\psi^{(2)} = uu$, $\Gamma = 1$, both having quantum numbers ($I = 1, I_z = +1, |j_z| = 0, \mathcal{P} = -, \mathcal{P}_x = -$). The $\Gamma = \gamma_3$ potential is attractive with an asymptotic value at around $2m(S)$, while the $\Gamma = 1$ potential is repulsive with an asymptotic value at around $m(S) + m(P_-)$. From (4.1) and (4.4) one can read off that the static-light meson content is essentially “orthogonal”: the $\Gamma = \gamma_3$ operator contains SS and P_-P_- combinations, whereas the $\Gamma = 1$ operator is exclusively made from SP_- combinations. While the corresponding $\Gamma = \gamma_3$ correlator yields the ground state in the ($I = 1, I_z = +1, |j_z| = 0, \mathcal{P} = -, \mathcal{P}_x = -$) sector, which closely resembles a pair of S mesons, the $\Gamma = 1$ operator mainly excites the first excitation, which is similar to an SP_- combination. The generated ground state overlap is, therefore, rather small and, consequently, very large temporal separations would be needed to extract the ground state potential. Presumably, the potential corresponding to the $\Gamma = 1$ operator has a small ground state contribution, which contaminates the first excited state potential. This is supported by the observation that the asymptotic value of the $\Gamma = 1$ potential is slightly lower than $m(S) + m(P_-)$. For a clean extraction of this first excited state an analysis of a 2×2 correlation matrix is needed.

From the 36 independent potentials one can also deduce a rule stating, whether a BB potential is attractive or repulsive. The rule is quite simple.

A BB potential is attractive, if the trial state is symmetric under meson exchange, repulsive, if the trial state is antisymmetric under meson exchange.

Here meson exchange means exchange of flavor, spin and parity. One can easily verify this rule for the examples discussed above: the operators (4.2) and (4.4) are symmetric under meson exchange and give rise to attractive potentials, while the operators (4.1) and (4.3) are antisymmetric under meson exchange and yield repulsive potentials. This more general rule is in agreement to what has been observed in quenched BB computations for SS potentials [1, 2].

5. Conclusions

I have presented results of an ongoing computation of BB potentials. Various channels characterized by the quantum numbers ($I, I_z, |j_z|, \mathcal{P}, \mathcal{P}_x$) have been investigated. The computations have been performed with dynamical, rather light quark masses ($mps \approx 340\text{MeV}$). The results have been interpreted in terms of individual S and P_- mesons. A simple rule has been established stating, whether a BB potential is attractive or repulsive.

The statistical accuracy of the correlation functions needs to be improved. BB systems are rather heavy and, hence, effective masses are quickly lost in noise. At the present level of statistics slight contamination from excited states cannot be excluded. To this end contractions are ongoing.

Future plans include studying the light quark mass dependence, the continuum limit and finite volume effects. Moreover, also BB_s and B_sB_s potentials could be computed. To treat the s quark as a fully dynamical quark, such computations should be performed on $N_f = 2 + 1 + 1$ flavor gauge field configurations currently produced by ETMC [16]. It would also be interesting to supplement the lattice computation by a perturbative calculation of BB potentials at small separations $R \lesssim 2$. Finally, one could use the obtained BB potentials as input for phenomenological considerations to answer e.g. the question, whether two B mesons are able to form a bound state.

Acknowledgments

I acknowledge useful discussions with Pedro Bicudo, William Detmold, Rudolf Faustov, Roberto Frezzotti, Vladimir Galkin, Chris Michael and Attila Nagy. This work has been supported in part by the DFG Sonderforschungsbereich TR9 Computergestützte Theoretische Teilchenphysik.

References

- [1] C. Michael and P. Pennanen [UKQCD Collaboration], Phys. Rev. D **60**, 054012 (1999) [arXiv:hep-lat/9901007].
- [2] W. Detmold, K. Orginos and M. J. Savage, Phys. Rev. D **76**, 114503 (2007) [arXiv:hep-lat/0703009].
- [3] G. Bali and M. Hetzenegger, talk by M. Hetzenegger at “XXVIIIth International Symposium on Lattice Field Theory”, Villasimius, Sardinia (2010).
- [4] K. Jansen, C. Michael, A. Shindler and M. Wagner [ETM Collaboration], JHEP **0812**, 058 (2008) [arXiv:0810.1843 [hep-lat]].
- [5] C. Michael, A. Shindler and M. Wagner [ETM Collaboration], arXiv:1004.4235 [hep-lat].
- [6] R. Frezzotti, P. A. Grassi, S. Sint and P. Weisz [Alpha collaboration], JHEP **0108**, 058 (2001) [arXiv:hep-lat/0101001].
- [7] R. Frezzotti and G. C. Rossi, JHEP **0408**, 007 (2004) [arXiv:hep-lat/0306014].
- [8] P. Weisz, Nucl. Phys. B **212**, 1 (1983).
- [9] R. Baron *et al.* [ETM Collaboration], arXiv:0911.5061 [hep-lat].
- [10] Ph. Boucaud *et al.* [ETM Collaboration], Phys. Lett. B **650**, 304 (2007) [arXiv:hep-lat/0701012].
- [11] P. Boucaud *et al.* [ETM collaboration], Comput. Phys. Commun. **179**, 695 (2008) [arXiv:0803.0224 [hep-lat]].
- [12] B. Blossier, M. Wagner and O. Pene [European Twisted Mass Collaboration], JHEP **0906**, 022 (2009) [arXiv:0903.2298 [hep-lat]].
- [13] R. Baron *et al.* [ETM Collaboration], arXiv:1005.2042 [hep-lat].
- [14] M. Wagner [ETM Collaboration], to be published.
- [15] M. Wagner and C. Wiese [ETM Collaboration], arXiv:1008.0653 [hep-lat].
- [16] R. Baron *et al.* [ETM Collaboration], JHEP **1006**, 111 (2010) [arXiv:1004.5284 [hep-lat]].

HU-EP-11/14, SFB/CPP-11-15

Static-static-light-light tetraquarks in lattice QCD*

MARC WAGNER

Humboldt-Universität zu Berlin, Institut für Physik, Newtonstraße 15,
D-12489 Berlin, Germany

I report on a lattice computation of the energy of a system of two light quarks and two static antiquarks as a function of the separation of the static antiquarks. In terms of hadrons such a system corresponds to a pair of B mesons and its energy to the hadronic potential. I present selected results for different isospin, spin and parity combinations of the individual B mesons mainly focusing on those channels relevant to determine, whether two B mesons may form a bound tetraquark state.

PACS numbers: 12.38.Gc, 13.75.Lb, 14.40.Nd.

1. Introduction

Lattice computations of the potential of a pair of static-light mesons (in the following also referred to as B mesons) are of interest, because they constitute first principles determinations of a hadronic force. Such potentials can e.g. be used as input for phenomenological calculations to determine, whether two B mesons may form a bound tetraquark state.

In the literature interactions between static-light mesons have been studied in the quenched approximation [1, 2, 3, 4, 5] and recently also with dynamical quarks [6, 7]. Here I report on the status of an investigation with two flavors of dynamical Wilson twisted mass quarks. Forces are not only studied between the lightest static-light mesons (denoted by S), but for the first time also first excitations are taken into account (denoted by P_-).

* Presented at “Excited QCD 2011”, 20–25 February 2011, Les Houches, France.

2. Trial states and quantum numbers

Quantum numbers of single static-light mesons as well as of pairs of static-light mesons (BB systems) have been discussed in detail in [6]. In the following I give a brief summary.

2.1. Static-light mesons

I consider static-light mesons made from a static antiquark \bar{Q} and a light quark $\psi \in \{u, d\}$ without non-trivial gluonic excitations. They can be labeled by the z -component of isospin $I_z = \pm 1/2$, the z -component of the light quark spin $j_z = \pm 1/2$ and parity $\mathcal{P} = \pm$. The $\mathcal{P} = -$ static-light meson (denoted by S , corresponding to B/B^* in [8]) is the lightest static-light meson. It is lighter by around 400 MeV than its parity partner with $\mathcal{P} = +$ (denoted by P_- , corresponding to B_0^* and B_1^*).

The corresponding static-light meson trial states are $\bar{Q}\gamma_5\psi|\Omega\rangle$ and $\bar{Q}\gamma_j\psi|\Omega\rangle$ for S mesons and $\bar{Q}\psi|\Omega\rangle$ and $\bar{Q}\gamma_j\gamma_5\psi|\Omega\rangle$ for P_- mesons, respectively.

For a more detailed discussion of static-light mesons I refer to [9, 10].

2.2. BB systems

The aim of this work is to compute the potential of a pair of B mesons as a function of their separation R (without loss of generality I choose the axis of separation to be the z axis). To this end one has to compute the energies of eigenstates of the QCD Hamiltonian containing two static antiquarks $\bar{Q}(\mathbf{r}_1)$ and $\bar{Q}(\mathbf{r}_2)$, $\mathbf{r}_1 = (0, 0, -R/2)$ and $\mathbf{r}_2 = (0, 0, +R/2)$, which define the positions of the two B mesons, and which will be surrounded by light quarks and gluons.

These BB states are characterized by the following five quantum numbers: isospin $I \in \{0, 1\}$, the z -component of isospin $I_z \in \{-1, 0, +1\}$, the absolute value of the z -component of the light quark spin $|j_z| \in \{0, 1\}$, parity $\mathcal{P} = \pm$ and “ x -parity” (reflection along the x -axis) $\mathcal{P}_x = \pm$.

I use BB trial states

$$(\mathcal{C}\Gamma)_{AB} \left(\bar{Q}_C(\mathbf{r}_1)\psi_A^{(1)}(\mathbf{r}_1) \right) \left(\bar{Q}_C(\mathbf{r}_2)\psi_B^{(2)}(\mathbf{r}_2) \right) |\Omega\rangle, \quad (1)$$

where the lower indices A , B and C denote spinor indices, $\mathcal{C} = \gamma_0\gamma_2$ is the charge conjugation matrix and Γ is a suitably chosen combination of γ matrices. Note that it is essential to couple the light degrees of freedom of both mesons in spinor space, because these degrees of freedom determine the quantum number $|j_z|$. Proceeding in a naive way by coupling light and static degrees of freedom in both B mesons separately will not result in a well defined angular momentum $|j_z|$ and, therefore, will mix different

BB sectors. To obtain $I = 0$, the flavors of the light quarks have to be chosen according to $\psi^{(1)}\psi^{(2)} = ud - du$, while for $I = 1$ three possibilities exist, $\psi^{(1)}\psi^{(2)} \in \{uu, dd, ud + du\}$. For a list of BB trial states and their quantum numbers I refer to [6], Table 1.

3. Lattice setup

I use $24^3 \times 48$ gauge field configurations generated by the European Twisted Mass Collaboration (ETMC). The fermion action is $N_f = 2$ Wilson twisted mass [11, 12] at maximal twist, where static-light mass differences are automatically $\mathcal{O}(a)$ improved [9]. The gauge action is tree-level Symanzik improved [13]. I use gauge coupling $\beta = 3.9$ and light quark mass $\mu_q = 0.0040$ corresponding to a lattice spacing $a = 0.079(3)$ fm and a pion mass $m_{PS} = 340(13)$ MeV [14]. For details regarding these gauge field configurations I refer to [15, 16].

In twisted mass lattice QCD at finite lattice spacing SU(2) isospin is explicitly broken to U(1), i.e. I_z is still a quantum number, but I is not. Moreover, parity \mathcal{P} has to be replaced by twisted mass parity $\mathcal{P}^{(tm)}$, which is parity combined with light flavor exchange. The consequence is that there are only half as many BB sectors in twisted mass lattice QCD as there are in QCD, i.e. QCD BB sectors are pairwise combined. Nevertheless, it is possible to unambiguously interpret states obtained from twisted mass correlation functions in terms of QCD quantum numbers. The method has successfully been applied in the context of static-light mesons [17] and is explained in detail for kaons and D mesons in [18]. For a more elaborate discussion of twisted mass symmetries in the context of BB systems I refer to an upcoming publication [19].

4. Selected numerical results

The potential of a pair of B mesons is extracted from the exponential falloff of correlation functions of trial states (1). As explained in subsection 2.2 the trial states differ by the spin coupling of the light quarks via the 4×4 matrix Γ (16 possibilities) and by their light quark flavor (4 possibilities). Consequently, there are $16 \times 4 = 64$ different correlation functions. This number can also be understood from the point of view of individual B mesons: since each of the two B mesons has 8 possibilities regarding quantum numbers ($I_z = \pm 1/2, j_z = \pm 1/2, \mathcal{P} = \pm$), there should be $8 \times 8 = 64$ BB correlation functions.

As outlined in subsection 2.2 the BB trial states (1) can be classified according to BB quantum numbers. However, to interpret the BB potential obtained from the correlation function of a specific trial state (1), it is

also useful to express this trial state in terms of individual B mesons, e.g.

$$\begin{aligned}\psi^{(1)}\psi^{(2)} &= ud - du, \quad \Gamma = \gamma_5 \quad \rightarrow \quad (-S_\uparrow S_\downarrow + S_\downarrow S_\uparrow - P_\uparrow P_\downarrow + P_\downarrow P_\uparrow)|\Omega\rangle \\ \psi^{(1)}\psi^{(2)} &= ud - du, \quad \Gamma = \gamma_0\gamma_5 \quad \rightarrow \quad (-S_\uparrow S_\downarrow + S_\downarrow S_\uparrow + P_\uparrow P_\downarrow - P_\downarrow P_\uparrow)|\Omega\rangle,\end{aligned}$$

where S and P denote creation operators for S and P_- mesons, respectively, and \uparrow and \downarrow indicate the orientation of the light quark spin. After linearly combining the two trial states via $\Gamma = \gamma_5 + \gamma_0\gamma_5$ to eliminate the P_-P_- contributions, one can extract an SS potential with quantum numbers $(I, I_z, |j_z|, \mathcal{P}, \mathcal{P}_x) = (0, 0, 0, -, +)$. Similarly, one can estimate a P_-P_- potential with the same quantum numbers by choosing $\Gamma = \gamma_5 - \gamma_0\gamma_5$. Results are shown in Figure 1(a). Further examples are discussed in [6].

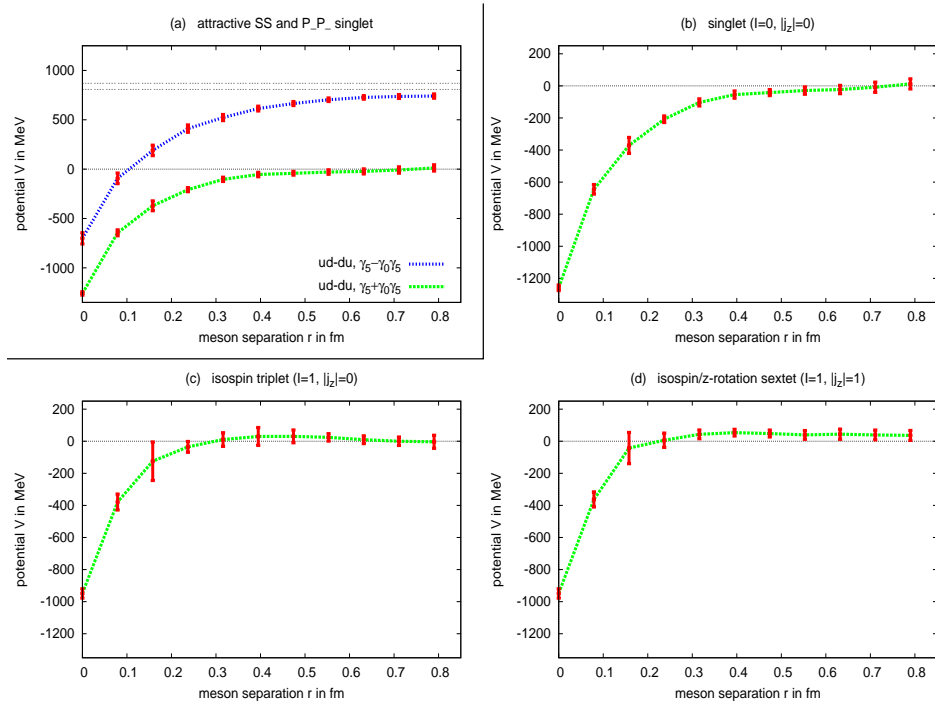


Fig. 1. BB potentials as functions of the meson separation. (a) SS potential and P_-P_- potential both with quantum numbers $(I, I_z, |j_z|, \mathcal{P}, \mathcal{P}_x) = (0, 0, 0, -, +)$. (b), (c), (d) Attractive SS singlet, isospin triplet and isospin/spin sextet.

BB potentials mainly differ in their asymptotic value at large meson separations, which is approximately $2m(S)$, $m(S) + m(P_-)$ or $2m(P_-)$ for SS , SP_- or P_-P_- combinations, respectively, and whether they are attractive or repulsive at small meson separations. Some of the potentials, even

though they differ in their quantum numbers, are exactly degenerate due to isospin symmetry ($I = 1$ triplets) or rotational symmetry around the z -axis ($|j_z| = 1$ doublets). In summary the number of attractive and repulsive BB potentials for SS , SP_- and P_-P_- combinations and their degeneracies are as follows:

SS potentials,	attractive: $1 \oplus 3 \oplus 6$	(10 states).
	repulsive: $1 \oplus 3 \oplus 2$	(6 states).
SP_- potentials,	attractive: $1 \oplus 1 \oplus 3 \oplus 3 \oplus 2 \oplus 6$	(16 states).
	repulsive: $1 \oplus 1 \oplus 3 \oplus 3 \oplus 2 \oplus 6$	(16 states).
P_-P_- potentials:	identical to SS potentials	(16 states).

Consequently, from the 64 trial states (1) one can extract 24 different potentials.

Of particular interest, when asking, whether two B mesons may form a bound tetraquark state, are attractive SS potentials. As stated above there are three different possibilities, a singlet, an isospin triplet and an isospin/spin sextet. The three potentials are shown in Figure 1(b) to 1(d). While the triplet and the sextet are rather similar, the singlet is significantly different: it is deeper and wider and, therefore, probably the best candidate to start investigations, whether there are bound BB tetraquark states. Such phenomenological investigations will be part of a subsequent publication.

5. Conclusions

I have presented selected results of a first principles lattice computation of BB potentials. Various channels characterized by the quantum numbers ($I, I_z, |j_z|, \mathcal{P}, \mathcal{P}_x$) have been investigated. Compared to existing publications the computations have been performed with rather light dynamical quark mass ($m_{PS} \approx 340$ MeV). The results have been interpreted in terms of individual S and P_- mesons. Future plans include studying the light quark mass dependence, the continuum limit as well as finite volume effects. Moreover, also BB_s and B_sB_s potentials could be computed. To treat the s quark as a fully dynamical quark, such computations should be performed on $N_f = 2 + 1 + 1$ flavor gauge field configurations currently generated by ETMC [20]. Finally, one should use the obtained BB potentials as input for phenomenological considerations to answer e.g. the question, whether two B mesons are able to form a bound tetraquark state.

Acknowledgments

I thank the organizers of “Excited QCD 2011” for the invitation to give this talk. I acknowledge useful discussions with Pedro Bicudo, William Det-

mold, Rudolf Faustov, Roberto Frezzotti, Vladimir Galkin, Chris Michael and Attila Nagy. This work has been supported in part by the DFG Sonderforschungsbereich TR9 Computergestützte Theoretische Teilchenphysik.

REFERENCES

- [1] C. Stewart and R. Koniuk, Phys. Rev. D **57**, 5581 (1998) [arXiv:hep-lat/9803003].
- [2] C. Michael and P. Pennanen [UKQCD Collaboration], Phys. Rev. D **60**, 054012 (1999) [arXiv:hep-lat/9901007].
- [3] M. S. Cook and H. R. Fiebig, arXiv:hep-lat/0210054.
- [4] T. Doi, T. T. Takahashi and H. Suganuma, AIP Conf. Proc. **842**, 246 (2006) [arXiv:hep-lat/0601008].
- [5] W. Detmold, K. Orginos and M. J. Savage, Phys. Rev. D **76**, 114503 (2007) [arXiv:hep-lat/0703009].
- [6] M. Wagner [ETM Collaboration], PoS **LATTICE2010**, 162 (2010) [arXiv:1008.1538 [hep-lat]].
- [7] G. Bali and M. Hetzenegger, PoS **LATTICE2010**, 142 (2010) [arXiv:1011.0571 [hep-lat]].
- [8] K. Nakamura *et al.* [Particle Data Group], J. Phys. G **37**, 075021 (2010).
- [9] K. Jansen, C. Michael, A. Shindler and M. Wagner [ETM Collaboration], JHEP **0812**, 058 (2008) [arXiv:0810.1843 [hep-lat]].
- [10] C. Michael, A. Shindler and M. Wagner [ETM Collaboration], JHEP **1008**, 009 (2010) [arXiv:1004.4235 [hep-lat]].
- [11] R. Frezzotti, P. A. Grassi, S. Sint and P. Weisz [Alpha Collaboration], JHEP **0108**, 058 (2001) [arXiv:hep-lat/0101001].
- [12] R. Frezzotti and G. C. Rossi, JHEP **0408**, 007 (2004) [arXiv:hep-lat/0306014].
- [13] P. Weisz, Nucl. Phys. B **212**, 1 (1983).
- [14] R. Baron *et al.* [ETM Collaboration], arXiv:0911.5061 [hep-lat].
- [15] Ph. Boucaud *et al.* [ETM Collaboration], Phys. Lett. B **650**, 304 (2007) [arXiv:hep-lat/0701012].
- [16] P. Boucaud *et al.* [ETM Collaboration], Comput. Phys. Commun. **179**, 695 (2008) [arXiv:0803.0224 [hep-lat]].
- [17] B. Blossier, M. Wagner and O. Pene [ETM Collaboration], JHEP **0906**, 022 (2009) [arXiv:0903.2298 [hep-lat]].
- [18] R. Baron *et al.* [ETM Collaboration], Comput. Phys. Commun. **182**, 299 (2011) [arXiv:1005.2042 [hep-lat]].
- [19] M. Wagner [ETM Collaboration], to be published.
- [20] R. Baron *et al.* [ETM Collaboration], JHEP **1006**, 111 (2010) [arXiv:1004.5284 [hep-lat]].

Lattice QCD signal for a bottom-bottom tetraquark

Pedro Bicudo*

Dep. Física and CFTP, Instituto Superior Técnico, Av. Rovisco Pais, 1049-001 Lisboa, Portugal

Marc Wagner†

*Johann Wolfgang Goethe-Universität Frankfurt am Main, Institut für Theoretische Physik,
Max-von-Laue-Straße 1, D-60438 Frankfurt am Main, Germany and
European Twisted Mass Collaboration (ETMC)*

Utilizing lattice QCD results for the potential of two static antiquarks and two dynamical quarks as well as quark model techniques for the dynamics of two heavy antiquarks in a cloud of two light quarks, we are provided with an accurate framework for the study of possibly existing heavy-heavy-light-light tetraquarks. Among the possible quantum numbers of such a system, we find binding in only one channel, the scalar isosinglet. Solving the Schrödinger equation for the displacement of the heavy antiquarks and taking systematic errors into account, we find an antibottom-antibottom-light-light bound state with a confidence level of around $1.8\sigma \dots 3.0\sigma$ and binding energy of approximately 30 MeV ... 57 MeV.

PACS numbers: 12.38.Gc, 13.75.Lb, 14.40.Rt, 14.65.Fy.

I. INTRODUCTION

Experimentally exotic hadrons have been searched for many years, because as soon as quarks were proposed in the sixties, it became clear that systems more complex than mesons and baryons could possibly exist. However, exotic hadrons are very elusive systems. They are much harder to observe experimentally, to understand by theoretical model calculations, and to simulate by means of lattice QCD than the conventional mesons and baryons. To confirm the existence or non-existence of exotic hadrons still remains an important problem in QCD.

A frequently discussed exotic multiquark is the tetraquark. It was already proposed in the seventies [1] as a bound state formed by two quarks and two antiquarks. There are several hadronic resonances, which are tetraquark candidates, e.g. σ , κ , D_{s0}^* or D_{s1} [2]. The most recent tetraquark candidate has been claimed by the BELLE Collaboration [3], observing in five different $\Upsilon(5S)$ decay channels two new charged bottomonium resonances Z_b with masses 10610 MeV and 10650 MeV and narrow widths of the order of 15 MeV, where the charge can only come from the presence of a light quark and a light antiquark. However, the tetraquark nature of these resonance is disputed [4].

Notice that the experimental particle physics collaborations are technically improving rather impressively. One decade ago SELEX at FNAL already studied the doubly charmed baryons. Presently, BELLE at KEK, CDF and DØ at FNAL, and LHCb at CERN have already observed bottom hadrons. Thus, they may possibly be able to search, not only for bottom-antibottom tetraquarks, but also for bottom-bottom tetraquarks, in

case sufficiently strong evidence is presented by theoretical calculations.

Tetraquark studies face several difficulties. (1) Mesons and baryons only decay strongly when the confining string breaks, a quark antiquark pair is created and either two mesons or a meson and a baryon are formed. In contrast to that, tetraquarks are directly open to meson-meson decay. (2) Moreover, tetraquarks are relativistic four-body systems, which are highly complex few-body systems. (3) And on the top of these technical difficulties no model (since the onset of QCD [1] up to the present) seems to be sufficiently well calibrated to address multiquark binding: different quark models, even when producing similar meson or baryon spectra, usually differ significantly in predictions for tetraquarks. Exceptions are heavy four-quark systems, say an exotic $c\bar{c}b\bar{b}$, but these are extremely hard to investigate experimentally.

An example of a rather complex system to study in lattice QCD is a tetraquark including a b and a \bar{b} quark. It is very interesting, due to the BELLE observation [3] of $B^*\bar{B}$ and $B^*\bar{B}^*$ tetraquark candidates. However, it couples to at least five decay channels as reported by BELLE. Therefore, we study here in a first step the theoretically simpler BB system. In the near future we plan to extend our investigations to the $B\bar{B}$ tetraquark. Notice that the observation of a $B\bar{B}$ system at BELLE suggests that a BB tetraquark may also be observable in present day laboratories.

A strategy to avoid many technical difficulties associated with tetraquark studies consists in searching for bound states rather than for resonances, which is e.g. appropriate, when two heavy antiquarks (or equivalently two heavy quarks) are involved. This strategy was already identified in the eighties [5]. On the one hand, it is plausible that any light tetraquark can only be treated as a resonance, because it couples to two-meson channels with identical quantum numbers, where at least one

*Electronic address: bicudo@ist.utl.pt

†Electronic address: mwagner@th.physik.uni-frankfurt.de

of the mesons is a pion or kaon. Due to chiral symmetry, these are very light mesons and, consequently, the tetraquark will have a rather light open decay channel. On the other hand the presence of two heavy antiquarks is sufficient to force all involved hadrons, i.e. the tetraquark and any two-meson channels with the same quantum numbers, to escape chiral symmetry. Moreover, the heavy antiquarks also reduce the technical complexity of the four quark system, since heavy antiquarks are non-relativistic. This in turn allows for the Born-Oppenheimer approximation: for the light quarks the heavy antiquarks can be regarded as static color charges; once the energy of the light quarks is determined, it can be utilized as an effective potential for the heavy antiquarks.

II. HEAVY ANTIQUARK-ANTIQUARK INTERACTION

A. Lattice QCD results

The major theoretical problem remaining is, to obtain the correct effective potential, which has been studied by lattice QCD methods mainly in the quenched approximation (cf. e.g. [6–10]). Only recently computations of this potential with dynamical sea quarks have been performed [11–13].

Here we use such dynamical results obtained with a comprehensive set of four quark operators of the form

$$(\mathcal{C}\Gamma)_{AB} \left(\bar{Q}_C(\mathbf{r}_1)\psi_A^{(1)}(\mathbf{r}_1) \right) \left(\bar{Q}_C(\mathbf{r}_2)\psi_B^{(2)}(\mathbf{r}_2) \right), \quad (1)$$

where \bar{Q} denotes a static quark operator, ψ a light antiquark operator, A, B and C are spin indices and $\mathcal{C} = \gamma_0\gamma_2$ is the charge conjugation matrix [11, 13]. While for the static antiquarks the only relevant variable is their separation, the two light u/d quarks can be combined in $8 \times 8 = 64$ different ways via the 4×4 matrix Γ and the light quark flavors $\psi^{(1)}\psi^{(2)} \in \{ud - du, uu, ud + du, dd\}$ (each light quark has two isospin, two spin and two parity degrees of freedom). Symmetries and quantum numbers of such four-quark states are explained in detail in [11].

In this work we focus on the two attractive channels between ground state static-light mesons (B and B^* mesons): a scalar isosinglet (cf. Fig. 1(a)) with corresponding four-quark creation operator

$$\psi^{(1)}\psi^{(2)} = ud - du , \quad \Gamma = \gamma_5 + \gamma_0\gamma_5 , \quad (2)$$

which is most attractive, and a vector isotriplet (cf. Fig. 1(b)) with corresponding four-quark creation operator e.g.

$$\psi^{(1)}\psi^{(2)} = ud + du , \quad \Gamma = \gamma_3 + \gamma_0\gamma_3 , \quad (3)$$

which is less attractive. Note that these operators have not only specific quantum numbers, but also exhibit a structure particularly suited, to excite the ground state

(a system composed at large $b\bar{b}$ separations of pseudoscalar B and/or vector B^* mesons, but not of excited positive parity mesons such as B_0^* or B_1^*) as explained in [11, 13]. Consequently, the resulting potential does not depend on the details of the used operators. In particular, no additional assumption about the physical structure of the four-quark state is made or entering the computation. The arrangement of the four quarks is decided by QCD dynamics, i.e. automatically realized in the lattice result according to QCD (cf. e.g. also recent lattice work on tetraquark candidates, where it has been demonstrated that operators similar to (1) generate significant overlap to a variety of different four-quark structures including mesonic molecules, diquark-antidiquark pairs or two essentially non-interacting mesons [14–17]).

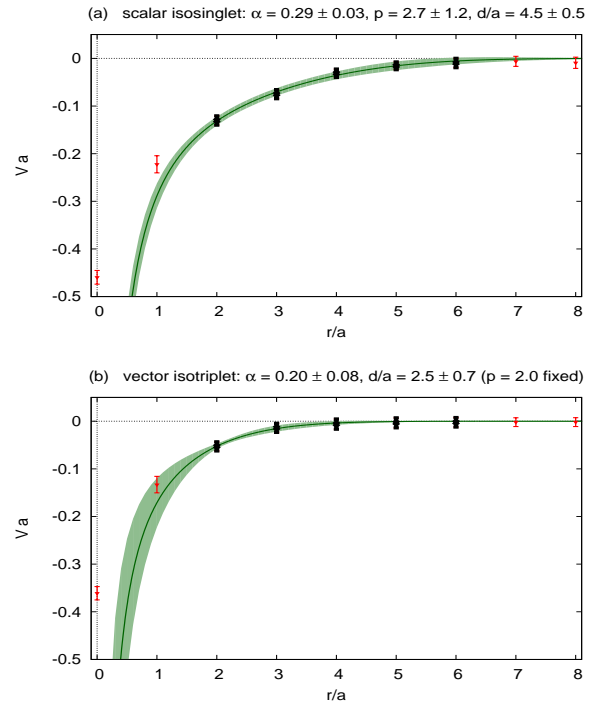


Figure 1: (Color online). The static antiquark-antiquark potential as a function of the separation in units of the lattice spacing $a \approx 0.079$ fm. (a) Three parameter fit (α, d, p) of ansatz (4) to the most attractive channel, the scalar isosinglet. (b) Two parameter fit ($\alpha, d; p = 2.0$ fixed) of ansatz (4) to the less attractive vector isotriplet.

For further details regarding the lattice computation of the heavy antiquark-antiquark interaction we refer to [11, 13].

B. Screening ansatz

To motivate an ansatz to fit the lattice results for these potentials, first remember that the pair of heavy antiquarks is immersed in a cloud of two light quarks.

The size of this cloud is crucial for the heavy antiquark-antiquark interaction. When the two antiquarks are much closer than twice the typical light quark cloud radius in a heavy-light meson, the antiquark-antiquark interaction is a typical diquark interaction (cf. Fig. 2(a)). However, when the separation of the two antiquarks becomes larger, the light quarks screen the heavy antiquark charges as in Fig. 2(b) and the antiquark-antiquark interaction vanishes.

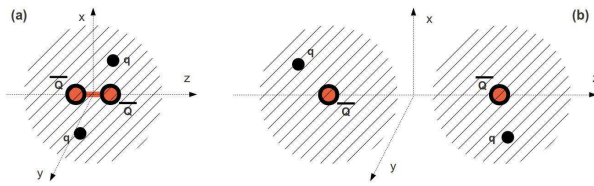


Figure 2: (Color online). Screening of the antidiquark flux tube interaction. We show two scenarios: (a) the heavy antiquarks are close and the screening of the light quarks has little effect on the antiquark-antiquark interaction; (b) the heavy quarks are well separated and their color charge is totally screened by the light quark wavefunctions.

The diquark interaction for systems containing only static quarks has also been studied by lattice QCD. Flux tubes have been observed for static baryons, static tetraquarks and static pentaquarks [18, 19]. It seems established that at large separations r the diquark potential is linear and confining $\sim \sigma r$. At small separations r the potential is rather Coulomb-like, i.e. $\sim -\alpha/r$. A similar system, which has been studied in even more detail by lattice methods is the “static-static meson” or static potential; here $\alpha \approx 0.3 \dots 0.4$, while $\sigma \approx (0.44 \text{ GeV})^2$ is estimated from quark model fits and often used to set the scale. For two heavy antidiquarks in a cloud of two light quarks we expect a similar Coulomb-like potential of order $-\alpha/r$ at small separations. At larger separations (in contrast to the purely static case) the potential should be screened by the light quarks, as discussed in the previous paragraph and illustrated in Fig. 2(b).

The screening of the heavy color charge is due to the decrease of the wave function ψ of the light quark with respect to its separation from the heavy quark. One expects this decrease to follow an exponential of a power law, i.e. $\psi(r) \propto \exp(-(r/d)^p)$, where d characterizes the size of the quark-antiquark system, i.e. a B meson. If the quark-antiquark interaction inside a B meson is dominated by a Coulomb-like term, the wave function is similar to that of a hydrogen atom, i.e. $p = 1$. In case the potential is rather linear, the non-relativistic Schrödinger equation is solved by Airy functions corresponding to $p = 3/2$. A similar, but relativistic treatment of the light quark yields $p = 2$ instead.

The above considerations suggest the following ansatz to model the heavy antiquark-antiquark potential:

$$V(r) = -\frac{\alpha}{r} \exp\left(-\left(\frac{r}{d}\right)^p\right), \quad (4)$$

where it is expected that $\alpha \approx 0.3 \dots 0.4$, d is around half the size of a B meson, i.e. $d \lesssim 0.5 \text{ fm}$, and $p \approx 1.0 \dots 2.0$.

C. Fitting procedure and results

We perform uncorrelated χ^2 minimizing fits of the ansatz (4) to the lattice results for the heavy antiquark-antiquark interactions shown in Fig. 1, i.e. we minimize

$$\chi^2 = \sum_{r=2a, \dots, 6a} \left(\frac{V(r) - V^{\text{latt}}(r)}{\Delta V^{\text{latt}}(r)} \right)^2 \quad (5)$$

with respect to the parameters α , d and p (V^{latt} denote the lattice results, ΔV^{latt} the corresponding statistical errors). Notice that data points for separations $r/a = 0$ and $r/a = 1$ are excluded from the fits, because they suffer from lattice discretization errors. For $r/a \geq 2$ it has been checked, that these discretization errors are negligible compared to the statistical errors by using different static quark actions [11]. On the other hand, data points for large separations have little relevance since the potential vanishes exponentially fast, due to screening, while the statistical error remains similar. Thus we utilize the points at distances $r/a = 2, 3, 4, 5, 6$ for our fits.

For the scalar isosinglet we are able to determine all three parameters α , d and p via fitting. For the vector isotriplet a three parameter fit is not stable; therefore, we only fit two parameters, α and d , while fixing the exponent to its expected value $p = 2.0$. The fits are also shown in Fig. 1, while numerical results are collected in Table I. Statistical errors for α , d and p have been determined via an elaborate Jackknife analysis starting on the level of the lattice correlation functions. In detail we proceeded as follows.

- (1) From the 480 available samples of the correlation functions of four quark operators (1) (corresponding to 480 gauge link configurations) we form 20 essentially independent bins by averaging each time over 24 consecutive gauge link configurations; this binning removes possibly existing correlations in Monte Carlo simulation time.
- (2) From these 20 bins we compute not only the average, but also 20 reduced samples, i.e. 20 correlation function averages over 19 of the available 20 bins, each time omitting a different bin.
- (3) On the average and on each reduced sample we compute the heavy antiquark-antiquark potential obtaining V^{latt} and $V^{\text{latt},\text{red},n}$, $n = 1, \dots, 20$, using standard lattice techniques (fitting constants to effective mass plateaus at sufficiently large temporal separations); these results are then used in a standard Jackknife analysis, to obtain a statistical error ΔV^{latt} .
- (4) The χ^2 minimizing fit of the ansatz (4) to lattice potential is not only performed for V^{latt} , but also for

the reduced samples $V^{\text{lat},\text{red},n}$, yielding (α, d, p) and $(\alpha^{\text{red},n}, d^{\text{red},n}, p^{\text{red},n})$ [or (α, d) and $(\alpha^{\text{red},n}, d^{\text{red},n})$]; as in step (3) a standard Jackknife analysis is used, to obtain statistical errors $(\Delta\alpha, \Delta d, \Delta p)$ [or $(\Delta\alpha, \Delta d)$].

The fit of the ansatz (4) to the lattice results is uncorrelated, because there are not sufficiently many lattice samples available, to estimate a covariance matrix appropriately. Note, however, that we use the same bins and reduced samples for all temporal separations of the correlation functions t and also for all spatial separations of the heavy antiquarks r . Therefore, these bins and reduced samples contain information about possibly existing correlations in t and in r , which in turn enters the resulting fit parameters α , d and p . In other words, although we do not minimize a correlated χ^2/dof , correlations are taken into account to some extent (cf. also [21], where in a similar context it has been demonstrated numerically that correlated and uncorrelated χ^2 minimization yield essentially identical results). Since we have only 2 [or 3] degrees of freedom (5 separations, 3 [or 2] fit parameters), not only $\chi^2/\text{dof} \ll 1$ but also $\chi^2 \lesssim 1$, which indicates consistency of the lattice data and our ansatz (4), even though we are currently not able, to determine a correlated χ^2/dof . Moreover, note that the resulting values for α , d and p are in agreement with phenomenological expectations.

Table I: χ^2 minimizing fit results of the ansatz (4) to the lattice static antiquark-antiquark potential; fitting range $2 \leq r/a \leq 6$; lattice spacing $a \approx 0.079$ fm

channel	α	d/a	p	χ^2/dof
scalar isosinglet	0.293(33)	4.51(54)	2.74(1.20)	0.35
vector isotriplet	0.201(77)	2.48(69)	2.0 (fixed)	0.06

III. HEAVY ANTIQUARK-ANTINUARK BINDING, EXISTENCE OF TETRAQUARKS

In Fig. 1 it is clear that, if the two \bar{Q} would be arbitrarily heavy, they would also go arbitrarily deep into the Coulomb potential. In this limit tetraquarks would have an arbitrarily large binding energy both in the scalar isosinglet and in the vector isotriplet channel. However, the heavy \bar{Q} have a finite mass and the question we now address is, whether the heavy quark mass is large enough, to bind our class of tetraquarks.

A. The antiquark-antiquark Hamiltonian

The potential of Eq. (4) with the fit parameters from Table I corresponds to the energy of a static-static-light-light four quark system minus the energy of a pair of

static-light ground state mesons. To obtain the energy of a heavy-heavy-light-light system, where the antiquarks have a heavy, but finite mass, one also needs to consider a kinetic term for the heavy antiquarks resulting in the Hamiltonian

$$H = \frac{\mathbf{p}^2}{2\mu} + 2m_B + V(r), \quad (6)$$

where μ is the reduced antiquark mass.

Notice that, because of screening, at large separations each heavy antiquark carries the mass of a B meson and thus $\mu = m_B/2$, whereas at small separations it carries just the energy of a heavy quark $\mu = m_b/2$. When investigating the existence of four quark bound states, we consider both mass values, which differ by around 5% ($m_B = 5279$ MeV [2], $m_b = 4977$ MeV in quark models [20]). Another possible source of systematic error is associated with the physical value of the lattice spacing. This error is introduced, when converting the “size parameter” d from dimensionless lattice units to physical units. We investigate the magnitude of this error, by using values for the lattice spacing determined by rather different scale setting procedures: $a = 0.079$ fm is used in many ETMC publications and is obtained from m_π , f_π and chiral perturbation theory [22], while $a = 0.096$ fm corresponds to identifying the lattice result for the Sommer parameter r_0 with its typical value 0.5 fm.

B. An analytical rule for heavy antiquark-antiquark binding

To get an analytical qualitative understanding, we first derive an approximate rule for the existence/non-existence of a bound state applying the Bohr-Sommerfeld relation corrected by the WKB approximation, to include the zero point energy of 1/2. For the radial equation in three dimensions we get,

$$4 \int_{c_1}^{c_2} dr \sqrt{2\mu \left(E - V(r) - \frac{l(l+1)}{2\mu r^2} \right)} = 2\pi \left(n + \frac{3}{2} \right), \quad (7)$$

where c_1 and c_2 are the classical turning points. Inserting (4), specializing to angular momentum $l = 0$ and integrating, yields the condition for having at least one bound state,

$$\mu ad \geq \frac{9\pi^2}{128 \times 2^{1/p} \Gamma^2(1 + 1/2p)}. \quad (8)$$

The right hand side of Eq. (8) has a rather moderate dependence on the exponent p . For example, when p increases from the expected values of 1.0 to 2.0, the right hand side only changes from 0.44 to 0.60. Thus the existence of a bound state mainly depends on the product of parameters μad . With the fit parameters for the scalar isosinglet from Table I and a bottom quark one roughly obtains $\mu ad \approx 2.5 \text{ GeV} \times 0.29 \times 4.5 \times 0.079 \text{ fm} \approx 1.3 \gg$

0.44...0.60, which is a strong indication for the existence of a bound state. A similar calculation for the vector isotriplet yields $\mu\alpha d \approx 0.5$, i.e. the existence of a bound state in this channel is rather questionable.

C. Numerical solution of Schrödinger's equation

Note, that the analytical estimates obtained in the previous subsection are rather crude, because e.g. the WKB approximation is questionable, when the potential is divergent at the origin as for a Coulomb-like potential. To investigate the existence of a bound state rigorously, we numerically solve the Schrödinger equation with the Hamiltonian (6). The strongest binding is expected in an s-wave, for which the radial equation is

$$\left[-\frac{\hbar^2}{2\mu} \frac{d^2}{dr^2} + 2m_B + V(r) \right] R(r) = ER(r) \quad (9)$$

with the wave function $\psi = \psi(r) = R(r)/r$. We impose Dirichlet boundary conditions $R(r_{\max}) = 0$ at sufficiently large r_{\max} (we checked that results are stable for $r_{\max} \gtrsim 10$ fm). The radial equation (9) can be solved by standard methods (e.g. 4th order Runge-Kutta shooting) up to arbitrary numerical precision.

In accordance with our analytical estimates we find binding for heavy bottom-bottom tetraquarks in the scalar isosinglet channel. The binding energy $E - 2m_B \approx 30$ MeV...57 MeV depends to some extent on the reduced mass (either $\mu = m_b/2$ or $\mu = m_B/2$) and on the value of the lattice spacing (either $a = 0.079$ fm or $a = 0.096$ fm). To compute the statistical error of $E - 2m_B$, we do a Jackknife analysis using the same bins and reduced samples as in section II C, when determining the parameters α , d and p of the potential ansatz $V(r)$ via χ^2 minimizing fits. Consequently, possibly existing correlations on the level of the lattice correlation functions are partly entering our final results for $E - 2m_B$ (as already discussed in section II C). These results are collected in Table II together with the “confidence for binding”, which is just the probability of a negative value for $E - 2m_B$ assuming a Gaussian distribution for the statistical error. Depending on the concrete choice for the reduced mass μ and the lattice spacing a the binding energy is negative by around $1.76\sigma \dots 3.00\sigma$. This confirms the existence of an heavy-heavy-light-light tetraquark with a confidence level of $\gtrsim 96\%$. The probability to find the two heavy antiquarks at separation r is proportional to $|R(r)|^2$ and shown in Fig. 3. The average separation is around 0.25 fm.

Solving Schrödinger's equation (9) for the vector isotriplet gives strong indication that the potential of this channel is too weak to generate a bound state, i.e. a tetraquark. The resulting wave function is essentially a plane wave with positive energy $E - 2m_B$ within more than 10σ .

Table II: Binding energy and confidence for the existence of a heavy-heavy-light-light tetraquark for the scalar isosinglet channel.

μ	a	$E - 2m_B$	confidence for binding
$m_b/2$	0.079 fm	-30(17) MeV	1.76σ , 96% binding
$m_b/2$	0.096 fm	-49(17) MeV	2.88σ , 100% binding
$m_B/2$	0.079 fm	-38(18) MeV	2.11σ , 98% binding
$m_B/2$	0.096 fm	-57(19) MeV	3.00σ , 100% binding

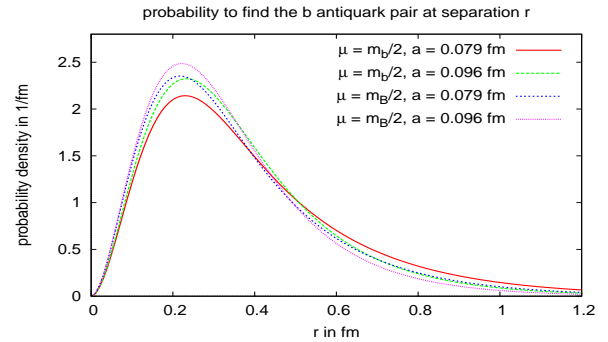


Figure 3: (Color online). Radial probability density $\propto |R(r)|^2$ for the separation of the heavy antiquarks (scalar isosinglet).

D. Discussion of systematic errors

Possible sources of systematic error include the concrete choice of values for the b quark mass m_b and the lattice spacing a . This has already been addressed in the previous subsection and included in the final results in a rather conservative way.

Moreover, the quality of the lattice results for the heavy antiquark-antiquark potential is not sufficient, to determine the parameters α , d and p of the potential ansatz by minimizing a correlated χ^2 . We minimize an uncorrelated χ^2 instead. Our statistical analysis of the binding energy $E - 2m_B$ (the central quantity studied in this work), however, is a single stringent Jackknife analysis starting already on the level of the lattice correlation functions. As discussed in section II C such an analysis partly accounts for potentially existing correlations in t and in r . A possibly remaining residual systematic error is expected to be small and to not alter the strong quantitative result (existence of an heavy-heavy-light-light tetraquark with a confidence level of $\gtrsim 96\%$) in a qualitative way.

Further possible systematic errors are not expected to weaken the binding.

- The static approximation of a ground state with bottom antiquarks is valid, since the bottom quark mass is a very hard scale compared with the scale Λ_{QCD} . Moreover, lattice computations of B mesons [23, 24] and b baryons [25] within the same lattice

setup showed that static quarks are a rather good approximation of bottom quarks.

- In lattice QCD finite volume effects are typically suppressed exponentially. Quantitatively this suppression depends on the extension of the periodic spatial volume L and the mass of the lightest particle, the pion, m_π and is proportional to $\exp(-m_\pi L)$. Even for rather simple quantities which can be computed very precisely, $m_\pi L \gtrsim 3\dots 4$ is usually a sufficient condition for the finite volume effects to be negligible compared to statistical errors. Therefore, for our results (where $m_\pi L = 3.3$), which exhibit sizeable statistical errors, we do not expect that finite volume effects play an important role. Moreover, the spatial extension of the lattice $L \approx 1.9$ fm seems large compared to the typical size of the tetraquark, which is related to $d \approx 4.51 a \approx 0.36$ fm and the average separation of the heavy antiquarks, which is ≈ 0.25 fm.
- In what concerns long range forces our Yukawa-like potential falls faster than the original one-pion-exchange Yukawa potential (OPEP). This happens, because our long range part of the potential has too much noise, to measure the small OPEP. We are only sensitive to the dominant exponential mode in our potential, ie the one due to screening. Notice pions can contribute to the interaction between our two light quarks, and can as well contribute to the pseudoscalar-vector BB^* or vector-vector B^*B^* interaction. In principle the OPEP should enhance the binding at least in some of the channels as it happens for the deuteron.

- Finally, the light u/d quark masses in the lattice computation are unphysically heavy (corresponding to $m_\pi \approx 340$ MeV). Decreasing the light quark masses to their physical values should increase the light cloud radius of a heavy-light meson and, therefore, lead to stronger binding (cf. Fig. 2(a)).

Nevertheless, the listed systematic errors should be investigated numerically in the future, to determine their exact effect on the bound state we predict.

IV. CONCLUSIONS

To summarize, we find strong indication for the existence of an antibottom-antibottom-light-light tetraquark bound state. This result is very promising with respect to further lattice QCD calculations with higher statistics or even lighter dynamical quarks, and for experimental searches of doubly bottom hadrons.

It would be most interesting, to extend the present investigation, to study tetraquark resonances such as the BELLE candidate including a b quark and a \bar{b} antiquark.

Acknowledgments

P.B. thanks the hospitality of IFT and FCT grants CERN/FP/116383/2010, CERN/FP/123612/2011.

M.W. acknowledges support by the Emmy Noether Programme of the DFG (German Research Foundation), grant WA 3000/1-1.

This work was supported in part by the Helmholtz International Center for FAIR within the framework of the LOEWE program launched by the State of Hesse.

-
- [1] R. L. Jaffe, Phys. Rev. D **15**, 267 (1977).
- [2] J. Beringer et al. [Particle Data Group], Phys. Rev. D86, 010001 (2012).
- [3] A. Bondar *et al.* [Belle Collaboration], Phys. Rev. Lett. **108**, 122001 (2012) [arXiv:1110.2251 [hep-ex]].
- [4] D. V. Bugg, Europhys. Lett. **96**, 11002 (2011) [arXiv:1105.5492 [hep-ph]].
- [5] J. L. Ballot and J. M. Richard, Phys. Lett. B **123**, 449 (1983).
- [6] C. Stewart and R. Koniuk, Phys. Rev. D **57**, 5581 (1998) [arXiv:hep-lat/9803003].
- [7] C. Michael and P. Pennanen [UKQCD Collaboration], Phys. Rev. D **60**, 054012 (1999) [arXiv:hep-lat/9901007].
- [8] M. S. Cook and H. R. Fiebig, arXiv:hep-lat/0210054.
- [9] T. Doi, T. T. Takahashi and H. Suganuma, AIP Conf. Proc. **842**, 246 (2006) [arXiv:hep-lat/0601008].
- [10] W. Detmold, K. Orginos and M. J. Savage, Phys. Rev. D **76**, 114503 (2007) [arXiv:hep-lat/0703009].
- [11] M. Wagner [ETM Collaboration], PoS LATTICE **2010**, 162 (2010) [arXiv:1008.1538 [hep-lat]].
- [12] G. Bali and M. Hetzenegger, PoS LATTICE **2010**, 142 (2010) [arXiv:1011.0571 [hep-lat]].
- [13] M. Wagner [ETM Collaboration], Acta Phys. Polon. Supp. **4**, 747 (2011) [arXiv:1103.5147 [hep-lat]].
- [14] J. O. Daldrop, C. Alexandrou, M. D. Brida, M. Gravina, L. Scorzato, C. Urbach and M. Wagner [ETM Collaboration], PoS LATTICE **2012**, 161 (2012) [arXiv:1211.5002 [hep-lat]].
- [15] C. Alexandrou, J. O. Daldrop, M. D. Brida, M. Gravina, L. Scorzato, C. Urbach and M. Wagner [ETM Collaboration], arXiv:1212.1418 [hep-lat].
- [16] M. Wagner, C. Alexandrou, J. O. Daldrop, M. D. Brida, M. Gravina, L. Scorzato, C. Urbach and C. Wiese [ETM Collaboration], arXiv:1212.1648 [hep-lat].
- [17] M. Wagner, C. Alexandrou, J. O. Daldrop, M. D. Brida, M. Gravina, L. Scorzato, C. Urbach and C. Wiese [ETM Collaboration], arXiv:1302.3389 [hep-lat].
- [18] N. Cardoso, M. Cardoso and P. Bicudo, Phys. Rev. D **84**, 054508 (2011) [arXiv:1107.1355 [hep-lat]].
- [19] N. Cardoso and P. Bicudo, arXiv:1209.1532 [hep-lat].
- [20] S. Godfrey and N. Isgur, Phys. Rev. D **32**, 189 (1985).
- [21] C. Michael and A. McKerrell, “Fitting correlated hadron mass spectrum data,” Phys. Rev. D **51**, 3745 (1995) [hep-lat/9412087].
- [22] R. Baron *et al.* [ETM Collaboration], JHEP **1008**, 097 (2010) [arXiv:0911.5061 [hep-lat]].

- [23] K. Jansen *et al.* [ETM Collaboration], JHEP **0812**, 058 (2008) [arXiv:0810.1843 [hep-lat]].
- [24] C. Michael *et al.* [ETM Collaboration], JHEP **1008**, 009 (2010) [arXiv:1004.4235 [hep-lat]].
- [25] M. Wagner *et al.* [ETM Collaboration], JHEP **1107**, 016 (2011) [arXiv:1104.4921 [hep-lat]].

Lattice investigation of heavy meson interactions

Björn Wagenbach¹, Pedro Bicudo², Marc Wagner^{1,3}

¹ Goethe-Universität Frankfurt am Main, Institut für Theoretische Physik,
Max-von-Laue-Straße 1, D-60438 Frankfurt am Main, Germany

² Dep. Física and CFTP, Instituto Superior Técnico, Av. Rovisco Pais, 1049-001 Lisboa,
Portugal

³ European Twisted Mass Collaboration (ETMC)

E-mail: wagenbach@th.physik.uni-frankfurt.de

Abstract. We report on a lattice investigation of heavy meson interactions and of tetraquark candidates with two very heavy quarks. These two quarks are treated in the static limit, while the other two are up, down, strange or charm quarks of finite mass. Various isospin, spin and parity quantum numbers are considered.

1. Introduction

We study the potential of two static quarks in the presence of two quarks of finite mass. While in [1, 2, 3] we have exclusively considered two static antiquarks and two light quarks ($\bar{Q}\bar{Q}ll$), where $l \in \{u, d\}$, here we also use s and c quarks, i.e. investigate $\bar{Q}\bar{Q}ss$ and $\bar{Q}\bar{Q}cc$, to obtain certain insights regarding the quark mass dependence of the static antiquark-antiquark interaction. We also discuss first steps regarding the static quark-antiquark case, i.e. $\bar{Q}\bar{Q}\bar{l}l$, $\bar{Q}\bar{Q}\bar{s}s$ and $\bar{Q}\bar{Q}\bar{c}c$.

$\bar{Q}\bar{Q}qq$ systems as well as $\bar{Q}\bar{Q}\bar{q}q$ systems have been studied also by other groups (cf. e.g. [4, 5, 6, 7, 8, 9, 10, 11, 12]).

2. Creation operators and trial states

The $\bar{Q}\bar{Q}qq$ and $\bar{Q}\bar{Q}\bar{q}q$ potentials $V(r)$ are extracted from correlation functions

$$C(t) \equiv \langle \Omega | \mathcal{O}^\dagger(t) \mathcal{O}(0) | \Omega \rangle \quad (1)$$

according to

$$V(r) =_{\text{large } t} V_{\text{eff}}(r, t) , \quad V_{\text{eff}}(r, t) \equiv \frac{1}{a} \ln \left(\frac{C(t)}{C(t+a)} \right), \quad (2)$$

where a is the lattice spacing and \mathcal{O} denote suitable creation operators, which are discussed in detail below. For an introduction to lattice hadron spectroscopy cf. e.g. [13].

2.1. Static-light mesons (“ B and \bar{B} mesons”)

The starting point are static-light mesons, which either consist of a static quark Q and an antiquark \bar{q} or of a static antiquark \bar{Q} and a quark q with $q \in \{u, d, s, c\}$. These mesons can be labeled by parity $\mathcal{P} = \pm$, by the z -component of the light quark spin $j_z = \pm 1/2$ ($j = 1/2$, because we do not consider gluonic excitations) and in case of $q \in \{u, d\}$ by the z -component

of isospin $I_z = \pm 1/2$ ($I = 1/2$). The lightest static-light meson has $\mathcal{P} = -$ and is commonly denoted by S , its heavier parity partner with $\mathcal{P} = +$ by P_- . The static-light meson S is an approximation for B/B^* , B_s/B_s^* and B_c listed in [14].

We use static-light meson trial states

$$\mathcal{O}|\Omega\rangle \equiv \bar{Q}\Gamma q|\Omega\rangle \quad (3)$$

with $\Gamma \in \{\gamma_5, \gamma_0\gamma_5, \gamma_j, \gamma_0\gamma_j\}$ for the S and $\Gamma \in \{1, \gamma_0, \gamma_j\gamma_5, \gamma_0\gamma_j\gamma_5\}$ for the P_- meson. For a more detailed discussion of static-light mesons cf. [15, 16].

2.2. $B\bar{B}$ systems

We are interested in the potential of two static-light mesons, i.e. their energy as a function of their separation r . W.l.o.g. we separate the mesons along the z -axis, i.e. their static antiquark \bar{Q} and quark Q are located at $\vec{r}_1 = (0, 0, +r/2)$ and $\vec{r}_2 = (0, 0, -r/2)$, respectively. The corresponding $B\bar{B}$ trial states are

$$\mathcal{O}|\Omega\rangle \equiv \Gamma_{AB}\tilde{\Gamma}_{CD}\left(\bar{Q}_C^a(\vec{r}_1)q_A^{(f_1)a}(\vec{r}_1)\right)\left(\bar{q}_B^{(f_2)b}(\vec{r}_2)Q_D^b(\vec{r}_2)\right)|\Omega\rangle \quad (4)$$

(A, B, \dots are spin indices, a, b color indices and $(f_1), (f_2)$ flavor indices). Since there are no interactions involving the static quark spins, one should not couple static spins and spins of finite mass, but contract the static spin indices with $\tilde{\Gamma} \in \{\gamma_5, \gamma_0\gamma_5, \gamma_3, \gamma_0\gamma_3, \gamma_1, \gamma_2, \gamma_0\gamma_1, \gamma_0\gamma_2\}$. This results in a non-vanishing correlation function independent of Γ .

The separation of the static quark and the static antiquark restricts rotational symmetry to rotations around the axis of separation, i.e. the z -axis. Therefore, and since there are no interactions involving the static quark spins, we can label states by the z -component of the light quark spin $j_z = -1, 0, +1$. For $j_z = 0$, i.e. for rotationally invariant states, spatial reflections along an axis perpendicular to the axis of separation are also a symmetry operation (w.l.o.g. we choose the x -axis). The corresponding quantum number is $\mathcal{P}_x = \pm$. \mathcal{P}_x can be used as a quantum number also for $j_z \neq 0$ states, if we use $|j_z|$ instead of j_z . Parity \mathcal{P} is not a symmetry, since it exchanges the positions of the static quark and the static antiquark. However, parity combined with charge conjugation, $\mathcal{P} \circ C$ is a symmetry and, therefore, a quantum number. When $q, \bar{q} \in \{u, d\}$, isospin $I \in \{0, 1\}$ and its z -component $I_z \in \{-1, 0, +1\}$ are also quantum numbers. In summary, there are up to five quantum numbers, which label $B\bar{B}$ states, $(I, I_z, |j_z|, \mathcal{P} \circ C, \mathcal{P}_x)$.

2.3. BB systems (and $\bar{B}\bar{B}$ systems)

We use BB trial states

$$\mathcal{O}|\Omega\rangle \equiv (\mathcal{C}\Gamma)_{AB}\tilde{\Gamma}_{CD}\left(\bar{Q}_C^a(\vec{r}_1)\psi_A^{(f_1)a}(\vec{r}_1)\right)\left(\bar{\psi}_D^b(\vec{r}_2)\psi_B^{(f_2)b}(\vec{r}_2)\right)|\Omega\rangle \quad (5)$$

with $\tilde{\Gamma} \in \{1, \gamma_0, \gamma_3\gamma_5, \gamma_1\gamma_2, \gamma_1\gamma_5, \gamma_2\gamma_5, \gamma_2\gamma_3, \gamma_1\gamma_3\}$ ($\mathcal{C} \equiv \gamma_0\gamma_2$ denotes the charge conjugation matrix). Arguments similar to those of the previous subsection lead to quantum numbers $(I, I_z, |j_z|, \mathcal{P}, \mathcal{P}_x)$. For a more detailed discussion cf. [1, 2].

3. Lattice setup

We use three ensembles of gauge link configurations generated by the European Twisted Mass Collaboration (ETMC) (cf. Table 1). For the $\bar{Q}\bar{Q}qq$ potentials we use $N_f = 2$ ensembles with lattice spacing $a \approx 0.079$ fm for $q \in \{u, d\}$ and an even finer lattice spacing $a \approx 0.042$ fm for $q \in \{s, c\}$, because in the latter case the potentials are quite narrow. Existing $\bar{Q}Q\bar{q}q$ results are

Ensemble	N_f	β	$(L/a)^3 \times (T/a)$	$a\mu_l$	$a\mu_\sigma$	$a\mu_\delta$	a	m_π
A40.24	2	3.90	$24^3 \times 48$	0.00400	-	-	0.079 fm	340 MeV
E17.32	2	4.35	$32^3 \times 64$	0.00175	-	-	0.042 fm	352 MeV
A40.24	2+1+1	1.90	$24^3 \times 48$	0.00400	0.15	0.19	0.086 fm	332 MeV

Table 1. ETMC gauge link ensembles used in this work.

rather preliminary and have been obtained exclusively with $q = c$ and the $N_f = 2+1+1$ ensemble with $a \approx 0.086$ fm. For details regarding these ETMC gauge link ensembles cf. [17, 18, 19, 20, 21].

Correlation functions have been computed using around 100 gauge link configurations from each of the three ensembles. We have checked that these correlation functions transform appropriately with respect to the symmetry transformations (1) twisted mass time reversal, (2) twisted mass parity, (3) twisted mass γ_5 -hermiticity, (4) charge conjugation and (5) cubic rotations. In a second step we have averaged correlation functions related by those symmetries to reduce statistical errors.

4. Numerical results

4.1. $\bar{Q}\bar{Q}qq$ potentials

In the following we focus on the attractive channels between ground state static-light mesons (S mesons). For $q \in \{u, d\}$ there is a more attractive scalar isosinglet ($qq = (ud - du)/\sqrt{2}$, $\Gamma = \gamma_5 + \gamma_0\gamma_5$ corresponding to quantum numbers $(I, |j_z|, \mathcal{P}, \mathcal{P}_x) = (0, 0, -, +)$) and a less attractive vector isotriplet ($qq \in \{uu, (ud+du)/\sqrt{2}, dd\}$, $\Gamma = \gamma_j + \gamma_0\gamma_j$ corresponding to quantum numbers $(I, |j_z|, \mathcal{P}, \mathcal{P}_x) = (1, \{0, 1\}, -, \pm)$). For $qq = ss$ there is only a single attractive channel, the equivalent of the vector isotriplet. To study also the scalar isosinglet with s quarks, we consider two quark flavors with the mass of the s quark, i.e. $qq = (s_1s_2 - s_2s_1)/\sqrt{2}$. Similarly we consider $qq = (c_1c_2 - c_2c_1)/\sqrt{2}$ to study a charm scalar isosinglet.

Proceeding as in [3] we perform χ^2 minimizing fits of

$$V(r) = -\frac{\alpha}{r} \exp\left(-\left(\frac{r}{d}\right)^p\right) \quad (6)$$

with respect to the parameters d (light isotriplet), (d, α) ($q = s$ or $q = c$) or (d, α, p) (light isosinglet) to the lattice results for the $\bar{Q}\bar{Q}qq$ potentials. The resulting functions $V(r)$ are shown in Figure 1.

To determine, whether the investigated mesons may form a bound state, i.e. a tetraquark, we insert the potentials shown in Figure 1 into Schrödinger's equation with reduced mass $\mu \equiv m(S)/2$ and solve it numerically (cf. [3] for details). While there is strong indication for a bound state in the light scalar isosinglet channel, there seems to be no binding for the light vector isotriplet, or when $q = s$ or $q = c$. To quantify these statements, we list in Table 2 the factor by which the reduced mass μ has to be multiplied to obtain a bound state with confidence level 1σ and 2σ , respectively (the factors ≤ 1.0 in the light scalar isosinglet indicate binding). These results clearly show that meson-meson bound states are more likely to exist for B mesons than for B_s or B_c mesons. In other words it seems to be essential for a tetraquark to have both heavy quarks (leading a large reduced mass μ) and light quarks (resulting in a deep and wide potential).

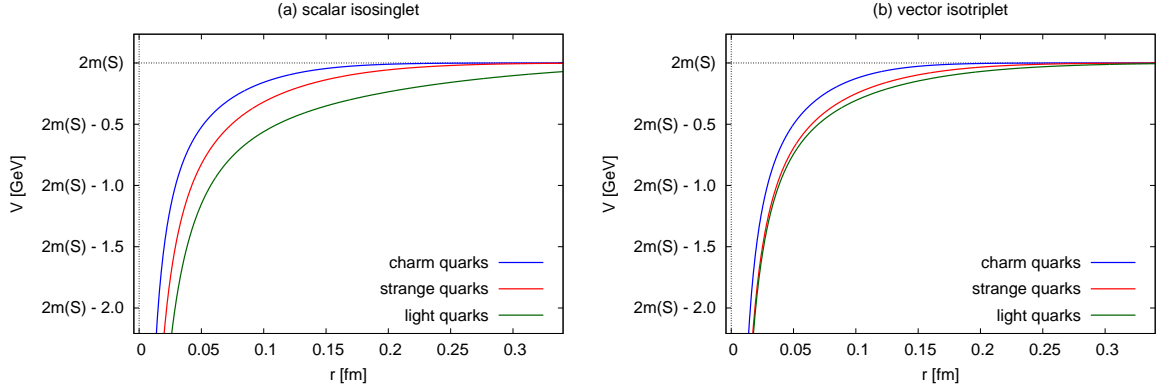


Figure 1. $\bar{Q}\bar{Q}qq$ potentials (6) for $q = u/d$, $q = s$ and $q = c$ (error bands are not shown). **(a)** Scalar isosinglet. **(b)** Vector isotriplet.

flavor	light		strange		charm	
confidence level for binding	1σ	2σ	1σ	2σ	1σ	2σ
scalar isosinglet	0.8	1.0	1.9	2.2	3.1	3.2
vector isotriplet	1.9	2.1	2.5	2.7	3.4	3.5

Table 2. Factors, by which the reduced mass $\mu = m(S)/2$ in Schrödinger's equation has to be multiplied to obtain a four-quark bound state with confidence level 1σ and 2σ , respectively.

4.2. $\bar{Q}Q\bar{q}q$ potentials

At the moment there are only preliminary results for $\bar{Q}Q\bar{q}q$ potentials corresponding to isospin $I = 1$ and $q = c$, i.e. $\bar{q}q = (\bar{c}_1c_2 - \bar{c}_2c_1)/\sqrt{2}$. Interestingly we observed that all these potentials are attractive, while in the $\bar{Q}\bar{Q}qq$ case only half of them are attractive and the other half is repulsive. This can be understood in a qualitative way by comparing the potential of $\bar{Q}Q$ and of $\bar{Q}\bar{Q}$ generated by one-gluon exchange. For $\bar{Q}\bar{Q}$ the Pauli principle applied to qq implies either a symmetric (sextet) or an antisymmetric (triplet) color orientation of the static quarks corresponding to a repulsive or attractive interaction, respectively. For $\bar{Q}Q$ no such restriction is present, i.e. all channels contain contributions of the attractive color singlet, which dominates the repulsive color octet.

$I = 0$ requires the computation of an additional diagram and u/d and s quarks are more demanding with respect to HPC resources than c quarks. We expect corresponding results to be available soon.

5. Conclusions

We have obtained insights regarding the quark mass dependence of $\bar{Q}\bar{Q}qq$ potentials, which suggest that tetraquark states with two heavy \bar{b} antiquarks seem to be more likely to exist, when there are also two light u/d quarks involved but not s or c quarks.

Preliminary results for $\bar{Q}Q\bar{q}q$ potentials indicate that there are only attractive channels, which is in contrast to the $\bar{Q}\bar{Q}qq$ case.

Acknowledgments

We thank Joshua Berlin, Owe Philipsen, Annabelle Uenver-Thiele and Philipp Wolf for helpful discussions. M.W. acknowledges support by the Emmy Noether Programme of the DFG (German Research Foundation), grant WA 3000/1-1. This work was supported in part by the Helmholtz International Center for FAIR within the framework of the LOEWE program launched by the State of Hesse.

References

- [1] M. Wagner [ETM Collaboration], PoS LATTICE **2010**, 162 (2010) [arXiv:1008.1538 [hep-lat]].
- [2] M. Wagner [ETM Collaboration], Acta Phys. Polon. Supp. **4**, 747 (2011) [arXiv:1103.5147 [hep-lat]].
- [3] P. Bicudo, M. Wagner, Phys. Rev. D **87**, no.11, 114511 (2013) [arXiv:1209.6274 [hep-ph]].
- [4] C. Stewart and R. Koniuk, Phys. Rev. D **57**, 5581 (1998) [hep-lat/9803003].
- [5] C. Michael *et al.* [UKQCD Collaboration], Phys. Rev. D **60**, 054012 (1999) [hep-lat/9901007].
- [6] M. S. Cook and H. R. Fiebig, [hep-lat/0210054].
- [7] G. Bali *et al.* [SESAM Collaboration], Phys. Rev. D **71**, 114513 (2005) [hep-lat/0505012].
- [8] T. Doi, T. T. Takahashi and H. Suganuma, AIP Conf. Proc. **842**, 246 (2006) [hep-lat/0601008].
- [9] W. Detmold, K. Orginos and M. J. Savage, Phys. Rev. D **76**, 114503 (2007) [hep-lat/0703009].
- [10] G. Bali *et al.* [QCDSF Collaboration], PoS LATTICE **2010**, 142 (2010) [arXiv:1011.0571 [hep-lat]].
- [11] G. Bali *et al.* [QCDSF Collaboration], PoS LATTICE **2011**, 123 (2011) [arXiv:1111.2222 [hep-lat]].
- [12] Z. S. Brown and K. Orginos, Phys. Rev. D **86**, 114506 (2012) [arXiv:1210.1953 [hep-lat]].
- [13] M. Wagner, S. Diehl, T. Kuske and J. Weber, arXiv:1310.1760 [hep-lat].
- [14] K. A. Olive *et al.* [Particle Data Group Collaboration], Chin. Phys. C, 38, 090001 (2014).
- [15] K. Jansen *et al.* [ETM Collaboration], JHEP **0812**, 058 (2008) [arXiv:0810.1843 [hep-lat]].
- [16] C. Michael *et al.* [ETM Collaboration], JHEP **1008**, 009 (2010) [arXiv:1004.4235 [hep-lat]].
- [17] P. Boucaud *et al.* [ETM Collaboration], Comput. Phys. Commun. **179**, 695 (2008) [arXiv:0803.0224 [hep-lat]].
- [18] R. Baron *et al.* [ETM Collaboration], JHEP **1008**, 097 (2010) [arXiv:0911.5061 [hep-lat]].
- [19] R. Baron *et al.* [ETM Collaboration], JHEP **1006**, 111 (2010) [arXiv:1004.5284 [hep-lat]].
- [20] K. Jansen *et al.* [ETM Collaboration], JHEP **1201**, 025 (2012) [arXiv:1110.6859 [hep-ph]].
- [21] K. Cichy, K. Jansen and P. Korcyl, Nucl. Phys. B **865**, 268 (2012) [arXiv:1207.0628 [hep-lat]].

